VIBRONIC INTERACTIONS IN THE
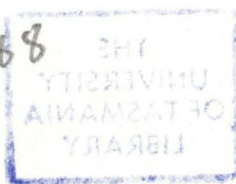## SPECTROSCOPY OF TRANSITION METAL COMPLEXES

by

Mark Julian Riley B.Sc.(Hons.)

A thesis submitted in fulfilment of the requirements
for the degree of Doctor of Philosophy

The Department of Chemistry
University of Tasmania
1987

graduating '88

This thesis contains no material which has been accepted for the award of any other degree or diploma in any University. To the best of my knowledge, this work contains no material previously presented by another person, except where due reference is made in the text.

Mark Riley

ACKNOWLEDGEMENTS

- "Camelot!"
- "It's only a model..."

        Monty Python and the Holy Grail.

ABSTRACT

This thesis is concerned with the effects of vibronic coupling in inorganic spectroscopy. The thesis is divided into two: a theoretical section which approaches the topic in general terms and an experimental section where examples of the phenomena described in the first section are taken from electron spin resonance and vibronic absorption spectroscopy of inorganic compounds.

The theoretical section examines the possible spectroscopic effects due to vibronic interaction. A numerical approach using the variational method has been employed to model these systems, although where ever possible simple approximate formulae are also given. Many illustrative calculations are given to test the validity of such formulae and several new expressions are presented.

The experimental section can be subdivided into investigations of ground state and excited state properties. In both cases the easiest way to study vibronic interactions is to vary the occupation of the vibronic levels by varying the temperature. This then leads to the temperature dependence of the physical properties that depend on the electronic character and geometry of the system.

The ground state properties of six coordinate Cu(II) complexes have been examined from the temperature dependent behaviour of their g-values. The experimental data of Cu(II) doped K_2ZnF_4, zinc Tutton salts, and NH_4Cl were reexamined, and interpreted in terms of the usual cubic Jahn-Teller Hamiltonian with additional strain terms included to account for the low symmetry of these systems.

The excited state properties were examined from the point of view of electronic absorption spectroscopy. The spectrum of square planar $CuCl_4^{2-}$ shows an unusual temperature dependence of both the intensity and band maxima which was rationalised in terms of the ground and excited state potentials respectively.

Vibronic interactions were found to be essential to the interpretation of the the molecular properties of the above metal complexes. They could also play an important role in biological molecules, as the active site in protein molecules often involves the change in geometry and/or electronic character around a transition metal centre.

CONTENTS

PART A: THEORY

3. WEAK VIBRONIC INTERACTION:
WORKING WITHIN THE ADIABATIC APPROXIMATION

4. STRONG VIBRONIC INTERACTION:
THE DYNAMIC JAHN-TELLER EFFECT

PRELIMINARIES:

0.1 KEY TO COMMONLY USED SYMBOLS

Unless otherwise stipulated, the commonly occurring symbols below will have the following meanings:

$\Omega_{ki} = \Psi_k \Phi_i$ . . The total vibronic wavefunction, Ω_{ki}; a product of the kth electronic, Ψ_k, and the ith vibrational, Φ_i, wavefunctions.

$\Psi_k = \Sigma\ a_{ik}\psi_i$ . . The kth electronic wavefunction, Ψ_k; a linear combination of the i electronic basis functions ψ_i.

$\Phi_i = \Sigma\ a_{ik}\phi_i$ . . The ith vibrational wavefunction, Φ_i; a linear combination of the i vibrational basis functions ϕ_i.

S, Q ..... The symmetry and normal coordinates.

ξ .... The dimensionless symmetry coordinates.

ρ, ϕ ..... The dimensionless polar coordinates.

Q_θ, Q_ε ... The dimensionless components of the e_g vibration.

A_1, A_2 ... The first and second order Jahn-Teller coupling constants.

K_2, K_3 ... The harmonic and anharmonic force constants.

ε .... The adiabatic potential surfaces.

$|\theta\rangle, |\varepsilon\rangle$ .. The tetragonal and orthorhombic components of a doubly degenerate electronic state.

β .... The warping parameter of the Jahn-Teller potential surface.

0.2 ABBREVIATIONS USED

AA   Adiabatic Approximation.

AOM   Angular Overlap Model.

A&B   Abragam and Bleaney (1970).

A&S   Abramowitz and Stegun (1972).

CDL   Cohen-Tannoudji, Diu and Laloe (1977).

ESR   Electron Spin Resonance.

HWHH Half Width at Half Height.

JT   Jahn-Teller.

LCAO Linear Combination of Atomic Orbitals.

LF   Ligand Field.

RMS   Root-Mean-Square.

SHO   Simple Harmonic Oscillator.

S&G   Silver and Getz (1974).

WDC   Wilson, Decius and Cross (1955).

0.3 THESIS ORGANISATION

This thesis is divided into two parts; a theoretical section where vibronic theory is considered quite generally, and an experimental section where the theory is applied to the spectroscopy of transition metal compounds. Appendices occur at the end of each chapter, and the references are organised in alphabetical order by author at the end of the thesis.

Within each chapter the equations, figures and tables are numbered so, for example, the first equation, figure and table of chapter 8, are referred to as (8.1), figure 8.1, and table 8.1 respectively. Note that equations are distinguished by brackets. Only pages containing text are numbered.

CHAPTER 1: INTRODUCTION

1.1 VIBRONIC APPROXIMATIONS

1.1.1 The Adiabatic Approximation.

The Schrödinger equation for a polyatomic system can be written as:

$$H_T(q,Q) \; \Omega_K(q,Q) \; = \; E_K \; \Omega_K(q,Q) \qquad (1.1)$$

where $\Omega_K(q,Q)$ denotes the Kth solution to the total Hamiltonian:

$$H_T(q,Q) \; = \; T_n(Q) \; + \; T_e(q) \; + \; V(q,Q) \qquad (1.2)$$

Here $T_n(Q)$ and $T_e(q)$ are the kinetic energy operators of the nuclei and electrons respectively and $V(q,Q)$ is the total potential energy of the system. In (1.2) it is assumed that rotation and translation of the molecule has been eliminated and the effects of spin are neglected.

Since this <u>vibrational-electronic</u>, or "vibronic", Hamiltonian is a three or more body problem for molecules, analytic solutions are not possible. For molecules with a large number of electrons numerical solutions, (possible in principle) are usually not accessible. Quite early on in the development of quantum mechanics Born and Oppenheimer (1927) made an approximation that decouples the motions of the nuclei and electrons and greatly simplifies the problem .

This <u>adiabatic approximation</u> is based on the fact that the nuclei are much heavier than the electrons, and this results in a large difference in their velocities. The electrons can be pictured as moving so much faster than the nuclei that the latter appear to be stationary. Approximately then, the "fast" electrons instantaneously attain a stationary electronic state for every position of the "slow" nuclei; or <u>the electrons adiabatically follow the motions of the</u> <u>nuclei</u>. To gain an idea of the magnitudes involved, the nuclei in the H_2^+ ion move approximately one millimetre for every metre the electrons

travel (Atkins 1982 pg 470). For other molecules with heavier nuclei this approximation is likely to be even better.

Mathematically, the adiabatic approximation assumes that the wavefunctions of (1.1) can be written as:

$$\Omega_{ki}(q,Q) = \Psi_k(q,Q)\Phi_{ki}(Q) \qquad (1.3)$$

where $\Psi_k(q,Q)$ is the kth electronic wavefunction that depends only parametrically on Q, and $\Phi_{ki}(Q)$ is the ith vibrational wavefunction which is independent of q, seeing the average field of the electrons in the kth electronic state.

Equation (1.3) represents the basic assumption of the adiabatic approximation; any wavefunction that can be written in this form can be said to belong to an adiabatic model (Ballhausen and Hansen 1972). It is important when considering various vibronic schemes to distinguish between the cases where the electronic state is well separated from others and (1.3) is a good approximation, and the cases of degeneracy or pseudo-degeneracy where it is not.

1.1.2 Non-Degenerate Electronic States.

There are many ways to use (1.3) in the solution of (1.1) and a number of different terminologies are used in the literature. This can cause some confusion, and for this reason the definitions of Ballhausen and Hansen (1972) are strictly followed. The four common adiabatic schemes are given below in order of increasing approximation. Equation (1.2) can be rewritten as:

$$H_T(q,Q) = T_n(Q) + H_e(q,Q) \qquad (1.4)$$

where $H_e(q,Q)$ is the electronic Hamiltonian, of which $\Psi_k(q,Q)$ is the kth eigenfunction.

ie $\qquad H_e(q,Q)\Psi_k(q,Q) = \varepsilon_k(Q)\Psi_k(q,Q) \qquad (1.5)$

Substituting (1.4) into (1.1), the equation for nuclear motion is:

$$[T_n(Q) + \varepsilon_k(Q) + \langle\Psi_k(q,Q)|T_n(Q)|\Psi_k(q,Q)\rangle]\Phi_{ki}(Q) = E_{ki}\Phi_{ki}(Q) \qquad (1.6)$$

$$(1.2)$$

Here the fact that Φ commutes with H_e, but Ψ does not commute with $T_n(Q)$, has been used (Longuet-Higgins 1961, equations 11,12; Fischer 1981, section 3.1). Equation (1.3) with Ψ and Φ determined by (1.5) and (1.6) represents the <u>Born-Huang</u> adiabatic approximation.

If the additional approximation is made that $\Psi(q,Q)$ does commute with $T_n(Q)$ (Piepho and Schatz 1983, section 3.2):

$$T_n(Q)\Psi(q,Q)\Phi(Q) \approx \Psi(q,Q)T_n(Q)\Phi(Q) \qquad (1.7)$$

then the matrix element in (1.6) disappears:

$$[T_n(Q) + \varepsilon_k(Q)]\Phi_{ki}(Q) = E_{ki}\Phi_{ki}(Q) \qquad (1.8)$$

Equation (1.3) together with (1.5), (1.8) is called the <u>Born-Oppenheimer</u> adiabatic approximation. The consequences of the approximation in (1.7) have recently been investigated in detail (Strickler 1976, Marechal 1985). It is concluded that $\Psi(q,Q)$ should be a slowly varying function of Q for (1.7) to be valid. In this approximation, (1.5) is solved for the pertinent range of Q, and the electronic energy $\varepsilon(Q)$ then plays the role of a potential surface for the nuclear motion in (1.8). This was the approximation made in the original work of Born and Oppenheimer (1927).

The electronic Hamiltonian of (1.4) can be written as:

$$H_e(q,Q) = H_e^O(q) + V'(Q) \qquad (1.9)$$
$$= [T_e(q) + V(q,Q_0)] + \left[\sum_n \left(\frac{\partial V}{\partial Q_n}\right)_o Q_n + \sum_{n,m} \left(\frac{\partial^2 V}{\partial Q_n \partial Q_m}\right)_o Q_n Q_m \right]$$

where $V(q,Q)$ has been expanded as a Taylor series about an equilibrium nuclear geometry Q_0. The electronic wavefunctions of (1.3) can then be approximated by:

$$\Psi_k(q,Q) = \Psi_k^O(q) + \sum_{l \neq k} \Psi_l^O(q) c_{lk}(Q) \qquad (1.10)$$

where $\Psi_k^O(q,Q)$ are the solutions to the electronic Hamiltonian H_e^O frozen at the equilibrium nuclear geometry (equation (1.13)), and the coefficients $c_{lk}(Q)$ can be found from first order perturbation theory using V' of (1.9) as the perturbation operator. The potential to be used in (1.8) is then the perturbation energy:

$$(1.3)$$

$$\varepsilon_k(Q) = \varepsilon_k(Q_o) + u_{kk} + \sum_{l \neq k} \frac{u_{kl} u_{lk}}{\varepsilon_k^o - \varepsilon_l^o} \tag{1.11}$$

where $u_{kl} = \langle \Psi_k^o(q) | V_e'(Q) | \Psi_l^o(q) \rangle$.

Equations (1.3),(1.10) that are found from (1.5),(1.8),(1.11) represent the <u>Herzberg-Teller</u> adiabatic approximation.

If only the first term of (1.10) is kept then we have:
$$\Psi_{ki}(q,Q) = \Psi_k^o(q) \Phi_{ki}(Q) \tag{1.12}$$
which is found from the solutions of

$$H_e^o(q) \Psi_k^o(q) = \varepsilon_k^o \Psi_k^o(q) \tag{1.13}$$

$$[T_n(Q) + \varepsilon_k^o + u_{kk}] \Phi_{ki} = E_{ki} \Phi_{ki} \tag{1.14}$$

Equations (1.12)-(1.14) constitutes the <u>crude</u> adiabatic approximation, and is the adiabatic approximation most commonly used in the literature.

The above four adiabatic schemes can be visualised as follows (Longuet-Higgins 1961):

i) In the <u>Born-Huang</u> approximation, the electronic wavefunctions are dependent both on the momenta and positions of the nuclei.

ii) In the <u>Born-Oppenheimer</u> approximation, the electronic wavefunctions are dependent only on the positions of the nuclei.

iii) In the <u>Herzberg-Teller</u> approximation, they depend on the nuclei only in a linear fashion.

iv) In the <u>crude adiabatic</u> approximation they are independent of the positions of the nuclei, which are assumed fixed at an equilibrium geometry.

All of the above adiabatic schemes are only valid when the potential surface $\varepsilon_k(Q)$ is well separated from those of other electronic states. If this is not the case, then the adiabatic separation implied in (1.3) is not a good approximation and the idea of a potential surface representing the geometry of a molecule loses its meaning. In this case " ...the notion of spatial structure of a polyatomic system loses

its physical sense." (Bersuker and Polinger 1982), or in the words of Woolley (1981): " Molecular structure is a metaphor.".

1.1.3 Degenerate Electronic States.

The general criterion for which the adiabatic schemes of the previous section are obeyed is given by:

$$h\nu \ll |\,\varepsilon_m - \varepsilon_k\,| \qquad (1.15)$$

where $h\nu$ is the energy of the vibrations of the electronic state Ψ_k at energy ε_k and ε_m is the energy of any other electronic state. If an electronic state Ψ_m is close in energy to that of Ψ_k, then the adiabatic approximation breaks down. The most dramatic example of this is the "Jahn-Teller" effect, when two or more electronic states are degenerate.

The following degenerate scheme is taken from Bersuker (1984a). Firstly the potential energy operator is expanded in terms of the normal coordinates Q about an equilibrium geometry.

$$V(q,Q) = V(q,Q_0) + \sum_n \left(\frac{\partial V}{\partial Q_n}\right)_0 Q_n + \sum_{n,m} \left(\frac{\partial^2 V}{\partial Q_n \partial Q_m}\right)_0 Q_n Q_m + \ldots \quad (1.16)$$

It should be noted that terms higher than second order are only qualitatively correct in view of the adiabatic approximation to be made (see Englman 1972 pg13).

The electronic Hamiltonian in the crude adiabatic approximation, (1.13), is then solved for the number (d) of degenerate (or near degenerate) states at the equilibrium geometry. The total wavefunction is then expressed as a linear combination of adiabatic vibronic wavefunctions:

$$\Omega(q,Q) = \sum_{k=1}^{d} \Psi_k(q)\Phi_{ki}(Q) \qquad (1.17)$$

When substituted into (1.1), a system of d coupled equations are obtained for the nuclear motion:

$$[T_n(Q) + u_{kk}(Q) + \varepsilon_k(Q_0)]\Phi_k + \sum_{m \neq k}^{d} [u_{km}(Q)\Phi_m(Q)] = E_k\Phi_k(Q) \qquad (1.18)$$

$$u_{km} = \langle \Psi_k(q) \,|\, V(q,Q) - V(q,Q_0) \,|\, \Psi_m \rangle, \qquad k=1,\ldots d.$$

When vibronic coupling is absent then all of the matrix elements u_{km} are zero, and the equations in (1.18) decouple. The crude adiabatic approximation of the previous section is then recovered, as the wavefunctions of (1.17) will consist of single terms. When vibronic coupling is present, as will be the case for close lying states, then the equations of (1.18) remain coupled.

The u_{km} terms in (1.18) are called vibronic coupling constants (or Jahn-Teller coupling constants in the case of degeneracy).As a consequence of the breakdown of the adiabatic approximation (ie the inability to express the wavefunctions in the form of eqution (1.3)), the vibronic equations in (1.18) must be solved numerically. However in some cases, where the coupling constants are large, the adiabatic approximation can again be recovered by making the electronic basis a varying function of the Jahn-Teller active coordinates (chapter 4). The derivation of (1.18) has used a linear combination of crude adiabatic wavefunctions as a basis and will be a good approximation as long as any electronic states that are not included are far away in energy (McLachlan 1961).

Finally it should be noted that the adiabatic approximation is not confined to systems of nuclei and electrons, but is a general principle used to separate fast and slow subsystems. For example it can also be applied to the separation of low and high frequency molecular vibrations (Mills 1984).

(1.6)

1.2 THE ADIABATIC POTENTIAL ENERGY SURFACES.

' "What is the use of a book", thought Alice,
"without pictures or conversation?" '   - Lewis Carroll.

The concept of potential energy surfaces arises out of the approximate description that the total wavefunction of the system can be written as a single product of the form given in equation (1.3). This equation implies that a vibronic state can be associated with a single potential potential surface which then determines its vibrational properties. As mentioned in the previous section this is not quite true in general, but is often a good approximation.

To illustrate some effects of vibronic coupling the electronic Hamiltonian is expanded in a Taylor series about a reference nuclear geometry as in (1.9), and the electronic wavefunctions are expanded as a linear combination of the crude adiabatic states Ψ^o of equation (1.13) which are the solutions of the electronic Hamiltonian at the reference geometry:

$$\Psi_k(Q) = \sum_i c_{ki}\psi_i^o \qquad (1.19)$$

Rather than using perturbation theory, as in the Herzberg-Teller approach, the coefficients c_{ki} are found by diagonalising the secular equation made from the matrix elements of the perturbation part of the electronic Hamiltonian, $V'(Q)$ in (1.9), in the crude adiabatic basis. For simplicity just three basis functions are considered and only 2nd order diagonal and 1st order off-diagonal terms are kept. The secular equation is then:

$$
\begin{vmatrix}
\varepsilon_1^o + \sum_a u_{11}^{aa}Q_a^2 - \varepsilon(Q) & \sum_a u_{12}^a Q_a & \sum_a u_{13}^a Q_a \\
\sum_a u_{21}^a Q_a & \varepsilon_2^o + \sum_a u_{22}^a Q_a + \sum_{a,b} u_{22}^{ab}Q_a Q_b - \varepsilon(Q) & \sum_a u_{23}^a Q_a \\
\sum_a u_{31}^a Q_a & \sum_a u_{32}^a Q_a & \varepsilon_3^o + \sum_a u_{33}^a Q_a + \sum_{a,b} u_{33}^{ab}Q_a Q_b - \varepsilon(Q)
\end{vmatrix}
\begin{pmatrix} c_1 \\ c_2 \\ c_3 \end{pmatrix} = 0
$$

where $u_{ij}^a = \langle \psi_i^o | \left(\dfrac{\partial V}{\partial Q_a}\right)_o | \psi_j^o \rangle$, $u_{ij}^{ab} = \langle \psi_i^o | \left(\dfrac{\partial^2 V}{\partial Q_a \partial Q_b}\right)_o | \psi_j^o \rangle$ (1.20)

(1.7)

This electronic secular equation is symmetric (strictly Hermitian) and the summations are over the 3N-6 coordinates of the molecule. Solving the secular equation will give three roots of a third order polynomial in $\varepsilon(Q)$. These roots are functions of the coordinates Q and represent the adiabatic potential surfaces.

Consider first the case where there are no off-diagonal terms in the secular equation. The diagonal terms are then solutions for the adiabatic potential surfaces. Notice that the ψ_1^0 state, which is taken as the ground electronic state, has no terms linear in Q, nor any cross terms of the form $Q_a Q_b$. This is because, as will be shown in section 2.2, the equilibrium geometry and normal coordinates can always be chosen in a manner to eliminate these terms. The concept of normal coordinates also allows group theory to be used in determining which of the terms in the adiabatic potentials of the other states will be non-zero.

The one dimensional potential surfaces in figure 1.1a are shown for a totally symmetric mode and a non-totally symmetric mode. As shown in chapter 3, the totally symmetric mode is allowed to have terms of any order in its potential, while the non-totally symmetric coordinate is allowed terms of even order only. This means that a potential energy surface can only be displaced with respect to the ground state equilibrium geometry along totally symmetric coordinates.

If the problem is now considered in two dimensions, there may be the additional non-zero cross quadratic terms in the excited state potentials. This situation is examined in section 3.7, and will only occur when the two coordinates are of the same symmetry and leads to the rotation of the excited state normal coordinates with respect to the ground state as shown in figure 1.2c.

The potential surfaces in the above cases will be true adiabatic functions and the electronic states may be labelled by the crude adiabatic basis functions as shown in figure 1a. The vibronic wavefunctions will then belong to only one of these potential surfaces, and can be found by simply adding the kinetic energy operator to the potential of each surface, which will then quantise the energy levels within the surface. Calculations of this sort are performed for many different potential surfaces in section 2.2.

However in general there will be off-diagonal terms in the secular equation (1.20) that will mix these crude adiabatic basis

(1.8)
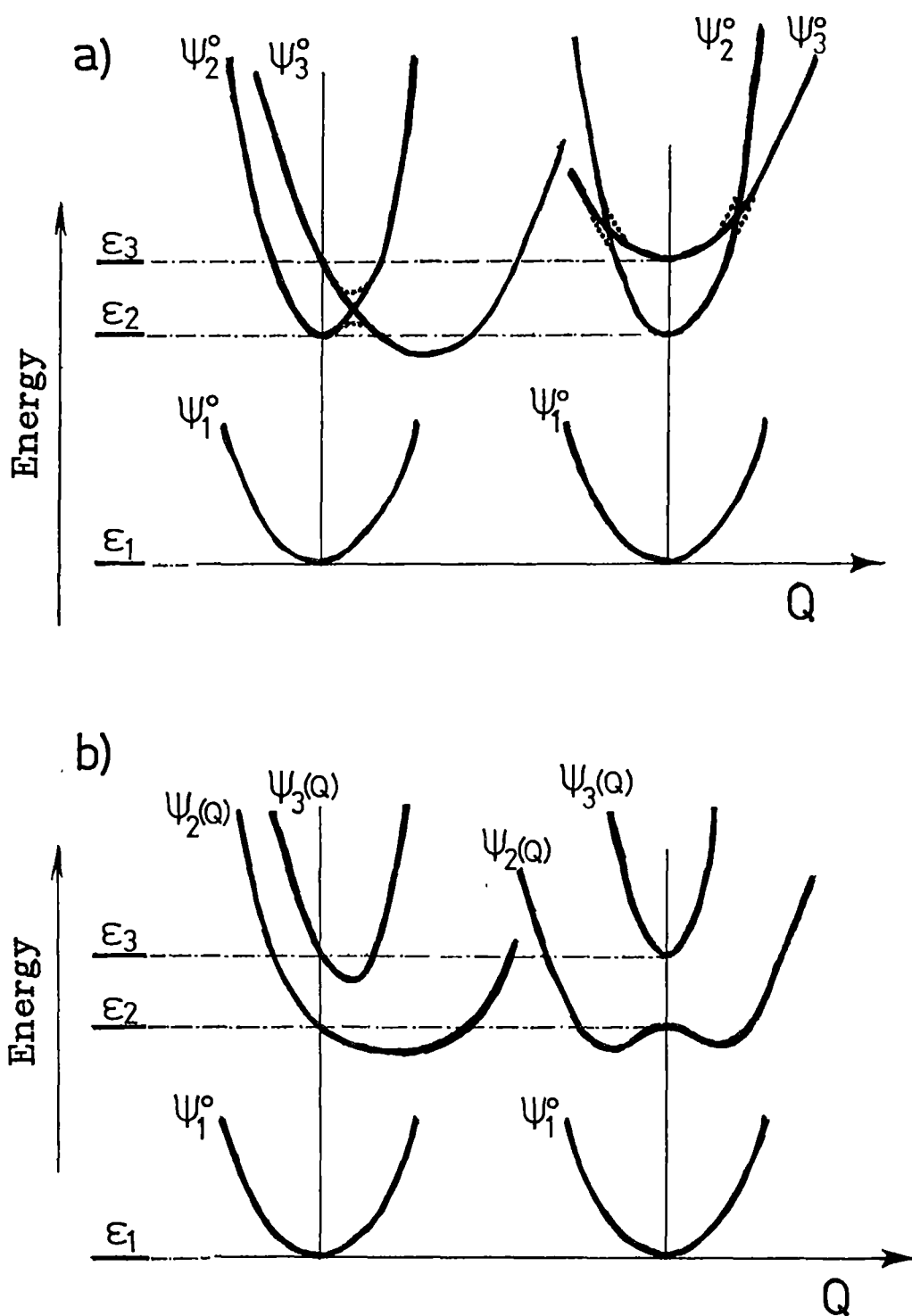
Figure 1.1 Adiabatic potential surfaces for a totally symmetric and a non-totally symmetric coordinate.
a) ————No interaction; ------Weak interaction.
b) Strong interaction.

functions. The coefficients involved u_{ij}^a ($i{\neq}j$) are called the first order vibronic coupling coefficients. Again, as discussed in section 3.4, group theory can be used to determine which of these coefficients are non-zero.

The dotted lines in figure 1.1a show the effect of weak coupling near a point of intersection, which leads to "avoided crossings". Figure 1.1b shows the same potentials with strong vibronic coupling. The lower surface of the non-totally symmetric mode forms a double minimum, and this is sometimes called the pseudo Jahn-Teller effect. The Jahn-Teller effect occurs in electronic states that are orbitally degenerate at a reference geometry (chapter 4). The adiabatic potential surfaces in the case of a doubly degenerate electronic state coupled by a doubly degenerate vibration (E×e) and two non-degenerate vibrations (E×(b+b)) are shown in figures 1.2 a and b respectively.

The adiabatic potential surfaces given above will be for an electronic state that is a linear combination of the basis functions which will vary with the molecular geometry. These electronic functions are indicated by $\Psi(Q)$ in figures 1b, 2a,b and they can be found by diagonalising the secular equation (1.20).

Since the electronic off-diagonal terms are functions of the nuclear coordinates, as well as the vibrational subsystem of the molecule, it follows that each vibrational state will couple the electronic basis functions to a different degree. This is then the breakdown of the adiabatic approximation. The electronic and vibrational parts of the Hamiltonian cannot be solved consecutively; the energy levels and wavefunctions are not simply the sum and product respectively of the two subsystems. Rather the secular equation must be solved in a <u>vibronic basis</u>.

The above point is not obvious but is extremely important to the topic of the thesis. A question that may be asked is: why is it not possible for the kinetic energy operator to be added to the adiabatic potential and the vibrational problem solved? This would lead to vibronic wavefunctions associated with only one particular potential surface that could be written as a single adiabatic product. The answer is: the act of diagonalising the electronic functions in the secular equation (1.20) to obtain an adiabatic potential, <u>introduces off-diagonal kinetic energy terms</u>. This is discussed in more detail in section 4.3. In general the only way to avoid this is to include the

(1.9)
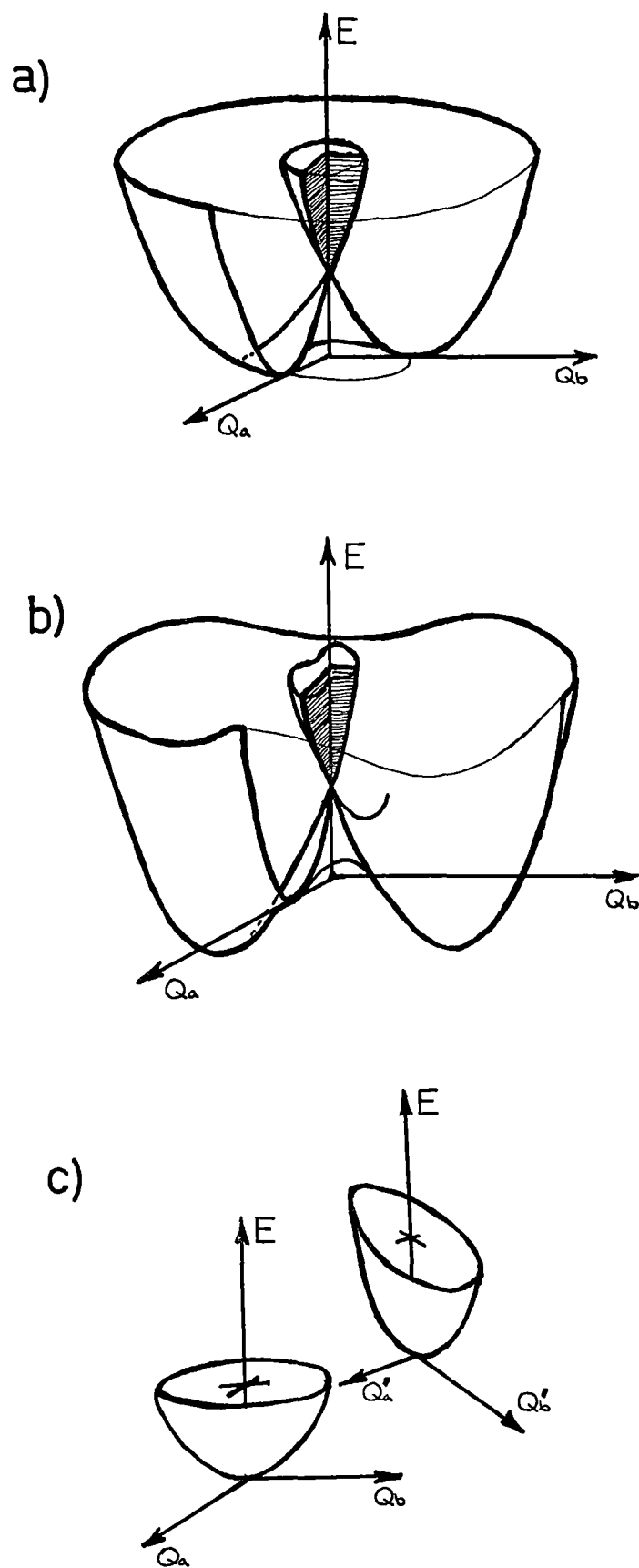
Figure 1.2 Adiabatic potential surfaces.
   a) Jahn-Teller effect (E⊗e).
   b) Jahn-Teller effect (E⊗(a⊕b)).
   c) Dushinsky effect.

kinetic energy operator in the secular equation and numerically diagonalise all terms simultaneously in what now must be a vibronic basis. The vibronic wavefunctions will not then be expressible as a simple adiabatic product of electronic and vibrational parts as in equation (1.3), but will be a linear combination of such products.

Such an approach is better than any of the adiabatic approximations given in the previous section. However, the importance of the adiabatic approximation is that it gives a physical meaning to electronic potential surfaces which form such an important concept in chemistry. Often the off-diagonal kinetic energy terms are small when the electronic states are well separated, and can be ignored. In this case the vibronic functions are expressible as an adiabatic product, and the potential surface determines their form. Sometimes even an electronic secular equation (1.20) need not be considered, and the electronic part of the wavefunction can be approximated as depending linearly on the coordinates, as is assumed in Herzberg-Teller theory (see section 3.4). It is important however, to realise when the adiabatic approximation is unrealistic and chapter 4 examines in detail some methods of going beyond the adiabatic approximation in the case of near or exact electronic degeneracy.

Chapter 2 will briefly discuss the electronic and vibrational subsystems, while chapter 3 will work within the framework of the adiabatic approximation to discuss the total vibronic system in the case of weak interaction. Chapter 4 will be concerned with calculations that go beyond the adiabatic approximation and chapter 5 will conclude the theoretical first half of the thesis with some discussion of electron spin resonance which is relevant to the studies in the experimental second half of this thesis.

(1.10)

CHAPTER 2 NO VIBRONIC INTERACTION: THE SUBSYSTEMS

The main concern of this thesis, introduced in the previous chapter, is the non-separability of the nuclear and electronic coordinates. However, it is constructive to first examine the two subsystems separately. This is then the assumption that the adiabatic approximation expressed by equation (1.3) holds, and that the vibrational and electronic equations can be solved separately.

In this chapter the electronic states are first considered with the nuclei assumed fixed at their equilibrium values. Following this, the vibrational states are then considered within a potential surface which corresponds simply to the energy of a _single_ electronic state as a function of the nuclear coordinates. The electronic and vibrational problems are then separate as they are dependent on only their own coordinates. The electronic states "see" a fixed nuclear geometry, while the vibrational states "see" the average field of the electrons of a particular electronic state.

Such a description is only valid when there is no interaction between the two subsystems. The effects of vibrational-electronic, or vibronic, interactions will be considered in the following chapters. The description of the vibrational and electronic states here will be very brief, but should serve to introduce some of the mathematical formalism which is to be used in this thesis.

2.1 ELECTRONIC STATES: "FIXED NUCLEI"

2.1.1 The problem.

The theoretical description of the electronic structure of transition metal complexes can be conveniently divided into two areas; ligand field theory and molecular orbital theory. In this chapter ligand field (LF) theory is briefly described; a full description is to be found in the texts of Ballhausen (1962), Figgis (1966), Gerloch (1983) and Lever (1984). LF theory can be thought of as a special case of MO theory, where the basis is truncated to include only the d-orbitals and the free ion parameters (ie Racah and zeta) are reduced

(2.1)

to compensate for the expansion of the d-orbitals on complexation, and covalency effects.

The many variants of LF theory differ in the way they parameterise the ligand field, and the earliest example of which was given by Bethe (1929) in what is now termed crystal field theory. Since then the usage of LF theory has become widespread among inorganic chemists and pervades much of the chemical thinking about transition metal ions. This popularity is due both to the simplicity of the model and the fact that it can explain a wide range of physical phenomena. The reasons why LF theory appears to work so well is usually rationalised (Gerloch and Slade 1973, pp1-16) as follows. i) Firstly, group theory can be used to describe the form of the splitting of the d-orbitals exactly, and the magnitude of this can be easily parameterised. ii) The bonding in a metal complex is usually based on the one centre, and the perturbation to the atomic d-orbitals is only slight when compared to atomic orbitals in more covalent compounds.

For the above reasons it is customary to start with the Hamiltonian of the free ion and then add to this the effect of the ligands. This Hamiltonian for i electrons in dimensionless units is (Lever 1984, pg2):

$$H = - \sum_i \nabla_i^2 - \sum_i \frac{Ze^2}{r_i} + \sum_{i>j} \frac{e^2}{r_{ij}} + \sum_i \zeta_i l_i s_i + V(x_i, y_i, z_i)$$

$$H = H_{KE} + H_{PE} + H_{IR} + H_{SO} + H_{LF} \qquad (2.1)$$

Here H_{KE} is the kinetic energy operator of the electrons,

H_{PE} is the potential energy operator of the electrons in a central field of a nucleus with an effective charge Z,

H_{IR} the inter-electron repulsion operator,

H_{SO} the spin-orbit coupling operator, and

H_{LF} the ligand field operator, describing the potential due to the nature and geometry of the ligands.

The first two terms of (2.1) are neglected in LF theory since it only adds a constant energy term whereas it is the energy differences that are of interest. Higher order terms can be included in (2.1), and Harriman (1978, appendix F) lists 35 such additional terms.

$$(2.2)$$

2.1.2 Variational and LCAO Methods.

Like the vibronic Hamiltonian, it is easy to write down the electronic Hamiltonian of a molecule, but its solution is usually impossible. The H_2^+ ion can be solved exactly within the adiabatic approximation (CDL, pp1148-99), but for all other cases additional approximations must be made. The variational method is a common approach that can be used to approximately solve the Hamiltonian (2.1).

The energy of a system whose wavefunction is Ψ, is given by:

$$E = <\Psi|H|\Psi>/<\Psi|\Psi> \qquad (2.2)$$

where the bra-ket notation introduced by Dirac (1958, sect.6) is used,

$$<\Psi|H|\Psi> = \int_{-\infty}^{\infty} \Psi^* H \Psi \, d\tau \, .$$

Supposing now that H is a Hamiltonian for which the Schrödinger equation cannot be solved. The variational theorem (Weissbluth 1978, pp290-4; CDL, pp1148-55) states that the energy calculated from a guessed wavefunction (Ψ_g) is equal to or higher than the true energy:

$$E \leqslant <\Psi_g|H|\Psi_g>/<\Psi_g|\Psi_g> \qquad (2.3)$$

This is very useful as Ψ_g can be varied to give the "best guess" wavefunction that minimizes the energy in (2.3). A common guess is to use a linear combination of the one electron orbitals or as it is better known, a linear combination of atomic orbitals (LCAO). However: ".. it must be emphasized that molecular electronic wavefunctions are not really linear combinations of atomic orbitals." (Harris and Bertolucci 1978), but is only a "good" guess.

Following Weissbluth (1978, pg293), the variational method is now applied to n LCAO basis functions.

$$\Psi = \sum_{i}^{n} a_i \psi_i \qquad (2.4)$$

where the n ψ_i are the antisymmetrised one electron wavefunctions of (2.2) and a_i are coefficients to be varied. Equation (2.2) is now rewritten as:

$$E \sum_{i,j}^{n} a_i^* a_j S_{ij} = \sum_{i,j}^{n} a_i^* a_j H_{ij} \qquad (2.5)$$

where $H_{ij} = <\psi_i|H|\psi_j>$ is usually called a matrix element (ME),
and $S_{ij} = <\psi_i|\psi_j>$ an overlap integral.
Differentiating both sides of (2.5) with respect to a single coefficient, a_k^* say:

$$\frac{\partial E}{\partial a^*_k} \sum_{i,j} a^*_i a_j S_{ij} + E \sum_j^n a_j S_{kj} = \sum_j^n a_j H_{kj} \qquad (2.6)$$

For the energy to be a minimum $\frac{\partial E}{\partial a^*_k} = 0$, and (2.6) becomes:

$$\sum_j^n a_j (H_{kj} - ES_{kj}) = 0 \qquad (2.7)$$

This is repeated for all other coefficients and a system of n homogeneous linear equations are obtained, the solutions for which only exist when (Spiegel 1971, pg348):

$$| \mathbf{H} - \mathbf{ES} | = 0 \qquad (2.8)$$

This is called the <u>secular equation</u>, which is a polynomial of degree n in E. If the basis in (2.4) is orthonormal, then $S_{ij} = \delta_{ij}$ and (2.9) becomes:

$$\begin{vmatrix} H_{11}-E & H_{12} & H_{13} & \cdots & H_{1n} \\ H_{21} & H_{22}-E & H_{23} & \cdots & \cdot \\ \cdot & & \cdot & & \cdot \\ H_{n1} & \cdot & \cdot & \cdot & \cdot & H_{nn}-E \end{vmatrix} = 0 \qquad (2.9)$$

Analytic solutions for the roots of polynomials are available only up to fourth order, however the solutions to cubics and quartics are especially difficult, (A&S, eq.3.8.2,3). Equation (2.9) is therefore usually solved (ie diagonalised) numerically, unless the symmetry of the system allows the determinant to be blocked along the diagonal (ie the basis wavefunctions were a good guess to the real wavefunctions).

2.1.3 Similarity Transforms and Bases.

The matrix forming the secular equation (2.9) is <u>Hermitian</u> (CDL, pg 120). A square matrix is Hermitian if it is equal to the complex conjugate of its own transpose, $A = (A^t)^*$. Some of the mathematical consequences of this are (Spiegel 1971, pp 342-50):

The <u>eigenvalues</u> (energies) are real.

The <u>eigenvectors</u> (wavefunctions) can be complex.

The basis may be changed by:

$$\psi = C\psi' \qquad (2.10)$$

(2.4)

where ψ, ψ' are column vectors of dimension n of the old and new bases respectively: and C is a (nxn) <u>unitary</u> matrix that expresses the old matrix in terms of the new. A matrix C is unitary if its inverse is equal to the complex conjugate of its transpose, $C^{-1} = (C^t)^*$. This means that if ψ is orthonormal, then so will be ψ'. Equation (2.9) then becomes:

$$(H_{ij} - E_{ii}) = \langle\psi_i|H|\psi_j\rangle - E_{ii} \qquad (2.11)$$
$$= \langle\psi_i'C^{-1}|H|C\psi_j'\rangle - E_{ii}$$
$$= \langle\psi_i'|H'|\psi_j'\rangle - E_{ii}$$
$$= (H_{ij}' - E_{ii}), \qquad H' = C^{-1}HC$$

The eigenvalues of (2.11) are exactly the same as those in (2.9), while the eigenvectors are now in terms of the new basis ψ'. (See Pease 1965, pp115-30.) The transformation of H to H' is called a <u>similarity transform</u>:

$$H' = C^{-1}HC \qquad (2.12)$$

If a particular similarity transform diagonalises (2.9):

$$B^{-1}HB = \text{diag}(E_1, E_2, \ldots, E_n) \qquad (2.13)$$

then $E_1, \ldots E_n$ are the n eigenvalues, and the eigenvectors (the coefficients of the linear combination of basis functions) are contained in the n columns of B.

Similarity transforms are very useful as a Hamiltonian may be composed of different parts whose matrix elements are most easily calculated in different bases. If this is the case, then matrix elements of each part of the Hamiltonian can be calculated in the most convenient basis, and then transformed into a common basis by (2.12). A similarity transform can also be used to construct a basis that removes a large off-diagonal matrix element, and such an approach is often used in Jahn-Teller problems (chapter 4).

LF theory solves (2.1) using the variational method with a LCAO of the valence shell orbitals as a basis. These are either the d or f one electron orbitals which form an orthonormal basis so the problem becomes that of calculating the matrix elements and diagonalising the secular equation (2.9). This last point can be quite a difficult "number-crunching" exercise for a computer when the basis size is large. The basis size is given by (Weissbluth 1978, pg 422):

$$\begin{pmatrix} n \\ k \end{pmatrix} = \frac{n!}{(n-k)!k!} \qquad (2.14)$$

where n is the number of spin orbitals (10 for a d , and 14 for an f orbital basis), and k is the number of electrons present. For a $d^5(f^7)$ configuration this gives a basis size of 252(3432).

Given these potentially large basis sizes, much ingenuity has been devoted to using group theoretical techniques to chose a basis that has the largest matrix elements on the diagonal of the secular equation. This allows the secular equation to be broken up into smaller matrices that can be diagonalised separately, small off-diagonal elements being either ignored or treated by perturbation theory. In this formalism the best basis to use is determined by the relative sizes of the terms in the Hamiltonian (2.1):

$$H_{LF} > H_{IR} > H_{SO} \quad \text{strong field scheme} \tag{2.15a}$$

$$H_{IR} > H_{SO} > H_{LF} \quad \text{weak field scheme (jj-coupling)} \tag{2.15b}$$

$$H_{IR} > H_{LF} > H_{SO} \quad \text{"} \quad \text{(Russell-Saunders coupling)} \tag{2.15c}$$

It should be emphasised that when the complete basis is used, all these schemes are equivalent, and will give identical results.

2.1.4 The calculation.

Formulae for evaluating the matrix elements in the above three schemes have been given by König and Kremer (1977) and Piepho and Schatz (1983) in terms of irreducible tensor methods. Gerloch and McMeeking (1975) have made freely available a program called CAMMAG, which performs ligand field calculations in a weak field $|JM_J>$ basis.

Apart from the irreducible tensor method, calculations in ligand field theory can also use the older methods of Condon and Shortley (1935). While this makes no elegant use of group theory, so in general a full basis must be used, it is conceptually simpler and easier to implement as computer program.

Programs were developed for the d^8 and d^9 cases using the methods of Condon and Shortley in a real d-orbital basis. This basis is used because it is the natural basis with which to parameterise the ligand field operator. With the angular overlap model, real analytic functions are available for any arrangement of ligands. Conversion of the AOM ligand field operator to other bases requires the use of spherical harmonics (Gerloch and McMeeking 1975). As well as this, it is easier to picture the spatial distribution of the electrons using real basis

functions, and "chemical intuition" from simple bonding arguments can be used.

The first step in solving the Hamiltonian (2.1) is to recognise that the operators involved are either one electron operators (H_{LF}, H_{SO}) or two electron operators (H_{IR}). All possible one electron and two electron matrix elements must be calculated at least once. This can be done <u>in the most convenient basis</u>, then, by the use of similarity transforms, these can be transformed into the required d-orbital basis. The matrix elements of the one electron spin-orbit coupling operator has been given by McGarvey (1966, pg144), the one electron angular overlap ligand field operator by Schäffer (1970), and the two electron interelectron repulsion operator by Griffith (1961, section 9.2), all in a real d-orbital basis.

The real d-orbital basis is really in the form of antisymmetrised products (or Slater determinants) of the one electron spin orbitals (Weissbluth 1978, chapter 11). The matrix elements of the secular equation in this many electron basis can be evaluated using the straightforward rules of one and two electron operators, (Condon and Shortley 1935, pp169-73; Golding 1969, pp25-38).

Diagonalisation of this matrix will give the eigenvalues (to compare with transition energies) and eigenvectors (to compare with transition intensities, magnetics, etc). The empirical parameters can then be varied to fit the experimental data. In general such parameters that fit experiment can be found and ligand field theory can then then be said to provide a good working model to account for those particular experimental properties. An immense amount of experimental work and ligand field analysis has been done to verify this, and in this sense it could be said that the "d" electronic properties of transition metal complexes are well understood.

2.2 VIBRATIONAL STATES: "AVERAGED ELECTRONS"

In studying the vibrations of a polyatomic molecule, it is implicitly assumed that the molecule can be described by point masses (the atoms) connected by forces (the bonds) that keep these atoms near their equilibrium position (the equilibrium molecular geometry). This description is essentially classical in nature, and indeed molecular vibrations can be studied by the analysis of the resonance frequencies of mechanical models (WDC, pg232).

In this section only vibrational coordinates are considered, ie it is assumed that there is no coupling with either electronic or rotational coordinates. Classical ideas are used to introduce the concept of normal coordinates, followed by the quantum mechanical description of the simple harmonic oscillator. The variational method is is then used to investigate systems with non-harmonic potentials.

2.2.1 Classical Concepts.

Normal Coordinates:

A non-linear(linear) molecule is said to be at <u>equilibrium</u> when all forces along all $n=3N-6(5)$ vibrational degrees of freedom on the system vanish:

$$\left(\frac{\partial V}{\partial q_i}\right)_0 = 0 \tag{2.16}$$

where V is the potential energy of the system and the equilibrium can be either stable or unstable (Goldstein 1980, pg243). If the potential energy is expanded in a Taylor series about this equilibrium geometry:

$$V = V(q_1, \ldots, q_n) + \sum_i \left(\frac{\partial V}{\partial q_i}\right)_0 q_i + \frac{1}{2} \sum_{i,j} \left(\frac{\partial^2 V}{\partial q_i \partial q_j}\right)_0 q_i q_j + \ldots \tag{2.17}$$

The first two terms can be made zero from (2.17) and a shift in the energy origin:

$$V = \frac{1}{2} \sum_{i,j} \left(\frac{\partial^2}{\partial q_i \partial q_j}\right)_0 q_i q_j + \ldots \quad i,j = 1, \ldots n \tag{2.18}$$

If the first term in (2.18) is positive the equilibrium is stable, and if the subsequent terms in the expansion are zero then the potential is harmonic. The contrary case, where the quadratic term is negative and higher terms are non-zero, occurs for example with a double minima potential. Here there is the paradoxical situation of

an equilibrium geometry which is classically unstable, yet is the quantum mechanical expectation value of the geometry (see section 2.2.3).

Assuming for the moment small harmonic vibrations about a stable equilibrium geometry, the classical energy the system is given by:

$$E = \sum_{i,j} [\ T_{ij} + V_{ij}\ ] \tag{2.19}$$

where $T_{ij} = \frac{1}{2}\ \dot{q}_i \dot{q}_j$, and $V_{ij} = \frac{1}{2} \left(\frac{\partial^2 V}{\partial q_i \partial q_j}\right)_0 q_i q_j$, represent the kinetic and potential energy of the system respectively.

Equation (2.19) can be written in matrix form (Weissbluth 1978, pg632), and diagonalised by a similarity transform, defining both the normal vibrational frequencies and the <u>normal coordinates Q.</u>

$$A^{-1}\ (T+V)\ A = D, \quad q = AQ \tag{2.20}$$

where $D = \text{diag}(\omega_1^2, \omega_2^2, ..)$ is the diagonal matrix of the squares of the frequencies. Such a transform must simultaneously diagonalise both the kinetic and potential energy terms, and the existence of such a transform A is shown by Goldstein (1980, chapter 6). The number of coordinates may be over specified, but this will only result in modes of zero frequency (WDC, pp22-25). Using the normal coordinates, (2.19) becomes:

$$E = \frac{1}{2} \sum_i^n [\ \dot{Q}_i^2 + \frac{1}{2}\ \omega_i^2 Q_i^2\ ] \tag{2.21}$$

Assuming for simplicity that all the modes are non-degenerate, then (2.21) becomes a set of n separate simple harmonic oscillator equations. Group theory can be used to determine the symmetries of the vibrations based on the point group symmetry of the equilibrium molecular geometry. This involves finding the irreducible representations from a set of characters found by performing the symmetry operations of the point group on a basis. This method is given in many texts (Vincent 1977, Harris and Bertolucci 1978). The normal coordinates are classified into the irreducible representations of the equilibrium geometry point group, even though at any instant in time the molecule will usually have no symmetry at all. For small displacements from the equilibrium geometry, these labels hold well, but become meaningless for large amplitudes (Landau and Lifshitz 1977, pg396).

(2.9)

The validity of normal coordinates only holds within the harmonic approximation, but is extremely useful as it allows the complex motion of a vibrating molecule to be described as a superposition of vibrational modes, each having a fixed frequency. It allows a $3N-6$ dimensional problem to be separated into one dimensional problems.

Normal Coordinate Analysis:

The standard method of treating molecular vibrations is called the GF matrix method and is well documented in the texts of Wilson etal (1955) and Cyvin (1968). Computer programs implementing this method are available (Fuhrer etal 1976). A brief outline is given here as the notation will be referred to at later stages. For a molecule of N atoms the vibrational Hamiltonian corresponding to (2.19) in matrix notation is:

$$H = \frac{1}{2} [\dot{x}^t M \dot{x} + x^t V x] \tag{2.22}$$

in terms of the $3N$ cartesian displacement vector x. Here M is the $3N \times 3N$ diagonal matrix of the masses of the atoms, and V is the $3N \times 3N$ matrix of the quadratic force constants: $V_{ij} = (\frac{\partial^2}{\partial x_i \partial x_j})_0$.

If the redundant coordinates are now removed by a transformation to the n ($=3N-6$) internal coordinates:

$$S = B x \tag{2.23}$$

by the $n \times 3N$ transformation matrix B. Here the internal coordinates S may be symmetry coordinates which will block diagonalise the GF matrix. Substituting into (2.22) one has (Cyvin 1968, pp54-62):

$$2H = [\dot{S}^t (B^{-1})^t M B^{-1} \dot{S} + S^t (B^{-1})^t V B^{-1} S] \tag{2.24}$$
$$= [\dot{S}^t G^{-1} \dot{S} + S^t F S]$$

where G is the $n \times n$ symmetrised kinetic energy matrix:

$$G = B M^{-1} B^t \tag{2.25}$$
$$G_{ij} = \sum_k \frac{1}{m_k} B_{ik} B_{jk}^\star$$

and F is the $n \times n$ symmetrised force constant matrix:

$$F_{ij} = (\frac{\partial^2 V}{\partial S_i \partial S_j})_0 \tag{2.26}$$

By definition, the n normal coordinates Q are those which make (2.24) diagonal. Let these be related to the internal coordinates by an $n \times n$ transformation L:

$$S = L Q \tag{2.27}$$

Substitution into (2.24) one gets:

$$2H = [\dot{Q}^t L^t G^{-1} L \dot{Q} + Q^t L^t F L Q]$$

(2.10)

$$= [\dot{Q}^t I \dot{Q} + Q^t \lambda Q] \tag{2.28}$$

where I is the n x n identity matrix and λ is diagonal. This then reduces to:

$$L^t G^{-1} L = I, \qquad L^t = L^{-1} G$$

$$L^t F L = \lambda \quad \text{or} \quad G F L = \lambda L \tag{2.29}$$

This is in the form of an eigenvalue equation, where λ are the n eigenvalues, and the columns of L contain the eigenvectors which will be the normal coordinates expressed in terms of the symmetry coordinates. Equation (2.29) can be solved by diagonalising the n x n matrix, GF (Cyvin 1968, Fuhrer 1976). For force constants given in mdyne$\overset{o}{A}^{-1}$, the vibrational frequencies v_k (in cm^{-1}) are related to the eigenvalues λ_k by (Fuhrer etal 1976, pg 187):

$$v_k = \frac{\lambda_k^{1/2}}{2\pi c} = (\lambda_k)^{1/2} \times 1302.8 \tag{2.30}$$

2.2.2 Quantum Concepts.

Schrodinger Formulation:

The Schrodinger equation corresponding to (2.21) for a one dimensional harmonic oscillator is given by (Cyvin 1968, pg 75):

$$H(\xi)\phi(\xi) = \frac{1}{2}\left(-\frac{\partial^2}{\partial\xi^2} + \xi^2 \right)\phi(\xi) = \frac{E}{hv}\phi(\xi) \tag{2.31}$$

whose nth eigenvalue is:

$$E_n = (n + \frac{1}{2}) hv \tag{2.32}$$

and nth eigenvector:

$$\phi_n(\xi) = (2^n n! \pi^{1/2})^{-1/2} . H_n(\xi) . \exp(- \frac{1}{2} \xi^2) \tag{2.33}$$

$H_n(\xi)$ is the nth Hermite polynomial, which can be defined by the following recurrence relationship (Schiff 1968, pg 70):

$$H_{n+1} = 2\xi . H_n(\xi) - 2n . H_{n-1}(\xi) \tag{2.34}$$

$$H_o(\xi) = 1, \qquad H_1(\xi) = 2\xi$$

The dimensionless coordinate ξ has been used for convenience. The relationships between the dimensionless coordinate, ξ, symmetry coordinate, S, and normal coordinate, Q, are given by Cyvin (1968, pg75):

(2.11)

$$\xi = xS = x/m\ Q \qquad\qquad (2.35)$$
$$x = 4\pi mc\omega/h = 1.722 \times 10^{-3} (M.h\nu)^{1/2} pm^{-1}$$

The symbol M in the constant x is the mass from the inverse of the appropriate G matrix element (equation 2.25) in amu, and $h\nu$ is the energy of the harmonic vibration in cm^{-1}.

The solutions of the Schrödinger equation, (2.31), given in (2.32), (2.33) have been derived in many texts, usually by the polynomial method (Schiff 1968, pp66-72; Flügge 1974, pp68-71). The Schrodinger equation and eigenvectors in terms of other coordinates are obtained by the appropriate substitution of (2.35). The eigenvalues remain the same for all coordinate systems.

Matrix Formulation:

A convenient geometric picture of a basis function is a vector in an infinite dimensional Hilbert space (Schiff 1968, pp163-4). Each dimension corresponds to a row in a column vector, the magnitude of which corresponds to the component of the vector along that axis in Hilbert space. Different orientations of the axes corresponds to different representations of the basis functions. If the axes are chosen so that each basis function is oriented directly along them, then the basis functions are eigenvectors of that particular Hamiltonian. The orthonormality of the basis functions can be interpreted as a set of unit vectors that are orthonormal in the geometric sense.

A unitary transform corresponds to a rotation of the axes in Hilbert space, rather than a change in the basis functions. An operator A can be thought of as a rotation of a basis function a_i so that it becomes the different basis function Aa_i. A matrix element, $\langle a_i|A|a_j\rangle$, is then the overlap of the two functions $\langle a_i|Aa_j\rangle$.

The variational method can be used in Hilbert space <u>where the explicit form of the basis functions need not be known</u>. As shown in section 2.1.2, the solutions to a variational problem are found by the following three steps:

1) Expanding the unknown wavefunctions in terms of the known basis functions.

2) Calculating the matrix elements of the Hamiltonian.

3) Diagonalising the secular equation.

The rest of this chapter examines the energy levels and wavefunctions of several sorts of non-harmonic potentials. The wavefunctions of these potentials are expanded as a linear combination of simple harmonic oscillator (SHO) basis functions, and solved with the variational method. The necessary matrix elements in a SHO basis are given in appendix 2.A1. After the secular equation is diagonalised numerically, the resulting eigenvalues will be in units of hν, and the eigenvectors will be linear combinations of the simple harmonic oscillator basis functions. A different basis could have equally well been used, for example, Davis and Heller (1979) have used Gaussian basis functions. Here a SHO basis is used for the convenience in which the matrix elements can be calculated.

2.2.3 Geometric Properties of the Wavefunctions.

As well as the energies of vibrational systems, other properties of the wavefunctions can also be of interest. In particular, geometric information about a particular vibrational state can be calculated from the wavefunction. A geometric quantity R is calculated as an expectation value or quantum mechanical average value of R in ϕ_n:

$$<R>_n = <\phi_n|R|\phi_n> \qquad (2.36)$$

The equilibrium geometry defined in (2.16) is the geometry where the potential is an extremum, usually a minimum. However the mean geometry as defined above in (2.36) need not necessarily be at the minimum of the potential. For a simple harmonic oscillator centred about $\xi=0$, the matrix elements in appendix 2.A1 show that the mean geometry $<\xi>_n$ will be zero in all vibrational levels. For a displaced SHO the mean geometry will be $<\xi+\xi_e>_n = <\xi>_n + <\xi_e>_n = \xi_e$ for all energy levels. Therefore in a SHO the equilibrium geometry always corresponds to the minimum in the potential, whereas for an anharmonic oscillator this need not be the case. If the anharmonic wavefunction is expressed as linear combination of N SHO basis functions then the expression for the geometry becomes:

$$\phi_n = \sum_{i=0}^{N} a_{i,n}|i>$$

$$<\xi>_n = <\phi_n|\xi|\phi_n> = \sum_{i=1}^{N} (2i)^{1/2} a_{i,n} a_{i-1,n} \qquad (2.37)$$

(2.13)

The fact that SHO wavefunctions always have a mean geometry identical to the potential energy minima is also obvious from their symmetric nature and will also be true for any even order potential. However for higher vibronic levels this mean geometry becomes increasingly the least probable geometry in the sense that the maximum of the probability density of the wavefunction move further away from the mean value. Indeed, in the odd numbered SHO wavefunctions there is a zero probability of finding the vibrational state at the equilibrium geometry.

A better measure of the amount of time that the wavefunction spends away from the mean geometry is the root-mean-squared (RMS) amplitude of the vibration. As above, this quantity is given as:

$$\langle \xi^2 \rangle_n^{1/2} = \langle \phi_n | \xi^2 | \phi_n \rangle^{1/2} \tag{2.38}$$

For a SHO the mean-squared amplitude is given by the appropriate matrix element from table 2.A1:

$$\langle \xi^2 \rangle_n = (n + \tfrac{1}{2}) \tag{2.39}$$

For a displaced SHO it is:

$$\langle (\xi+\xi_e)^2 \rangle = ((n + \tfrac{1}{2}) + \xi_e) \tag{2.40}$$

In an anharmonic oscillator, the mean-squared geometry must be found from a variational calculation:

$$\langle \xi^2 \rangle_n = \sum_{i=0}^{N-2} a_{i,n} a_{i+2,n} \sqrt{(i+1)(i+2)} + \sum_{i=0}^{N} a_{i,n}^2 (i + \tfrac{1}{2}) \tag{2.41}$$

Examples of the use of the above equations are made in the following sections with wavefunctions from anharmonic potentials. As a word of warning, it should be remembered that it is the squared geometry that is calculated as an expectation value. For temperature dependent calculations, it is the square root of the Boltzmann average of the mean square values that should be taken, not the Boltzmann average of the RMS values which in general will give a different (and wrong) answer.

(2.14)

2.2.4 Anharmonic Potentials.

In this section one dimensional anharmonic potentials are considered, where the higher order terms in (2.18) are restricted to being wholly within the one coordinate:

$$V(\xi) = \sum_i [\ k_{2i}\xi_i^2 + k_{3i}\xi_i^3 + k_{4i}\xi_i^4 + \ ..\ ]\ , \quad k_{ni} = \frac{1}{n!}\left(\frac{\partial^n V}{\partial \xi_i^n}\right)_0 \qquad (2.42)$$

The case where cross terms cause anharmonic coupling between the two modes, will be considered in section 3.7. The solution of the vibrational Hamiltonian with the potential given by (2.42) can be made either by perturbation theory or the variational method. Perturbation theory gives algebraic approximate expressions for the energies and wavefunctions (appendix 2.A2), but is suitable only for small anharmonic terms. The variational method gives answers to arbitrary accuracy, but must be solved numerically. Here both methods are investigated to see under what conditions perturbation theory holds. Numerical test data is given in appendix 2.A2.

Cubic anharmonicity: Cubic anharmonicity is a common correction made to normal coordinates involving bond stretching. This is simply due to the potential energy of a molecule increasing more for a bond compression than for a bond elongation (Harris and Bertolucci 1978, pg106). A negative cubic anharmonicity then approximates the behaviour of the more realistic Morse potential (Herzberg 1950, pg90) for the lowest few levels. With both kinetic and potential energy operators, the vibrational Hamiltonian is then:

$$H = \frac{1}{2}\ P(\xi)^2 + \frac{1}{2}\ \xi^2 + k_3\xi^3; \quad P(\xi)^2 = -\frac{\partial^2}{\partial\xi^2} \qquad (2.43)$$

Figure 2.1a shows the energies obtained both from the variational method and perturbation theory. Similarly, the mean and root-mean-squared values of the coordinate are shown in figures 2.1b,c. As is well known the vibrational energy intervals become smaller both with increasing anharmonicity, and with increasing quantum number. The energies calculated from perturbation theory are a good approximation up to $k_3 = -0.04$, but the wavefunction properties show poorer agreement. In the unlikely case of a positive cubic anharmonicity, the

(2.15)
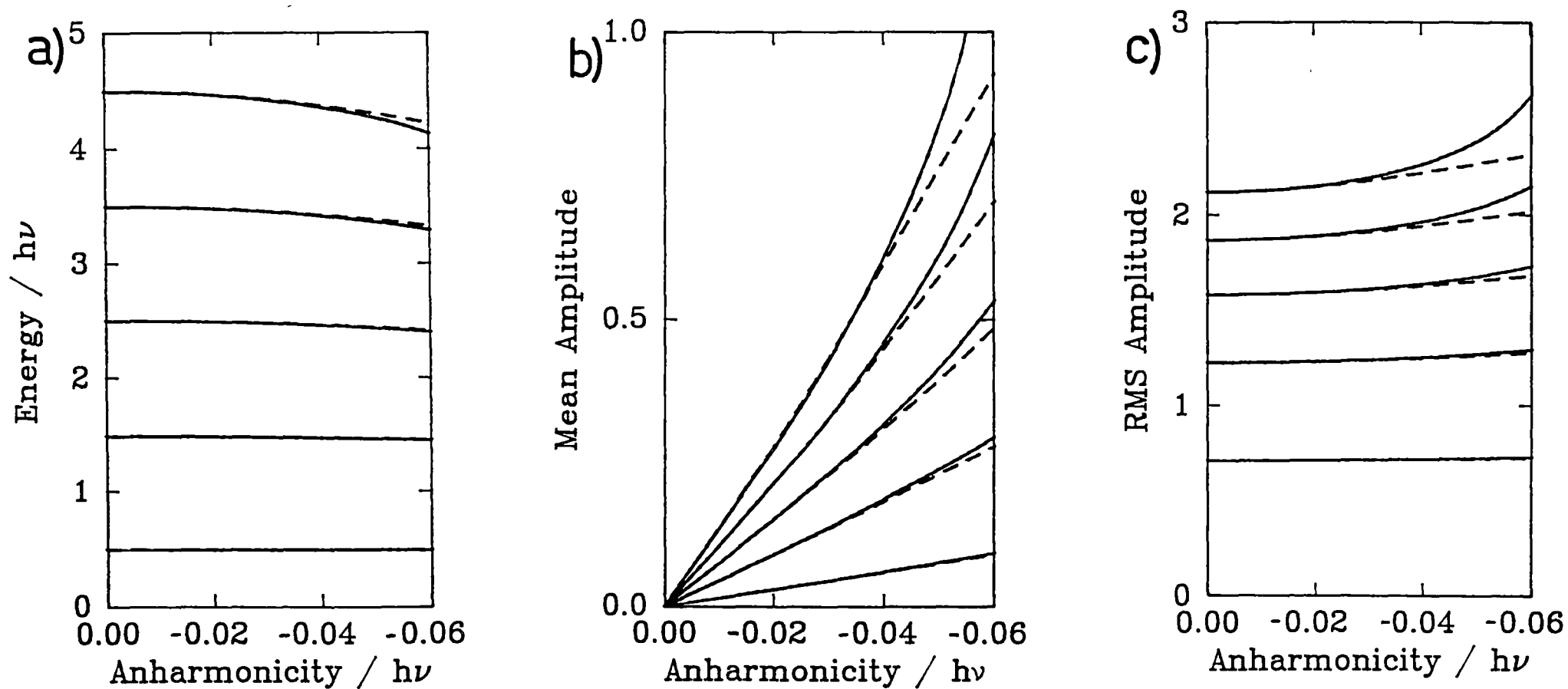
Figure 2.1 Cubic anharmonicity:

———Variational method.———Perturbation theory.

a) Energy levels, b) Mean geometry, c) RMS geometry.

energies and RMS values will remain the same, while the mean values will be negative.

Care must be used when calculating for large values of k_3, or when large basis sizes are used, as the cubic term in (2.43) will eventually cause the potential to turn over. In this case, "unbound states" will be calculated outside the potential. They can be identified either by varying the basis size, in which case they will shift in energy (as they try to approach negative infinity), or by calculating the RMS value of the coordinate which will be unreasonably large. This situation can be avoided by adding a quartic term to (2.43).

Quartic anharmonicity: Quartic anharmonicity is the lowest non-zero anharmonicity that can occur in "even" vibrations. An "even" vibration can be defined as a vibration where a positive displacement along the normal mode is equal to a negative displacement, within a rotation of the molecule. For example, the orthorhombic component of the octahedral e_g vibration (figure 4.2) is an even vibration, while the tetragonal component is not. Thus while the tetragonal component can have any power of anharmonicity, the orthorhombic or "even" component can only have even orders of anharmonicity.

For quartic anharmonicity the Hamiltonian is then:
$$H = \frac{1}{2} P(\xi)^2 + \frac{1}{2} \xi^2 + k_4 \xi^4 \qquad (2.44)$$
The energy and RMS amplitudes as a function of the quartic anharmonicity k_4 are shown in figures 2.2a,b. The mean geometry will always be zero due to the symmetry of the wavefunctions. When k_4 is negative the energy levels become closer, corresponding to a softening of the potential. A positive k_4 corresponds to a "stiffening" of the potential, which causes increasing energy intervals and decreasing RMS amplitudes. Perturbation theory holds well only for k_4 in the range $-0.01 \rightarrow 0.01$, for the lowest levels, but again the energies are a better approximation than the RMS values. As in the cubic case, a large negative quartic anharmonicity will cause the potential to turn over. The potential of $k_4 = -0.01$ is shown in figure 2.3 along with the vibronic probability functions which identify the fifth level as an "unbound state". In practise, care must be taken in all cases where the highest order anharmonicity is negative, whether even or odd.
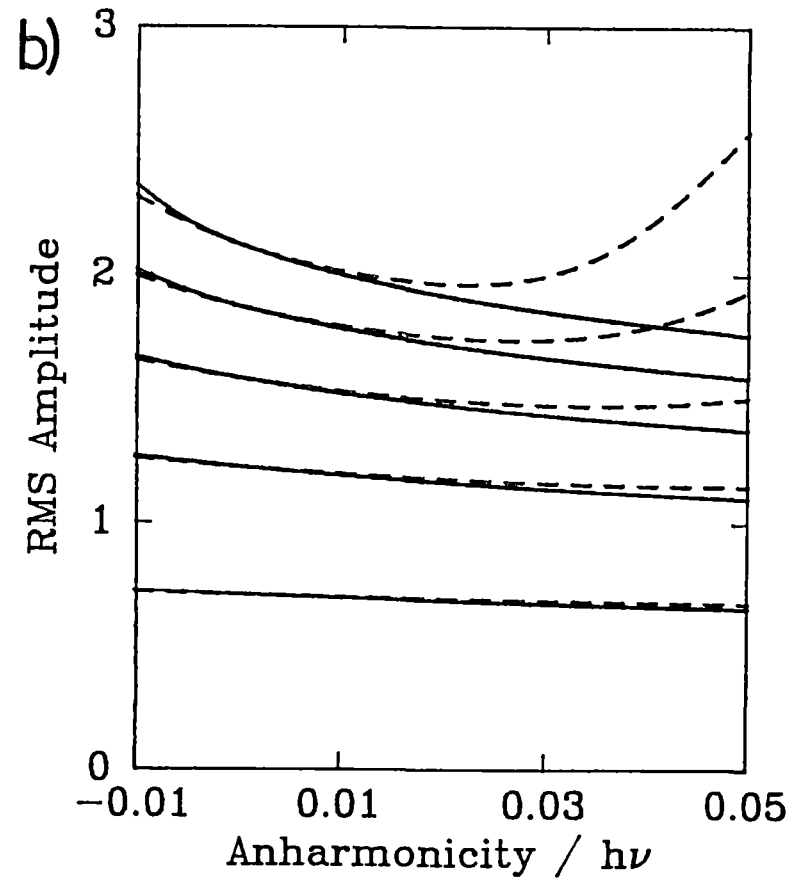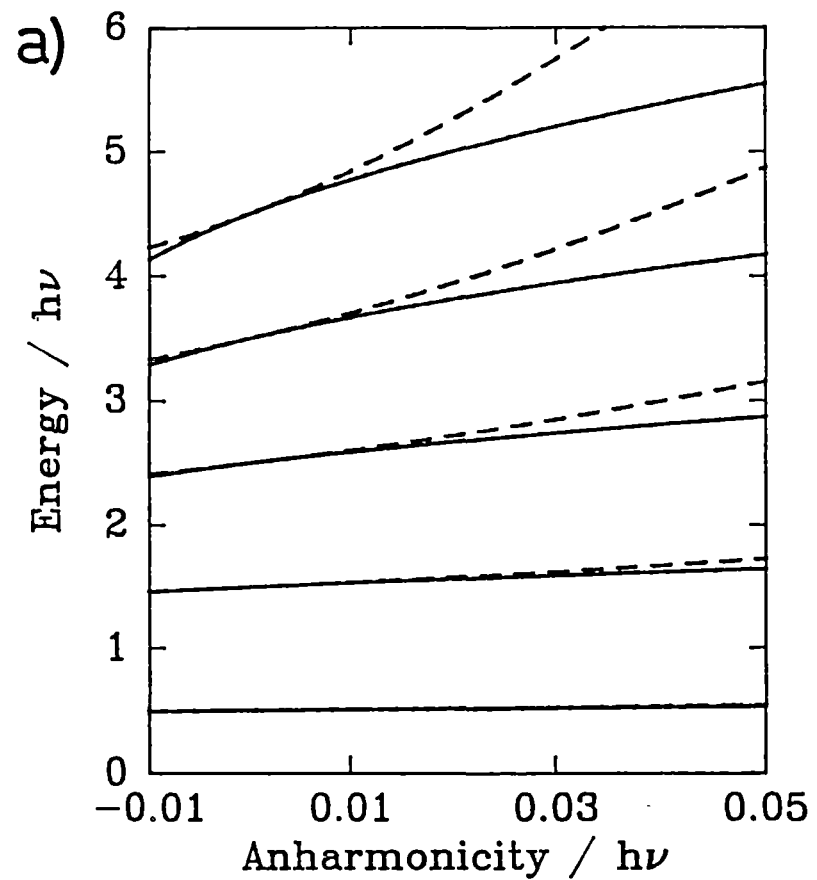
Figure 2.2 Quartic anharmonicity:

————Variational method. — — —Perturbation theory.

a) Energy levels, b) RMS geometry,
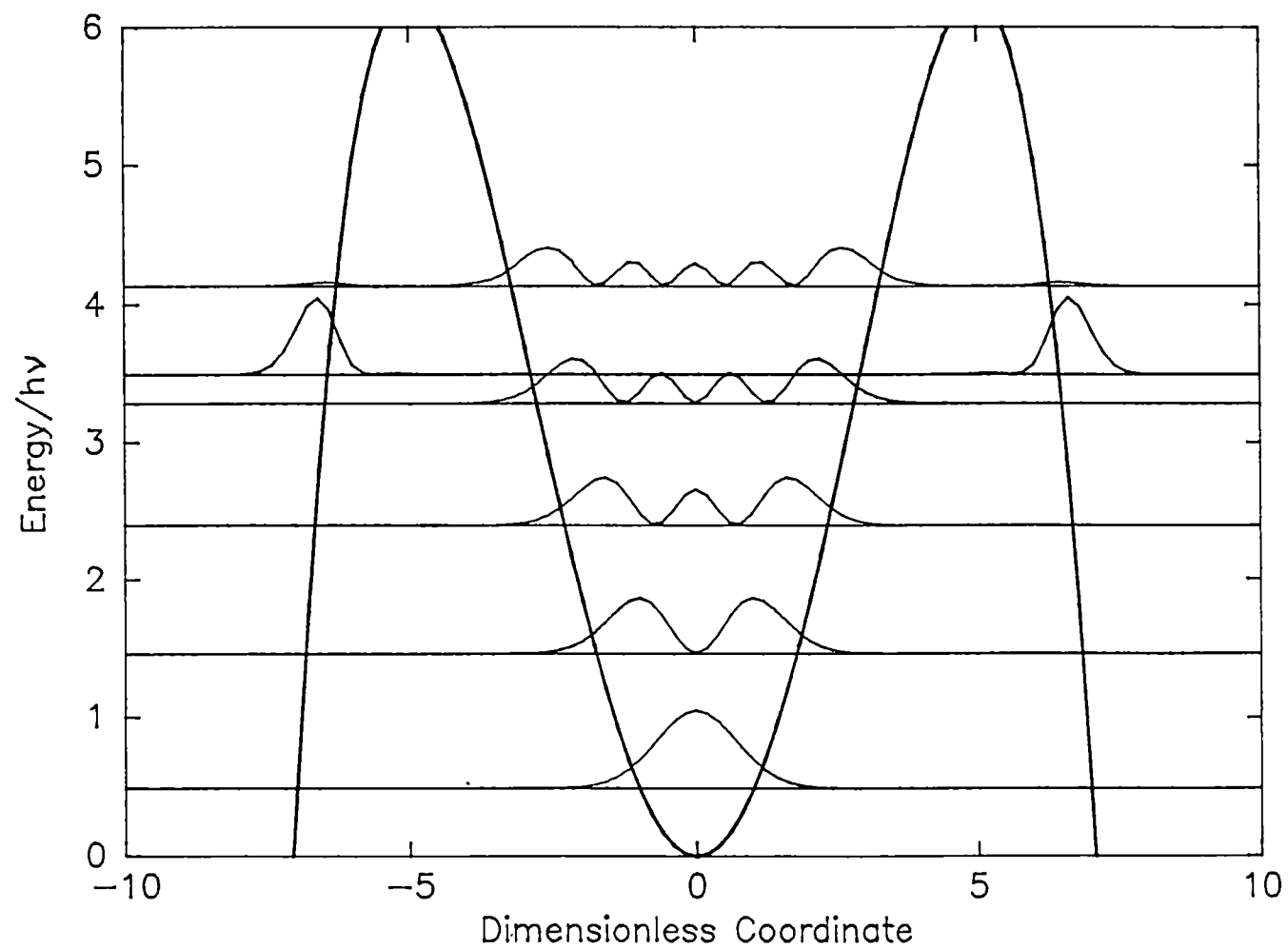
Figure 2.3 A potential surface with quartic anharmonicity. The fifth highest level is "unbound".

The quartic oscillator: The pure quartic oscillator has been studied by Chan and Stelman (1963a), who proposed that while such a potential is unlikely to be found in nature, it may provide better basis functions than the SHO for some systems. To this end, they calculated the matrix elements of ξ, ξ^2, ξ^3, ... with the eigenvectors found from solving the quartic oscillator. However, when repeating their calculation it was found that while the same eigenvalues were reproduced, the wavefunctions were not. Exhaustive tests in double precision on two different computers with two different diagonalisation routines gave consistent eigenvectors that were different from those of Chan and Stelman (1963a). It is concluded that the Jacobi rotation method of diagonalisation that they used was the source of their inaccurate eigenvectors.

Double Minima Potentials: Often the potential along a vibrational coordinate cannot even be approximately described by a harmonic parabola. While anharmonicity implies a small perturbation to the harmonic potential, completely non-harmonic potentials may also be encountered. This situation can occur in molecules which undergo inversion, large amplitude motions or hindered rotation (Papousek and Aliev 1982; Maruani and Serre 1983). Other phenomena related to such potentials are hydrogen bonding (Somorjai and Hornig 1962) and spectroscopic properties of metalloproteins (Bacci 1984).

The general potential considered here is given by:

$$V(\xi) = \sum_{i=0}^{6} \xi^i + \alpha \exp(-\beta\xi^2) \qquad (2.45)$$

and must be solved by the variational method, as these potentials will be far from harmonic.

Double minima potentials have been studied thoroughly by Somorjai and Hornig (1962). Potential 1 of their work is shown in figure 2.4a and is used here as a test case. It is obtained by using the potential parameters $k_2 = -2.63$; $k_4 = 0.32875$ in equation (2.45). Note the very small separation of the first two vibrational levels and the symmetric/antisymmetric nature of the wavefunctions. This is the so called "inversion" splitting, as found in ammonia, the magnitude of which depends on the barrier height.

If a very small linear term ($k_1 = 0.01$) is added to the potential to make the minima inequivalent in figure 2.4b. The energy levels are only slightly perturbed, but the wavefunctions are greatly changed,

(2.17)
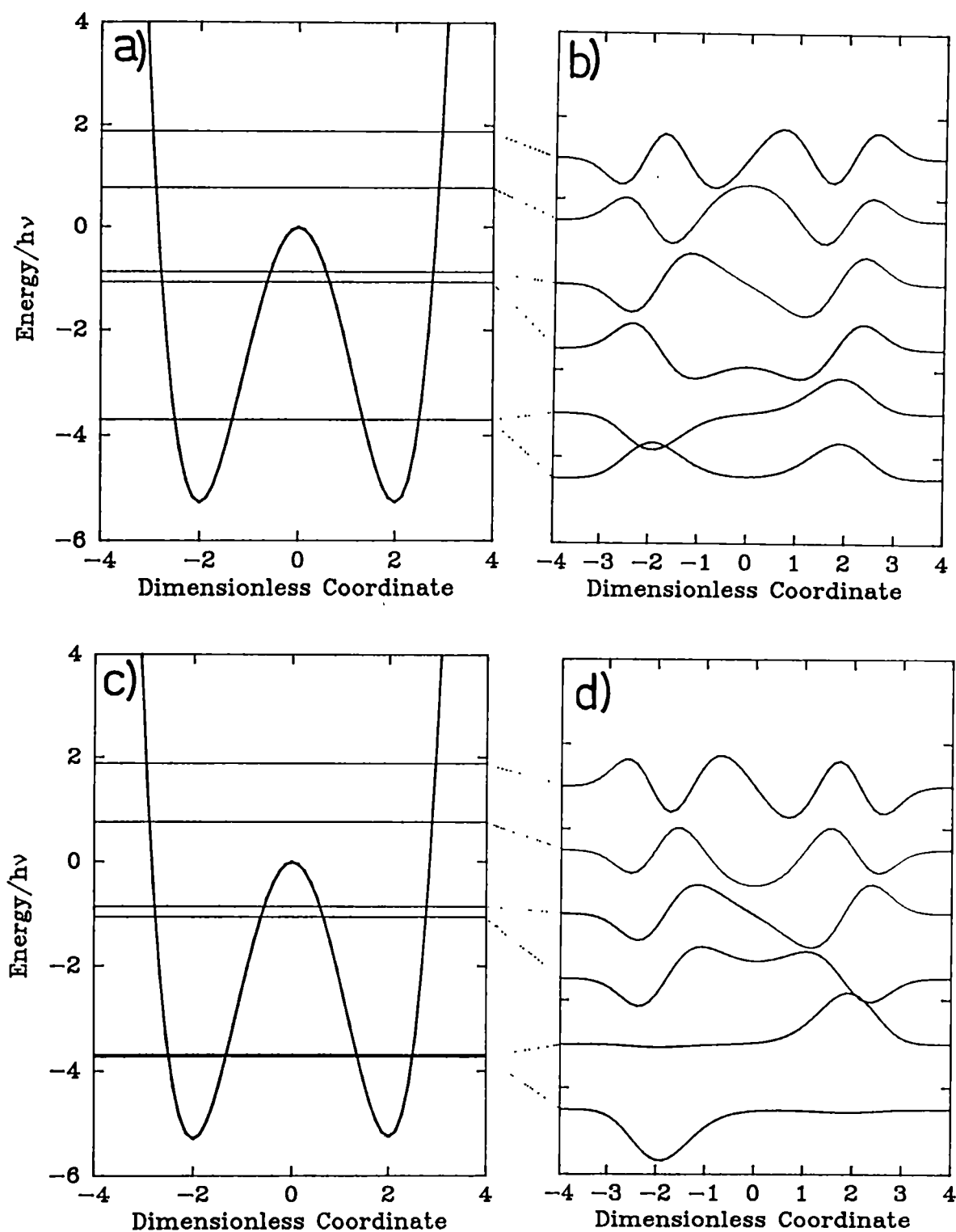
Figure 2.4 Double Minimum Potentials.

a) Symmetric minima: $V(\xi) = -2.63\xi^2 + 0.32875\xi^4$.

b) Wavefunctions of the symmetric potential.

c) Asymmetric double minima; $V(\xi) = 0.01\xi - 2.63\xi^2 + 0.32875\xi^4$.

d) Wavefunctions of the asymmetric potential.

each state becoming localised in one of the two minima. This is exactly analogous to the "vibronic enhancement of small perturbations" found in Jahn-Teller systems (see chapter 4).

Alternatively a double minimum potential may be constructed from a quadratic term and the Gaussian in (2.45). Chan and Stelman (1963b) have given methods of calculating the matrix elements between SHO functions and Gaussians. Exact agreement was found with their published results except for large (100 x 100) basis sizes. In this case round off errors caused unpredictable results when their recursive method of calculating matrix elements was used. Their other suggested method, of calculating the diagonal elements explicitly by their equation 5 and using their "diamond rule" for off-diagonal elements, was used with no problems in round off error.

APPENDIX 2.A1 HARMONIC OSCILLATOR MATRIX ELEMENTS (HOMEs)

$\underline{H}$armonic $\underline{O}$scillator $\underline{M}$atrix $\underline{E}$lements of powers of the normal coordinate are an often calculated quantity and methods for doing this can be found in almost any quantum mechanical text. Some of the methods that have been used are:

        1.) direct integration (Flügge 1974, pp80-84),

        2.) the use of generating functions (Schiff 1968, pg72),

and 3.) the use of ladder operators (CDL, pp496-505).

However, the above methods have the disadvantage that they become increasingly difficult for HOMEs of higher orders of the normal coordinate. Shaffer and Krohn (1976) give the HOMEs $\langle n|\xi^p|m\rangle$ up to p=7. Here, a new method is presented based on a recursive relation and HOMEs up to p=30 have been calculated. A list of the non-zero HOMEs up to p=10 is given in Table 2.A1.

The general HOME to be evaluated is:

$$\langle n|\xi^p|m\rangle \qquad p\geq 0 \qquad\qquad\qquad (2.A1)$$

Here ξ is the dimensionless coordinate introduced in section 2.2.2. In anticipation of a recursive relation the HOME's for p=0,1,2 are calculated. For p=0 we have:

$$\langle n|m\rangle = 1 \quad n=m$$
$$\qquad\quad = 0 \quad n\neq m \qquad\qquad\qquad (2.A2)$$

from the orthonormal properties of harmonic oscillator wavefunctions. Following method 3 above, the creation (a^+) and annihilation (a) operators (CDL pp481-503) are introduced:

$$a^+ = \frac{1}{\sqrt{2}}(\xi-ip)$$
$$a = \frac{1}{\sqrt{2}}(\xi+ip) \qquad\qquad\qquad (2.A3)$$

where p is the conjugate momentum to ξ. Equation (2.A3) has the following properties:

$$\xi = \frac{1}{\sqrt{2}}(a^+ + a) \qquad\qquad\qquad (2.A4a)$$
$$a|n\rangle = \sqrt{n}|n-1\rangle \qquad\qquad\qquad (2.A4b)$$
$$a^+|n\rangle = \sqrt{n+1}|n+1\rangle \qquad\qquad\qquad (2.A4c)$$
$$[a,a^+] = 1 \qquad\qquad\qquad (2.A4d)$$

It can be seen that the effect of the operator a (a^+) is to annihilate (create) a quantum when acting on $|n\rangle$. They are also known

as step or ladder operators in the literature. It is a simple matter to calculate HOMEs for lower powers of p:

p=1: $\langle n|\xi|m\rangle = \langle n|\frac{1}{\sqrt{2}}(a^+ + a)|m\rangle$ (from (2.A4a))

$$= \sqrt{1/2}\,\langle n|a^+|m\rangle + \sqrt{1/2}\,\langle n|a|m\rangle$$

$$= \sqrt{(m+1)/2}\,\langle n|m+1\rangle + \sqrt{m/2}\,\langle n|m-1\rangle \quad \text{(from (2.A4b,c))}$$

$$= \sqrt{(m+1)/2} \quad \text{for } m=n-1,$$

$$\sqrt{m/2} \qquad \text{for } m=n+1. \tag{2.A5}$$

p=2: $\langle n|\xi^2|m\rangle = \frac{1}{2}\langle n|(a^+a^+ + a^+a + aa^+ + aa)|m\rangle$

$$= \frac{1}{2}\sqrt{(m+1)(m+2)}\,\langle n|m+2\rangle + (m+\tfrac{1}{2})\langle n|m\rangle + \frac{1}{2}\sqrt{m(m-1)}\,\langle n|m-2\rangle$$

$$= \frac{1}{2}\sqrt{(m+1)(m+2)} \quad \text{for } m=n-2,$$

$$(m+\tfrac{1}{2}) \qquad \text{for } m=n,$$

$$\frac{1}{2}\sqrt{m(m-1)} \qquad \text{for } m=n+2. \tag{2.A6}$$

However to calculate $\langle n|\xi^8|m\rangle$ becomes very tedious as $(a^+ + a)^8$ must be expanded into 256 terms because the order of operation is important as by (2.A4d) these terms do not commute.

Since the functions $|n\rangle$ are a complete set we have the closure identity:

$$\sum_n |n\rangle\langle n| = 1 \tag{2.A7}$$

and applying this to (2.A1) we get:

$$\langle n|\xi^p|m\rangle = \langle n|\xi^{p-1}\cdot(\sum_r |r\rangle\langle r|)\cdot\xi|m\rangle \tag{2.A8}$$

from (2.A5), this HOME is non-zero only when $r = m \pm 1$.

$$\text{HOME} = \langle n|\xi^{p-1}|\cdot(|m-1\rangle\langle m-1| + |m+1\rangle\langle m+1|)\cdot\xi|m\rangle$$

$$= \langle n|\xi^{p-1}|m-1\rangle\langle m-1|\xi|m\rangle + \langle n|\xi^{p-1}|m+1\rangle\langle m+1|\xi|m\rangle$$

which leads to the desired recursive relationship:

$$\langle n|\xi^p|m\rangle = \sqrt{m/2}\,\langle n|\xi^{p-1}|m-1\rangle + \sqrt{(m+1)/2}\,\langle n|\xi^{p-1}|m+1\rangle \tag{2.A9}$$

With this simple expression, a HOME of ξ^p can easily be calculated from the HOMEs of ξ^{p-1}. This is a far simpler method of calculating matrix elements than has been given previously in the literature.

To find explicit expressions for the higher order matrix elements still involves a certain amount of manipulation as the expression must be simplified at each step by collecting terms. To do this a program

(2.20)

was written using REDUCE, a symbolic language for algebraic manipulation, the results up to p=30 were obtained. It is probably unlikely that HOMEs for p=30 are actually needed, however when simulating spectra it is useful to fit the potential to a power series. In this situation higher order HOMEs than those published (up to p=7, Shaffer and Krohn 1976) may well be necessary.

Closed formulas have recently been developed (Morales etal 1984) for evaluating any particular matrix element. The general HOME has been shown to be given by:

$$\langle n|\xi^p|m\rangle = \frac{p!}{2^{p/2+z}}\left(\frac{m!}{n!}\right)^{1/2}\sum_{\alpha=0}^{[n,z]} 2^\alpha \binom{n}{\alpha} (m-n+\alpha)!\,(z-\alpha)!]^{-1} \qquad (2.A10)$$

Equation (2.A10) is defined for $n\leqslant m$ and $z = \frac{1}{2}(p+n-m)$, $[n,z]$ denotes the smaller of n and z, and $\binom{n}{\alpha}$ is a binomial coefficient. In the special case of diagonal elements this expression reduces that previously given by Cyvin (1968, pg75):

$$\langle n|\xi^{2p}|n\rangle = \frac{(2p)!}{2^{2p}p!}\sum_{\alpha=0}^{[n,p]} 2^\alpha \binom{p}{\alpha}\binom{n}{\alpha} \qquad (2.A11)$$

where only even powers of the coordinate ξ are non-zero. These formulae could be used instead of the explicit expressions given in table 2.A1 but are more cumbersome in practice.

The non-zero matrix elements of the kinetic energy operator are given by (Heilbronner 1956):

$$\langle n|\;P(\xi)^2\;|n-2\rangle = -\frac{1}{2}\sqrt{n(n-1)} \qquad (2.A12)$$

$$\langle n|\;P(\xi)^2\;|n\rangle\; = (n+\frac{1}{2}) \qquad P(\xi)^2 = -\frac{\partial^2}{\partial\xi^2}$$

$$\langle n|\;P(\xi)^2\;|n+2\rangle = -\frac{1}{2}\sqrt{(n+1)(n+2)}$$

TABLE 2.A1 Matrix elements of $\langle n|\xi^p|m\rangle$ p=0-10

p	m	$\langle n|\xi^p|m\rangle$
0	n	2^0
1	n-1	$2^{-1/2}\ [n]^{1/2}$
	n+1	$2^{-1/2}\ [n+1]^{1/2}$
2	n-2	$2^{-1}\ [n(n-1)]^{1/2}$
	n	$2^{-1}\ .(2n+1)$
	n+2	$2^{-1}\ [(n+1)(n+2)]^{1/2}$
3	n-3	$2^{-3/2}\ [n(n-1)(n-2)]^{1/2}$
	n-1	$2^{-3/2}\ [n]^{1/2}\ .3n$
	n+1	$2^{-3/2}\ [n+1]^{1/2}\ .3(n+1)$
	n+3	$2^{-3/2}\ [(n+1)(n+2)(n+3)]^{1/2}$
4	n-4	$2^{-2}\ [n(n-1)\ ..\ (n-3)]^{1/2}$
	n-2	$2^{-2}\ [n(n-1)]^{1/2}\ .2(2n-1)$
	n	$2^{-2}\ .3(2n^2+2n+1)$
	n+2	$2^{-2}\ [(n+1)(n+2)]^{1/2}\ .2(2n+3)$
	n+4	$2^{-2}\ [(n+1)\ ..\ (n+4)]^{1/2}$
5	n-5	$2^{-5/2}\ [n(n-1)\ ..\ (n-4)]^{1/2}$
	n-3	$2^{-5/2}\ [n(n-1)(n-2)]^{1/2}\ .5(n-1)$
	n-1	$2^{-5/2}\ [n]^{1/2}\ .5(2n^2+1)$
	n+1	$2^{-5/2}\ [n+1]^{1/2}\ .5(2n^2+4n+3)$
	n+3	$2^{-5/2}\ [(n+1)\ ..\ (n+3)]^{1/2}\ .5(n+2)$
	n+5	$2^{-5/2}\ [(n+1)\ ..\ (n+5)]^{1/2}$
6	n-6	$2^{-3}\ [n(n-1)\ ..\ (n-5)]^{1/2}$
	n-4	$2^{-3}\ [n(n-1)\ ..\ (n-3)]^{1/2}\ .3(2n-3)$
	n-2	$2^{-3}\ [n(n-1)]^{1/2}\ .15(n^2-n+1)$
	n	$2^{-3}\ .15(4n^3+6n^2+8n+3)$
	n+2	$2^{-3}\ [(n+1)(n+2)]^{1/2}\ .15(n^2+3n+3)$
	n+4	$2^{-3}\ [(n+1)\ ..\ (n+4)]^{1/2}\ .3(2n+5)$
	n+6	$2^{-3}\ [(n+1)\ ..\ (n+6)]^{1/2}$
7	n-7	$2^{-7/2}\ [n(n-1)\ ..\ (n-6)]^{1/2}$
	n-5	$2^{-7/2}\ [n(n-1)\ ..\ (n-4)]^{1/2}\ .7(n-2)$
	n-3	$2^{-7/2}\ [n(n-1)(n-2)]^{1/2}\ .21(n^2-2n+2)$
	n-1	$2^{-7/2}\ [n]^{1/2}\ .35(n^3+2n)$
	n+1	$2^{-7/2}\ [n+1]^{1/2}\ .35(n^3+3n^2+5n+3)$
	n+3	$2^{-7/2}\ [(n+1)\ ..\ (n+3)]^{1/2}\ .21(n^2+4n+5)$

TABLE 2.A1 (cont.)

	$n+5$	$2^{-7/2}\,[(n+1)\,..\,(n+5)]^{1/2}\,.7(n+3)$
	$n+7$	$2^{-7/2}\,[(n+1)\,..\,(n+7)]^{1/2}$
8	$n-8$	$2^{-4}\,[n(n-1)\,..\,(n-7)]^{1/2}$
	$n-6$	$2^{-4}\,[n(n-1)\,..\,(n-5)]^{1/2}\,.4(2n-5)$
	$n-4$	$2^{-4}\,[n(n-1)\,..\,(n-3)]^{1/2}\,.14(2n^2-6n+7)$
	$n-2$	$2^{-4}\,[n(n-1)]^{1/2}\,.28(2n^3-3n^2+7n-3)$
	n	$2^{-4}\,.35(2n^4+4n^3+10n^2+8n+3)$
	$n+2$	$2^{-4}\,[(n+1)(n+2)]^{1/2}\,.28(2n^3+9n^2+19n+15)$
	$n+4$	$2^{-4}\,[(n+1)\,..\,(n+4)]^{1/2}\,.14(2n^2+10n+15)$
	$n+6$	$2^{-4}\,[(n+1)\,..\,(n+6)]^{1/2}\,.4(2n+7)$
	$n+8$	$2^{-4}\,[(n+1)\,..\,(n+8)]^{1/2}$
9	$n-9$	$2^{-9/2}\,[n(n-1)\,..\,(n-8)]^{1/2}$
	$n-7$	$2^{-9/2}\,[n(n-1)\,..\,(n-6)]^{1/2}\,.9(n-3)$
	$n-5$	$2^{-9/2}\,[n(n-1)\,..\,(n-4)]^{1/2}\,.18(2n^2-8n+11)$
	$n-3$	$2^{-9/2}\,[n(n-1)(n-2)]^{1/2}\,.42(2n^3-6n^2+13n-9)$
	$n-1$	$2^{-9/2}\,[n]^{1/2}\,.63(2n^4+10n^2+3)$
	$n+1$	$2^{-9/2}\,[n+1]^{1/2}\,.63(2n^4+8n^3+22n^2+28n+15)$
	$n+3$	$2^{-9/2}\,[(n+1)\,..\,(n+3)]^{1/2}\,.42(2n^3+12n^2+31n+30)$
	$n+5$	$2^{-9/2}\,[(n+1)\,..\,(n+5)]^{1/2}\,.18(2n^2+12n+21)$
	$n+7$	$2^{-9/2}\,[(n+1)\,..\,(n+7)]^{1/2}\,.9(n+4)$
	$n+9$	$2^{-9/2}\,[(n+1)\,..\,(n+9)]^{1/2}$
10	$n-10$	$2^{-5}\,[n(n-1)\,..\,(n-9)]^{1/2}$
	$n-8$	$2^{-5}\,[n(n-1)\,..\,(n-7)]^{1/2}\,.5(2n-7)$
	$n-6$	$2^{-5}\,[n(n-1)\,..\,(n-5)]^{1/2}\,.45(n^2-5n+8)$
	$n-4$	$2^{-5}\,[n(n-1)\,..\,(n-3)]^{1/2}\,.30(4n^3-18n^2+44n-39)$
	$n-2$	$2^{-5}\,[n(n-1)]^{1/2}\,.105(2n^4-4n^3+16n^2-14n+9)$
	n	$2^{-5}\,.63(4n^5+10n^4+40n^3+50n^2+46n+15)$
	$n+2$	$2^{-5}\,[(n+1)(n+2)]^{1/2}\,.105(2n^4+12n^3+40n^2+66n+45)$
	$n+4$	$2^{-5}\,[(n+1)\,..\,(n+4)]^{1/2}\,.30(4n^3+30n^2+92n+105)$
	$n+6$	$2^{-5}\,[(n+1)\,..\,(n+6)]^{1/2}\,.45(n^2+7n+14)$
	$n+8$	$2^{-5}\,[(n+1)\,..\,(n+8)]^{1/2}\,.5(2n+9)$
	$n+10$	$2^{-5}\,[(n+1)\,..\,(n+10)]^{1/2}$

APPENDIX 2.A2   Perturbation Formulae for a Harmonic Oscillator.

If a harmonic oscillator is perturbed by small anharmonic terms in the potential, then perturbation theory can be used to find the approximate correction to the unperturbed energy levels and wavefunctions. The Hamiltonian to be solved in dimensionless units is given by:

$$H = H_o + H' \qquad (2.A13)$$

Here $H_o = \frac{1}{2} (- \frac{\partial^2}{\partial\xi^2} + \xi^2)$ is the unperturbed SHO Hamiltonian, and

$$H' = a_0 + a_1\xi + a_2\xi^2 + a_3\xi^3 + a_4\xi^4$$

is the perturbation which is considered small with respect to H_o.

From the solution of H_o, the unperturbed energies and wavefunctions are respectively:

$$E_n = (n + \tfrac{1}{2}) h\nu; \quad |n\rangle \qquad n = 0,1,2.. \qquad (2.A14)$$

The explicit form of these wavefunctions have been given in (2.33).
The approximate energies of the Hamiltonian in (2.A13) can be found using second order perturbation theory (see Schiff 1968, pg 247) and are given by:

$$E_n = (a_0 - \tfrac{1}{2}a_1^2) + (h\nu + a_2 - \tfrac{1}{2}a_2^2)(n + \tfrac{1}{2})$$

$$- a_3^2 \frac{15}{4} (n^2 + n + \tfrac{11}{30}) + a_4 \frac{3}{4} (2n^2 + 2n + 1)$$

$$- a_4^2 \frac{1}{8} (34n^3 + 31n^2 + 59n + 21) \qquad (2.A15)$$

The corresponding approximate wavefunctions of (2.A13) are given by:

$$\Phi_n = N \sum_{i=n-8}^{n+8} c_i |n\rangle; \quad N = [\sum_i c_i^2]^{-1/2} \quad (i > 0) \qquad (2.A16)$$

The expressions for the coefficients c_i, will be very long and cumbersome when there is more than one non-zero perturbation term in (2.A13), because of the cross terms in the second order perturbation expressions. For the special cases where only a cubic (a_3) or only a

quartic (a_4) perturbation is present, the coefficients are as given in table 2.A2. It is these approximate expressions in equations (2.A15) and (2.A16) that were used in section 2.2.4, and compared with the exact results of the variational methods.

TABLE 2.A2   The Wavefunction Coefficients

i	c_i cubic perturbation ($a = a_3$)	
n-6	$a^2 (18.8)^{-1} [n(n-1)..(n-5)]^{1/2}$	$.1$
n-4	$a^2 (4.8)^{-1} [n(n-1)(n-2)(n-3)]^{1/2}$	$.(4n-3)$
n-3	$a (3.\sqrt{8})^{-1} [n(n-1)(n-2)]^{1/2}$	$.1$
n-2	$a^2 (2.8)^{-1} [n(n-1)]^{1/2}$	$(7n^2 - 19n + 1)$
n-1	$a (1.\sqrt{8})^{-1} [n]^{1/2}$	$.3n$
n	1	
n+1	$a (1.\sqrt{8})^{-1} [n+1]^{1/2}$	$.-(3n+3)$
n+2	$a^2 (2.8)^{-1} [(n+1)(n+2)]^{1/2}$	$.(7n^2 + 33n + 27)$
n+3	$a (3.\sqrt{8})^{-1} [(n+1)(n+2)(n+3)]^{1/2}$	$.-1$
n+4	$a^2 (4.8)^{-1} [(n+1)...(n+4)]^{1/2}$	$.(4n + 7)$
n+6	$a^2 (18.8)^{-1} [(n+1)...(n+6)]1/2$	$.1$

i	c_i quartic perturbation ($a = a_4$)	
n-8	$a^2 (32.16)^{-1} [n(n-1)..(n-7)]^{1/2}$	$.1$
n-6	$a^2 (24.16)^{-1} [n(n-1)..(n-5)]^{1/2}$	$.(12n-22)$
n-4	$a^2 (16.16)^{-1} [n(n-1)..(n-3)]^{1/2}$	$.(32n^2 - 132n + 112)$
	$+ a (4.4)^{-1} [n(n-1)..(n-3)]^{1/2}$	$.(4n - 2)$
n-2	$a^2 (8.16)^{-1} [n(n-1)]^{1/2}$	$.-(4n^3 + 210n^2 - 214n + 156)$
	$+ a (2.4)^{-1} [n(n-1)]^{1/2}$	$.(4n-2)$
n	1	
n+2	$a^2 (8.16)^{-1} [(n+1)(n+2)]^{1/2}$	$.-(4n^3 - 166n^2 - 718n - 600)$
	$+ a (2.4)^{-1} [(n+1)(n+2)]^{1/2}$	$.-(4n + 6)$
n+4	$a^2 (16.16)^{-1} [(n+1)..(n+4)]^{1/2}$	$.(32n^2 + 208n + 288)$
	$+ a (4.4)^{-1} [(n+1)..(n+4)]^{1/2}$	$.-1$
n+6	$a^2 (24.16)^{-1} [(n+1)..(n+6)]^{1/2}$	$(12n + 38)$
n+8	$a^2 (32.16)^{-1} [(n+1)..(n+8)]^{1/2}$	$.1$

(2.23)

APPENDIX 2.A3 NUMERICAL TEST DATA

Test data is given here for the exact numerical eigenvalues, mean and root mean squared amplitudes for several vibrational levels of an anharmonic oscillator. These were calculated by the variational method using a basis of 70 SHO functions. The potential energy operator is constructed from a sixth order polynomial so that the Hamiltonian is:

$$H = -\frac{1}{2}\frac{\partial^2}{\partial\xi^2} + \sum_{n=0}^{6} a_n \xi^n \qquad (2.A17)$$

The potential coefficients are arbitrarily chosen as those which give a least squares fit to the curve given in figure 2.A1. This curve is actually a detail from the IR spectrum of Nujol in the hydrogen stretch region (see inset of figure 2.A1) which has been arbitrarily dimensioned. The source of this curve along with the quality of the fit is unimportant, but results in the potential coefficients in table 2.A3 which, when substituted into (2.A17), gives the numerical test data in table 2.A4.
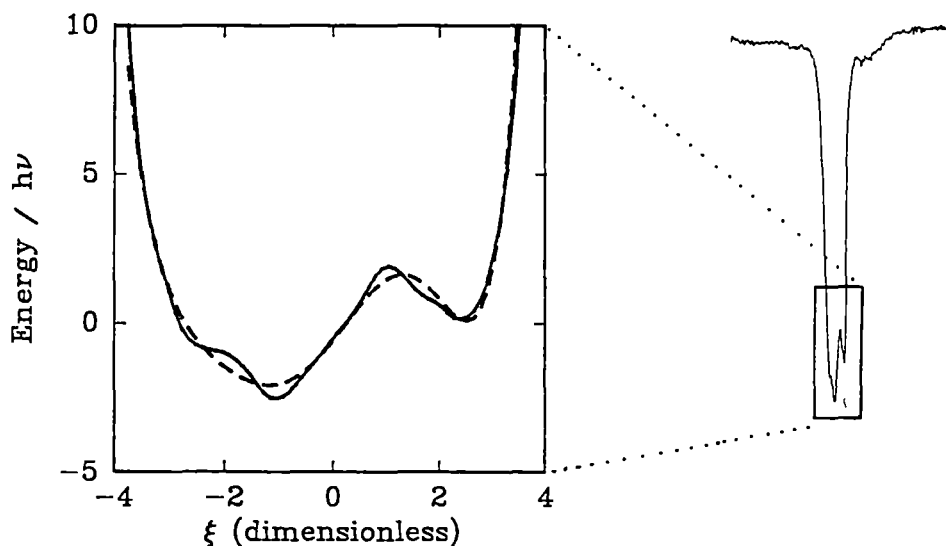
Figure 2.A1 ——— Arbitrarily dimensioned Nujol IR spectrum.
——— Least squares fit to a sixth order polynomial.

TABLE 2.A3 Potential Coefficients

n	a_n
0	−0.57762
1	2.30767
2	0.41713
3	−0.59221
4	−0.14409
5	0.03909
6	0.01373

TABLE 2.A4 Numerical Test Data

Level	Energy/hv	$\langle \xi \rangle$	$\langle \xi^2 \rangle^{1/2}$
1	−1.43913	−1.28371	1.42782
2	−0.02976	−1.21555	1.64112
3	1.07495	1.33027	2.02175
4	1.45977	−0.13957	1.97881
5	2.64788	−0.16042	1.91259
6	3.78543	0.02445	2.09134
7	5.09141	−0.11736	2.17380
8	6.56163	−0.16527	2.23651
9	8.16156	−0.19448	2.29710
10	9.88462	−0.21940	2.35160

CHAPTER 3   WEAK VIBRONIC INTERACTIONS:
WORKING WITHIN THE ADIABATIC APPROXIMATION.

This chapter considers weak vibronic coupling which causes the electronic part of an adiabatic vibronic wavefunction to vary as a function of the nuclear coordinates. The use of adiabatic functions greatly simplifies the calculation of vibronic spectra as the transitions will occur between the potential surfaces of only two electronic states. This chapter is concerned with the calculation of such vibronic spectra within the adiabatic approximation.

After some introductory concepts relevant to vibronic transitions and group theory, the normal modes are divided into those in which the transition moment depends on the nuclear coordinates and those in which it does not. These will be called the coupling and non-coupling coordinates respectively. The following sections detail the way that the total spectrum can then be calculated using the variational method. Also discussed is the alternative approach of a moments analysis, where the spectral properties can be found in a convenient manner. Analytic formulae are then derived for some properties of vibronic spectra within a harmonic approximation. Finally, several interesting and unusual effects in vibronic spectra are explored.

3.1 VIBRONIC TRANSITIONS

The vibronic spectrum of a non-linear molecule will consist of transitions between only two potential surfaces in an n (=3N-6) dimensional hyperspace. In an absorption spectrum a single vibronic transition can be denoted by:

$$|\Psi_g i_1\, i_2\, \cdot\, \cdot\, i_n> \rightarrow |\Psi_e j_1\, j_2\, \cdot\, \cdot\, j_n> \qquad (3.1)$$

where Ψ_g, Ψ_e are the ground and excited electronic states and $i_1,\ldots i_n$; $j_1,\ldots j_n$ are the respective quantum numbers of the n normal vibrations. The energy of this transition will be:

$$E_{j_1 j_2 \cdots j_n}^{i_1 i_2 \cdots i_n} = E_o + E(j_1,j_2 \cdots j_n) - E(i_1,i_2 \cdots i_n) \qquad (3.2)$$

where E_o is the vertical energy separation of the potential surfaces and $E(i_1,\ldots i_n)$; $E(j_1,\ldots j_n)$ are the vibrational energy levels within

the potential surfaces of the ground and excited states. The intensity of this transition is given by (Roche and Jaffe 1976):

$$I_{j_1,j_2\cdots j_n}^{i_1,i_2\cdots i_n} \propto |\ <i_1 i_2 \cdots i_n|\ M_{ge}(Q)\ |j_1 j_2 \cdots j_n>\ |^2 \qquad (3.3)$$

where $M_{ge}(Q)$ is the electronic transition moment in the electron dipole approximation:

$$M_{ge}(Q) = <\Phi_g(Q)|\ e\Sigma_p r_p\ |\Phi_e(Q)> \qquad (3.4)$$

In any electronic transition there are clearly an enormous number of vibronic transitions. For example, in a medium size molecule of six atoms, if it is assumed that in each normal mode there will be non-zero transitions from the lowest vibronic level in the ground state to five excited state vibronic levels, then there will be $5^{12} \approx 2.4 \times 10^8$ individual vibronic transitions in the spectrum.

However, a great simplification can be made if it is assumed that the normal coordinates are the same in both electronic states. This then assumes that there is no rotation of the normal coordinates in the excited state (the effects on the vibronic spectrum when this occurs is examined in section 3.7.2). The consequence of this assumption is that all terms in the vibronic Hamiltonian that are attributable to different normal modes commute with each other. This means that <u>the total vibronic spectrum is the convolution of the vibrational spectra of each normal mode</u>.

A proof of this statement has been given by O'Brien (1981; 323-37). The importance of this statement is that the vibronic spectrum can be calculated separately for each normal mode. In the six atom example given above, there will still be ~2.4×10^8 vibronic transitions in the spectrum, but only 5x12 = 60 transitions need to be calculated, the rest follow by convolution (for simplicity all vibrations are considered non-degenerate). By convolution it is meant that each vibronic transition in one normal mode acts as a vibronic origin for the vibronic spectra of all other normal modes.

In this approach the electronic transition moment in equation (3.3) can be expanded about the ground state equilibrium geometry, $Q=0$, in terms of the normal coordinates:

$$M_{ge}(Q) = M(0) + \sum_n \left(\frac{\partial M(Q)}{\partial Q_n}\right)_0 Q_n + \ldots$$
$$= M(0) + \sum_n M^n(Q_n) \qquad (3.5)$$

The cross terms in (3.5) disappear in the absence of the Dushinsky effect, and the energy and intensity of the vibronic transition in (3.1) are then given respectively as:

$$E_{j_1,j_2\cdots j_n}^{i_1,i_2\cdots i_n} = E_0 + \sum_n (E(j_n) - E(i_n)) \qquad (3.6)$$

$$I_{j_1,j_2\cdots j_n}^{i_1,i_2\cdots i_n} \propto |M(0)|^2 \prod_n |<i_n|j_n>|^2$$
$$+ \sum_k \left[|<i_k|M^k(Q)|j_k>|^2 \cdot \prod_{n \neq k} |<i_n|j_n>|^2 \right] \qquad (3.7)$$

These equations then replace (3.2) and (3.3) in the convolution approach and represent the deflation of the problem from an n-dimensional one to n one-dimensional problems. The first and second terms on the right hand side of equation (3.7) represent the allowed and forbidden components of the transition. In equations (3.6) and (3.7) the subscript n, in the sums and products, runs over all the n normal coordinates, and k denotes only those that are vibronically active (ie $M^k(Q_k) \neq 0$). The part of the electronic transition moment that does not depend on the nuclear coordinates, $M(0)$, can be taken outside of the integral over the vibrational wavefunctions in (3.7). Methods of evaluating these integrals are given in sections 3.3 and 3.4.

(3.3)

3.2 GROUP THEORY

"Just the ability to describe the symmetry of a physical object
may be sufficient reason for many people to learn the rudiments
of point symmetry groups (eg to amaze ones friends by announcing
that a tennis ball has D_{2h} point symmetry)."   - Flurry (1983)

3.2.1 Molecular Point Groups and Selection Rules.

A complete set of symmetry operations that takes a molecule into
itself forms a mathematical group called a molecule point group. Group
theory can formalise the intuitive use of symmetry arguments that are
of such fundamental importance in chemistry.

The chemical applications of group theory given in the texts of
Cotton (1963), Vincent (1977) and Harris and Bertolucci (1978) include
the formation of spectral selection rules and the construction of
symmetry adapted functions. More advanced applications of group theory
include the use of irreducible tensor methods in the simplification of
matrix elements (Köning and Kremer 1977; Piepho and Schatz 1983).

The application of group theory to quantum mechanics depends on
the fact that the Hamiltonian of a molecule transforms as totally
symmetric in the point group of the molecule (Cotton 1963, chapter 5;
Piepho and Schatz 1983, section 8.9). This means that the Hamiltonian
is invariant to any of the symmetry operations of the point group. If
this was not so, the molecule point group would be lowered by the
invariant terms in the Hamiltonian until it became so.

Group theory gives information about integrals such as:

$$\int_{-\infty}^{\infty} \psi_a^* \, P \, \psi_b \, d\tau \equiv \langle a|P|b \rangle \tag{3.8}$$

The wavefunctions ψ_a, ψ_b and the operator P can form a basis for the
irreducible representations Γ_a, Γ_b, Γ_p of a particular point group.
The integral in (3.8) will be non-zero if the direct product of these
irreducible representations contains the totally symmetric irreducible
representation of the point group:

$$\langle a|P|b \rangle \neq 0 \text{ only if } \Gamma_a \times \Gamma_b \times \Gamma_p \supset \Gamma_{tot.sym.} \cdots \tag{3.9}$$

When the operator is the Hamiltonian of the system then, since H is always totally symmetric, the rule in (3.9) reduces to:

$$<a|H|b> \neq 0 \text{ only if } \Gamma_a \times \Gamma_b \supset \Gamma_{tot.sym.} + . . \qquad (3.10)$$

This is extremely important as it shows that in a variational calculation a matrix element can only connect basis functions of the same symmetry. It is therefore very desirable to have basis functions that are symmetry adapted to the problem being solved. This decreases the computational task and has the added advantage of increasing one's insight into the problem.

To form selection rules from equation (3.9), a model must first be invented to describe the system which can then be used to give the relevant integrals. The rule expressed by (3.9) may then be used to determine whether these integrals are non-zero, thus forming the selection rules. These selection rules often "break down" but this is always due to an inadequate model rather than a failure of group theory.

For example, selection rules can be made for the polarisation of the transitions between two electronic states of a particular molecule in the electric dipole approximation. However, these selection rules will be wrong if the intensity of the transition is mainly derived from a magnetic dipole mechanism or from vibronic coupling. In this case the wrong integrals were considered, rather than group theory failing to evaluate them correctly.

3.2.2 Non-Rigid Molecules: Inversion-Permutation Groups.

The point group symmetry of molecules refers to the equilibrium nuclear geometry of the molecule, and assumes that there are only small departures from this configuration. Difficulties arise in the case of non-rigid molecules where there can be several equivalent configurations separated by energy barriers. Examples of such molecules include those with internal rotation (ethane), ring puckering (cyclopentane) and inversion (ammonia). The theory of inversion-permutation groups was developed by Longuet-Higgins (1963) to deal with these types of situations. It is noted that dynamic Jahn-Teller

systems are also examples of non-rigid molecules and must be clas-
sified in terms of inversion-permutation symmetry groups (see Bersuker
and Polinger 1982, pp92-3; also section 4.4.3).

Ammonia provides a good example of a non-rigid molecule, as there
are two equivalent minima at a C_{3v} geometry which are separated by a
barrier of ~2000 cm^{-1} at the D_{3h} planar configuration (Papousek and
Aliev 1983, chapter 25). As discussed in section 2.2.5, this sort of
double minima potential results in near degenerate pairs of vibra-
tional levels below the height of the barrier. The energy separation
between these pairs of levels are often referred to as the inversion
splitting. If the C_{3v} point group was used to calculate the ground
state vibrational properties of ammonia then this inversion splitting
would not be predicted. However, if the inversion-permutation group is
used (which is isomorphic to the D_{3h} point group), the inversion
splittings will be correctly calculated.

The inversion barrier in phosphine PH_3 is ~11,000 cm^{-1} and the
inversion splitting has been calculated to be ~10^{-16} cm^{-1} (Spirko etal
1986). This splitting has not been detected experimentally so the
molecule can be considered as having a rigid C_{3v} geometry with no loss
of information. However, if an ultra high resolution experiment was
able to detect these splittings, they would have to be interpreted in
terms of a D_{3h} permutation-inversion symmetry group (Papousek and
Aliev 1983, pg244).

A general criterion for the use of an inversion-permutation group
of a non-rigid molecule, in preference to a molecular point group of a
rigid molecule, is when the experimental technique is capable of
detecting the effects of the quantum mechanical tunnelling between the
equivalent configurations (ie inversion splittings). This in turn
depends on whether the tunnelling can occur on the time scale of the
experiment. [Note: This is a very loose sort of criterion as the
inversion splitting increases as the vibrational levels approach the
barrier height, and therefore the probability of tunnelling increases
(Papousek and Aliev 1983, pg 76).]

For example, in a calculation/experiment involving the electronic
Hamiltonian of a non-rigid molecule the molecular point group of the
rigid molecule is sufficient to describe the system, as electrons are
very fast on the time scale of nuclear motions. For vibrational
calculations/experiments this may not be sufficient, depending on the

(3.6)

barrier height between equivalent geometries, as the time scale of vibrations are slower. For isomer separation where the time scale is long (of the order minutes), the system should be described by the appropriate inversion-permutation group (Flurry 1983, pg 114).

When one thinks of the "geometry" of a non-rigid molecule one must specify the time scale of the "geometry". In the case of ammonia, the geometry along the inversion coordinate at any instant of time is given by the C_{3v} point group. However, the time average (or expectation value, see section 2.2.3) of the geometry will correspond to the inversion-permutation group isomorphic to the D_{3h} point group. It is therefore often a matter of preference as to how one defines geometry. It is important to realise, however, that if one wishes to describe ammonia in the C_{3v} point group, the Hamiltonian of the molecule is of C_{3v} symmetry. This means that NH_3 will be described by a potential surface that has a single minimum at C_{3v} geometry, and the fact that it can invert will be completely lost. If one wishes to describe the ground state of ammonia as a double minimum potential, the Hamiltonian (and therefore mean geometry) is of D_{3h} symmetry.

3.2.3 Selection Rules for Adiabatic Potential Surfaces.

Group theory can be used to determine the possible forms of the adiabatic potential surfaces along a normal coordinate of particular symmetry. Here non-degenerate coordinates are assumed; degenerate coordinates are considered in chapter 4. The adiabatic potential surface along a single normal coordinate is given by (1.9):

$$\varepsilon_k(Q) = \langle \Psi_k | H_e(q,Q) | \Psi_k \rangle$$

$$= \varepsilon_k(Q_o) + \langle \Psi_k | \left(\frac{\partial V}{\partial Q} \right)_o Q + \frac{1}{2} \left(\frac{\partial^2 V}{\partial Q^2} \right)_o Q^2 + \ . \ . \ | \Psi_k \rangle$$

$$= \varepsilon_k(Q_o) + u_{kk}^1 Q + u_{kk}^2 Q^2 + \ . \ . \tag{3.11}$$

$$\text{where} \qquad u_{kk}^n = \langle \Psi_k | \frac{1}{n!} \left(\frac{\partial^n V}{\partial Q^n} \right)_o | \Psi_k \rangle \tag{3.12}$$

The first term gives the energy of the adiabatic potential at the equilibrium geometry, and the remaining terms give the shape of the

(3.7)

potential in terms of a power series in the normal coordinate. Group theory can now be used to determine which of the coefficients in (3.12) are non-zero. Since the Hamiltonian of the system must transform as totally symmetric, this means that each of the $u_{kk}^n Q^n$ terms in the expansion must also be totally symmetric. This will only be true when u_{kk}^n transforms the same as Q^n, ie as $[\Gamma_Q]^n$. Since the coefficients (integrals) in (3.12) must themselves transform as totally symmetric to be non-zero, this will only be possible when $[\Gamma_Q]^n$ contains the totally symmetric representation:

$$u_{kk}^n \neq 0 \text{ only when } [\Gamma_Q]^n \supset \Gamma_{tot.sym.} + \cdot \cdot \qquad (3.13)$$

If Γ_Q is a_{1g} then $[\Gamma_Q]^n$ is always totally symmetric and therefore all coefficients in the adiabatic potential (3.11) are allowed to be non-zero. However, if Γ_Q is non-totally symmetric only even orders of $[\Gamma_Q]^n$ are totally symmetric. Therefore, by group theory, <u>the adiabatic potential along a non-totally symmetric coordinate may only be composed of even order terms</u>.

This immediately means that <u>an excited state potential surface of a molecule can only be displaced from the ground state equilibrium geometry along totally symmetric coordinates</u>. This is because a displacement requires a non-zero linear term in the potential (3.11). Displacements that have been given to potentials along non-totally symmetric coordinates in the literature (for example Ballhausen 1977, figure 7) are without question incorrect.

Perhaps an easier way of stating this is: since the total Hamiltonian of the system must transform as totally symmetric in the molecular point group, there is nothing in this Hamiltonian that can lower the symmetry of the molecule. Therefore there cannot be a displacement along a non-totally symmetric coordinate as this would lower the symmetry of the molecule. As will be discussed in detail in section 4.2, this is true even for Jahn-Teller systems. In an ideal Jahn-Teller system, the quantum mechanical mean geometry is always the high symmetry undistorted geometry; it takes terms of low symmetry in the Hamiltonian to produce a (static) distortion.

3.3 NON-COUPLING MODES

A non-coupling normal coordinate of an electronic transition will be defined as one where the intensity of the vibronic transitions between the potential surfaces does not depend on the coordinate. The electronic transition moment can then be taken outside of the integral over these vibrational coordinates in the expression for the intensity in equation (3.7). This is often called the Condon approximation (Roche and Jaffe 1970).

The intensity due to a non-coupling coordinate is then given by:

$$I_j^i \propto M^2 \cdot |<i|j>|^2 \tag{3.14}$$

where M represents either the pure electronic transition moment or the induced intensity of a false origin due to a coupling mode. The $|<i|j>|^2$ term is called the Franck-Condon factor, the square of the Franck-Condon overlap integral. This determines the intensity distribution among the vibrational components of the electronic transition. The total intensity of the transition is constant and does not depend on the ground or excited state potential surfaces nor the temperature of the system. The intensity distribution among the vibrational components of the spectrum, however, depends on all of the above factors.

3.3.1   Selection Rules for the Vibrational Fine Structure.

Since the electronic transition moment in (3.14) does not depend on the nuclear coordinates, the electric dipole selection rules for the electronic transition depends only on the electronic states. The selection rules can be easily found from (3.9) using the symmetry of the ground and excited wavefunctions and the electric dipole moment. Examples of such calculations are found in the texts of Harris and Bertolucci (1978, section 5-4) and Lever (1984, section 4.2). What is of interest in this section is the selection rules for the individual vibronic transitions that make up the vibrational fine structure of the electronic transition.

In section 3.2.3 it was shown that only totally symmetric modes may have displaced potentials. This fact can now be used to determine

the form of the wavefunctions. From appendix 2.A1 it can be seen that the matrix elements of powers of a normal coordinate can only connect simple harmonic oscillator basis functions of the same parity (evenness or oddness). Therefore, if the wavefunctions are expanded in a SHO basis in a variational calculation, they can be a linear combination of any SHO basis functions for a totally symmetric potential. In a non-totally symmetric potential however, odd numbered vibronic states will be a linear combination of odd SHO basis functions, and even states will be a combination of even functions. From their explicit form in equation (2.36), a SHO wavefunction with an even quantum number will be an even function of the coordinates, while those with odd quantum numbers will be an odd function of the coordinates. Since any integral of an odd function will be zero, a Franck-Condon overlap integral will only be non-zero between two even wavefunctions or two odd wavefunctions. This leads to the following selection rules (Herzberg 1966, pp151-2):

$$\Delta n = 0, \pm 1, \pm 2, \ldots \qquad (Q: TS) \qquad (3.15)$$

for transitions between potentials of a totally symmetric coordinate, and

$$\Delta n = 0, \pm 2, \pm 4, \ldots \qquad (Q: non-TS) \qquad (3.16)$$

for transitions between potentials of a non-totally symmetric coordinate. These selection rules are completely general, and do not assume harmonic potentials. They are based on the following line of reasoning:

Symmetry of Q → Possible dependence of the potential on Q.

→ Possible dependence of the wavefunctions on Q.

→ Selection rules for the Franck-Condon overlaps.

An alternative approach is to consider the symmetry of the wavefunctions directly. The Franck-Condon integral, $<i|j>$, will be non-zero if the direct product, $\Gamma_i \times \Gamma_j$, contains the totally symmetric irreducible representation. The lowest vibrational level of each electronic state ($i=0$, or $j=0$) will transform, or have the same symmetry, as the normal coordinate. The symmetry of the higher vibrational levels can be obtained from direct products. These will be totally symmetric for even quantum numbers, and have the same symmetry as the lowest state for odd quantum numbers. These are the same considerations that are used to determine the symmetry species of vibrational overtone levels (WDC, section 7.3). Finding the symmetry

(3.10)

of higher levels of degenerate vibrations is more complex, but may be found using the formula of WDC (pg153, equation 13). The direct product of the irreducible representations of the ground and excited vibronic states gives the symmetry of the Franck-Condon overlap integral. This will be non-zero only when it transforms as totally symmetric and the same selection rules as given by equations (3.15) and (3.16) result.

Figures 3.1-3.4 illustrate these selection rules for transitions from the lowest level of a harmonic ground state to the various different excited state potential surfaces given in the figure captions. Several vibrational probability functions are also shown with the potentials. The spectra have been calculated with the methods given in section 3.5, and the ground and excited state potentials have been chosen so that the energy separation of their minima is the same in all cases.

Figure 3.1 shows identical ground and excited state potential surfaces which results in a spectrum that consists of the single $n_g=0 \rightarrow n_e=0$ transition which is called the electronic origin. Figure 3.2 shows a typical cross section of a potential surface along a totally symmetric coordinate. The potential is displaced due to the odd linear term in the potential. The selection rule in equation (3.15) is operating, although the vibrational "progression" is finite in length. The higher members of the progression, while group theoretically non-zero, are calculated to have a vanishingly small intensity.

Figure 3.3 shows a typical cross section of the potential along a non-totally symmetric coordinate. The excited state potential is harmonic and undisplaced with respect to the ground state, but with a harmonic frequency that is half that of the ground state. Here, a very short progression in two quanta of the non-totally symmetric mode is seen, following the selection rule in (3.16). Calculations show that for harmonic potentials, even when the excited state frequency is half that of the ground state, the $\Delta n = 0$ origin contains ~ 95% of the intensity (Herzberg 1966, pp152-3).

Figure 3.4 shows a double minima excited state potential surface, which again has a progression in two quanta. However, this spectrum has more in common with the intensity pattern of figure 3.2 than

(3.11)
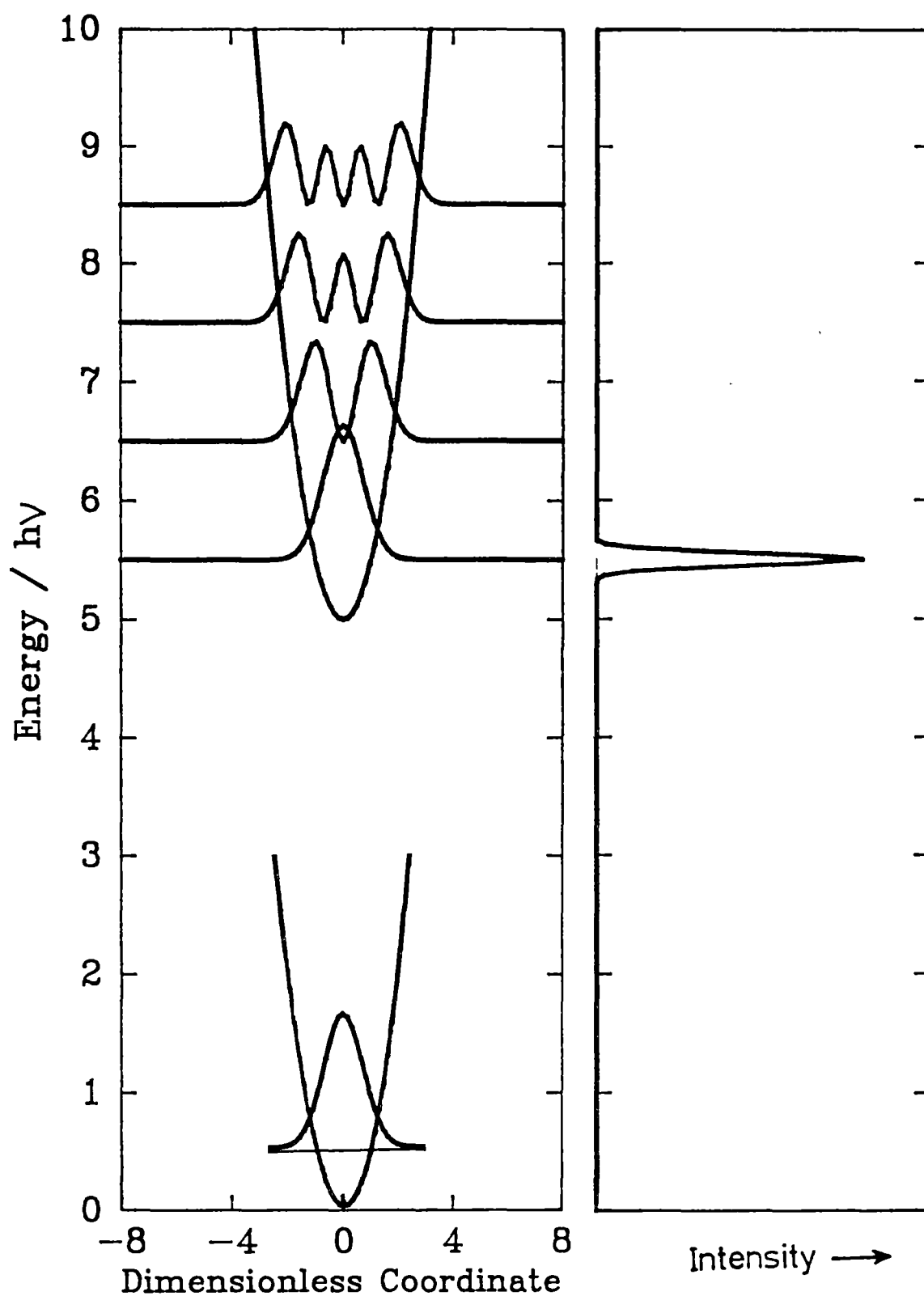
Figure 3.1 The spectrum due to transitions between the potential surfaces: $V_g(\xi) = 0.5\xi^2$; $V_e(\xi) = 5.0 + 0.5\xi^2$.
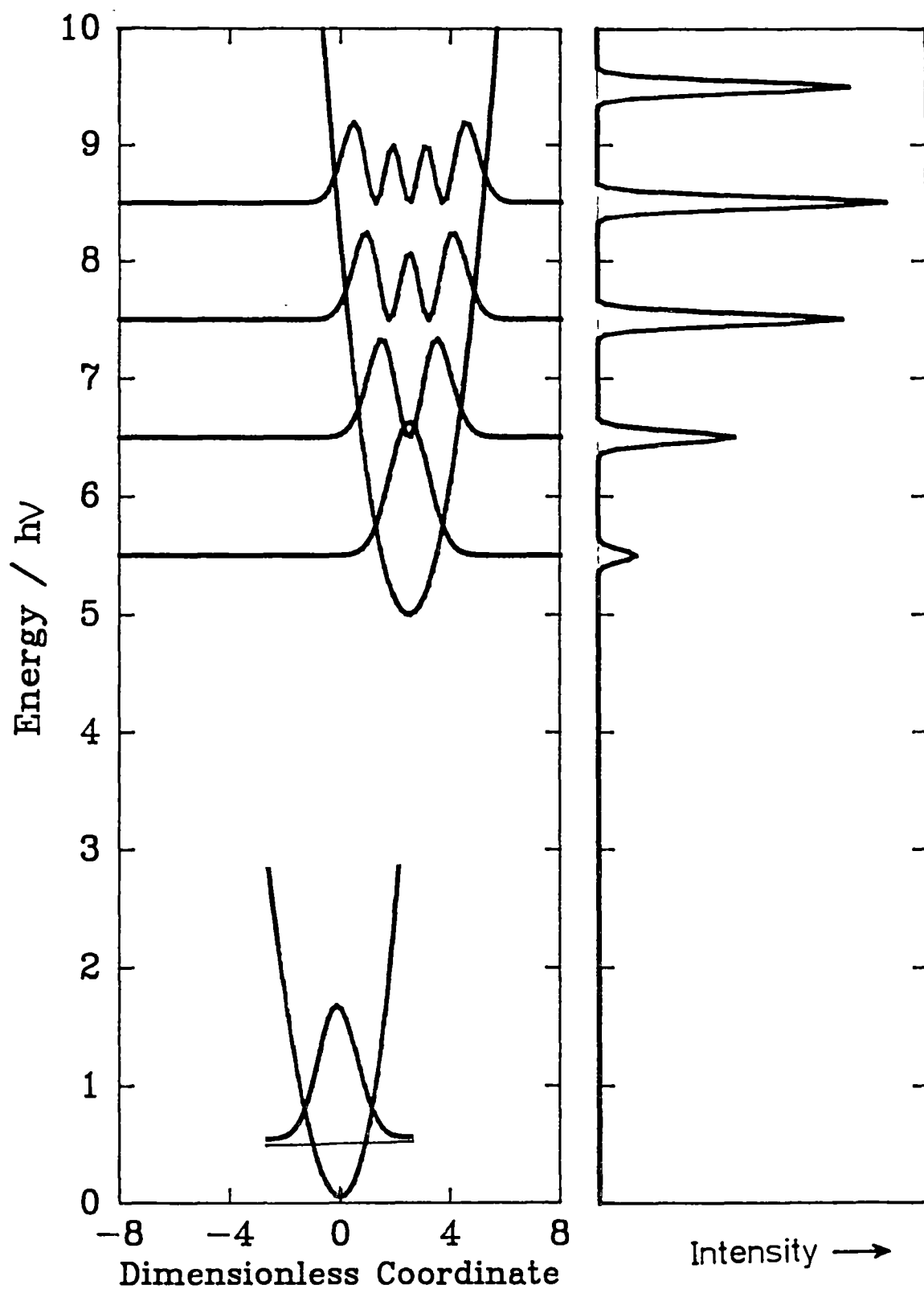
Figure 3.2 The spectrum due to transitions between the potential surfaces: $V_g(\xi) = 0.5\xi^2$; $V_e(\xi) = 5.0 + 0.5(\xi-2)^2$.
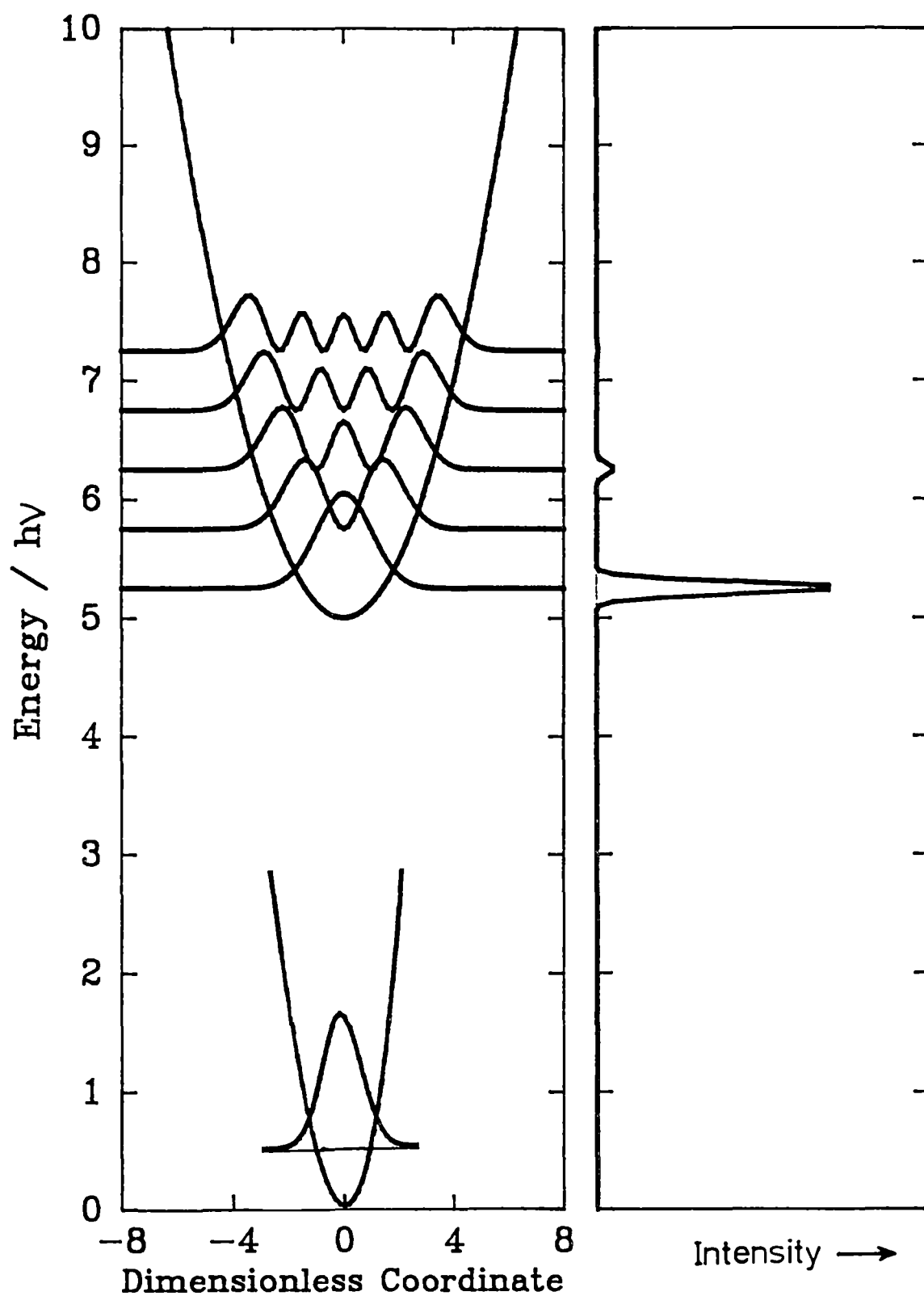
Figure 3.3 The spectrum due to transitions between the potential surfaces: $V_g(\xi) = 0.5\xi^2$; $V_e(\xi) = 5.0 + 0.125\xi^2$.
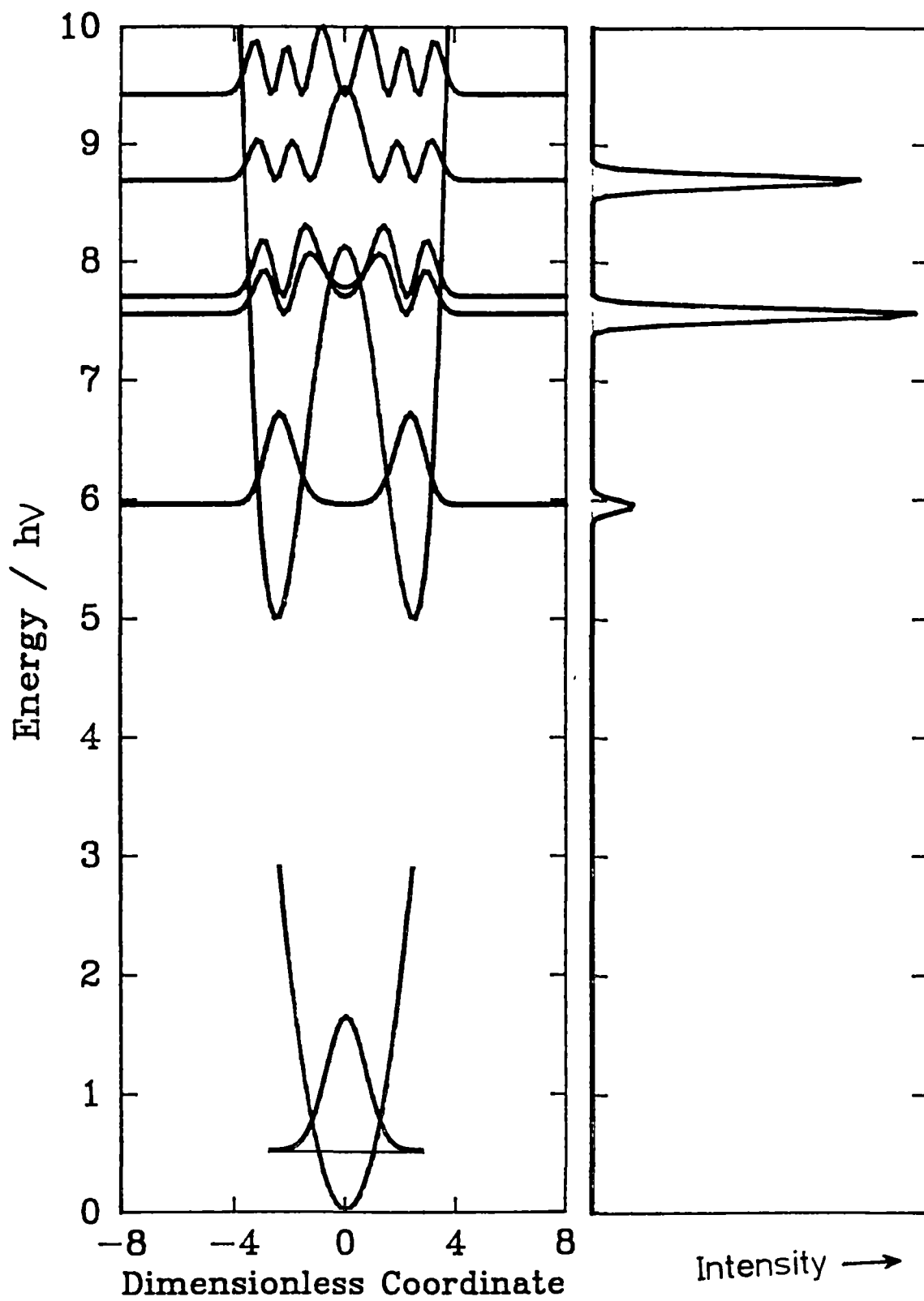
Figure 3.4 The spectrum due to transitions between the potential surfaces: $V_g(\xi) = 0.5\xi^2$; $V_e(\xi) = 8.125 - \xi^2 + 0.08\xi^4$.

figure 3.3. This is because the vibrational levels below the barrier occur in symmetric/antisymmetric pairs which are separated by a small "inversion" splitting. The energy separation of these pairs is approximately harmonic and is typical of a displaced parabola as in figure 3.2. The spectral lines with intensity in figure 3.4 are the transitions to the symmetric wavefunctions, which are the lower of the pair. Transitions from the symmetric ground state to the antisymmetric excited states are calculated to be zero, as required by group theory.

The temperature dependence of the above spectra is shown in figure 3.5. Although the overall intensity of the transitions does not vary, the intensity distribution within the different vibrational components can be temperature dependent. The mean energy of the transitions change if the ground and excited states do not have the same harmonic frequency (figures 3.5c,d); and the mean halfwidth will also change if the potentials are not identical in the ground and excited states (figures 3.5b,c,d).

3.3.2 Franck-Condon Analysis.

A Franck-Condon analysis derives the displacement of the excited state potential from the observed spectrum. This can be done by fitting the experimental intensities of the vibrational components in the Franck-Condon progression to those values calculated by varying the displacement of the potential surfaces. The displacement of the excited state potential surface with respect to the ground state can be related to the change of geometry that occurs in the molecule when it is electronicly excited. One of the first quantitative calculations of this sort was performed by Craig (1950) on the $^1A_{1g} \rightarrow {}^1B_{2u}$ absorption spectrum of benzene, where it was found that in this transition the C-C bond lengths all expand by 3.7pm.

The Franck-Condon overlap integrals necessary for such a calculation can be evaluated by the variational method to be discussed in section 3.5. However, if the potential surfaces are assumed to be harmonic (but may be both displaced and have different frequencies), then a recursion formula is available to evaluate these integrals. For transitions from the lowest vibrational level in the ground state to the nth vibrational level of the excited state, the overlaps are given by (Henderson etal 1964a):

$$(3.12)$$
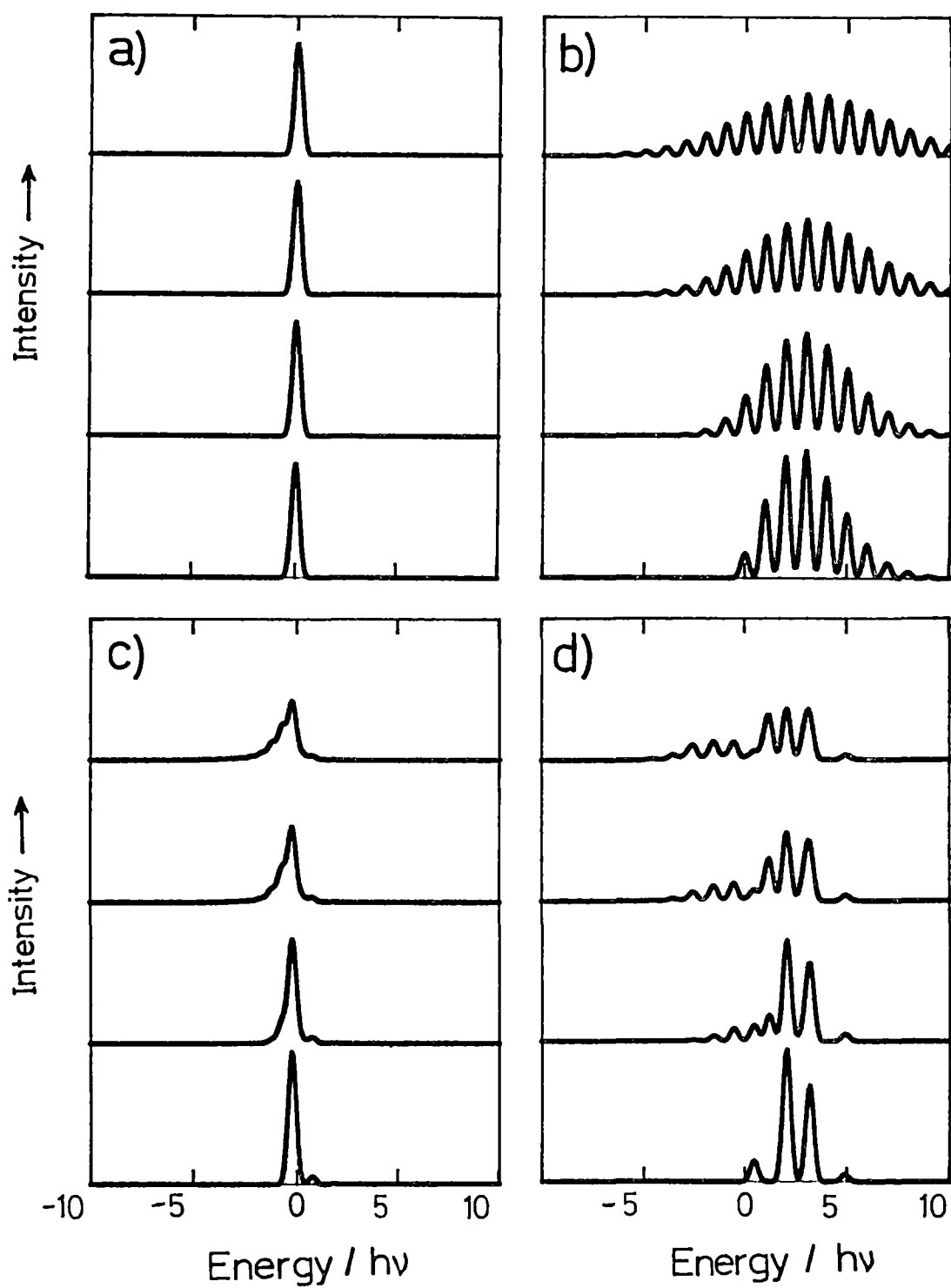
Figure 3.5 The temperature dependence of the allowed spectra with the potentials taken from figures 3.1-4 shown in a) - d) respectively. The temperatures are 0, 100, 200, 300 K from bottem to top.

$$<0|n+1> = \frac{-2\delta D<0|n> - (2n)^{1/2}(\delta^2-1)<0|n-1>}{(\delta^2+1)[2(n+1)]^{1/2}} \qquad (3.17)$$

$$\text{where } <0|0> = \left(\frac{2\delta}{(1+\delta^2)}\right)^{1/2} \exp(-0.5\rho^2),$$

$$\delta = \left(\frac{h\nu_g}{h\nu_e}\right)^{1/2}, \quad \rho = D/(1+\delta^2)^{1/2}, \quad D \equiv \Delta\xi = 1.722\times10^{-3}(M h\nu_g)^{1/2}\Delta S\,(a_{1g})$$

Here ΔS refers to the change in a symmetry coordinate (in pm), and M is the inverse of the G matrix element appropriate to this symmetry coordinate (in amu) (Moule 1977, eq32; Yersin etal 1980). This expression is defined for absorption; for emission, $h\nu_g$ and $h\nu_e$ should be interchanged in the expression for δ, and $h\nu_g$ should be replaced by $h\nu_e$ in the expression for D ($\Delta\xi$). This is because the displacement of the final state potential surface is measured from the initial equilibrium geometry. The displacement is always measured in this way because the kinetic energy in the problem is assumed to be unchanged from its value in the initial state. This is the basic premise of the Franck-Condon approximation: the potential surface changes before the (kinetic energy of the) vibrations have "realised" what has happened. An excellent discussion of this point has been given by Mulliken (1971).

This general problem of solving overlap integrals between the wavefunctions of harmonic oscillators with different frequencies centred at different equilibrium geometries was solved as early as 1930 by Hutchisson. The recursive formula of (3.17) was later derived by Ansbacher (1959). This equation has been "rediscovered" quite regularly since then (see Waldenstrom and Naqvi 1982 and 22 references within) and frequent misprints in the literature (ie Yersin etal 1980; Lever 1984, pg181) have caused some confusion. For this reason equation (3.17) has been tested very thoroughly. Table 3.1 gives sample overlaps calculated in 4 different ways, for the parameters $\delta = 1.1$, D = 1.0. These parameters can be dimensioned in the manner to be given in section 3.5. For example, in the case of the a_{1g} mode of $CuCl_4^{2-}$ with a ground state frequency of 275 cm^{-1}, they correspond to an excited state potential with a frequency of 227.2727 cm^{-1} that is displaced by 5.8815 pm.

Table 3.1 Test data D=1.0, δ=1.1

n	I	II	III	IV
0	0.7957168	0.79572	0.7957168	-0.79572
1	-0.5601108	-0.56011	-0.5601108	-0.56011
2	0.2253231	0.22532	0.2253231	-0.22532
3	-0.0481150	-0.048115	-0.0481150	0.04811
4	0.0016081	0.0016080	0.0016080	0.00161
5	-0.0045955	-0.0045955	-0.0045955	-0.00460
6	0.0011811	0.0011811	0.0011811	0.00118
7	-0.0000900	-0.0000900	-0.0000901	0.00009

The data in column I of table 3.1 was obtained from the recursive relation (3.17). The figures in column II were taken from the tables of Henderson etal (1964b, pg74). Column III was calculated from the explicit formula for the overlaps (Waldenstrom and Naqvi 1982), which in the present notation are:

$$<0|n> \; = \; <0|0> \; (2^n n!)^{-1/2} \left(\frac{\delta^2-1}{\delta^2+1}\right)^{n/2} H_n\left(\frac{D\delta}{(\delta^4-1)^{1/2}}\right) \qquad (\delta > 1) \qquad (3.18a)$$

$$<0|n> \; = \; <0|0> \; (2^n n!)^{-1/2} \left(\frac{1-\delta^2}{1+\delta^2}\right)^{n/2} i^n H_n\left(\frac{i\,D\delta}{(1-\delta^4)^{1/2}}\right) \qquad (\delta < 1) \qquad (3.18b)$$

Here $H_n(x)$ is the nth Hermite polynomial, i is $\sqrt{-1}$, and all other quantities are as previously defined. The figures in column IV are the results of a variational calculation. [Note: the sign of the overlaps are not correctly reproduced because the eigenvectors obtained from a matrix diagonalisation are unique only within a sign change. In practise this causes no problems, as only the square of the overlap is ever needed.]

A useful simplification can be achieved if it is assumed that the ground and excited state frequencies are the same. Equation (3.17) then reduces to:

$$\frac{<0|j>}{<0|0>} = \frac{D^{2n}}{2^n n!} \qquad (3.19)$$

where the quantities are as previously defined. In most cases equation (3.19) can be used instead of (3.17), as the difference in the frequencies will have only a small effect on the intensity distribution.

(3.14)

3.4 COUPLING MODES

For forbidden electronic transitions, the Condon approximation of the previous section becomes invalid and the intensity gained through vibronic coupling causes the electronic transition moment to be dependent on the nuclear geometry, and therefore temperature, of the system. The normal modes where this occurs will be called coupling modes and the form of this dependence is investigated in this section.

3.4.1 Herzberg-Teller Theory.

Vibronic coupling is usually derived in the Herzberg-Teller approach (Albrecht 1960). This treats the nuclear motion as a perturbation using the electronic wavefunctions appropriate to the equilibrium nuclear geometry (see section 1.2):

$$|\Psi_g(Q)> = |\Psi_g^0> + \sum_{s \neq g} c_{gs}(Q) |\Psi_s^0> \qquad (3.20)$$

$$|\Psi_e(Q)> = |\Psi_e^0> + \sum_{t \neq e} c_{et}(Q) |\Psi_t^0>$$

where $|\Psi_g(Q)>$, $|\Psi_e(Q)>$ refer to the ground and excited state electronic wavefunctions respectively, and $|\Psi_g^0>$, $|\Psi_e^0>$ are the solutions to the Hamiltonian H_e^0 in the crude adiabatic approximation of equation (1.19). From first order perturbation theory, the coefficients $c(Q)$ are:

$$c_{gs}(Q) = \frac{<\Psi_g^0|H'|\Psi_s^0>}{(E_s - E_g)}, \qquad c_{et}(Q) = \frac{<\Psi_e^0|H'|\Psi_t^0>}{(E_t - E_e)} \qquad (3.21)$$

the integrals being over electronic coordinates only, and

$$H' = H - H_e^0 = \sum_a \left(\frac{\partial H}{\partial Q_a}\right)_0 Q_a + \sum_{a,b} \left(\frac{\partial^2 H}{\partial Q_a \partial Q_b}\right)_0 Q_a Q_b + \ldots \qquad (3.22)$$

In general the inducing coordinate, Q, can be of any symmetry although here only non-totally symmetric modes are considered. This is because the vibronic coupling in transition metal complexes is usually most apparent in the symmetry forbidden transitions of centrosymmetric complexes. The excited ligand field states are coupled to higher electronic states of ungerade symmetry (usually charge transfer

(3.15)

states) by vibrations of ungerade (therefore non-TS) symmetry. The effects of vibronic coupling via totally symmetric vibrations has been observed by Craig and Small (1969).

In the present case then, the quadratic terms of the form Q^2 in (3.22) will be zero, as this term will only couple electronic states which have the same symmetry as the zeroth order wavefunctions $|\Psi_g^0>$ and $|\Psi_e^0>$. Cross terms of the form $Q_a Q_b$ can be non-zero if two different vibrations of the same symmetry are coupled to the same electronic state. This results in a Dushinsky rotation which will be considered in section 3.7. In what follows only the linear terms of (3.22) are kept and the transition moment is then given by:

$$M_{ge}(Q) = <\Psi_g^0|e\Sigma r|\Psi_e^0> + \sum_t c_{et}(Q)<\Psi_g^0|e\Sigma r|\Psi_t^0>$$
$$+ \sum_s c_{gs}(Q)<\Psi_s^0|e\Sigma r|\Psi_e^0> + \sum_{s,t} c_{gs}(Q)c_{et}(Q)<\Psi_s^0|e\Sigma r|\Psi_t^0> \qquad (3.23)$$

For strictly forbidden transitions the first term is zero. For the remaining terms, consideration of the energy denominator of the coefficients (3.21) shows that the second term will be the largest, and usually the following two are set to zero. However, as pointed out by Orlandi and Siebrand (1973), the size of the coefficients $c_{gs}(Q)$ depends on the matrix element as well as the energy difference. Vibronic calculations by Ziegler and Albrecht (1974) on benzene show that vibronic coupling in the ground state gives small but significant contributions to the transition moment. This may even be more important for a metal complex such as $CuCl_4^{2-}$ where $(E_t - E_e) \sim 15,000 \text{ cm}^{-1}$ and $(E_s - E_g) \sim 30,000 \text{ cm}^{-1}$; whereas for benzene $(E_t - E_e) \sim 10,000 \text{ cm}^{-1}$ and $(E_s - E_g) \sim 50,000 \text{ cm}^{-1}$. If a particular transition is vibronically allowed by a single vibration (from group theory arguments) along a particular coordinate Q_k, then (3.23) becomes:

$$M_{ge}(Q_k) = C_1 Q_k + C_2 Q_k^2 \qquad (3.24)$$

where $C_1 = \sum_{t \neq e} \dfrac{<\Psi_e^0|(\frac{\partial H}{\partial Q})_0|\Psi_t^0>}{(E_t - E_e)} <\Psi_g^0|e\Sigma r|\Psi_t^0> + \sum_{s \neq g} \dfrac{<\Psi_g^0|(\frac{\partial H}{\partial Q})_0|\Psi_s^0>}{(E_s - E_g)} <\Psi_s^0|e\Sigma r|\Psi_e^0>$

and $C_2 = \sum_{t \neq e} \dfrac{<\Psi_e^0|(\frac{\partial H}{\partial Q})_0|\Psi_t^0>}{(E_t - E_e)} \sum_{s \neq g} \dfrac{<\Psi_g^0|(\frac{\partial H}{\partial Q})_0|\Psi_s^0>}{(E_s - E_g)} <\Psi_s^0|e\Sigma r|\Psi_t^0>$

Here the normal coordinate Q_k has been taken out of the integral over electronic coordinates in (3.22). If mixing into the ground state is ignored, then C_2 and the second term of C_1 are zero and the usual case of a linear dependence of the transition moment on Q is recovered.

The vibronic calculation of Ziegler and Albrecht (1974) on benzene has shown that a linear dependence of (3.24) holds fairly well for at least two root-mean-squared displacements of the inducing coordinate. It is usual in the study of centrosymmetric transition metal complexes to set the quadratic term in (3.24) to zero as the coefficient "steals" intensity from a charge transfer to charge transfer type transition which is also parity forbidden like the d-d transitions. However, as will be discussed in appendix 9.A3, semi-empirical intensity calculations suggest that such a contribution can be important for low frequency, large amplitude coupling vibrations. In this case the molecule can be viewed as having a static distortion at the RMS amplitude of this coordinate.

Finally it is noted that the whole Herzberg-Teller approach has been recently criticized since it neglects coupling by nuclear momenta due to the breakdown of the adiabatic approximation (Orlandi and Siebrand 1972, 1973, Orlandi 1973). Since the relative contribution of this effect is roughly of the order $h\nu/(E_t - E_e)$, the Herzberg-Teller theory described here is for weakly coupled electronic states that are well separated in energy. For degenerate or near degenerate electronic states the kinetic energy operator must be included on a par with the potential energy terms in a variational calculation on a vibronic basis. This approach will be described in chapter 4.

3.4.2 Vibronic Selection Rules.

Vibronic selection rules are important in centrosymmetric transition metal complexes where the spectrum is electric dipole forbidden, as all the intensity comes from the "false" or vibronic origins of the coupling modes. These selection rules can be obtained from the integrals in the coefficients of equation (3.24). If only the vibronic coupling in the excited state is considered, then the conditions for these coefficients to be non-zero are found by using (3.9):

$$(3.17)$$

$$\Gamma_e \times \Gamma_Q \times \Gamma_t \supset A_{1g} \qquad (3.25)$$

$$\Gamma_g \times \Gamma_r \times \Gamma_t \supset A_{1g} \qquad (3.26)$$

where Γ_g, Γ_e, Γ_t, Γ_Q, Γ_r are the irreducible representations of respectively the ground, excited and "lending" electronic states, the coupling mode and the electronic vector of the incident light. Equation (3.25) represents the coupling of the excited state to a "lending" state and (3.26) determines whether this lending state is itself allowed in r polarisation. As implied by (3.26) the vibronic origin then takes on the polarisation properties of the lending state.

If the symmetry of these intermediate lending states is not of interest, then (3.25) and (3.26) can be combined to give:

$$\Gamma_g \times \Gamma_e \times \Gamma_Q \times \Gamma_r \supset A_{1g} \qquad (3.27)$$

It should be borne in mind when using (3.27) as a vibronic selection rule, that it is a necessary but not sufficient condition for vibronic intensity to occur. In particular it assumes that the intermediate states Ψ_t of the appropriate symmetry exist, and that the integrals as expressed in (3.25) and (3.26), while group theoretically non-zero, are of non-vanishing magnitude. It can also be noted that ground state vibronic coupling will give exactly the same overall selection rule (3.27). However the intermediate states Ψ_s may be different to those found to mix with the excited state; in equations (3.25), (3.26) Γ_s would replace Γ_t and Γ_g and Γ_e would be exchanged.

3.4.3 Vibrational Fine Structure and Temperature Dependence.

For coupling modes, the electronic transition moment cannot be factored out of the integration over nuclear coordinates as in the Condon approximation (3.14). The part that is a function of Q must remain inside the integral over the vibrational wavefunctions. The intensity of such a forbidden electronic transition, where only the linear terms in (3.24) are kept, is given by:

$$I_j^i \propto |\langle i | M_{ge}(Q) | j \rangle|^2 \qquad (3.28)$$
$$\propto c_1^2 \cdot |\langle i | Q | j \rangle|^2$$

Here, instead of the square of a Franck-Condon overlap as in (3.14), the intensity is proportional to the square of $\langle i|Q|j\rangle$ which will be called the _inducing overlap_. There are other approaches such as the r-centroid method of Noda and Zare (1982) where the Franck-Condon overlap can be kept for a forbidden (or non-Condon) transition, but this will not be introduced to avoid the confusion of additional terminologies.

If Q is a non-totally symmetric coordinate then, since $\langle i|Q|j\rangle$ must transform as totally symmetric to be non-zero, the irreducible representation of $\langle i|j\rangle = [\Gamma_Q]^{i+j}$ must transform as Γ_Q. Using the same arguments as in section 3.3.2, this condition is fulfilled when the difference (or sum) of the vibrational quantum numbers ($\Delta n = j-i$) in the transition is odd. The selection rules for individual vibronic transitions is then as given by Herzberg (1966, pg176):

$$\langle i|Q|j\rangle \neq 0 \text{ if } \Delta n = \pm 1, \pm 3, \pm 5, \ . \ . \quad (Q: \text{non-TS}) \qquad (3.29)$$

As shown in the previous section, the non-totally symmetric potentials are required to be undisplaced, and for harmonic type potentials this results in a very short vibrational progression. The most prominent by far will be the $\Delta n = \pm 1$ transitions. This becomes exact if the ground and excited state potentials are harmonic with the same frequency, as is easily seen by considering the non-zero harmonic oscillator matrix elements of $\langle i|Q|j\rangle$ in table 2.A1.

In the unusual situation where a totally symmetric mode is inducing intensity , the condition $[\Gamma_Q]^{i+j} = \Gamma_Q$ is always met. The selection rules for individual vibronic transitions is then:

$$\langle i|Q|j\rangle \neq \text{zero if } \Delta n = 0, \pm 1, \pm 2, \ . \ . \quad (Q: \text{TS}) \qquad (3.30)$$

As noted by Roche and Jaffe (1976, pg177) a totally symmetric mode can only induce intensity when the transition is already partly allowed. The reasoning is as follows. If the transition is symmetry forbidden then the intensity of the transition is zero at the equilibrium geometry ($M_{ge}(0) = 0$). Since a totally symmetric mode does not change the symmetry of a molecule, it follows that $M_{ge}(Q)$ will be zero for any value of Q.

(3.19)

It is therefore impossible for totally symmetric vibrations to contribute intensity in the symmetry forbidden transitions of centrosymmetric metal complexes. This also follows from the vibronic selection rule in (3.27). The electronic "d" states are made of molecular orbitals that are even functions, so Γ_g, Γ_e are gerade. The symmetry of the electric field vector will always be ungerade because it is odd with respect to the inversion symmetry element. This means that the symmetry of the coupling vibration, Γ_Q, must also be ungerade to fulfill the conditions in (3.27) and so Γ_Q cannot be totally symmetric.

Figure 3.6 illustrates the temperature dependent spectra calculated for transitions between the same potentials as that given in figures 3.1 to 3.4. The only difference between this and figure 3.5 is that Q is now considered a coupling coordinate. It is assumed that the electronic transition is forbidden at the equilibrium nuclear geometry and the electronic transition moment depends linearly on Q. The intensity of each vibronic transition is given by (3.28) rather than (3.14).

These spectra can be directly compared to those in figure 3.5, the main difference between these allowed and forbidden spectra being the large increase in the intensity with temperature in the latter case. This is because the electronic moment depends on the nuclear coordinates, making the intensity dependent on the population of the ground state vibrational levels (see section 3.6). In addition, the most intense vibronic transition in the spectra of figure 3.6 is not the vertical transition as in figure 3.5, since this is at the geometry where the transition is forbidden. Instead, the most intense vibronic lines occur in the wings of the spectrum, and a "hole" in the spectrum appears at this vertical transition. When this vertical transition is missing, it is often called a "non-Condon" effect (Herzberg 1966, pp172-3; Hennecker etal 1979).

It should be noted that the spectra shown in figure 3.6 would not be observed in practice, as each of the vibronic lines in these spectra would act as vibronic origins for a totally symmetric progression of the molecule. In addition, the hypothetical spectrum shown in figure 3.6b could not possibly occur, as this spectrum is due to a totally symmetric coordinate which cannot be rigorously forbidden at the equilibrium nuclear geometry, for the reasons given above.

(3.20)
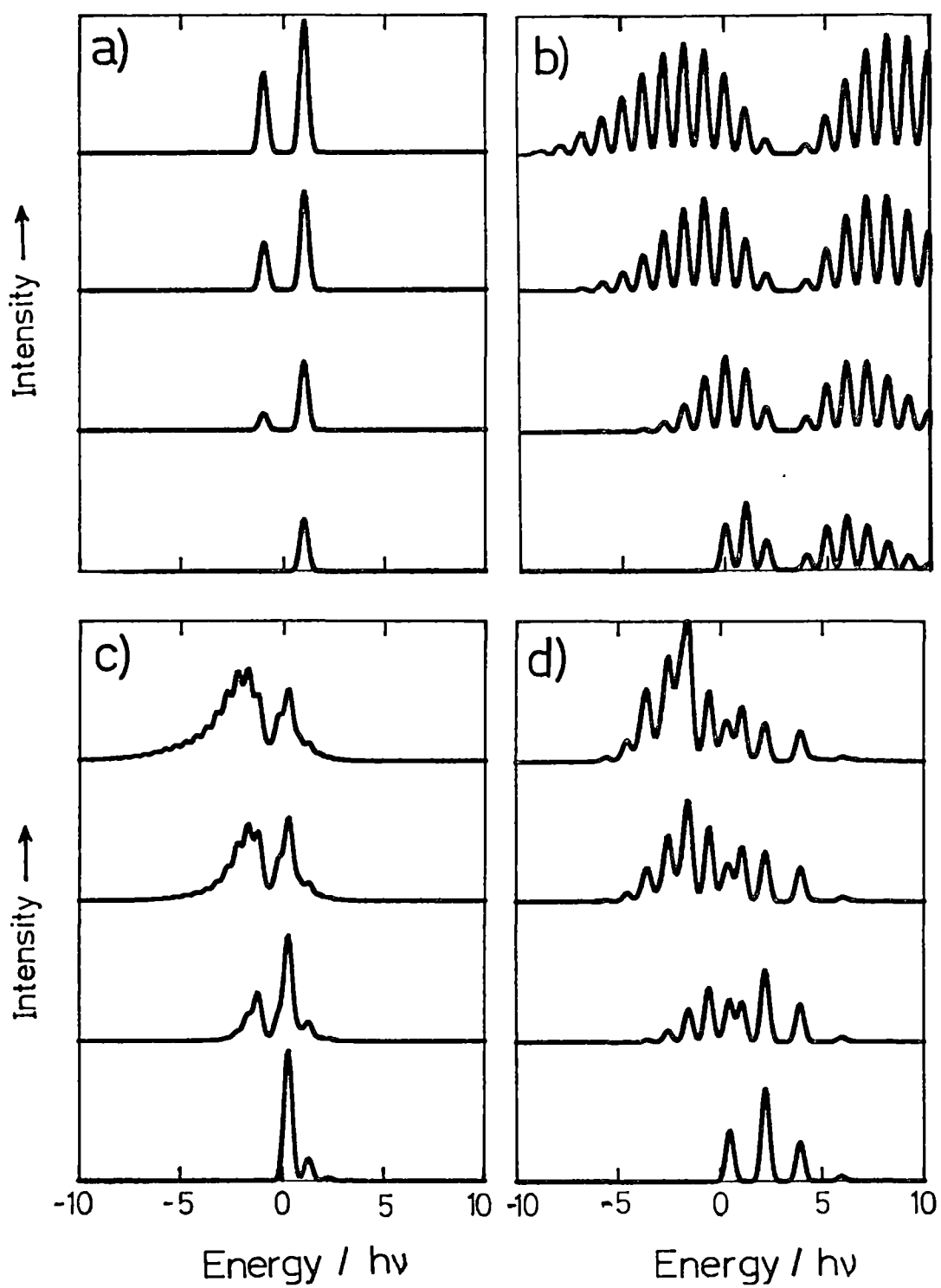
Figure 3.6 The temperature dependence of the vibronically induced spectra with the potentials taken from figures 3.1-4 shown in a) - d) respectively. The temperatures are 0, 100, 200, 300 K from bottem to top.

3.5 NUMERICAL SIMULATION OF THE TOTAL SPECTRUM

> "Well," said Owl, "the customary procedure
> in such cases is as follows."
> "What does Crustimoney Proseedcake mean?"
> said Pooh. "For I am a Bear of Very Little
> Brain, and long words Bother me."   -A.A.Milne

To find the position and intensity of vibronic transitions be-
tween two adiabatic potential surfaces, the energy and wavefunctions
of the vibrational levels within each potential must be calculated.
This is most easily done within a variational calculation (section
2.1.2), and this approach has been described in detail by Lohr (1970).
The Hamiltonian of the one dimensional adiabatic potential surfaces
considered in this thesis can be expressed in the general form:

$$H(\xi) = -\frac{1}{2}\frac{\partial^2}{\partial\xi^2} + \sum_{p=0}^{6} a_p\xi^p + A\exp(-B\xi^2) \qquad (3.31)$$

ξ is a dimensionless coordinate which can be related to the
symmetry or normal coordinates by equation (2.35). The vibrational
Hamiltonian in (3.31) is in units of the harmonic frequency of the
basis functions. When it can be expressed in terms of the symmetry coor-
dinates, the Hamiltonian in (3.31) becomes (see equation 2.35 for the
definition of x):

$$H(S) = -\frac{1}{2}\frac{h\nu}{x^2}\frac{\partial^2}{\partial S^2} + \sum_{p=0}^{6} h\nu\, x^p a_p S^p + h\nu\, A\exp(-h\nu x^2 B S^2) \qquad (3.32)$$

However, in all variational calculations in this thesis, the
dimensionless form of (3.31) is used. This is the customary procedure
in the literature and is more straightforward than to especially
dimension the Hamiltonian of each normal coordinate before the cal-
culation. Any dimensioned quantity that is desired (ie root-mean-
square geometry, excited state displacement) can be found by using
equation (2.35) after the calculation.

To find the energy levels and wavefunctions of the vibrational
levels in the ground and excited states, the wavefunctions of both

states are expanded as a linear combination of <u>the same</u> N harmonic oscillator basis functions:

$$|i> = \sum_{n=0}^{N} c_{ni}\phi_n \qquad\qquad |j> = \sum_{n=0}^{N} c_{nj}\phi_n \qquad\qquad (3.33)$$

The matrix elements of the kinetic and potential energy operators of (3.31) can be evaluated by the formulae given in appendix 2.A1 in a harmonic basis that is centred at the ground state equilibrium nuclear geometry. As discussed in section 3.3.2, this is done because it is absorption spectra that are of interest and the kinetic energy operator retains the ground state value in the excited state. For an emission spectrum the wavefunctions would be expanded in terms of SHO basis functions centred at the excited state equilibrium geometry.

The secular equations are diagonalised by standard techniques (Smith etal 1976) resulting in N energy levels in (non-integral) units of hv, and N columns of the coefficients c_n of (3.33) in the eigenvector matrix. The basis size should in principle be infinite but is truncated to N and, as previously discussed in section 2.2, care must be taken that N is large enough to properly converge all the wavefunctions that are of interest. The calculation is performed separately for both ground and excited states and, since their wavefunctions were expanded in the same basis, the overlaps necessary for the calculation of the intensities are given by:

$$<i|j> = \sum_{n=0}^{N} C_{ni}C_{nj} \qquad\qquad (3.34)$$

$$<i|\xi|j> = \sum_{n=1}^{N} (n/2)^{1/2} [C_{ni}C_{n-1j} + C_{n-1i}C_{nj}] \qquad\qquad (3.35)$$

$$<i|\xi^2|j> = \sum_{n=2}^{N} \frac{1}{2}(n(n-1))^{1/2} [C_{ni}C_{n-2j} + C_{n-2i}C_{nj}]$$
$$+ \sum_{n=0}^{N} (n+\frac{1}{2}) C_{ni}C_{nj} \qquad\qquad (3.36)$$

A similar calculation can be performed for all normal modes, and then the spectrum is convoluted. As described previously, this involves calculating a huge number of transitions as each vibronic line between potentials of one normal coordinate serves as an origin for

all other normal coordinates. In practice the ground and excited state potentials of most normal coordinates are similar and their spectra will consist of a single line as shown in figure 3.1. Therefore, usually the spectra due to only one or two normal modes need be considered in simulating the complete spectrum.

The intensity of a single vibronic transition for a particular dimensionless coordinate ξ_n is given by:

$$I_{j_n}^{i_n} = (E_o + E(j_n) - E(i_n)) \; P_i^n(T) \; |<i_n|M^n(\xi)|j_n>|^2 \qquad (3.37)$$

The convoluted spectra due to all n (=3N-6) normal modes for a single vibronic transition is then given by:

$$I_{j_1 j_2 \cdots j_n}^{i_1 i_2 \cdots i_n} = \Delta E \; \prod_n P_i^n(T) \; |<i_n|M^n(\xi)|j_n>|^2 \qquad (3.38)$$

The energy factor ΔE is the energy of the transition:

$$\Delta E = E_o + \sum_n (E(j_n) - E(i_n)) \qquad (3.39)$$

and E_o is the pure electronic transition energy. Equations (3.37) and (3.39) are defined for absorption; the energy factor must be raised to the fourth power for emission (Yersin et al 1980). The temperature factor, which gives the fractional Boltzmann population of the ground state level $|i_n>$ of energy $E(i_n)$, is:

$$P_i^n(T) = \exp(-E(i_n)/kT) \; / \; \sum_i \exp(-E(i_n)/kT) \qquad (3.40)$$

It is defined such that $\sum_i P_i^n(T) = 1.0$ for all n and T. The electronic transition moment in (3.38) is expressed in terms of dimensionless coordinates and the total transition moment can be found by using equations (3.34)-(3.36).

There is no need to convert the electronic transition moment back to dimensioned form of (3.24) as only the relative, not absolute, intensities are of interest. It is customary to normalise the total spectrum at zero Kelvin to unity (Lohr 1970). It then suffices to know the ratio of allowed to forbidden character, or the the ratio of first

(3.23)

to second order dependence of the transition moment rather than the absolute value of the coefficients in (3.24).

Having the energy and intensity of all vibronic transitions in the spectrum, it is now possible to construct the total spectrum in the form of a stick diagram. However, in a real spectrum the vibronic lines have finite width which can be simulated by giving each transition a Gaussian lineshape. The source of these finite linewidths need not concern us here. A Gaussian can be fully characterised by an intensity, I, position, P, and halfwidth, HWHH, of the vibronic line. These three parameters correspond to the integrated area, the peak, and the half width at half height of the Gaussian. Whenever a halfwidth is referred to in this thesis, it refers to this half width at half height. The Gaussian line shape as a function of the energy E in terms of the above parameters is given by (A&S equation 26.2.9):

$$G(E) = \frac{I}{HWHH} \left(\frac{\ln 2}{\pi}\right)^{1/2} \exp\left[-\left(\frac{E-P}{HWHH}\right)^2 \ln 2 \right] \qquad (3.41)$$

The lineshape in (3.41) is calculated for all transitions in the convoluted spectrum and summed to give the total spectra shown in figures 3.1-6. It is interesting to notice that, while it is assumed that the halfwidth of the individual transitions are temperature independent (this is certainly an oversimplification), the resolution of the spectra decreases with increasing temperature, as is observed experimentally. This is caused by the congestion of the enormous number of spectral lines present at higher temperatures.

(3.24)

3.6 MOMENTS ANALYSIS

The simulation of vibronic spectra outlined in the previous section is a straightforward task for a computer. These calculated spectra can then be fitted to the experimental spectrum by varying the adiabatic potential surfaces. If a unique set of potential surfaces are found, then this allows one to draw conclusions about the geometry, bonding and electronic properties of the particular electronic states involved.

However, while thousands of vibronic transitions may be calculated to high accuracy, often the experimental spectrum may be quite featureless. In this case, the structure of the calculated spectrum can be either deliberately "washed out" by adding a large halfwidth to each vibronic transition, or else a moments analysis can be done. The zero, first, second,... moments of a spectrum can be related to the bulk spectral properties of intensity, mean energy, mean halfwidth,... respectively.

This is very useful because, as noted by O'Brien (1981, pg 332), "Given a complicated spectrum in which many modes of vibration are involved, it is always difficult and frequently impossible to make an unambiguous fit to a set of phonon frequencies and coupling strengths, but it is often possible to extract the first few moments of the spectrum from the experimental data, and they can then be used as a set of parameters to which any theoretical fit must conform." A moments analysis is then a useful bridge between theory and experiment in much the same manner as the spin Hamiltonian used in the study of ESR spectroscopy.

3.6.1 The Intensity, Mean Energy and Mean Halfwidth.

If $f(E)$ is a function describing a lineshape such as a spectrum, then the mth moment is defined as (A&S, pg 928):

$$\mu_m = \int E^m f(E) \, dE \qquad (3.42)$$

The intensity I, mean energy $\bar{E}$, and the variance σ^2, are related to the moments in the following manner (Kubo and Toyozawa 1955; Markham 1959; Prassides and Day 1984):

$$I = \mu_0 \qquad (3.43)$$

$$\bar{E} = \mu_1 / \mu_0 \qquad (3.44)$$

$$\sigma^2 = \mu_2 / \mu_0 - \bar{E}^2 \qquad (3.45)$$

For a Gaussian distribution, the halfwidth (HWHH) is related to the variance by:

$$\bar{H} = (2\ln 2)^{1/2} \sigma \qquad (3.46)$$

Higher order properties such as the skewness, kurtosis, etc of a spectrum can be related to the higher moments (Lohr 1970).

The moments of a continuous experimental spectrum can be extracted by numerical integration, but for a discontinuous distribution, such as is calculated theoretically, the moments are given by:

$$\mu_m = \sum_i f_i(E) \cdot (E_i)^m \qquad (3.47)$$

Equation (3.47) can then be used to determine the properties in (3.43)-(3.46) from a calculated spectrum represented by equations (3.38) and (3.39). The summation in (3.47) will be over all vibronic transitions and therefore is over all quantum numbers of all normal coordinates.

If k of the m normal coordinates are responsible for inducing intensity and the electronic transition moment is separated into allowed and forbidden parts, then the expression for the total intensity becomes:

$$I_{TOT}(T) \propto M(0) \prod_n \sum_{i_n} P_i^n(T) \sum_{j_n} |<i_n|j_n>|^2$$

$$+ \sum_k \sum_{i_k} P_i^k(T) \sum_{j_k} |<i_k|M^k(\xi_k)|j_k>|^2 \cdot \prod_{n \neq k} \sum_{i_n} P_i^n(T) \sum_{j_n} |<i_n|j_n>|^2$$

$$\propto M(0) \prod_n I_n(T) + \sum_k I_k(T) \cdot \prod_{n \neq k} I_n(T)$$

$$\propto A + \sum_k I_k(T) \qquad (3.48)$$

Here A is the temperature independent part of the intensity due to the allowed component of the spectrum. $I_n(T)$ and $I_k(T)$ correspond to the contribution from the non-coupling and coupling modes respectively:

(3.26)

$$I_n^-(T) = \sum_{i_n} P_i^n(T) \sum_{j_n} |<i_n|j_n>|^2 \qquad (3.49)$$

$$I_k(T) = \sum_{i_k} P_i^k(T) \sum_{j_k} |<i_k|M^k(\xi_k)|j_k>|^2 \qquad (3.50)$$

The intensity due to the non-inducing modes, $I_n(T)$, contributes nothing to the temperature dependence of the intensity as, by the orthonormal properties of the wavefunctions, equation (3.49) will be summed to 1.0. However, it is very important to include these terms in the expressions for the mean energy and halfwidth below. The expression for the total intensity given in (3.48) is normalised to 1.0 at zero Kelvin:

$$A + \sum_k I_k(T=0) = 1.0 \qquad (3.51)$$

The mean energy (which will also be the maximum of the spectrum if the total spectrum is symmetric, such as a Gaussian) is given by (Markham 1959):

$$\bar{E}(T) = \bar{E}_1 + \bar{E}_2 + \bar{E}_3 + \ldots \qquad (3.52)$$

where $\bar{E}_m = \dfrac{I_m(T) \, \Delta E}{I_m(T)}$ and $\Delta E = E(j_m) - E(i_m)$ is the energy difference between the states $|j_m>$ and $|i_m>$. The analogous relationship for the halfwidth (HWHH) is:

$$H(T) = H_1 + H_2 + H_3 + \ldots \qquad (3.53)$$

$$\text{where } H_m = \left[2\ln2 \, \frac{I_m(T) \, (\Delta E - \bar{E}_m)^2}{I_m(T)} \right]^{1/2}$$

$\bar{E}_m$ is given by (3.52) above and the $I_m(T)$ terms are given by either (3.50) if the mode is "active" (m=k), or (3.49) if it is not (m=n). However, it is should be pointed out that in general the spectra due to the inducing modes will be non-Gaussian. The expression for the halfwidth in (3.53) is only valid for Gaussian distributions, and the contribution due to the inducing modes will usually be overestimated.

It is very important to realise that the terms subscripted i,j in (3.52) and (3.53) are to be included in the summation over i and j in

equations (3.49) or (3.50). It can be seen that the denominators of these equations will be equal to unity if the mode is "inactive" ($m \neq k$).

While (3.48) only gives the _relative_ intensity, equations (3.52) and (3.53) give the _absolute_ mean energy and halfwidth respectively. The problem remains to evaluate the overlaps in (3.49),(3.50). This can be done either by the variational methods of section 3.5 using equations (3.34)-(3.36), or by analytic formulae that are valid if the adiabatic potentials are restricted to certain forms.

3.6.2 Some Analytic Formulae.

Analytic formulae for the temperature dependence of the intensity, band shift and halfwidth of symmetry forbidden transitions are given in this section. The details of their derivation are given in appendix 3.A2. The normal modes in this section are subscripted "k" if they are coupling modes, or "n" if they are non-coupling modes.

I. _Intensity_: The temperature dependence of the intensity of an electronically forbidden spectrum is determined solely by the form of the ground state potentials of the inducing modes. Proof of this statement is given in appendix 3.A1. If the electronic transition moment in (3.48) depends only linearly on the k "active" normal modes, then the intensity is given by (Kubo and Toyozawa, 1955):

$$I(T) = \sum_k I_k(0) \coth(X_k), \quad \text{where } X_k = (h\nu_k/2kT) \qquad (3.54)$$

The total intensity of the spectrum in (3.54) is the sum of the contributions of the individual inducing modes. If the electronic transition moment in (3.48) contains quadratic terms then the intensity is given by (Fussgaenger etal 1965):

$$I(T) = \sum_k I_{1k}(0) \coth(X_k) + I_{2k}(0) \coth^2(X_k) \qquad (3.55)$$

where I_{1k}, I_{2k} are determined by the relative size of the coefficients in (3.24). The conditions for the appearance of these quadratic terms were discussed in section 3.4.1. In the remaining equations given in this section, a linear dependence of the electronic transition moment on Q is assumed. Equations (3.54) and (3.55) have been derived assuming a harmonic ground state for the inducing modes. As shown in

(3.28)

appendix 3.A1 the excited state potentials, as well as the ground and excited state potentials of the non-coupling modes (Lohr 1969), may take any form.

II. <u>Band-shift</u>: The shift of the band maximum from that expected for a pure vertical electronic transition is given by:

$$E(T) = \sum_{k} h\nu_{k} \tanh(X_{k}) + \frac{1}{4} \sum_{n} h\nu_{n}(\delta_{n}-1)\coth(X_{n}) \qquad (3.56)$$

where $\delta_{n} = \left(\dfrac{h\nu'_{n}}{h\nu_{n}}\right)^{2}$, $h\nu'_{n}$ being the excited state frequency.

Equation (3.56) is derived assuming that the potentials of all modes in both the ground and excited states are harmonic. In addition, the excited state potential of the k inducing modes must be undisplaced and have the same frequency as the ground state. The n non-inducing modes may have their excited state potential displaced or with a different frequency.

III. <u>Halfwidth</u>: The variation in halfwidth is given by:

$$H(T) = \sum_{k} h\nu_{k}(2\ln2)^{1/2}\text{sech}(X_{k})$$

$$+ \sum_{n} h\nu_{n}\left[2\ln2[S\delta_{n}\coth(X_{n}) + \frac{1}{8}(\delta_{n}-1)^{2}\coth^{2}(X_{n})] \right]^{1/2} \qquad (3.57)$$

where $S = \frac{1}{2}D^{2}\delta_{n}$ is called the Huang-Rys factor, D the displacement of the surfaces, and all other definitions are as before. The Huang-Rys factor given here is dimensionless and conforms with the definition given by Markham (1959; eq 10.23). It represents the energy difference between the excited state potential minima and the vertical transition energy in units of the ground state frequency, and is therefore analogous to the Jahn-Teller stabilization energy (E_{JT}). Equation (3.57) is only valid under the same conditions as given for (3.56).

The first term in equations (3.56) and (3.57), which are due to the inducing modes, have not previously appeared in the literature.

(3.29)

Their derivation is given in appendix 3.A2. Some general comments can now be made concerning the above expressions:

i)   No use of symmetry has been made and in general, the inducing modes may be of any symmetry. However, the usual case is that the inducing mode is non totally symmetric, and is then <u>required</u> by group theory to be undisplaced (see section 3.2.3). The approximations made in the derivation of (3.56) and (3.57) are then fully justified.

ii)   The intensity in equations (3.54) and (3.55) is due entirely to the inducing modes.

iii) The shift in the mean energy that is due to the k inducing modes, goes from $h\nu_k$(0K) to 0 (∞K); ie at low temperature only the 0$\rightarrow$1 transition will be observed, while at high temperature a nearly equal number of n$\rightarrow$n+1 and n$\rightarrow$n-1 transitions will occur, which will average to a mean of zero. A maximum band shift of less than $h\nu_k$ is therefore expected as a result of an inducing mode.

iv)   The shift in the mean energy due to the non-inducing modes will only appear if the frequencies are different in the ground and excited states.

v)   The halfwidth due to the inducing modes will grow from 0 (at 0K) to $(2\ln2)^{1/2}h\nu_k$ (at ∞K). The non-inducing modes will give a finite bandwidth at 0K, the most important factor being the displacement of the surfaces D.

The equations (3.54)-(3.57) are only valid within the harmonic approximations that were made, so anharmonicity will dramatically change the temperature dependence. Dreybrodt and Fussgaenger (1965) have derived an expression for the temperature dependence of the intensity for a vibration with quartic anharmonicity using perturbation theory. However, this is very cumbersome and is valid only over a limited range. A more profitable approach can be pursued with the variational method previously described. This allows one to not only extract the properties of non-harmonic potentials, but also provides a check on the above formulae.

3.6.3 Some Applications.

The simulated allowed spectra shown in figure 3.5 were subjected to a moments analysis, and the variation of the intensity, mean energy and mean halfwidth with temperature are shown in figure 3.7. This figure shows how the various properties of the spectra can be represented in a very straightforward manner. Briefly, it can be seen that the intensity is constant for all four cases, the mean energy becomes red-shifted and the halfwidth increases with temperature.

The moments analysis of the inducing spectra in figure 3.6, which have been calculated using the same potentials as in the allowed case, are shown in figure 3.8. The increase in the intensity with temperature is identical for all four cases as they all have the same harmonic ground state potential and this intensity follows the "coth rule" of equation (3.54). The deviations from the "coth rule" that occur if there is anharmonicity in the ground state potential of the coupling mode or a non-linear dependence of the transition moment, is investigated in chapter 9.

In all four cases the mean energy of the spectrum becomes red shifted with increasing temperature. In both the allowed and forbidden cases the effect is only slight for harmonic potentials of the same frequency (cases 1,2), is larger for an excited state with a reduced frequency (case 3), but is most pronounced for the double well excited state potential (case 4). It has been shown by Lohr (1970) that if the frequency of the coupling modes in the excited state are larger than in the ground state, the spectrum can become blue shifted with increasing temperature.

The increase in the halfwidth with temperature shows similar trends, although the largest temperature dependence comes from the displaced potential (case 2). For reasons already given, the halfwidth variation of the non-harmonic modes are misleading as they do not correspond to the true halfwidth; however, the general trend remains qualitatively valid.

Different potential surfaces with various types of anharmonicity or displacements could give endless variations on the above examples, but space does not permit their inclusion here. Further examples are considered in chapter 9.

(3.31)
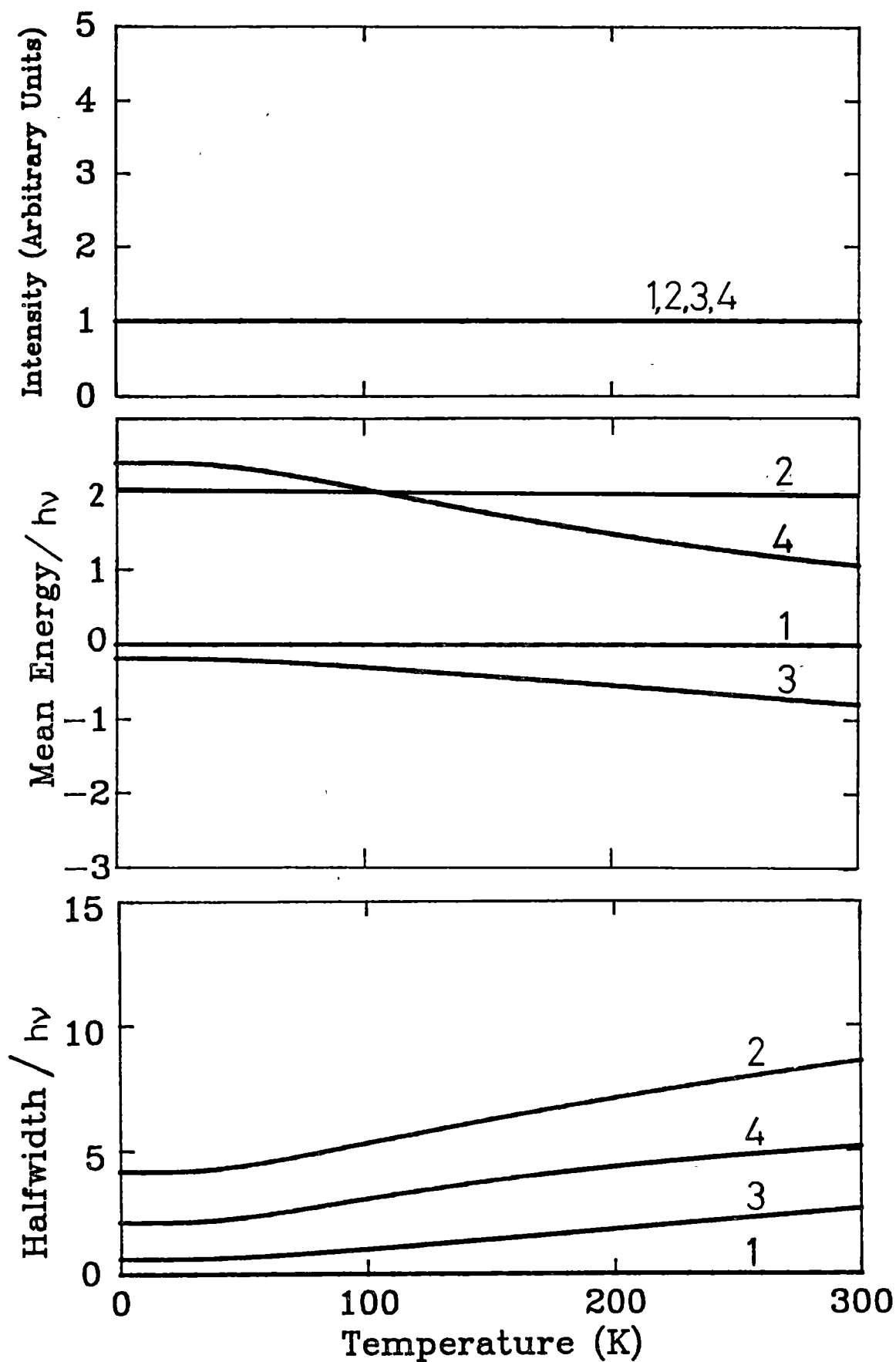
Figure 3.7 Moments analysis of the allowed spectra shown in figure 3.5.
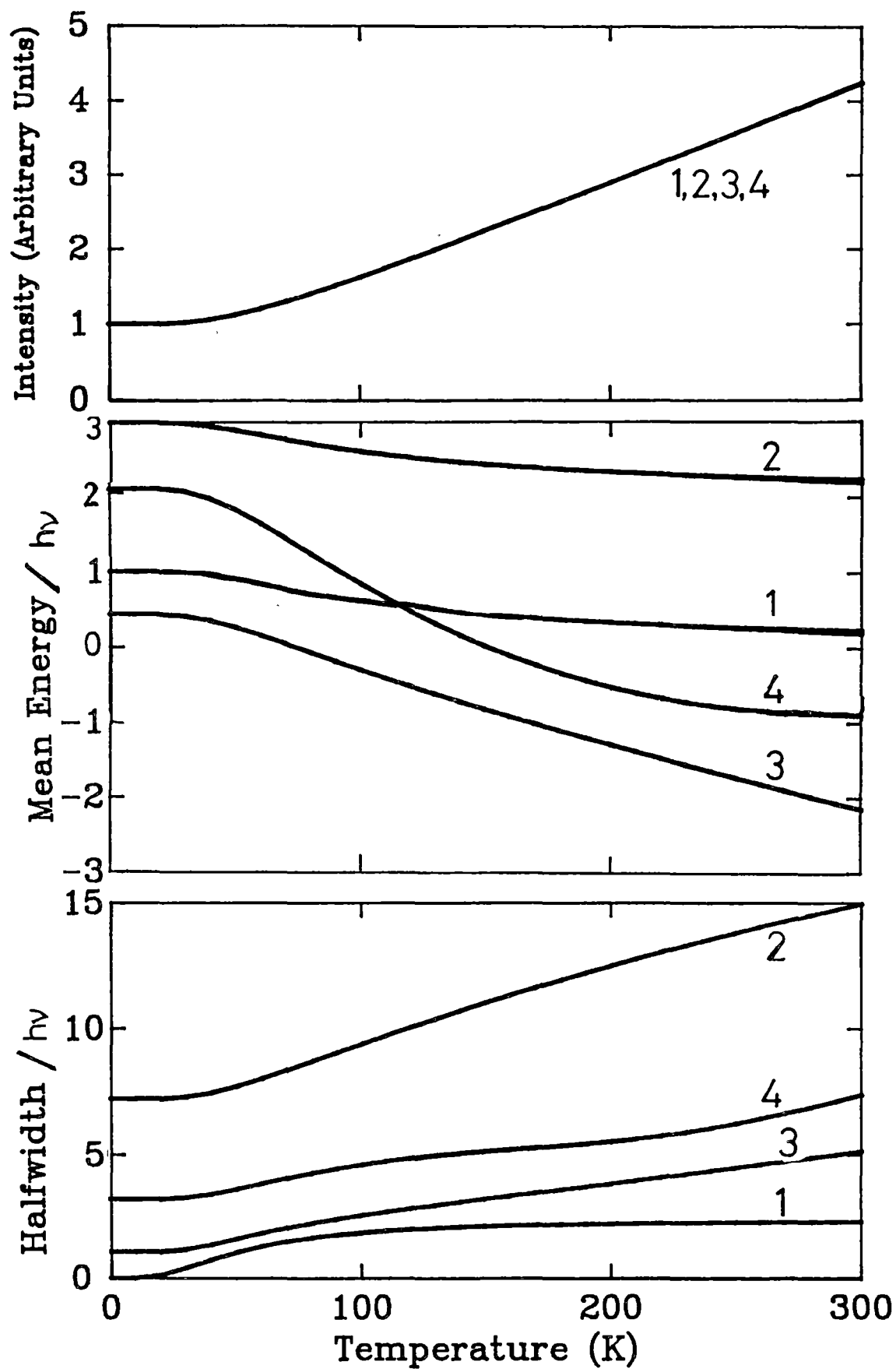
Figure 3.8 Moments analysis of the forbidden spectra shown in figure 3.6.

3.7 ADDITIONAL EFFECTS

3.7.1 MIME: Missing Mode Effect.

Recently a new "effect" has been coined for the appearance of a vibrational progression in the absorption or emission spectrum of a molecule which has an energy interval that cannot be associated with any of the totally symmetric vibrational frequencies of the molecule. This "missing mode effect" or MIME (Tutt etal 1982; 1983; 1987) is more convincing in emission spectra as the ground state vibrational frequencies that should appear in the spectrum can be observed directly from Raman spectroscopy.

Tutt etal (1982) have considered such a case where a 550cm^{-1} progression observed in the emission spectra of $W(CO)_5 py$ did not correspond to any of the totally symmetric vibrations, the closest of which are the 432 and 599 cm^{-1} modes. This puzzling observation was interpreted using the "semiclassical" theory of electronic transitions (Heller 1981), as being due to the excited state potential being displaced along both these totally symmetric coordinates. In this section it is shown that this type of calculation can be done both more easily and accurately with the well known procedure of calculating Franck-Condon overlaps.

In their semiclassical approach the Frank-Condon overlap is proportional to the recurrence of the time evolving wave packet to its original position on the final potential surface. This recurrence is only partial when a damping factor is included to give the vibronic lines a finite halfwidth. The time evolution of the wave packet on a two dimensional surface is the product of the time evolution of the separate modes (O'Brien 1981). The fourier transform from the time to the frequency domain then gives a spectrum with a vibrational interval that is different than either of the separate vibrations. This "missing mode" vibration is not simply the average of the two separate vibrations, and indeed can be smaller than either, but must not be larger than both of the separate vibrations (Tutt etal 1983).

The above arguments are illustrated in figure 3.9a where the time evolution of the total and separate vibrations are shown. The steep fall of the recurrence times are due to the damping factor which
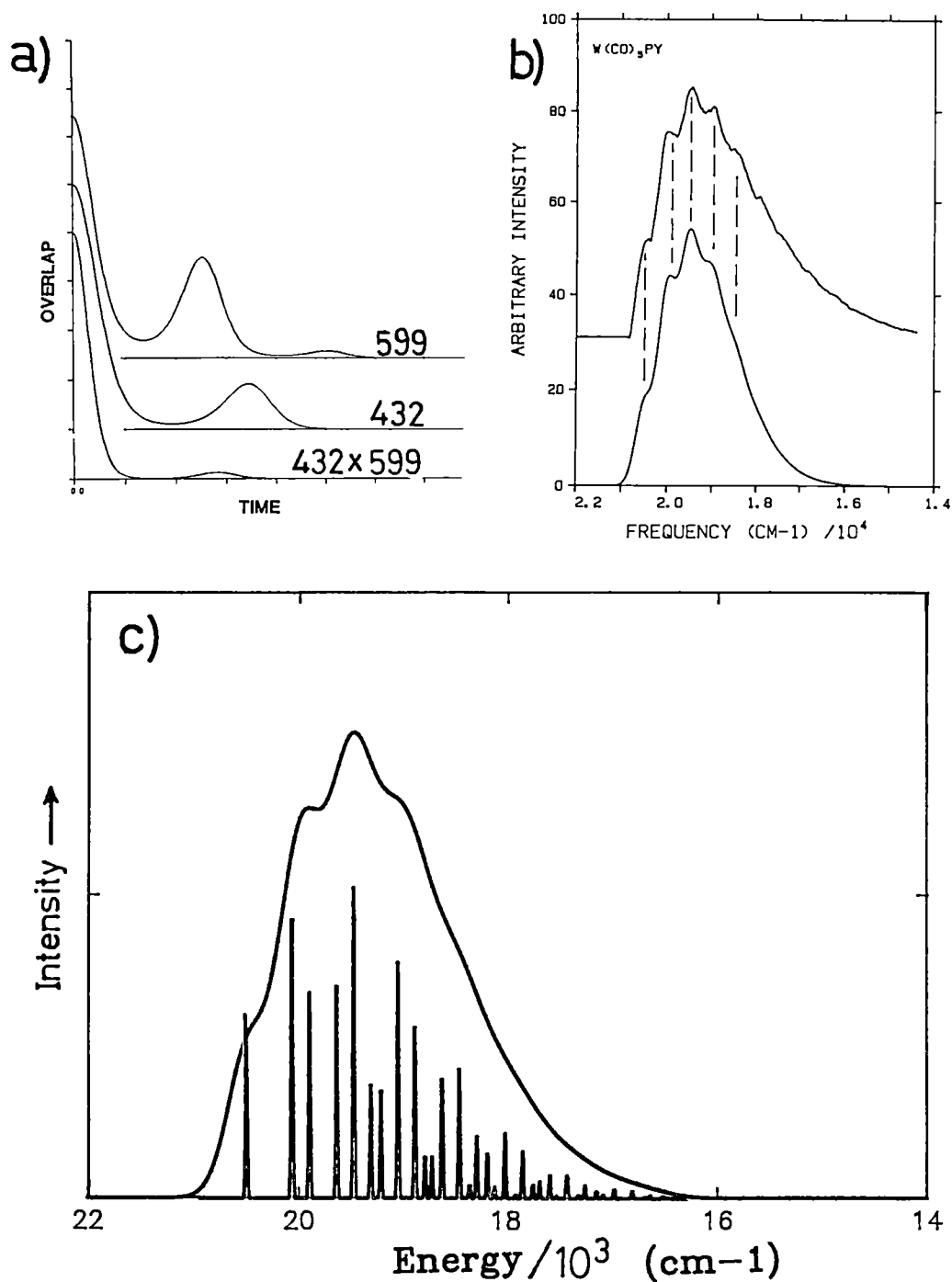
Figure 3.9 MIME: The missing mode effect.

Figures a), b) have been taken from Tutt etal (1982).

a) Time evolution of the semiclassical wavepackets.

b) Experimental and semiclassically calculated spectrum of $W(CO)_5py$.

c) The exact Franck-Condon spectrum calculated from (3.58) and (3.59).

represents the relaxation of the system into other vibrational modes. Transforming into the frequency domain in figure 3.9b, the role of this damping factor is seen to broaden the vibronic lines. The resulting spectrum shows the progression in $\bar{v}$ = 550 cm^{-1} that was observed in W(CO)$_5$py. These figures have been taken from Tutt etal (1982) which were calculated using the frequencies $\bar{v}_1$= 432 cm^{-1}, $\bar{v}_2$= 599 cm^{-1}; the dimensionless displacements d$_1$= 1.82, d$_2$= 1.55; and the electronic origin E$_0$= 20,500 cm^{-1}.

While this analysis provides a convincing explanation for the experimental observations, it is given in the unfamiliar (or new) language of semiclassical spectroscopy. This approach gives an approximation to the exact quantum mechanical behaviour in a variational calculation. A variational calculation with a two dimensional harmonic oscillator basis could have equally been used to calculate the Franck-Condon overlaps and hence the spectrum. Since in the present case there are no matrix elements connecting the two coordinates, this is equivalent to doing two one dimensional calculations and convoluting the resulting spectra. Indeed, a variational calculation is in itself unnecessary since analytic formulae are available for the Franck-Condon factors of displaced oscillators. From equation (3.19), the energy and intensity of the low temperature emission spectrum from the excited to ground state, |00> → |mn>, is given by:

$$E_{m,n} = E_0 + m\bar{v}_1 + n\bar{v}_2 \qquad (3.58)$$

$$I_{m,n} = I_{0,0} \left(\frac{E_{m,n}}{E_{0,0}}\right)^4 \left(\frac{<00|mn>}{<00|00>}\right)^2 \qquad (3.59)$$

$$\left(\frac{<00|mn>}{<00|00>}\right)^2 = \frac{D_1^{2m} D_2^{2n}}{2^m 2^n m! n!} \quad \text{(D is defined as in equation (3.19))}$$

The energy factor in (3.59) is raised to the fourth power because we are dealing with emission (Yersin etal 1980). The stick diagram of the spectrum calculated using equations (3.58) and (3.59) with the same parameters as Tutt etal (1982), is shown in figure 3.9c. The addition of a Gaussian lineshape (HWHH=250cm^{-1}) to each of these lines results in a spectrum which is almost identical to that calculated by semiclassical methods. In fact, any differences in the two spectra must result from the inadequancy of the semiclassical method

as it only approximates the exact spectrum given in figure 3.9c calculated from equations (3.58), (3.59).

The Franck-Condon spectrum shows the MIME frequency for exactly the same reasons as the semiclassical spectrum, the resolution or halfwidth of the lines (or damping factor) does not allow the underlying structure to be observed. The resolved line spectrum of figure 3.9c could also be approximately calculated by semiclassical methods by setting the damping factor to zero.

In summary, for the missing mode effect to occur, two conditions must be present. First, there must be a displacement along at least two normal coordinates (ie there must be two or more totally symmetric modes); and second, the spectrum must not be fully resolved. Although this phenomena has recently been explained semiclassically, the MIME effect is a general molecular property and need not be calculated in this manner. It is felt that the usual time independent Franck-Condon method are more accessible and easier to use. However, the semiclassical approach is very useful conceptionally when considering the dynamics of the problem, especially the source of spectral resolution.

3.7.2 The Dushinsky Effect: The Electron's Revenge.

The Dushinsky effect (Dushinsky 1937; Kupka and Cribb 1986) is the name given to the unusual intensity distribution among the vibronic transitions between two electronic states where the normal coordinates are rotated in one electronic state, with respect to those of the other. This can then be described as a case where the electronic states (or the different sets of averaged electrons) couple the vibrational coordinates (nuclear motions). This electronic-vibrational coupling ("electrational"?) is in a sense the opposite case to the vibrational-electronic (vibronic) coupling that is the main thrust of this thesis. However it is relevant to the present work in that the unusual intensity distributions that result may be confused with vibronic effects. In addition, if both the Dushinsky effect and vibronic coupling are present, novel cancellation effects can also occur.

As discussed in section 2.2.1, for any particular electronic state, normal coordinates can always be found. These normal coordinates need not be the same in each electronic state as has been

(3.34)

assumed up to now. However, since the normal coordinates of a particular electronic state must span the complete 3N-6 coordinate space of the molecule, a set of normal coordinates in one electronic state can always be expressed as a linear combination of the normal coordinates in another.

Consider the adiabatic potential surface of a particular non-degenerate electronic state $|m>$ which is not coupled to any other electronic state. This surface is then expanded about a reference geometry Q_o:

$$V_m(Q) = V_m(Q_o) + \sum_i <m| \left(\frac{\partial V}{\partial Q_i} \right)_o |m> Q_i + \frac{1}{2} \sum_{i,j} <m| \left(\frac{\partial^2 V}{\partial Q_i \partial Q_j} \right)_o |m> Q_i Q_j +$$

If only the two normal modes Q_a, Q_b are considered this becomes:

$$V_m(Q) = E_o + u_a Q_a + u_b Q_b + u_{aa} Q_a^2 + u_{bb} Q_b^2 + u_{ab} Q_a Q_b + .. \tag{3.60}$$

The reference geometry, Q_o, is usually taken as the equilibrium ground state geometry so that the linear terms in (3.60) are zero in the ground state. Similarly, the normal coordinates can be chosen so that the quadratic cross term in (3.60) is also zero in the ground state (see section 2.2.1). This need not be the case in the excited electronic states but group theory can be used to determine when these terms can be non-zero. As seen previously, the linear terms in (3.60) are non-zero only for the normal coordinates Q_a that are totally symmetric. The quadratic term is the harmonic force constant when a=b and a cross term when a≠b. This cross term u_{ab} will only be non-zero when the direct product of the irreducible representations of the coordinates contain the totally symmetric representation. This will only be true when the two coordinates a and b are of the same symmetry (regardless of whether a or b are degenerate or not). It is this cross term that gives rise to the Dushinsky rotation, the normal coordinates in this electronic state are "mixed" when expressed in terms of the ground state coordinates.

The expansion of the potential in (3.60) can be continued where the diagonal cubic terms represent the anharmonicity, but the cubic and higher cross terms cause difficulties. Their inclusion means that the excited state coordinates can no longer be expressed as a linear

(3.35)

combination of the ground state coordinates but are related by a non-linear transform. Curvilinear coordinates must then be used, but this case will not be considered further here (Gans 1977).

If terms only up to second order are kept in (3.60), then the linear combination of the normal coordinates can be expressed as a rotation of the normal coordinates in the excited state with respect to the ground state. For only two normal coordinates this can be expressed by (Doktorov etal 1979):

$$\begin{bmatrix} Q'_a \\ Q'_b \end{bmatrix} = \begin{bmatrix} \cos\theta & \sin\theta \\ -\sin\theta & \cos\theta \end{bmatrix} \begin{bmatrix} Q_a \\ Q_b \end{bmatrix} + \begin{bmatrix} d_a \\ d_b \end{bmatrix} \tag{3.61}$$

The coordinates Q'_a, Q'_b, and Q_a, Q_b correspond to those of the excited and ground states respectively. The angle θ is the Dushinsky rotation angle of the excited state coordinates as shown in figure 3.10. It can be related to the potential constants in (3.60) by substituting (3.61) into (3.60), and with some algebra it is found:

$$\tan 2\theta = \frac{k_{ab}}{k_{aa} - k_{bb}} \tag{3.62}$$

This is equivalent to an expression given by Small (1971).

So far it has been assumed that there is no vibronic coupling present, and it is again stressed that vibronic coupling is not necessary for the Dushinsky effect to be occur. However, if it is present, and the excited state is coupled to the intermediate states $|m\rangle$, then the u_{ab} of equation (3.60) is then given by (Lee 1985; Small 1971):

$$u_{ab} = \frac{1}{2} \langle e| \frac{\partial^2 V}{\partial Q_a \partial Q_b} |e\rangle + \sum_{m \neq e} \frac{\langle e| \frac{\partial V}{\partial Q_a} |m\rangle \langle m| \frac{\partial V}{\partial Q_b} |e\rangle}{E_e - E_m} \tag{3.63}$$

The existence of both the Dushinsky rotation and vibronic coupling as expressed above can lead to constructive and destructive interference in the spectrum and a detailed study of this has been given by Small (1971) and Henneker etal (1983). Here only the first term in (3.63) is considered and the absorption spectrum was simulated for transitions between two two-dimensional potential surfaces for three typical cases:

1) The ground state potential surface is harmonic and is characterised by the two vibrations $\bar{v}_a$, $\bar{v}_b$ of different frequencies. The excited state potential is identical and undisplaced with respect to the ground state.

2) As in the case above, except the excited state potential surface is displaced along both the normal coordinates.

3) The ground state is as above, the excited state potential is undisplaced and harmonic with respect to one normal mode and a double well potential with respect to the other.

Cases 1) and 3) above are typical behaviour for two non-totally symmetric normal modes, while case 2) is typical for a two totally symmetric normal modes. In all the above cases, the spectra were calculated for different angles of Dushinsky rotation. The transition is assumed to be allowed and the spectra was simulated using the energy levels and wavefunctions determined by the variational method as described in section 3.5. Only transitions from the lowest vibrational level of the ground electronic state were included, which corresponds to a low temperature spectrum. In all cases the vibronic transitions were given a halfwidth (HWHH) of 50 cm^{-1} and the separation of the electronic origins was held at 20,000 cm^{-1}. A cross section of the ground and excited state potential surfaces at the energy of their lowest vibrational level is also given for each spectrum.

The calculated spectrum of the potentials of case 1) are shown in figure 3.10. The harmonic vibrations are $\bar{v}_a$= 200 cm^{-1}, $\bar{v}_b$= 500 cm^{-1} and as expected the spectrum with no rotation of the excited state potential consists of a single vibronic line corresponding to the (0,0) → (0,0) transition. As the Dushinsky rotation is applied, additional transitions are calculated to be non-zero, but the intensity is very low. In real systems the difference in the ground and excited state frequencies would also caused transitions of comparable intensity in progressions of two excited state quanta (see section 3.3.1)

What is of particular interest in figure 3.10 is that the spectrum is composed of two "harmonic" vibrations with a frequency intermediate to the two ground state frequencies. These calculated excited state frequencies are shown in figure 3.11 as a function of the Dushinsky angle θ. At $\theta = 0^{\circ}$ and $\theta = 90^{\circ}$, the coupling term u_{ab}

Figure 3.10   The Dushinsky effect. The vibronic Hamiltonian is given by:

$$H = -\frac{1}{2}\left(\frac{\partial^2}{\partial a^2} + \frac{5}{2}\frac{\partial^2}{\partial b^2}\right) + \frac{1}{2}\left(a^2 + \frac{5}{2}b^2\right), \quad h\nu = 200 \text{ cm}^{-1}.$$

The ground and excited states are shown by dashed and solid lines respectively.
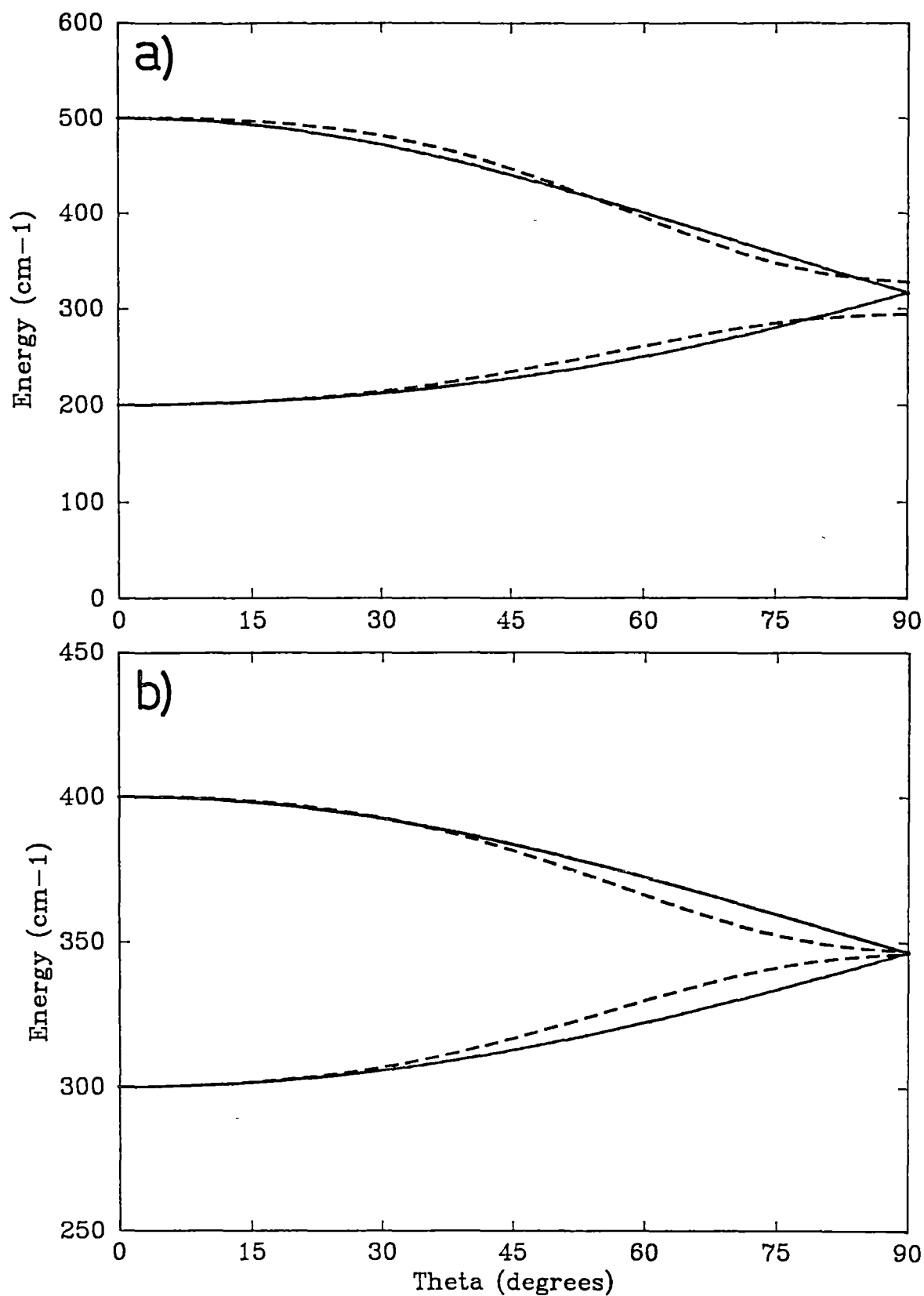
Figure 3.11 The harmonic energy intervals as a function of the Dushinsky angle.
————— Exact calculation; — — — — — Approximate expression in (3.65).
The vibrational Hamiltonians are those given in figures 3.10 (a) and 3.12,13 (b).

disappears and the Franck-Condon factors may be calculated exactly from the analytic expression previously given by equation (3.17). At θ = 0° the excited state vibronic energy levels are those of the ground state, while at θ = 90°, the excited state vibronic levels are given by:

$$\bar{v}'_a = \bar{v}'_b = \sqrt{K}\ \bar{v}_a \qquad (3.64)$$

At all other angles the energy levels and Franck-Condon factors must be calculated numerically. However, an approximate expression for these excited state frequencies is given by:

$$\bar{v}'_a = [\ 1 + \lambda_a - \tfrac{1}{2}\lambda_a^2 - \tfrac{1}{2}\lambda_{ab}^2[K/(K^2-1)]\ ]\ \bar{v}_a \qquad (3.65)$$

$$\bar{v}'_b = [\ 1 + \lambda_b - \tfrac{1}{2}\lambda_b^2 + \tfrac{1}{2}\lambda_{ab}^2(1/(K^2-1))\ ]\ \bar{v}_b$$

$$K = \bar{v}_b/\bar{v}_a; \quad \lambda_a = \tfrac{1}{2}(K-1)\sin^2\theta; \quad \lambda_b = \lambda_a/K; \quad \lambda_{ab} = \tfrac{1}{2}(1-K)\sin2\theta.$$

These approximate formulas are compared with the exact calculations in figure 3.11. Equation (3.64) and (3.65) were derived by scaling the coordinates and 2nd order perturbation theory respectively, but space does not permit details here.

When considering case 2) above, there arises an ambiguity in the way the displacement of the excited state surfaces can be defined. The displacement as defined in (3.61) corresponds to a displacement after the rotation. Similarly a displacement before the rotation can be defined by:

$$\begin{pmatrix} Q'_a \\ Q'_b \end{pmatrix} = \begin{pmatrix} \cos\theta & \sin\theta \\ -\sin\theta & \cos\theta \end{pmatrix} \begin{pmatrix} Q_a + d_a \\ Q_b + d_b \end{pmatrix} \qquad (3.66)$$

The simulated spectra for both these cases are given in figure 3.12 and 3.13 respectively. These spectra were calculated for potentials with the harmonic frequencies: $\bar{v}_a$ = 300 cm^{-1}, $\bar{v}_b$ = 400 cm^{-1} and the displacements d_a = 2.5, d_b = 1.0.

As in the undisplaced case, a harmonic vibrational spacing is calculated, where the harmonic interval is intermediate between the ground state frequencies. However, in this case, the vibronic transitions are far more visible due to the Franck-Condon envelope. These harmonic intervals are the same for a particular value of the
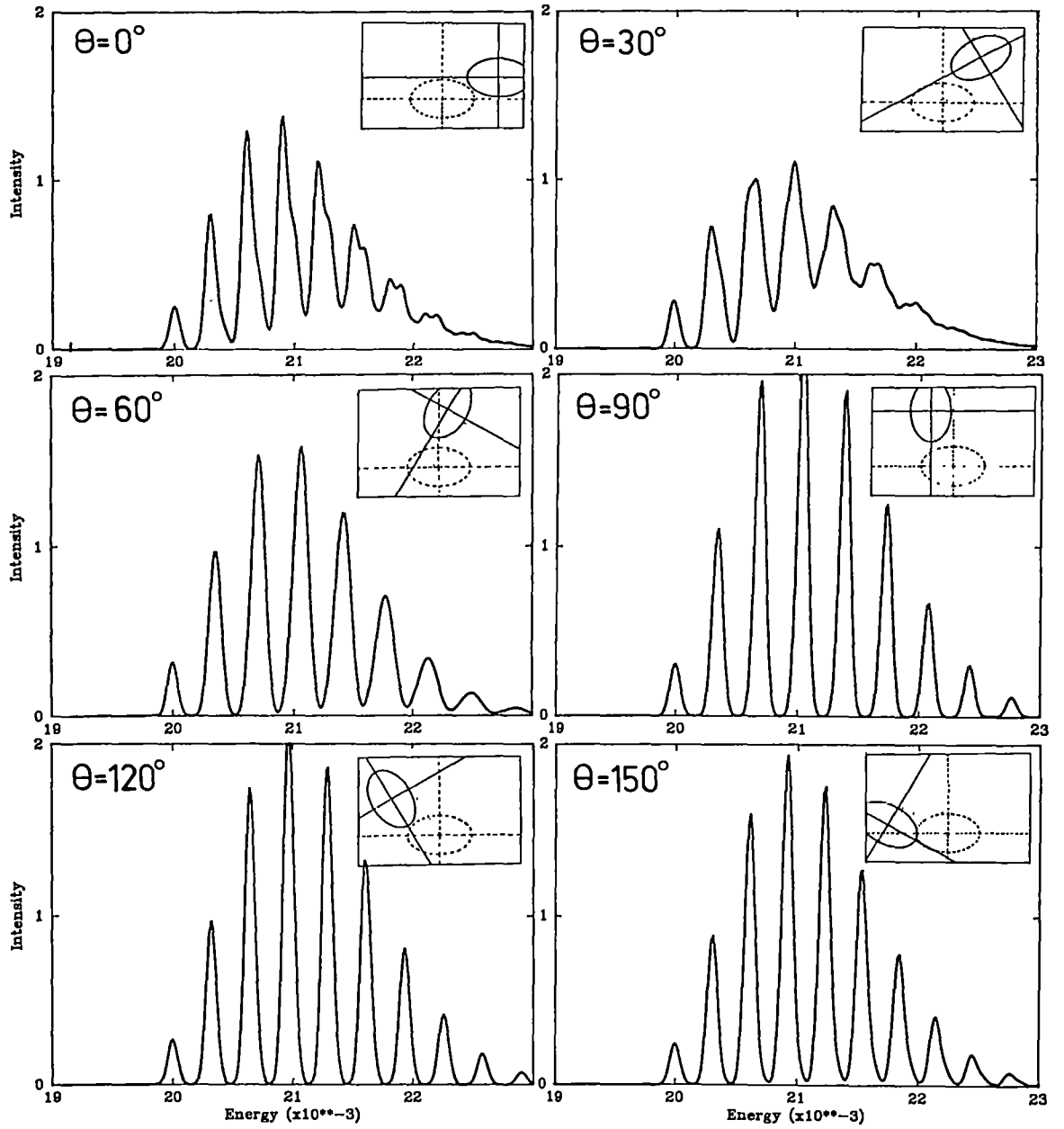
Figure 3.12 The Dushinsky rotation using equation (3.61).
The ground state Hamiltonian is given by:

$$H = -\frac{1}{2} \left(\frac{\partial^2}{\partial a^2} + \frac{4}{3} \frac{\partial^2}{\partial b^2}\right) + \frac{1}{2}(a^2 + \frac{4}{3} b^2); \quad h\nu = 300 \text{ cm}^{-1}.$$

The excited state displacements are : $d_a = 2.5$, $d_b = 1.0$.
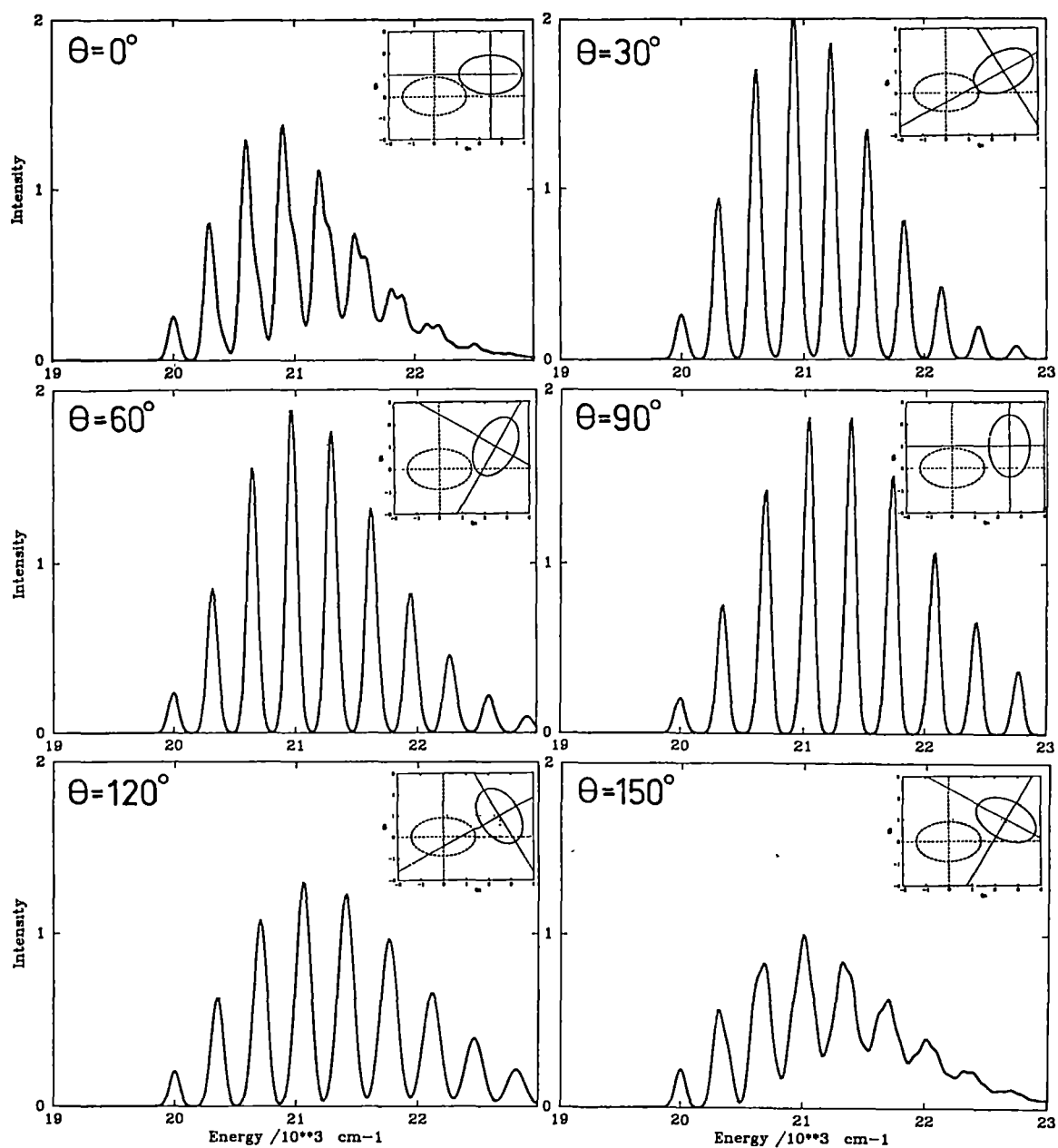
Figure 3.13 The Dushinsky rotation using equation (3.65).
The vibronic Hamiltonians are the same as that given in figure 3.12.

Dushinsky angle, regardless of whether equation (3.61) or (3.66) is used. The exact values and those obtained from (3.65) are shown in figure 3.11b. For angles in the interval 90-180°, the behaviour is the reflection of that shown in the 0-90° range.

While the harmonic intervals are identical for a particular rotation in figures 3.12 and 3.13, the intensity pattern differs substantially. This may seem surprising at first since the potentials are related. For example, the potential surfaces at $\theta = 30^\circ$ in figure 3.12 are identical to those at $\theta = 150^\circ$ in figure 3.13, except that the ground and excited states are interchanged. This then stresses the importance that the kinetic energy operator has in determining the observed fine structure. The spectra shown for the angles 0-180° in figure 3.12 will correspond to the emission spectra with the potential surfaces given in 180-0° in figure 3.13, and vice versa. Inspection of these spectra shows that there is a lack of the expected mirror image symmetry between such absorption and emission spectra. Craig and Small (1971) have observed such a lack in mirror symmetry between the absorption and emission spectra of phenanthrene.

In the third case to be considered, the potentials are undisplaced and have a double minimum as a function of one coordinate. The intensity pattern of the vibronic structure changes considerably with the rotation angle, however it is not possible to derive simple expressions for this non-harmonic structure.

The spectra due to the rotation of harmonic potentials in cases 1) and 2) have harmonic frequencies which are intermediate to those calculated with the potential with no rotation. Often, depending on the rotation angle and the displacement of the surfaces, only one of these progressions will dominate. In this respect it could be said that the Dushinsky rotation causes a true "missing mode effect", where a vibrational progression can be observed whose interval does not correspond to either of the harmonic frequencies of the potential. The MIME effect studied by Tutt etal (1982, 1983, 1987) is essentially the result of constructive interference of many vibronic transitions, whereas the structure observed here is due to "real" energy levels and does not depend on the resolution of the spectrum.

(3.39)
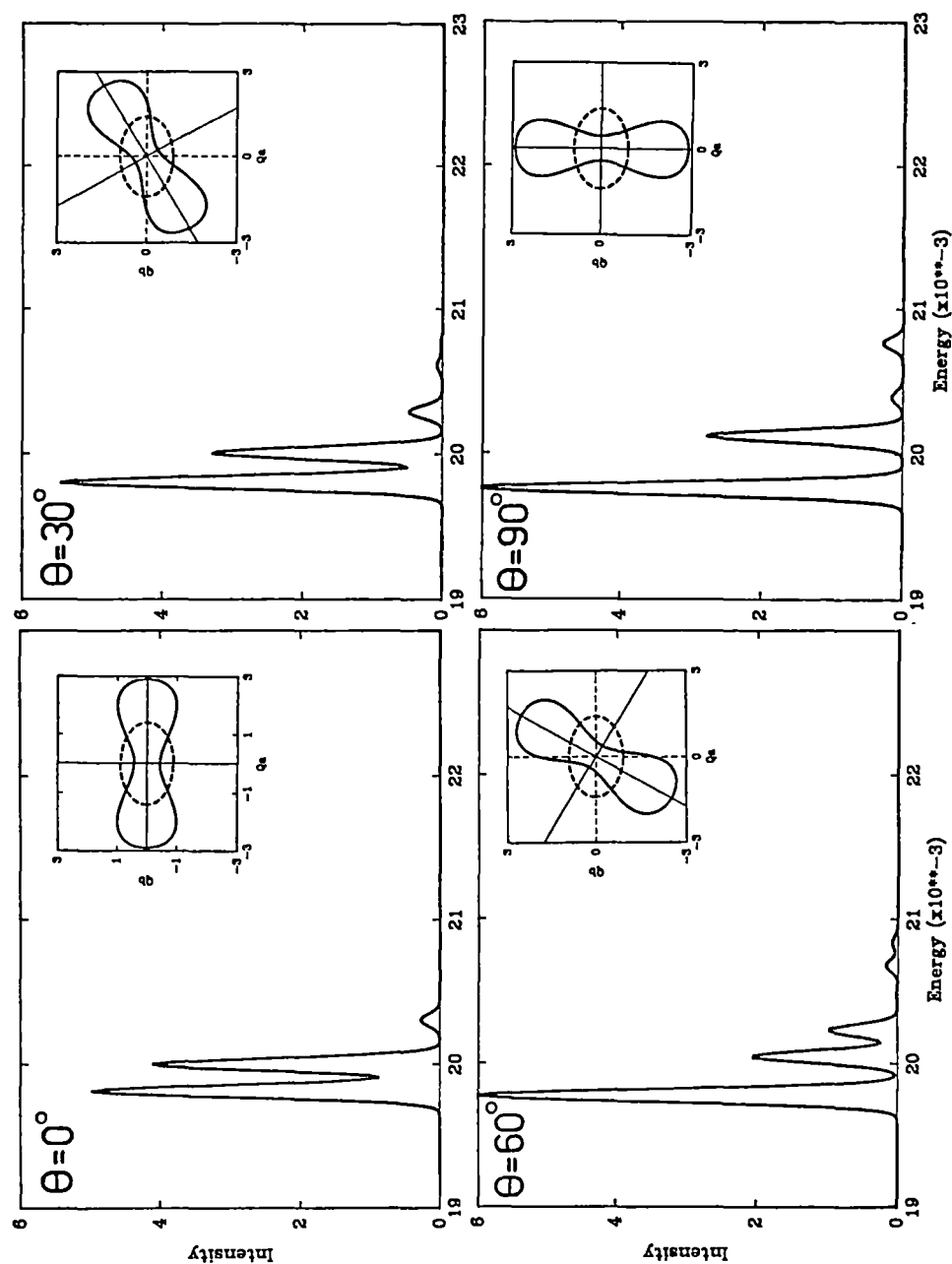
Figure 3.14 The Dushinsky effect where there ia a double minimum along one coordinate. The excited state vibronic Hamiltonian is given by:
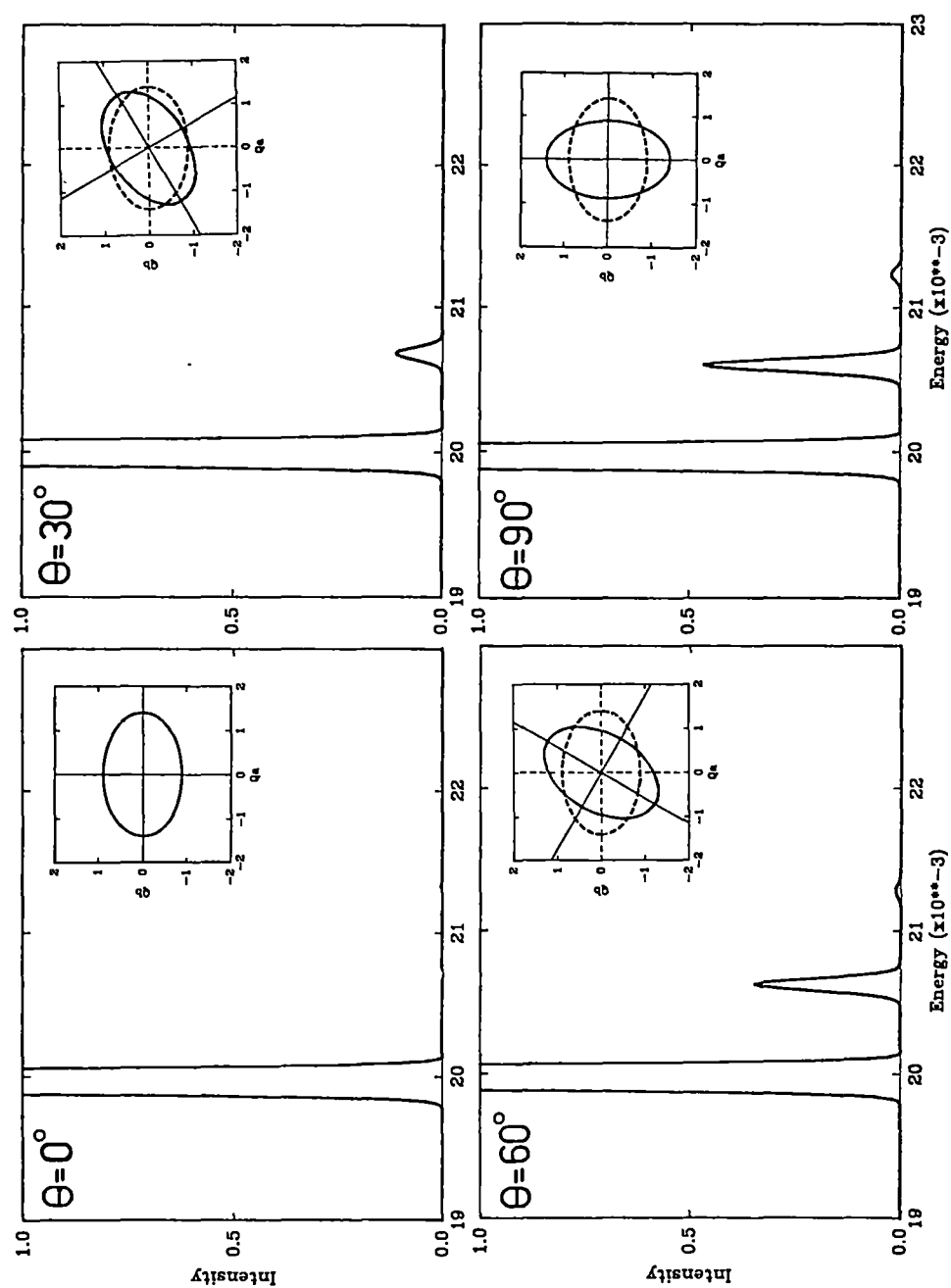
$$H = -\frac{1}{2}\left(\frac{\partial^2}{\partial a^2} + \frac{5}{2}\frac{\partial^2}{\partial b^2}\right) + \frac{1}{2}\left(-a^2 + \frac{a^2}{16} + \frac{5}{2}b^2\right), \quad h\nu = 200 \text{ cm}^{-1}.$$

The ground state potential is that given in figure 3.10.

In summarising this chapter, the importance of the kinetic energy operator should be stressed. Studying the form of the adiabatic potential surfaces gives the static, but incomplete, view of a molecular system. A full understanding of the vibrational or electronic properties of a molecule requires the consideration of the dynamics of the system. This is examined in more detail in the study of the dynamic Jahn-Teller effect in the following chapter.

(3.40)

APPENDIX 3.A1: **PROOF: THE TEMPERATURE DEPENDENCE OF THE INTENSITY DEPENDS ONLY ON THE GROUND STATE POTENTIAL.**

It was shown by Lohr (1969) that the derivation of the "coth rule" in equation (3.54) requires that the ground state is harmonic and that there is only a linear dependence of the electric transition moment on normal coordinate of the inducing mode. This will now be extended to show that _any_ temperature dependence of the intensity depends only on the ground state where both the ground and excited state potentials may be anharmonic, and the electronic transition moment may be an _arbitrary_ function of the normal coordinate.

The intensity of a transition is given by (3.50). For clarity only one inducing mode is considered. [This may be easily extended to many modes.]

$$I(T) \propto \sum_i P_i(T) \sum_j |<i|M(\xi)|j>|^2 \qquad (3.A1)$$

The ground and excited state vibrational wavefunctions $|i>, |j>$ are expanded in terms of a harmonic oscillator basis $|\phi_n>$:

$$|i> = \sum_{n=0}^{\infty} a_{ni}|\phi_n> ; \qquad |j> = \sum_{n=0}^{\infty} b_{nj}|\phi_n> \qquad (3.A2)$$

The coefficients a,b are found as eigenvectors of a secular equation and will form orthonormal sets. This makes it possible to express the excited state functions $|j>$ in terms of the ground state functions:

$$|j> = \sum_{i=0}^{\infty} c_{ij}|i> \qquad \text{where } c_{ij} = \sum_{n=0}^{\infty} a_{in}b_{nj} \qquad (3.A3)$$

Assuming that the normal coordinate spaces in the ground and excited states will be connected at most by a displacement and rotation (Albrecht 1960, footnote 19), the coefficients c will also form an orthonormal set. Substituting (3.A3) into the part of the intensity expression dependent on the j excited states:

$$\sum_j |<i|M(\xi)|j>|^2 = \sum_j |<i|M(\xi)|\sum_i c_{ij}|i>|^2$$

$$= \sum_j |\sum_k c_{i+k,j}<i|M(\xi)|i+k>|^2, \quad i+k \geqslant 0$$

$$= \sum_j \left[\sum_k \left[c^2_{i+k,j} |<i|M|i+k>|^2 + \sum_{m \neq k} c_{i+k,j} c_{i+m,j} <i|M|i+k><i|M|i+m> \right] \right]$$

$$= \sum_k (\Sigma c^2_{i+k,j}) |<i|M|i+k>|^2 + \sum_k \sum_{m \neq k} (\Sigma c_{i+k,j} c_{i+m,j}) <i|M|i+k><i|M|i+m>$$

By the orthonormality of the rows and columns of c the summation over j in the first parentheses is equal to one and in the second equal to zero:

$$= \sum_k |<i|M(\xi)|i+k>|^2, \quad i+k \geqslant 0. \tag{3.A4}$$

Substitution into (3.A1) results in the desired relationship where the intensity is independent of the excited state. [Note: It is recognised that the electronic transition moment $M(\xi)$ will be different for transitions to different electronic states. However, if two electronic transitions are vibronically allowed by the same vibration, then they should show the same temperature dependent intensity as it is determined solely by the ground state potential.]

Alternatively, the closure relationship (Albrecht 1960, eq.6) can be used in the summation over j in (3.61) to give:

$$<i|M(\xi) \sum_j |i+k><i+k| M(\xi)|i> = <i|M(\xi)^2|i> \tag{3.A5}$$

This again results in the temperature dependence of the intensity being determined by a Boltzmann distribution over the ground state levels.

This is a different way of thinking about the temperature dependence of the intensity, instead of transition probabilities between vibronic levels as in (3.A1), we now have the average (or quantum-mechanical mean) value of the square of the electronic transition moment in the ground state levels. For example, if the electronic transition moment has a linear dependence on a normal coordinate, then the relative intensity at certain temperature will be _equal_ to the relative mean-square value of this coordinate at this temperature.

APPENDIX 3.A2: ANALYTIC FORMULA IN THE HARMONIC APPROXIMATION.

The equations (3.54)-(3.57) in section 3.6.2 are derived assuming harmonic potentials. The "coth rule" in equation (3.54) has previously been given by Albrecht (1960), but a short derivation in the present notation follows.

It is assumed that the ground state wavefunctions are harmonic oscillator functions and that the transition moment depends linearly on ξ. The non-zero matrix elements of (3.A4) are when $k=\pm 1$ and the intensity is then given by:

$$
\begin{aligned}
I(T) &= A \sum_i P_i(T) \; (|<i|\xi|i-1>|^2 + |<i|\xi|i+1>|^2) \\
&= \frac{A}{2} \sum_i X^i [1-X] \; (2i+1), \quad \text{where } X = \exp(-h\nu/kT) \\
&= \frac{A}{2} [1-X] \; (2\sum_i (i+1)X^i - \sum_i X^i) \\
&= \frac{A}{2} \left(\frac{1+X}{1-X}\right) \\
&= I_o \coth(h\nu/2kT) \qquad\qquad\qquad\qquad\qquad (3.A6)
\end{aligned}
$$

The relationship for a second order dependence of the transition moment on ξ has been given by Fussgaenger (1965). The derivation follows a similar course as that of (3.A6) above. If the electronic transition moment is given by: $M(\xi) = a\xi + b\xi^2$, then from (3.A1) one has:

$$
\begin{aligned}
I(T) &\propto \sum_i P_i(T) \left(a^2 [\; |<i|\xi|i-1>|^2 + |<i|\xi|i+1>|^2 \;] \right. \\
&\qquad \left. + b^2 [\; |<i|\xi^2|i-2>|^2 + |<i|\xi^2|i>|^2 + |<i|\xi^2|i+2>|^2 \;] \right) \\
&\propto \sum_i X^i [1-X] \frac{1}{2} \left(a^2(2i+1) + 3b^2(i^2+i+1/2) \right) \\
&\propto \frac{a^2}{2} \left(\frac{1+X}{1-X}\right) + \frac{3b^2}{4} \left(\frac{1+X}{1-X}\right)^2 \\
I(T) &= I_{o1}\coth(h\nu/2kT) + I_{o2}\coth^2(h\nu/2kT) \qquad\qquad (3.A7)
\end{aligned}
$$

where $I_{o1}/I_{o2} = \frac{2}{3} (a/b)^2$ and $I_{o1} + I_{o2} = 1.0$.

In deriving (3.A6), (3.A7) the following identities have been used:

$$\sum_i X^i = (1-X)^{-1} \text{ where } X = \exp(-h\nu/kT)$$

$$\sum_i iX^i = X \cdot (1-X)^{-2}$$

$$\sum_i i^2 X^i = X(X+1) \cdot (1-X)^{-3}$$

For the remainder of this appendix a linear dependence of the electronic transition moment is assumed. The expressions for the non-inducing contribution to the band maxima (3.56) and halfwidth (3.57) have also previously been given, (Kubo and Toyozawa 1955; Markham 1959; Prassides and Day 1984) and will not be elaborated on. The inducing mode contributions to these quantities, however, have not previously appeared in the literature and their derivation follows:

The energy of the band maxima is given by (3.52); and if again only one mode is considered:

$$E(T) = \sum_i P_i(T) \sum_j |\langle i|\xi|j\rangle|^2 (E(j)-E(i)) \Big/ \sum_i P_i(T) \sum_j |\langle i|\xi|j\rangle|^2$$

Assuming now that the ground and excited state potential surfaces have the same harmonic frequency; and letting E_o represent the electronic origin:

$$E(T) = \sum_i P_i(T) \frac{1}{2} [\, i(E_o-h\nu) + (i+1)(E_o+h\nu) \,] \Big/ \frac{1}{2}\left(\frac{1+X}{1-X}\right)$$

$$= E_o + h\nu \sum_i X^i (1-X)^2 / (1+X)$$

$$E(T) = E_o + h\nu \tanh(h\nu/2kT) \tag{3.A8}$$

The halfwidth (halfwidth at half height) from (3.53) is:

$$H(T) = [2\ln2]^{1/2} \sigma \text{ where}$$

$$\sigma^2 = \sum_i P_i(T) \sum_j |\langle i|\xi|j\rangle|^2 (E(j)-E(i)-E(T))^2 \Big/ \sum_i P_i(T) \sum_j |\langle i|\xi|j\rangle|^2$$

Assuming again equal frequencies in the ground and excited states:

$$\sigma^2 = (h\nu)^2 \sum_i P_i(T) \left[(i(1+\tanh(\tfrac{x}{2}))^2 + (i+1)(1-\tanh(\tfrac{x}{2}))^2 \right] \Big/ \left(\frac{1+X}{1-X}\right)$$

where $x = h\nu/kT$, $X = \exp(-x)$

$$= [h\nu \, \text{sech}(\tfrac{x}{2})]^2 \, \sum_i P_i(T) \, [i\exp(x) + (i+1)\exp(-x)] \, / \left(\frac{1+X}{1-X}\right)$$

$$= [h\nu \, \text{sech}(\tfrac{x}{2})]^2 \, (1-X)^2 \, \sum_i X^i (iX^{i-1} + (i+1)X^{i+1}) \, / \left(\frac{1+X}{1-X}\right)$$

$$= [h\nu \, \text{sech}(\tfrac{x}{2})]^2$$

$$H(T) = (2\ln 2)^{1/2} \, h\nu \, \text{sech}(h\nu/2kT) \tag{3.A9}$$

In the above derivations all summations have been from 0 to ∞ and use has been made of the relations between hyperbolic functions (Abramowitz and Stegun 1964, section 4.5). Note: To be consistent with other parts of the thesis the label i denotes the ground vibrational states; it should not be confused with the imaginary i which does not appear in this appendix.

CHAPTER 4:   STRONG VIBRONIC INTERACTION:
THE DYNAMIC JAHN-TELLER EFFECT.

4.1 INTRODUCTION AND SOME OBJECTIONS.

This chapter is concerned with a particular breakdown of the adiabatic approximation that occurs with electronic states at the point of degeneracy. This breakdown is commonly known as the Jahn-Teller effect, and has typically been stated as:

Apart from two specific exceptions, a molecule in a degenerate electronic state will be unstable and the nuclei of the molecule will displace themselves so that the symmetry of the system is lowered and the degeneracy is removed. The exceptions are when the degeneracy is either in a linear molecule or is the Kramer's spin degeneracy that occurs in systems with an odd number of electrons.

The above is an existence theorem and can say nothing about the magnitude of the distorting forces. It has been shown, however, that the coupling of degenerate spin levels with molecular distortions will be very much weaker than the case of orbital degeneracy (Jahn 1938). The above formulation of the Jahn-Teller effect does not reflect the full subtlety of the problem. In particular it contains the following two statements:

     1) The molecule spontaneously distorts from high symmetry.

and   2) The degeneracy of the system is removed.

These statements, if taken literally, are incorrect or at the best misleading (Bersuker 1975 pg358). There are three objections that can be made against the Jahn-Teller effect formulated in the above manner.

    These objections arise because the non-adiabatic nature of the Jahn-Teller effect has not been appreciated. The electronic and vibrational states of the system become inexorably mixed and cannot be described by a simple Born-Oppenheimer product as in equation (1.3). The concept of vibronic states existing on a single potential surface then loses physical meaning. In particular the adiabatic potential at the point of degeneracy can be shown to be singular (see section

(4.1)

4.3.1). This means that, at the point of high symmetry, a "Q-dependent electronic state" is meaningless and the stability argument in statement 1) cannot be used (Perlin and Wagner 1984, pg11).

In addition, it is well known that the vibronic Hamiltonian must reflect the full symmetry of the system, and transforms as totally symmetric in the molecular point group (section 3.2.1). This means that there is nothing in the Hamiltonian that can lower the symmetry of the system. The expectation values of the nuclear coordinates in all vibronic states will correspond to the high symmetry, undistorted geometry. This is again contrary to statement 1).

For the same reason there can be no terms in the Hamiltonian that can remove the degeneracy of the system. The symmetry of the vibronic states will be the same whether the Jahn-Teller effect is present or not. The hypothetical electronic degeneracy is then replaced by a vibronic degeneracy, the overall degeneracy of the system does not change contrary to statement 2).

The distortion and degeneracy removal that is characteristic of the Jahn-Teller formulation above can only occur when there is some external perturbation present. As this is often the case in the solid state due to the existence of random crystal strains, this distortion and degeneracy removal is often observed. However, it is important to realise that formally the Jahn-Teller effect alone cannot be responsible for its appearance.

The objections outlined above are well known and these points have previously been made by many others (for example: Sturge 1967, pp106,111; A&B, pg791; Ham 1972, pp14-16; Englman 1970, pp5-7; Bersuker 1975, pg376; Perlin and Wagner 1984, pg11; Bersuker 1984a, pg35). In this chapter some of the subtleties of the problem are presented and the above objections will become clearer. Only the Jahn-Teller case of a doubly degenerate electronic state coupled by a doubly degenerate vibration (the E×ε problem) is considered. The problem is presented from both a static and dynamic viewpoint, following the classic papers of Öpik and Pryce (1957) and Longuet-Higgins etal (1958) respectively. Cooperative effects between the Jahn-Teller centre and the lattice are not considered, although some discussion of this point is given in section 5.4 in connection with vibronic relaxation. It has been shown that multimode effects can often be

represented by a single effective mode (O'Brien 1972; O'Brien and Evangelou 1980). Although the theory of the present chapter is quite general, it is especially developed for the case of octahedrally coordinated Cu(II) ions which are to be studied in the subsequent chapters.

The literature published on the Jahn-Teller effect is enormous, a bibliographic review by Bersuker (1984b) contains several thousand references. Several texts (Englman 1972; Bersuker 1984a; Perlin and Wagner 1984) are available as well as many general reviews (Sturge 1967; Bersuker 1975). Specialist reviews also exist dealing with optical spectroscopy (O'Brien 1981), vibrational spectroscopy (Koningstein 1980), electron spin resonance (Ham 1972; Bates 1978), solid state structures (Reinen and Friebel 1979) as well as theoretical aspects (Longuet-Higgins 1961; Liehr 1963; Judd 1974; Bersuker and Polinger 1982).

4.2 THE STATIC VIEWPOINT: ADIABATIC POTENTIAL SURFACES.

To clarify the objections made in the previous section it is necessary to start by considering the adiabatic approximations discussed in chapter 1. The electronic part of the vibronic wavefunction can be expanded in terms of the electronic states that are d-fold degenerate at the point of high symmetry Q_0:

$$\Omega = \sum_{k=1}^{d} \psi_k(q,Q_0) \cdot \Phi_{ki}(Q) \qquad (4.1)$$

By expanding the potential about this high symmetry configuration, the difference between the potential at an arbitrary geometry and the high symmetry geometry can then be considered as a perturbation in a secular equation:

$$| V'_{ij} - \varepsilon \delta_{ij} | = 0, \quad i,j = 1, \; .. \; d. \qquad (4.2)$$

$$V'_{ij} = \langle \psi_i | \; V(q,Q) - V(q,Q_0) \; | \psi_j \rangle$$

$$V' = \sum_a \left(\frac{\partial V}{\partial Q_a}\right)_0 (Q_a - Q_{ao}) + \frac{1}{2} \sum_{a,b} \left(\frac{\partial^2 V}{\partial Q_a \partial Q_b}\right)_0 (Q_a - Q_{ao})(Q_b - Q_{bo})$$

The solution to this electronic part of the problem gives the adiabatic potentials $\varepsilon(Q)$. The Jahn-Teller theorem is really concerned about the geometric nature of these adiabatic potentials, and can be restated as:

If Q_{ao} (a=1,.. 3N-6) is a point where d of the adiabatic potentials $\varepsilon_i(Q_a)$, i=1,.. d coincide, then none of these d surfaces will have a minimum at this point. The exceptions are linear molecules and Kramer's degeneracy (Bersuker 1984a).

This is very easy to prove: For there to be a minimum at Q_{ao} there must be no linear terms in the potential. It can be shown that in degenerate electronic states there will always be such a linear term for all molecular point groups. From (4.2) the linear terms are:

$$V'_{ij} = \langle \psi_i | \left(\frac{\partial V}{\partial Q_a}\right)_0 (Q_a - Q_{ao}) | \psi_j \rangle$$

(4.4)

$$= A \ (Q_a - Q_{ao}), \quad A = \langle \psi_i | \left(\frac{\partial V}{\partial Q_a} \right)_0 | \psi_j \rangle \qquad (4.3)$$

The matrix elements A can be shown to be non-zero using the usual arguments from group theory. The direct product of the irreducible representations of ψ_i, ψ_j, Q_a must contain the totally symmetric representation of this to be true. [$\left(\frac{\partial V}{\partial Q_a} \right)_0$ transforms the same as Q_a since V _must_ transform as totally symmetric.]

$$\Gamma(\psi_i) \times \Gamma(Q_a) \times \Gamma(\psi_j) \supset A_{1g}$$
$$\text{or} \quad [\Gamma(\psi)^2] \supset \Gamma(Q_a) \qquad (4.4)$$

The brackets [ ] denote the symmetric direct product (Harris and Bertolucci 1978; eq 4.21). [It should be noted that for double point groups, or systems with an odd number of electrons, it is the antisymmetric direct product that should be taken (Jahn 1938).]

Equation (4.4) is trivially true when Q_a is the totally symmetric coordinate, but this has the same effect on all the d degenerate electronic states in the secular equation (4.2) and so does not remove the degeneracy but simply displaces it. This effect can be removed by a change in the origin of the totally symmetric coordinate. Not counting this trivial case, Jahn and Teller (1937) showed that there will always exist a normal mode of suitable symmetry to make (4.4) true for non-linear molecules. They proved this by considering all possible molecular point groups. Therefore, where the adiabatic potentials of a non-linear molecule are at a point of degeneracy, they cannot simultaneously be at a minimum.

4.2.1 The Linear Jahn-Teller Effect.

For the case of a doubly degenerate E electronic state, the symmetric direct product of (4.4) can be found from published tables (Harris and Bertolucci 1978):

$$[E^2] = A_1 + E \qquad (4.5)$$

This then identifies the doubly degenerate e vibration as the Jahn-Teller active mode. In this electronic state, the Jahn-Teller theorem states that there will be linear terms in the potential along this normal coordinate and the secular equation in (4.2) can now be written out in the electronic subspace composed of the two components θ, ε of the degenerate E electronic state up to first order:

$$\begin{vmatrix} -A_1 Q_\theta - \varepsilon & A_1 Q_\varepsilon \\ A_1 Q_\varepsilon & A_1 Q_\theta - \varepsilon \end{vmatrix} = 0, \quad A_1 = \left\langle \theta \left| \left(\frac{\partial V}{\partial Q} \right)_0 \right| \theta \right\rangle \qquad (4.6)$$

Only four of the possible eight matrix elements are non-zero and these can be replaced by a single constant A_1, as the four matrix elements will be equal within a sign change. This is a consequence of the Wigner-Eckart theorem which says that any operator acting within an irreducible representation of a group can be written as a product of a reduced matrix element and a set of vector coupling coefficients (Bill 1984, pg714). In the present case the reduced matrix element is A_1 and is commonly called the linear (or first order) Jahn-Teller coupling constant. The vector coupling coefficients must transform as the components of the direct product:

$$E^2 = A_1 + A_2 + E \qquad (4.7)$$

With the usual choices of phase (Koster etal 1963; Ham 1972, pg18; A&B, pg799) these coefficients are:

$$I = \begin{bmatrix} 1 & 0 \\ 0 & 1 \end{bmatrix} \quad (A_1) \qquad -\sigma_z = \begin{bmatrix} -1 & 0 \\ 0 & 1 \end{bmatrix} \quad (E_\theta) \qquad (4.8)$$

$$\sigma_y = \begin{bmatrix} 0 & -i \\ i & 0 \end{bmatrix} \quad (A_2) \qquad \sigma_x = \begin{bmatrix} 0 & 1 \\ 1 & 0 \end{bmatrix} \quad (E_\varepsilon)$$

The σ labels have been used because they they provide a convenient way to remember the coefficients as they correspond to the Pauli spin matrices (Schiff 1968, pg206).

Within the angular overlap model (Bacci 1978), these linear coupling terms can be calculated explicitly, and are in full agreement with (4.6):

$$\left\langle \theta \left| \frac{\partial V}{\partial Q_\theta} \right| \theta \right\rangle = -\left\langle \varepsilon \left| \frac{\partial V}{\partial Q_\theta} \right| \varepsilon \right\rangle = -\left\langle \theta \left| \frac{\partial V}{\partial Q_\varepsilon} \right| \varepsilon \right\rangle = -\left\langle \varepsilon \left| \frac{\partial V}{\partial Q_\varepsilon} \right| \theta \right\rangle = \frac{\sqrt{3}}{2} \frac{\partial e}{\partial R} (\sigma)$$

$$\left\langle \theta \left| \frac{\partial V}{\partial Q_\varepsilon} \right| \theta \right\rangle = \left\langle \varepsilon \left| \frac{\partial V}{\partial Q_\varepsilon} \right| \varepsilon \right\rangle = \left\langle \theta \left| \frac{\partial V}{\partial Q_\theta} \right| \varepsilon \right\rangle = \left\langle \varepsilon \left| \frac{\partial V}{\partial Q_\theta} \right| \theta \right\rangle = 0 \qquad (4.9)$$

The solution of the secular equation in (4.6) gives the two adiabatic potential surfaces:

$$\varepsilon^\pm = \pm |A_1| (Q_\theta^2 + Q_\varepsilon^2)^{1/2} = \pm |A_1| \, \rho \qquad (4.10)$$

Here the polar coordinates ρ, ϕ defined in figure 4.2, have been used:

$$Q_\theta = \rho \cos\phi \qquad\qquad (4.11)$$

$$Q_\varepsilon = \rho \sin\phi$$

A plot of the two potential surfaces of equation (4.10) gives the conical intersection in figure 4.1a that is characteristic of these systems. It should be noticed that the + and − surfaces expressed by (4.10) are the stalactite and stalagmite respectively and are both singular at the point of high symmetry. Figure 4.1a implies that the molecule will not be stable on the lower potential surface. However, this "distortion" does not go on forever but is stopped by the "restoring forces" or bonding in the molecule. Higher terms then just linear must be considered in the expansion of the potential energy operator.

These higher order terms are classified into those that take the totally symmetric coefficient in (4.8) and those that do not. The former are called invariants (Piepho and Schatz 1983, pg304) and can be thought of as the usual potential energy terms or force constants in the absence of any Jahn-Teller effect, and will be labelled K terms to differentiate them from the A coupling terms. If the second order invariants, or harmonic terms, of the potential are included then the secular equation in (4.6) becomes:

$$| \mathbf{H} - \varepsilon \mathbf{I} | = 0 \qquad\qquad (4.12)$$

$$\mathbf{H} = \mathbf{H}_o + \mathbf{H}_{JT}$$

$$\mathbf{H}_o = \tfrac{1}{2} K_2 (Q_\theta^2 + Q_\varepsilon^2)\, \mathbf{I} \;\; ; \quad \mathbf{H}_{JT} = A_1 (\sigma_x Q_\varepsilon - \sigma_z Q_\theta)$$

The invariants are kept in $\mathbf{H}_o$, and the coupling terms in $\mathbf{H}_{JT}$. The K_2 constant is equal to the vibrational energy of the harmonic oscillator basis functions, or the hypothetical frequency of the e_g vibration of the molecule in the absence of vibronic interactions. It is often referred to in the literature as simply hν. In the variational calculations of chapter 2, the dimensionless potential coefficients were in units of hν, whereas in this chapter all the coefficients are in units of cm^{-1}. The adiabatic terms that result from diagonalising (4.12) are:

$$\varepsilon^\pm = \tfrac{1}{2} K_2 \rho^2 \pm |A_1| \rho \qquad\qquad (4.13)$$

(4.7)
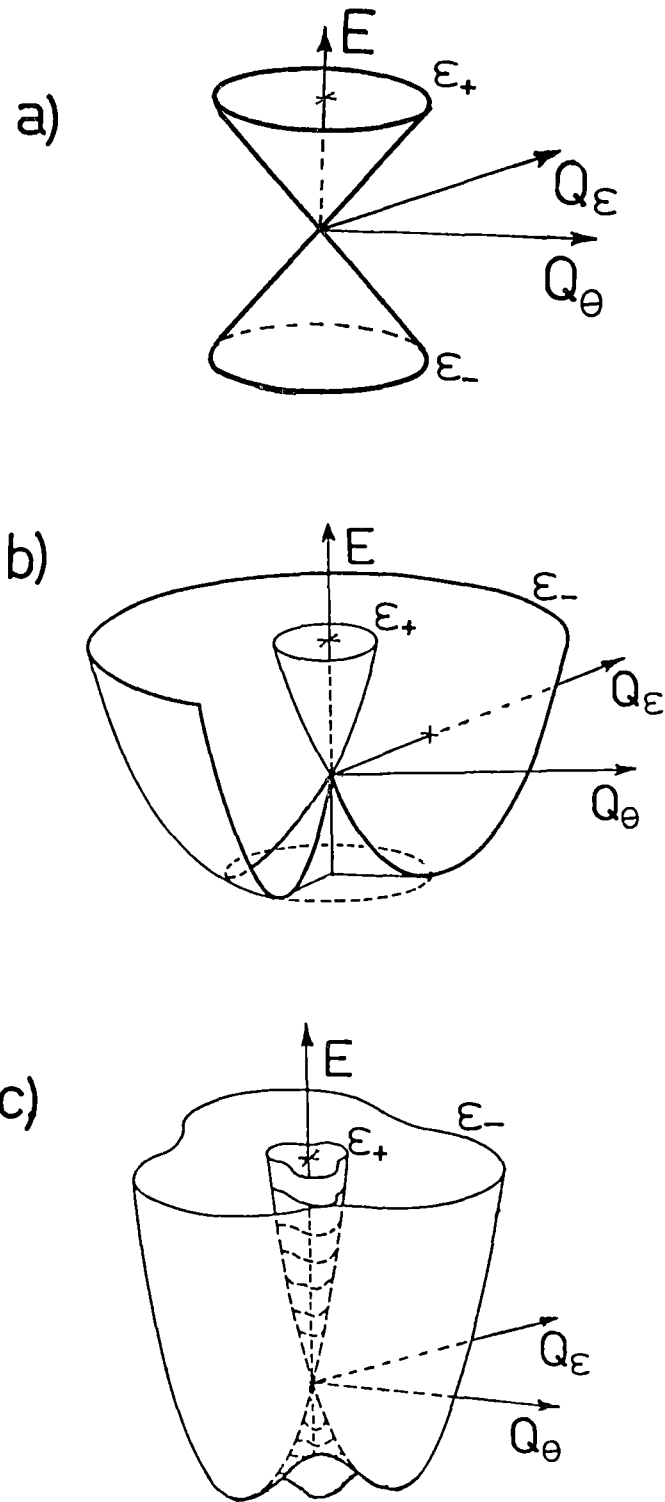
Figure 4.1 The Adiabatic Potential Surfaces.
a) Conical intersection of the linear terms: equation (4.10).
b) The Mexican hat potential: equation (4.13).
c) The warped Mexican hat: equation (4.17).

This gives the familiar form of the Mexican hat potential surface as shown in figure 4.2, where the symmetry coordinates of the e_g vibration of an octahedral molecule are also given. A new electronic basis can be obtained from the eigenvectors of the diagonalisation:

$$\psi^+ = \sin\frac{\phi}{2} \, |\theta\rangle + \cos\frac{\phi}{2} \, |\varepsilon\rangle \qquad (4.14)$$
$$\psi^- = \cos\frac{\phi}{2} \, |\theta\rangle - \sin\frac{\phi}{2} \, |\varepsilon\rangle$$

The eigenvector matrix in (4.14) represents a similarity transform that converts the potential energy terms in the Hamiltonian (4.12) into diagonal form. This corresponds to a rotation of the electronic basis by $\phi/2$; or equivalently, a rotation of the electronic operators by ϕ (Rorison and O'Brien 1984). The two electronic wavefunctions ϕ^+, ϕ^- "belong" to the upper ε^+ and lower ε^- potential surfaces respectively. However if the linear coupling constant A_1 as defined by (4.6) and (4.7), is negative then this order is reversed and ψ^+ belongs to the lower surface (Ham 1972 pg25; Reinen and Friebel 1979, pg6).

4.2.2 The Warping Terms: Second Order Coupling and Anharmonicity.

It is well known that this Mexican hat potential surface shows a higher symmetry than the C_{3v} factor group of the vibronic space indicates (Bersuker and Polinger 1982; O'Brien 1984). This results in the artificial degeneracy of the A_1, A_2 vibronic states. The inclusion of higher order terms in the potential will remove these artificial degeneracies, and the resulting Hamiltonian is then given by:

$$| \, H - \varepsilon I \, | = 0 \qquad (4.15)$$

where $\quad H = H_o + H_{JT}$

$$H_o = [\, \tfrac{1}{2}K_2(Q_\theta^2 + Q_\theta^2) + K_3 Q_\theta (Q_\theta^2 - 3Q_\varepsilon^2) \,] \begin{pmatrix} 1 & 0 \\ 0 & 1 \end{pmatrix}$$

$$H_{JT} = [A_1 Q_\theta - A_2(Q_\theta^2 - Q_\varepsilon^2)] \begin{pmatrix} -1 & 0 \\ 0 & 1 \end{pmatrix} + [A_1 Q_\varepsilon + 2A_2 Q_\theta Q_\varepsilon] \begin{pmatrix} 0 & 1 \\ 1 & 0 \end{pmatrix}$$

Equation (4.15) can be rewritten by changing to polar coordinates:

$$H_o = [\, \tfrac{1}{2}K_2\rho^2 + K_3\rho^3\cos 3\phi \,] \begin{pmatrix} 1 & 0 \\ 0 & 1 \end{pmatrix} \qquad (4.16)$$

(4.8)
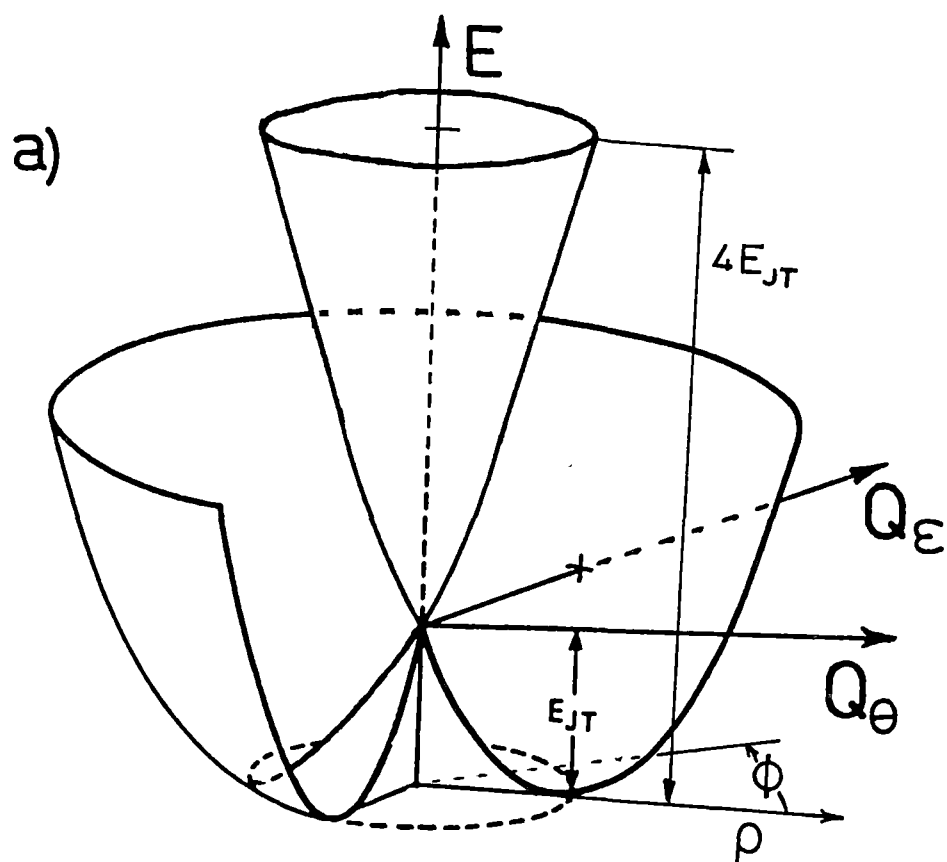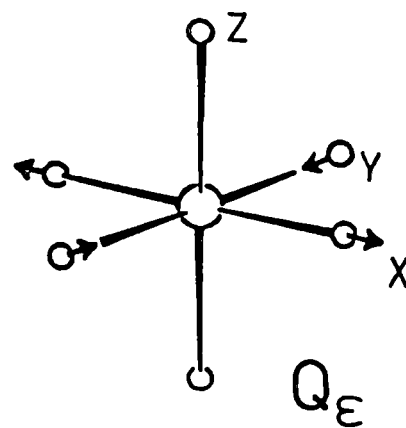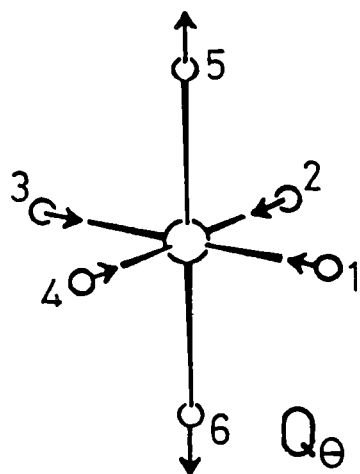
Figure 4.2 a) The cartesian and polar coordinates of the Mexican hat.
b) The symmetry coordinates of the e_g vibration in an octahedral molecule.

$$H_{JT} = [A_1\rho\cos\phi + A_2\rho^2\cos2\phi]\begin{bmatrix} -1 & 0 \\ 0 & 1 \end{bmatrix} + [A_1\rho\sin\phi + A_2\rho^2\sin2\phi]\begin{bmatrix} 0 & 1 \\ 1 & 0 \end{bmatrix}$$

Diagonalisation of the secular equation will give the adiabatic potential surfaces:

$$\epsilon^{\pm} = \frac{1}{2}K_2\rho^2 + K_3\rho^3\cos3\phi \pm \rho[\ A_1^2 + A_2^2\rho^2 - 2A_1A_2\rho\cos3\phi\ ]^{1/2} \qquad (4.17)$$

and the wavefunctions:

$$\psi^+ = \sin(\tfrac{z}{2})\ |\theta> + \cos(\tfrac{z}{2})\ |\epsilon> \qquad (4.18)$$

$$\psi^- = \cos(\tfrac{z}{2})\ |\theta> - \sin(\tfrac{z}{2})\ |\epsilon>$$

As noted by Bersuker (1975; pg367), $z \neq \phi$ unless A_2 is zero:

$$z = \tan^{-1}\left(\frac{A_1\sin\phi + A_2\rho\sin2\phi}{A_1\cos\phi - A_2\rho\cos2\phi}\right) \qquad (4.19)$$

Equations (4.17) and (4.19) have differing signs to those given by Bersuker (1975, pg 367) and Bersuker (1984a, pg47). This is due to the different phase conventions that have been used and will be discussed in section 4.2.4.

The lower adiabatic potential surface of (4.17) is shown in figure 4.3a. It can be seen that the potential surface now has the full C_{3v} symmetry required. It is noted here that anharmonic, K_3, and the second order coupling, A_2, terms have the same qualitative effect of warping the potential surface so that three minima result. If the Hamiltonian in (4.15) is transformed by the similarity transform of the linear case (4.14), then the diagonal warping terms are:

$$V_W(\rho,\phi) = (-K_3\rho^3 \pm A_2\rho^2)\ \cos3\phi \qquad (4.20)$$

If the off-diagonal terms are ignored and the radial coordinate ρ is replaced by the minimum of the Mexican hat potential ρ_0, then (4.20) becomes (Bill 1984, pg718):

$$V_W(\phi) \sim \beta\cos3\phi, \quad \beta = -K_3\rho_0^3 \pm A_2\rho_0^2, \quad \rho_0 = A_1/K_2 \qquad (4.21)$$
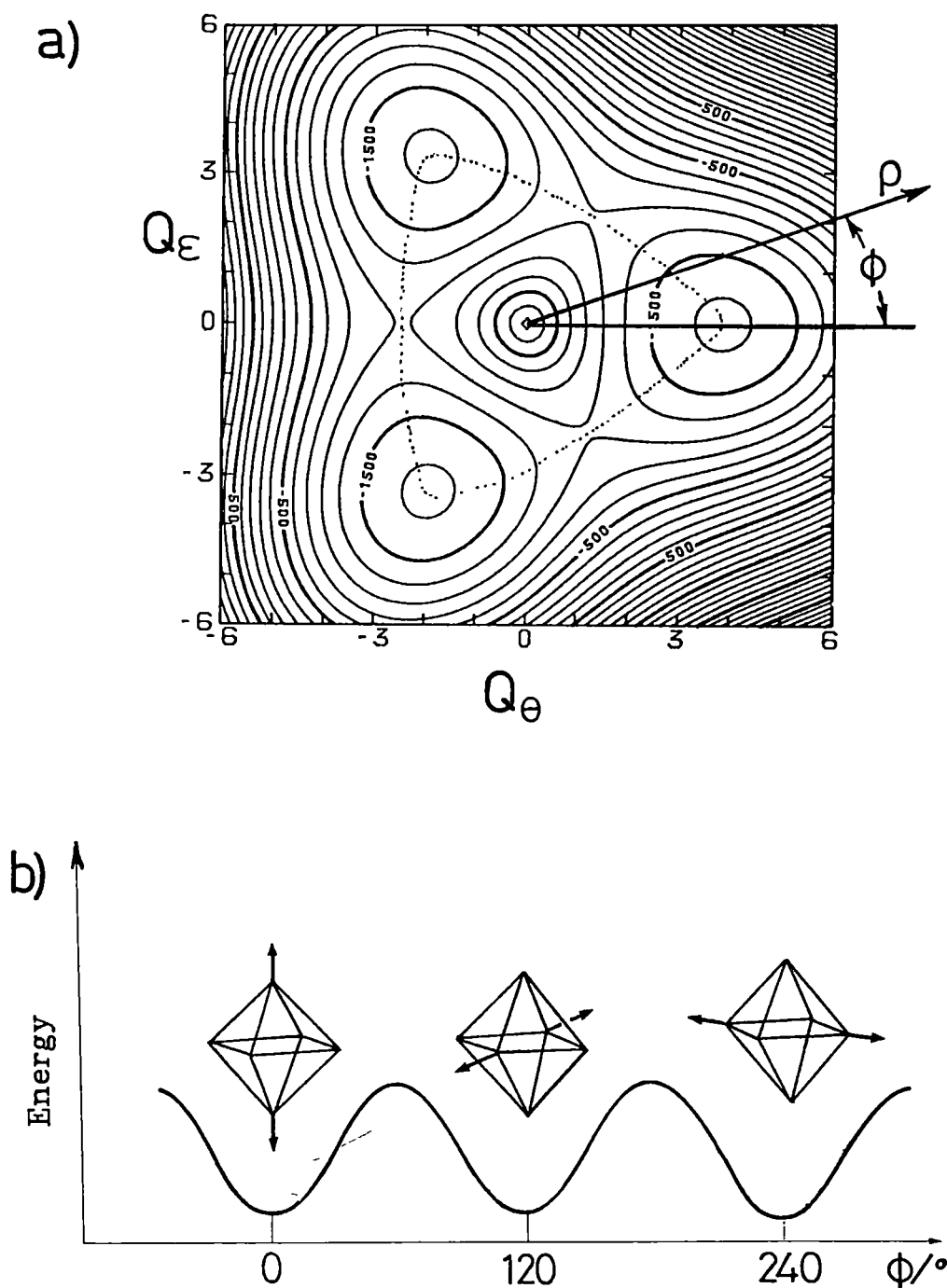
Figure 4.3 The lower adiabatic surface of the warped Mexican hat potential.
a) Contour plot of equation (4.17), using the parameters:

$K_2 = 300cm^{-1}$, $A_1 = 900cm^{-1}$, $A_2 = 33.33cm^{-1}$ ($\beta = 300cm^{-1}$).

b) Angular potential along the path of least energy (dotted line in a).
The minima correspond to tetragonally elongated geometries.

The positive sign in front of A_2 in (4.21) is appropriate for Cu(II) complexes. The barrier height between the three equivalent wells is then approximately 2β, although, it should be noted that the least energetic path between the minima is far from circular (figure 4.3a) as implied from setting $\rho = \rho_0$ in (4.21). Figure 4.3b shows that the movement along the angular coordinate causes linear combinations of the e_g vibrational components in figure 4.2 that result in a pseudo-rotation motion of the molecule through the three possible tetragonal elongations.

The octahedral Cu^{2+} ion is most often found in a tetragonal elongated geometry, as in the three minima shown in figure 4.1c. These minima result at an elongated geometry for $K_3 < 0$ (as expected for a bond stretch cubic anharmonicity) or $A_2 > 0$ when the two effects are considered separately in (4.21). A mixture of these and other factors (Deeth and Hitchman 1986) will be probably be physically responsible for the warping, although it is usual to set $K_3 = 0$ as it causes computational difficulties (O'Brien 1981; pg342). Figure 4.4 shows the effect that even quite a small anharmonicity has on the potential surfaces at large values of ρ. As discussed in section 2.2, this sort of dissociative potential will cause erroneous results in a variational calculation. The second order coupling constant can be used to warp the potential without causing it to turn over, as long as:

$$|A_2| < \frac{1}{2} K_2 \tag{4.22}$$

An additional difference between the anharmonic and second order coupling terms is the effect it has on the energy separation of the lower and upper adiabatic surfaces shown in figure 4.2. From (4.17), the warping due to the anharmonic terms is the same in both lower and upper surfaces and their separation is $4E_{JT}$. For second order coupling, however, this warping is out of phase and the energy separation becomes $4E_{JT} + 2\beta$.

4.2.3 The Strain Terms: Systems of Lower than Cubic Symmetry.

It has been appreciated for some time that the effects of even small random crystal strains can be very large on the wavefunctions in the cubic Exe case (Ham 1972). The "strain" that is to be considered in the experimental examples of the following chapters is large and in
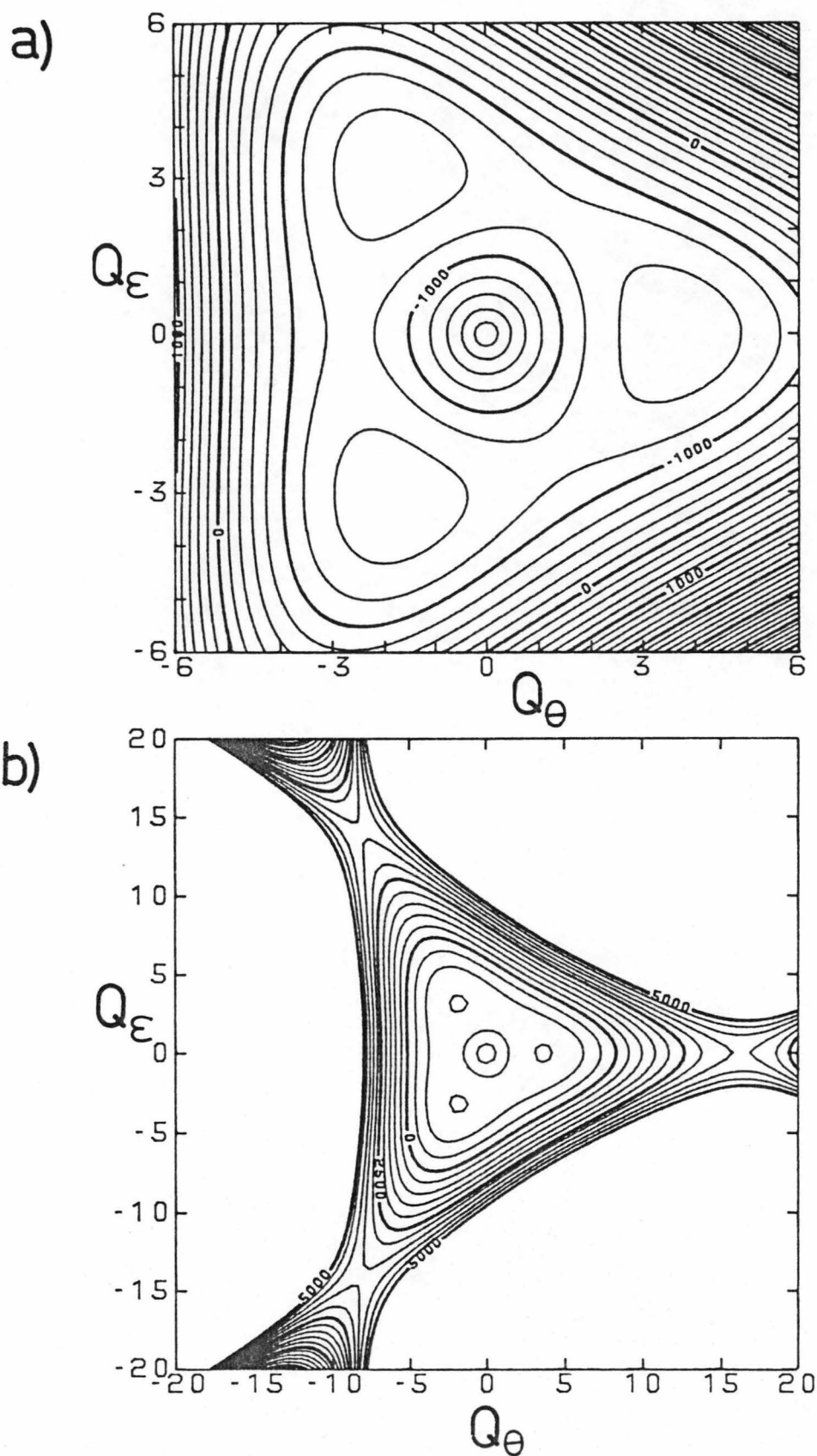
Figure 4.4 The effect of anharmonicity on the lower adiabatic potential. Potential parameters: $K_2 = 300cm^{-1}$, $A_1 = 900cm^{-1}$, $K_3 = -5cm^{-1}$ ($\beta = 135cm^{-1}$). a) Three equivalent minima; b) Dissociative channels at higher values of ρ.

well defined directions, formally reducing the problem to one of lower than cubic symmetry. These low symmetry terms are called strain terms because the formalism is similar to that of small strain terms in the cubic case. The origin of these strain terms need not be considered here, but they can either be due to the low symmetry of a host lattice, or to the different bonding characteristics of inequivalent ligands.

The E×e problem is reduced to a (A+A)×(a+a) problem for a general strain in the Q_θ-Q_ε plane. In terms of the cubic electronic basis functions, the strain Hamiltonian is given by (Ham 1972, pg21):

$$H_{ST} = \begin{bmatrix} -S_\theta & S_\varepsilon \\ S_\varepsilon & S_\theta \end{bmatrix} \qquad (4.23)$$

Here S_θ, S_ε are the tetragonal and orthorhombic components of the strain respectively and can be expressed as:

$$S_\theta = S \cos\phi_S \qquad (4.24)$$
$$S_\varepsilon = S \sin\phi_S$$

where S, ϕ_S are the magnitude and direction of the strain respectively in the Q_θ- Q_ε plane.

The $|\theta\rangle$, $|\varepsilon\rangle$ electronic basis functions will transform as A_1 and B_1 in tetragonal symmetry, and as A and A in orthorhombic symmetry. From group theory, considering the possible first order coupling constants in (4.9), there will be three independent non-zero values in tetragonal symmetry, and six in orthorhombic symmetry. For the second order coupling constants the number of independent non-zero constants becomes five and nine respectively. In addition to this, the problem will also require more harmonic and anharmonic force constants to describe the now non-degenerate vibrational modes. In general it would be impossible to find a unique set of these parameters by fitting experimental data.

Feiner (1981) has argued that a similarity transform can remove the orthorhombic component of the strain, thus reducing the number of independent parameters. However his argument is strictly incorrect as the kinetic energy operators are neglected in the total Hamiltonian. Such a similarity transform, while removing the orthorhombic strain, will produce additional off-diagonal terms from the kinetic energy operator. The arises from the fact that the kinetic energy operators do not commute with rotations in the Q_θ-Q_ε plane (section 4.3.1). The effect of these additional off-diagonal terms will be small if the

orthorhombic component of the strain is small compared to the tetragonal component, but even in tetragonal symmetry the problem is over parameterised.

The most useful simplification that can be made in low symmetry problems is to assume that the strain terms are sufficiently small that H_{ST} can be considered as a perturbation on the cubic Hamiltonian (4.15). This seems to be the only feasible approach to such an over-parameterised problem, and has been previously adopted by Feiner (1981), although he considered only tetragonal strain with first order coupling. Including the kinetic energy operator, the most general form of the Exe Hamiltonian then becomes:

$$H = H_o + H_{JT} + H_{ST} \qquad (4.25)$$

$$H_o = [\frac{K_2}{2} (P_\theta^2 + P_\varepsilon^2 + Q_\theta^2 + Q_\varepsilon^2) + K_3 Q_\theta (Q_\theta^2 - 3Q_\varepsilon^2)] I$$

$$H_{JT} = - [A_1 Q_\theta - A_2 (Q_\theta^2 - Q_\varepsilon^2)] \sigma_z + [A_1 Q_\varepsilon + 2A_2 Q_\theta Q_\varepsilon] \sigma_x$$

$$H_{ST} = -S_\theta \sigma_z + S_\varepsilon \sigma_x$$

$$P_\theta^2 = - \frac{\partial^2}{\partial Q_\theta^2} , \quad P_\varepsilon^2 = - \frac{\partial^2}{\partial Q_\varepsilon^2}$$

4.2.4 A Respite: Phase Conventions.

It is often confusing to find in the literature that different signs are often used in the expressions given in the previous sections for the coupling constants, adiabatic potentials and wavefunctions. Up to this point, the choice has been made to be consistent with the phase conventions in Koster etal (1963). This means that the cubic Hamiltonian in (4.15) is identical to that given by: A&B (equations 21.39,43,44); Ham (1972, equations 2.2.1,6,7); Bill (1984 equation 1); Bersuker and Polinger (1984, equations 37,41). The adiabatic potential and wavefunctions also agree with the above workers with the exception of Bersuker and Polinger (1984) where the third term on the RHS of their equation 53 should be negative as in (4.17).

Note that these conventions are different from those used by the often cited references O'Brien (1964) and Bersuker (1984a). This

discrepancy arises because they have defined the first order coupling constants $A_1 = - \langle \theta | \frac{\partial V}{\partial Q_\theta} | \theta \rangle$ rather than that given in (4.10). [In addition the O'Brien (1964) Hamiltonian operates on the electronic basis ($| \varepsilon \rangle$, $| \theta \rangle$) rather than the usual ($| \theta \rangle$, $| \varepsilon \rangle$) basis.] These authors have later (see Rorison and O'Brien (1984), Bersuker and Polinger (1984)) conformed with the usual convention.

The sign of the linear coupling constant will affect the signs in both the adiabatic potentials and wavefunctions. For example, compare Bersuker (1984a) equations 2.5, 2.12 with the equations (4-.17), (4.19) given earlier. However, it is important to realise that with these standard conventions, the sign of the linear coupling constant in the case of octahedral copper(II) is negative. This has been pointed out by Abragam and Bleaney (1970, p806-7), Setser etal (1975, tableII) and Reinen and Friebel (1979, pg6).

However, in the literature, the vast majority of the Jahn-Teller studies of octahedral Cu(II) complexes have defined the first order coupling constant to take positive values. Since the theory outlined in this chapter is to be applied to such complexes, the linear coupling constant will also be be defined positive. Similarly, since the $| \theta \rangle$, $| \varepsilon \rangle$ electronic states are hole functions in Cu(II), the strain terms will also take the opposite sign. The most general vibronic Hamiltonian to be considered in this thesis is then given by:

$$H = H_o + H_{JT} + H_{ST} \qquad (4.26)$$

$$H_o = [\frac{K_2}{2}(P_\theta^2 + P_\varepsilon^2 + Q_\theta^2 + Q_\varepsilon^2) + K_3 Q_\theta (Q_\theta^2 - 3Q_\varepsilon^2)] \; \mathbf{I}$$

$$H_{JT} = [A_1 Q_\theta + A_2 (Q_\theta^2 - Q_\varepsilon^2)] \, \sigma_z - [A_1 Q_\varepsilon - 2A_2 Q_\theta Q_\varepsilon] \, \sigma_x$$

$$H_{ST} = S_\theta \sigma_z - S_\varepsilon \sigma_x$$

The adiabatic potentials cartesian and polar coordinates are:

$$\varepsilon^{\pm} = \frac{K_2}{2}(Q_\theta^2 + Q_\varepsilon^2) + K_3 Q_\theta (Q_\theta^2 - 3Q_\varepsilon^2) \qquad (4.27)$$

$$\pm [\; (A_1 Q_\theta + A_2 (Q_\theta^2 - Q_\varepsilon^2) + S_\theta)^2 + (A_1 Q_\varepsilon - 2A_2 Q_\theta Q_\varepsilon + S_\varepsilon)^2 \;]^{1/2}$$

(4.13)

$$= \frac{K_2}{2}\rho^2 + K_3\rho^3\cos3\phi \pm [\ A_1^2\rho^2 + A_2^2\rho^4 + S^2 + 2A_1A_2\rho^3\cos3\phi$$

$$+ 2SA_1\rho\cos(\phi-\phi_s) + 2SA_2\rho^2\cos(2\phi+\phi_s)\ ]^{1/2}$$

The adiabatic wavefunctions are now:

$$\begin{bmatrix} \psi^+ \\ \psi^- \end{bmatrix} = \begin{bmatrix} \cos(z/2)\ |\theta> - \sin(z/2)\ |\epsilon> \\ \sin(z/2)\ |\theta> + \cos(z/2)\ |\epsilon> \end{bmatrix} \qquad (4.28)$$

$$\tan z = [(A_1\rho\sin\phi - A_2\rho^2\sin2\phi + S_\epsilon)\ /\ (A_1\rho\cos\phi + A_2\rho^2\cos2\phi + S_\theta)]$$

In (4.28) the adiabatic wavefunction ψ^- corresponds to the lower adiabatic potential ϵ^-. The above three equations are to be used throughout the remainder of the thesis. Only the vibronic Hamiltonian in (4.26) is really needed in the numerical solution of the system, although equations (4.27) and (4.28) are useful when considering the problem from a static point of view.

(4.14)

4.3 DYNAMIC VIEWPOINT: THE KINETIC ENERGY OPERATOR

When the kinetic energy operator in (4.26) is taken into account, the system is no longer treated as static as in the previous section, but is now called the dynamic Jahn-Teller effect. This is not simply a study of hopping between static distortions, but rather the numerical solution of the secular equation of the vibronic Hamiltonian. This results in discrete energy levels and vibronic wavefunctions where the electronic and vibrational parts are mixed such that it is impossible to express them as an adiabatic product.

The adiabatic potentials in the previous section were found by diagonalising the 2x2 electronic secular equation via a similarity transform to form uncoupled potential surfaces. If this is attempted when the kinetic energy operator is included, one find that the secular equation cannot be made diagonal. The dynamic Jahn-Teller effect can then best be described by a pair of coupled (second order differential) equations, and the resulting vibronic wavefunctions cannot be said to be associated with only one potential surface.

However, if there is strong Jahn-Teller coupling so that the adiabatic potential surfaces are well separated, then the coupling between these surfaces is small and the adiabatic approximation can approximately be recovered by using a wavefunction that varies with the nuclear geometry. That is, the vibronic wavefunction can approximately be written as a single adiabatic product as in (1.3):

$$\Omega^- = \Psi^- . \Phi^-$$
(4.29)

where the electronic part of the wavefunction Ψ^- is given by (4.28). However, an exact solution requires the coupled equations to be solve numerically, and the vibronic wavefunctions are then expressed as linear combinations of two adiabatic products:

$$\Omega = |\theta>.\Phi_\theta + |\varepsilon>.\Phi_\varepsilon$$
(4.30)

4.3.1 The Effect on the Adiabatic Potentials.

The effect that the kinetic energy operator has on the adiabatic potentials can best be illustrated by considering the linear case of equation (4.12). Including the kinetic energy operator and expressed

in polar coordinates, the Hamiltonian becomes (Rorison and O'Brien 1984):

$$H = H_o + H_{JT}$$ (4.31)

$$H_o = -\frac{1}{2}\left(\frac{\partial^2}{\partial\rho^2} + \frac{1}{\rho}\frac{\partial}{\partial\rho} + \frac{1}{\rho^2}\frac{\partial^2}{\partial\phi^2} - \rho^2\right)\begin{bmatrix} 1 & 0 \\ 0 & 1 \end{bmatrix}$$

$$H_{JT} = A_1\begin{bmatrix} -\rho\cos\phi & \rho\sin\phi \\ \rho\sin\phi & \rho\cos\phi \end{bmatrix}$$

acting on the electronic basis $\begin{pmatrix} |\theta\rangle \\ |\varepsilon\rangle \end{pmatrix}$.

Applying the similarity transform given by (4.14) to (4.31) one finds:

$$H' = SHS^{-1}$$ (4.32)

$$= H_o + A_1\rho\begin{bmatrix} -1 & 0 \\ 0 & 1 \end{bmatrix} + \frac{1}{2\rho^2}\begin{bmatrix} \frac{1}{4} & -\frac{\partial}{\partial\phi} \\ \frac{\partial}{\partial\phi} & \frac{1}{4} \end{bmatrix}$$

which acts on $\psi' = S\psi$.

$$\psi' = \begin{bmatrix} \psi^+ \\ \psi^- \end{bmatrix} = \begin{bmatrix} \sin(\frac{\phi}{2})|\theta\rangle + \cos(\frac{\phi}{2})|\varepsilon\rangle \\ \cos(\frac{\phi}{2})|\theta\rangle - \sin(\frac{\phi}{2})|\varepsilon\rangle \end{bmatrix}$$ (4.33)

The important point to note about equation (4.33) is that, while the linear Jahn-Teller coupling terms are made diagonal, additional off-diagonal terms appear from the kinetic energy operator. This arises from the fact that the kinetic energy operator does not commute with the trigonometric terms in the similarity transform (4.32). For example $[\partial^2/\partial\phi^2, \cos(\frac{\phi}{2})] = \partial^2/\partial\phi^2 \cos(\frac{\phi}{2}) - \cos(\frac{\phi}{2}) \neq 0$.

The effect of these additional terms can best be illustrated by a plot of the adiabatic potentials. These plots ignore any off-diagonal terms, so it should be realised that the resulting surfaces are still coupled. A plot of the diagonal terms of (4.31) before the similarity transform are shown in figure 4.5a. These are sometimes called "diabatic" potential surfaces (Thompson etal 1985). A plot of the adiabatic potentials after the similarity transform, but ignoring the last term in (4.33) which arises from the kinetic energy operator,

(4.16)
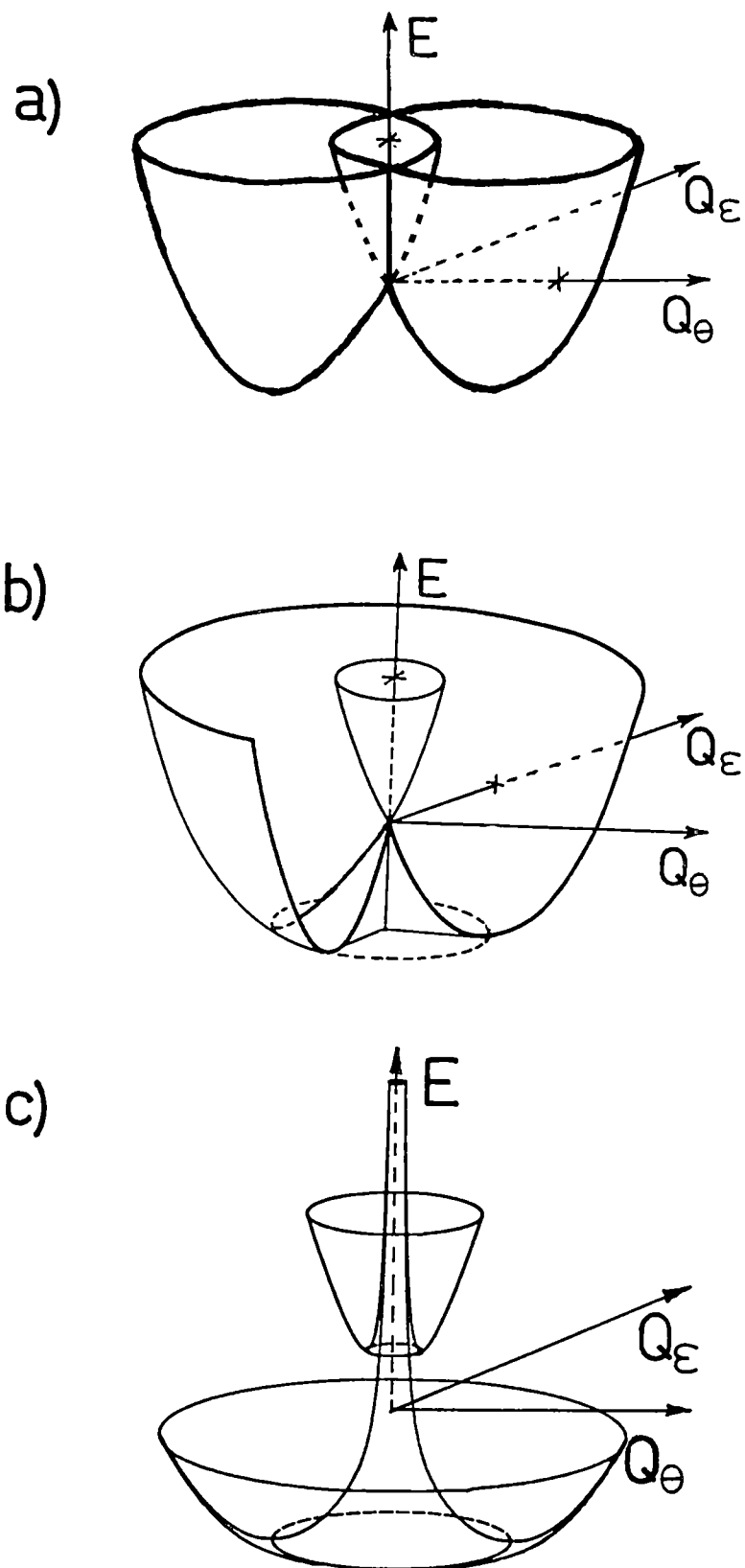
Figure 4.5 The (E⊗e) Jahn-Teller potentials with linear coupling.
a) The diabatic surfaces: the diagonal terms of the potential energy operator before the similarity transform.
b) The adiabatic surfaces: the diagonal terms of the potential energy operator after the similarity transform.
c) As in b), but including the potential terms due to the kinetic energy operator after the similarity transform.

results in the popular "Mexican hat" potential shown in figure 4.5b. A plot of the adiabatic potentials including all the diagonal terms in (4.33) is shown in figure 4.5c. The ρ^{-2} term causes the potentials to become infinite at the high symmetry configuration, thus illustrating the origin of objection 1) in section 4.1. The study of Thompson etal (1985) has shown that the vibronic wavefunctions passed through this point of singularity "unharmed", clearly contrary to what would be expected for a classical particle on the potential. This singular potential also illustrates the "centrifugally stabilised Slonczewski resonances" (Slonczewski 1963; Englman 1972, pp30-2), where metastable states are proposed for the upper potential surface.

It is a moot point as to which of the three potentials in figure 4.5 is the most "real", as they all neglect an invisible (unplottable) off-diagonal term. In an interesting study by Thompson etal (1985), the Hamiltonians corresponding to all three of these potentials were solved numerically and compared with the exact values. Their results showed that the third potential shown in figure 4.5c gives results closest to the exact values, and in this sense this potential with a singularity could be said to be more realistic than the usual "Mexican hat" potential. Further comments have been made by Perlin and Wagner (1984, pp12-18).

4.3.2 The Nature of the Problem.

In the most general form of the E×e Jahn-Teller Hamiltonian considered here the Hamiltonian in (4.26) must be solved. This represents a system of two coupled equations:

$$(H_{\theta\theta} - E)\Phi_\theta(Q) + H_{\theta\varepsilon}\Phi_\varepsilon(Q) = 0 \qquad (4.34)$$
$$H_{\varepsilon\theta}\Phi_\theta(Q) + (H_{\varepsilon\varepsilon} - E)\Phi_\varepsilon(Q) = 0$$

To solve equation (4.34), the vibrational part of the wavefunctions Φ_θ, Φ_ε that are based on the $|\theta\rangle$, $|\varepsilon\rangle$ electronic states respectively, are expanded in a series of N/2 basis functions. Equation (4.34) then becomes a large (N×N) secular equation in the N dimensional vibronic space. This secular equation can then be diagonalised numerically resulting in the vibronic eigenvalues and eigenfunctions. A brief description of how this is done is given in the following section.

4.4 THE CALCULATION

4.4.1 Basis Functions and Basis Size.

The vibronic basis functions for the solution of the $E \times e$ Jahn-Teller problem can be written as

$$|\lambda \, m \, n\rangle = |\lambda\rangle|m\rangle|n\rangle \qquad (4.35)$$

where $\lambda = \theta, \varepsilon$ represents the electronic wavefunctions and m, n are the quantum numbers for a two dimensional harmonic oscillator basis expressed as a product of two one dimensional SHO's. This vibrational basis was chosen rather than the two dimensional SHO functions expressed in polar coordinates because it is more straightforward to evaluate the matrix elements in this basis. [However, see Rorison and O'Brien 1984.]

The pth vibrational level of a two dimensional HO has a degeneracy of (p+1) functions: $|p\rangle|0\rangle$, $|p-1\rangle|1\rangle$, ... $|1\rangle|p-1\rangle$, $|0\rangle|p\rangle$. When n_v of the vibrational levels are included in both the electronic components of the basis, the total basis size of the vibronic functions is given by:

$$N = \sum_{p=0}^{n_v} 2(p+1) = (n_v+1)(n_v+2) \qquad (4.36)$$

An estimate of the number of vibrational levels that need to be included in the vibronic basis can be achieved using classical arguments. For example, the lowest vibronic wavefunction may be centred on the trough, $\rho_0 = 3$, of a Jahn-Teller surface, but could extend as far as $\rho = 4$. It is then necessary that the basis functions, from which this wavefunction is constructed, should also extend at least this far. If this extension is connected with the root-mean-square amplitude of the vibrational basis then the following equation can be used as a guideline.

$$n_v = (\rho_0 + 1)^2 - 1 \qquad (4.37)$$

Here ρ_0 is the Jahn-Teller radius expressed in dimensionless units as in equation (4.22). For $\rho_0 = 4$, a value typical of strong Jahn-Teller coupling, then $n_v = 24$ and the total basis size is N = 650. If higher vibronic levels are required then a larger basis must be used.

(4.18)

Equation (4.37) should only be used as a rough guide, the best way of to tell if the basis is large enough is to examine the eigenvalues as the basis size is increased. The eigenvalues will then converge to a constant value (from above), however it should noted that the eigenvalues are known to converge more quickly than eigenvectors (Barentzen etal 1981, section 4). Adler-Golden (1985) has used the more sophisticated approach of using semi-classical trajectories to determine a minimum basis size which can then have both an upper and lower cutoff. This approach has not been used here as it means that the calculated eigenvalues are not necessarily always an upper limit to the true eigenvalues, making it difficult to determine a convergence criteria.

Another common method of reducing the basis size necessary in a variational calculation is to scale the basis functions. However, it can be shown using the methods of Balsa etal (1983) that this approach cannot be applied to Jahn-Teller systems, as the linear term is dominant in the potential. A shift in the origin, which would be an obvious simplification in the case of a non-degenerate electronic state, will not be helpful in the present case unless a large strain is present, and such a case is considered in the following section.

4.4.2 Redefining the Origin.

A shift in the origin of the vibronic basis functions will only be advantageous when the strain strongly localises the wavefunctions of interest near a particular minimum. If this is the case, then these wavefunctions will converge with a smaller basis; however, for higher avefunctions that are delocalised, the convergence will become much slower than if the basis functions at the undistorted geometry were used. If a large enough basis size is used, the calculation will give identical results for the basis functions based on any origin.

In the present case the change in origin has been restricted to lie along the tetragonal coordinate only, as in the cases to be studied, it is the tetragonal strain that dominates the potential surface. The shift of the origin along the orthorhombic coordinate also causes an added complication as it not only changes the coefficients in the Hamiltonian (4.26), but also causes new terms to appear.

(4.19)

Making the following coordinate change:

$$Q'_\theta = Q_\theta - Q^o_\theta \qquad (4.38)$$

$$Q'_\varepsilon = Q_\varepsilon$$

the Hamiltonian in (4.26) can then be rewritten as:

$$\begin{vmatrix} H_{\theta\theta} & H_{\theta\varepsilon} \\ H_{\varepsilon\theta} & H_{\varepsilon\varepsilon} \end{vmatrix} \qquad \begin{aligned} H_{\theta\theta} &= H_o + AA0 + AA1 Q'_\theta + AA2(Q'^2_\theta - Q'^2_\varepsilon) \qquad (4.39) \\ H_{\varepsilon\varepsilon} &= H_o + BB0 + BB1 Q'_\theta + BB2(Q'^2_\theta - Q'^2_\varepsilon) \\ H_{\theta\varepsilon} &= H_{\varepsilon\theta} = AB0 + AB1 Q'_\varepsilon + AB2 Q'_\theta Q'_\varepsilon \end{aligned}$$

Here H_o is given in (4.26) and the coefficients take the values given in table 4.1 when the origin is either at the undistorted $(0, 0)$ or tetragonal $(Q^o_\theta, 0)$ geometry. Note that the vibrational part of the Hamiltonian, H_o, is the same as when the origin is not shifted, and the kinetic energy operator is not effected by a shift in the origin (Schiff 1968, pg191).

Table 4.1 Coefficients of Equation (4.39).

ORIGIN	$(0, 0)$	$(Q^o_\theta, 0)$
AA0	S_θ	$S_\theta + A_1 Q_o + (\frac{1}{2}K_2 + A_2)Q^2_o + K_3 Q^3_o$
AA1	A_1	$A_1 + (K_2 + 2A_2)Q_o + 3K_3 Q^2_o$
AA2	A_2	$A_2 + 3K_3 Q_o$
BB0	$-S_\theta$	$-S_\theta - A_1 Q_o + (\frac{1}{2}K_2 - A_2)Q^2_o + K_3 Q^3_o$
BB1	$-A_1$	$-A_1 + (K_2 - 2A_2)Q_o + 3K_3 Q^2_o$
BB2	$-A_2$	$-A_2 + 3K_3 Q_o$
AB0	$-S_\varepsilon$	$-S_\varepsilon$
AB1	$-A_1$	$-A_1 - 2A_2 Q_o$
AB2	$2A_2$	$2A_2$

4.4.3 The Secular Equation and Symmetry Blocking.

Since from (4.36) the problem involves the diagonalisation of large matrices, symmetry is used wherever possible to "uncouple" the matrix into diagonal blocks. For the case of linear Jahn-Teller coupling, Longuet-Higgins etal (1958) defined a good half-odd integral quantum number j, that allowed the secular equation of size N, to be

factored into $2(n_v + 1)$ separate blocks (figure 4.6a). Since all of the levels are doubly degenerate, only half of the number of functions in each block need be considered. For a particular value of j, the secular equation is a real tridiagonal symmetric matrix (Thompson etal 1985):

$$
\begin{vmatrix}
h\nu(j+1/2) & A_1\sqrt{(j+1/2)} & 0 & 0 & \cdots \\
A_1\sqrt{(j+1/2)} & h\nu(j+3/2) & -A_1\sqrt{1} & 0 & \cdots \\
0 & -A_1\sqrt{1} & h\nu(j+5/2) & A_1\sqrt{(j+3/2)} & 0 \\
0 & 0 & A_1\sqrt{(j+3/2)} & h\nu(j+7/2) & -A_1\sqrt{2} \\
\cdot & \cdot & & 0 & -A_1\sqrt{2} & h\nu(j+9/2)
\end{vmatrix}
\qquad (4.40)
$$

The fact that this can be done is due to the linear Hamiltonian having a symmetry that is higher than required by group theory (Rorison and O'Brien 1984). When warping terms are included, j ceases to be a good quantum number, and the vibronic wavefunctions are classified by the A_1, A_2 or E irreducible representations in the C_{3v} factor group. The warping terms also remove the artificial degeneracy of the A_1, A_2 levels that occurs in the linear case (O'Brien 1964), as shown in figure 4.14a.

The factor group reflects the symmetry of the potential surface and can be found by dividing the the molecules point group by the kernal symmetry (Ceulemans etal 1984). The kernal symmetry is the first subgroup where all the Jahn-Teller active coordinates become totally symmetric. The symmetry of an octahedral complex in the Q_θ-Q_ε plane is O_h at the origin, D_{4h} along the Q_θ axis, and D_{2h} for any other position. The kernal symmetries are then D_{2h} or D_2 for an octahedral or tetrahedral molecule respectively. The factor group is then given by $O_h/D_{2h} = T_d/D_2 = C_{3v}$. Terms in the Hamiltonian also must transform as A_1, A_2 or E representations and so cannot mix states of different symmetry. With appropriate symmetry adapted basis functions the NxN secular equation can then be factored into one of size N/2 and two of size N/4.

If the symmetry of the system is lowered by tetragonal strain then the factor group is $D_{4h}/D_{2h} = C_s$, again reflecting the symmetry of the potential surface. The vibronic wavefunctions can then be labelled as transforming as the A' or A'' representations and the secular equation can be divided into two blocks of half the original

(4.21)
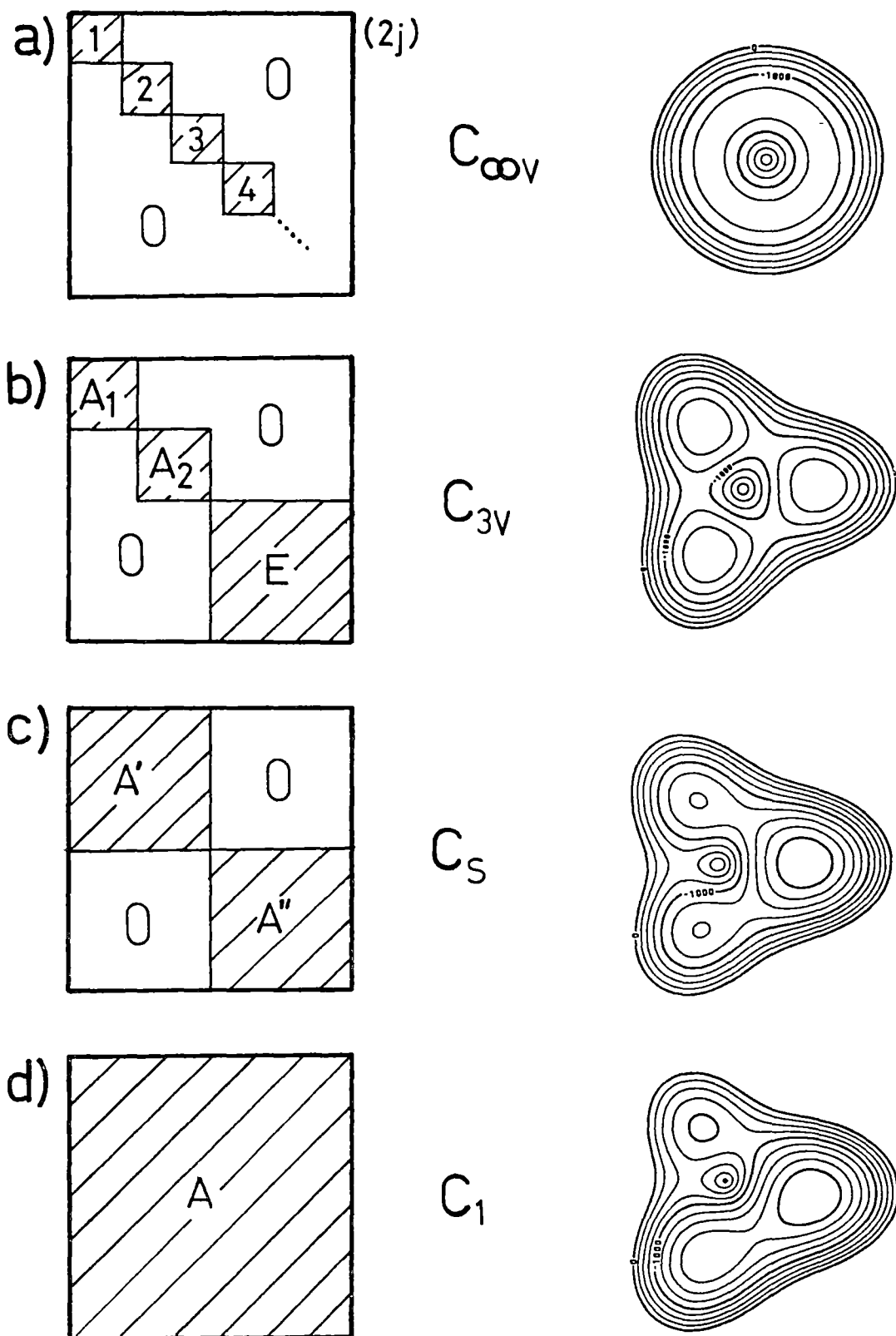
Figure 4.6 The factor group symmetry of the vibronic functions and the adiabatic potential surfaces:
a) Linear coupling; b) + Warping terms;
c) + Tetragonal strain; d) + Orthorhombic strain.

size. If the orthorhombic component of the strain is non-zero however, then the factor group is $D_{2h}/\ D_{2h}= C_1$. All vibronic wavefunctions will then transform as the same irreducible representation A. This means that all basis functions can be mixed and the secular equation cannot be factored. These four cases are illustrated schematically in figure 4.6, where the secular equation can be symmetry blocked in the factor group which is also isomorphic with the point group of the adiabatic potentials.

It remains to create symmetry adapted basis functions that transform as the irreducible representations of the vibronic states. For the important case of tetragonal strain, this can be done simply by reordering the basis functions already given in section 4.4.1. Simple symmetry considerations of the product functions (4.35) shows which will transform as A' or A''. An easy way to describe this is to give the values $\theta = 0;\ \varepsilon = 1$ for the electronic basis and then the following conditions apply:

$$\lambda \quad + \text{ n even } \quad \rightarrow \quad |\lambda mn\rangle \text{ transforms as A'} \qquad (4.41)$$

$$\lambda \quad + \text{ n odd } \quad \rightarrow \quad |\lambda mn\rangle \text{ transforms as A''.}$$

4.4.4 Matrix Elements and Diagonalisation.

The actual implementation of a computer program to solve a variational problem must do two main things: calculate the matrix elements of the vibronic Hamiltonian, and diagonalise the resulting secular equation. This section briefly describes the Fortran 77 program JTVIB which was written to solve the general (Exe) vibronic Hamiltonian of equation (4.26).

The vibrational part of the basis has been chosen as a product of one dimensional harmonic oscillator basis functions due to the ease with which the matrix elements can be calculated. These matrix elements are simply the product of the one dimensional matrix elements given by the explicit expressions in table 2.A1. For example, the anharmonic term in (4.26) between $|001\rangle$ and $|011\rangle$ is given by:

$$\langle 001| \ K_3 Q_\theta (Q_\theta^2 - 3Q_\varepsilon^2) \ |011\rangle = K_3 (\langle 0|Q_\theta^3|1\rangle\langle 1|1\rangle - 3\langle 0|Q_\theta|1\rangle\langle 1|Q_\varepsilon^2|1\rangle)$$

$$= -3/\sqrt{2} \ K_3$$

This sort of calculation must be made for all terms in the Hamiltonian between all basis functions and a sample 6×6 portion of the secular equation is shown in table 4.2, although it should be

(4.22)

noted that in a typical calculation the secular equation will be of the order 1000×1000. It can be seen from table 4.2 that when $S_\varepsilon = 0$, the matrix can be split in half using the bases $|\theta00\rangle$, $|\theta10\rangle$ and $|\varepsilon01\rangle$ transforming as A' and $|\varepsilon00\rangle$, $|\varepsilon10\rangle$ and $|\theta01\rangle$ transforming as A'' in agreement with (4.41) . Matrices up to about 250×250 can be diagonalised by standard routines (Smith etal 1976), but for larger matrices problems are encountered with both storage requirements and processor time limitations.

Table 4.2 Sample Portion of the Secular Equation

	$\lvert\theta00\rangle$	$\lvert\varepsilon00\rangle$	$\lvert\theta10\rangle$	$\lvert\varepsilon10\rangle$	$\lvert\theta01\rangle$	$\lvert\varepsilon01\rangle$
$\langle\theta00\rvert$	$1+S_\theta$	$-S_\varepsilon$	$\frac{1}{\sqrt2}A_1$	0	0	$-\frac{1}{\sqrt2}A_1$
$\langle\varepsilon00\rvert$	$-S_\varepsilon$	$1-S_\theta$	0	$-\frac{1}{\sqrt2}A_1$	$-\frac{1}{\sqrt2}A_1$	0
$\langle\theta10\rvert$	$\frac{1}{\sqrt2}A_1$	0	$2+A_2+S_\theta$	$-S_\varepsilon$	0	A_2
$\langle\varepsilon10\rvert$	0	$-\frac{1}{\sqrt2}A_1$	$-S_\varepsilon$	$2-A_2-S_\theta$	A_2	0
$\langle\theta01\rvert$	0	$-\frac{1}{\sqrt2}A_1$	0	A_2	$2-A_2+S_\theta$	$-S_\varepsilon$
$\langle\varepsilon01\rvert$	$-\frac{1}{\sqrt2}A_1$	0	A_2	0	$-S_\varepsilon$	$2+A_2-S_\theta$

Condensed storage algorithms have been employed (Pissanetsky 1984, pp20-23,252) as most of the elements of large secular equation will be zero. These algorithms allow operations on the matrix where only the non-zero upper triangular elements are stored. The diagonalisation is performed by the Lanczos algorithm which is ideally suited for use with a matrix in condensed storage. The Lanczos algorithm has been discussed by many workers (Cullum and Willoughby 1981; Parlett 1980; Bjorck etal 1981), and the subroutines used in the present program were EA14ZD, EA14WD from the Harwell libraries (Parlett and Reid 1980). Minimal changes in common block storage and I/O format were made to enable to allow the routines to run on a FORTRAN 77 compiler. A random starting vector (O'Brien and Evangelou 1980) was used in the present case as there is little overlap of the lowest eigenvalues with the lowest basis functions for the case of strong linear coupling. With the program described above the lowest eigenvalues and eigenvectors of matrices of the order 4000×4000 could be obtained.

(4.23)

4.5 THE ANSWERS

4.5.1 The Energy Levels.

The energy levels of a E×e linear Jahn-Teller system are shown in figure 4.7 as a function of the first order coupling constant A_1. There are many interesting features in this figure. On the extreme left the energy levels are that of an unperturbed two dimensional harmonic oscillator; while on the extreme right, in the regime of strong linear coupling, the levels can be approximately described by radial and angular quantum numbers. In the intermediate region the energy levels are observed to undergo curious oscillations, a detailed section of this is shown in figure 4.8a. This nodal structure is unusual as the apparent degeneracies are in fact all "near misses" (Thorson and Moffitt 1968). This phenomena has lead to the discovery of isolated "exact" solutions for E×e coupling (Judd 1977; 1979), and in turn to an analytic formulation of the linear Jahn-Teller problem (Reik 1984; Reik and Doucha 1986).

The angular and radial type vibrational energy levels at the strong coupling end of figure 4.7 can be understood in terms of the adiabatic potential surfaces. The potential in the radial direction remains harmonic with the same curvature as the unperturbed case. The potential in the angular direction on the other hand is zero and the energy levels are determined solely by the kinetic energy operator in exactly the same manner as rotation energy levels are quantised. Using the radial and angular quantum numbers m and j, the energy levels are approximately given by (Longuet-Higgins etal 1958):

$$E(m,j) = -E_{JT} + (m + \tfrac{1}{2}) h\nu + \frac{h\nu}{2\rho_0^2} j^2; \quad E_{JT} = A_1^2/(2h\nu) \qquad (4.42)$$

This approximate formula is shown with the exact calculations in figure 4.8b, and the agreement at high coupling strengths shows how good this approximate description of independent radial and angular motions becomes.

At intermediate coupling strengths the spacing between levels of adjacent m quantum number are far from harmonic as shown in figure 4.9 and such irregular spacings have often been cited as evidence of the

(4.24)
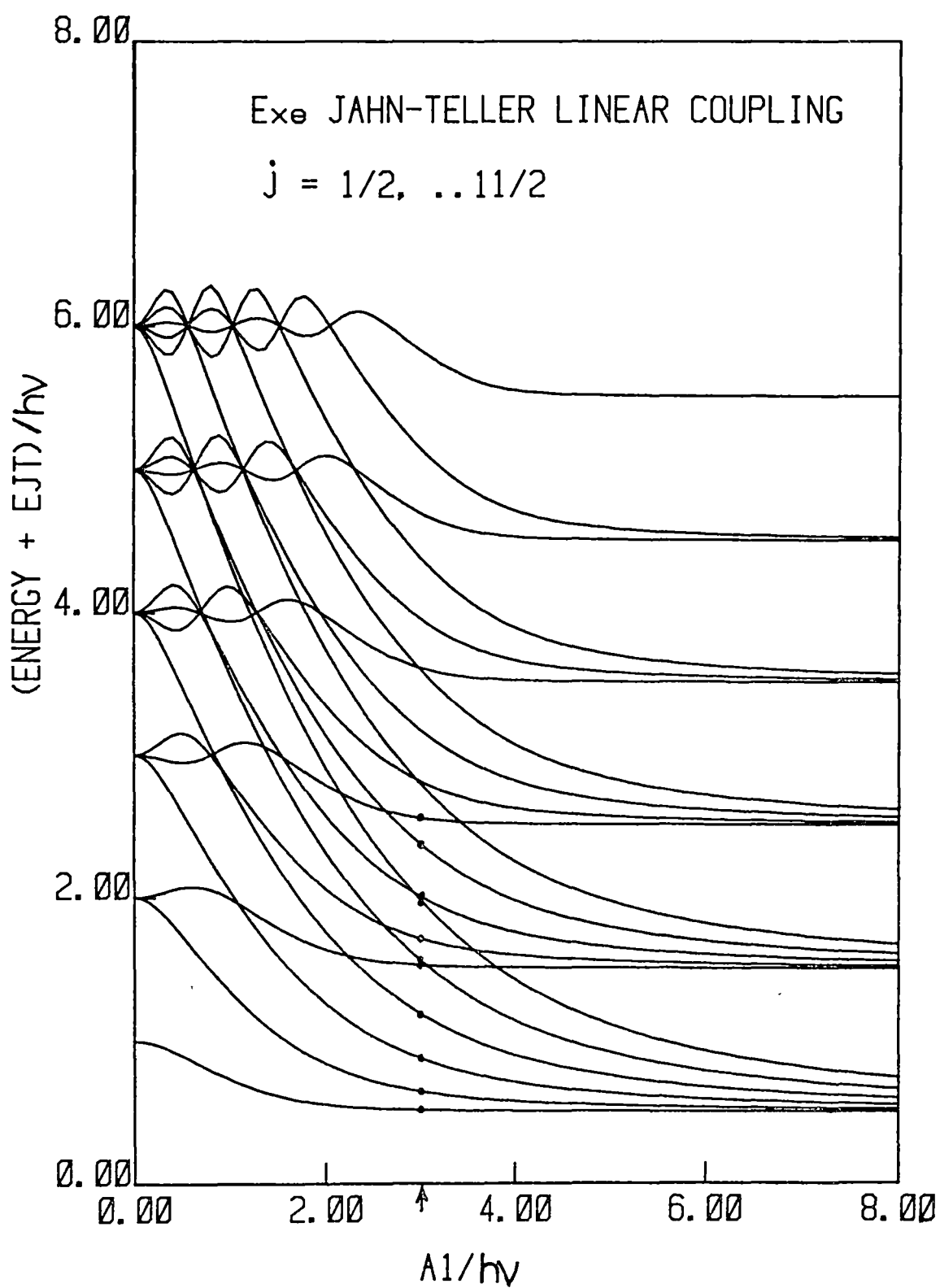
Figure 4.7 The E⊗e energy levels as a function of the linear coupling constant. The wavefunctions of the levels marked with a solid circle are shown in figures 4.11, 4.12.
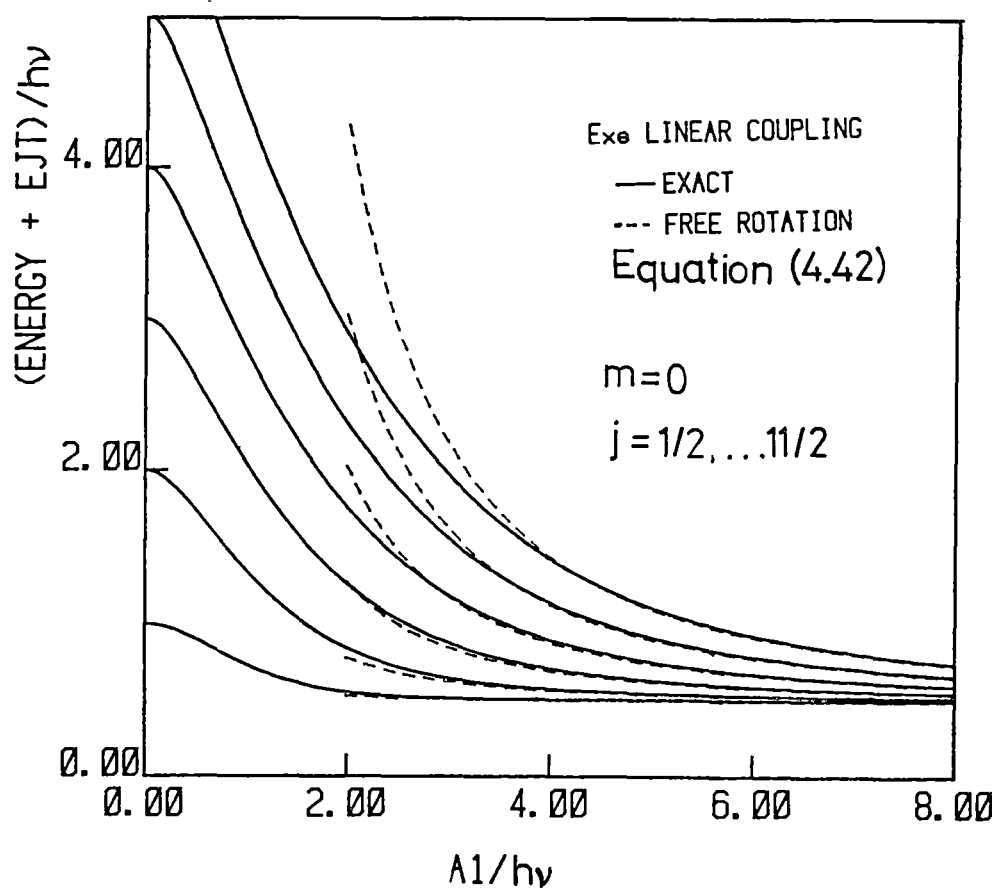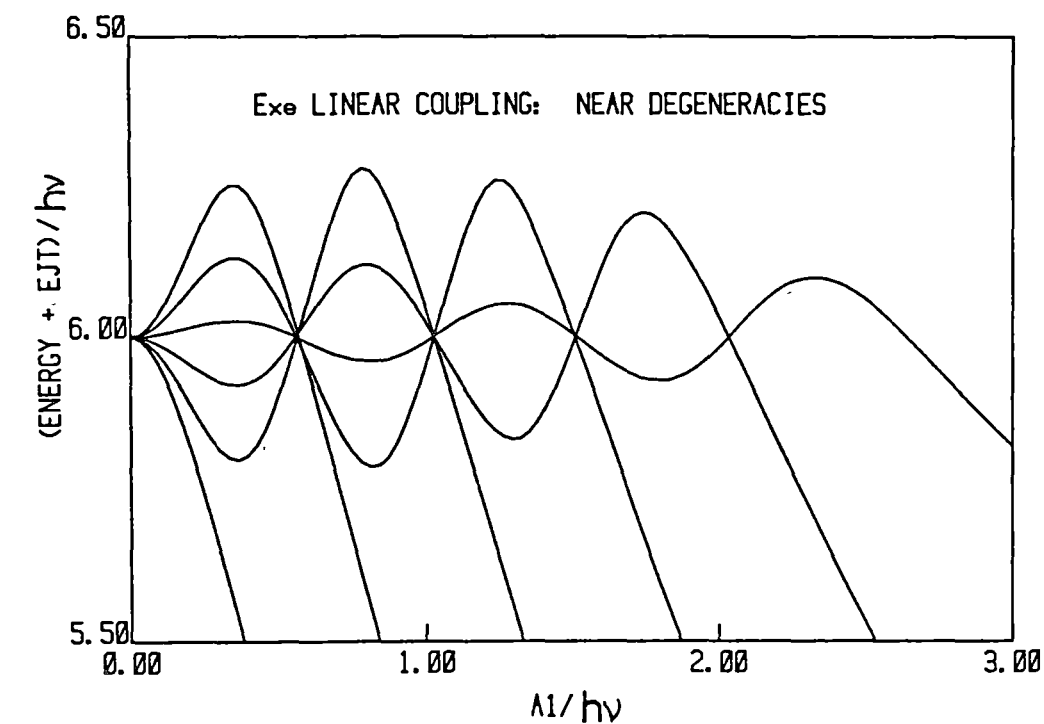
Figure 4.8 The E⊗e energy levels.
a) The near degeneracies in the nodal structure.
b) The pseudo-rotational levels in the zero point radial vibration.

Jahn-Teller effect in optical spectroscopy (Struck and Herzfeld 1966). Figure 4.9 also shows the expected intensity pattern for an optical transition to an excited doubly degenerate excited state for a particular value of the coupling strength ($A_1/h\nu = 2.25$). The spectrum is calculated from the square of the projection of the lowest vibrational level of the harmonic ground state on to the calculated excited state wavefunctions (Longuet-Higgins etal 1958). This results in a spectrum with a characteristic double maxima that one might expect from applying the Franck-Condon principle classically. Such unevenly spaced vibronic structure with a double maxima has been observed in the $^4A_2 \rightarrow ^2E(D)$ (Laiho and Treshchalov 1981) and $^4A_2 \rightarrow ^2E(G)$ (unpublished work) transitions of tetrahedral $CoCl_4^{2-}$.

However, the linear E×e case is highly idealised and such a spectrum as shown in figure 4.9 would be unlikely to be observed in practice. Anharmonicity (O'Brien 1964) and second-order coupling (Sakamoto 1982) in the Hamiltonian in (4.26) will greatly effect the energy levels and split the artificial degeneracy of the A_1, A_2 states. Figure 4.14a shows the energy levels relative to the ground vibronic state as a function of the second order coupling constant for a particular (fixed) value of linear coupling.

The ground vibronic state always remains an orbital doublet, the next excited state splits into singlets of A_1 and A_2 symmetry. [These symmetry labels should not be confused with the first and second order coupling constants, which unfortunately have the same symbols.] For strong second order coupling the barrier between the equivalent minima (2β) is high and the energy levels approach triple degeneracy. If these minima correspond to tetragonal elongations in a Cu(II) complex, then the second order coupling constant is positive and the lower singlet that approaches three fold degeneracy with the ground state doublet is then of A_2 symmetry. A different choice in the signs of the first and second order coupling constants can result in this lowest excited singlet having A_1 symmetry (Englman 1972, pg36; Setser etal 1975, table II). The behaviour of the energy levels as a function of strain has been given by Englman and Halperin (1970) and Feiner (1981). Similar calculations are shown in figure 4.14b.
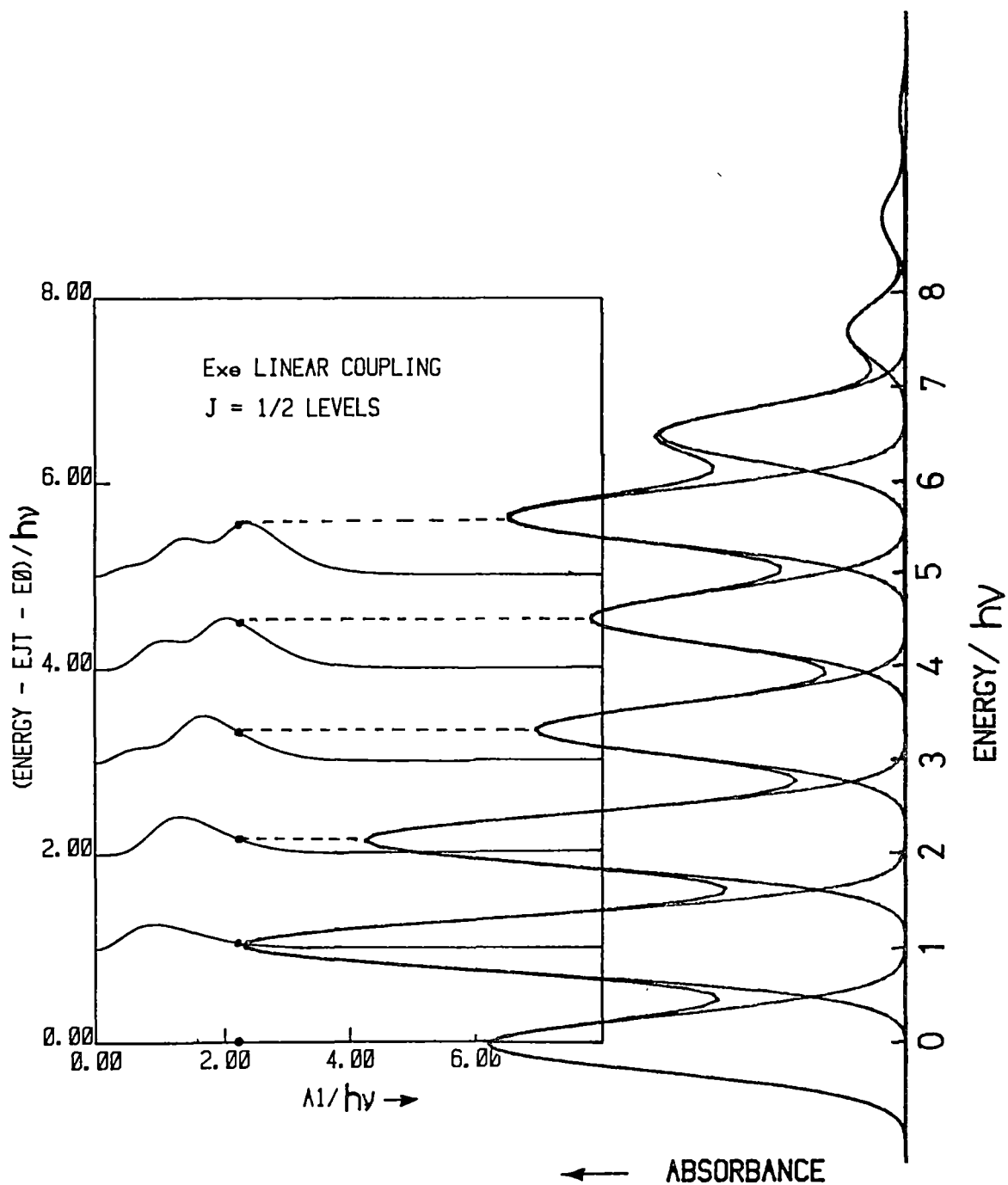
Figure 4.9 The A → E optical transition at $A_1/h\nu$ = 2.25. Note that the energy intervals are not harmonic, and the intensity distribution is non-Gaussian.

4.5.2 The Wavefunctions.

The shape of the adiabatic potential surfaces in section 4.2 were useful in visualising Jahn-Teller phenomena from a static viewpoint. Similarly, the probability plots of the wavefunctions are useful for visualising dynamic phenomena. However, a complete plot of a vibronic wavefunction would require six dimensions. This is the three dimensional geometric space of the molecule in which the electron(hole) density of an electronic state is usually shown, the two dimensional $Q_\theta - Q_\varepsilon$ space of the vibrational wavefunctions and a dimension to express the probability amplitude.

The difficulties in displaying such a wavefunction can be avoided by plotting the electronic and vibrational parts of the vibronic wavefunction separately. This involves integrating over the part that is not to be displayed. The vibronic wavefunction and the probability functions of the electronic and vibrational parts can be given by:

$$\Omega = \sum_{m,n} (a_{\theta mn} |\theta mn> + a_{\varepsilon mn} |\varepsilon mn>) \tag{4.43}$$

$$<\Omega|\Omega>_{el}(x,y,z) = \sum_{m,n} [\sum_\lambda a_{\lambda mn} |\lambda>]^2 . <m|m><n|n>$$

$$= <A^2><\theta|\theta>(x,y,z) + 2<AB><\theta|\varepsilon>(x,y,z) + <B^2><\varepsilon|\varepsilon>(x,y,z)$$

$$<A^2> = \sum_{m,n} a^2_{\theta mn}, \quad <AB> = \sum_{m,n} a_{\theta mn} a_{\varepsilon mn}, \quad <B^2> = \sum_{m,n} a^2_{\varepsilon mn}$$

$$<\Omega|\Omega>_{vib}(Q_\theta, Q_\varepsilon) = \sum_\lambda [\sum_{m,n} a_{\lambda mn} |m>|n>]^2 . <\lambda|\lambda>$$

$$= \sum_{m,n} [(a^2_{\theta mn} + a^2_{\varepsilon mn}) <m|m>(Q_\theta)<n|n>(Q_\varepsilon)]$$

Here $|\theta>(x,y,z)$, $|\varepsilon>(x,y,z)$ are the conventional real d-orbitals evaluated at the point (x,y,z) in the molecular coordinate system; and $|m>(Q_\theta) |n>(Q_\varepsilon)$ is the product of two one-dimensional harmonic oscillator functions (equation (2.36)) evaluated at the points Q_θ and Q_ε.

The electronic and vibrational parts of the vibronic wavefunctions are shown in figures 4.10 and 4.11 respectively. These plots have been made using the spherical and polar coordinate subroutines

(4.26)
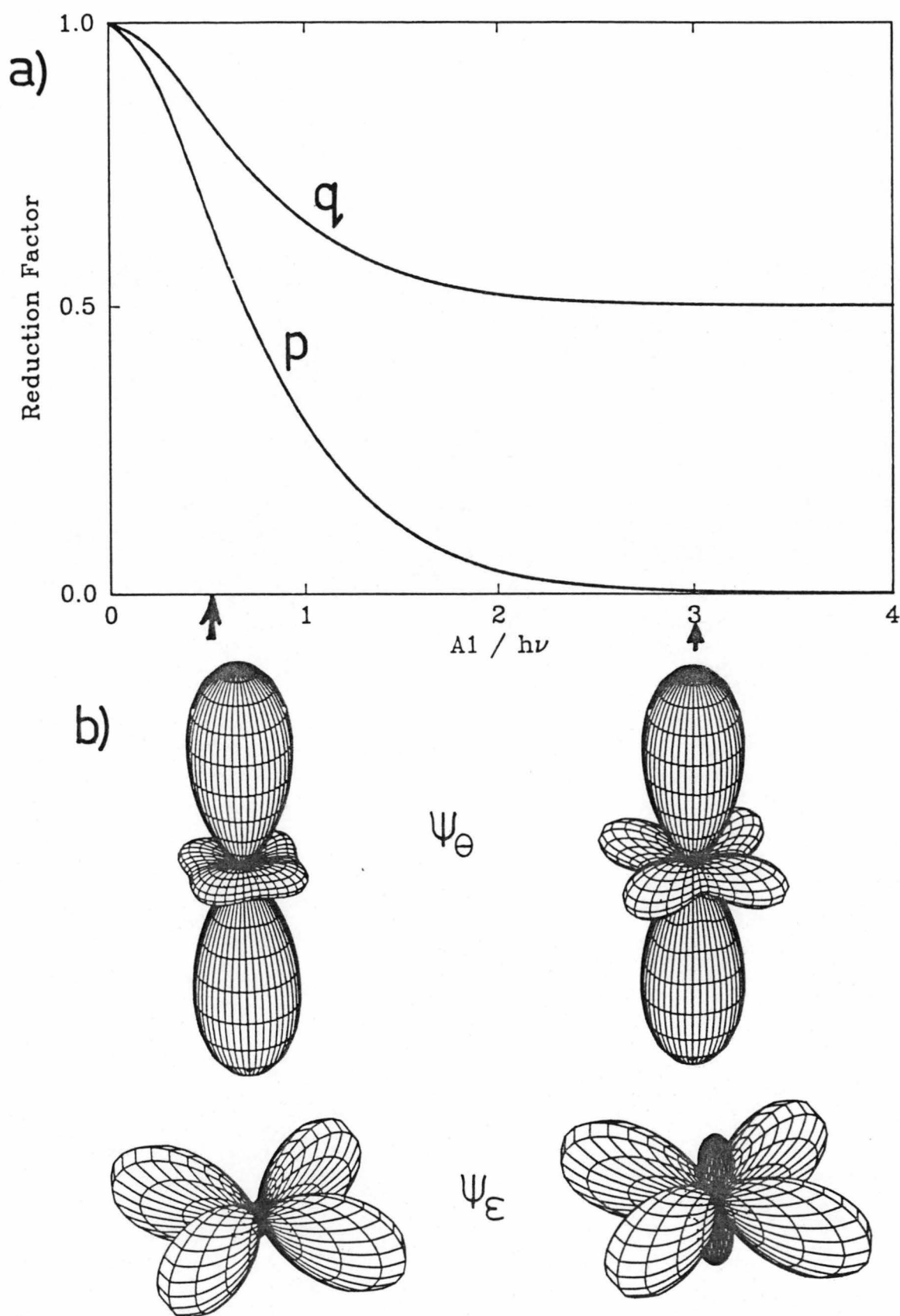
Figure 4.10 The Ham reduction factors for linear coupling.
a) The reduction factors q and p as a function of $A_1/h\nu$.

b) The explicit form of the electronic probability functions
for the values shown by the arrows above.

Energy / $h\nu$
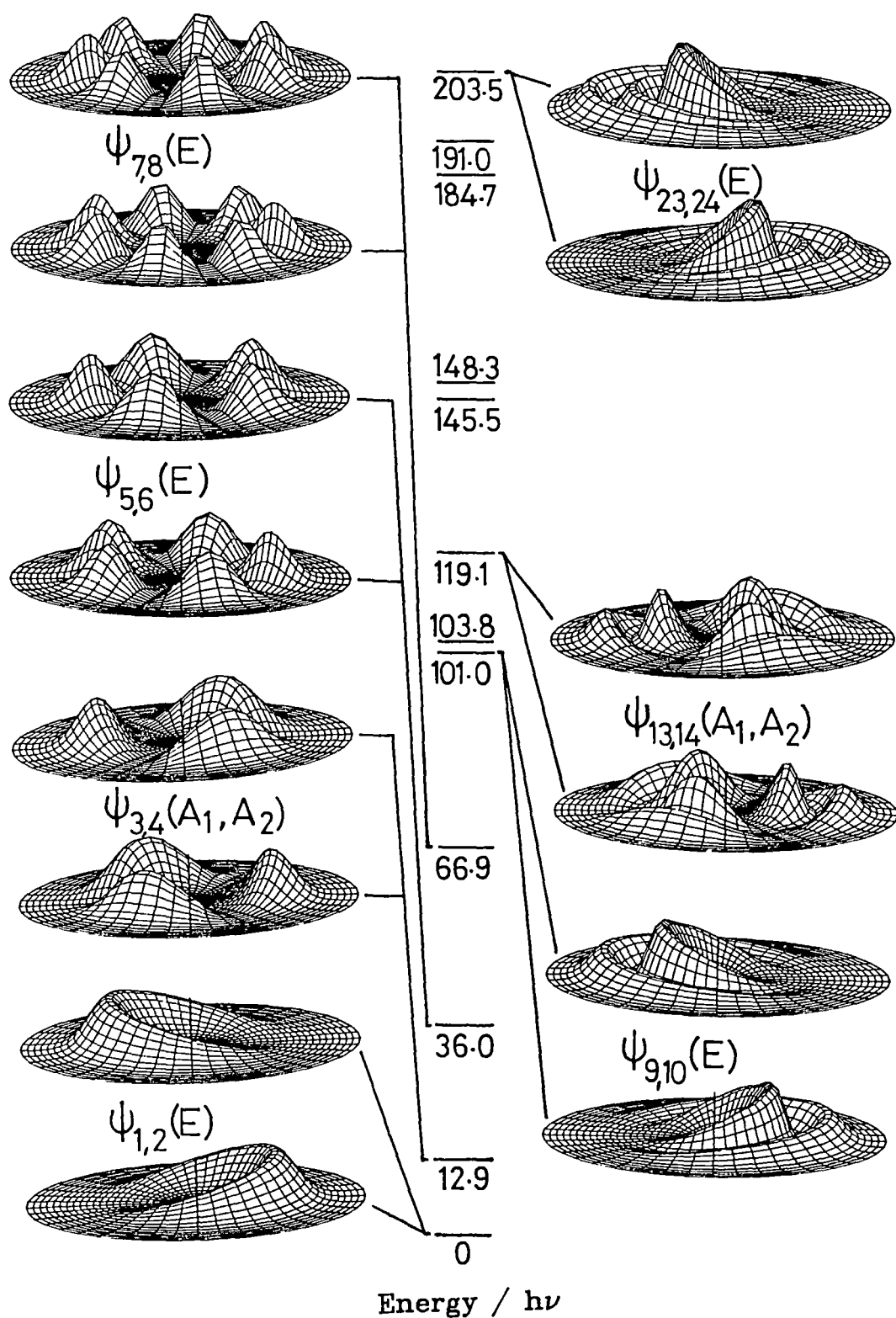
Figure 4.11 The vibrational part of the vibronic probability functions for linear coupling ($A_1/h\nu = 3.0$), see the solid circles in figure 4.7. Each probability function has $2j$ nodes along the angular coordinate.

respectively from the <PLOT79> library (McIntosh and Beebe 1979). The electronic part of the probability functions are shown in figure 4.10 for the two components of the ground vibronic doublet for weak and strong linear coupling. There is a close connection between these plots and the vibronic reduction (or Ham) factors which can be considered as the reduced matrix elements of the electronic part of the vibronic functions (Ham 1972). These reduction factors have been given by Ham (1972, p32), which in the present formalism for a ground vibronic doublet Ω_θ, Ω_ε in the case of linear coupling are:

$$q = \langle \Omega_\theta | \ \sigma_z \ | \Omega_\theta \rangle = \langle A^2 \rangle - \langle B^2 \rangle \qquad (4.44)$$

$$p = i \langle \Omega_\theta | \ \sigma_y \ | \Omega_\varepsilon \rangle = 2q - 1$$

These reduction factors can be used in a (2x2) spin Hamiltonian of a purely electronic basis. Apart from reducing the electronic quantities, the vibrational parts of the wavefunctions do not need to be used. This is called the two state model (Bill 1984, pp719-21), but this is often found to be inadequate when higher order and strain terms in the Hamiltonian make it necessary to include higher vibronic states in the spin Hamiltonian. The three state model (Setser etal 1975) and six state model (Setser and Estle 1978) then require additional reduction factors, and the use of this type of formalism quickly loses it's attractiveness. In the experimental systems to be studied here, there are large strain terms so that the wavefunctions are far from the cubic basis functions in these models. This would then require an "n" state model, where n is large, to construct accurate wavefunctions for all thermally populated levels using many reduction factors. For these reasons this approach of using reduction factors in a large spin Hamiltonian will not be considered further. In chapter 5 it is assumed that the strain terms sufficiently remove the degeneracy of the vibronic levels that the Zeeman operator can be applied separately to each level.

For the singlet vibronic levels, the electronic part of the probability functions, shown in figure 4.12a, are isotropic combinations of the $d(z^2)$ and $d(x^2-y^2)$ orbitals that have equal lobes along all three molecular axes. It is interesting to note that it is impossible to produce such a probability function from the square of a

(4.27)

static mixture of $d(z^2)$ and $d(x^2-y^2)$ orbitals, so they represent true dynamic wavefunctions. This will result in an isotropic g-tensor for such a state, although in practice it is often difficult to distinguish between such a case and the rapid exchange between equivalent static states.

The vibrational part of the vibronic probability functions is shown in figure 4.11 for a linear coupling of $A_1= 300cm^{-1}$, $K_2= 100cm^{-1}$. The approximate radial and angular quantum numbers of (4.42) is reflected in the nodal structure as there are m nodes in the radial direction similar to that of a harmonic oscillator, and 2j nodes in the angular direction for the pairs of degenerate levels. The ground state vibronic wavefunctions are in agreement with those given by Thompson etal (1985, fig7). However, these functions do not display the full symmetry of the problem as the two components of the degenerate levels are prevented from mixing. Although the variational calculation has been done in real space, this is only because real d orbitals were used in the electronic basis. In general electronic (and therefore vibronic) states will be complex Hermitian, and any linear combination of the eigenvectors Ω_θ, Ω_ε of the two components of a degenerate level will also be eigenvectors of these levels. When the vibronic space is considered complex then the combinations that reveal the symmetry of the wavefunctions are given by:

$$\Omega_1 = \frac{1}{\sqrt{2}} (\Omega_\theta + i\, \Omega_\varepsilon)$$

$$\Omega_2 = \frac{1}{\sqrt{2}} (\Omega_\theta - i\, \Omega_\varepsilon) \qquad \text{where } i \text{ is } \sqrt{-1}.$$

(4.45)

These wavefunctions are shown in figure 4.12b and can be compared with those in figure 4.11. The linear combinations of (4.45) will also cause the electronic part of the vibronic functions to become isotropic, identical to that calculated for singlet levels (figure 4.12b). This is in contrast to the anisotropic electronic probability functions that are calculated from vibronic wavefunctions that have not been symmetrised. This refinement is completely unnecessary in any practical application of the wavefunctions, as the Ω_θ, Ω_ε wavefunctions remain perfectly correct.

As might be expected, the effect that warping terms have on the wavefunctions is to localised them about the three minima of the

a)
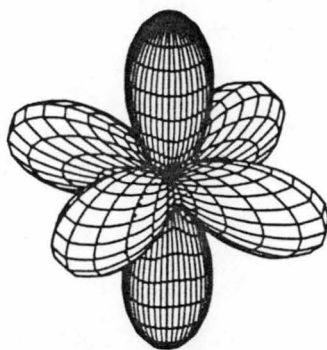
b)
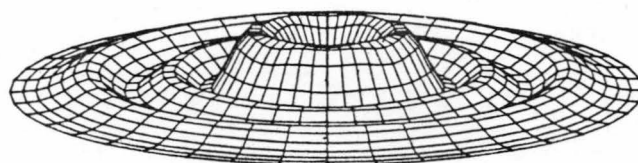
$$\psi_{23,24}(E)$$
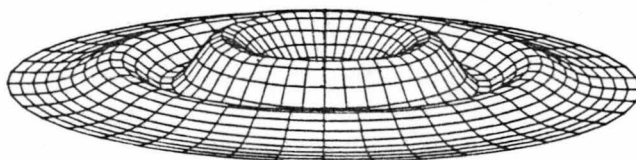
$$\psi_{9,10}(E)$$
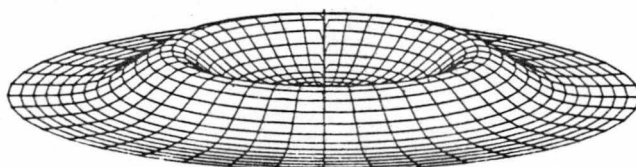
$$\psi_{1,2}(E)$$

Figure 4.12 The symmetrised vibronic probability functions.
a) The electronic part, which is the same for all vibronic levels. This isotropic function has equal lobes along the molecular axes.
b) The vibrational part, which all have the full $C_{\infty V}$ symmetry.

The higher excited angular vibrations are almost identical except for a slight increase in the mean radial amplitude, $\langle \rho \rangle$, which corresponds to a centrifugal distortion.

potential as shown in figure 4.13. These numerically calculated vibrational probability functions are very close to linear combinations of SHO functions ψ_1, ψ_2, ψ_3 based in the minima at $\phi = 0°$, $120°$, $240°$ respectively. The appropriate linear combinations are also shown in figure 4.13 and these functions are the basis in the three state model (Bill 1984, pg722). It can be seen from figure 4.13, that these functions are a very good approximation to the true wavefunctions in this particular case where there is strong linear coupling with large warping terms.

4.5.3 Expectation Values.

Other quantities of interest can be calculated from the vibronic wavefunctions other than just the $\langle A^2 \rangle$, $\langle AB \rangle$, $\langle B^2 \rangle$ electronic coefficients given in (4.43). The expectation value of the cartesian coordinates can easily be found by using simple harmonic oscillator matrix elements (appendix 2.A1). One can find for example:

$$\langle Q_\theta \rangle = \langle \Omega | \, Q_\theta \, | \Omega \rangle$$

$$= \sum_{\lambda, m, n} a_{\lambda m n} \sum_{\lambda' m' n'} a_{\lambda' m' n'} \langle \lambda | \lambda' \rangle \langle m | Q_\theta | m' \rangle \langle n | n' \rangle$$

$$= \sum_\lambda \sum_{n=0}^{n_v} \sum_{m=1}^{n_v} (2m)^{1/2} \, a_{\lambda m n} a_{\lambda m-1 n}$$

Similarly $\langle Q_\varepsilon \rangle$, $\langle Q_\theta^2 \rangle$, $\langle Q_\varepsilon^2 \rangle$, etc can be calculated. However, expectation values of geometric quantities such as $\langle \rho \rangle$, $\langle \phi \rangle$, $\langle \sin\phi \rangle$, etc cannot be calculated directly in the above manner, as analytic expressions for the matrix elements in this basis do not exist, and the integrals must be evaluated numerically. Gauss-Hermite quadrature (Carnahan etal 1969; chapter 2) was chosen to save the calculation of exponentials in the expressions for the harmonic oscillator wavefunctions. The abscissae and weighting factors were taken from the tabulations of Stroud and Secrest (1966; table 5). Expectation values of the following quantities were calculated: $\langle \Omega | \Omega \rangle$, $\langle \rho \rangle$, $\langle \phi \rangle$, $\langle \sin\phi \rangle$, $\langle \cos\phi \rangle$, $\langle \cos^2(\phi/2) \rangle$, $\langle \sin^2(\phi/2) \rangle$, $\langle z \rangle$, $\langle \sin z \rangle$, $\langle \cos z \rangle$, $\langle \cos^2(z/2) \rangle$, $\langle \sin^2(z/2) \rangle$. The results were checked by using both 20 and 30 point quadrature formula and numerical test data is given in appendix 4.A1.

a)
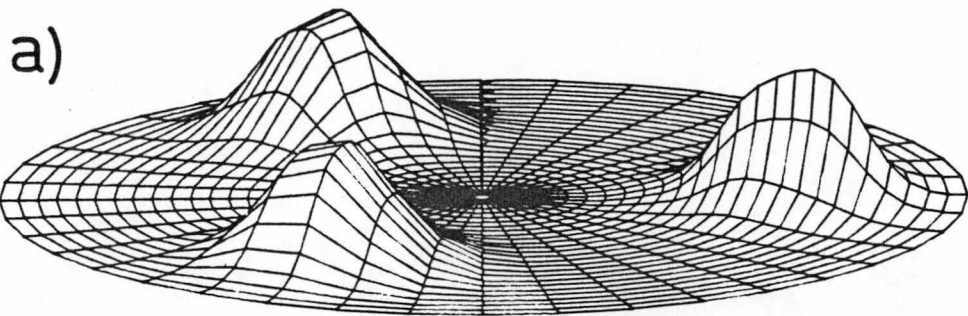
$\psi_3^2(A_2)$ Energy = 0.28 cm^{-1}; $\psi = 3^{-1/2}(\psi_1 + \psi_2 + \psi_3)$.

b)

$\psi_2^2(E_\epsilon)$ Energy = 0 cm^{-1}; $\psi = 2^{-1/2}(\psi_3 - \psi_2)$.

c)
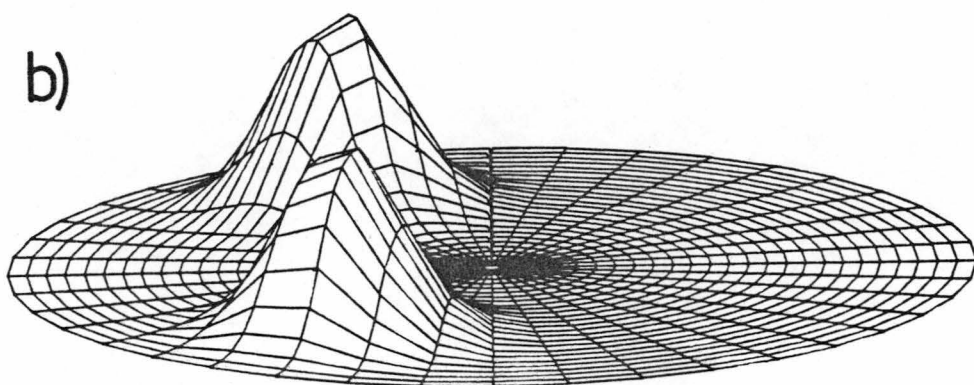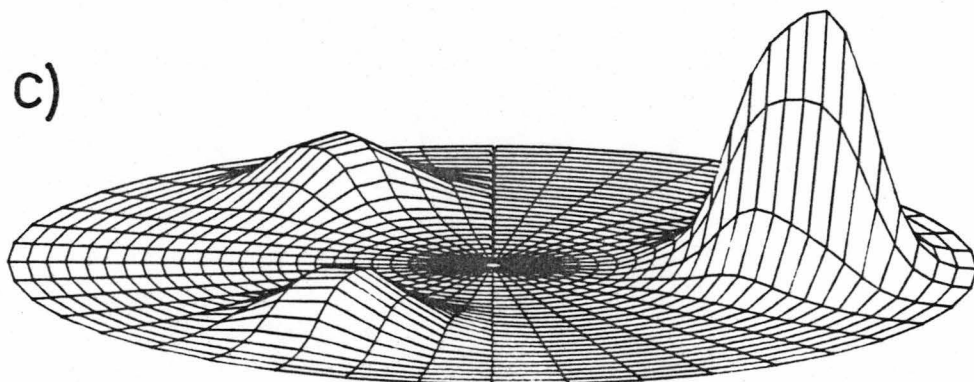
$\psi_1^2(E_\theta)$ Energy = 0 cm^{-1}; $\psi = 6^{-1/2}(2\psi_1 - \psi_2 - \psi_3)$.

Figure 4.13 The effect of the warping terms on the three
lowest wavefunctions. The potential is that of figure 4.3a.
The approximate wavefuntions of the three state model are also shown.

4.6 APPROXIMATE METHODS

Many approximate methods have been devised to simplify the computational task of solving the vibronic Hamiltonian in (4.26) exactly. Here three different approaches are briefly described:

1.) An obvious simplification that can be made in the limit of strong first order coupling, is to ignore the upper adiabatic potential surface. This has been done by Thompson etal (1985, scheme ii) when they considered only the lower surface in figure 4.5c. The calculation is difficult to implement numerically although a reduction of the basis size by half is achieved.

2.) In the next level of approximation, only the angular coordinate of the lower potential surface is considered important in determining the electronic properties of the vibronic functions, which can then be calculated from (4.28). The natural basis to use for this circular cross-section of the Jahn-Teller surface is a Fourier series of sine and cosine functions. This has been done for the Exe case with anharmonicity (O'Brien 1964), and anharmonicity with tetragonal strain (Englman and Halperin 1970). In this approximation, if there is no warping or strain terms, then the basis is diagonal with the energy levels simply that of a free rotor given by (4.42).

A computer program, CIRCLE, was written to perform such calculations and contains two improvements to Englman and O'Brien's methods. First, centrifugal and vibrational-rotational coupling type terms have been included to improve the free rotation basis functions (CIRCLE I); and second, the similarity transform that includes the strain terms (4.28) is used (CIRCLE II). Space does not permit a detailed description, but some example calculations comparing these methods with the exact results are shown in figure 4.14.

3.) In a further simplification, the potential near a single minimum can be approximated by a harmonic parabola. This has been done by Englman (1972, equation 3.25) in the case where a small strain localises the ground state in one of the minima caused by the warping terms. The case where a large strain dominates the potential has been

(4.30)
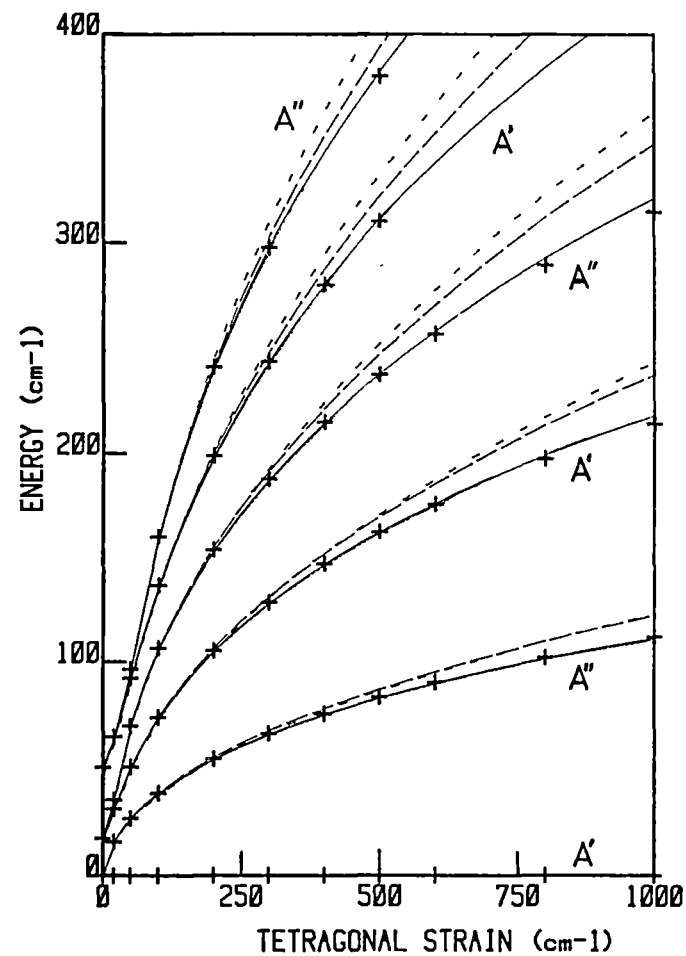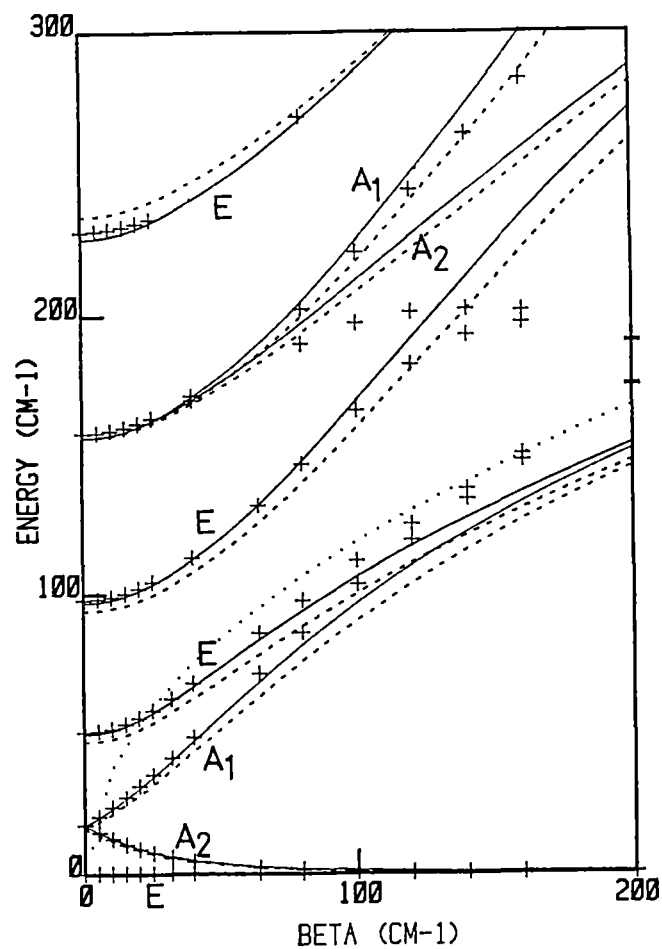
Figure 4.14 Comparison of some approximate methods with exact results.

Parameters: $h\nu = 250 cm^{-1}$, $A_1 = 1000 cm^{-1}$. + Exact values.

a) Energy levels as a function of the warping term β.
  ∙∙∙ Harmonic Model   --- O'Brien Model   — Circle I.

b) Energy levels as a function of the tetragonal strain.
  --- Englman Model   ∙∙ Circle I Model   — Circle II.

given by Kurzynski (1977, equation 2.7). The intermediate case where both strain and anharmonic terms determine the form of this harmonic potential is given in section 6.4.3.

In addition to the above approximations, it has recently been found that semiclassical methods are able to provide reasonable agreement to the eigenvalues of the Exe vibronic Hamiltonian (Zwanziger etal 1986). In addition, the resulting classical trajectories appear to be a promising approach to studying multimode and cooperative effects.

(4.31)

APPENDIX 4.A1   NUMERICAL TEST DATA

Exact numerical eigenvalues of the vibronic Hamiltonian of equation (4.26) for a range of parameters are available in the literature for first order coupling (Longuet-Higgins etal 1958) and first and second order coupling (Sloane and Silbey 1972; Sakamoto 1982). In the tables below, the exact numerical eigenvalues and several wavefunction properties are given for the lowest five levels of the vibronic Hamiltonian (4.26) with two sets of parameters.

These parameters correspond to the "best fit" values found for the $K_2Zn[Cu]F_4$ (chapter 6) and $K_2Zn[Cu](H_2O)_6(SO_4)_2$ (chapter 7) systems and are given here as numerical test data. A basis size of n_v = 26, and 30 point Hermite quadrature has been used in these calculations.

<div align="center">

TABLE 4.A1 Numerical Test Data.

</div>

$K_2 = 220 \text{ cm}^{-1}$ (=hv) $\qquad A_1 = 673 \text{ cm}^{-1}$ $\qquad S_\theta = -541 \text{ cm}^{-1}$

$K_3 = -1.799 \text{ cm}^{-1}$ $\qquad A_2 = 0.0 \text{ cm}^{-1}$ $\qquad S_\varepsilon = 0.0 \text{ cm}^{-1}$

Energy/cm^{-1}	$\langle A^2\rangle$	$\langle B^2\rangle$	$\langle AB\rangle$	$\langle Q_\theta\rangle$	$\langle Q_\varepsilon\rangle$	$\langle Q_\theta^2\rangle$	$\langle Q_\varepsilon^2\rangle$
1 -1380.1	0.9689	0.0311	0.0000	-2.718	0.000	7.890	1.733
2 -1318.0	0.9234	0.0766	0.0000	-2.527	0.000	6.932	4.332
3 -1239.1	0.8975	0.1025	0.0000	-2.415	0.000	6.531	5.842
4 -1154.5	0.8740	0.1260	0.0000	-2.302	0.000	6.317	6.859
5 -1150.9	0.9583	0.0417	0.0000	-2.654	0.000	8.441	2.300

	$\langle\rho\rangle$	$\langle\phi\rangle$	$\langle\cos\phi\rangle$	$\langle\sin\phi\rangle$	$\langle\cos^2(\frac{\phi}{2})\rangle$	$\langle\sin^2(\frac{\phi}{2})\rangle$
1	3.0236	180.0	-0.9000	0.0000	0.0500	0.9500
2	3.2839	180.0	-0.7695	0.0000	0.1153	0.8847
3	3.4468	180.0	-0.7059	0.0000	0.1471	0.8529
4	3.5647	180.0	-0.6471	0.0000	0.1764	0.8236
5	3.0562	180.0	-0.8597	0.0000	0.0702	0.9298

	$\langle z\rangle$	$\langle\cos z\rangle$	$\langle\sin z\rangle$	$\langle\cos^2(\frac{z}{2})\rangle$	$\langle\sin^2(\frac{z}{2})\rangle$
1	180.0	-0.9360	0.0000	0.0320	0.9680
2	180.0	-0.8456	0.0000	0.0772	0.9228
3	180.0	-0.7941	0.0000	0.1030	0.8970
4	180.0	-0.7473	0.0000	0.1263	0.8737
5	180.0	-0.9140	0.0000	0.0430	0.9570

(4.32)

TABLE 4.A2 Numerical Test Data.

$K_2 = 300$ cm^{-1} (=$h\nu$) $A_1 = 900$ cm^{-1} $S_\theta = -1000$ cm^{-1}
$K_3 = 0.0$ cm^{-1} $A_2^1 = 33.33333$ cm^{-1} $S_\varepsilon = 55$ cm^{-1}

Energy/cm^{-1}	$<A^2>$	$<B^2>$	$<AB>$	$<Q_\theta>$	$<Q_\varepsilon>$	$<Q_\theta^2>$	$<Q_\varepsilon^2>$
1 -2127.1	0.8633	0.1366	0.3334	-2.242	2.754	5.518	8.374
2 -2055.6	0.8772	0.1228	-0.3115	-2.271	-2.592	5.647	7.746
3 -1940.0	0.9086	0.0914	0.1673	-2.238	1.383	5.908	6.530
4 -1862.3	0.8886	0.1114	-0.0937	-2.311	-0.790	5.831	8.470
5 -1821.5	0.8505	0.1495	0.3439	-2.191	2.799	6.276	8.653

	$<\rho>$	$<\phi>$	$<\cos\phi>$	$<\sin\phi>$	$<\cos^2(\frac{\phi}{2})>$	$<\sin^2(\frac{\phi}{2})>$
1	3.6464	129.9	-0.6212	0.7468	0.1894	0.8106
2	3.5750	227.6	-0.6436	-0.7147	0.1782	0.8218
3	3.3532	155.5	-0.7433	0.3679	0.1283	0.8717
4	3.6179	194.6	-0.6812	-0.2244	0.1594	0.8406
5	3.7291	126.5	-0.5634	0.7646	0.2183	0.7817

	$<z>$	$<\cos z>$	$<\sin z>$	$<\cos^2(\frac{z}{2})>$	$<\sin^2(\frac{z}{2})>$
1	137.5	-0.7263	0.6663	0.1368	0.8631
2	219.3	-0.7538	-0.6223	0.1231	0.8769
3	158.8	-0.8158	0.3340	0.0921	0.9079
4	191.6	-0.7762	-0.1871	0.1119	0.8881
5	135.7	-0.7006	0.6871	0.1497	0.8503

A careful examination of the above tables can yield much information about the systems. In table 4.A1, the expectation values of all properties that are antisymmetric with respect to the Q_θ axis are zero, due to the symmetric nature of the wavefunctions in this system which has a zero orthorhombic strain term. The potential is dominated by a single minimum and approximate angular and radial quantum numbers can be assigned to these levels.

In table 4.A2, the potential has three inequivalent minima, and the minima in which the wavefunctions are predominately localised can be identified by the expectation values of the coordinates. It is interesting to compare the adiabatic wavefunctions given by (4.28) to the exact values by comparing $<A^2>$, $<B^2>$, $<AB>$ with $<\sin^2(\frac{z}{2})>$, $<\cos^2(\frac{z}{2})>$, $\frac{1}{2}<\sin z>$ respectively. The agreement is quite close in both cases due to the relatively large separation of the adiabatic potentials which allows the vibronic wavefunctions to be mainly associated with the lower Mexican hat surface. Note that if z was set equal to ϕ then there would not be this agreement.

(4.33)

APPENDIX 4.A2   SOAP FILMS: A JAHN-TELLER ANALOGUE.

An interesting classical analogy to the lower surface of the warped Mexican hat potential exists in the soap films that form on a wire frame in the shape of a cube. When such a frame is withdrawn from a container of soapy water, a film will form that connects all sides of the cube (see figure 4.A1). The free energy of the film is proportional to the surface area (Almgren and Taylor 1976), and can be thought of as the potential energy of the system. This potential energy will minimise by minimising the surface area in the same way that a film enclosing a volume of gas will form a spherical bubble.

In the case of a cubic frame, the soap film "spontaneously distorts" from a high symmetry to adopt one of three equivalent lowest energy configurations. These "geometries" are shown in figure 4.A1a, where the central square can be normal to either of the X, Y or Z axes. These three positions are similar to the three equivalent minima in the warped Mexican hat shown in figure 4.3. This analogy becomes stronger if "bondlengths" are defined as in figure 4.A1a so that the low energy configurations correspond to tetragonal elongations. The normal coordinates Q_θ, Q_ε can now be defined in exactly the same manner as for an octahedral ML_6 molecule in figure 4.2b.

Although the soap film cannot be distorted along the Q_θ coordinate, it can pass between equivalent minima via orthorhombic distortions. This pathway is indicated by dotted lines in the Q_θ-Q_ε plane in figure 4.A1b, where the lowest energy configurations are marked X, Y, Z. The surface area ($\propto$ energy) of a unit cube is given in figure 4.A1c for movement along this triangular path, clearly showing the three stable configurations as equivalent minima. The soap film will remain at the one configuration that is formed originally as long as the frame is kept still.

The behaviour that is being observed here is analogous to the static Jahn-Teller effect. There is no kinetic energy in the system corresponding to the kinetic energy operator in the Hamiltonian (4-.26). Kinetic energy can be provided, however, by shaking the wire frame, and higher energy films will form. A movement backwards and forwards parallel to the X or Y axes in figure 4.A1a will cause the orthorhombic motion shown by the arrows in figure 4.A1b. If enough
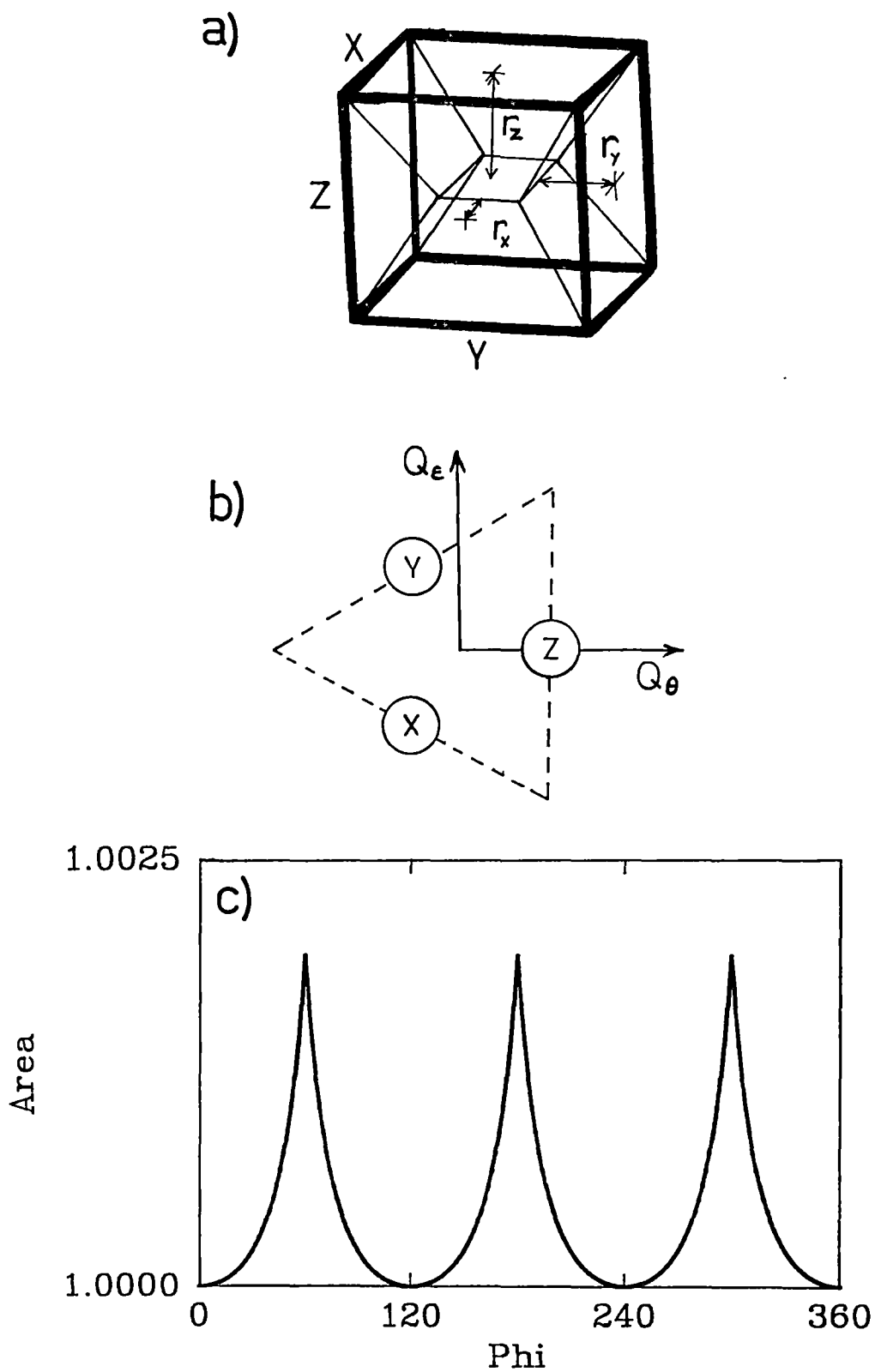
Figure 4.A1 a) The soap film that forms on a cubic frame.

b) The three equivalent geometries of the film, with the central square
   normal to the X, Y or Z axes. The interconversion pathway is shown.

c) The surface area of the unit cube following the dashed line above.

energy is supplied so that the barrier at the corner of the triangular path is crossed, then a different configuration will result with the central square parallel to X or Y.

If a large and constant kinetic energy is added then a dynamical system will result, and the time-averaged geometry will be that of the origin in the Q_θ-Q_ε plane in figure 4.A1b. This is the symmetrical configuration where the soap films meet at the centre of the cube; however, at any instant of the time, the "geometry" of the film will be close to the dotted line in figure 4.A1b.

The soap film on a cube has many similarities to the cubic E×e Jahn-Teller system and analogies can also be drawn with strain modified Jahn-Teller cases. Squashing the cube into a square prism by making four parallel edges shorter than the other eight, corresponds to a positive tetragonal strain. One of the minima in the cubic case is made lower than the others as shown in figure 4.A2a. The converse case, where the four edges are made longer, corresponds to a negative tetragonal strain and is shown in figure 4.A2b. By making the three sets of four parallel edges unequal, forming a rectangular prism, will cause the three minima to all be inequivalent and the "potential" corresponds to Mexican hat with both tetragonal and orthorhombic components of strain (figure 4.A2c).

These three cases where the cube is perturbed are interesting because ground state potential surfaces of real systems have been found that strongly resemble these potentials. In the second half of this thesis, potentials have been found for copper(II) doped into the hosts $ZnGeF_6 \cdot 6H_2O$, NH_4Cl and $K_2Zn(SO_4)_2 \cdot 6H_2O$ that are qualitatively similar to those given in figures 4.A2 a-c respectively. This again illustrates the usefulness of adapting a high symmetry formalism to the low symmetry situations that are most commonly found in nature.

.
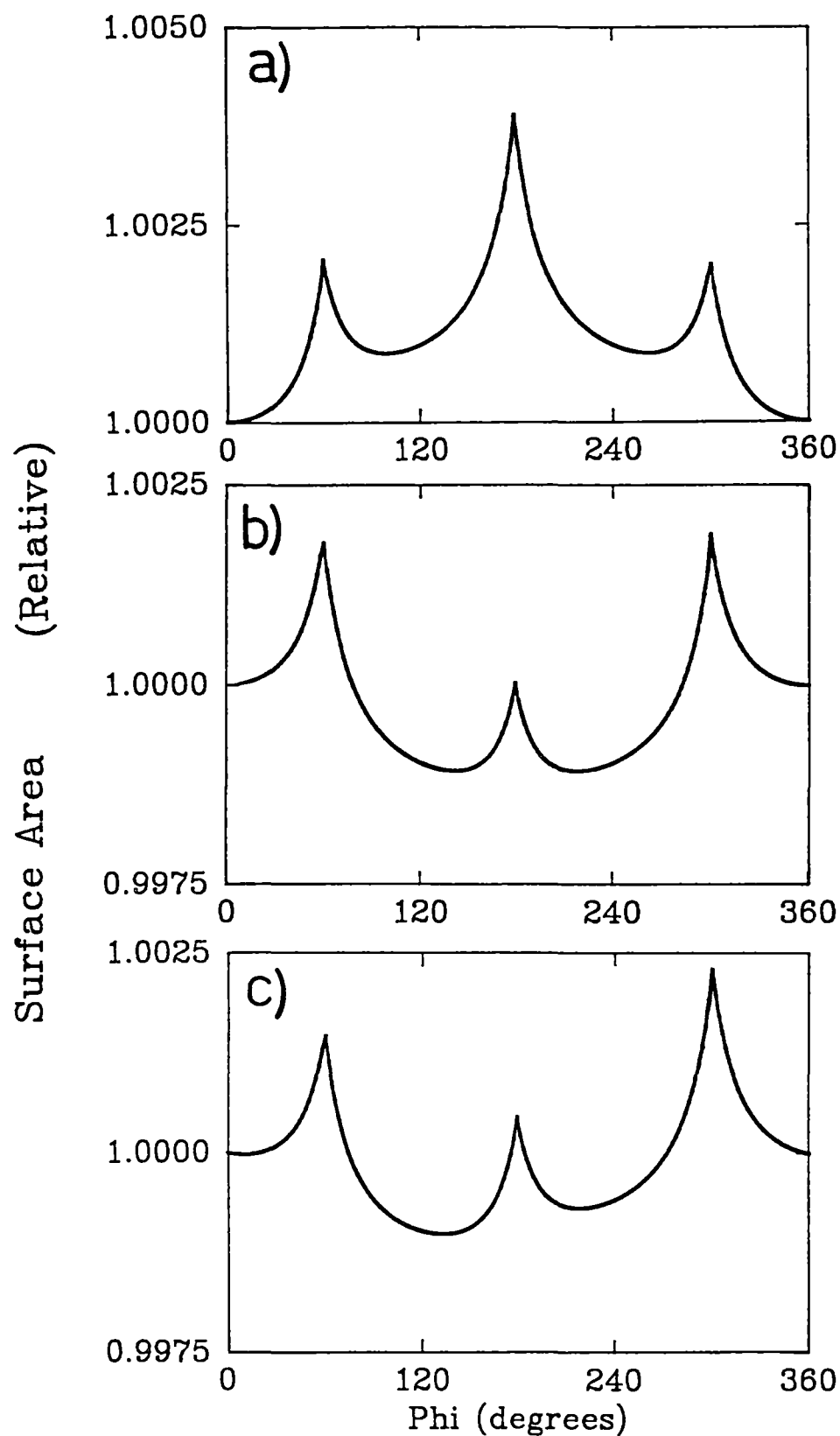
Figure 4.A2   The "cubic" case of figure 4.A1c, subject to
"strain" from unequal sides of the wire frame:
a) X=Y=1.05, Z=1.00; b) X=Y=1.00, Z=1.05; c) X=1.02, Y=1.00, Z=1.05.

CHAPTER5: ELECTRON SPIN RESONANCE

5.1 THE CALCULATION OF g-VALUES AT A FIXED GEOMETRY

Electron spin resonance spectra are usually interpreted in terms of a spin Hamiltonian rather than the real Hamiltonian of the system. It is an effective Hamiltonian which involves only spin operators, and acts on the wavefunctions of a system that are expressed as effective spin functions:

$$H_s = \beta \; S.g.H$$
$$= \beta \; (g_x S_x H_x + g_y S_y H_y + g_z S_z H_z) \qquad (5.1)$$

This expression is for the magnetic field along the principal axes of the g-tensor or g-ellipsoid and all symbols have their usual meanings (McGarvey 1966). A more complete spin Hamiltonian will also include the additional terms involving the hyperfine, superhyperfine, and for systems with spin greater than $\frac{1}{2}$, the zero-field splitting tensors (A&B, chapter 3). This section will only be concerned with the calculation of the g-values, and further, only for systems of spin $\frac{1}{2}$. Such a case arises for isolated Kramers doublets, and of particular interest is copper (II) compounds in octahedral coordination.

For an $S = \frac{1}{2}$ system the fictitious spin functions are then $|+\frac{1}{2}>$, $|-\frac{1}{2}>$ and evaluating the spin Hamiltonian (5.1) in this basis gives:

$$
\begin{array}{c}
 \\
<+\frac{1}{2}| \\
<-\frac{1}{2}|
\end{array}
\left[
\begin{array}{cc}
|+\frac{1}{2}> & |-\frac{1}{2}> \\
\frac{1}{2}g_z\beta H_z & \frac{1}{2}g_x\beta H_x - \frac{i}{2}g_y\beta H_y \\
\frac{1}{2}g_x\beta H_x + \frac{i}{2}g_y\beta H_y & -\frac{1}{2}g_z\beta H_z
\end{array}
\right] \qquad (5.2)
$$

The above matrix elements of the spin operators in (5.1) can be found from the Pauli spin matrices in equation (4.8).

The "real" Hamiltonian of the system is the Zeeman operator:

$$H_{zee} = (kL + g_e S) \beta H \qquad (5.3)$$

where again the symbols taking their usual meanings (A&B, pg50). The corresponding "real" wavefunctions can be labelled $|+>$, to be associated with the spin function $|+\frac{1}{2}>$ with mainly $m_s = +\frac{1}{2}$, and $|->$ to be associated with the $|-\frac{1}{2}>$ function.

The use of the Zeeman operator (5.3) only within the pair of ground state wavefunctions $|+>$, $|->$ is call the first order Zeeman effect (Mabbs and Machin 1973, chapter 3), and is tantamount to assuming that the magnetic field does not mix in higher excited states. This is a very good approximation for isolated Kramers doublets as the perturbations of the ligand field and spin-orbit coupling on the d-orbital basis are of the order $10,000 \text{cm}^{-1}$ and 1000cm^{-1} respectfully, while the perturbation due to the magnetic field is of the order $\sim 1 \text{cm}^{-1}$.

This approximation can breakdown when there are low lying electronic states, and the second order Zeeman formula (from perturbation theory) must be used (Mabbs and Machin 1973). A similar effect can happen when there are close lying _vibronic_ states with different electronic character to that of the ground state. This will be considered in the following section.

As an alternative to using perturbation formula, the Zeeman Hamiltonian (5.3) can be evaluated simultaneously with the other (ligand field etc) terms. In the present case this is unnecessary, as the use of (5.3) on the wavefunctions $|+>$, $|->$ _after_ evaluating the other perturbations is a good approximation. The action of the Zeeman Hamiltonian (5.3) on $|+>$, $|->$ can then be equated with that of the spin Hamiltonian (5.1) on $|+\frac{1}{2}>$, $|-\frac{1}{2}>$:

$$g_x \beta S_x H_x = (k_x L_x + g_e S_x) \beta H_x = \mu_x H_x \qquad (5.4)$$
$$g_y \beta S_y H_y = (k_y L_y + g_e S_x) \beta H_y = \mu_y H_y$$
$$g_z \beta S_z H_z = (k_z L_z + g_e S_z) \beta H_z = \mu_z H_z$$

By comparing the matrix elements of the above equations and using (5.2) the following equations can be found:

$$g_x = 2 <+| k_x L_x + g_e S_x |-> = 2 <+| \mu_x |-> \qquad (5.5)$$
$$g_y = 2i<+| k_y L_y + g_e S_y |-> = 2i<+| \mu_y |->$$
$$g_z = 2 <+| k_z L_z + g_e S_z |+> = 2 <+| \mu_z |+>$$

It can be seen in (5.5), that if the $|+>$, $|->$ wavefunctions are equivalent to the $|+\frac{1}{2}>$, $|-\frac{1}{2}>$ spin functions, then the absence of orbital angular momentum will cause the g-values to be isotropic and equal to g_e, the value for a free electron. The "g-shifts" are then a direct measure of the orbital angular momentum in the wavefunctions $|+>$, $|->$. The fact that these shifts are usually small in copper(II) complexes is due to the "quenching" of the orbital angular momentum by the ligand field which removes the degeneracy of the $d(x^2-y^2), d(xy)$

and d(xz),d(yz) pairs of orbitals. Spin-orbit coupling, however, mixes these states so the quenching is not complete.

In arriving at equations in (5.5) many aspects of the problem have been glossed over to keep the argument simple. The following points need to be considered:

i) What if the reference frame is not along the principal directions?

ii) How can the wavefunctions $|+\rangle$, $|-\rangle$ be calculated?

iii) What is the effect of the Zeeman Hamiltonian mixing vibronic states?

5.1.1 The g-tensor.

When the g-values of a compound are either measured experimentally or calculated theoretically, the principal axes may not be known, and off-diagonal elements of the g-tensor can be non-zero. Equation (5.1) can then be more fully written as:

$$\mathbf{H_s} = \beta \ \mathbf{S.g.H}$$
$$= \beta \ (S_x \ S_y \ S_z) \begin{bmatrix} g_{xx} & g_{xy} & g_{xz} \\ g_{yx} & g_{yy} & g_{yz} \\ g_{zx} & g_{zy} & g_{zz} \end{bmatrix} \begin{bmatrix} H_x \\ H_y \\ H_z \end{bmatrix} \qquad (5.6)$$

$\mathbf{g}$ is usually referred to as the g-tensor, and although in a strict mathematical sense $\mathbf{g}$ is not a tensor (A&B, pp651-3), the common usage of referring to a g-tensor will be kept.

For molecules of low symmetry, $g_{ij} \neq g_{ji}$ and it is impossible to diagonalise the g-tensor by a coordinate transform (Wertz and Bolton 1972, section 7.4; Gerloch and McMeeking 1975). The $\mathbf{g}^2$ tensor, however, is symmetric and the principal directions will be the same as for the $\mathbf{g}$-tensor. The sign of the principal g-values obtained from the square-root of the diagonalised elements of the $\mathbf{g}^2$-tensor, remains ambiguous. For the present case of Cu(II), the small shifts from the free electron value of g_e= 2.0023 imply that these values will always be positive.

The elements of the $\mathbf{g}^2$-tensor, which is the matrix product of $\mathbf{g}$ in (5.6) and its transpose (Wertz and Bolton 1972, pg136), can be calculated from (Gerloch and McMeeking 1975):

$$g^2_{\alpha\beta} = 2 \sum_{i=+,-} \sum_{j=+,-} \langle i|\mu_\alpha|j\rangle \ \langle j|\mu_\beta|i\rangle \qquad (5.7)$$

(5.3)

where μ_α is the αth component of the magnetic dipole moment operator in (5.4). Diagonalisation of this calculated g^2-tensor gives eigenvectors, which are the principal axes expressed as a linear combination of the reference axes, and eigenvalues which will be the squares of the principal g-values. It remains to have the explicit wavefunctions for the calculation of the matrix elements in (5.7).

5.1.2 The Wavefunctions.

The "real" wavefunctions $|+>$, $|->$ to be used in the previous calculations are most conveniently obtained by a ligand field calculation. For Cu(II) compounds this means that the matrix elements of the ligand field and spin-orbit operators are evaluated in, say , a real d-orbital spin basis and the resulting 10×10 secular equation is diagonalised. The lowest Kramers doublet is then used in either (5.5) or (5.7) to calculate the g-values.

Alternatively, the wavefunctions can be obtained from perturbation theory, then explicit expressions for $|+>$, $|->$, and hence the g-values, can be found without the need for a matrix diagonalisation. For centrosymmetric six-coordinate Cu(II), the zero order ground state Ψ_0 will be a mixture of the $d(x^2-y^2)$ and $d(z^2)$ orbitals:

$$\Psi_0^+ = A\ (x^2-y^2)^+ + B\ (z^2)^+ \tag{5.8}$$
$$\Psi_0^- = A\ (x^2-y^2)^- + B\ (z^2)^-$$

The mixing of the d(xy), d(xz), d(yz) orbitals into this ground state by spin-orbit coupling can be achieved by perturbation theory, giving the following wavefunctions (Bleaney etal 1955c):

$$|+> = N^{-1/2}\ [\ \Psi_0^+ + i\alpha d_{yz}^- - \beta d_{xz}^- + i\gamma d_{xy}^+\ ] \tag{5.9}$$
$$|-> = N^{-1/2}\ [\ \Psi_0^- + i\alpha d_{yz}^+ + \beta d_{xz}^+ - i\gamma d_{xy}^-\ ]$$

where $N = (1 + \alpha^2 + \beta^2 + \gamma^2)$.

First order perturbation theory gives for the coefficients:

$$\alpha = \frac{1}{2}\ u\ (-A-\sqrt{3}B) \tag{5.10}$$
$$\beta = \frac{1}{2}\ v\ (-A+\sqrt{3}B)$$
$$\gamma = \frac{1}{2}\ w\ (2A)$$

while second order perturbation theory gives:

$$\alpha = \frac{1}{2} \left[u(-A-\sqrt{3}B) + \frac{1}{2}uv(-A+\sqrt{3}B) + \frac{1}{2}uw(2A) \qquad \right] \qquad (5.11)$$

$$\beta = \frac{1}{2} \left[v(-A+\sqrt{3}B) + \frac{1}{2}vw(2A) \qquad + \frac{1}{2}uv(-A-\sqrt{3}B) \right]$$

$$\gamma = \frac{1}{2} \left[w(2A) \qquad + \frac{1}{2}uw(A-\sqrt{3}B) + \frac{1}{2}vw(-A+\sqrt{3}B) \right]$$

The other coefficients are $u = \dfrac{k_x^2 \zeta}{E_{yz}}$, $v = \dfrac{k_y^2 \zeta}{E_{xz}}$, $w = \dfrac{k_z^2 \zeta}{E_{xy}}$; E_{xy} is the energy of the excited state d_{xy} etc, and ζ is the spin-orbit coupling constant.

It is important to realise that the above wavefunctions are derived for six coordinate Cu(II) assuming that it remains in the Q_θ-Q_ε plane of the octahedral e_g vibration. In this situation only the spin orbit coupling causes the mixtures of the d_{xy}, d_{xz}, d_{yz} orbitals into the ground state Ψ_o, <u>not</u> the low symmetry component of the ligand field.

Since the Cu(II) complex remains centrosymmetric in the Q_θ- Q_ε plane, it follows that the principal axes of the g-tensor lie along the molecular axes. Explicit expressions for the g-values may then be derived by substituting the appropriate wavefunction coefficients in (5.9) and then evaluating (5.5). The g-values that result from the first order wavefunctions are given by (Hitchman 1970):

$$g_x = g_e + 2 u (A+\sqrt{3}B)^2 \qquad (5.12)$$

$$g_y = g_e + 2 v (A-\sqrt{3}B)^2$$

$$g_z = g_e + 2 w (2A)^2$$

The g-values that result from the second order wavefunctions are given by:

$$g_x = g_e + 4\alpha(-A-\sqrt{3}B) - 4(\beta^2 + \beta\gamma + \gamma^2) \qquad (5.13)$$

$$g_y = g_e + 4\beta(-A+\sqrt{3}B) - 4(\gamma^2 + \gamma\alpha + \alpha^2)$$

$$g_z = g_e + 4\gamma(2A) - 4(\alpha^2 + \alpha\beta + \beta^2)$$

[Note: In deriving the expressions in (5.13), factors of the type $\frac{\alpha}{N}$ appear which are made $\sim \alpha$. This means that the above expressions are accurate only up to second order in α.]

These expressions have been previously given for the ground state in the form: $\Psi_o = \frac{1}{3} \left(ad(x^2) + bd(y^2) + cd(z^2) \right)$ by Bleaney etal

(1955c). The expressions in (5.12), (5.13) are needed directly in terms of the A^2, AB, B^2 coefficients when vibronic effects are considered, for reasons to be explained in the following section. The expansion of (5.12) is obvious and will not be given, but the expansion of (5.13) is quite messy. The necessary algebraic manipulation was done by the computer program REDUCE2, resulting for example in the following inelegant expression for g_x:

(5.14)

$$g_x = g_e + \frac{1}{4}[-u^2v^2-u^2vw-u^2w^2+3uv^2w-4uv^2+2uvw+4uv+8uw^2-8uw+8u-3v^2w^2+6v^2w$$
$$-4v^2+8vw-16w^2].A^2 + \frac{\sqrt{3}}{2}[-u^2v^2-u^2vw-u^2w^2+2uv^2w+uvw^2+2uvw+4uw^2$$
$$-4uw+8u-2v^2w+4v^2-4vw^2-4vw].AB + \frac{1}{4}[-3u^2v^2-3u^2vw-3u^2w^2+3uv^2w$$
$$+12uv^2+6uvw^2+6uvw-12uv+24u-3v^2w^2-6v^2w-12v^2].B^2$$

Friebel etal (1976) have taken the expressions in (5.11) and (5.13) and have kept terms only up to second order in α, β, γ (which is entirely valid in light of the previous approximation concerning 1/N), and arrived at the following expressions:

(5.15)

$$g_x = g_e + 4u - 2(v^2+w^2) - (uv-vw+wu)$$
$$- (2u+(2w^2-v^2)-(2uv+vw-wu)).cos\phi + \sqrt{3}\ (2u+v^2-(vw+wu)).sin\phi$$

$$g_y = g_e + 4v - 2(w^2+u^2) - (vw-wu+uv)$$
$$- (2v+(2w^2-u^2)-(2uv+wu-vw)).cos\phi - \sqrt{3}\ (2v+u^2-(uw+wv)).sin\phi$$

$$g_z = g_e + 4w - 2(u^2+v^2) - (wu-uv+vw)$$
$$+ (4w+(u^2+v^2)-(2uv+wu+vw)).cos\phi - \sqrt{3}\ ((u^2-v^2)-(vw-wu)).sin\phi$$

Here the problem has been formulated in terms of the Jahn-Teller angular coordinate ϕ, and the coefficients of the previous equations are related by:

$$<cos\phi> = <cos^2(\phi/2)> - <sin^2(\phi/2)> = <A^2> - <B^2> \qquad (5.16)$$
$$<sin\phi> = 2\ <sin(\phi/2).cos(\phi/2)> \qquad = 2<AB>$$

The expressions in (5.13)-(5.15) above can now be compared to the results of an "exact" calculation. This will give an idea under what conditions these perturbation expressions can be applied. Table 5.1 shows the results for a pure $d(z^2)$ [A=0,B=1] and and a pure $d(x^2-y^2)$

(5.6)

[A=1,B=0] ground state with the parameters: $k_x = k_y = k_z = 0.9$; $E_{xy} = E_{xz} = E_{yz} = \Delta E$; $\zeta = 830 \text{cm}^{-1}$.

It can be seen from table 5.1 that, as would be expected, the expressions from perturbation theory are closer to the exact values when the excited states are higher in energy and the perturbation is therefore smaller. As this energy is raised (ie > 60,000 cm^{-1}), all orders of perturbation agree with the exact values. In the more realistic situation, corresponding to $\Delta E = 10,000 \text{ cm}^{-1}$, it can seen from table 5.1 that first-order perturbation theory gives values which are only qualitatively correct, but the second order expressions generally agree with the exact values to two decimal places. It is interesting to note that the second order expressions of Friebel etal (1976) in equation (5.15) are closer to the exact values than those of Bleaney etal (1955c) in equation (5.14). As indicated previously the inclusion of terms higher than second order are not justified within the level of approximation, and this seems to be borne out in the results of table 5.1.

The choice of one of the above methods for calculation of g-values is a balance between the accuracy that is desired and the ease of calculation. The explicit expressions from perturbation theory are easy to use but are only really correct to two decimal places. As another example on a real system, figure 5.1 shows the temperature dependent g-values of $Cu(II)/K_2ZnF_4$ (chapter 6), where 1st, 2nd order, and exact expressions are used.

<div align="center">

TABLE 5.1

</div>

$\Delta E/\text{cm}^{-1}$		1st Order (5.12)	2nd Order (5.14)	2nd Order (5.15)	"Exact"
g_z:	5,000 (z^2)	2.0023	1.9551	1.9481	1.9435
	(x^2-y^2)	3.0780	2.9585	2.9514	2.8982
	10,000 (z^2)	2.0023	1.9897	1.9888	1.9856
	(x^2-y^2)	2.5401	2.5094	2.5085	2.4982
	20,000 (z^2)	2.0023	1.9990	1.9989	1.9979
	(x^2-y^2)	2.2712	2.2634	2.2633	2.2614
$g_x = g_y$:	5,000 (z^2)	2.8091	2.7076	2.7006	2.6595
	(x^2-y^2)	2.2712	2.2060	2.1989	2.1822
	10,000 (z^2)	2.4057	2.3795	2.3786	2.3700
	(x^2-y^2)	2.1368	2.1196	2.1187	2.1137
	20,000 (z^2)	2.2040	2.1973	2.1972	2.1955
	(x^2-y^2)	2.0695	2.0651	2.0650	2.0638

<div align="center">

(5.7)

</div>
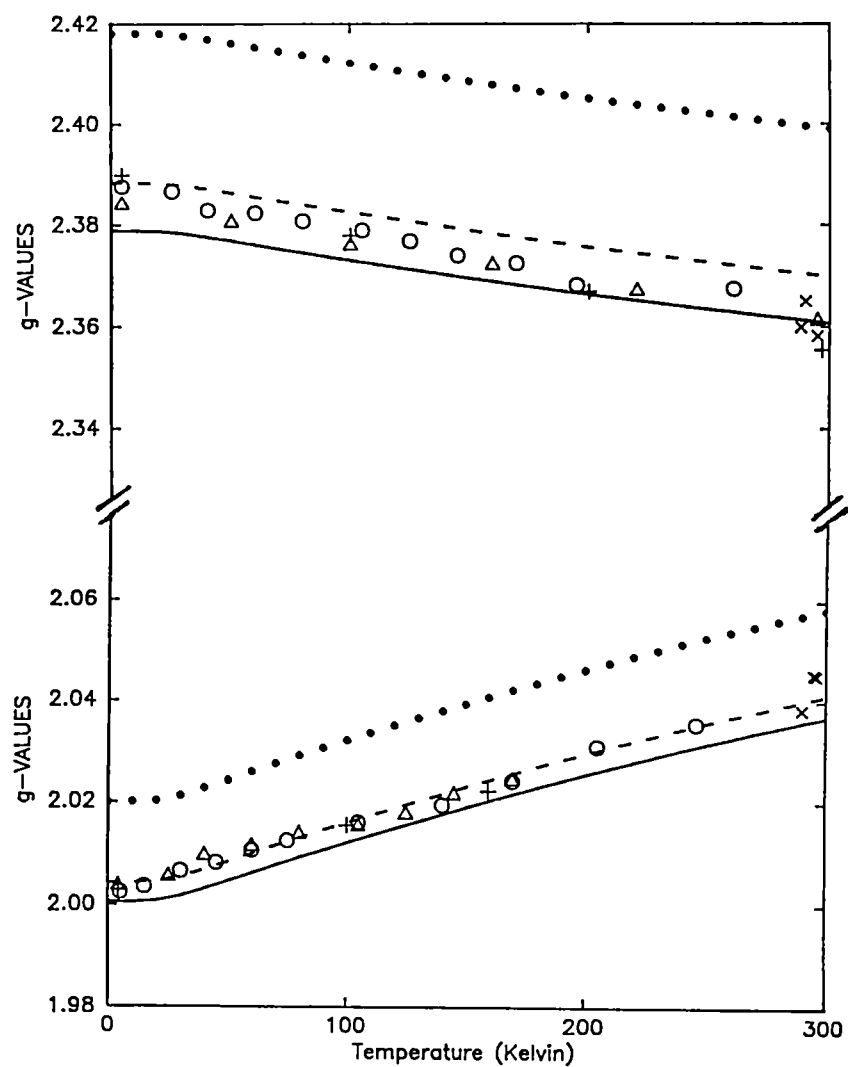
Figure 5.1 Calculation of the g-values of $Cu(II)/K_2ZnF_4$ with the parameters of Riley etal (1986) using:

First order perturbation theory (equation 5.12): ....
Second order perturbation theory (equation 5.15): - - - -
"Exact" diagonalisation: ━━━━━

5.2 THE CALCULATION OF THE g-VALUES IN DYNAMIC SYSTEMS

Although the calculation of g-values in a fixed electronic state is well understood, the problem becomes more complex when considering the vibronic (implying dynamic) states. This is especially true where the electronic properties of a system are "non-rigid" and vary according the vibronic state it is in.

The vibronic coupling of the Jahn-Teller effect represents such a situation, and two distinct aspects of the problem will be discussed. Firstly there is the case of the Jahn-Teller effect in crystals of cubic symmetry where the ground state will retain its degeneracy as a vibronic doublet. Secondly, and of particular interest to the present study, is the case of lower than cubic symmetry where the problem becomes formally that of the pseudo Jahn-Teller effect. This second case is somewhat more straightforward to treat as far as the calculation of the g-values is concerned, as all the vibronic levels are singlets. Another incentive to examine this second case in detail closely is that while little theoretical work has previously been attempted, there is a wealth of experimental data available.

5.2.1 Jahn-Teller Effect: Cubic Symmetry.

Although there is much literature dealing with the ESR of cubic Jahn-Teller systems (A&B; Ham 1972; Sester and Estle 1978; Bill 1984), these systems were not well understood until the contributions of O'Brien (1964) and Ham (1965, 1968). Typically there are three basic types of ESR spectra that are observed in such systems (A&B, pg 826):

1) A superposition of three axially symmetric spectra corresponding to vibronic singlets at static tetragonal elongations.

2) A single anisotropic spectrum of a vibronic doublet similar to that of an ^2E_g electronic state in full cubic symmetry in the absence of the Jahn-Teller effect.

3) A single isotropic ESR spectrum of a vibronic singlet.

Since the ground state in the Exe case is always a vibronic doublet in the absence of strain, the last spectrum will only occur for finite temperatures.

The occurrence of the above spectra depends both on the random strain Δ_s and the separation 3Γ of the ground vibronic doublet from the lowest excited vibronic singlet. Ham (1972) has stressed that the role of the random strain is particularly important in these cases as strong Jahn-Teller coupling can amplify the effects of even the smallest strain. For the case of copper, with a large Jahn-Teller coupling constant, the following two cases may be distinguished:

a) $\Delta_s \gg 3\Gamma$ where a static Jahn-Teller spectrum of type 1 is expected.

b) $3\Gamma \gg \Delta_s$ where a dynamic, but still anisotropic, spectrum of type 2 is expected.

The former case a) was investigated by O'Brien (1964) where it was shown that a random strain could isolate the complex at a tetragonal geometry in any of the three wells of the warped Mexican hat. At higher temperatures the population of the other wells occurs. Either the population or exchange with these states, or a combination of both, will give rise to an isotropic spectrum at higher temperatures. An example of this is given by Cu(II) / $ZnSiF_6 \cdot 6H2O$ (Dang ctal 1974), who have shown that the observed coexistence of both the anisotropic and isotropic spectra over a temperature range is consistent with either of the above population or averaging mechanisms.

The second case b) has been examined by Ham (1965, 1968, 1972) who realised the implications of the fact that the Jahn-Teller effect does not lift the total degeneracy of a system, rather the electronic degeneracy is replaced by a vibronic degeneracy. The ESR spectrum of the ground vibronic doublet is then similar to that of an electronic doublet in octahedral symmetry without the Jahn-Teller effect. This situation was encountered in Cu(II) / CaO (Coffman 1968). At first the Jahn-Teller effect seems strangely absent, but its effect is to cause a vibronic reduction factor, q, to appear in the spin Hamiltonian (A&B, eq 21.71; Ham 1972, eq 2.3.15):

$$\mathbf{H_s} = g_1\beta \mathbf{S.H} \ \mathbf{I} + \frac{1}{2}qg_2\beta[-(3S_zH_z - \mathbf{S.H}) \ \sigma_z + \sqrt{3}(S_xH_x - S_yH_y) \ \sigma_x] \quad (5.17)$$

The symbols $\mathbf{I}$, σ_z, σ_x are the 2×2 unit and Pauli spin matrices (equation (4.8)) respectively. In this case the spin Hamiltonian in (5.17) acts on a 4×4 basis ("two state model"), rather than the 2×2 basis of singlets given by equation (5.1) in the previous section. The ESR spectrum will be characterised by two frequencies which will

become equal along the body diagonal of the cube in the molecular coordinate system (A&B, pp803-4). The ESR lineshape will be influenced by both the random strain (Ham 1972, pp35-6) and the motional averaging, which is dependent on the magnetic field direction (Ham 1972, pg55). Population or exchange with the higher vibronic singlet with a spectrum of type 3 will give rise to an isotropic signal at higher temperatures.

These two cases of a) a static vibronic singlet spectrum, and b) a dynamic vibronically reduced doublet spectrum, represent limiting cases of the same problem. A formulation that covers both these cases is the "three state" model, and has been successfully applied to Cu(II) / MgO, CaO (Reynolds etal 1974, Reynolds and Boatner 1975). This approach has also been extended to a "six state" model (Sester and Estle 1978), although the increase in the number of reduction factors makes this hard to use in practice. Each reduction factor will be different between different vibronic levels, and it is usual to approximate their values according to the strength of the coupling. [It is noted here that within the framework of the present numerical approach all such reduction factors are implicitly evaluated and a "N (>1000) state" model could be used if desired. However the this type of calculation is not the main interest here so this will not be pursued.]

An orbital singlet in a linear Exe Jahn-Teller system will have an isotropic g tensor. The wavefunctions will be composed of 50% character of each of the electronic basis functions, but the product of their electronic coefficients will be zero because of the orthogonality of the vibrational parts of the wavefunction. This can be verified from direct calculations and is easily understood when the expectation value of the electronic coefficients are expressed as trigonometric functions. Integrating over a singlet wavefunction that will be delocalised around the Mexican hat potential, one finds:

$$\langle A^2 \rangle - \langle B^2 \rangle = \langle \cos^2(\phi/2) \rangle - \langle \sin^2(\phi/2) \rangle = \langle \cos\phi \rangle = 0$$

$$\langle AB \rangle = \langle \cos(\phi/2).\sin(\phi/2) \rangle = \langle \sin\phi \rangle = 0$$

Using the the normality of the wavefunctions one then finds $\langle A^2 \rangle = \langle B^2 \rangle = 0.5$, while $\langle AB \rangle = 0$.

If these values are then substituted into the perturbation expressions of (5.15) (noting that u = v = w), then all principal g values become equal and are given by (Reinen and Friebel 1979):

$$g_{iso} = g_e' + 4u - 5u^2 \qquad (5.18)$$

This equation is only appropriate for vibronic singlets, whereas the ground state of an E×e Jahn-Teller system is a vibronic doublet. Although the spectrum of this doublet will be anisotropic Abragam and Bleaney (1970, pg 828) and Ham (1970, pg 55) have shown that fast vibronic relaxation between the lowest levels that are split by strain, will result in an averaged spectrum that is identical to the isotropic spectrum of a singlet.

5.2.2 The Pseudo Jahn-Teller Effect: Low Symmetry.

The large value of strain implied in a system of low symmetry will lift the degeneracy of the electronic states involved, so formally there will not be a Jahn-Teller effect present. However it seems reasonable to assume that if there is a strong Jahn-Teller coupling in cubic symmetry, there will also be strong vibronic coupling in lower symmetry. The approximation is made that the strain terms can be simply added to the cubic part of the vibronic Hamiltonian. As discussed in section 4.2.3, this is not entirely valid as the coupling constants and force constants of the two electronic states are not now required to be equal by symmetry. However, this seems the only tractable approach for such systems and can be partly justified by the fact that it can successfully explain the experimental systems considered in the following chapters.

An important consequence of the strain terms in the Hamiltonian is that the degeneracy of all the vibronic levels are removed (excepting Kramers degeneracy). They are all singlets of A′, A′′ or A symmetry if there is tetragonal or orthorhombic strain respectively. The fact that only singlets occur in such systems means the approximation can be made that the Zeeman operator does not mix the different vibronic levels. This will still be good approximation as the energy separations are of the order $100cm^{-1}$, and any such mixing that does occur will have only a minor effect as the electronic properties between neighbouring levels do not usually differ greatly. This is tantamount to saying that each vibronic level will have its own set of g-values and, in the limit of fast vibronic relaxation, a Boltzmann

average over these levels will result in the single set of g-values that is observed.

The usual approach to calculating ESR parameters in a system of lower than cubic symmetry is to consider the problem from the "static" Jahn-Teller viewpoint, by ignoring the kinetic energy term in the Hamiltonian (4.26). However, the Jahn-Teller effect is not completely "quenched", and departures from a rigid electronic state that can occur experimentally for the zero Kelvin and temperature dependent spectrum, are explained by the "zero-point motion" and "averaging over two or more static geometries" respectively. Such phenomena can only be properly explained within a dynamic model, and such a model that reproduces the experimental observables will yield much information about the coupling of nuclear and electronic motions that is the subject of this thesis. The following section shows how the numerical vibronic calculations of chapter 4 can be used to calculate dynamic ESR parameters.

5.2.3 The Calculation of g-values in Dynamic Systems.

The vibronic Hamiltonian (4.26) can be solved for a particular set of parameters describing the potential and kinetic operators of the pseudo Jahn-Teller problem (see chapter 4). The result is then a series of n levels with energy E_n and wavefunctions:

$$\Omega_n = |\theta\rangle \left(\sum_{i=1}^{n} a_i |\phi_i\rangle \right) + |\epsilon\rangle \left(\sum_{i=1}^{n} b_i |\phi_i\rangle \right) \qquad (5.19)$$

The basis functions are comprised of two electronic states $|\theta\rangle$, $|\epsilon\rangle$ and N (>1000) vibrational states $|\phi_i\rangle$. These wavefunctions contain both the geometric and electronic properties that are necessary for the g-value calculations. In order to determine the electronic properties, the wavefunctions are integrated over the vibrational coordinates, and in terms of the coefficients of (5.8):

$$\langle A^2 \rangle = \sum_i a_i^2; \qquad \langle B^2 \rangle = \sum_i b_i^2; \qquad \langle AB \rangle = \sum_i a_i b_i \qquad (5.20)$$

Note: i=1,2,..N; $\langle A^2 \rangle + \langle B^2 \rangle = 1$.

(5.12)

Similarly the expectation values of geometric properties can be found from the wavefunctions: $\langle\rho\rangle$, $\langle\phi\rangle$, $\langle Q_\theta\rangle$, $\langle Q_\varepsilon\rangle$, $\langle\cos\phi\rangle$, $\langle\sin^2(\phi/2)\rangle$, ... etc (section 4.5.3). These geometric factors can be used to establish the energy of the excited triplet electronic states which will be different for each ground vibronic state. Alternatively, a mean energy can be used depending on how sophisticated a model is desired.

The electronic coefficients in (5.20) can be substituted into a g-value expression such as (5.12), but care must be taken to use only the exact product expressions given. The dynamic electronic coefficients in (5.20) will obey the Schwartz inequality (CDL, pg165):

$$\langle AB\rangle^2 \leqslant \langle A^2\rangle\langle B^2\rangle \qquad (5.21)$$

instead of the equality that would be obeyed if these coefficients were replaced by their static values. As an example, in systems with only tetragonal strain present in addition to the usual cubic Jahn-Teller terms, $\langle AB\rangle$ will be calculated to be zero. So when using (5.12) the appropriate expressions are:

$$g_x = g_e + 2u(\langle A^2\rangle + 3\langle B^2\rangle) \qquad (5.22)$$
$$g_y = g_e + 2v(\langle A^2\rangle + 3\langle B^2\rangle)$$
$$g_z = g_e + 8w(\langle A^2\rangle)$$

It is obvious that this must be so, as otherwise g_x would not equal g_y and rhombic g-values would result without any rhombic strain. Equation (5.22) is equivalent to calculating the g-values expected for a pure $d(z^2)$ and pure $d(x^2-y^2)$ electronic state and then using the fractional probability of each electronic state from the vibronic calculation to calculate the vibronic g-values. In other words the "cross term" disappears, and this approach was the one made in Riley etal (1986), using the second order expressions in (5.15).

This point is important as it has sometimes been erroneously concluded that the tetragonal strain in a Jahn-Teller system, which gives a mixture of $d(x^2-y^2)$ and $d(z^2)$ electronic states, will lead to rhombic g-values (Bill 1984, pg760). Rhombic g-values require an orthorhombic term in the vibronic Hamiltonian and cannot be a result of just tetragonal strain. The Schwartz inequality, (5.21), and the above arguments can be visualised in several ways. The vibronic

(5.13)

wavefunctions in the tetragonal problem can be classified as either A′
or A′′ in the C_s factor group:

$$|A′\rangle = a_{1g}|A_{1g}\rangle + b_{1g}|B_{1g}\rangle \qquad (5.23)$$
$$|A′′\rangle = b_{1g}|A_{1g}\rangle + a_{1g}|B_{1g}\rangle$$

The symbols a_{1g}, b_{1g}, A_{1g}, B_{1g} represent the irreducible repre-
sentations of the vibrational and electronic basis functions in the
D_{4h} point group. In both cases the vibrational functions connected to
each electronic function are of different symmetry, so the product
<AB> within each vibronic state must, by symmetry, be equal to zero.

Alternatively, (5.21) can be explained by examining the vibronic
probability functions in figure 6.6. The wavefunctions are symmetric
about the Q_θ (or in this case $Q(a_{1g})$) axis. From equation (4.28) it
can be seen that the $d(x^2-y^2)$ state changes sign about this axis.
Therefore <A> = 0, even though $\langle A^2\rangle \neq 0$, similar to the mean and RMS
geometry of an undisplaced harmonic oscillator.

To again stress the point, in the <u>electronic</u> wavefunctions that
are at a fixed geometry in (5.8), the coefficients A and B have
definite values that represent the mixture of $d(z^2)$ and $d(x^2-y^2)$
orbitals. However in the <u>vibronic</u> wavefunctions of (5.17), the in-
tegration over vibrational coordinates leaves only the electronic
coefficients $\langle A^2\rangle$, $\langle B^2\rangle$, and <AB> available for use.

Considering briefly the case of an orthorhombic component of the
strain, the symmetry of the vibronic states are classified all of A
symmetry in the factor group C_1:

$$|A\rangle = a_g|A_g\rangle \qquad (5.24)$$

Both the vibrational and electronic basis functions are totally
symmetric in the D_{2h} point group, and the cross term <AB> will be non-
zero. This is entirely expected, as it is needed to produce rhombic g-
values. A plot of the wavefunctions (or potential surface) will lose
the mirror symmetry about the Q_θ axis of before and therefore <A> ≠ 0.

The electronic properties in (5.20) can be used in the first
(5.12) or second (5.15) order perturbation formula for the calculation
of the g-values. For an "exact" calculation however, additional care
must be taken. Each vibronic state is an orbital singlet, but a
Kramers doublet. Since there are no spin operators in the vibronic
Hamiltonian of (4.26), each vibronic state of the form (5.19) can be
labeled either a pure spin = $+\frac{1}{2}$ or $-\frac{1}{2}$. However, it is impossible to
determine the electronic coefficients of the vibronic functions to

(5.14)

form a (static) purely electronic wavefunction to substitute into the ligand field calculation. The following circuitous approach is taken.

The pure spin-orbital pairs $(z^2)^+, (z^2)^-$ and $(x^2-y^2)^+, (x^2-y^2)^-$ are separately put into the ligand field matrix. The two resulting 8×8 complex Hermitian matrices can each be split into two 4×4 matrices, because the spin-orbit coupling matrix for d spin-orbitals can be split into two, and there are no off-diagonal ligand field matrix elements. This later point is true because the only states that are coupled by the ligand field in the Q_θ-Q_ε plane are the $d(z^2)$ and $d(x^2-y^2)$ orbitals, and this term has already appeared in the Jahn-Teller Hamiltonian as the orthorhombic strain S_ε. In a sense then, the vibronic states are pre-diagonalised with respect to the ligand field.

The energy of the excited electronic triplet states are given by:

$$E_{yz} = \Delta E + A_1(T) \left(-\frac{1}{2} \langle Q_\theta \rangle + \frac{\sqrt{3}}{2} \langle Q_\varepsilon \rangle \right) \qquad (5.25)$$

$$E_{xz} = \Delta E + A_1(T) \left(-\frac{1}{2} \langle Q_\theta \rangle - \frac{\sqrt{3}}{2} \langle Q_\varepsilon \rangle \right)$$

$$E_{xy} = \Delta E + A_1(T) \langle Q_\theta \rangle$$

The quantities $\langle Q_\theta \rangle$, $\langle Q_\varepsilon \rangle$ are expectation values calculated from the vibronic functions (section 4.5.3), ΔE is the energy baricentre of the triplet state above the ground state, and $A_1(T)$ can be viewed as a linear coupling constant in a T×e Jahn-Teller problem. The energy ΔE is kept constant for all vibronic levels to keep the average g-value constant.

The different expectation values for the geometry in each vibronic state means that the energies of the excited triplet orbitals $d(xy)$, $d(xz)$, $d(yz)$ will also differ for each vibronic level. Four 4×4 complex Hermitian matrices must then be evaluated <u>for each vibronic level</u>, and four eigenvectors similar to (5.9) result:

$$|+(z^2)\rangle, \quad |-(z^2)\rangle, \quad |+(x^2-y^2)\rangle, \quad |-(x^2-y^2)\rangle \qquad (5.26)$$

where the orbital in brackets indicates the main component, with small mixtures of the excited triplet electronic states. The vibronic wavefunctions would be:

$$|+\rangle = A|+(x^2-y^2)\rangle + B|+(z^2)\rangle$$
$$|-\rangle = A|-(x^2-y^2)\rangle + B|-(z^2)\rangle$$

except that the coefficients A, B <u>are unknowable</u>. However, the evaluation of the Zeeman Hamiltonian (5.5) gives for example:

$$g_x = 2A^2 <+(x^2-y^2)|\mu_x|-(x^2-y^2)> \qquad (5.27)$$
$$+ 2AB<+(x^2-y^2)|\mu_x|-(z^2)>$$
$$+ 2AB<+(z^2)|\mu_x|-(x^2-y^2)>$$

$$+ 2B^2<+(z^2)|\mu_x|-(z^2)>$$

where the coefficients are now known from equation (5.20). [Note: $<BA>$ = $<AB>$ since all coefficients in equation (5.19) are real.] From the wavefunctions in (5.26), the coefficients given in (5.20), and equations of the form (5.27), the principal g-values for each vibronic level can be calculated. The full g-tensor does not need be calculated and diagonalised since the principal axes are assume coincident with the molecular axes. A Boltzmann average over populated levels will then give the calculated g-values at a particular temperature.

The calculation of dynamic g-values outlined in this section requires the numerical solution of a vibronic Hamiltonian that includes the kinetic energy operator of the system. Such a calculation is often beyond the level of sophistication in reported studies and dynamic effects are often quoted as an "O'Brien mechanism" (O'Brien 1964) being active to provide an appropriate dynamic mixture of the electronic functions due to the zero point motion about a minimum of the potential (Reddy and Srinivasan 1966; Hagan and Trappeniers 1970). Alternatively, a static model has sometimes been used where a dynamic averaging between two orthorhombic static distortions is said to account for such a mixture (Reinen and Krause 1981). In either case, such arguments can lead to an incorrect interpretation of the systems.

(5.16)

5.3 CALCULATING HYPERFINE PARAMETERS

The coupling of the electron spin with the nuclear magnetic moment results in hyperfine structure in the ESR spectrum. This is represented in the spin Hamiltonian by an additional term:

$$H_s = \beta \ S.g.H + S.A.I \qquad (5.28)$$

Here **A** is the hyperfine tensor analogous to the **g** tensor that was described in section 5.1. For the case of copper, which has a nuclear spin of 3/2, the above spin Hamiltonian will act on an 8×8 basis composed of the fictitious spin functions that are characterised by electron and nuclear spin quantum numbers. The principal hyperfine values can be found by calculating all the elements of the **A** tensor and then diagonalising.

Since the electronic Zeeman term is much larger than the hyperfine splitting, the off-diagonal hyperfine interaction connecting the two different electron spin states can be neglected. This means that the two terms in (5.28) can be calculated separately in a 2×2 electronic spin and a 4×4 nuclear spin basis respectively. The principal values and axes of both the **g** and **A** tensors can then be found separately, and the principal axes of the hyperfine tensor need not necessarily be parallel with those of the g-tensor (A&B, pg169).

Analogous to the calculation of the **g** tensor given in section 5.1, the "real" Hamiltonian of the system and the spin-orbital ground state wavefunction, are required. The matrix elements of the real system are then equated to those of the effective spin Hamiltonian to give the elements of **A**. The real Hamiltonian, or hyperfine operator, can be found in the texts of Ham (1972, eq 2.1.9) or Abragam and Bleaney (1970, eq 17.61) and the calculation is straightforward using the methods of sections 5.1-2.

As with the g-values, approximate formulae for the principal hyperfine values can be obtained from perturbation theory. Bleaney etal (1955c) have derived such expressions up to second order. However, as explained at length in section 5.2.3, such expressions must be fully expanded if they are to be used with the wavefunction

coefficients from dynamical systems. The appropriate expressions given to first order are:

$$(5.29)$$

$$A_x/P\alpha' = -K + 4u + [\tfrac{1}{7}(2-3v)-2u].(A^2 - B^2) + \sqrt{3}[\tfrac{1}{7}(-2+2w+v)+2u].AB$$

$$A_y/P\alpha' = -K + 4v + [\tfrac{1}{7}(2-3u)-2v].(A^2 - B^2) + \sqrt{3}[\tfrac{1}{7}(-2+2w+u)+2v].AB$$

$$A_z/P\alpha' = -K + 4w + [\tfrac{1}{7}(3(u+v)-4)+4w].(A^2 - B^2) + \sqrt{3}[\tfrac{1}{7}(u-v)].AB$$

Here P is a scaling factor representing the average distance of the electron spin from the nucleus, α' is a constant less than 1 that represents the unpaired spin density in the metal d-orbitals, and K represents the contribution due to the unpaired spin density in the metal s orbitals. These above parameters take the values 0.036 cm^{-1}, 0.75 and 0.43 respectively for copper(II) complexes (Hitchman 1985b); and other symbols in equation (5.29) are as defined in section 5.1.2.

TABLE 5.2 Hyperfine Test Data

	1st Order Pert. (eq 5.29)			2nd Order Pert. (Bleaney etal)			2nd Order Pert. (keeping only 2nd order terms)		
	A_x	A_y	A_z	A_x	A_y	A_z	A_x	A_y	A_z
$Cu(NH_3)_4^{2+}$	-25	-25	-193	-24	-24	-194	-24	-24	-195
Cs_2CuCl_4	29	29	-16	35	35	-40	37	37	-37
$(enH_2)_2CuCl_6$	59	9	-31	51	20	-51	54	22	-46
CuF_6^{4-}	-39	-39	18	-47	-47	25	-45	-45	26

Equation (5.29) has also been determined by second order perturbation theory, analogous to equation (5.15) for the g values, but as these formulae are quite lengthy they will not be reproduced here. Example calculations are shown in table 5.2 that compare the three perturbation formulae. The parameters used have been taken from Hitchman (1985b), and the hyperfine constants are given in units of $\times 10^{-4}$ cm^{-1}. It can be seen from the table that while the two second order expressions give similar results, the first order expressions in

(5.29) do not. This is especially the case in tetrahedral complexes (second and third examples above) where the excited electronic states are at low energy.

Analogous to the isotropic g-values given by (5.18), isotropic hyperfine values can be found (A&B, pg802):

$$A_{iso}/P\alpha' = - (1 - 2u^2)K + 4u - \frac{34}{21} u^2 \qquad (5.30)$$

As with the isotropic g-values, this equation is only appropriate for a vibronic singlet, or motional averaging within a vibronic doublet. In the following section the vibronic relaxation effects, which cause this motional averaging, is considered in more detail.

(5.19)

5.4 RELAXATION EFFECTS IN JAHN-TELLER SYSTEMS

The calculation of g-values and hyperfine values given in the previous sections are for the individual vibronic eigenstates of the molecule. If rapid relaxation between these levels is assumed then the observed magnetic properties will be the Boltzmann average of the properties of the individual levels.

It is important to note that vibronic relaxation is quite different from spin lattice relaxation. In the former case the relaxation is between vibronic levels of the same spin, while in the later it is between different spin states. The conditions under which averaging from vibronic relaxation will occur has been carefully studied by Kurzynski (1977), and it was concluded that if τ_v is the vibronic relaxation time and τ_s the spin-lattice relaxation time, where τ_v is always $\ll \tau_s$, then the following inequalities must be obeyed:

$$\tau_s^{-1} \ll \nu; \qquad \Delta\nu \ll \tau_v^{-1} \qquad\qquad (5.31)$$

In the first inequality, ν is the frequency of the transition between spin states within one vibronic state and is then the condition for slow spin-lattice relaxation. The spin-lattice relaxation is usually slow in the cases studied in this thesis (Bersuker 1984a, pg115) and is not of direct interest. In the second inequality $\Delta\nu$ is the difference between ν's for different vibronic states and is the condition for fast vibronic relaxation or "motional averaging".

A rapid relaxation between between vibronic levels are implicit in studies where the magnetic properties vary smoothly with temperature. Such a situation was found by Griller and Preston (1979) who determined the energy of the out-of-plane bending vibration of the isopropyl radical from the temperature dependence of the hyperfine values. Similarly, the temperature dependence of the g-values of $K_2Zn[Cu]F_4$ can be used to determine the form of the ground state potential surface (chapter 6).

The above two cases are examples where the ground state potential is characterised by a single minimum. Rapid relaxation will occur between the different vibrational levels within the one well, and simple thermal averaging in these cases is a good approximation. However, if there are several minima in the potential, the relaxation between vibronic wavefunctions that are localised in different minima

can be much slower. This can lead to abrupt changes of the magnetic properties with temperature that do not follow a Boltzmann type law. The classic case of this is observed in the anisotropic to isotropic collapse of the ESR spectrum of $Zn[Cu]SiF_6.6H_2O$ as discussed in section 5.2.

Such a situation can also occur in systems of less than cubic symmetry. The experimental ESR spectra of Cu(II) doped Tutton salts and NH_4Cl are also characteristic of a potential surface with more than one minimum. These cases are considered in detail in chapters 7 and 8. The remainder of this chapter examines the way that vibronic relaxation effects can be incorporated into the molecular model that has been developed so far.

5.4.1 Causes of Vibronic Relaxation.

Rapid vibronic relaxation means that the rate of the transitions between the vibronic levels is much faster than the timescale of the ESR experiment. These transitions are due to the coupling of the molecular energy levels with the phonon continuum (Ham 1972, section 2.5; Gauthier and Walker 1976). In principle then, the continuous phonon spectrum should be included within the Jahn-Teller vibronic calculation. However, such a multimode calculation is impossible within the variational approach given in chapter 4.

Gauthier and Walker (1976) have used thermal Green function techniques to study the coupling of the ground vibronic ^2E state to the phonon continuum in the linear Jahn-Teller approximation. The present approach is to consider the Jahn-Teller coupling of the electronic E state only with the internal molecular vibrations of e symmetry. This then assumes that the low energy lattice phonons are only weakly coupled with the molecular Jahn-Teller system. The "isolated molecule" type calculations given in chapter 4 can then be kept, and although the lattice phonons are not considered explicitly, their existence are required to provide a relaxation mechanism between the vibronic levels of the molecule.

(5.21)

5.4.2 Lineshape Calculations.

The effects of vibronic relaxation on the lineshape of an ESR spectrum is identical to that of "motional narrowing" or "chemical exchange" in NMR spectra (Carrington and McLachlan 1967, chapter 12). The theory in both ESR and NMR is usually developed from the modified Bloch equations or density matrix theory (Heinzer 1971; Poole and Farach 1972, chapter 16; Kaplan and Fraenkel 1980). Here the results from the density matrix formalism are simply presented. The details behind these results are quite complex, and the above references can be consulted for additional information.

Considering now a particular problem where there are n_k vibronic levels each with their own magnetic properties. The energy of these levels and their properties can be calculated using the methods given in chapter 4 and sections 5.2, 5.3 respectively. In each level the ESR spectrum will consist of n_j lines representing the hyperfine transitions. If it is assumed that there will only be relaxation between levels of the same nuclear spin as well as electron spin, the problem can be solved separately for each hyperfine line (Binsch 1975, pg 52). The spectral lineshape is then given by (Heinzer 1971):

$$Y(v) \propto \text{Real} \left\{ - Q \sum_{j}^{n_j} M_j^{-1} P \right\} \qquad (5.32)$$

Here Q is a row vector of length n_k with elements all 1.0, P is a column vector containing the fractional populations of the n_k levels. The nxn matrix M can be decomposed into the parts dependent and independent of frequency:

$$M_j = B_j + i\, vI \qquad (5.33)$$

I is the nxn unit matrix and the elements of B are given by:

$$B_{pp}^j = -i\, v_{pj} - 1/T_{2p} - \sum_{r \neq p}^{n_k} K_{rp} \qquad (5.34)$$

$$B_{pq}^j = K_{pq}$$

Throughout this section the symbol i will represent the imaginary quantity $\sqrt{-1}$. The symbol T_{2p} represents the effective transverse

(5.22)

relaxation time (in seconds) of the spin in level p. In the present case it is just treated as a parameter to give the line widths of the spectrum in the absence of vibronic relaxation. It is therefore an effective relaxation constant which contains contributions from many line broadening mechanisms and instrumental factors (Binsch 1975, pg 48; Sandstrom 1982, pg 15). If the half width at half height of a Lorentzian ESR line is W Gauss, then the following relationship holds:

$$T_2 = (2\pi\beta gW)^{-1} \tag{5.35}$$

where g is the g value of the transition and $\beta = 1.4 \times 10^6$ is the Bohr magneton in units of Hertz/Gauss.

The symbol K_{rp} in equation (5.34) represents the rate of relaxation or exchange between the vibronic levels r and p. It is a first order rate constant in units of s^{-1}. K_{rp} is related to K_{pr} by the equilibrium condition: $P_r K_{rp} = P_p K_{pr}$, where P_r is the fractional population of the rth level (Heinzer 1971; Sandstrom 1982, pg 19).

The frequency v_{pj} is the energy of the Zeemann transition between hyperfine levels j in the vibronic state p, evaluated at a particular reference magnetic field. A value near the centre of the spectrum is usually taken (Kaplan and Fraenkel 1980, pg 25). Since the g-shifts in Cu(II) compounds are small, the reference field will be taken as the resonance field of a free electron at the microwave frequency of the spectrometer.

A spectrum calculated from (5.32) would involve inverting a complex n×n matrix at each frequency, which may be up to 1000 values for a typical spectrum. However, the decomposition of equation (5.32) into (5.33) may be exploited in the following manner given by Binsch (1968). The complex non-Hermitian matrix B can be made diagonal by a similarity transform:

$$U_j^{-1} B_j U_j = \Lambda_j \tag{5.36}$$

Here Λ_j is a column vector containing the n_k complex eigenvalues of B_j, While U_j is an n×n matrix containing the complex eigenvectors in columns. Equation (5.32) then reduces to:

$$Y(v) \propto - \text{Real} \left\{ \sum_j^{n_j} \sum_k^{n_k} S_{jk} (\Lambda_{jk} + iv)^{-1} \right\} \tag{5.37}$$

where S_j is a vector of the shape function whose elements are:

$$S_{jk} = \sum_m^{n_k} Q \ (U_j)_{mk} \ \sum_n^{n_k} (U_j^{-1})_{kn} \ P_n \qquad\qquad (5.38)$$

The use of equation (5.37) means that B needs to be diagonalised only once for each spectrum, saving an enormous amount of computer time. However, the second summation in (5.38) requires the solution of a system of complex linear equations.

It is usual to present an ESR spectrum as the derivative of the absorption, which from (5.37) gives:

$$\frac{d}{d\nu} Y(\nu) = - \ \text{Imag} \left\{ \sum_j^{n_j} \sum_k^{n_k} S_{jk} \ (\ \Lambda_{jk} - i\nu \ )^{-2} \right\} \qquad (5.39)$$

All parameters in matrix M, and therefore the spectral functions in (5.37) and (5.39), are measured in Hertz. These can easily be changed to field swept absorption or derivative curves for the appropriate microwave frequency of the spectrometer.

The following physical interpretation can be made of equations (5.37) and (5.38) (Binsch 1968, Heinzer 1971): The relative intensity of the spectral line jk is determined by the real part of S_{jk}, while the width and position are determined from the real and imaginary parts of Λ_{jk} respectively.

5.4.3 The Vibronic Rate Constants.

The vibronic rate constants, K in equation (5.34), will vary with temperature as the rate of transitions between the levels depends on the temperature of the phonon bath (Ham 1972). This dependence has been found to closely follow an Arrhenius law:

$$K_{ab} = \nu_o \exp(\ -E_{ab}/ \ kT \ ) \qquad\qquad (5.40)$$

where K_{ab} is the relaxation rate between states a and b separated by the "activation" energy E_{ab}. This is the same dependence for the rate constants as in motional averaging problems in NMR spectroscopy (Carrington and McLachlan 1967, pg210; Binsch 1975, pp75-6).

The exponential factor in (5.40) can be interpreted as the relative probability of finding the molecule in the bth state; or equivalently, to the probability of the phonon continuum exciting the

(5.24)

upward transition (Ham 1970, pg 55). The energy, E_{ab}, is then just the energy separation of the two levels, except for levels that are localised in different minima of the potential surface, where the "rate determining" step may be the excitation to a higher vibronic level that is delocalised over both wells.

This can be explained by the following arguments: All vibronic levels of the isolated molecule are initially orthogonal, and therefore direct overlap between them is zero. However, the coupling with the phonon bath causes the vibronic levels and wavefunctions, to be "smeared", and this allows transitions to take place as finite overlap of the wavefunctions occurs (Reynolds and Boatner 1975). Clearly a much greater overlap would be expected for wavefunctions within the same minimum, as the probability density of the their wavefunctions are in closer proximity. For wavefunctions in separate minima, the smearing of the wavefunctions will create only a small amount of overlap as the probability density of the unperturbed wavefunctions are far from each other.

The relaxation rate constant between two states that are localised in different minima is then better described by equation (5.40) with the energy E_{ab} being the height of the barrier between the minima, rather than their energy separation. This corresponds to a real transition to a level near the top of the barrier that is delocalised over both wells thus providing a pathway for relaxation to the level in the other minimum (Ham 1972, pg 56). The Arrhenius form of equation (5.40) is then easy to understand in terms of a classical rate of passage over a barrier.

The "random strain" introduced by Ham (1972) provides such a "phonon bath" for a relaxation pathway in cubic Jahn-Teller systems. This is in addition to the role the random strain plays in explaining the anisotropic g-values at low temperature in such systems. The calculation of line shapes of cubic systems have been made (Sester et al 1975) assuming some explicit form of the random strain. In the following section the lineshape formalism previously described is used to illustrate some of the effects that can result from relaxation in Cu(II) ESR spectra.

(5.25)

5.4.4 Example Calculations of Relaxation Effects.

Using the methods outlined in section 5.4.2, the general program EXCHGE was written for the simulation of spectral lineshapes. This is essentially the same program as that described by Heinzer (1971) except that it will calculate spectra for systems with up to 60 levels, each with an arbitrary number of hyperfine components. Library routines from EISPACK (Smith etal 1975) and LINPACK (Dongarra etal 1979) were used for the complex matrix diagonalisation and solution of the linear equations.

Two experimental examples will be considered:

   1) The variation of the hyperfine line widths and their temperature dependence in $Cu(II)/K_2Zn(SO_4)_2 \cdot 6H_2O$.

   2) The anisotropic to isotropic collapse of the ESR spectrum of Cu(II) doped into a cubic host with a random strain.

The lineshape simulation of the above cases are merely illustrative and will only consider a small number of levels. The relaxation rates between pairs of levels are assumed to take the Arrhenius form of (5.40) where the "activation energy" is simply the energy difference between the levels, unless otherwise stipulated.

The simple two level model of Silver and Getz (1974) will be used for the temperature dependence of $Cu(II)/K_2Zn(SO_4)_2 \cdot 6H_2O$. The levels are characterised in table 5.3 for the magnetic field directed along the x molecular axis:

TABLE 5.3

n	E_n/cm^{-1}	g_{xn}	$A_{xn} (\times 10^{-4} cm^{-1})$
1	0.0	2.42	96
2	75.0	2.15	20

The temperature dependence of the principal g and hyperfine values have been observed to follow the Boltzmann averaging that is expected for fast vibronic relaxation (Silver and Getz 1974). However, since the hyperfine values of the different levels vary, the frequency
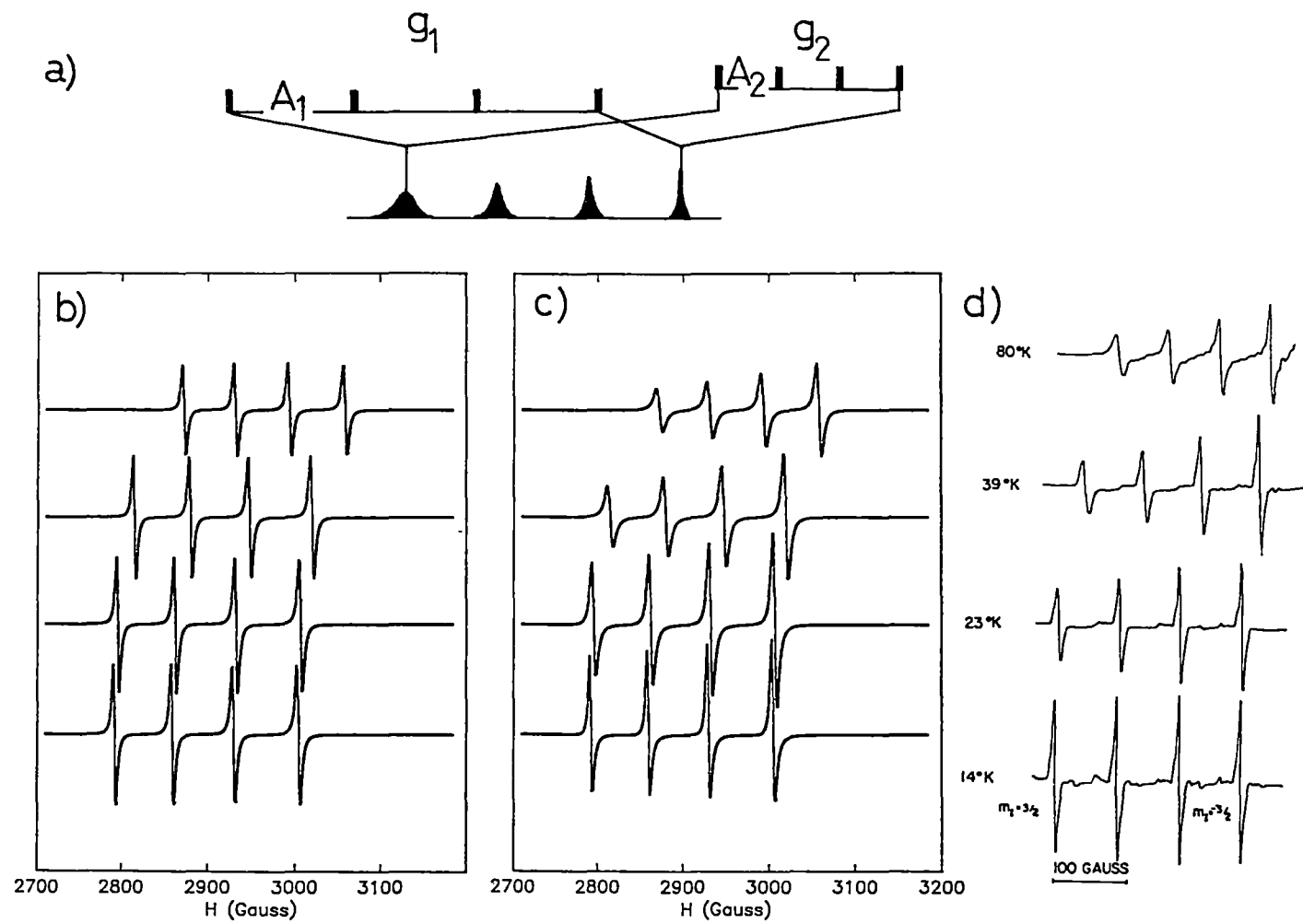
(5.26)

Figure 5.2 The low field spectrum of Copper(II) doped $K_2Zn(SO_4)_2 \cdot 6H_2O$.

a) The relaxation mechanism.

b) Simulated spectra with $K = 10^{15} S^{-1}$

c) Simulated spectra with $K = 6.5 \times 10^{10} \exp(-120/kT) S^{-1}$

d) Experimental spectra (from Silver and Getz 1974).

difference between the different levels will vary with the hyperfine transition. This will result a in different broadening of each hyperfine line if the relaxation rate is comparable to these frequency differences. This is illustrated schematically in figure 5.2a.

If the vibronic relaxation between levels is very fast, then there would be no contribution to the line widths from the relaxation. This is shown in figure 5.2b where, although the g and hyperfine values "change" with temperature, the halfwidths of the lines do not. This spectrum was simulated using the data in table 5.3 with an intrinsic halfwidth, W, of 3 Gauss and a relaxation time of 10^{15} Hz that satisfies the conditions of fast vibronic relaxation expressed by equation (5.31): $K = \tau_v^{-1} \gg \Delta v$.

In the other extreme, if there were no vibronic relaxation, then the spectra due to individual levels will by seen as these levels become thermally populated. The relaxation rate that will reproduce the observed experimental spectrum must be fast enough to "motional average" the spectra due to each level, but not so fast that it does not contribute to the halfwidths of the individual lines.

The simulated spectra shown in figure 5.2c were obtained with the temperature dependent relaxation rate given by equation (5.40) using the parameters found by Silver and Getz (1974): $v_o = 6.5 \times 10^{10} s^{-1}$ and $E_{12} = 120$ cm^{-1}. The simulated spectrum can be seen to compare well with the experimental spectrum of Silver and Getz in figure 5.2d.

A hypothetical cubic system is now considered. It is assumed that random strain will localise the molecule in one of the minima of a warped Mexican hat potential. A system for a strain directed along the z molecular axis is characterised by the three levels in table 5.4:

<p align="center"><u>TABLE 5.4</u></p>

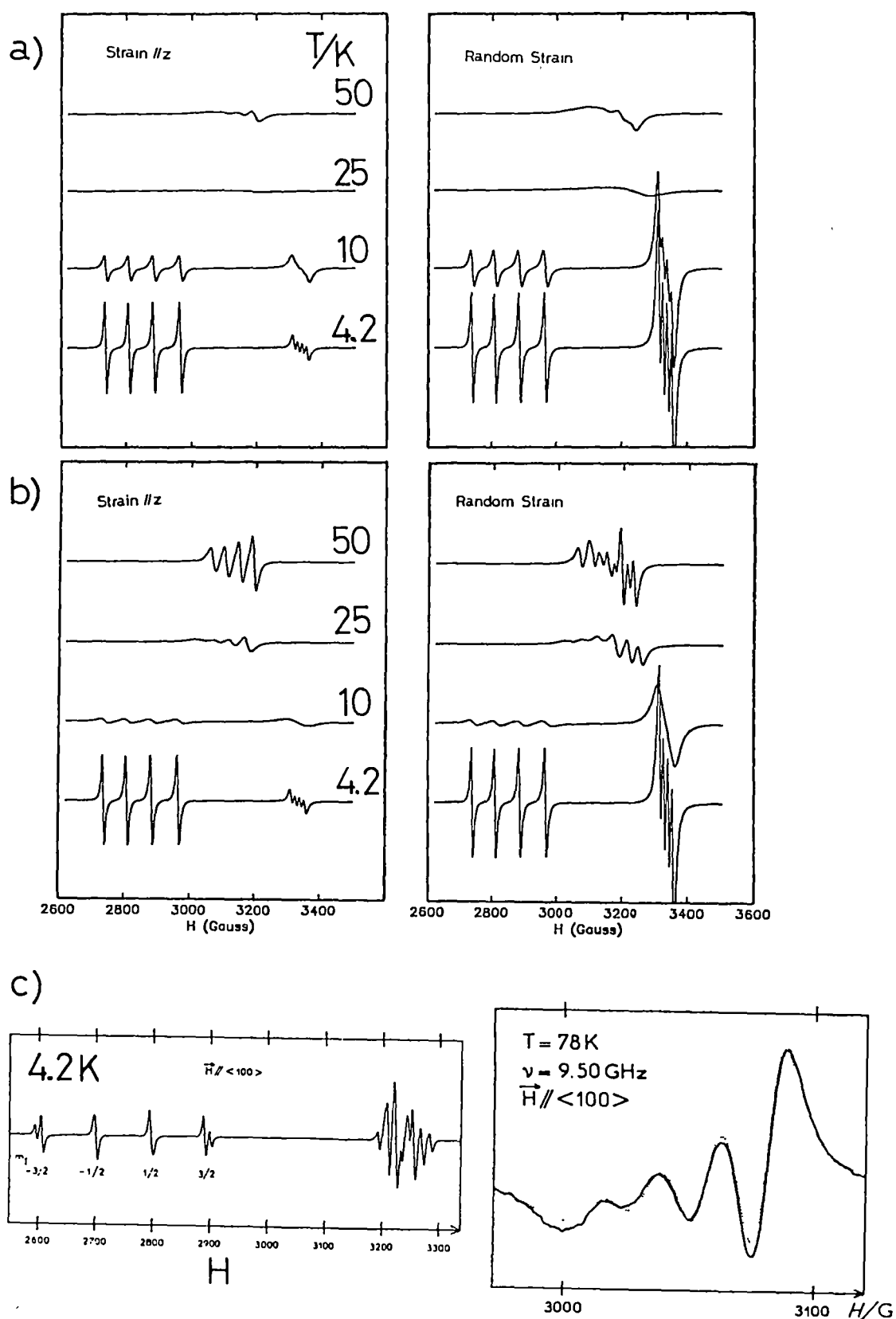| n	E_n/cm^{-1}	g_{xn}	g_{yn}	g_{zn}	A_{xn}	A_{yn}	A_{zn}
1	0	2.1	2.1	2.42	14	14	107
2	5	2.1	2.42	2.1	14	107	14
3	10	2.42	2.1	2.1	107	14	14

<p align="center">(5.27)</p>

Figure 5.3 The hypothetical spectrum of table 5.4.

a) Simulated spectra with $K = 1 \times 10^{10} \exp(-50/kT)$ s^{-1}.

b) Simulated spectra with $K = 5 \times 10^{10} \exp(-50/kT)$ s^{-1}.

c) Experimental spectrum of $Cu(II)/ZnSiF_6 \cdot 6H_2O$. (Taken from Dang etal 1974.)

These parameters are taken from the low temperature spectrum of Cu(II)/ZnSiF$_6$.6H$_2$O (Dang etal 1974). The spectra due to these levels are shown on the left hand side of figures 5.3a,b. Here the magnetic field is parallel to the z molecular axis and the relaxation rates are given by an activation energy of 50cm^{-1} with the pre-exponential factors of v_o = 1 x 10^{10}s^{-1} and 5 x 10^{10}s^{-1} respectively for figures a and b. The high field lines at low temperature are due to the small thermal population of the excited levels. It can be seen at about 25K the two sets of lines collapse to a single set.

In a real system the strain will randomly localise the molecule into different wells. This means that sites with the levels 1,2,3 permutated in table 5.4 are equally likely. Since the vibronic relaxation is assumed to be intramolecular only, the resulting spectrum is the same as that calculated from table 5.4 with the magnetic field along x, y, and z simultaneously appearing in the same spectrum. The temperature dependent spectra for this random strain, with the magnetic field directed along a principal axis, are also shown in figures 5.3a,b. The experimental spectrum of copper doped Zn(SiF$_6$).6H$_2$O is shown in figure 5.4c for comparison (Dang etal 1974).

The main temperature dependent features are correctly reproduced by the simulation. These are the anisotropic to isotropic collapse of the spectrum, and the unequal halfwidths of the hyperfine lines in the isotropic spectra. However no attempt is made to fit the experimental spectrum as the real situation in this molecule is likely to be considerably more complicated. A similar case of exchange narrowing occurs in the orthorhombic to tetragonal coalescence of the ESR spectrum of a copper centre in NH$_4$Cl. This is considered in detail in chapter 8.

In the following three chapters, the theory in the previous chapters is applied to the interpretation of the temperature dependent g-values of copper complexes. In these three chapters, complexes of increasingly low symmetry are considered: tetragonal and orthorhombic complexes with identical ligands in chapters 6 and 7 respectively, and mixed ligand complexes in chapter 8. A general concern of this thesis is whether the Jahn-Teller formalism, which is really only appropriate to cubic systems, can be successfully applied to low symmetry compounds.

6.1   INTRODUCTION

6.1.1 "Octahedral" Copper.

A static six coordinate copper complex cannot be rigorously octahedral according to the Jahn-Teller theorem because it has a doubly degenerate electronic ground state. The highest static symmetry that is allowed is tetragonal, where the distortion can either be an elongation or compression of the octahedron. A dynamic CuL_6 system, on the other hand, may have a time averaged octahedral geometry but this can only occur in cubic crystal systems where the barriers along the angular coordinate of the Mexican hat potential is small. Such behaviour has been observed, for example, in Cu(II)/CaO (Boatner etal 1977).

The tetragonal distortion that is observed experimentally is most commonly an elongation. This corresponds to the warping terms in the potential forming minima at ϕ = 0, 120 and 240° in the Mexican hat potential surface. Yamatera (1979) has shown that the alternative tetragonal compression is less stable.

The crystal structure determination of CuL_6 systems can often reveal a compressed geometry which actually results from either a time average or space average of elongated octahedra (Bertini etal 1979). A true compressed CuL_6 geometry, however, can often be found in doped

systems where the symmetry of the host lattice may impose a compression that is greater than the intrinsic tendency of Cu(II) to elongate.

These systems are of special interest as the deviation of $g_{||}$ from the value expected from a pure $d(z^2)$ ground state is quite sensitive to the small mixture of $d(x^2-y^2)$ caused by vibronic coupling. In addition, the balance of the strain and warping terms can result in a potential that is relatively shallow and anharmonic. This then will be sensitive to the temperature of the system. Both the low temperature g-values and their temperature dependence make copper in a compressed octahedral geometry ideal for the study of vibronic coupling effects.

6.1.2   Examples of Compressed Octahedra.

An early ESR study of a system that was interpreted as due to compressed octahedra was reported by Hayes and Wilkins (1964), in conjunction with the theoretical study of O'Brien (1964). Later studies also found compressed octahedra for Cu(II) doped into the following hosts: $Ba_2Zn(HCO_2)_6.4H_2O$ (Reddy and Srinivasan 1966); CsCl (Hagen and Trappeniers 1973); Ba_2ZnF_6 (Friebel etal 1976); and K_2ZnF_4 (Reinen and Krause 1980). In these studies no attempt was made to quantitatively interpret the effects of vibronic coupling, all simply commenting that an "O'Brien mechanism" is likely to be present. It is the subject of this chapter to make such a quantitative study of the temperature dependence of the $Cu(II)/K_2ZnF_4$ system.

In the previous study of Reinen and Krause (1980), it was recognised that relatively large vibronic mixtures of $d(x^2-y^2)$ were involved, but it could not be determined whether this was due to a single minimum at $\phi = 180^{\circ}$, or dynamic exchange between two orthorhombic minima at $\phi = 180 \pm x^{\circ}$. Other examples of a compressed octahedral geometry occur in mixed ligand systems, such as $Cu(II)/NH_4Cl$, but their treatment is considerably more complicated and the study of this system is left to chapter 8.

(6.2)

6.1.3. Experimental

The K_2ZnF_4 host lattice consists of layers of ZnF_6^{4-} polyhedra connected by four common corners, as shown in figure 6.1.
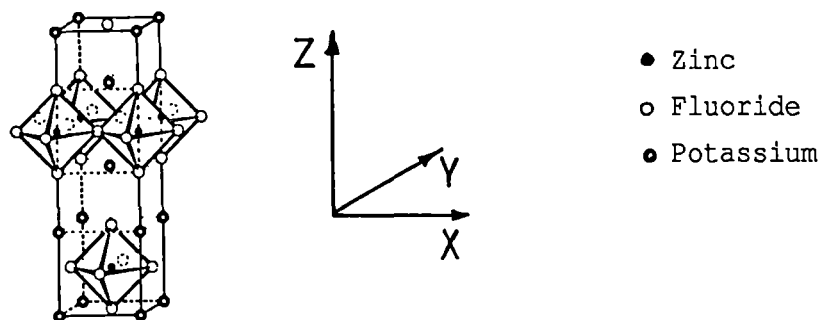
FIGURE 6.1 The Structure of K_2ZnF_4 (from Reinen and Krause 1981).

The axial flouride bonds are only slightly shorter than the equatorial Zn-F = 202pm(2x), 203pm(4x) (Herdtweck and Babel 1980), and although ZnF_6^{4-} is nearly octahedral, it is apparently the fact that the four equatorial flouride ligands are shared while the two axial ones are not, which makes this a compressed octahedral site.

The ESR spectrum of $Cu(II)/K_2ZnF_4$ was measured by M.A. Hitchman in the temperature range 4-300K at both X and Q band. The tetragonal g-tensor was found to lie with $g_\parallel$ aligned along the z molecular axis in figure 8.1, with $g_\perp$ showing no angular dependence in the (001) plane.

The g-values at 4.2K, $g_\parallel$ = 2.0030(5), $g_\perp$ = 2.390(5), are characteristic of a $d(z^2)$ ground state. As the temperature is raised, $g_\parallel$ is observed to increase while $g_\perp$ decreases, as shown in figure 6.3. Many different samples where used and this served to provide an estimate of the uncertainties in the recorded g-values (Hitchman 1986). The measurement of $g_\parallel$ was considerably more precise than $g_\perp$ and is also more sensitive to vibronic coupling. For these reasons, in addition to the fact that the dependence of $g_\parallel$ shows other interesting features, the emphasis in this study has been to reproduce the features of $g_\parallel$, while keeping within the constraint of broadly reproducing $g_\perp$.

(6.3)

The system shows considerable hyperfine structure; in particular, there is coupling with the axial and equatorial ligands. The latter is usually indicative of a $d(x^2-y^2)$ component in the ground state. A low temperature hyperfine analysis has been reported by Hitchman et al (1986), but because of broadening effects the temperature dependence could not easily be studied and is not considered here.

The electronic spectrum of the doped $Cu(II)/K_2ZnF_4$ system has been measured by Reinen and Krause (1981) who observed the following transitions that are typical of a compressed copper geometry:

$$d(z^2) \rightarrow d(x^2-y^2) \quad : \quad 5,200 \text{ cm}^{-1}$$
$$\rightarrow d(xz), d(yz): \quad 9,000 \text{ cm}^{-1}$$
$$\rightarrow d(xy) \quad : \quad 10,500 \text{ cm}^{-1}$$

The pure K_2CuF_4 compound has also been the subject of many optical absorption and MCD studies. The assignments of Laiho (1975) agree with those of the doped compound above, but disagree with the works of Kleeman and Farge (1975) and Ferre etal (1979). These later studies place the lower transition at 900 cm^{-1}. However, this conflicts strongly with the degree of distortion in the complex and conventional ideas about bonding. The electronic spectrum of the pure compound is interesting as the middle transition shows considerable vibrational fine structure.

A similar study of the low temperature absorption spectrum of the doped system would be very interesting as the vibrational structure may be even more resolved. The structure on this transition would be expected to involve progressions in two totally symmetric, and one Jahn-Teller active, vibrations. These three vibrations would be of a_{1g}, a_{1g} and e_g symmetry in the D_{4h} point group, corresponding to the vibrations of a_{1g}, $e_g(\theta)$ and t_{2g} symmetry respectively in the parent octahedral group (ie the Jahn-Teller active vibration will not correspond to either of the pseudo Jahn-Teller vibrations of the present problem). Such a study would provide very detailed information about the geometry of the complex in this excited state.

(6.4)

6.2 METHOD

6.2.1 The Vibronic Hamiltonian.

The method used here to calculate the temperature dependent g-values is to treat the CuF_6^{4-} centre in the K_2ZnF_4 lattice as a discrete unit. Multimode effects are then ignored. The vibronic Hamiltonian of the Exe Jahn-Teller system is used with a tetragonal strain component added to account for the low symmetry of the host.

The vibronic Hamiltonian to be solved is given by the equation (4.26) from chapter 4. Here only the first order electronic coupling is included, and the warping of the Mexican hat potential was achieved by the anharmonicity of the e_g vibration. It was found that the small size of the anharmonicity constant that was required did not cause the computational difficulties that were outline in section 4.2.2. Both the second order electronic coupling, A_2, and the orthorhombic strain, S_θ, in the vibronic Hamiltonian are set to zero for the present problem.

A basis size of 506 was found to be sufficient for this problem. Since the vibronic Hamiltonian has tetragonal symmetry, the methods outlined in section 4.4 have been used to symmetry block the secular equation. Diagonalisation was performed by both Householder and Lanczos algorithms, giving identical results.

6.2.2 Calculation of the g-values.

The calculation of the g-values in this study is very straightforward. The vibronic wave functions can be found by solving the vibronic Hamiltonian. From these the electronic properties can be calculated by the methods of section 5.2. These are the $<A^2>$ and $<B^2>$ coefficients which are the fraction of the $d(z^2)$ and the $d(x^2-y^2)$ basis functions in the vibronic wavefunction. As discussed in section 5.2.3, since there is no orthorhombic component of the strain, the crossterms $<AB>$ will be zero.

A single average value for the energy of the excited electronic triplet states was taken, $E(T) = 9,500$ cm^{-1}, as well as an isotropic

orbital reduction factor, k = 0.9. This means that, in the present approach, the g-values of the vibronic states depend <u>only</u> on their electronic composition, not on any geometric properties of the wavefunctions.

Using a value of 830 cm^{-1} for the spin-orbit coupling constant, the parameters in the second order perturbation expressions of equation (5.15) are then calculated to be u = 0.0704. These expressions can then give the expected g-values for pure $d(z^2)$ and $d(x^2-y^2)$ electronic states:

$$g_{\parallel}(z^2) \quad = 1.987 \qquad g_{\perp}(z^2) \quad = 2.395 \qquad (6.1)$$
$$g_{\parallel}(x^2-y^2) = 2.531 \qquad g_{\perp}(x^2-y^2) = 2.123$$

The observed g-values will then be:

$$g_{\parallel} = g_{\parallel}(z^2) \langle A^2 \rangle + g_{\parallel}(x^2-y^2) \langle B^2 \rangle \qquad (6.2)$$
$$g_{\perp} = g_{\perp}(z^2) \langle A^2 \rangle + g_{\perp}(x^2-y^2) \langle B^2 \rangle$$

Substituting the low temperature g-values given in section 6.1.3, and the g-values expected for the pure electronic basis functions, the equations in (6.2) can be solved to give the following electronic composition of the lowest vibronic level:

$$\langle A^2 \rangle = 0.97; \qquad \langle B^2 \rangle = 0.03 \qquad (6.3)$$

Since $\langle A^2 \rangle + \langle B^2 \rangle$ must always equal 1.0, the equations in (6.2) can be solved separately, both roughly giving the same result. The values in (6.3) are for the more accurate $g_{\parallel}$ values. It is also clear from (6.2) that $g_{\parallel}$ is more sensitive to vibronic coupling. For a particular value of $d(x^2-y^2)$ mixed into the predominantly $d(z^2)$ ground state, the shift of $g_{\parallel}$ is much greater than $g_{\perp}$ from the values of a pure $d(z^2)$ ground state. This also explains why $g_{\parallel}$ is observed to be more temperature dependent than $g_{\perp}$.

It was shown in figure 5.1 of chapter 5, that the use of the second order perturbation expressions is quite a good approximation to the "exact" calculation for the present system. Comparison of the first, second and exact calculations in figure 5.1 indicates that the perturbation expressions will slightly underestimate the orbital reduction parameter k. For simplicity this effect is ignored and the

(6.6)

second order perturbation expressions are used with the electronic coefficients obtained from the vibronic wavefunctions.

The calculation of the g-values for finite temperatures can be done in one of two ways. Either the g-values of all the thermally populated levels can be calculated from (6.2) and then a Boltzmann average taken; alternatively a Boltzmann average can be taken of the electronic properties $<A^2>$ and $<B^2>$ and then the g-values calculated from (6.2). Both methods will give identical results. It is the former, however, that is strictly correct. It is not the electronic properties of the system that are averaged, but rather the g-values, or more strictly, the ESR spectrum, that is averaged. This is because of the fast vibronic relaxation or "motional narrowing" that occurs on the ESR timescale. An hypothetical "fast" experiment could verify this by detecting the electronic properties of each vibronic level, though in practise this would be difficult as the electronic properties of the levels only differ slightly.

6.2.3 Estimation of the Parameters.

Four parameters in the vibronic Hamiltonian need to be specified:
A_1:   The linear coupling constant.
K_2, K_3: The force constant and anharmonicity of the e_g vibration.
S_θ: The magnitude of the tetragonal strain.

The features which may be observed experimentally are: the low temperature g-values, the temperature dependence of the g-values and the optical spectrum. The optical spectrum can give the transition between the two Jahn-Teller potential surfaces directly. This transition is approximately $d(z^2) - d(x^2-y^2)$ in the present system and has been observed at 5,200 cm^{-1} (Reinen and Krause 1981). In terms of the potential parameters this corresponds to the energy:

$$\Delta E = 4 \; E_{JT} + 2 \; |S_\theta|; \quad E_{JT} = A_1^2 / (2K_2) \tag{6.4}$$

The low temperature g-values, on the other hand, are determined by the zero point vibration which in turn is mainly dependent on the relative magnitude of S_θ and K_3. This is for a particular set of the

(6.7)

magnetic parameters: k, ζ, E(T) that have already been chosen in the previous section to give (6.1).

Where g(average) is determined by these magnetic parameters, the anisotropic part of the g-tensor ($g_\perp - g_\parallel$) is determined by the relative mixture of the $d(z^2)$ and $d(x^2-y^2)$ electronic basis functions in the vibronic states. The lowest state must contain the correct mixture given in (6.3) to reproduce the low temperature g-values, while the higher vibronic states must have both the correct mixtures and energies above the ground state to reproduce the temperature dependence of the g-values.

Although it has been shown here that the experimental observables are related to the parameters of the vibronic Hamiltonian in a complex manner, a systematic approach can reveal a unique set of these parameters that "fits" experiment.

(6.8)

6.3 RESULTS

6.3.1 Fitting the Parameters

The transition energy to the upper Jahn-Teller is determined by three parameters in (6.4). Figure 6.2a shows sets of these three parameters that fit the observed transition energy by satisfying (6.4). It can be seen that the fit is most sensitive to the linear coupling constant A_1. For reasonable values of hv and S_θ, the linear coupling constant, A_1, must lie in the range 600-900 cm^{-1}.

Another experimental observable that can be used is the Jahn-Teller radius ρ_0 which can be determined from X-ray structural data. For pure K_2CuF_4 this equals ~35pm (Reinen and Krause 1981), but because of cooperative effects this is likely to be larger than for a discrete CuF_6^{4-} centre. From the study of mixed crystals at various concentrations a value of ρ_0 ~27.5pm was concluded by Reinen and Krause (1981) for an infinitely dilute crystal. This dimensioned Jahn-Teller radius is related to both A_1 and hv by the following expression:

$$A_1 = \rho_0 x \, hv; \quad x = 1.722 \times 10^{-3} [M.hv]^{1/2} \qquad (6.5)$$

The values of A_1 and hv that satisfy (6.5) when $\rho_0 = 27.5pm$ is shown as a dashed line in figure 6.2a. Intersections of the dashed and full lines represent possible solutions that simultaneously satisfy both ρ_0 and ΔE.

The next easiest experimental observable to fit is the low temperature g-values, and figure 6.2b shows the values of S_θ and β that reproduce $g_{\parallel}(0)$ for several values of hv. For each value of hv, the linear coupling constant that reproduces ρ_0 is taken (ie the dashed line in figure 6.2a). However, an arbitrary point along these plots will not fit either ΔE or the temperature dependent g-values. As with A_1 and S_θ in figure 6.2a, β and S_θ are near linearly related. Plots of β and S_θ, chosen to fit both the low temperature and temperature dependent g-values, versus ΔE, A_1 and hv are shown in figure 6.2c. Here, at $\Delta E = 5,200cm^{-1}$, there are sets of A_1 and hv that appear to fit all the experimental data.
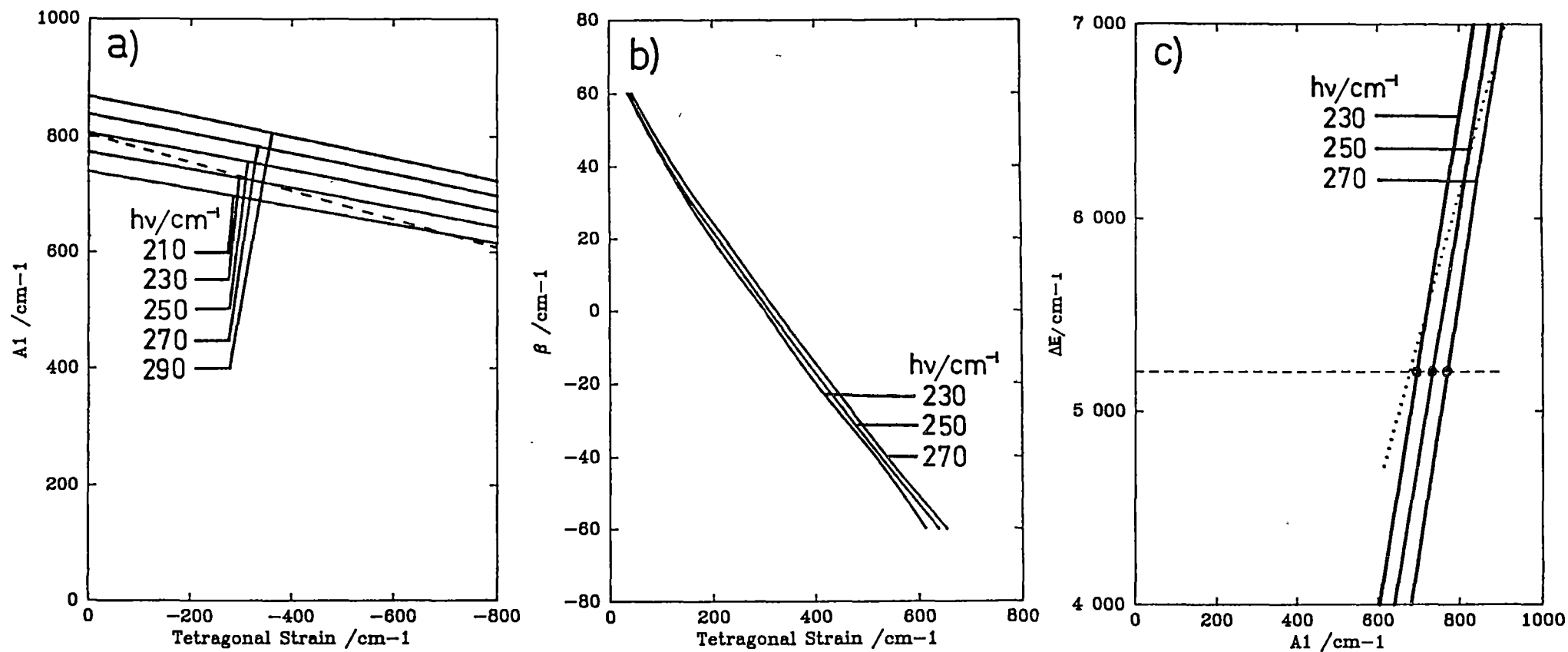
Figure 6.2 Fitting the Parameters.

a) To fit $\Delta E = 5,200$ cm^{-1}, — — — — $(h\nu, A_1)$ to fit $\rho_o = 27.5$pm.

b) To fit $g_{||}(0) = 2.0030$ and $\rho_o = 27.5$pm.

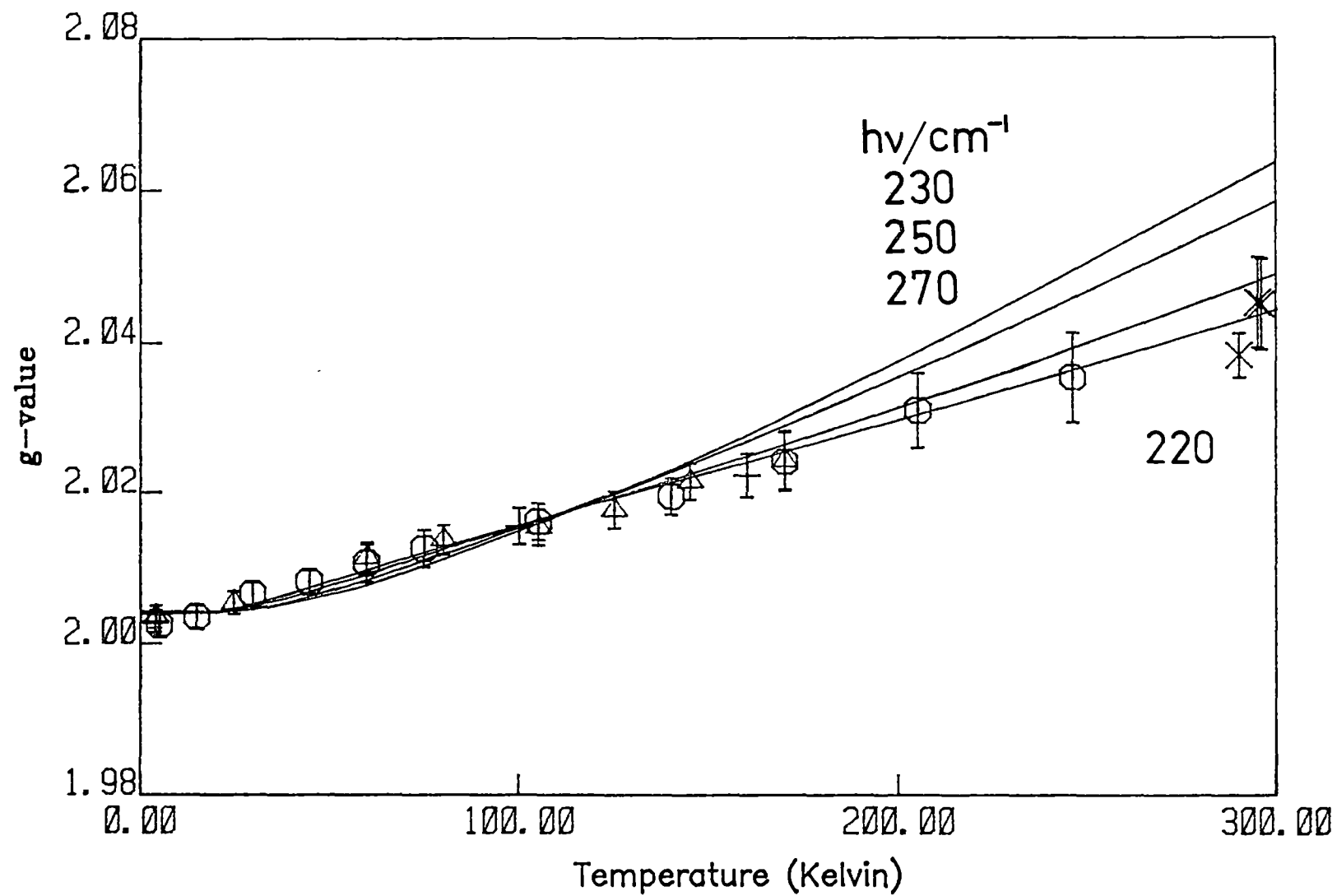c) To fit $g_{||}(0) = 2.0030$; — — —$(h\nu, A_1)$ to fit ΔE, ·······$(h\nu, A_1)$ to fit ρ_o.

Figure 6.3 The Temperature Dependence of $q_\parallel$.

From the potentials with the parameters marked ● in figure 6.2c.

If the extra information that ρ_0 ~27.5pm is used, then this gives the dotted line in figure 6.2c. The intersection of the dotted and dashed lines occurs at a frequency of $h\nu$ ~220 cm^{-1} and $A_1 = 673$ cm^{-1}. When these are related back to figures 6.2a and 6.2b, the unique values of $S_\theta = -541$ cm^{-1} and $\beta = 51.5$ cm^{-1} respectively, are obtained.

However, the value of ρ_0 was estimated using many approximations, and it would be preferable to determine it by independent means. This is done by calculating the temperature dependent g-values for other pairs of $(A_1, h\nu)$ that intersect the dashed line in figure 6.2c. Plots obtained using these values are shown in figure 6.3.

It can be seen that while the low temperature g-values and the general temperature dependences are reproduced, only one set gives the inflection in the curve of $g_\parallel$ at low temperature. This particular set also corresponds to that predicted using $\rho_0 = 27.5$ cm^{-1}. The final parameters obtained are then fully consistent with all the experimental data and are in a sense overdetermined. This, coupled with the sensitivity of the fit shown in the following section, suggests that parameters of this system can be determined uniquely.

6.3.2 Sensitivity of the Fit.

The sensitivity of the fit to the parameters determined in the previous section are briefly discussed here. The lower adiabatic potential surface of the best fit potential is shown in figure 6.5a. The angular cross section of this surface at constant $\rho = \rho_0$, is shown in figure 6.5b. However, it should be noted that the least energy path around the two dimensional surface is far from circular, and figure 6.5b is only a schematic representation to display the calculated energy levels.

Of all the parameters that define the potential surface, it is the warping parameter that is most difficult to independently quantify, as it is a composite parameter resulting from many competing mechanisms of which the anharmonicity will be just one (Deeth and Hitchman, 1986). This warping parameter can be conveniently described by β $(\sim -K_3\rho_0^3)$ where 2β is the barrier height between equivalent minima of the warped Mexican hat in the absence of strain. In a sense β is a parameter used to "fine tune" the potential into the shape desired.
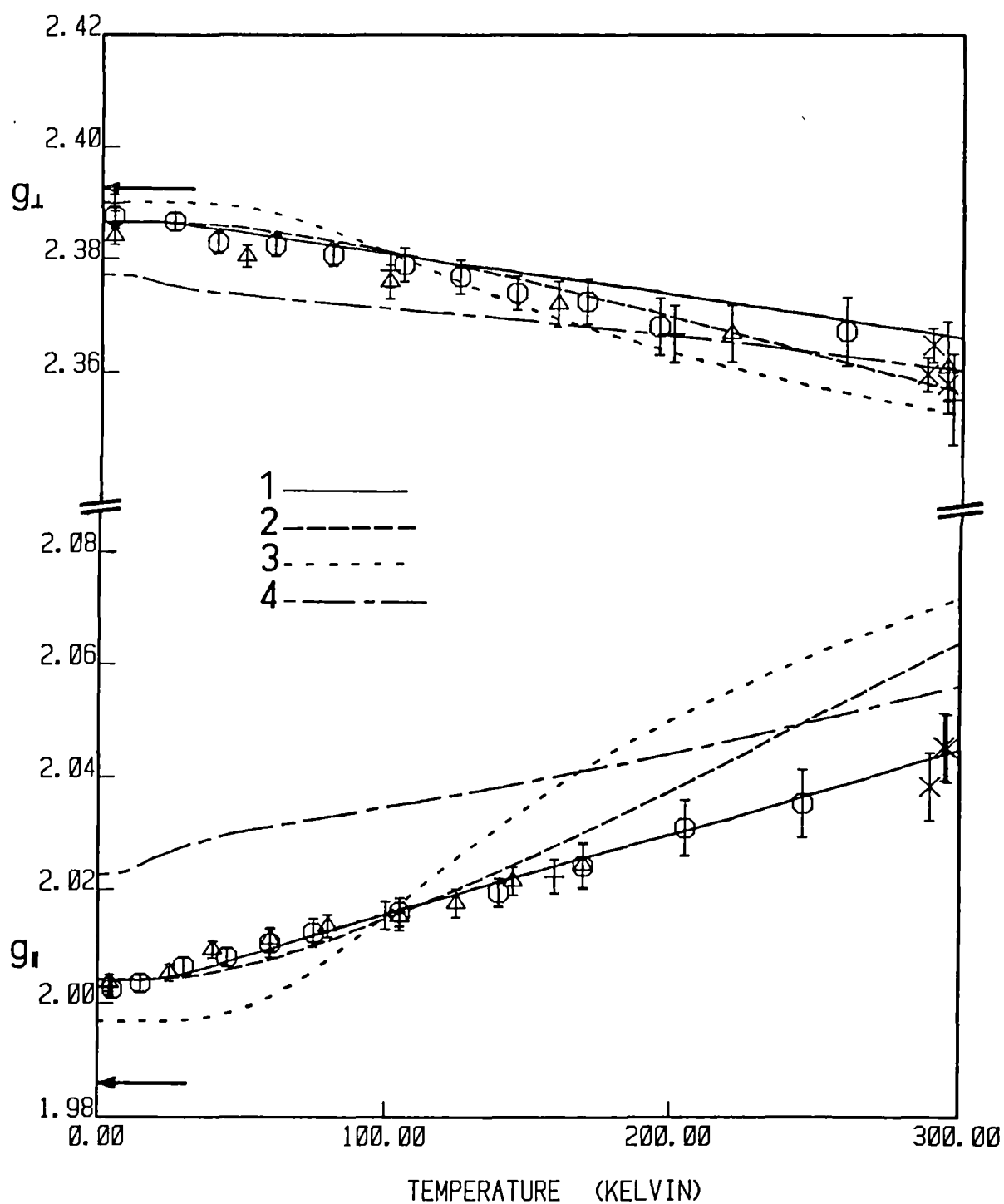
(6.10)

Figure 6.4 Experimental and Calculated g-values.

Curve 1: Best fit calculation. Parameters for all curves given in text.

The temperature dependent g-values for $\beta = 0$ and 100 cm^{-1} are shown in curves 3 and 4 respectively in figure 6.4, where the other parameters are kept at the values given in (6.5). It can be seen that these values fit neither the low temperature g-values nor their temperature dependence. The value of β can then be said to be well fixed at ~ 50cm^{-1} for this system assuming the values of all the other parameters.

The best fit linear coupling constant $A_1 = 673$cm^{-1} ($V = 75$cm^{-1}pm^{-1}) is somewhat lower than that determined by the optical spectra and structure of pure copper (II) flouride complexes, $A_1 = 816$cm^{-1} ($V = 100$cm^{-1}pm^{-1}) (Reinen and Krause, 1981). Again it is not at all surprising that the best fit value of A_1 for this doped system is less than in the pure cases, as cooperative effects would tend to increase A_1 in the latter case. If a larger value of A_1 is used with the other parameters chosen to fit the low temperature g-values and optical spectra ($A_1 = 770$cm^{-1}; $h\nu = 270$cm^{-1}; $S_\theta = -400$cm^{-1}; $\beta = 12$cm^{-1}), then curve 2 in figure 6.4 results. [Note: Slightly different values of these parameters were erroneously given in figures 6 & 7 of Riley etal (1986).] However, this curve does not reproduce the temperature dependence of the g-values. The angular potential obtained using these parameters is shown in figure 6.5c and can be compared directly with the best fit potential, clearly illustrating why the temperature dependence of this does not fit using this potential.

The inflection in $g_{\parallel}$ at ~ 60K implies that there must be angular vibrations of quite low energy. This occurs for particular values of S_θ and β which result in a highly anharmonic potential along the angular coordinate. The best fit potential in figure 6.5b has such a low lying level (62cm^{-1}) when compared to the potential in figure 6.5c (~ 100cm^{-1}).

These low lying levels could only be found for quite a low frequency of the e_g vibration, $h\nu = 220$ cm^{-1}. This hypothetical frequency of the CuF_6^{4-} unit in the absence of vibronic interactions or strain, is substantially lower that that observed in the $Ni(H_2O)_6^{2+}$ (305cm^{-1}) or $Zn(H_2O)_6^{2+}$ (278cm^{-1}) by Jenkins and Lewis (1981). However, such a low value appears necessary to fit all the experimental observables in the present study.

(6.11)
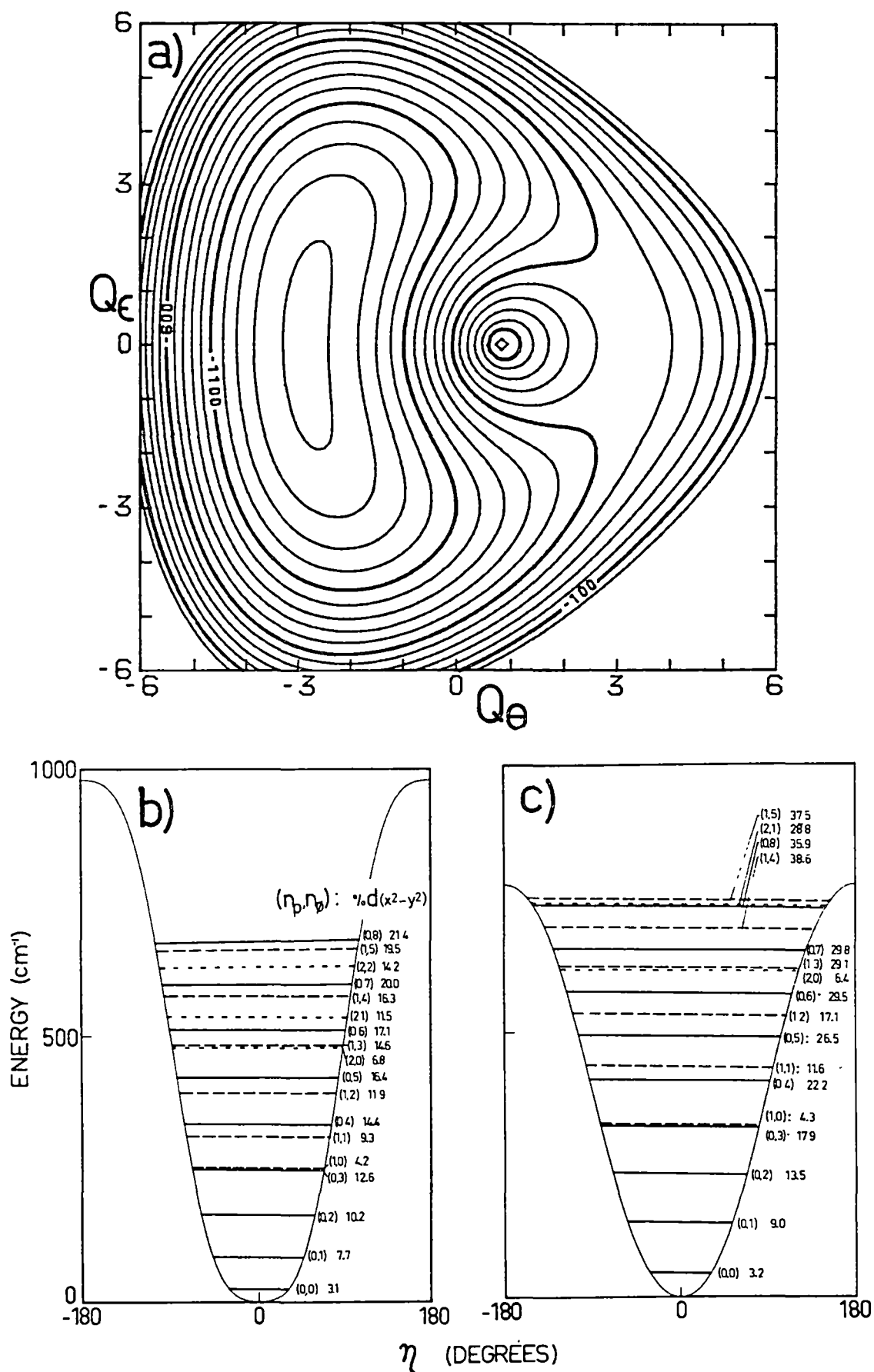
Figure 6.5 The Potential Surfaces.

a) Contour plot of the best fit potential surface.

b) Plot of the above potential at constant ρ_o.

c) Plot of the potential surface that gives curve 2 of figure 6.4.

6.4 DISCUSSION

6.4.1. The Best Fit Parameters.

The parameters that were found to best fit experiment are:

$$A_1 = 673 \text{ cm}^{-1} \quad (V = 75.0 \text{ cm}^{-1}\text{pm}^{-1}) \tag{6.6}$$
$$h\nu = 220 \text{ cm}^{-1} \quad (f = 0.54 \text{ mdyne}\text{Å}^{-1})$$
$$K_3 = -1.8 \text{ cm}^{-1} \quad (\beta = 51.4 \text{ cm}^{-1})$$
$$S_\theta = -541 \text{ cm}^{-1}.$$

The additional values on the right are equivalent ways of expressing these parameters in alternative units. Other quantities of interest are:

$$E_{JT} = 1029 \text{ cm}^{-1}$$
$$\rho_0 = 3.0591 \qquad (= 27.5\text{pm})$$

The vibronic energy levels and wavefunctions calculated for these parameters are shown in figures 6.6 and 6.7. The energy levels are shown inside the circular cross section of the lower Jahn-Teller surface at constant ρ_0. The zero point vibration energy of the radial vibration has been subtracted from these levels.

Approximate radial and angular quantum numbers (n_ρ, n_ϕ) are given to each level and the members with 0,1,2 radial quanta are shown, as full, dashed and dotted lines respectively. These approximate quantum numbers can be understood if the vibrational part of the vibronic wavefunctions are plotted explicitly. These are shown in figure 6.6 as probability functions in the Q_θ-Q_ε plane. As in a simple harmonic oscillator, the 0,1,2... quantum numbers correspond to 0,1,2... nodes in the wavefunctions along the radial or angular coordinates.

Also shown, next to the energy levels, is the percentage of the $d(x^2-y^2)$ orbital in the predominantly $d(z^2)$ wavefunctions. For higher quanta of the angular vibration, this mixture quickly increases. Even though each vibronic function is symmetric about $\phi = 180^\circ$ as required by symmetry, the more delocalised they become, the more $d(x^2-y^2)$ character is mixed in dynamically. The radial vibration, however, is much less effective in mixing in $d(x^2-y^2)$ as the two surfaces of the
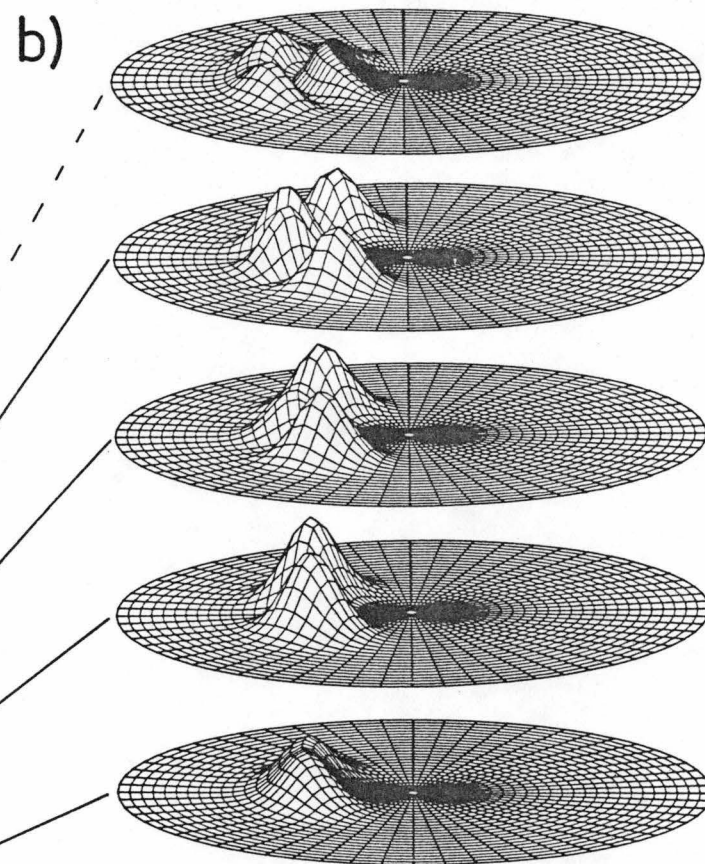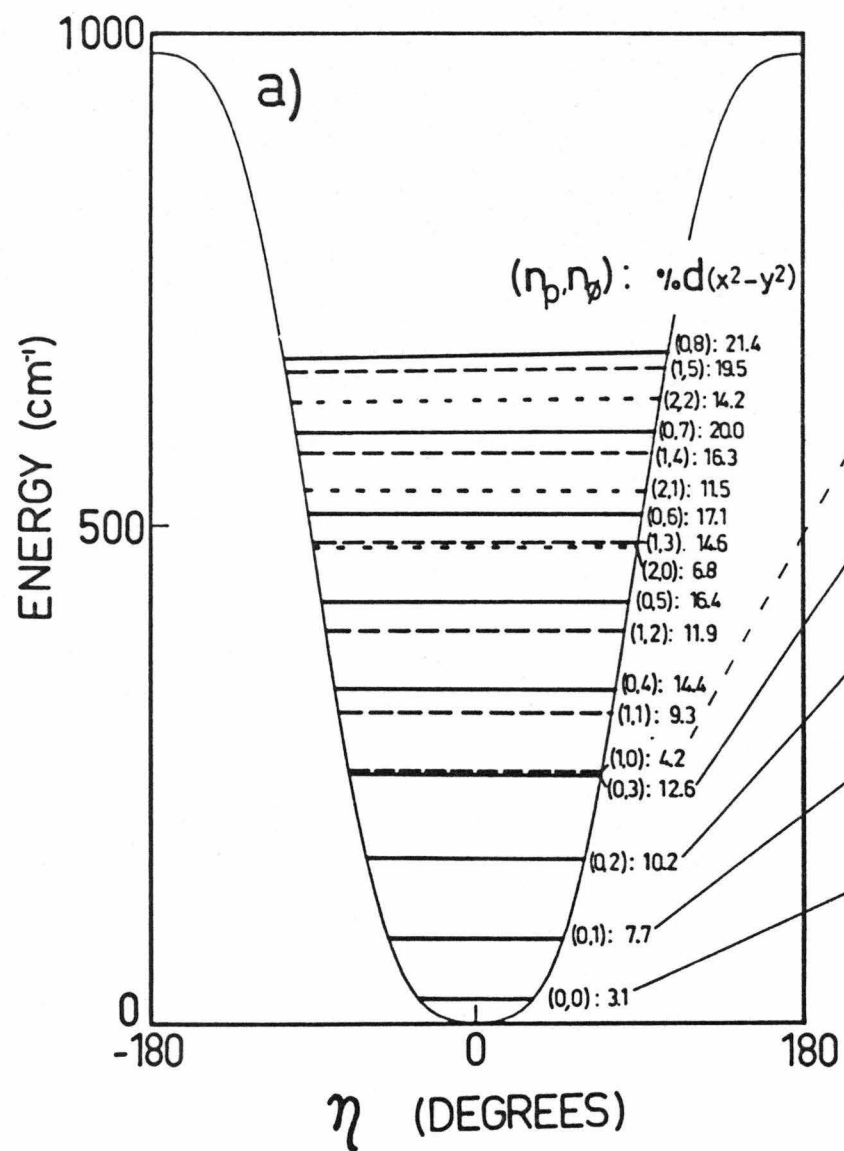
Figure 6.6 Best Fit Potential Surface and Wavefunctions.

a) Energy levels and approximate quantum numbers.

b) The vibrational part of the vibronic wavefunctions.
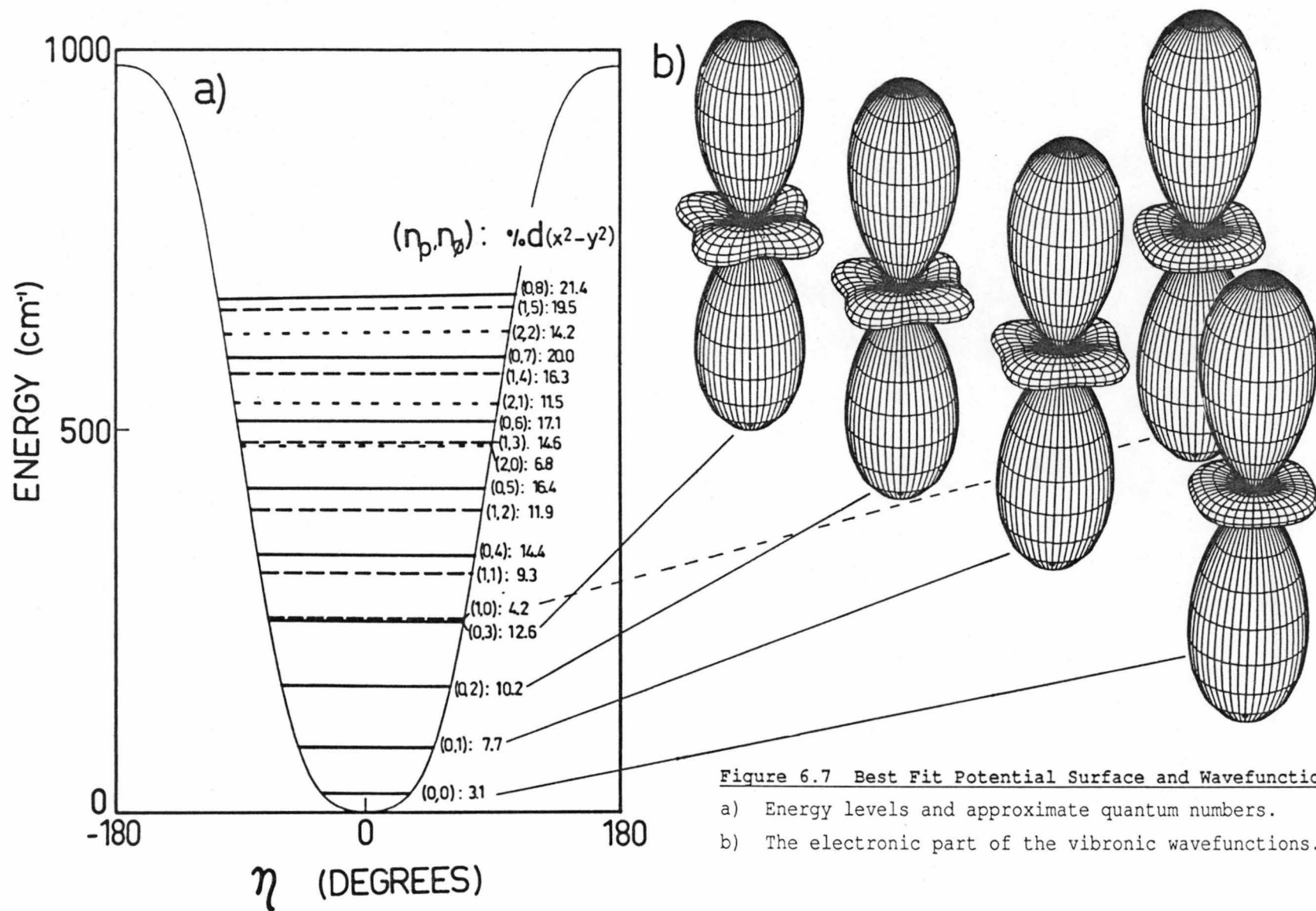
Figure 6.7 Best Fit Potential Surface and Wavefunctions.

a) Energy levels and approximate quantum numbers.

b) The electronic part of the vibronic wavefunctions.

Mexican hat potential are separated by a large amount in these strong Jahn-Teller coupling systems.

The electronic composition of the vibronic levels can also be illustrated by considering the electronic part of the wavefunctions explicitly, as shown in figure 6.7. The lowest level is nearly a pure $d(z^2)$ orbital, with the ~3% $d(x^2-y^2)$ causing only a small protuberance along the x and y axes. For the higher levels, as a greater mixture of $d(x^2-y^2)$ is involved, these lobes grow. With the first excited radial vibration (1,0), the almost pure $d(z^2)$ orbital is again calculated.

6.4.2 Comparison with other Calculations.

The present calculations indicate that there is only a single minimum at $\phi = 180^\circ$, therefore ruling out the alternative explanation of rapid exchange between two orthorhombic minima for the low temperature g-values in this system made by Reinen and Krause (1981). Although there have not been other quantitative determinations of the coupling constants of CuF_6^{4-} from experiment, several theoretical studies have been carried out. The results of these studies are given in table 6.1 in terms of the units that are used here.

<u>TABLE 6.1   Vibronic Constants of CuF_6^{4-}</u>

	Present Work.	Liehr & Ball.(1958)	Pelikan etal (1985)	Shashkin & Goddard (1986)
METHOD	Experiment	Crystal Field	CNDO/INDO	HF-CI Cluster Model
$h\nu/cm^{-1}$	220	210	681	270
A_1/cm^{-1}	673	693	427	702
E_{JT}/cm^{-1}	1029	1142	134	1075
β/cm^{-1}	51.5	200	4	674

With the exception of the study by Pelikan etal (1985), and the values of β, good agreement was found with the calculated values. This gives some confidence to the values obtained in the present study,

especially as the work of Shashkin and Goddard (1986) appeared after the completion of the present work (Riley etal 1986).

6.4.3 An Approximate Harmonic Model.

A contour plot of the lower potential surface of the best fit parameters is shown in figure 6.5a. Here it can be seen that near the minimum of the potential the curvature is very much less in the angular direction than along the radial coordinate. This results in the energy of the angular vibration being much less than that of the radial vibration.

A much simpler approach than solving the vibronic equations as given above would be to consider just this angular coordinate with a harmonic potential. The variation of the adiabatic electronic function in the angular coordinate is then given by:

$$\Psi = \sin\frac{z}{2} \, d(z^2) + \cos\frac{z}{2} \, d(x^2-y^2) \qquad (6.7)$$

$$z = \tan^{-1}[A_1Q_\varepsilon/(A_1Q_\theta+S_\theta)]$$

For strong Jahn-Teller coupling $(E_{JT} \gg S_\theta)$, z can be replaced by the angle ϕ of the Mexican hat potential. The mean angular amplitude of the vibrations in such a harmonic angular potential centred at 180° will be zero as required by group theory, but the mean squared angular amplitude be non-zero. If the angle η is defined as $\phi - 180^\circ$, then for small values of η one has:

$$Q_\varepsilon/\rho_o = \sin \eta \sim \eta \qquad (6.8)$$

The mean square angular amplitude for the nth vibrational level is then given by:

$$\langle\eta^2\rangle_n = (n+\tfrac{1}{2}) \, (\rho_o x)^{-2} \qquad (6.9)$$

Here ρ_o is given in picometers and x has been given in equation (6.5), where the vibrational frequency, $h\nu$, to be used in x is the energy of the angular vibration in cm^{-1}.

Using equations (6.2) and (6.7) the g-values are given by:

$$g = g(z^2) \, \langle\cos^2(\tfrac{\eta}{2})\rangle + g(x^2-y^2) \, \langle\sin^2(\tfrac{\eta}{2})\rangle \qquad (6.10)$$

(6.14)

The dynamical quantities can be approximated using (6.8):

$$<\cos^2(\tfrac{\eta}{2})> \sim 1 - \frac{<\eta^2>}{4}; \qquad <\sin^2(\tfrac{\eta}{2})> \sim \frac{<\eta^2>}{4}$$

when η is small and given in radians. The temperature dependent g-values are then:

$$g_{\parallel} = g_{\parallel}(z^2) + 2[g_{\parallel}(x^2-y^2) - g_{\parallel}(z^2)](2\rho_o x)^{-2}\coth(h\nu/2kT) \qquad (6.11)$$

$$g_{\perp} = g_{\perp}(z^2) + 2[g_{\perp}(x^2-y^2) - g_{\perp}(z^2)](2\rho_o x)^{-2}\coth(h\nu/2kT)$$

These equations are easily derived from (6.10) using the methods of section 3.6 and are analogous to the expressions for temperature dependence of the intensity of parity forbidden electronic transitions. The frequency, $h\nu$, of this angular vibration can be found from (6.10) using the low temperature g-values, or equivalently, using (6.8) with the wavefunctions in (6.3). If the experimentally determined value of ρ_o = 27.5pm is used then one finds:

$$h\nu = [8\times(1.722\times10^{-3})^2\times19\times(27.5)^2<A^2>]^{-1}$$
$$= 100 \text{ cm}^{-1}$$

This value of 100 cm^{-1}, which reproduces the low temperature g-values, also roughly gives their temperature dependence. This is shown in figure 6.8 with several other harmonic potentials. The fact that the overall behaviour of this system can be modelled with these harmonic potentials is not surprising considering the single minimum and well localised wavefunctions that were obtained in the more sophisticated calculations. However, the harmonic model is incapable of reproducing the subtler features of the temperature dependence, such as the inflection in $g_{\parallel}$ observed at low temperatures. It would need a very anharmonic potential to reproduce such a feature.

In addition to this it is difficult to directly relate the harmonic model to the physical properties or parameters arrived at in solving the vibronic equations. The lower adiabatic potential in polar coordinates is given by:

(6.15)
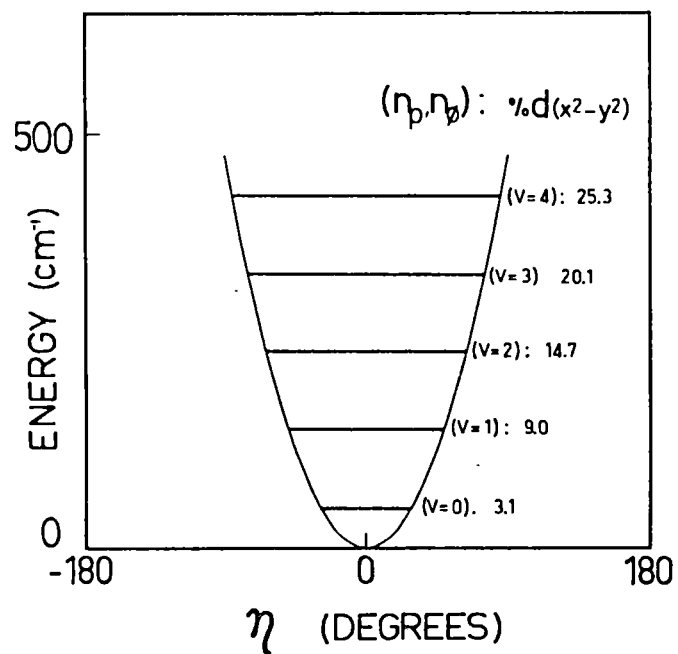
Figure 6.8 The Harmonic Approximation.

a) Potential, angular quantum numbers and %d(x^2-y^2) for harmonic vibration of 95cm^{-1}.

b) Experimental and calculated g-values for potentials with hv = 80, 95, 110 cm^{-1}.
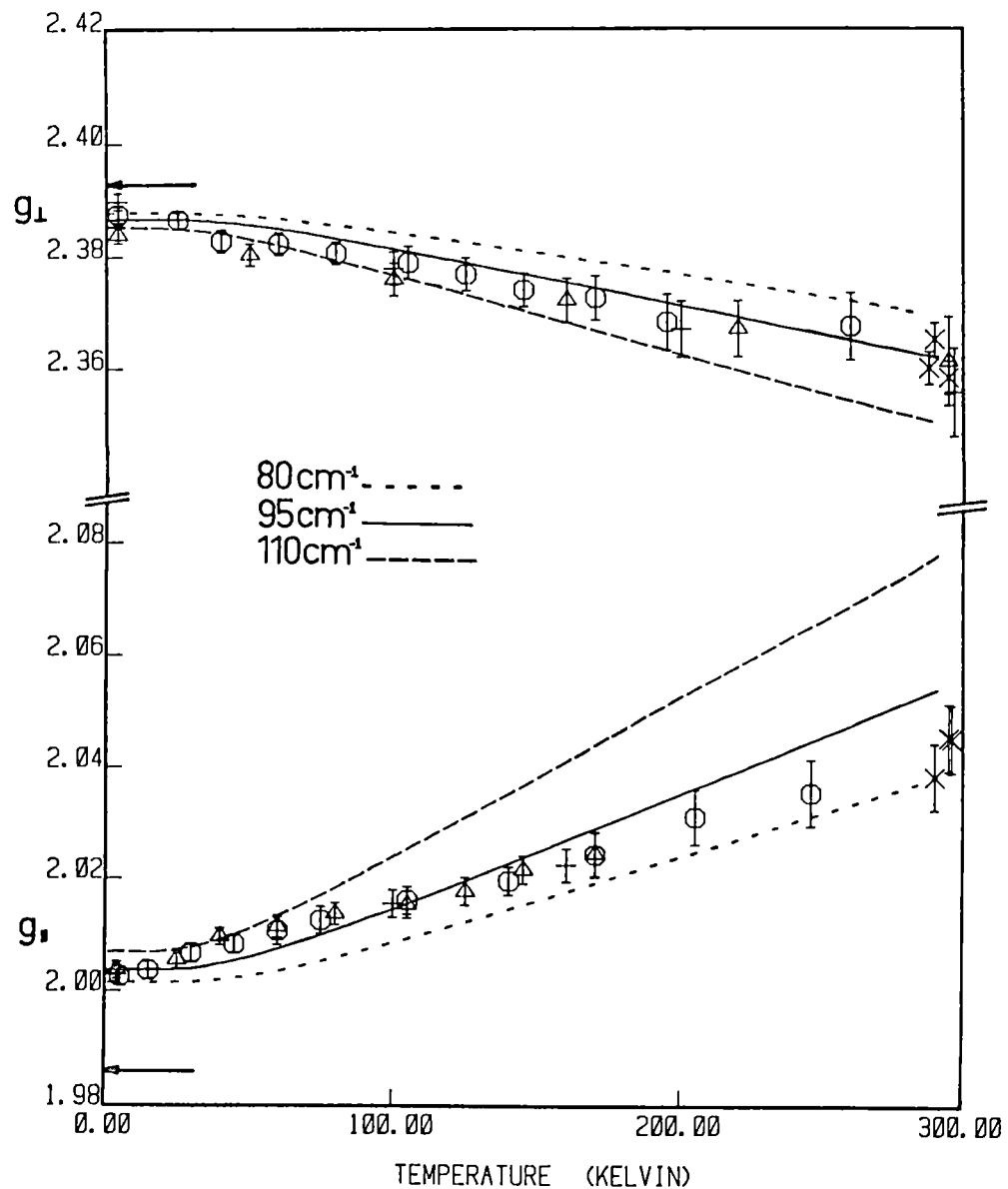
$$\varepsilon^- = \tfrac{1}{2}h\nu\rho^2 - \beta\cos3\phi - [A_1^2\rho^2 - 2A_1 S_\theta\rho\cos\phi + S_\theta^2]^{1/2} \qquad (6.12)$$

If the approximations $\cos x \sim 1-x^2/2$ and $[1-x]^{1/2} \sim 1-x/2$ are used, and (6.12) is minimised with respect to ρ, then the angular potential is:

$$\varepsilon^- = -E_{JT} - \beta - S_\theta + \tfrac{1}{2}K(\phi-180)^2 \qquad (6.13)$$

$$K = [A_1\rho S_\theta/(A_1\rho+S_\theta) - 9\beta]$$

For $S_\theta \ll E_{JT}$ this gives $K = [S_\theta - 9\beta]$ as given in Riley etal (1986). Similar formulae have been given by Kurzynski (1975, 1977). If the best fit values are substituted into the above expressions, the value of $h\nu = 8$ cm^{-1} is calculated for the angular vibration. Since this is far from the 100 cm^{-1} that was required to fit the experimental data, it can be seen that the parameters of the two approaches are not easily related.

The actual energies of these (approximately) angular vibrations calculated from the vibronic Hamiltonian, are shown in figure 6.5b. The first to fourth energy intervals are 62, 79, 85, 87 cm^{-1} respectively.

$$(6.16)$$

6.5 CONCLUSIONS

It has been found that the temperature dependent ESR spectrum of $K_2Zn[Cu]F_4$ could be well reproduced by molecular models that are strictly applicable only to isolated CuF_6^{4-} species. The copper centre in the crystal lattice will really have its ground electronic states coupled by the phonon continuum of e_g symmetry. However, O'Brien (1983) has shown that multimode effects can be closely approximated by a single effective vibration. It has also been assumed that the potential surface itself is temperature independent. At higher temperatures a slight increase in the g-values could be expected from the thermal expansion of the host lattice.

The anharmonicity, or warping terms, in the potential are also likely to be influenced by the continuous nature of the lattice in two dimensions. It has been argued by Deeth and Hitchman (1986) that such lattices will tend to reduce the anharmonicity. This is borne out by the relatively low value of β (=50 cm^{-1}) required to reproduce the g-values of this system.

A simple harmonic model of the system was found to qualitatively reproduce the temperature dependent g-values. However, the more sophisticated approach of solving the strain perturbed E x e Hamiltonian was necessary to quantitatively reproduce all the experimental data.

The success of treating $K_2Zn[Cu]F_4$, as described in this chapter, has prompted the further studies of the more complex low symmetry and mixed ligand systems discussed in the following chapters.

CHAPTER 7 COPPER(II) DOPED TUTTON SALTS

7.1 INTRODUCTION

The family of Tutton salts given in table 7.1 have the general composition expressed by $X_2M(YO_4)_2 \cdot 6H_2O$, where the symbol X represents a monovalent cation and Y is either sulphur or selenium. These compounds contain discrete $M(H_2O)_6^{2+}$ units, where the metal ion, M^{2+}, is surrounded by a distorted octahedra of six water molecules and has a local D_{2h} symmetry. Following the pioneering work of Bleaney etal (1955b), it was Silver and Getz (1974) who showed that the ESR spectrum of Cu(II) doped $K_2Zn(SO_4)_2 \cdot 6H_2O$ was an example of the Jahn-Teller effect. They carefully examined the temperature dependence of the spin Hamiltonian parameters and developed a model that could account very well for the observed experimental behaviour.

This model, which is essentially a Boltzmann average over three (energetically) non-equivalent static distortions, has subsequently been used to interpret the ESR spectra of similar systems containing the $Cu(H_2O)_6^{2+}$ ion (Petrashen etal 1980; Zaitdinov etal 1976, 1983; De etal 1984; Rubin etal 1984); as well as crystal structures (Hathaway etal 1981; Alcock etal 1984).

As Silver and Getz (1974) have themselves appreciated, the model is basically a static one whose strength lies in the ability to correctly reproduce temperature dependent ESR parameters. However, it is felt that already several workers have carried this model too far and have drawn erroneous conclusions about the nature of the ground state potential surface. In this chapter the experimental ESR spectrum of four representative copper doped Tutton salts and copper doped $Zn(GeF_6) \cdot 6H_2O$ is reexamined in terms of a fully dynamical model.

7.1.1 Experimental.

The temperature dependent g-values for copper doped $X_2Zn(SO_4) \cdot 6H_2O$, where $X = NH_4^+$, K^+, Cs^+, Rb^+ and $Zn(GeF_6) \cdot 6H_2O$ are shown as points in figures 7.3-7.7. The different sources of the data

X	Y	M	R_z[b]	R_y	R_x	$<R>$[c]	ρ_o[d]	Temp.	Ref.
*NH4	S	Cu	196.1(5)	209.5(5)	221.9(5)	209.2	25.8	RT	1
*"	"	"	196.6(1)	207.2(1)	223.0(1)	208.9	26.6	?e)	2
*"	"	"	196.7(2)	204.1(2)	225.0(2)	208.6	29.4	215e)	3
*"	"	"	197.0(1)	201.2(1)	227.8(2)	208.7	33.4	145e)	"
ND4	"	"	192.7(6)	208.1(7)	224.2(6)	208.3	31.5	293	4
"	"	"	194.1(4)	204.8(6)	229.9(5)	209.6	36.8	250	"
"	"	"	195.1(4)	202.4(6)	232.5(4)	210.0	39.6	203	"
"	"	"	194.4(5)	200.8(5)	231.8(6)	209.0	40.0	150	"
"	"	"	195.0(4)	200.6(4)	231.8(5)	209.1	39.7	123	"
"	"	"	194.8(5)	199.6(5)	230.3(6)	208.2	38.5	50	"
"	"	"	195.1(4)	201.1(4)	230.4(6)	208.9	37.8	5	"
K	"	"	194.3(2)	206.9(2)	227.8(2)	209.7	33.8	RT	5
Rb	"	"	195.7(3)	203.1(3)	230.7(3)	209.8	36.9	RT	6
"	"	"	197.8(5)	200.0(5)	231.7(5)	209.8	37.9	77	7
Cs	"	"	196.6(5)	200.4(4)	231.5(5)	209.5	38.3	RT	8
"	"	"	201(4)	200(1)	231(2)	210.6	35.2	77	9
?Tl	"	"	195.7	201.7	231.7	209.7	38.6	RT	10
?NH4	Se	"	199.0(5)	203.1(5)	223.7(5)	208.6	26.5	295	11
*K	"	"	193.6(2)	204.4(2)	229.7(2)	209.2	37.1	RT	12
*NH4	S	Zn	207.5(1.2)	211.7(1.2)	212.9(1.2)	210.7	5.7	RT	13
*K	"	"	203.2(4)	212.6(5)	213.3(4)	209.7	11.3	RT	14
*NH4	S	Ni	203(2.5)	203(3.5)	205(2.5)	–	–	RT	15
*"	"	"	203.6(1.2)	208.3(1.2)	208.5(1.2)	206.8	5.5	RT	16
*"	"	"	204.8(9)	205.5	206.5(5)	205.6	1.7	2	17
*DH4	"	"	203.8(3)	206.2(3)	206.6(3)	205.5	3.0	2	17
K	"	"	202.1(2)	207.8(2)	208.7(2)	206.2	7.2	RT	18
*NH4	"	Mg	205.1(5)	207.3(5)	208.3(5)	206.9	3.3	RT	19
?K	"	"	205.6(?)	210.3(?)	211.8(?)	209.2	6.5	RT	20
NH4	"	Mn	215.0(6)	219.3(6)	220.0(6)	218.1	5.4	RT	21
*NH4	"	Cd	224.1(7)	229.7(7)	229.8(7)	227.9	6.5	RT	22
*NH4	"	V	212(1)	216(1)	216(1)	214.7	4.6	RT	23
*NH4	"	Fe	208.6(7)	213.6(7)	215.6(7)	212.6	7.2	RT	"
*NH4	"	Co	207.0(4)	210.6(4)	210.7(3)	209.4	4.2	RT	"

NOTES FOR TABLE 7.1:

a) All compounds are isostructural, monoclinic space group $P2_1/a$ with $Z=2$. The standard deviation in the last figure is given in brackets.

b) In the crystallographic notation R_z=M-O(9), R_y=M-O(7), R_x=M-O(8); except for the structures marked *, where R_y=M-O(8), R_x=M-O(7); or ? where a different notation has been used. The molecular coordinate system has been chosen so $R_z < R_y < R_x$. Therefore the principal axis z corresponds to a tetragonal compression, with a positive rhombic distortion. In terms of the e_g vibrational coordinates, this means Q_θ 0, $Q_\epsilon > 0$. The "static" geometry is therefore in the second quadrant ($90 < \phi < 180$) of the Jahn-Teller surface.

c) $<R> = \frac{1}{3} \sum_i R_i$, is the mean bondlength.

d) $\rho_0 = [\sum_i 2(R_i - <R>)^2]^{1/2}$, is the Jahn-Teller radius.

e) The temperatures 215, 145K quoted are taken from Hathaway etal (1981). Their original reference (3) gives them as 203, 123K respectively. Reference 3 also suggest that the structure reported in (2), has been done below room temperature, and so has been marked ?. Reference 2 does not quote a temperature.

REFERENCES FOR TABLE 7.1:

1) Montgomery and Lingafelter (1966a).
2) Brown and Chidambaram (1969). (neutron)
3) Alcock etal (1984). Note: Data at ~150K (Duggan etal 1979) has not been given as this reference says it is inaccurate.
4) Hathaway and Hewat (1984). (neutron powder)
5) Robinson and Kennard (1972). (neutron)
6) Van der Zee (1972). (neutron)
7) Smith etal (1975). (neutron)
8) Shields and Kennard (1972). (neutron)
9) Shields etal (1972b).
10) Shields etal (1972a). (neutron)
11) Monge and Gutierrez-Puebla (1981).
12) Whitnall etal (1975a). (neutron)
13) Montgomery and Lingafelter (1964a).
14) Whitnall etal (1975b). (neutron)
15) Grimes etal (1963). (two dimensional data)
16) Montgomery and Lingafelter (1964b).
17) Fender etal (1986).
18) Hodgeson etal (1975). (neutron)
19) Margulis and Templeton (1962).
20) Kannon and Viswamitra (1965).
21) Montgomery etal (1966).
22) Montgomery and Lingafelter (1966b).
23) Montgomery etal (1967).

are indicated by different symbols and were obtained from the following published studies:

$\times$ Bagguley and Griffiths (1952) [K]
$\triangle$ Bleaney etal (1955b)　　　　　[K]
$\diamondsuit$ Silver and Getz (1974)　　　[K]
$+$ Zaitdinov etal (1976)　　　- [Ge]
$\square$ Petrashen etal (1980)　　　$[NH_4, Cs, Rb]$
$\bigcirc$ Wan Mohamed (1985)　　　$[K, NH_4]$

From these studies the following features are well known:

1) In all cases <g> is temperature independent and coincides for all the Tutton salts hosts, having a value of 2.20. In the case of $Zn(GeF_6).6H_2O$, <g> = 2.226.

2) In all cases the principal axes of the **g** and **A** tensors coincide and are temperature independent, remaining directed along the the Cu-O bonds.

3) The temperature dependence of the g-values varies with the host lattice.

4) In the case of the Tutton salts, the principal g-values are rhombic, two being strongly temperature dependent while the third remains essentially temperature independent.

5) In the case of the Tutton salts, the "apparent tetragonal axis" changes by 90 degrees between low and room temperature. At low temperature the rhombic g-values can be loosely described as being close to a tetragonal elongation, while at higher temperatures they become better described by a tetragonal compression.

6) In the case of $Cu(II)/Zn(GeF_6).6H_2O$, the g-values are tetragonal up to a phase transition at 190K. The g-values are typical of a $d(x^2-y^2)$ ground state, but are strongly temperature dependent.

7) In the case of $K_2Zn(SO_4)_2.6H_2O$, the relative hyperfine linewidths show a strong temperature dependence.

7.1.2 The Silver and Getz Model.

In previous studies, the temperature dependent ESR spectrum of copper(II) doped Tutton salts has been explained in terms of the Silver and Getz (1974) model. This model uses the three static elongated distortions that correspond to the minima of the warped Mexican

(7.2)

hat where their degeneracy has been lifted by the low site symmetry of the lattice. The g-values are given by an equation of the form (Petrashen etal 1980):

$$g_x(T) = N_1 g_{x1} + N_2 g_{x2} + N_3 g_{x3} \tag{7.1}$$
$$g_y(T) = N_1 g_{y1} + N_2 g_{y2} + N_3 g_{y3}$$
$$g_z(T) = N_1 g_{z1} + N_2 g_{z2} + N_3 g_{z3}$$

$$N_n = \exp(-\delta_{1n}/kT) \; / \; [\Sigma_i \exp(-\delta_{1i}/kT)]; \quad N_1 + N_2 + N_3 = 1.0.$$

The symbols g_{x1}, N_1 for example, represent the g-value and fractional population respectively at a static rhombic geometry of site 1. In the original treatment of Silver and Getz (1974), it was assumed that only the population of the two lowest sites was important, and that the magnetic properties were the same in both sites with an interchange of the x and y axes:

$$g_x(T) = N_1 g_{x1} + N_2 g_{y1} \tag{7.2}$$
$$g_y(T) = N_1 g_{y1} + N_2 g_{x1}$$
$$g_z(T) = g_{z1}$$

Inherent in equations (7.1) and (7.2) is the assumption that the transitions occur between the three wells at a rate that is fast compared to the ESR time scale. This fast vibronic relaxation results in motional averaging and the observed magnetic properties are a Boltzmann weighted average of the individual sites.

The values of g_i are equal to those obtained from the low temperature spectrum when $N_1 = 1$, $N_2 = 0$. From the populations N_1, N_2 that fit the the experimental data, the energy differences between the wells $\delta_{1,2}$ can be found and such values are given in table 7.2. Also included in table 7.2 are the estimates of the energy of the higher well $\delta_{1,3}$ obtained from crystallographic data, and the "activation energy" for transitions between wells 1 and 2 in $K_2 Zn(SO_4)_2 \cdot 6H_2O$. This latter value was obtained by Silver and Getz (1974) from an analysis of the hyperfine linewidths in a manner described in section 5.4.4.

$$\tag{7.3}$$

Table 7.2: Parameters from the Silver and Getz Model.

Compound	$\delta_{1,2}$	$\delta_{1,3}$	$E_{1,2}$	Reference
$K_2Zn(SO_4)_2 \cdot 6H_2O$	75	450	120	Silver & Getz (1974)
	75	~1125*	-	Petrashen etal (1978)
$Rb_2Zn(SO_4)_2 \cdot 6H_2O$	175	~1000*	-	"
$(NH_4)_2Zn(SO_4)_2 \cdot 6H_2O$	230	~1050*	-	"
$Cs_2Zn(SO_4) \cdot 6H_2O$	290	~1000*	-	"
$ZnGeF_6 \cdot 6H_2O$	154	-	160	Zaitdinov (1976, 1983)

* Obtained from the crystal structure, the rest from ESR data.

Table 7.3: Vibrational Data for $M(H_2O)_6^{2+}$.

Complex	$\nu(e_g)/cm^{-1}$	$\nu(a_{1g})/cm^{-1}$	Temp/K	Reference
$Ni(H_2O)_6SiF_6$	305	405	15	Jenkins & Lewis (1981)
$Ni(H_2O)_6TiF_6$	302,323,334	402	15	"
$Fe(H_2O)_6SiF_6$	296	379	15	"
$Mg(H_2O)_6SiF_6$	300	374	15	"
$Zn(H_2O)_6SiF_6$	278	380	15	"
$Mn(H_2O)_6TiF_6$	260	-	103	Choudhury etal (1985)
$Zn(H_2O)_6TiF_6$	254,268	396	110	"

Table 7.4: Estimation of the Strain Parameters.

	NH_4^+	K^+
ΔR_x (pm)	2.2 (1.2)	3.6 (0.5)
ΔR_y (pm)	1.0 "	2.9 "
ΔR_z (pm)	-3.2 "	-6.5 "
Q_θ (pm)	-5.54	-11.3
Q_ε (pm)	1.20	0.70
Q_θ a)	-0.701	-1.425
Q_ε	0.152	0.089
S_θ (cm^{-1}) b)	-630	-1280
S_ε (cm^{-1})	140	80
$-S_\theta / S_\varepsilon$	4.5	16

a) The coordinates are made dimensionless by using equation (2.35).
b) The strain is calculated using $A_1 = 900cm^{-1}$ ($V=113cm^{-1}pm^{-1}$).

7.2 METHOD

Contrary to the Silver and Getz model usually adopted, a dynamic approach has been taken, where the full pseudo-Jahn-Teller vibronic Hamiltonian is solved numerically. A single set of parameters are used to describe the kinetic and potential energy operators of an isolated $Cu(H_2O)_6^{2+}$ ion. The observed temperature dependence in the different host lattices are then fitted by allowing the tetragonal and orthorhombic components of the strain to vary. It will be shown that these strain terms compare favourable with the geometry of the host lattice where a crystal structure has been done.

7.2.1 The Calculation.

The vibronic Hamiltonian is that of the usual Jahn-Teller E⊗e problem with additional strain terms to account for the low symmetry of the host lattice. This vibronic Hamiltonian is given by (4.26) which has the inherent approximation that the strain terms will not destroy the symmetry of the cubic part of the Hamiltonian.

Anticipating a relatively large value for the warping terms in the present systems, the second order coupling constant has been used to parameterise this effect. This term has been used instead of the anharmonicity because of the computational difficulties that are encountered for a large anharmonic constant (section 4.2.2).

7.2.2 Estimation of the Parameters.

K_2: The quadratic force constant, K_2, which is equal to the energy of the hypothetical e_g vibration, $h\nu$, in the absence of vibronic coupling, is held fixed at $300cm^{-1}$ from the vibrational data obtain for other metal hydrates. Table 7.3 shows the assignments given to the Raman active e_g and a_{1g} vibrations for several non Jahn-Teller ions. The assignments of Jenkins and Lewis (1981) are preferred, because the spectrum has been taken at a lower temperature and is in keeping with the usual value of $300cm^{-1}$ that is used for the e_g vibration in vibronic calculations on the $Cu(H_2O)_6^{2+}$ ion (Williams et al 1969; O-'Brien 1964).

(7.4)

$\underline{A_1}$: The linear Jahn-Teller coupling constant for $Cu(H_2O)_6^{2+}$ has previously been given values of $812cm^{-1}$ (Williams etal 1969), and $1300cm^{-1}$ (O'Brien 1964). The value of O'Brien is probably too large as it is inconsistent with the electronic spectrum. Bill (1984, pg791) gives a value of $960\ cm^{-1}$ for the (CuO_6) sub-unit, found from an average of the structural data of 15 pure compounds. An estimate from simple bonding arguments (Deeth and Hitchman 1986) gives $A_1 = 625cm^{-1}$, when values of $r_o = 210pm$, $\Delta' = 11,500cm^{-1}$, $h\nu = 300cm^{-1}$ are used in their equation for V.

A_1 may be fixed from experiment from the observed transition to the upper Jahn-Teller surface in the electronic spectrum. This transition has been observed at $\Delta E \sim 7,500cm^{-1}$ in pure copper Tutton salts (Hitchman and Waite 1976). Cooperative effects may make this larger than that in an isolated complex, but this can be taken as an upper limit. Neglecting orthorhombic strain and second order coupling terms this energy is given by:

$$\Delta E \approx 4E_{JT} + 2S_\theta, \quad E_{JT} = A_1^2/(2h\nu) \qquad (7.3)$$

Anticipating values for S_θ of the order $\sim 500-1000\ cm^{-1}$, equation (7.3) gives a value of A_1 in the range $\sim 900-1000\ cm^{-1}$. A value of $A_1 = 900cm^{-1}$ is used in this investigation.

$\underline{A_2}$: The value of A_2 determines the barrier height, 2β, between equivalent wells of the warped Mexican hat:

$$\beta = A_2\rho_o^2, \quad \rho_o = A_1/K_2 \qquad (7.4)$$

This parameter is traditionally hard to quantify; previous estimates for $Cu(H_2O)_6^{2+}$ have been $\beta = 450cm^{-1}$ (Williams etal 1969) and $\beta = 600cm^{-1}$ (O'Brien 1964). The "activation energy" for the transition between the two lowest wells in $Cu(II)/K_2Zn(SO_4)_2.6H_2O$ was found by Silver and Getz (1974) to be $E_{1,2} = 120\ cm^{-1}$, but this is not equal to the barrier height as has sometimes been implied (Hathaway 1983). This activation energy represents the energy of a relaxation pathway, usually a vibronic state that is delocalised over both wells (section 5.4). Even if this value could be equated with the barrier height between wells, it does not provide a direct measure of β, as the strain terms will decrease the barrier height that occurs in the cubic case (Reinen and Krause 1981, figure 14).

A value of $\beta = 300cm^{-1}$ ($A_2 = 33.3\ cm^{-1}$) was found to give an excited vibronic level at an energy in rough agreement to $E_{1,2}$ for the

(7.5)

copper doped potassium salt when the strain terms are included. It should be noted however that this value is far from certain and will be further discussed below.

Strain: Ham (1972, pp110-3) has shown that the effect of the strain from a host lattice can be viewed in terms of the displacement $(Q_\theta^O, Q_\varepsilon^O)$ along the e_g coordinates in the absence of the Jahn-Teller effect. By expanding this displacement and making a change of variable he arrived at:

$$H_{ST} = A_1 (Q_\theta^O \sigma_z - Q_\varepsilon^O \sigma_x) \qquad (7.5)$$

which is then added to the cubic Hamiltonian. A comparison with equation (4.26) gives $S_\theta = A_1 Q_\theta^O$, $S_\varepsilon = A_1 Q_\varepsilon^O$, where A_1 is the linear coupling constant.

Equation (7.5) is only strictly valid in the case of linear coupling and where the force constants of the host compound are equal to the guest species (Ham 1968). However, since we are dealing with a strong Jahn-Teller effect and the vibrations of the zinc host are quite similar (see table 7.3), equation (7.5) should be valid within the experimental uncertainties to follow.

Using the data for the known zinc structures in table 7.1, the strain terms that result from using a value of $A_1 = 900 \text{cm}^{-1}$ are shown in table 7.4. The uncertainties are large, even if the error estimate for the change in bondlength is taken as the standard deviation of the bondlength given in the crystal structure. Due to this large uncertainty in the quite small changes of bondlength involved, the strain components are left as variables in this treatment. A qualitative comparison of these values with those derived from fitting the ESR data will then test the self-consistency of the present model.

$$(7.6)$$

7.3 RESULTS

7.3.1 Fitting the Parameters.

After solving (diagonalising) the vibronic Hamiltonian, the g-values can be calculated from the wavefunctions in a manner previously described in section 5.2.3. In all cases the average g-value is ~2.20, and this effectively fixes the value for the baricentre of the excited triplet state ΔE in equation (5.25) and the isotropic orbital reduction factor k. If ΔE is held at ~11,900cm^{-1} from the experimentally observed spectrum of the pure copper compounds (Hitchman and Waite 1976), then a value of k = 0.88 must be used to give <g>=2.20. These parameters are now fixed and do not enter the fitting procedure.

It it should be noted that the g-values are calculated by diagonalising the ligand field matrix rather than by using the usual perturbation formula. These latter formula tend to overestimate the mixture of the excited triplet states through spin-orbit coupling and consequently a lower value of k is typically reported for these type of compounds (Waite and Hitchman 1976).

The low symmetry effects of the host lattice can best be appreciated by examining figure 7.1. Here the the g-values are calculated for the lowest vibronic state with the cubic parameters fixed at the values given earlier, while the tetragonal compression is allowed to vary. The ratio $-S_\theta/\beta < 9$ is in the regime where there are two equivalent lowest energy minima on the potential surface symmetric about $\phi = 180^{\circ}$ (Reinen and Krause 1981). The circular cross-section of the strain perturbed warped Mexican hat potential at constant $\rho = \rho_o$ is shown in figure 7.1b. A small positive orthorhombic strain S_ε has been used to make the minimum in the second quadrant ($90^{\circ}<\phi<180^{\circ}$) the lowest in energy which in turn defines the order of the low temperature g-values as $g_x > g_y > g_z$.

For a small tetragonal strain, the lowest wavefunction is nearly centred at $\phi = 120^{\circ}$, corresponding to a tetragonal elongation along the x axis. The g-values are then nearly tetragonal with g < g . As the tetragonal strain is increased, this has two effects on the potential: 1) the minima of the two wells move towards $\phi = 180^{\circ}$, and 2) the barrier between the wells decreases. Both these points tend to make

(7.7)
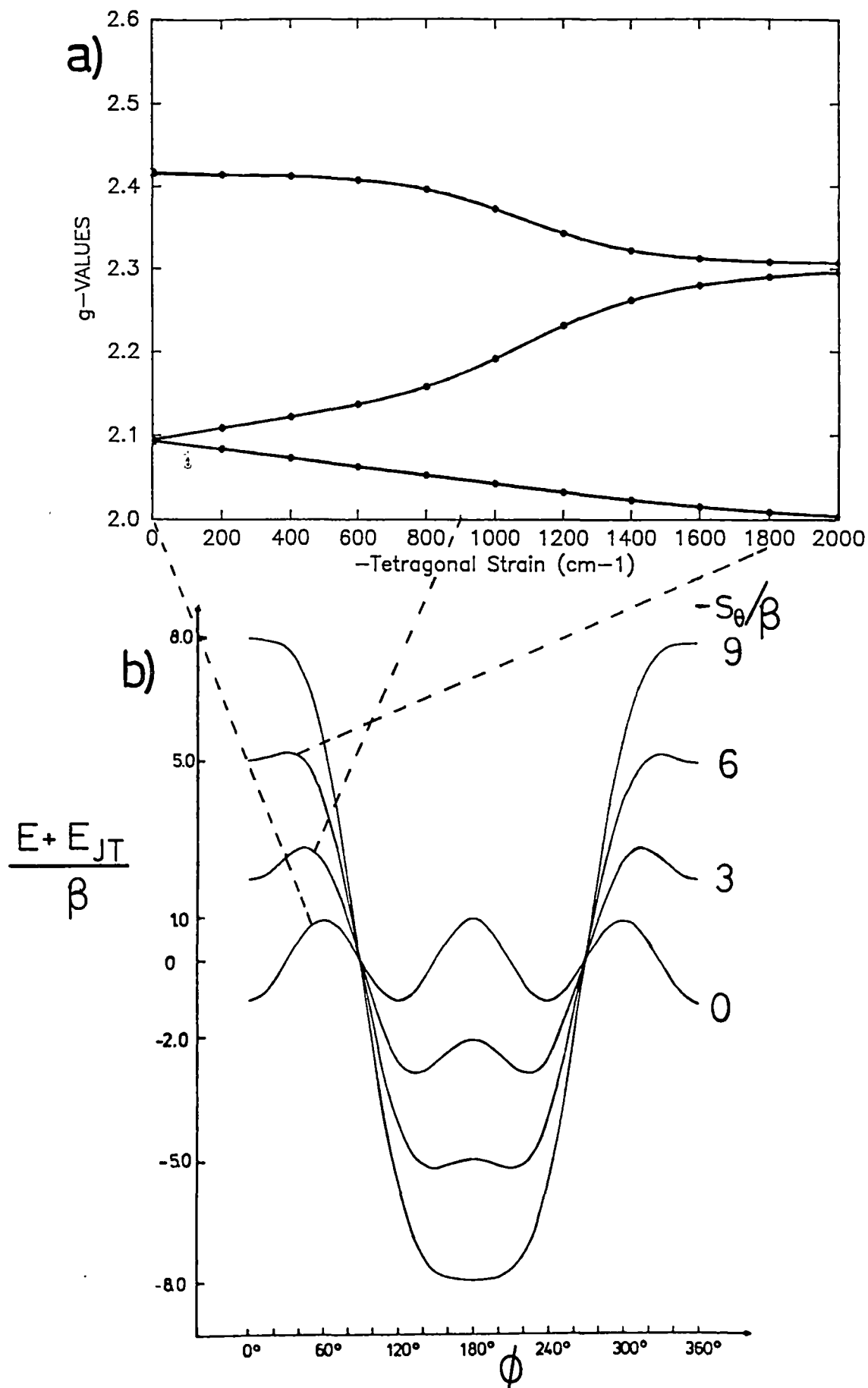
Figure 7.1: a) The low temperature g-values as a function of S_θ. $h\nu = 300 cm^{-1}$, $A_1 = 900 cm^{-1}$, $A_2 = 33.3 cm^{-1}$, $S_\varepsilon = 5 cm^{-1}$.

b) The lower adiabatic Jahn-Teller surface along the angular coordinate, as a function of the tetragonal strain.
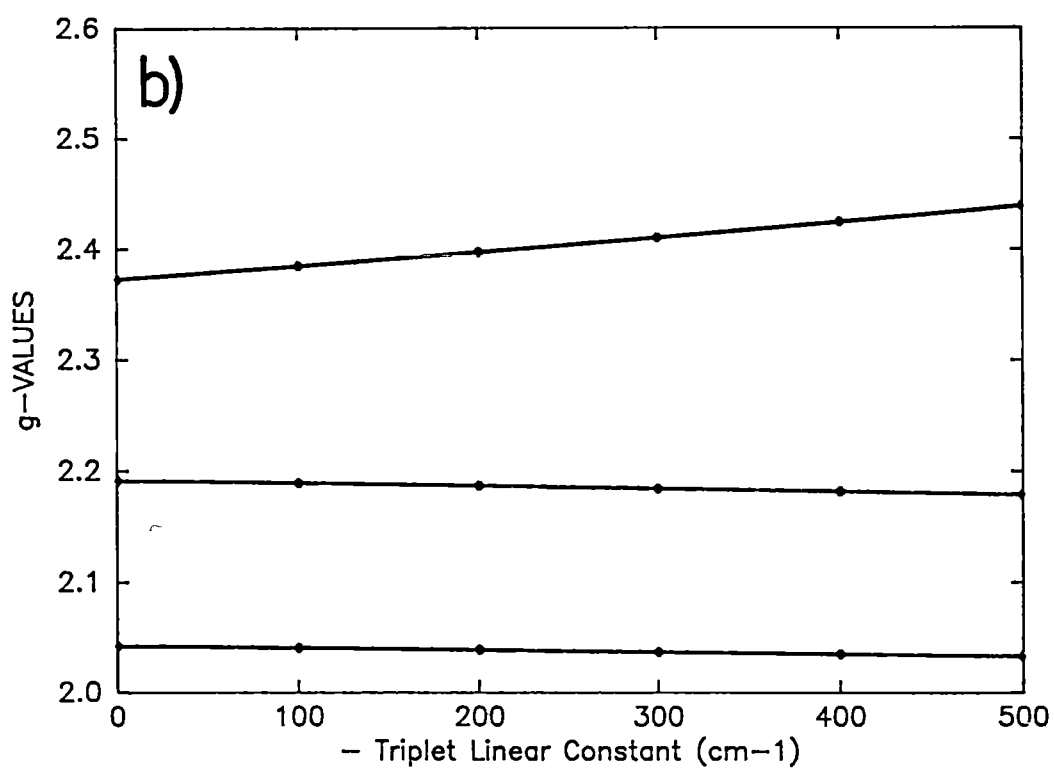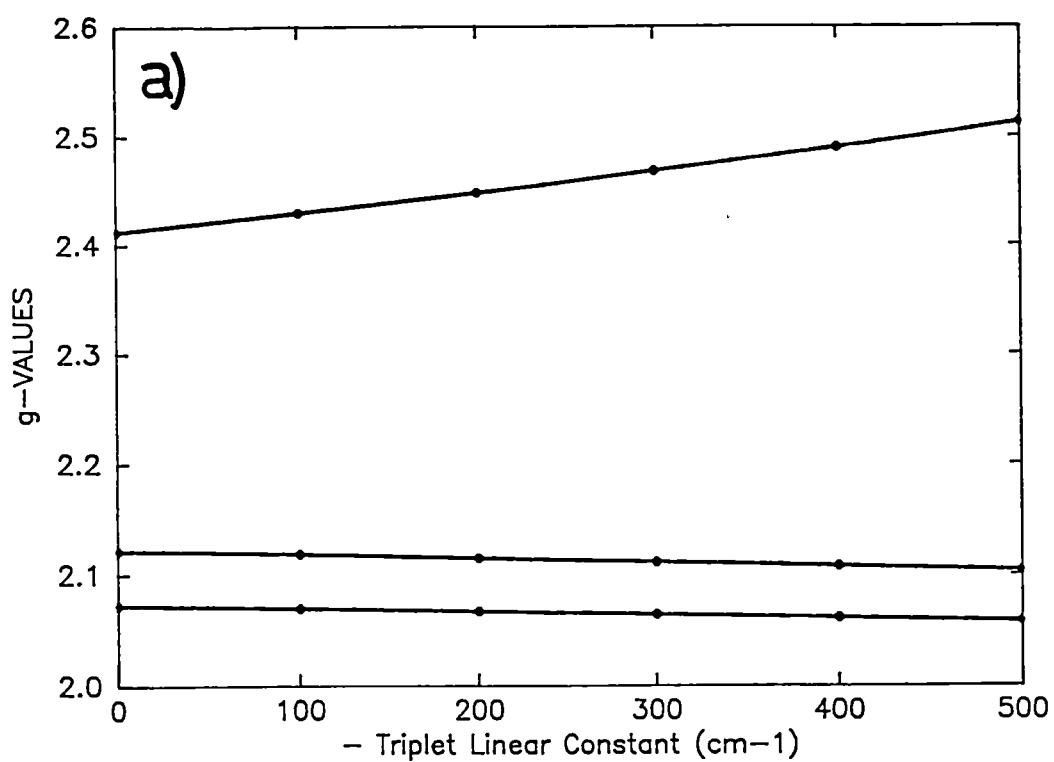
Figure 7.2: The low temperature g-values as a function of $A_1(T)$. Cross section of figure 7.1a at: a) $S_\theta = -400$ cm^{-1}; and b) $S_\theta = -1000$ cm^{-1}.

the g-values correspond more to a tetragonal compression, after passing through a rhombic stage. The first can be thought of as a static effect as the wavefunction closely follows the minima of the well which corresponds to a particular static geometry. The second is a dynamic effect, as the wavefunction becomes delocalised over both wells as the barrier decreases. In the limiting case where $S_\theta/\beta > 9$, there is a single minima near $\phi = 180^\circ$ corresponding to a compression along the z axis, and almost tetragonal g-values will result.

The observed low temperature g-values can be compared to those calculated in figure 7.1a and the position of the lowest energy well can be found. The value of the tetragonal strain that roughly fits the rhombicity of the g-values will in general give the highest g-value too low and the lowest g-value too high. This is due to the fact that the energy of the excited triplet states d(xy), d(xz), d(yz) have been assumed the same. These levels are now allowed to differ according to equation (5.25) and the calculated geometry of the vibronic states. The anisotropy of the excited triplet can be controlled by the linear coupling constant $A_1(T)$ in equation (5.25), and the effect of varying this is shown in figure 7.2 for different values of S_θ. As might be expected, the general effect is to increase the spread of the g-values.

The splitting of the triplet states experimentally observed is approximately 1,500 cm^{-1} (Hitchman and Waite 1976) which, using the present set of parameters ($\rho_0 = A_1/h\nu = 3$), would give $A_1(T) \sim 330 cm^{-1}$. However, the energy of these triplet states will also be determined by: the low symmetry strain terms, the anisotropic pi-bonding of the water ligands and the variation of the orbital reduction factors with bondlength. For this reason the coupling constant, $A_1(T)$, will be an effective value that incorporates many different factors that effect the mixture of the triplet states into the ground vibronic states. The approach taken here has been to use a single isotropic value for the orbital reduction factor, k, and a single value for the triplet baricentre, ΔE, in all five $Cu(H_2O)_6^{2+}$ complexes; and allowing the coupling constant, $A_1(T)$, to vary. The values that fit the experimental data fall in the range $-150:-300 cm^{-1}$ and are shown in table 7.5. These values both agree in sign and magnitude with the splitting observed in the electronic spectrum.

(7.8)

After the low temperature g-values have been fitted by varying the tetragonal strain, the temperature dependence of the g-values can be fitted by varying the orthorhombic component of the strain. The best fit calculations are shown in figures 7.3-7.7, along with a plot of their four lowest probability functions. As can be seen, good agreement can be made with all the experimental data. It should be stressed that exactly the same Jahn-Teller parameters for the cubic part of the Hamiltonian have been used, and only the strain has been varied to correspond to the different host lattices. A list of the parameters used is given in table 7.5. The values obtained for the strain and those independently calculated from the known crystal structures in table 7.4 are in close agreement. In both cases the strains derived from the crystal structures are too large. This may be due to an overestimate of the linear coupling constant. A value of A_1 = 750 cm^{-1} (V=95cm^{-1}pm^{-1}) would give closer agreement, but would predict the lowest electronic transition from equation (4) to be at 4750-5750 cm^{-1}. The electronic spectrum is considered to be a more accurate measure of A_1, as it does not have the uncertainties of the structural data, and the value of $A_1 \sim 900$ cm^{-1} is kept.

7.3.2 Sensitivity of the Fit.

The linear coupling constant, A_1, and the harmonic frequency, hν, can be fixed with some certainty. However, the warping parameter of the Mexican hat potential surface is not easy to quantify and this is often reported in the literature as "the least improbable" value (Englman 1972, pg315). Given these uncertainties, it is of interest to consider the sensitivity of the experimental fit to the value of β in the present cases.

First, it is instructive to consider the case where there is no warping term at all, and attempt to fit the observed experimental data using only linear coupling and strain terms in the potential. The strain components in the vibronic Hamiltonian (4.26) can be written in terms of a magnitude S, and a direction ϕ_s in the Q_θ-Q_ε plane given in equation (4.24). The lower surface of the Mexican hat potential takes the following form after diagonalising the potential operators (equation 4.27):

$$V(\rho, \phi) = \frac{1}{2}h\nu\rho^2 - [A_1^2\rho^2 + 2A_1\rho S\cos(\phi-\phi_s) + S^2]^{1/2} \quad (7.6)$$

Figure 7.3a: Experimental and calculated g-values of $Cu/K_2Zn(SO_4)_2 \cdot 6H_2O$.

Figure 7.3b: The four lowest vibronic probability functions.

4 $E = 265 \text{ cm}^{-1}$; $g_x = 2.247$; $g_y = 2.322$; $g_z = 2.035$.
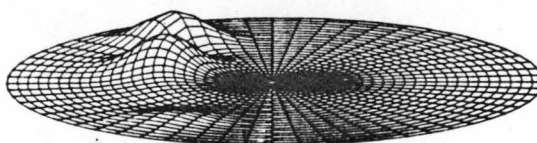
3 $E = 187 \text{ cm}^{-1}$; $g_x = 2.357$; $g_y = 2.222$; $g_z = 2.039$.
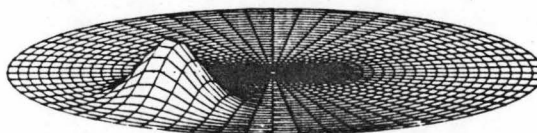
2 $E = 72 \text{ cm}^{-1}$; $g_x = 2.161$; $g_y = 2.411$; $g_z = 2.039$.

1 $E = 0 \text{ cm}^{-1}$; $g_x = 2.417$; $g_y = 2.150$; $g_z = 2.045$.

Figure 7.4a: Experimental and calculated g-values of $Cu/Rb_2Zn(SO_4)_2 \cdot 6H_2O$.

Figure 7.4b: The four lowest vibronic probability functions.

4 $E = 299\ cm^{-1}$; $g_x = 2.435$; $g_y = 2.125$; $g_z = 2.060$.

3 $E = 216\ cm^{-1}$; $g_x = 2.407$; $g_y = 2.169$; $g_z = 2.034$.

2 $E = 153\ cm^{-1}$; $g_x = 2.151$; $g_y = 2.425$; $g_z = 2.043$.

1 $E = 0\ cm^{-1}$; $g_x = 2.435$; $g_y = 2.131$; $g_z = 2.054$.

Figure 7.5a: Experimental and calculated g-values of $Cu/(NH_4)_2Zn(SO_4)_2 \cdot 6H_2O$.
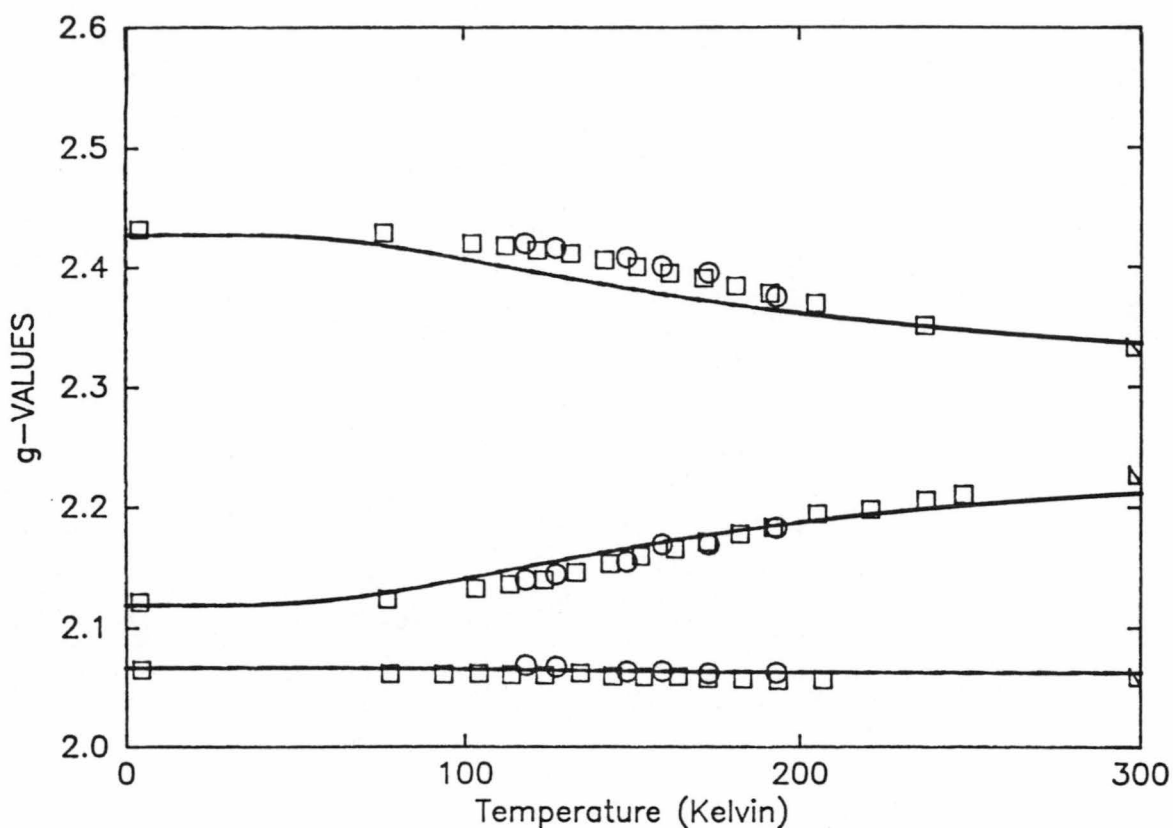
Figure 7.5b: The four lowest vibronic probability functions.

4 $E = 291$ cm^{-1}; $g_x = 2.426$; $g_y = 2.112$; $g_z = 2.074$.

3 $E = 235$ cm^{-1}; $g_x = 2.414$; $g_y = 2.143$; $g_z = 2.074$.

2 $E = 181$ cm^{-1}; $g_x = 2.134$; $g_y = 2.422$; $g_z = 2.057$.

1 $E = 0$ cm^{-1}; $g_x = 2.427$; $g_y = 2.119$; $g_z = 2.067$.
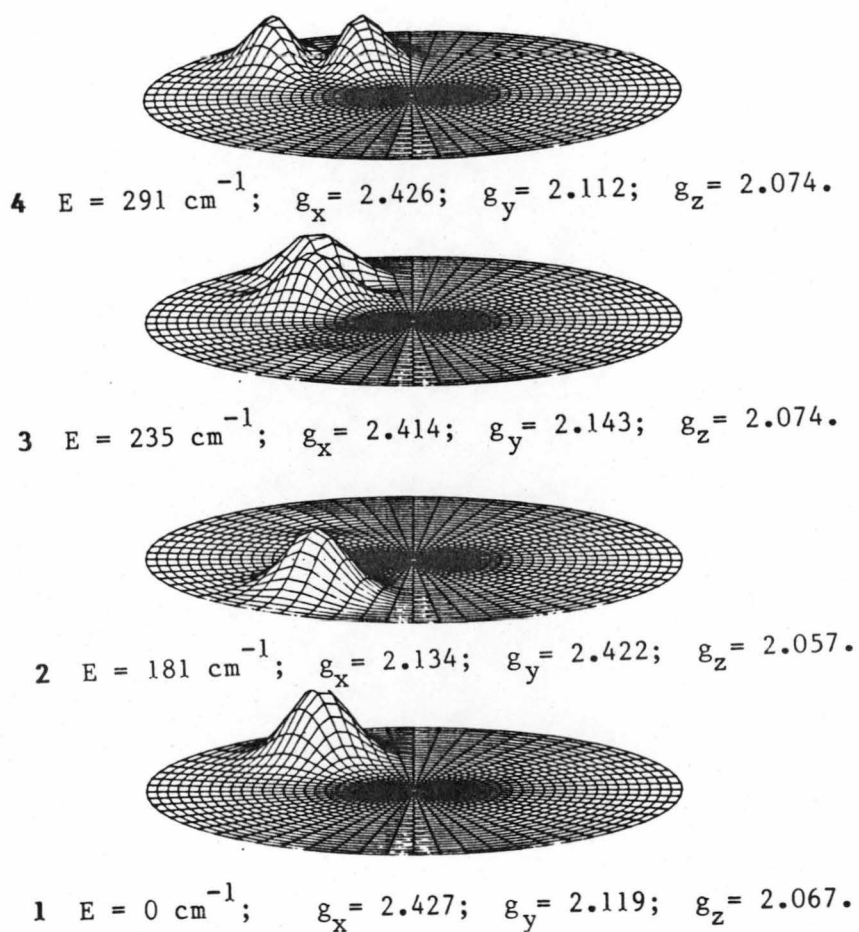
Figure 7.6a: Experimental and calculated g-values for $Cu/Cs_2Zn(SO_4)_2 \cdot 6H_2O$.

Figure 7.6b: The four lowest vibronic probability functions.

4 $e = 293$ cm^{-1}; $g_x = 2.304$; $g_y = 2.243$; $g_z = 2.060$.

3 $E = 292$ cm^{-1}; $g_x = 2.269$; $g_y = 2.280$; $g_z = 2.060$.

2 $E = 235$ cm^{-1}; $g_x = 2.434$; $g_y = 2.139$; $g_z = 2.051$.

1 $E = 0$ cm^{-1}; $g_x = 2.447$; $g_y = 2.117$; $g_z = 2.062$.

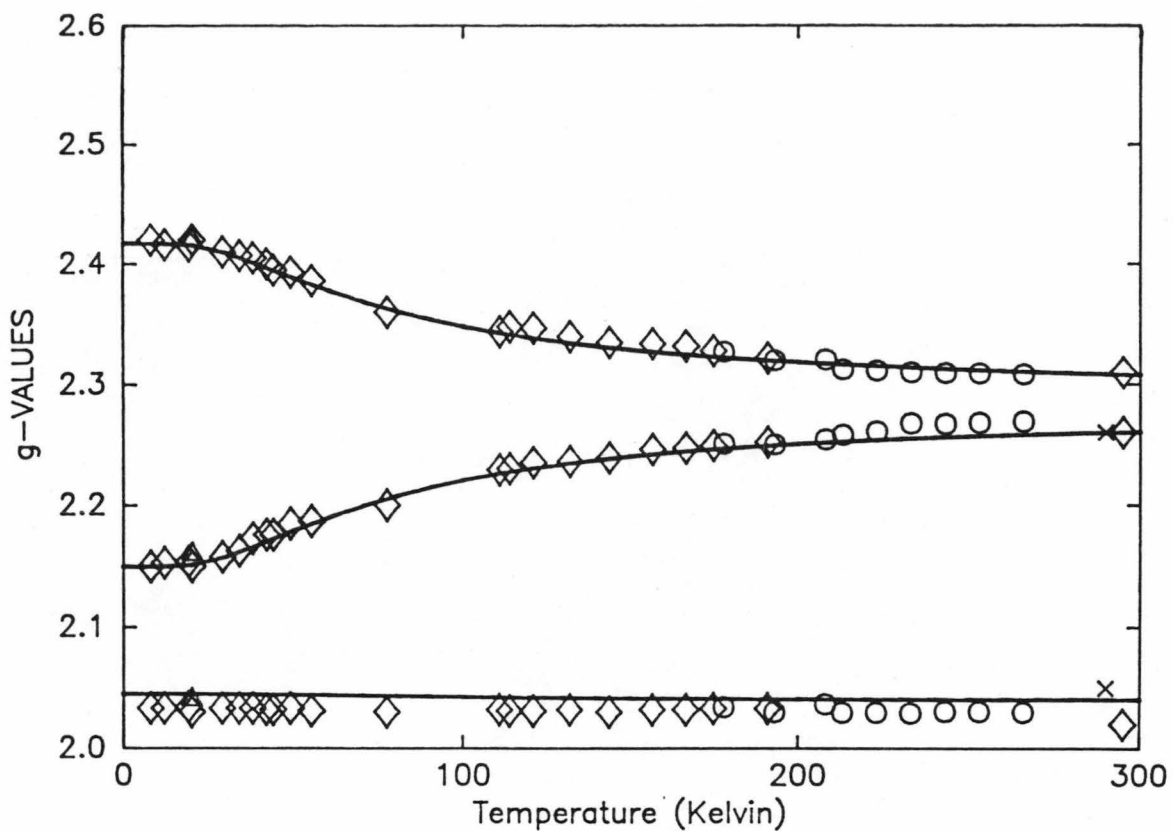**Figure 7.7a**: Experimental and calculated g-values for Cu/Zn(GeF$_6$).6H$_2$O.

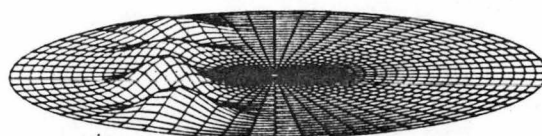**Figure 7.7b**: The four lowest vibronic probability functions.
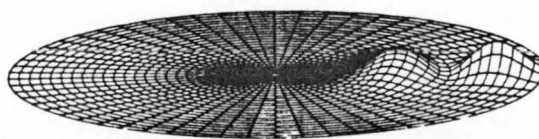
4 E = 257 cm^{-1};   g$_x$= 2.102;   g$_y$= 2.102;   g$_z$= 2.471.
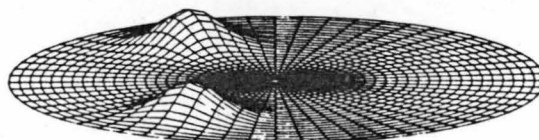
3 E = 147.1 cm^{-1};   g$_x$= 2.277;   g$_y$= 2.277;   g$_z$= 2.109.
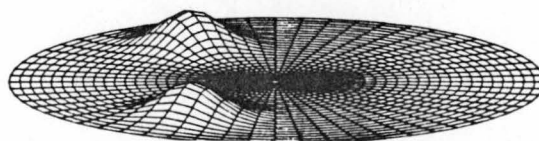
2 E = 147.0 cm^{-1};   g$_x$= 2.277;   g$_y$= 2.277;   g$_z$= 2.109.
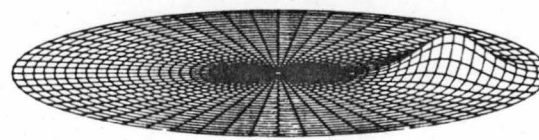
1 E = 0 cm^{-1};   g$_x$= 2.100;   g$_y$= 2.100;   g$_z$= 2.474.

For a particular magnitude of the strain, the components S_θ, S_ε can be chosen, via equation (4.24), to cause the potential to have a minimum at the value ϕ_s. The approach then is to choose these components to give a value of ϕ_s that correctly reproduces the low temperature g-values, and then to vary the magnitude, S, in an attempt to fit the temperature dependence of the g-values.

Figures 7.8 and 7.9 show the calculated g-values for the strain parameters S=100 and 400 cm^{-1} respectively, where a value of $\phi_s \sim 135^\circ$ has been chosen to approximately fit the low temperature g-values of Cu(II)/K$_2$Zn(SO$_4$)$_2$.6H$_2$O. At room temperature in figure 7.8a, the value of g_x has decreased too much, while g_y has not increased enough. The lowest g-value, g_z, instead of remaining approximately constant, has increased substantially. The g-values at 300K are approaching an isotropic value, following the behaviour of the increasingly delocalised vibronic functions shown in figure 7.8b. Figure 7.9 shows qualitatively the same behaviour except, as the localised nature of the probability functions indicate, the larger strain means that the change towards an isotropic spectrum is more gradual. Again, both the calculated rise in g_z, and the temperature dependence of g_x and g_y do not follow the experimentally observed behaviour.

The existence of a warping term in the potential is then necessary, _within the present model_, to reproduce the experimental observables; the strain terms alone are insufficient. An estimate of the magnitude of this warping can be found in two ways:

In the first approach, the strain parameters can be taken from the structural data of the host compounds and thereby used to find β, as both β and S_θ mainly determine the low temperature g-values. The fitted value of the strains (table 7.5) were found to be somewhat smaller than those obtained from the structural studies (table 7.4), implying that β could be similarly underestimated. If just the tetragonal strain is considered, then Reinen and Krause (1981) have shown that the angular position of the potential minimum is determined by the ratio $S_\theta/3\beta$. Using this and the data given in tables 7.4, 7.5, this gives the values $\beta \sim 380$ and 340 cm^{-1} for the K$^+$, and NH$_4^+$ hosts respectively.

The second way to estimate a value of β is from the relaxation rate determined from the variation of the hyperfine halfwidths. This

(7.10)

Figure 7.8a No warping terms. $S = 100 \text{ cm}^{-1}$; $\phi_S = 135°$.
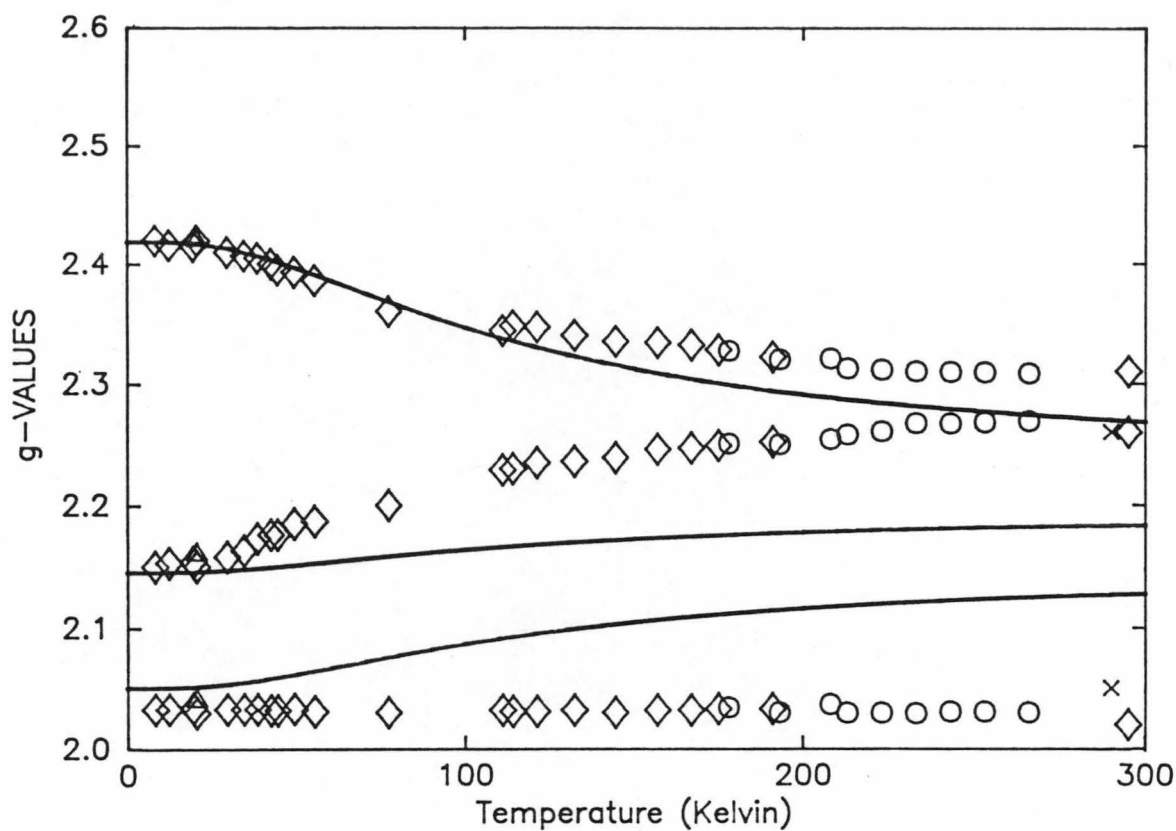
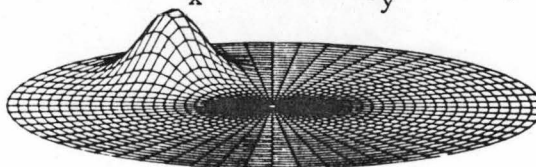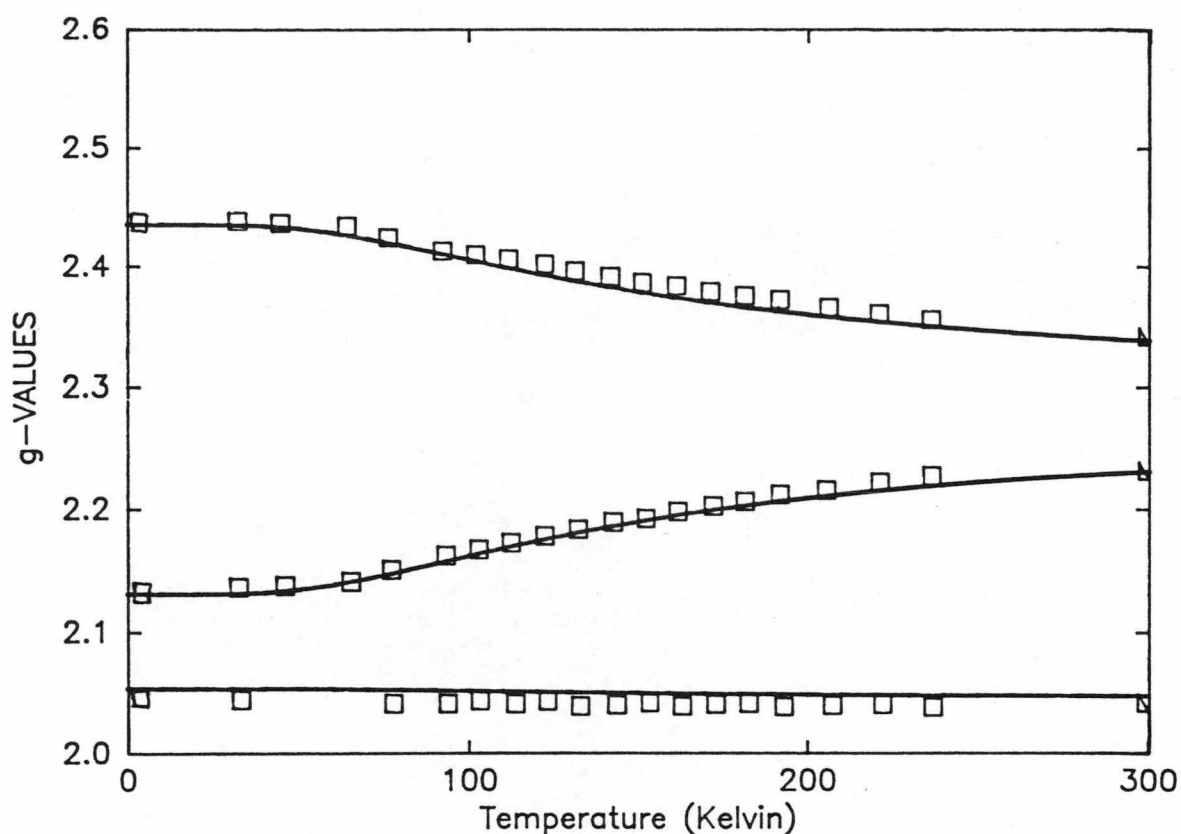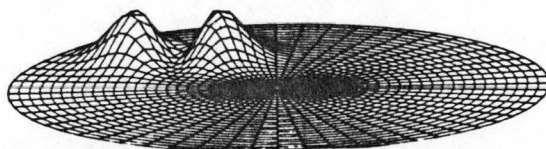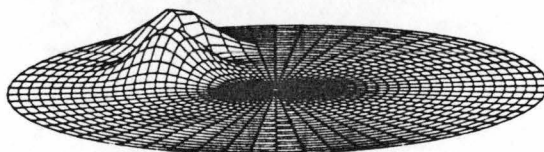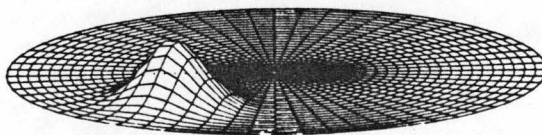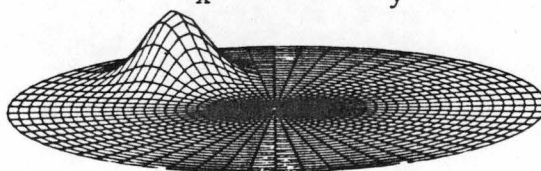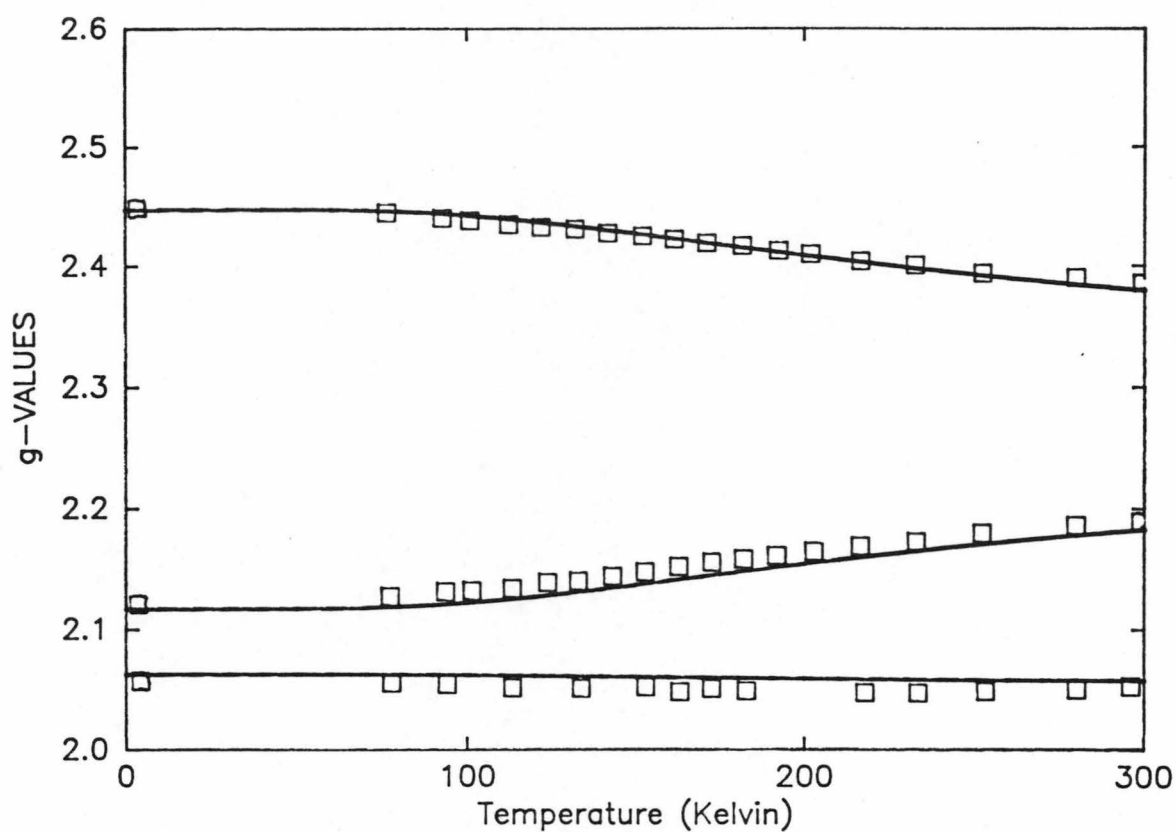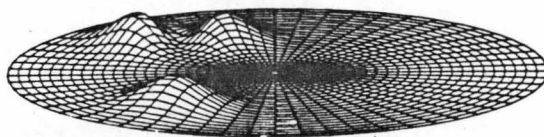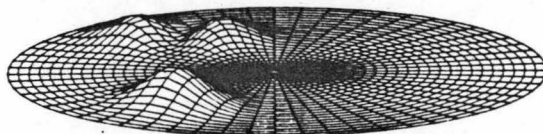**Figure 7.8b** The four lowest vibronic probability functions.
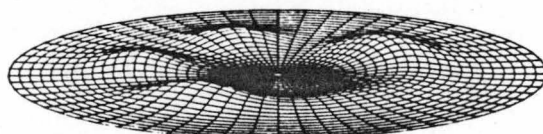
4 $E = 142 \text{ cm}^{-1}$; $g_x = 2.174$; $g_y = 2.208$; $g_z = 2.178$.
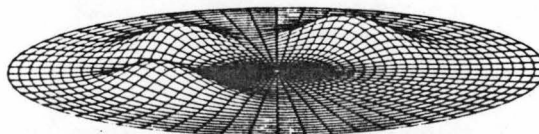
3 $E = 104 \text{ cm}^{-1}$; $g_x = 2.272$; $g_y = 2.181$; $g_z = 2.121$.

2 $E = 56 \text{ cm}^{-1}$; $g_x = 2.339$; $g_y = 2.164$; $g_z = 2.087$.

1 $E = 0 \text{ cm}^{-1}$; $g_x = 2.419$; $g_y = 2.145$; $g_z = 2.051$.

Figure 7.9a No warping terms. $S = 400 \text{ cm}^{-1}$; $\phi_s = 135^{\circ}$.
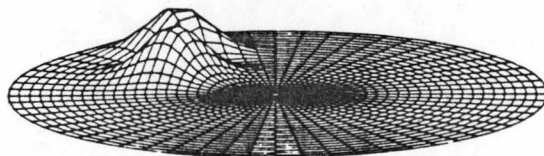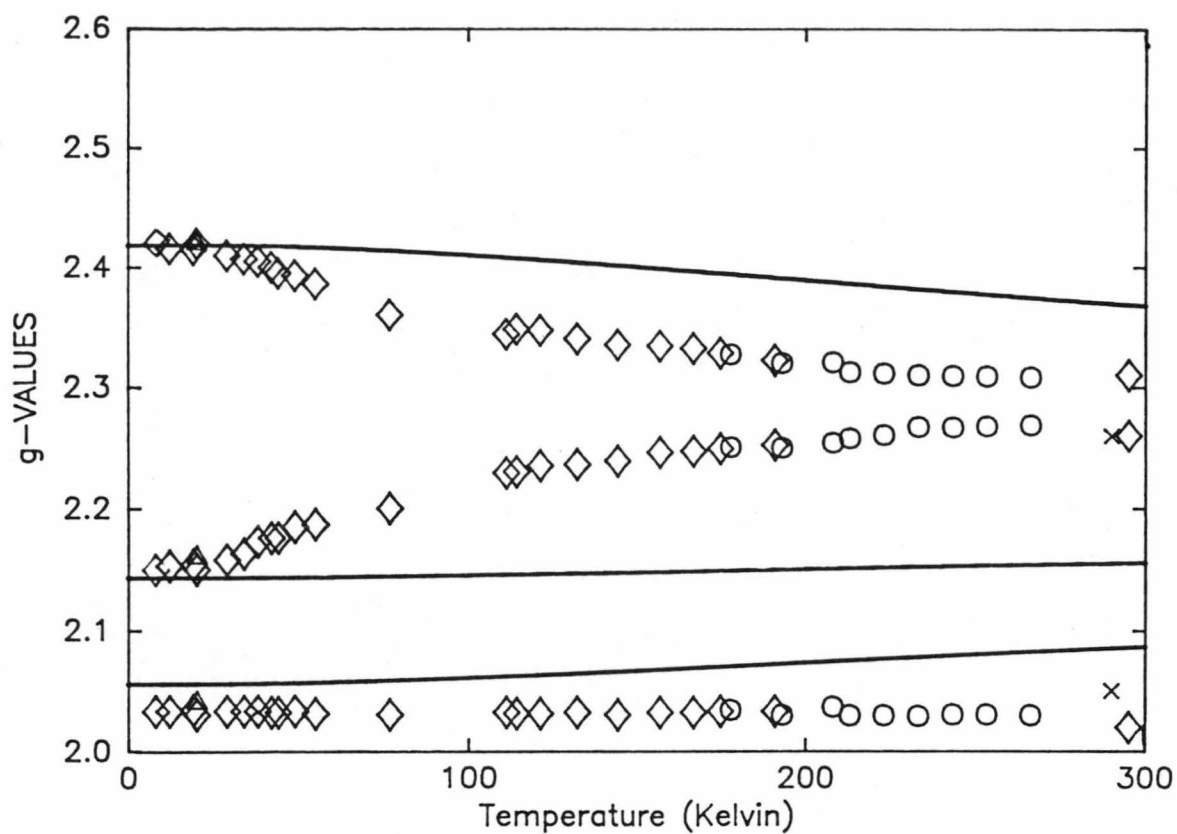

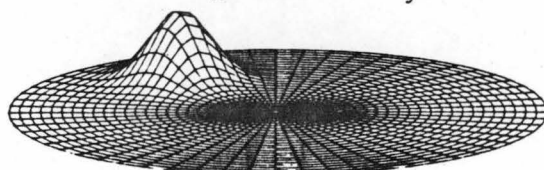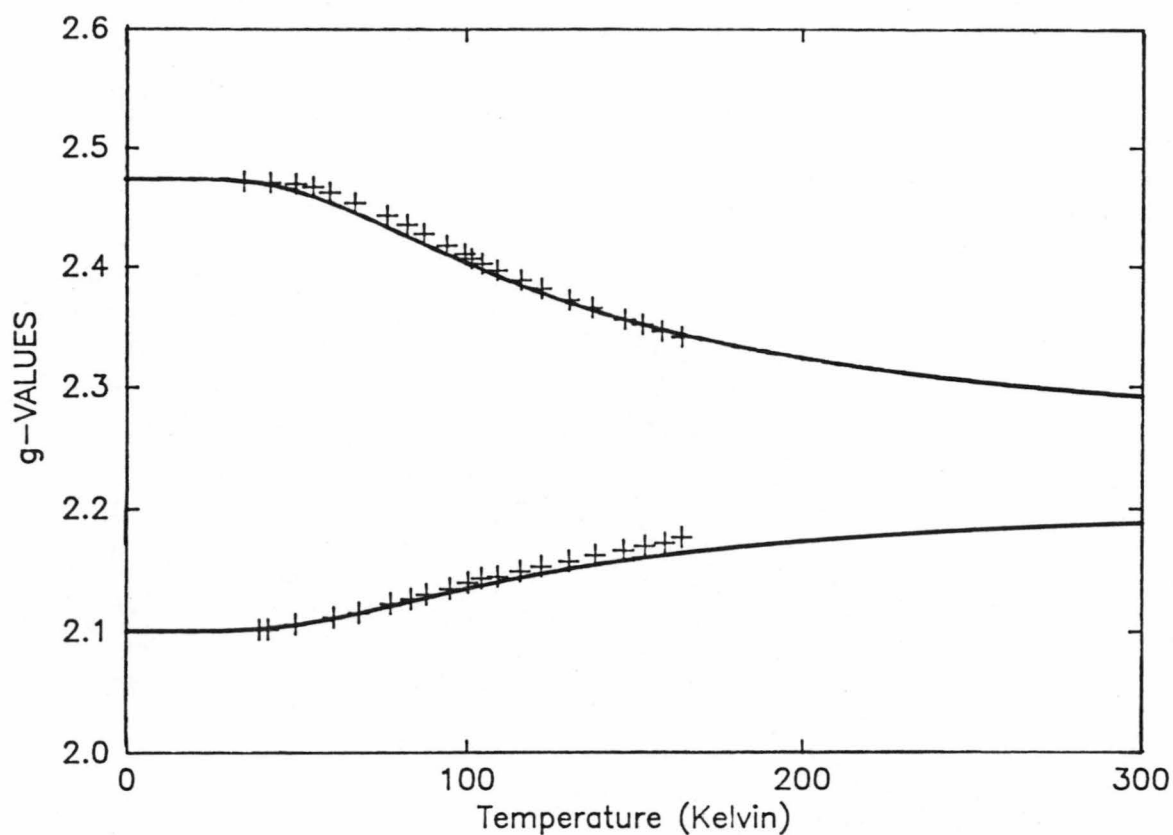**Figure 7.9b** The four lowest vibronic probability functions.
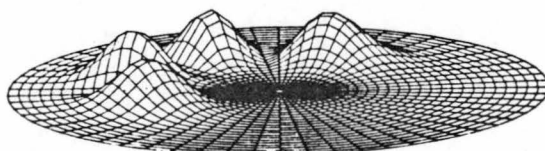
4 $E = 296 \text{ cm}^{-1}$; $g_x = 2.339$; $g_y = 2.163$; $g_z = 2.104$.
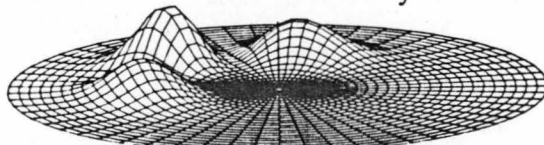
3 $E = 205 \text{ cm}^{-1}$; $g_x = 2.365$; $g_y = 2.156$; $g_z = 2.088$.
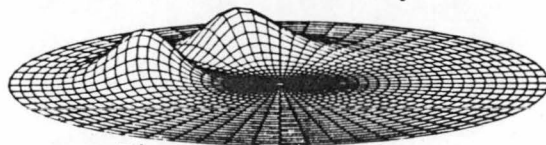
2 $E = 108 \text{ cm}^{-1}$; $g_x = 2.389$; $g_y = 2.150$; $g_z = 2.073$.
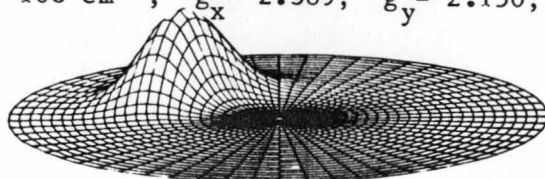
1 $E = 0 \text{ cm}^{-1}$; $g_x = 2.419$; $g_y = 2.143$; $g_z = 2.056$.

has been shown (Silver and Getz 1974; Zaitdinov etal 1983) to approximately follow an exponential dependence given by (5.40) over the temperature range ~ 10-80 K. The "activation energy", E_{12}, has been interpreted as a barrier height between the two lowest wells and has been found to be 120 cm^{-1} for the K$^+$ host (Silver and Getz 1974); 160 cm^{-1} for the Zn(GeF$_6$).6H$_2$O host (Zaitdinov 1983); and 420 cm^{-1} for Cu(H$_2$O)$_6^+$ in solution (Poupko and Luz 1972). In the present case, for A_2= 33.3 cm^{-1}, the barrier height in the absence of strain at the Jahn-Teller radius ρ_o, is approximately given by 2β ~ 600 cm^{-1}. However, the inclusion of a negative tetragonal strain greatly reduces this value, and using the data for the K$^+$ host a barrier height of ~280 cm^{-1} is found.

The energy E_{12} is more correctly interpreted as the energy interval to the lowest lying excited vibronic state that is delocalised over both wells to provide a relaxation pathway (William etal 1969). From figures 7.3b and 7.7b, it can be seen from the vibronic probability plots that such vibronic levels exist in the correct region to be interpreted in terms of E_{12}, although the energy levels are calculated too high in both cases. A smaller value of β only marginally improves this agreement.

The value of β ~ 300 cm^{-1} (A_2= 33.3 cm^{-1}) is a compromise between both the above methods of estimation. A larger value of β would require a larger value of the tetragonal strain to fit the low temperature g-values. This then causes disagreement with the S_θ/S_ε ratio from the structural data. Alternatively, if the orthorhombic component of the strain is then increased to give agreement with this ratio, then the temperature dependence of the g-values will not be reproduced. A value of β~300 cm^{-1} gives a S_θ/S_ε ratio that closely agrees with the structural data and fits the g-values (tables 7.4,5).

It should be stressed that it is not really appropriate to give a precise value of β because of the approximations already made in the model. In particular it is likely that the strain will destroy the cubic form of the warping terms in the vibronic Hamiltonian and the "real" warping parameters may be very different. A value of β ~ 300 $\pm$ 100 cm^{-1} seems a reasonable estimate for the present system.

(7.11)

Table 7.5: The Best Fit Parameters.

Cubic parameters:

$h\nu = 300$ cm^{-1} ($f = 0.95$ mdyneA^{-1})

$A_1 = 900$ cm^{-1} ($V=113$cm^{-1}pm^{-1})

$A_2 = 33.3$ cm^{-1} ($\beta = 300$ cm^{-1})

$k = 0.88$ $\Delta E = 11,900$ cm^{-1}

	K^+	Rb^+	NH_4^+	Cs^+	$(GeF_6)^{2-}$
S_θ (cm^{-1})	-1000	-800	-550	-650	100
S_ε (cm^{-1})	55	110	120	200	0
$-S_\theta/S_\varepsilon$	18	7.3	4.6	3.2	-
A_1 (T)	-170	-250	-170	-300	-130

Table 7.6: Predicted Zn-O bondlengths in the Host Lattices.

	K^+	Rb^+	NH_4^+	Cs^+	$(GeF_6)^{2-}$
Q_θ^0 (dim'less)	-1.111	-0.889	-0.611	-0.722	0.111
Q_ε^0 (dim'less)	0.061	0.122	0.133	0.222	0.0
Q_θ^0 (pm)	-8.78	-7.02	-4.83	-5.71	0.88
Q_ε^0 (pm)	0.48	0.97	1.05	1.76	0.0
R_x (pm)	212.8	212.5	211.9	212.5	209.7
R_y (pm)	212.3	211.5	210.9	210.8	209.7
R_z (pm)	204.9	205.9	207.2	206.7	210.5

7.4 DISCUSSION

7.4.1 Comparison with the Silver and Getz model.

Silver and Getz (1974) have seemed almost apologetic that their simple model works so well, and ended their paper with the hope that their work would ".. stimulate further theoretical work on this crystal in order to elucidate the role of the excited vibronic states". The present investigation represents the start of such a study, and it is now of interest to compare the two approaches.

From figures 7.3-7.7 it is clear why the Silver and Getz (S&G) model has been so successful. The probability functions of the vibronic levels show that the lowest levels are strongly localised within single wells. The properties of these levels are then close to what would be expected for an ion with a static geometry representing the minimum of the appropriate well. The gross features of the observed temperature dependence are then principally determined by the relative population of the two levels that are localised in the two lowest wells. The higher of these two levels may not be the lowest excited level, as calculated for the Cs^+ host (figure 7.6), so it is not the case that other vibronic levels are unimportant because they are thermally inaccessible. However, the g-values calculated for these other levels do not differ greatly from those of the lowest level in each well, and their effect on the overall temperature dependence will be minimal.

This is illustrated in figure 7.10 for the two extreme cases of the K^+ and Cs^+ hosts. Here the full lines shows the results of the present method as previously given which includes ~60 vibronic levels in a Boltzmann average over all levels up to 1,500 cm^{-1} above the ground state. The dashed line is for the same calculation using just the two vibronic levels that are most closely localised in each well. These levels are the 1st and 2nd and the 1st and 4rd levels respectively for the K^+ and Cs^+ hosts. The dotted line is the Silver and Getz model (equation 7.2) using the parameters given in table 7.2 and the low temperature g-values. It can be seen that in both cases the full calculation and the S&G model agree very well. The use of only

(7.12)
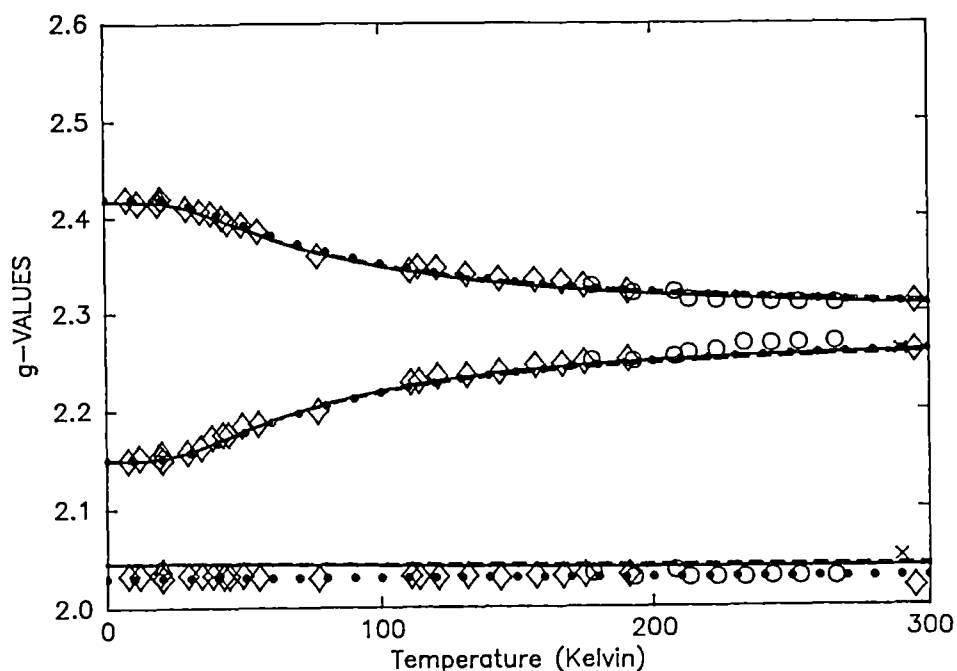
Figure 7.10a: g-values of $Cu/K_2Zn(SO_4)_2 \cdot 6H_2O$ calculated using:
Silver & Getz model (g_x=2.42; g_y=2.15; g_z= 2.03; $\delta_{1,2}$= 75cm^{-1})
Including only the vibronic states 1 and 2 from figure 7.3b.
Including all states up to 1500 cm^{-1}.
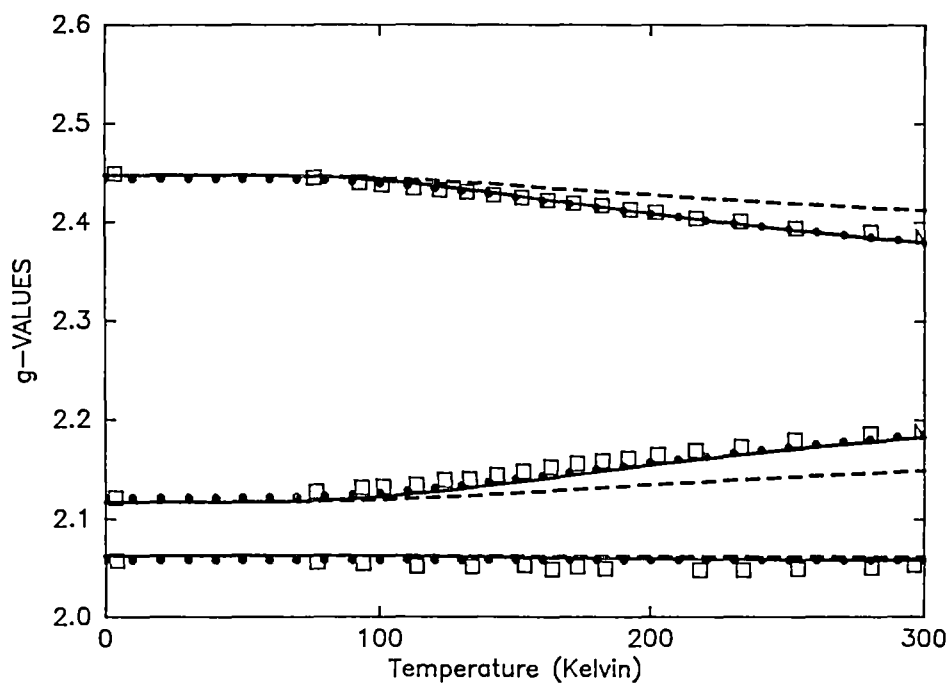
Figure 7.10b: g-values of $Cu/Cs_2Zn(SO_4)_2 \cdot 6H_2O$ calculated using:
Silver & Getz model (g_x=2.444; g_y=2.121; g_z=2.067; $\delta_{1,2}$= 290cm^{-1})
Including only the vibronic states 1 and 4 from figure 7.6b.
Including all states up to 1500 cm^{-1}.

two levels (dashed line) agrees well in the K^+ host, as the wavefunctions are completely localised in the separate wells (see figure 7.3b), therefore closely resembling the static nature of the S&G model. In the Cs^+ host, however, the use of only two levels (dashed line) results in a large deviation from the full calculation. Inspecting the wavefunctions (figure 7.6b) shows that there is, in fact, no level that is fully localised in the higher well. Including all the levels however (full line) results in the correct behaviour. The two level S&G model appears to be a better approximation for the K^+ host system rather than the Cs^+ host.

The biggest difference between the g-values calculated using the Silver and Getz model and the present approach is due to the fact that the S&G model uses the experimental low temperature g-values so that better agreement is obtained for the lowest g-value. Another, very subtle, difference is that the full model predicts that the lowest g-value should very slightly _decrease_ with increasing temperature, rather than stay the same in the S&G two well model, or increase in the S&G three well model. This change however is very slight and would be difficult to observe experimentally. The present model does not require the experimental low temperature g-values, as these values come out of the calculation. The g-values may even be predicted with some confidence in similar systems if the structure of the host compound is known.

The purpose of this work is not to improve an already very good model, but rather to investigate the physical meaning behind it, and in particular the differences between the values of the parameters obtained from the two approaches. From the g-values given for the lowest wavefunctions in figures 7.3-7.7, it can be seen that the Silver and Getz assumption that the two wells have equivalent magnetic properties, is not quite true. This means in the present model these levels must be somewhat closer than those in the S&G model to achieve the same temperature dependence. This energy interval is not the same as the strain, as has been assumed by some authors (Petrashen et al 1980), or even the energy difference of the well minima. The strain is just one of many terms that go to make up the potential, and the energy levels which result must be calculated numerically. The present model should give a better estimate of both components of the "true" strain. In the S&G model the tetragonal strain is found from the

(7.13)

population of the third (highest) well; whereas in the present method it is fixed by the low temperature g-values, or equivalently, the angular position of the minima in the Jahn-Teller surface. This means that the tetragonal strain can be found much more accurately with the present model if a value of beta is assumed.

Silver and Getz (1974) have estimated a value of $E_{13} \sim 450$ cm^{-1} from the temperature dependence of the lowest g-value, g_3, in the K$^+$ salt. Petrashen etal (1980) have realised that this is too low to be consistent with the crystal structure of the host, and have estimated a value of $E_{13} \sim 1125$ cm^{-1}. The present value of $S_\theta \sim 1000$ cm^{-1} is in good agreement with the value of Petrashen etal (1980), because as discussed before, in general $S_\theta < E_{13}$. Since the K$^+$ salt has the most rhombic low temperature g-values in the four Tutton salts discussed, it follows if β is kept constant, that it must have the highest value of the tetragonal strain. This is found to be the case using the present model, but the third level has a much higher energy than that given by Silver and Getz (1974). These workers have stressed that their value of 450 cm^{-1} is only very approximate, based on the data in the 310-350K range in figure 7.11b. The very definite rise in the lowest g-value that they observed in this range requires explanation as such a rise is unexpected with the strain parameters found in the present work.

This discrepancy prompted the thermogravimetric analysis of the host compound $K_2Zn(SO_4)_2.6H_2O$ shown in figure 7.11a. The host compound loses four waters at ~333K and a further two ~20° higher. Silver and Getz observed no change in the g-values until ~310K, and a phase transition prior to water loss may explain the rise until 333K; certainly their published points at 340 and 350K should be viewed with some suspicion.

7.4.2 Prediction of the Host Geometry.

It is now possible to predict the Zn-O bondlengths of the host compounds where the crystal structure determination has not been carried out, from the strain parameters that have been derived from the temperature dependent ESR data. These predictions are given in table 7.6, and a brief description of the calculation follows.
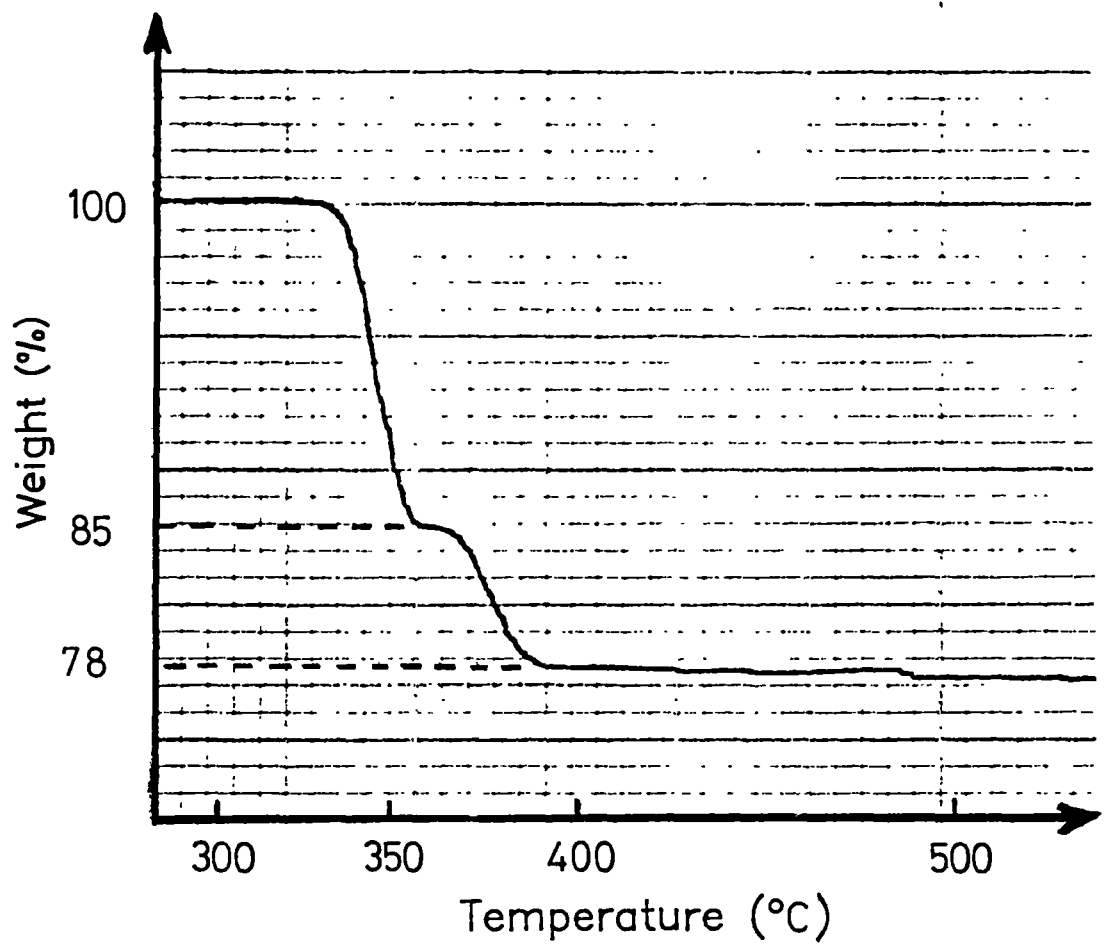
Figure 7.11a: Thermogravimetric analysis of $K_2Zn(SO_4)_2 \cdot 6H_2O$.
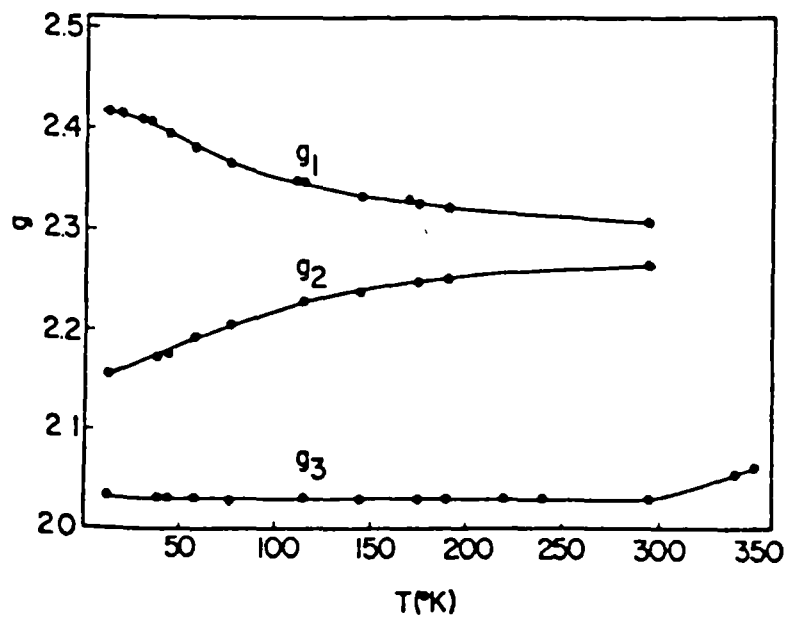
Figure 7.11b: g-value data of Silver and Getz (1974).

First equation (7.5) is used with a value of $A_1 = 900$ cm^{-1} to find the shift in the origin of the host Q_θ^0, Q_ε^0 that is responsible for the ESR derived strain values. This origin is then converted to dimensioned coordinates using the relationship given by equation (2.35). The change in the individual bondlengths can then be calculated by the following expressions:

$$\Delta R_x = -\frac{1}{\sqrt{12}} \, Q_\theta^0 + \frac{1}{2} \, Q_\varepsilon^0 \qquad\qquad (7.6)$$

$$\Delta R_y = -\frac{1}{\sqrt{12}} \, Q_\theta^0 - \frac{1}{2} \, Q_\varepsilon^0$$

$$\Delta R_z = \frac{1}{\sqrt{3}} \, Q_\theta^0$$

The overall bondlengths can then be calculated by using $<R>=210$ pm found from an average of the bondlengths in the two known zinc crystal structures in table 7.1.

The final results, listed in table 7.6, show excellent agreement with the two known structures (K^+, NH_4^+ salts). Further, the Cs^+ salt is predicted to be the host with the largest rhombic distortion, and the Rb^+ salt to have a tetragonal compression intermediate to the known K^+ and NH_4^+ structures. The $Zn(GeF_6) \cdot 6H_2O$ host is predicted to have only a very small tetragonal elongation in the low temperature phase. However, this compound is known to be isomorphic with $MgSiF_6 \cdot 6H_2O$ (Zaitdinov 1983), which is monoclinic in the low temperature phase (Syoyama and Osaki 1972). Because the tetragonal strain is positive and reinforces one of the wells due to the warping, a small orthorhombic strain from the host would have little effect on what would essentially be a tetragonal ESR spectrum. Therefore, while it is unlikely that the bondlengths along the x and y molecular axes will be equal as given in table 7.6, the present method is not capable of distinguishing this.

(7.15)

7.5 CONCLUSIONS

The ESR properties of the $Cu(H_2O)_6^{2+}$ ion in various host lattices can be successfully described from the point of view of the dynamic Jahn-Teller effect where the effects of strain imposed on the system by the host lattice partially quenches the dynamic properties. The approximation that the Jahn-Teller part of the problem keeps its cubic symmetry, while drastic, has resulted in a model that is capable of explaining the very different temperature dependence of the $Cu(H_2O)_6^{2+}$ ion observed in five different host lattices with a _single set_ of parameters. The experimentally fitted strain parameters are shown to be physically more realistic than those found using the Silver and Getz model. It allows certain predictions to be made about the structure of the unknown zinc host lattices.

The reason why the Silver and Getz model works so well appears to be due to the fact that the calculated vibronic wavefunctions are at well defined localised geometries. The observed temperature dependence of the ESR spectrum can then be closely approximated by the rapid equilibrium between these static configurations rather than a delocalisation in the electronic and structural sense that occurs in cubic Jahn-Teller cases.

(7.16)

APPENDIX 7.A1   THE TEMPERATURE DEPENDENCE OF THE CRYSTAL STRUCTURES

The crystal structures of the pure copper Tutton salts are quite interesting in that they apparently show a substantial temperature dependence of the Cu-O bondlengths (see table 7.1). An analysis of the anisotropic temperature factors (Duggan etal 1979) show that the bonds that have the greatest temperature dependence also have the largest root-mean-square amplitudes in the direction of the Cu-O bond. Since x-ray measurements occur over a long time scale, a thermal average of vibronic levels will be observed. For dynamic systems such as these, the geometry can be quite different in each vibronic level. The electron density that is observed corresponds to that of many different individual levels, resulting in an average value of the geometry with a large thermal ellipsoid.

Such a postulated large thermal ellipsoid along the Cu-L axis in dynamic Jahn-Teller systems has often been puzzlingly absent. For example the thermal ellipsoid of the nitrogen atom in cubic $K_2Pb[Cu(NO_2)_6]$ was found to be nearly isotropic (Isaacs and Kennard 1969) where clearly an anisotropic one would be expected for what is thought to be a dynamic system. However, a careful study by Cullen and Lingafelter (1971) on the same molecule, found that the RMS amplitude of the N atom was slightly greater in the direction parallel to the Cu-N perpendicular to it. Considering just the internal vibrations, this is unexpected since bond bending amplitudes are in general greater than bond stretching. Cullen and Lingafelter (1971) were able to derive a value for the Jahn-Teller radius from from these temperature factors alone, and similar work has been carried out by Ammeter etal (1979). The above discussion is to show that while anisotropic thermal parameters are to be expected, the effect may be quite small since the bulk of the ellipsoid contains the external motions of the crystal lattice.

The geometric properties of the present doped systems cannot really be investigated experimentally. However, their hypothetical geometries can be calculated for the potentials that reproduce the ESR data, and then compared to the observed behaviour of the pure structures. These geometries of the $Cu(H_2O)_6^{2+}$ ion in the zinc hosts are given in table 7.7 for the NH_4^+, K^+ and $Zn(GeF_6).6H_2O$ compounds.

(7.17)

The geometric properties of the first four vibronic levels have been calculated directly as expectation values from the wavefunctions shown in figures 7.3-7.7. The value of the Jahn-Teller radius, $\rho_0 \sim 30$ pm, does not vary appreciable within the individual levels, but is significantly less than the value of ~36 pm seen in the pure Tutton salts. [This value was found from the average of the four low temperature copper Tutton salt structures in table 7.1]. This may be due to cooperative effects in the pure compounds. It is also interesting to note that ρ is greater than the classical Jahn-Teller radius $\rho_0 = A_1/h\nu$ which gives $\rho_0 = 3$, or 23.7 pm when dimensioned. This is because the warping causes the minima of the wells to be at slightly larger values of ρ.

Table 7.7 also shows the temperature dependence of these geometric properties, where they are given a Boltzmann average. The geometry does not actually "average" in this sense, a perfect X-ray machine would see the thermal ellipsoids of all the vibronic levels as they are populated. However, since the root-mean-square amplitudes are of the same order of magnitude as the change in the bondlengths in the different vibronic states, an average of these ellipsoids will be seen, the mean of which will be temperature dependent.

These calculated values are seen to behave in much the same qualitative manner as that observed in the pure copper Tutton salts. At low temperatures the geometry is close to that of an tetragonal elongation along x; and as the temperature is increased, ΔR_x decreases, ΔR_y increases and ΔR_z stays much the same.

Duggan et al (1979) have suggested that the temperature dependence of the g-values can be solely explained by this apparent variation in the bondlengths that is due to the fluxional properties of the complex itself. Indeed they adopted this model "... especially as it is difficult to understand why the alternative explanation of $d(x^2-y^2)$ and $d(z^2)$ mixing should be so temperature dependent". They have misunderstood the situation as it is just this mixing, or vibronic coupling, that causes a potential surface that gives rise to the apparent "fluxional" behaviour of the complex.

The apparent variation of the Jahn-Teller radius "ρ_0" is also shown in table 7.7. These values were calculated from the temperature averaged bondlengths, and decreases in magnitude with increasing temperature, similar to what is observed in the pure Tutton salts

(7.18)

Table 7.7: Predicted Cu-O Bondlengths in Zinc Hosts.

Rb^+	$\langle\Delta R_x\rangle$	$\langle\Delta R_y\rangle$	$\langle\Delta R_z\rangle$	$\langle\rho_o\rangle$*
level: 1	16.6	-6.7	-9.9	29.6
2	-5.5	15.7	-10.2	28.7
3	14.3	-4.0	-10.3	28.2
4	16.6	-6.9	-9.6	30.1
NH_4^+				
1	17.0	-7.4	-9.6	30.1
2	-6.6	16.5	-9.9	29.5
3	15.7	-5.8	-9.9	29.3
4	16.8	-7.7	-9.2	30.5
$Zn(GeF_6).6H_2O$				
1	-8.7	-8.7	17.3	30.5
2	4.2	4.2	-8.4	30.4
3	4.2	4.2	-8.3	30.5
4	-8.5	-8.5	17.1	29.6
Rb^+	"ΔR_x"	"ΔR_y"	"ΔR_z"	"ρ_o"**
Temp. 0K	16.6	-6.7	-9.9	29.6
100	14.3	-4.3	-10.0	25.4
200	10.8	-0.7	-10.0	20.9
300	9.1	0.9	-10.1	19.3
NH_4^+				
0	17.0	-7.4	-9.6	29.5
100	15.3	-5.7	-9.6	26.8
200	11.7	-2.0	-9.6	21.6
300	9.7	-0.1	-9.6	19.3
$Zn(GeF_6).6H_2O$				
0	-8.6	-8.6	17.3	30.5
100	-6.1	-6.1	12.3	21.3
200	-3.3	-3.3	6.7	11.6
300	-2.2	-2.2	4.5	7.8

* The changes in the bondlengths are calculated from the expectation values of the Q_θ, Q_ε coordinates and equation (7.6). $\langle\rho_o\rangle$ is an _expectation value_ calculated directly from the vibronic wavefunctions.

** The changes in the bondlength are a Boltzmann's average over the vibronic levels. "ρ_o" is then calculated from these changes in bondlength.

structures. Alcock etal (1984) have commented on, but could not give an explanation for, this observation which seems contrary to the usual assumption of a temperature independent potential surface. The explanation is, of course, that the value of ρ_o is not decreasing with increasing temperature, but remains relatively constant as can seen from the expectation values of the individual levels. It only appears to be decreasing when it is calculated from the temperature averaged bondlengths that are obtained from the X-ray structures. One can also imagine the situation of a purely dynamic Jahn-Teller effect where a crystal structure will give equal bondlengths and ρ_o will then be calculated to be zero. In other words, X-ray crystallography cannot give a direct measure of ρ_o, and a "ρ_o" calculated from the bondlengths that are an average will appear to decrease as the temperature rises. While structural experiments cannot give the Jahn-Teller radius of dynamic systems from the bondlengths, they can do so from an analysis of the RMS amplitudes of the bondlengths.

The previous points can be illustrated by considering the $Zn(GeF_6) \cdot 6H_2O$ case in table 7.7. The first wavefunction has the expectation values of $<Q_\theta> = 30.0pm$, $<Q_\epsilon> = 0.0pm$, while the second has $<Q_\theta> = 14.5pm$, $<Q_\epsilon> = 0.0pm$. By calculating "ρ_o" from these values, we have "ρ_o" = 30.0pm for the first and "ρ_o" = 14.5pm for the second wavefunction. While the first value is close to the real (expectation) value ($<\rho_o> = 30.5pm$), the second is a long way off ($<\rho_o> = 30.4pm$). The apparent "ρ_o" is calculated too small for the second wavefunction because, as can be seen from figure 7.7b, $<Q_\epsilon^2>^{1/2} \neq 0$ although $<Q_\epsilon> = 0$ from the equal amount of the probability function at positive and negative regions of Q_ϵ.

Expressed mathematically, this is because:

$$<\rho_o> = < \Omega \mid \rho_o \mid \Omega > = < [\; \sum_i 2(\; R_i - <R> \;)^2 \;]^{1/2} > \qquad (7.A1)$$

$$\neq [\; \sum_i 2(\; <R_i> - <R> \;)^2 \;]^{1/2} = "\rho_o"$$

since in general $<X^2>^{1/2} \neq <X>$. Care must therefore be taken when interpreting the "average" geometry of the crystal structures of dynamical systems.

APPENDIX 7.A2   IMPLICATIONS FOR THE ELECTRONIC SPECTRUM

Since electronic transitions are very fast, the electronic spectrum of systems such as those considered here will not be the spectrum from an averaged geometry; rather a different electronic spectrum would be expected from each vibronic level. The superposition of the transitions from all the populated ground state vibronic levels will give rise to the observed spectrum. It is therefore pertinent to ask whether any temperature dependent effects would be expected from these dynamic systems.

Consider the case of the $K_2Zn(SO_4)_2 \cdot 6H_2O$ host, where there are two close lying levels that approximately correspond to tetragonal elongations along x and y respectively. In the lower well there will be transitions to the excited triplet states: $d(y^2-z^2) \rightarrow d(yz)$ and $d(y^2-z^2) \rightarrow d(xy), d(xz)$ at the energies $\Delta E - A_1(T)$ and $\Delta E + \frac{1}{2} A_1(T)$ respectively. [Here ΔE is the energy of the triplet baricentre above the ground state, and $A_1(T)$ is the linear coupling constant of the triplet state in equation (5.25).] In the second, higher well the transitions will be $d(x^2-z^2) \rightarrow d(xz)$ and $d(x^2-z^2) \rightarrow d(xy), d(yz)$ at the same energies. Therefore exactly the same spectrum would be expected from each well although the transition to the higher energy doublet would be to $d(xy)$, $d(xz)$ in one well and to $d(xy)$, $d(yz)$ in the other.

The population of other levels will change these energies but, as long as the discussion is kept in the e_g vibrational space, the overall baricentre of the triplet levels will remain the same and the effect of other levels with different geometries will be to simply broaden the spectrum. Therefore the spectrum is essentially temperature independent of the dynamic effects of the e_g vibrations. Much greater temperature dependent effects would be expected from the ungerade vibrations that induce intensity in these centrosymmetric compounds.

It should be noted that they are dangers involved in interpreting the electronic spectrum (at low or high temperatures) in terms of the geometry taken from a room temperature crystal structure. In dynamic systems the crystal structure will give an "averaged" geometry rather than the true geometry of the individual vibronic levels.

CHAPTER 8   THE ESR OF Cu(II) DOPED NH$_4$Cl.

8.1 INTRODUCTION

The ESR spectrum of Cu(II) doped NH$_4$Cl has been extensively studied following the early works of Zaripov and Chirkin (1964) and Trappeniers and Hagen (1965). The experimental ESR spectrum can be very complicated as up to three different copper centres can be observed, depending on the conditions of crystal growth. The temperature dependent principal g-values obtained by many studies are shown in figure 8.1a. The main concern of these studies have been twofold:

i) To determine the exact location and coordination of the copper centres.

ii) To explain the unusual temperature dependence of the spin Hamiltonian parameters of these centres.

It is now well established that in the first two centres the Cu(II) ion occupies an interstitial site in the face centred position of four chloride ions in the CsCl type structure of NH$_4$Cl. The charge compensation is accomplished by the substitution of two NH$_4^+$ ions in the trans positions by either two H$_2$O or two NH$_3$ molecules, as shown in figure 8.1b. The copper ion is then six coordinate and the two types of species: trans-Cu(H$_2$O)$_2$Cl$_4^{2-}$ [centre (I)] and trans-Cu(NH$_3$)$_2$Cl$_4^{2-}$ [centre (II)], can be selectively obtained in crystals grown from acidic or basic solutions respectively (Hagan and Trappeniers 1970). These conclusions are unequivocal from the ENDOR studies of Boettcher and Spaeth (1974a,b), and thus supercede the earlier interpretations of Pilbrow and Spaeth (1967a,b) (NH$_4^+$ vacancies) and Bechtle etal (1971) (off centred position of Cu(II)). The coordination of centre (III) however, which has always be observed in conjunction with at least one of the other centres, has not been determined. The present study suggests a mixed coordination: trans-Cu(H$_2$O)(NH$_3$)Cl$_4^{2-}$ for centre (III).
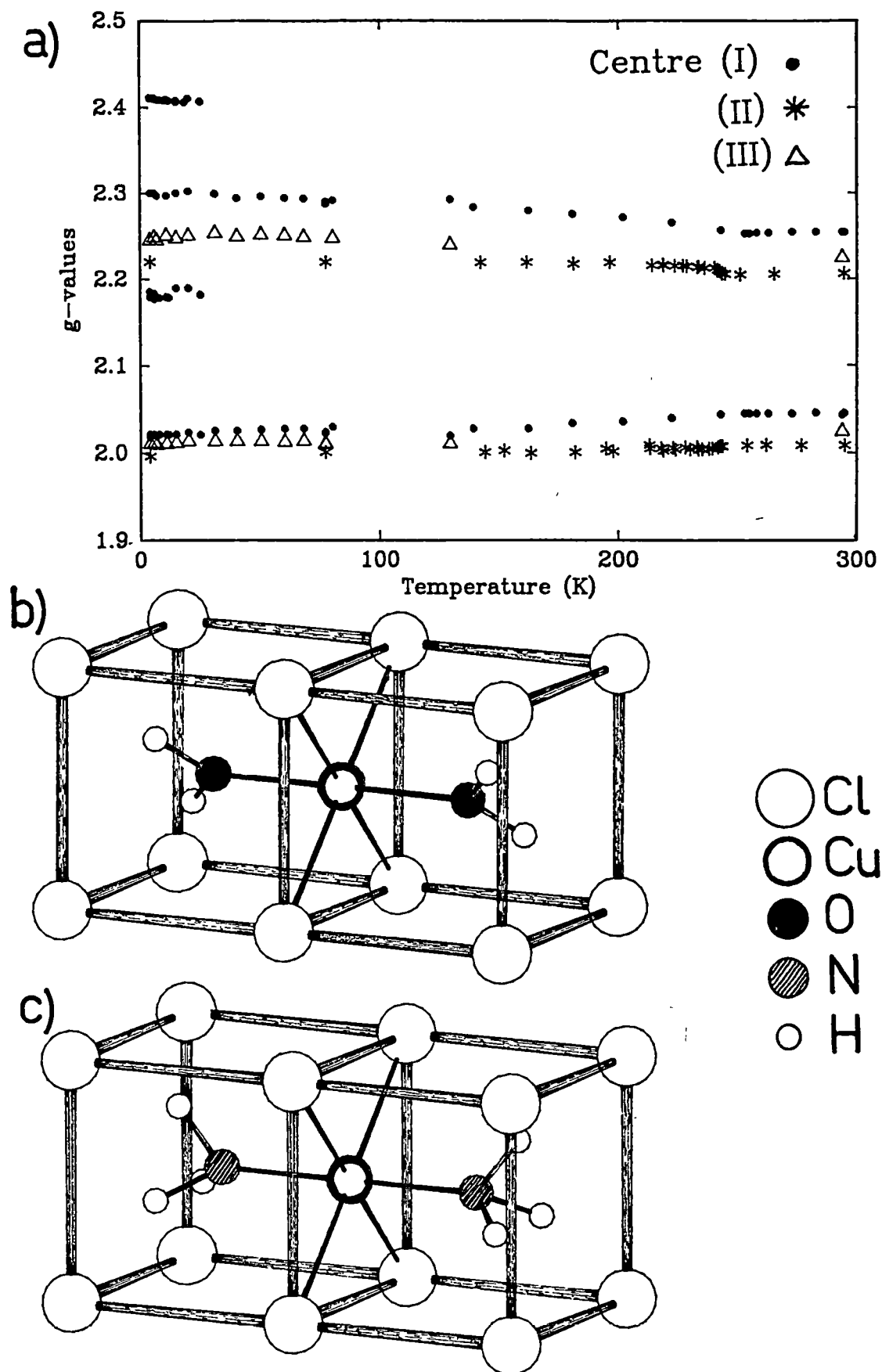
Figure 8.1 Cu(II)/NH₄Cl Centres.

a) Principal g-values of all centres.

b) Geometry of Centre (I).

c) Geometry of Centre (II).

The interpretation of the temperature dependence of these systems is more controversial. There are two separate features observed in this temperature dependence. At T_λ = 242.9K, there is an order-disorder phase transition that greatly influences the g values of the system, and this has been the subject of many studies (Pilbrow and Spaeth 1967a,b; Hagen and Trappeniers 1973; Van der Valk and Trappeniers 1977). In addition, at temperatures far from this phase transition, other dramatic temperature dependent effects are also observed. While the former is due, to some extent, to the bulk properties of the host crystal, the latter can be interpreted as due to the molecular properties of the Cu(II) guest species. It is this latter form of the temperature dependence that is of interest in the present study.

At low temperatures (<12K) the ESR spectrum of centre (I) $[Cu(H_2O)_2Cl_4^{2-}]$ has orthorhombic g-values (Bechtle etal 1971). At higher temperatures this spectrum is observed to collapse into a tetragonal spectrum with $g_\parallel < g_\perp$, usually typical of a compressed octahedral environment. This tetragonal spectrum is then also temperature dependent with $g_\parallel$ increasing and $g_\perp$ decreasing until the lamda point where abrupt changes occur. The spectrum of centres (II) and (III) are similar except that they remain tetragonal at all temperatures and their temperature dependence is not as marked as in centre (I).

The local coordination of the Cu(II) ions in figures 6.1b and 6.1c are of effective D_{4h} symmetry for the centres (I) and (II) respectively. This is because pi-bonding does not enter into the ^2E_g ground state and the axial ligands will therefore have an effective cylindrical symmetry even though geometrically this is not so. Centre (III) will have an effective C_{4v} symmetry if it has the suggested $Cu(H_2O)(NH_3)Cl_4^{2-}$ mixed coordination. A spin Hamiltonian with either D_{4h} or C_{4v} symmetry will give rise to a tetragonal g-tensor, so the fact that centre (I) shows orthorhombic g-values at low temperatures clearly needs explanation. In addition to this, from the purely static picture of the centres in figures 6.1b,c, these g-values would be expected to be temperature independent. Again this is not the case, the order of the temperature dependence of the tetragonal g-values being centre (I) > centre (III) > centre (II). Both of the above puzzling aspects of the temperature dependence can be quantitatively

(8.2)

explained by departing from a purely static model and considering the vibronic interactions of the centres. This model is essentially the Jahn-Teller Mexican hat potential surface perturbed by the different bonding characteristics of the axial ligands.

Although the Jahn-Teller theorem is not strictly applicable to mixed-ligand systems such as those considered here, it is convenient to apply the formalism developed in the previous chapters to this problem. Reasonable values of the potential and coupling parameters can be deduced from simple bonding arguments in what would be otherwise a very underdetermined problem in these low symmetry systems. The solution of the vibronic equations then allows all the above experimental data to be explained in a straightforward manner.

8.1.1 The Crystal Structure of Ammonium Halides.

The ammonium halides undergo a number of well-known phase transitions (Perry and Lowndes 1969) which are summarised below:

TABLE 8.1 AMMONIUM HALIDE STRUCTURES

Lattice type	NaCl	CsCl	"tetragonal"	CsCl
NH_4^+ ions	disordered	disordered	antiparallel ordering	parallel ordering
NH_4Cl NH_4Br NH_4I	I -- 457.7K -- II -------- 242.9K -------- III I -- 411.2K -- II -- 235K -- IIIa - 78K - IIIb IIIa - 105K - IIIb I -- 255.8K -- II -- 232K -- IIIa			

In this study, it is the NH_4X lattices with the CsCl type structure that are of interest. Here the NH_4^+ ions occupy the body centred sites in a cubic Cl^- lattice. The N-H bonds point directly at the chloride ions, and the two possible orientations, A and B, of the ammonium ions are shown in figure 8.2a.

The order-disorder transition, that occurs at $T_\lambda=243K$ in NH_4Cl, is associated with the orientation of the ammonium ions. At low temperature the NH_4^+ ions are parallel to each other as shown in figure

(8.3)
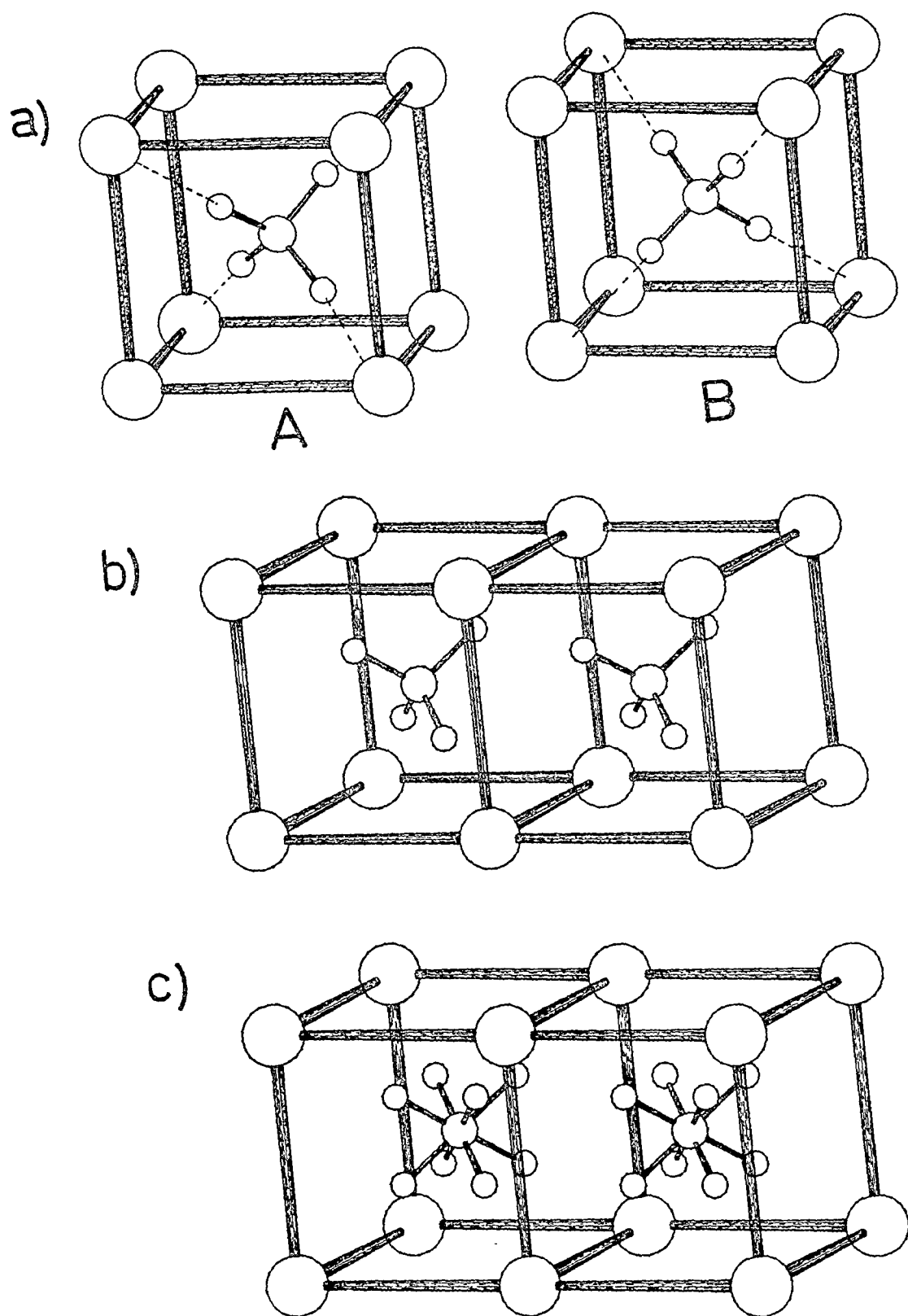
Figure 8.2   The NH$_4$Cl Structure in the CsCl type Phase.

a)   The two possible orientations of the ammonium ions.

b)   The ordered phase (T < 243K).

c)   The disordered phase (243 < T < 458K).

8.2b. In this case there is translational symmetry between the ammonium ions which will be either all A, or all B. Above T_λ there is an equal probability of finding the ammonium ion in the A or B orientation, and these will be randomly distributed in the lattice. This is called the disordered CsCl phase and is shown in figure 8.2c. In NH_4Br and NH_4I there exists an additional phase where the ordering is antiparallel (A-B-A-B...) along two axes and parallel along the third (either A-A-A-A... or B-B-B-B...). In this phase the lattice is then tetragonal, although the departure from cubic symmetry is very small (Perry and Lowndes 1969).

As well as the reorientation of the NH_4^+ ions, there also coexists a first order phase transition at T_λ (Slichter etal 1971). This is observed as a discontinuity in the thermal expansion of the NH_4Cl lattice which also shows both hysteresis and sample dependence (Fredericks 1971).

A temperature and pressure dependent ESR study of Cu(II)/ND_4Cl has shown that this change in the lattice constant is at least partly responsible for the change in the magnetic properties around T_λ. Any change in the g-values around T_λ must therefore include lattice effects as well as "local" changes around the Cu(II) centres, as was well appreciated in the early work of Pilbrow and Spaeth (1967a,b).

The study of Kuroda and Kawamori (1971) can therefore be criticised as they have interpreted the change in the g-values of centre (II) at T_λ as due to the order-disorder transition of the ammonia ligands. This treatment is over simplistic as it ignores the abrupt change in the lattice constants and, in addition, it is unlikely that the reorientation of the NH_3 ligand bound to copper would be the same as the NH_4^+ ion in the lattice. The ENDOR studies of Boettcher and Spaeth (1974a,b) imply that the NH_3 ligands rotate about the Cu-N axis even down to 1.6K.

Similarly, the reasoning by Watanabe and Abe (1975a,b) that centre (I) must have a NH_4^+ nearest neighbour to explain the abrupt changes observed at T_λ, is not necessarily true. An explanation of the observed changes at T_λ is beyond the scope of this thesis. Here, the temperature dependence of the ESR spectrum only below ~230K is considered. It is then assumed that the local dynamics of the Cu(II) centres, rather that the bulk crystal properties, can account for the observed experimental behaviour.

(8.4)

8.1.2 Previous Interpretations of the Cu(II)/NH$_4$Cl System.

The literature on this system is extensive. Some of the more important previous studies are summarised below.

Pilbrow and Spaeth (1967a,b) concluded from their studies that centre (I) consisted of Cu(II) in a square of Cl$^-$ ions with one NH$_4^+$ nearest neighbour, one NH$_4^+$ vacancy nearest neighbour and one NH$_4^+$ vacancy remote. Centre (II) was then thought to be due to the Cu(II) ion having two NH$_4^+$ vacancies axial. While this was later shown to be wrong, they correctly argued that vibronic contributions would influence the temperature dependence, as would the change in the lattice constant at T$_\lambda$.

Hagen and Trappeniers (1970) first correctly recognized the nature of the Cu(II) sites as due to Cu(H$_2$O)$_2$Cl$_4^{2-}$ and Cu(NH$_3$)$_2$Cl$_4^{2-}$ entities in centres (I) and (II) respectively, from analysing the hyperfine and superhyperfine structure.

Betchle etal (1971) were the first to report the orthorhombic g-values of centre (I) at low temperature. They postulated that this was due to the Cu(II) ion occupying an off-centre position in the Cl$^-$ square. The orthorhombic → tetragonal transition of the spectrum was then said to be due to rapid exchange between the four equivalent off-centred positions.

Hagan and Trappeniers (1973) examined the temperature dependence of centre (I) in the range 77-300K with no knowledge of the orthorhombic spectrum discovered at lower temperatures. Remarkably, they independently concluded from a lineshape analysis that the previously assumed tetragonal spectrum was actually orthorhombic (g$_x$- g$_y$ =0.01 at 77K), and was likely to be an averaged spectrum of inequivalent orthorhombic centres. Further, they proposed that the Cu(H$_2$O)$_2$Cl$_4^{2-}$ species may intrinsically tend to assume an orthorhombic symmetry by vibronic interactions.

Freeman and Pilbrow (1974) further developed the off-centred model of Betchle etal (1971).

Boettcher and Spaeth (1974a,b) conducted a thorough ENDOR study of both centres. They confirmed the presence of axial H_2O and NH_3 ligands in centres (I) and (II) respectively. In centre (I) they showed that the (110) plane must be a mirror plane of the charge distribution (see figure 8.1b). The off-centred model was therefore shown to be wrong. Boettcher and Spaeth concluded that the orthorhombic spectrum observed at low temperatures was due to the two H_2O ligands ligands both being coplanar in the (110) plane. At higher temperatures the thermally activated reorientation of these ligands would occur about the (001) axis between the two possible (110) planes. In this "hopping" model, the reorientation of the two molecules are required to remain in phase (ie stay coplanar) to reproduce the tetragonal ESR spectrum observed at higher temperatures. Although they were understandably not entirely happy with this interpretation, this was the only model which they could see was able to account for all their experimental observables.

Watanabe and Abe (1975a,b) have argued that having the H_2O ligands coplanar in the (110) plane is inconsistent with the NH_4Cl structure in the ordered phase. Despite the ENDOR evidence they have kept the Pilbrow and Spaeth model (adjacent NH_4^+, adjacent NH_4^+ vacancy, remote NH_4^+ vacancy), instead of the H_2O coordination. They felt it necessary to keep this model to provide a mechanism for the change of the ESR spectrum at the order-disorder temperature. However as discussed in the previous section this is an invalid argument. They then proposed that the low temperature orthorhombic spectrum was due to the Cu(II) ion being in the centre of a rhombus of Cl^- ions. At higher temperatures, the tetragonal spectrum was then said to be due to the vibrations of the Cl^- rhomb on a fast timescale that results in an averaged tetragonal ESR spectrum corresponding to an averaged square geometry.

8.1.3 Sources of Experimental Data.

The experimental data to be used in this chapter is shown in figures 8.3. The sources of this data are indicated by the use of the following symbols:

☐ Pilbrow and Spaeth (1967a,b)
✳ Kuroda and Kawamori (1971)
+ Hagen and Trappeniers (1973)
△ Boettcher and Spaeth (1974a,b)
◇ Valk and Trappeniers (1977)
○ Hitchman (1986)
● Steffen and Reinen (1986)

Several comments can be made about this data:

1) Only the data for temperatures below 230K is included.

2) In all centres the principal z axis of the g-tensor was found to be parallel to the [100] and equivalent directions in the crystal. The x and y axes in centre (I) were found to be parallel to [110] or [1$\bar{1}$0] and equivalent directions in the crystal.

3) The data provided by Hitchman (1986), Steffen and Reinen (1986) have not previously been reported, and reflects the special interest of the present study in the orthorhombic → tetragonal transition of the spectrum of centre (I).

4) While "pure" centres (I) and (II) are possible from the growth conditions, centre (III) has never been observed in isolation. Both the studies of Pilbrow and Spaeth (1967a) and Hagan and Trappeniers (1970) observed all three centres in crystals grown from neutral solutions, while Steffen and Reinen (1986) observed centre (III) in conjunction with centre (I). Such behaviour is entirely consistent with centre (III) arising from $Cu(H_2O)(NH_3)Cl_4^{2-}$ entities, as if both H_2O and NH_3 were available for axial ligation then a statistical mixture of centres would result.

5) The tetragonal spectrum of centre (I) disappears below 10-20K (Bechtle et al 1971; Boettcher and Spaeth 1974; Hitchman 1986), although Steffen and Reinen (1986) observed a small tetragonal signal even at 4.2K. However these signals are not included here as they are probably caused by a small number of centres with neighbouring copper sites due to a high concentration of dopant.

(8.7)
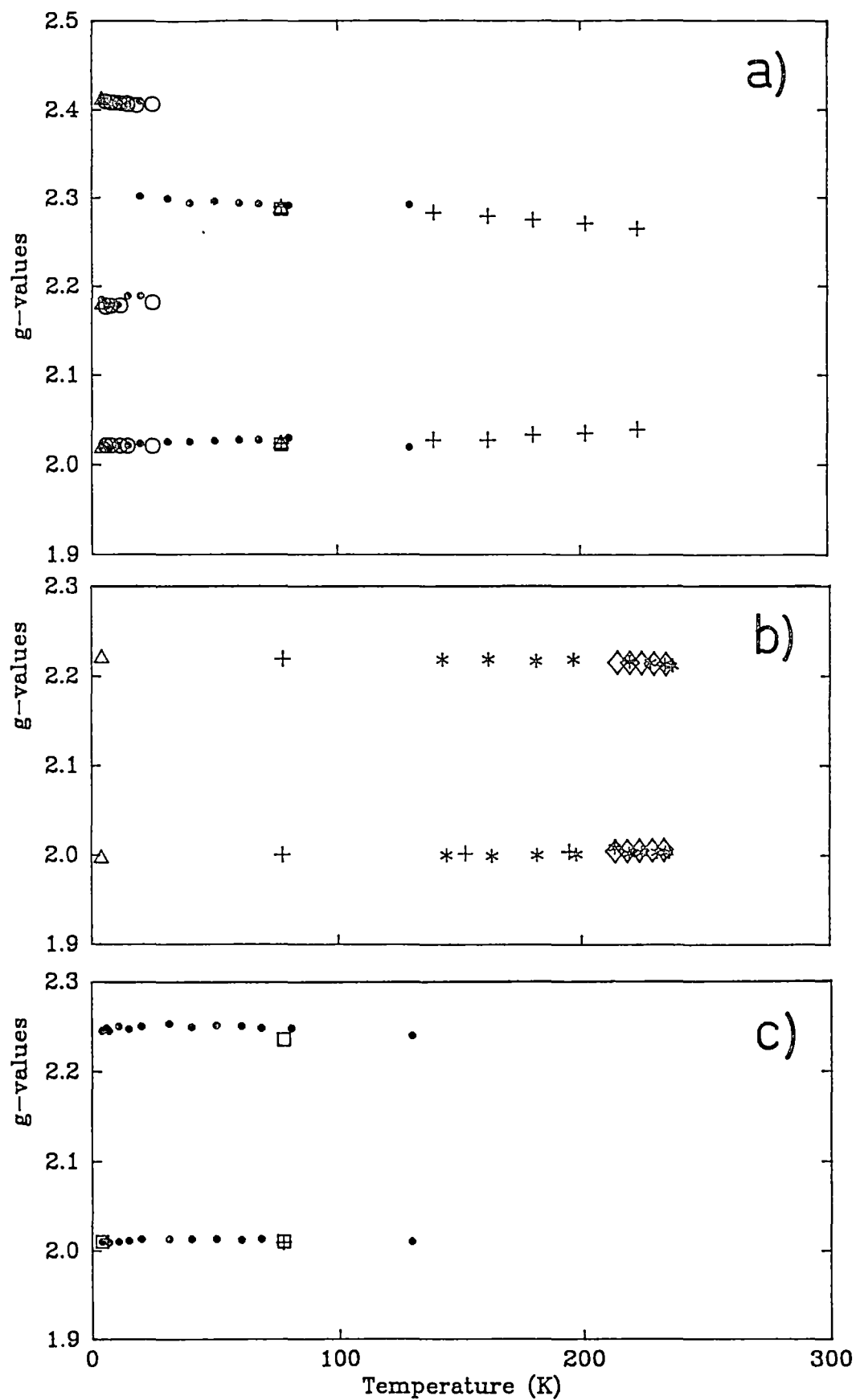
Figure 8.3 Principal g-values of Cu(II)/NH$_4$Cl Centres.
a) Centre (I);   b) Centre (II);   c) Centre (III).

8.2 METHODS

In the present study, a vibronic coupling model is used to explain the temperature dependent effects in $Cu(II)/NH_4Cl$, which can be loosely described as due to a pseudo-Jahn-Teller effect. This model then assumes that the temperature dependent effects are a result of the local dynamics of the isolated $CuX_2Cl_4^{2-}$ species, and so is only appropriate up to the phase transition which is an external effect.

The experimental temperature dependent ESR spectra have many similarities with the $Cu(II)/K_2ZnF_4$ and $Cu(II)/$ zinc Tutton salts systems described in chapters 6 and 7. The methods used in this chapter are also similar, although a special emphasis in this chapter is made on the different levels of interpretation that are possible.

The basic coordination of the copper as $trans-Cu(H_2O)_2Cl_4^{2-}$ for centre (I) and $trans-Cu(NH_3)_2Cl_4^{2-}$ for centre (II) is assumed from the ENDOR studies of Boettcher and Spaeth (1974a,b). From simple bonding arguments the stronger σ perturbation of the axial ligands compared to the equatorial Cl^- ligands, would be expected to produce a compressed octahedral geometry about the Cu(II) ion. This can equivalently be thought of as a tetragonal uniaxial strain superimposed onto the normal Mexican hat potential surface. It has been shown by Reinen and Krause (1981) that for certain values of the warping parameter and the tetragonal compression, the lower potential surface can have two equivalent minima at orthorhombic geometries.

It is proposed that in centre (I) such a situation exists, and at low temperatures "random strain" will freeze the molecule into one of these minima, giving rise to the observed orthorhombic spectrum. The geometry at this minimum corresponds to short bonds to the two water molecules and two chloride ions, and longer ones to the other two chloride ions. As the temperature is raised the minimum that is slightly higher in energy will be populated. The geometry at this minimum is the same as that of the lower, except that the bondlengths of the two equivalent chloride ions are interchanged. Rapid vibronic relaxation between these levels that is sufficiently fast will result in the "tetragonal" spectrum that is observed at higher temperatures. In practice there is a transition region between 4.2-20K where the orthorhombic spectrum disappears, with accompanying broadening, to be

replaced by the "motionally narrowed" tetragonal spectrum. The spectrum will then have discontinuous g-values as a function of temperature. This temperature region is interesting because, whereas a Boltzmann averaged spectrum can give information about the energy levels of the system, the temperature dependent relaxation rates can given information about the barrier heights between different minima and therefore providing a more rigorous test for any molecular model.

For centre (II), the same arguments as above can be used, the only difference being that the NH_3 ligands represent a stronger axial compression. This then results in a single minimum on the potential surface which gives an ESR spectrum corresponding to a tetragonal compression over the entire temperature range. The deviation of $g_\parallel$ from that expected for a pure $d(z^2)$ ground state, as well as the small temperature dependence is then due to vibronic effects within the one well, analogous to the $Cu(II)/K_2ZnF_4$ case studied in chapter 6.

For centre (III), although the coordination is not known, the following facts strongly suggest that it will be $Cu(H_2O)(NH_3)Cl_4^{2-}$:

a) It appears in crystals grown from neutral solutions.

b) It always coexists with either of the other centres.

c) It has an average g-value intermediate between that of the other two centres. This implies that it has an intermediate covalency and/or energy of the excited triplet states.

d) It has a $g_\parallel$ intermediate between the other two centres. This implies the vibronic coupling due to the zero point vibration in a single well is larger than in centre (II).

e) It has a temperature dependence intermediate between the other two centres.

It will be shown that good agreement with the experimental g-values can be obtained for centre (III), when the potential and coupling parameters are transferred from the other centres, and strain terms appropriate for axial $(H_2O)(NH_3)$ ligands are used.

The interpretation of the ESR data for the centres will be given in the following levels of approximation in order of increasing "reality":

i) The Silver and Getz (1974) model is used, which is essentially a "static" model. The energy levels and magnetic properties are left as free parameters, and although a good fit can be obtained with

experiment, it will be shown that these energies and magnetic properties do not necessarily correspond to the real physical situation. This static approach can be misleading when used for these systems.

The following two models include the effects of the vibrations and are therefore true dynamic models:

ii) A one-dimensional vibronic coupling model is used, where the $d(z^2)$ and $d(x^2-y^2)$ electronic states are coupled by a vibration of orthorhombic symmetry. This is then the $(A+B) \times b$ vibronic problem, that has been previously used by Sorokin and Chirkin (1979) on the $Cu(II)/NH_4Br$ system.

iii) The full two dimensional $E \times e$ vibronic problem is solved, assuming that the system can be adequately be described as having a potential surface of six equivalent ligands, and the effects of the inequivalence of the equatorial and axial ligands is incorporated into the model in the form of strain parameters.

In principle the full two dimensional $(A+B) \times (a+b)$ vibronic Hamiltonian should be solved. This then has many more force constants and coupling constants that the low symmetry of the system really requires. However, as discussed in section 4.2.3, this leads to a very underdetermined problem, where a set of parameters cannot be found to give a unique fit to the experimental data.

From the above it can be seen that as well as the study of the $Cu(II)/NH_4Cl$ system, this chapter is also concerned with the different "levels of interpretation" that can be applied to such a system. In particular, it will be shown that after a certain stage, the essential chemistry of a molecular system can be understood, and that more "rigorous" extensions to a model will not change one's understanding or picture of the problem in any way. One must then ask if a more "complete" model is in any sense more correct, if when what one is neglecting in a simple model does not have any effect on the interpretation.

(8.10)

8.3 PARAMETERS

The interface between theory and experiment is often a case of developing a theoretical model with a number of parameters which represent physical properties of the system, and then "fitting" the model to reproduce experiment. In the following sections the magnitudes of the relevant parameters are estimated independently of the vibronic model by using the electronic spectrum, normal coordinate analysis and the AOM. Exact values of these parameters are not desired, but rather an idea of the range of chemically acceptable values that can be expected.

8.3.1 The Electronic Spectrum.

The electronic spectrum is useful in estimating the strength of the linear Jahn-Teller coupling constant as well as the energies of the excited triplet states that are necessary for the calculation of the g-values. Since electronic transitions occur on a time scale that is fast compared to the rate of relaxation between vibrational levels of the electronic ground state, they will reflect the underlying static structure of the molecule. The electronic spectrum of samples containing centre (I) were measured over the temperature range 60-300K using a Cary 17 spectrometer with a Cryodyne 22 closed cycle refrigerator. It was found that the transition energies are essentially temperature independent, although the spectrum both broadens and increases in intensity with temperature. Kuroda and Kawamori (1971) found similar behaviour in a study of centre (II).

The <u>low</u> temperature g-values can give the d-orbital mixture of the ground electronic state, which will reflect the geometry of the complex. For centres (II) and (III), the electronic ground state is approximately a pure $d(z^2)$ hole and the expected ordering of their electronic states is given in figure 8.4. For centre (I) this mixture is found to be (see section 8.3.4):

$$\psi_1 = 0.97 \ d(z^2) - 0.24 \ d(x^2-y^2) \qquad (8.1)$$

At first this might also appear to correspond to a compressed geometry of a mainly $d(z^2)$ ground state. In actual fact it is almost exactly orthorhombic, midway between compressed and elongated

geometries. This can be shown by expressing (8.1) in terms of the equivalent d orbital basis $d(y^2)$ and $d(x^2-z^2)$. The wavefunction in these two bases are related by:

$$\psi_1 = \sin\frac{\phi}{2} \; d(z^2) + \cos\frac{\phi}{2} \; d(x^2-y^2) \qquad (8.2)$$

$$= \sin\frac{1}{2}(\phi-120) \; d(y^2) + \cos\frac{1}{2}(\phi-120) \; d(x^2-z^2)$$

Here the wavefunction coefficients are described by the angle ϕ of the Jahn-Teller Mexican hat. The change of basis in (8.2) corresponds simply to a shift in the origin by 120°, and when the wavefunction is written in both bases one has:

$$\psi_1 = 0.97 \; d(z^2) - 0.24 \; d(x^2-y^2) \qquad (8.3)$$

$$= 0.28 \; d(y^2) + 0.96 \; d(x^2-z^2)$$

___ $^2B_{2g}$ (xy)	___ $^2B_{1g}$ (xy)	___ ^2E_g (xy,yz)
	___ $^2B_{3g}$ (yz)	
___ ^2E_g (xz,yz)	___ $^2B_{2g}$ (xz)	___ $^2B_{2g}$ (xz)
___ $^2B_{1g}$ (x^2-y^2)	___ ^2A_g (Ψ_2)	___ $^2A_{1g}$ (y^2)
___ $^2A_{1g}$ (z^2)	___ ^2A_g (Ψ_1)	___ $^2B_{1g}$ (x^2-z^2)
D_{4h} (Compressed) $\phi = 180^\circ$	D_{2h} (Orthorhombic) $\phi = 150^\circ$	D_{4h} (Elongated) $\phi = 120^\circ$
Centres (II),(III)	Centre (I)	

FIGURE 8.4 The d-d Electronic Spectrum of Cu(II)/NH$_4$Cl.

Even though (8.1) is mainly $d(z^2)$, it can be seen from (8.3) that it actually corresponds to a wavefunction of orthorhombic geometry. This is in agreement with the observed near equal separation of the low temperature g-values ($g_x-g_y \sim g_y-g_z$). It is therefore misleading to assign the spectrum of centre (I) as transitions from a $d(z^2)$ ground state as given by Billing etal (1970) in table 8.2 below. However, the three components of the equally split triplet state that might be

(8.12)

expected for the ordering as given in the centre of figure 8.4 were not observed in the spectrum, but rather a single broad band at 12,500 cm^{-1} with a shoulder at 11,400 cm^{-1}. Each component of the triplet state is vibronically allowed by available inducing vibrations and so should be equally likely to be observed.

The reason why all three split components are not observed is because the description given by figure 8.4 is based on the linear Jahn-Teller effect, which is too simplistic for these low symmetry systems. The vibration that corresponds to the tetragonal component of the e_g vibration is quite different to that of an octahedral complex. As shown in the following section, it corresponds to a movement of the axial ligands ~6 times that of the equatorial ligands. When this is considered, the wavefunction in (8.1) would correspond more to a compressed geometry, with the excited state ordering given on the LHS of figure 8.4. These are the assignments given in table 8.2.

TABLE 8.2 Electronic Spectra of Cu(II)/NH$_4$Cl.

Bands/cm^{-1}	Temp./K	Assignment	Reference
Centre(I) 9300(sh) 11000(sh) 12300	300K	$d(z^2) \rightarrow$? $\rightarrow$? $\rightarrow$ d(xz),d(yz)	Billing etal (1971).
9300(sh) 11400(sh) 12500	60K	$\psi_1 \rightarrow \psi_2$ $\rightarrow$ d(xz),d(yz) $\rightarrow$ d(xy)	Present Work.
Centre(II) 9600(sh) 14200	300K	$d(z^2) \rightarrow$? $\rightarrow$ d(xz),d(yz)	Billing etal (1970).
9500(sh) 13700 40000(calc)	100K	$d(z^2) \rightarrow d(x^2-y^2)$ $\rightarrow$ d(xz),d(yz) $\rightarrow$ d(xy)	Kuroda and Kawamori (1971).
[Cu(II)/NH$_4$Br] 9600 13380 28900(vs)	300K	$d(z^2) \rightarrow d(x^2-y^2)$ $\rightarrow$ d(xz),d(yz) $\rightarrow$ d(xy)	Trappeniers etal (1978).

The spectrum of centre (II) only shows a single peak in the region where the triplet states are expected. The studies referenced in table 8.2 assume that this is the $d(z^2) \rightarrow d(xz),d(yz)$ transition and

(8.13)

argue that the $d(z^2) \rightarrow d(xy)$ transition is not observed. Kuroda and Kawamori (1971) have calculated this transition to occur at 40,000 cm^{-1}, which seems far too high for a d-d transition.

In the present study, the $d(z^2) \rightarrow d(xy)$ transition is assumed to be unresolved from the $d(z^2) \rightarrow d(xz), d(yz)$ transition at 14,000 cm^{-1}. This is not surprising as the bands are very broad and a splitting of only 1,000 cm^{-1} was observed in centre (I). In centre (II) the tetragonal compression is associated mainly with the movements of the axial NH_3 ligands, and as these do not form pi bonds, they would have little effect on the anisotropy of the triplet states.

The electronic transitions will not be averaged over the vibronic levels as an ESR spectrum is when it undergoes rapid exchange. Each vibronic level will have its own electronic spectrum. The two lowest orthorhombic levels of centre (I) will have virtually the same electronic spectrum except for the interchange of the x and y molecular axes. The spectra for these two levels will be identical except for the assignments, the electronic spectrum will then be virtually temperature independent, except for the usual red-shift due to the vibronically active vibrations.

8.3.2 The Vibrational Potential.

In this section the hypothetical vibrations of the $CuX_2Cl_4^{2-}$ complex in the complete absence of vibronic interactions are derived approximately. To do this the valence force constants of several non-Jahn-Teller complexes are used. Table 8.3 shows the experimental frequencies and symmetrised force constants of the stretching vibrations of a number of such complexes. Three vibrations are required to determine the three valence stretch force constants simultaneously.

The experimental frequencies were obtained from the references indicated by the bracketed numbers following their values. The symmetrised force constants have been calculated using the appropriate elements of the G matrix given by Cyvin (1968; pp 125, 131), where the approximation is made that the $t_{1u}(s)$ and $e_u(s)$ stretching vibrations do not mix with the bending vibrations of the same symmetry. The relationships given by Cyvin (1968, pp126,131) are then used to find the valence stretch force constants given in table 8.4. Here f_{rr} and

TABLE 8.3 Vibrational Frequencies and Force Constants.[a]

Octahedral Complex	$\nu(a_{1g})$	$F(a_{1g})$	$\nu(e_g)$	$F(e_g)$	$\nu(t_{1u})$	$F(t_{1u})$
$Zn(H_2O)_6^{2+}$	380(1)	1.531	278(1)	0.819	364(2)	1.113
$Ni(H_2O)_6^{2+}$	405(1)	1.739	305(1)	0.986	333(3)	0.922
$Zn(NH_3)_6^{2+}$	340(4)	1.157	235(4)	0.553	300(5)	0.718
$Ni(NH_3)_6^{2+}$	370(5)	1.371	265(5)	0.703	335(5)	0.883
Square Planar	$\nu(a_{1g})$	$F(a_{1g})$	$\nu(b_{1g})$	$F(b_{1g})$	$\nu(e_u s)$	$F(e_u s)$
$CuCl_4^{2-}$	275(6)	1.579	195(6)	0.794	290(6)	1.15

a) Frequencies in cm^{-1}, force constants in mdyne/Å.

(1) Jenkins and Lewis (1981) (4) Schmidt and Muller (1976)
(2) Nakagawa and Shimanouchi (1964) (5) Schmidt and Muller (1975)
(3) Adams and Trumble (1974) (6) McDonald and Hitchman (1986)

TABLE 8.4 Valence Stretch Force Constants.

Complex	f_r (mdyne/Å)	f_{rr} (mdyne/Å)	f'_{rr} (mdyne/Å)
$Zn(H_2O)_6^{2+}$	1.08	0.12	-0.03
$Ni(H_2O)_6^{2+}$	1.08	0.13	0.16
$Zn(NH_3)_6^{2+}$	0.93	0.10	0.04
$Ni(NH_3)_6^{2+}$	0.90	0.11	0.02
$CuCl_4^{2-}$	1.11	0.20	0.04

f'_{rr} refer to the stretch-stretch interactions of cis and trans bonds respectively.

The valence force constants are all reasonably consistent for the three types of ligands and two types of coordination. This then gives some justification to the drastic assumption that the stretch valence force constants of the mixed ligand complex, $CuX_2Cl_4^{2-}$, can be approximated by a single set of values. These valence force constants will be taken as $f_r = 1.0$ mdyne/$\overset{o}{A}$, $f_{rr} = 0.11$ mdyne/$\overset{o}{A}$ and $f'_{rr} = 0.03$ mdyne/$\overset{o}{A}$, the average of the values in table 8.4. In a normal coordinate analysis then, the off-diagonal elements of the F matrix are zero and vibrations of the same symmetry will be mixed only by the off-diagonal terms in the G matrix.

The three vibrations of interest are those which are the a_{1g} and e_g vibrations in the parent octahedral group. The basis functions for the symmetry coordinates are shown below in figure 8.5. The non-zero elements of the G and F matrices are given by:

$$G_{11} = \frac{1}{3} \left(\frac{2}{m(Cl)} + \frac{1}{m(X)} \right) \qquad F_{11} = f_r + 4f_{rr} + f'_{rr} \qquad (8.4)$$

$$G_{22} = \frac{1}{3} \left(\frac{1}{m(Cl)} + \frac{2}{m(X)} \right) \qquad F_{22} = f_r - 2f_{rr} + f'_{rr}$$

$$G_{33} = \frac{1}{m(Cl)} \qquad\qquad\qquad F_{33} = f_r - 2f_{rr} + f'_{rr}$$

$$G_{12} = \frac{\sqrt{2}}{3} \left(\frac{1}{m(X)} - \frac{1}{m(Cl)} \right)$$
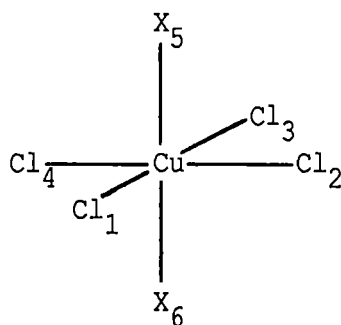
$$a_{1g}: \quad S'_1 = \frac{1}{\sqrt{6}} \left(r_1 + r_2 + r_3 + r_4 + r_5 + r_6 \right)$$

$$a_{1g}: \quad S'_2 = \frac{1}{\sqrt{12}} \left(2r_5 + 2r_6 - r_1 - r_2 - r_3 - r_4 \right)$$

$$b_{1g}: \quad S'_3 = \frac{1}{2} \left(r_1 - r_2 + r_3 - r_4 \right)$$

FIGURE 8.5   The D$_{4h}$ Coordinate System.

(8.15)

Substituting values into (8.4), the resulting vibrational frequencies and eigenvectors (arbitrarily normalised to unity) are:

$$\nu_1 = 326 \text{ cm}^{-1}; \quad S_1 = c_{11}S_1' + c_{12}S_2'; \quad c_{11}=0.8, \ c_{12}=0.6 \qquad (8.5)$$
$$\nu_2 = 225 \text{ cm}^{-1}; \quad S_2 = c_{21}S_1' + c_{22}S_2'; \quad c_{21}=0.384, \ c_{22}=0.923$$
$$\nu_3 = 197 \text{ cm}^{-1}; \quad S_3 = S_3'$$

Similar results are found for $X = NH_3$ since the force constants are the same and the mass difference of NH_3 and H_2O is small, and in view of the approximations made, the ν_2 and ν_3 vibrations can be considered the same. By substituting the symmetry coordinates into (8.5) it can be found that for the symmetry coordinate S_2, the axial ligands move about six times the distance of the chloride ions, instead of twice the distance for S_2' as would be the case for ligands of equal mass.

The vibrations for several other hypothetical octahedral copper complexes can also be found in a similar manner:

	$\nu(a_{1g})/\text{cm}^{-1}$	$\nu(e_g)/\text{cm}^{-1}$
$Cu(H_2O)_6^{2+}$	372	276
$CuCl_6^{4-}$	265	197
CuF_6^{4-}	362	269

The frequencies calculated in this section, with all the approximations made, are estimated to be "correct" only to within about 25%. However, they provide a rough estimate of the values of the potential constants to be used in the vibronic Hamiltonian.

8.3.3 The Coupling Constants.

In this section the various vibronic coupling constants are derived assuming a certain radial dependence of the AOM parameters. The reader is again asked to bear with the many approximations used here; this section is to gain some form of chemical insight into the effects of the non-equivalent ligands on the problem, rather than to obtain exact quantities. The coordinates obtained in equation (8.5) can be used to derive the linear coupling constants of the problem by the methods of Bacci (1979). These are:

$$\begin{array}{c} \quad\quad |A_{1g}\rangle \quad\quad\quad\quad |B_{1g}\rangle \\ \begin{array}{c} \langle A_{1g}| \\ \langle B_{1g}| \end{array} \left[\begin{array}{cc} C_1 S_1 + C_2 S_2 & C_3 S_3 \\ C_3 S_3 & C_4 S_1 + C_5 S_2 \end{array} \right] \end{array} \quad\quad (8.6)$$

$$C_1 = \frac{1}{\sqrt{12}} (\sqrt{2} c_{11} - c_{12}) \frac{\partial e_\sigma(Cl)}{\partial r} + \frac{2}{\sqrt{6}} (c_{11} + \sqrt{2} c_{12}) \frac{\partial e_\sigma(H_2O)}{\partial r}$$

$$C_2 = \frac{1}{\sqrt{12}} (\sqrt{2} c_{21} - c_{22}) \frac{\partial e_\sigma(Cl)}{\partial r} + \frac{2}{\sqrt{6}} (c_{12} + \sqrt{2} c_{22}) \frac{\partial e_\sigma(H_2O)}{\partial r}$$

$$C_3 = -\frac{\sqrt{3}}{2} \frac{\partial e_\sigma(Cl)}{\partial r}$$

$$C_4 = \frac{\sqrt{3}}{2} (\sqrt{2} c_{11} - c_{12}) \frac{\partial e_\sigma(Cl)}{\partial r}$$

$$C_5 = \frac{\sqrt{3}}{2} (\sqrt{2} c_{21} - c_{22}) \frac{\partial e_\sigma(Cl)}{\partial r}$$

In the cubic case where $e_\sigma = e_\sigma(Cl) = e_\sigma(H_2O)$; $c_{11} = c_{22} = 1$; $c_{12} = c_{21} = 0$; then the above coupling constants reduce to those given by Bacci (1979):

$$C_2 = -C_3 = -C_5 = \frac{\sqrt{3}}{2} \frac{\partial e_\sigma}{\partial r}; \quad C_1 = C_4 = \frac{3}{\sqrt{2}} \frac{\partial e_\sigma}{\partial r}.$$

Here C_2, C_3 and C_5 correspond to the linear Jahn-Teller coupling constants; and C_1, C_4 to the linear terms in the potential of the totally symmetric mode.

To evaluate the coupling constants in (8.6), the way in which the AOM parameters change with the bondlength must first be specified. For the hypothetical $CuX_2Cl_4^{2-}$ unit before vibronic interactions, the bondlengths will approximately be $r(Cu-Cl) = 252pm$, $r(Cu-OH_2) = 210pm$ and $r(Cu-NH_3) = 225$ pm. [These values are estimated from the average of the six bondlengths in the structures of $CuCl_2$ (Wells 1949), several copper Tutton salts (Bill 1984, pg791) and $Cu(NH_3)_6Cl_2$ (Distler and Vaughan 1967).] At these bondlengths, the AOM parameters have been estimated to be $e_\sigma(Cl) = 3250cm^{-1}$, $e_\sigma(H_2O) = 4000cm^{-1}$ and $e_\sigma(NH_3) = 4500cm^{-1}$ (Hitchman 1986). If the additional approximation is made that the AOM parameters are proportional to the inverse fifth power of the bondlength (Hitchman 1982), then one finds:

$$\frac{\partial e_\sigma(Cl)}{\partial r} = -65 cm^{-1} pm^{-1}; \quad\quad\quad\quad (8.7)$$

$$\frac{\partial e_\sigma(H_2O)}{\partial r} = -95 cm^{-1} pm^{-1}; \quad \frac{\partial e_\sigma(NH_3)}{\partial r} = -100 cm^{-1} pm^{-1}.$$

Substituting these values into (8.6) with the coefficients given in (8.5), the coupling constants are then given by:

$$
\begin{array}{cc}
|A_{1g}> & |B_{1g}> \\
\end{array}
\left[
\begin{array}{cc}
-860\ Q_1 - 370\ Q_2 & 390\ Q_3 \\
390\ Q_3 & -190\ Q_1 + 680\ Q_2
\end{array}
\right]
\qquad
\begin{array}{cc}
|A_{1g}> & |B_{1g}> \\
\end{array}
\left[
\begin{array}{cc}
-900\ Q_1 - 400\ Q_2 & 390\ Q_3 \\
390\ Q_3 & -190\ Q_1 + 690\ Q_2
\end{array}
\right]
$$

The coupling constants on the left and right above are for centres (I) and (II) respectively. Here the coupling parameters are given in units of cm^{-1}, appropriate for the dimensionless coordinates given by Q.

It can be seen that in this D_{4h} problem the coordinates Q_1 and Q_2, both which transform as a_{1g}, do not couple the $d(z^2)$ $|A_{1g}>$ and $d(x^2-y^2)$ $|B_{1g}>$ electronic basis functions. However, anharmonic coupling between the vibrations will formally cause them all to be coupled (Pelikan etal 1985). From the eigenvectors in (8.5) the Q_1 and Q_2 coordinates are mainly associated with the S'_1 and S'_2 basis functions or the a_{1g} and $e_g(\theta)$ coordinates of the parent octahedral complex. The approximation is now made that the effect of S_1 on the potential will be relatively small and is neglected. Following Bill (1984, pg759), a change in the origin will then give for the linear coupling matrix:

$$
H_{JT} = \left[
\begin{array}{cc}
-A_{1a}Q_a & A_{1b}Q_b \\
A_{1b}Q_b & A_{1a}Q_a
\end{array}
\right]
\tag{8.8}
$$

where $A_{1a} = 525cm^{-1}$, $A_{1b} = 390cm^{-1}$ for centre (I) and $A_{1a} = 540cm^{-1}$, $A_{1b} = 390cm^{-1}$ for centre (II). The strain Hamiltonian can be found by evaluating the energies of the $d(z^2)$ and $d(x^2-y^2)$ orbitals at the hypothetical geometry before the vibronic interaction. In terms of the AOM, this is given by $2[e_\sigma(X)-e_\sigma(Cl)]$ which results in the following tetragonal strain terms for the centres (I), (II), and (III):

$$
H_{ST}^{I} = \left[
\begin{array}{cc}
-750 & 0 \\
0 & 750
\end{array}
\right]
\qquad
H_{ST}^{II} = \left[
\begin{array}{cc}
-1250 & 0 \\
0 & 1250
\end{array}
\right]
\qquad
H_{ST}^{III} = \left[
\begin{array}{cc}
-1000 & 0 \\
0 & 1000
\end{array}
\right]
\tag{8.9}
$$

The harmonic vibrational part of the Hamiltonian is given by the vibrational frequencies of the previous section:

$$
H_o = \tfrac{1}{2}h\nu_a(\ P_a^2 + Q_a^2\ ) + \tfrac{1}{2}h\nu_b(\ P_b^2 + Q_b^2\ )
\left[
\begin{array}{cc}
1 & 0 \\
0 & 1
\end{array}
\right]
\tag{8.10}
$$

Here Q_a and Q_b represent the dimensionless form of the symmetry coordinates S_2 and S_3 respectively, while P^2 and $h\nu$ represent the respective kinetic energy term and vibrational frequency of these coordinates.

The form of the lower adiabatic potential without the strain terms ($H_o + H_{JT}$) for centre (I) is shown in figure 8.6a. The effect that the different frequencies and coupling constants have on the Mexican hat potential surface can be seen quite clearly. This is the surface typically found in the Ex(b+b) vibronic problem (see Herzberg 1966, fig.14). Figure 8.6b shows the adiabatic potential of the total Hamiltonian ($H = H_o + H_{JT} + H_{ST}$) of the low symmetry (A+B)x(a+b) problem, using the strain terms of centre (I). The lowest levels in this potential surface will be very sensitive to the warping terms in the potential. These will be considered at a later stage as it is not feasible to estimate such terms independently from experiment.

The similarity of the coupling constants of the axial ligands in (8.7) can justify the use of a single set of coupling parameters for all three of the systems. Already in the previous section, it was shown that a single set of vibrational parameters is likely to be a good approximation. The most important terms in the vibronic Hamiltonian that distinguish between the different centres are then the strain terms given in (8.9). In the numerical calculations to follow, it is hoped that the same vibronic Hamiltonian, except for differing strain terms, will be able to effectively account for all three centres.

The accuracy of the actual values derived is doubtful. The electronic transitions can be calculated from the derived parameters:

$$\psi_1 \rightarrow \psi_2 \quad : \quad 4E_{JT} + 2 \, |S_\theta| \qquad\qquad (8.11)$$
$$\rightarrow \psi(T) \quad : \quad 2e_\sigma(Cl) + e_\sigma(X) + E_{JT} + |S_\theta|$$

Using the effective values $h\nu = 200 \text{ cm}^{-1}$ and $E_{JT} = 500 \text{ cm}^{-1}$, this gives:

	Centre (I)/cm^{-1}	Centre (II)/cm^{-1}
$\psi_1 \rightarrow \psi_2$	3,500	4,500
$\rightarrow \psi(T)$	11,250	12,250

(8.19)
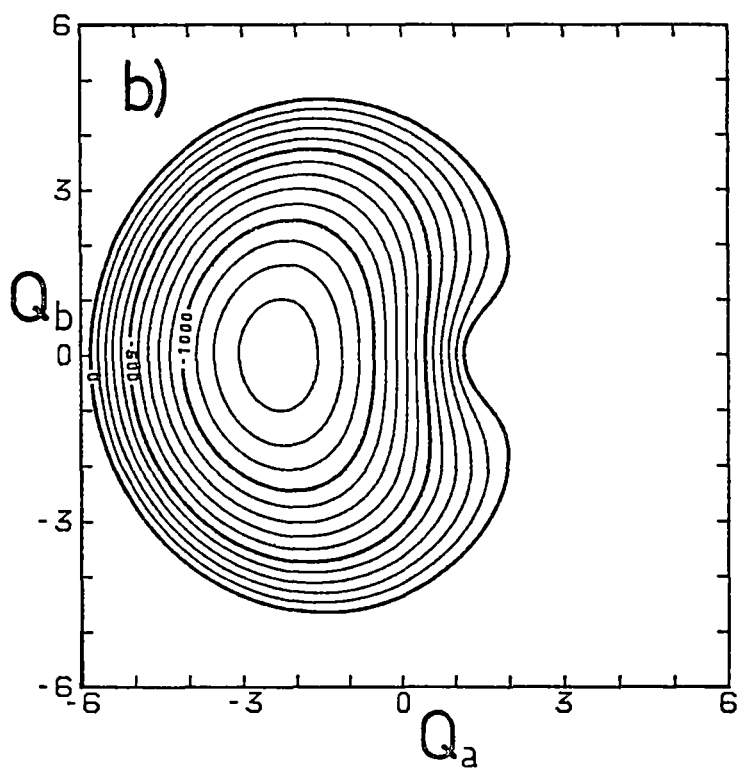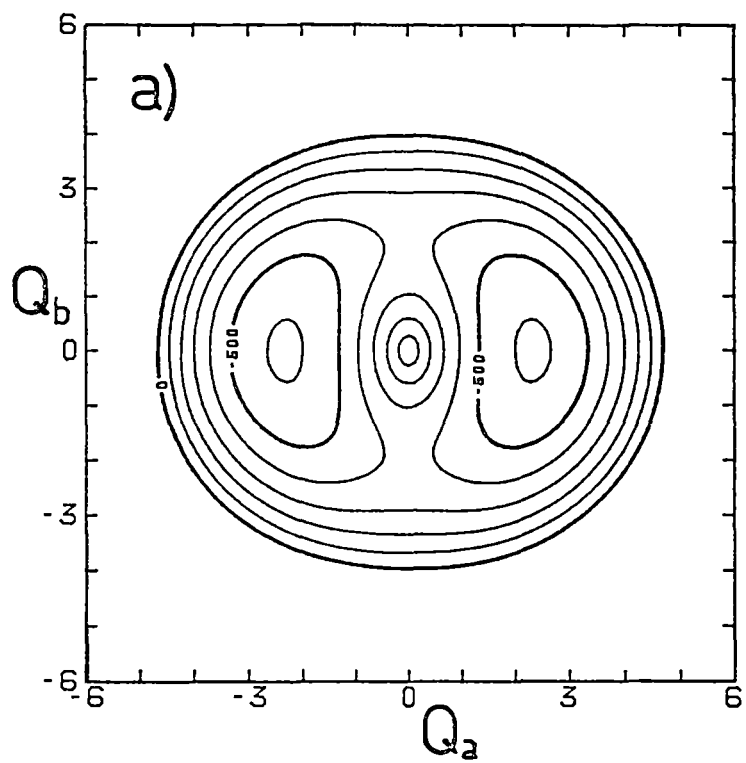
Figure 8.6   The Lower Adiabatic Potential Surface.

a)   E⊗(a⊕b) Jahn-Teller Surface.

b)   (A⊕B)⊗(a⊕b) psuedo Jahn-Teller Surface.

Although the energy of the triplet state is reasonable reproduced, it would appear that the AOM model underestimates the Jahn-Teller coupling constants in these systems.

8.3.4 Magnetic Properties.

The low temperature g-values and <g> (the average g-value) are shown in table 8.5 below for the three centres. The average g-value is less for centre (II) than for centre (I) as expected because of the larger energy separation of the triplet state. If the experimental energies are taken (and an intermediate value assumed for centre (III)), then the orbital reduction factor can be calculated from:

$$\langle g \rangle = g_o + 4u - 5u^2; \qquad u = \frac{k^2 \lambda}{E(T)} \qquad (8.12)$$

TABLE 8.5 Low Temperature g-values.

	Centre (I)	Centre (II)	Centre (III)
g_x	2.411	2.220	2.247
g_y	2.179		
g_z	2.018	1.996	2.010
$\langle g \rangle$	2.202	2.145	2.168
$E(T)/cm^{-1}$	12,200	14,000	13,100
u	0.0529	0.0374	0.0438
k (8.12)	0.88	0.80	0.83
k (exact)	0.90	0.81	0.84

The average g-value can also be calculated from applying the Zeeman operator to the wavefunctions found from a ligand field diagonalisation using the methods given in section 5.1. The isotropic k values calculated in this manner to reproduce the observed average g-values are also given in table 8.5, showing that the perturbation formula underestimates these values. These reduction factors are exactly as expected since NH_3 forms more covalent complexes than H_2O.

The low temperature orthorhombic g-values of centre (I) are principally determined by the static mixture of the electronic part of its lowest vibronic state, as this wavefunction is localised around a single minimum. This static electronic mixture is given by equation

(8.20)

(8.2) and the g-values can be calculated from this wavefunction using the second order perturbation expressions of (5.15) using an isotropic k value:

$$g_x = <g> - [2u - u^2] (\cos\phi + \sqrt{3}\sin\phi)$$ (8.13)
$$g_y = <g> - [2u - u^2] (\cos\phi - \sqrt{3}\sin\phi)$$
$$g_z = <g> + [4u - 2u^2] \cos\phi$$

When the low temperature g-values from table 8.5 are substituted into the above expressions, the value of ϕ that best reproduces the g-values is 152°. This value does not exactly reproduce the orthorhombic g-values but is the best value found by a least squares fit when an isotropic u is used. The approximate static electronic wavefunction is then:

$$\phi = 0.9703 \, d(z^2) - 0.2419 \, d(x^2-y^2)$$ (8.14)

8.4 RESULTS

8.4.1 The Silver and Getz Model.

The Silver and Getz model (Silver and Getz 1974) will be briefly described here for centres (I) and (II) to show some of the shortcomings of this model when applied to the present system. The model is described by the set of equations given by (7.1). If assumptions are made about the geometry of the levels then the g-values of each level can be simply related to each other. Schematically these geometries are shown below where the dotted, dashed and solid lines refer to short, medium and long bonds respectively.
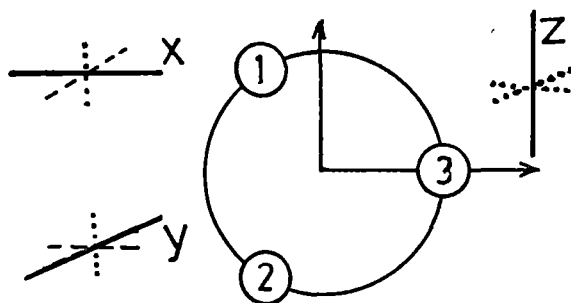
The g-values of the two lowest levels can be related by an interchange of the x and z axes.

$$g_{x1} = g_{y2} = g_x; \qquad g_{y1} = g_{x2} = g_y; \qquad g_{z1} = g_{z2} = g_z.$$

The third level will approximately have the following g-values:

$$g_{x3} = g_{y3} = g_z; \qquad g_{z3} = \tfrac{1}{2}(g_x + g_y)$$

A least squares fit of the five independent parameters is shown in figure 8.7a where the experimental points between 4.2 and 77K have been omitted. The fitted parameters are:

$$g_x = 2.448 \qquad E_1 = 0$$
$$g_y = 2.128 \qquad E_2 = 5.3 \ cm^{-1}$$
$$g_z = 2.015 \qquad E_3 = 294 \ cm^{-1}$$

One conclusion of the Silver and Getz model would be that the orthorhombic g-values change dramatically between 0-30K, and that the lowest temperature g-values would be different to that observed at 4.2K. This conflicts with what is observed because the S&G model assumes a Boltzmann average of the levels from the motional averaging

(8.22)
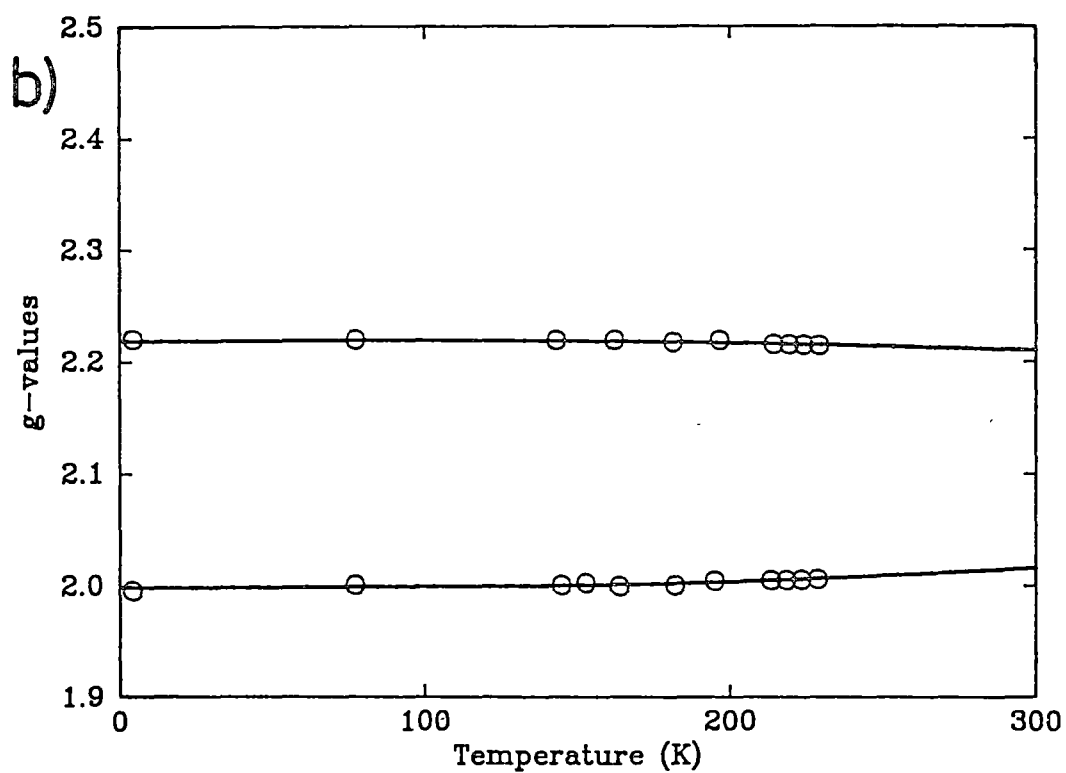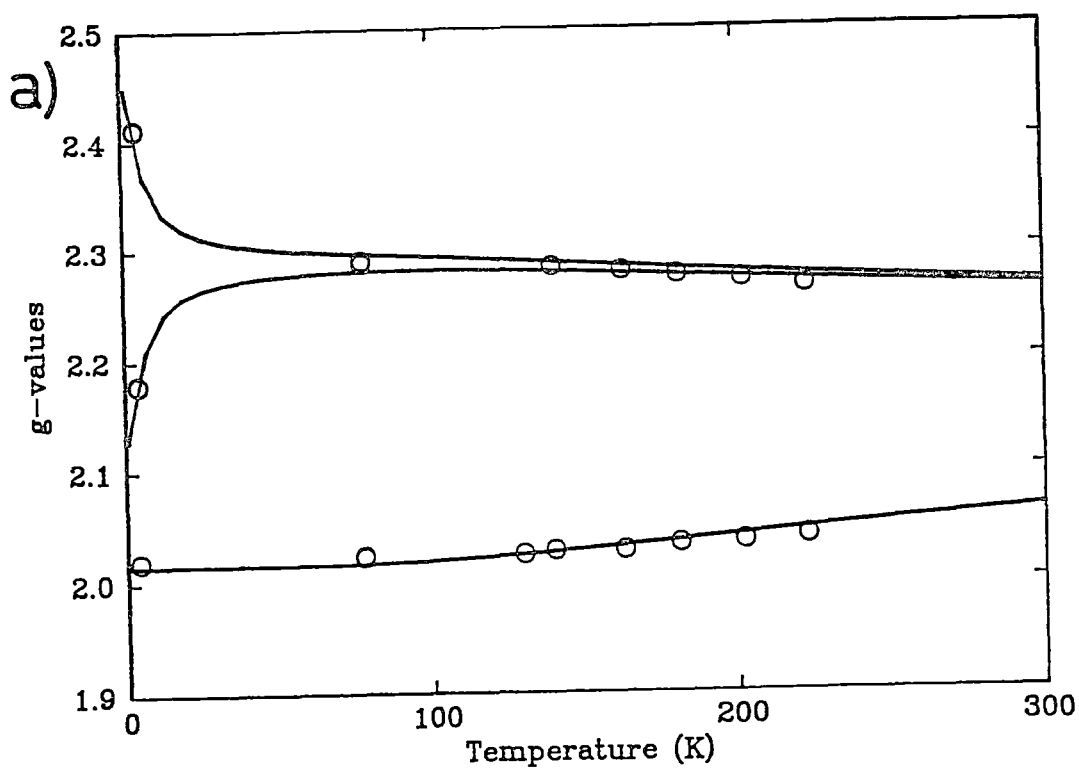
Figure 8.7 The Silver and Getz Model.
a) Centre (I); b) Centre (II).

of the spectrum. This motional narrowing, which results from fast vibronic relaxation, is considered in the following section.

The model would also imply that the higher temperature dependence of the tetragonal spectrum results from the population of a level with a geometry elongated along z. The Jahn-Teller model, which is to be discussed in section 8.4.3, implies that the population of higher levels within and over the two minima of the levels 1 and 2 will also contribute to this temperature dependence.

In centre (II) the g-values are tetragonal at all temperatures, and the Silver and Getz model requires only two levels:

$$g_\parallel(T) = N_1 g_{\parallel 1} + N_2 g_{\perp 1}$$

$$g_\perp(T) = N_1 g_{\perp 1} + N_2 g_{\parallel 1} \qquad (8.15)$$
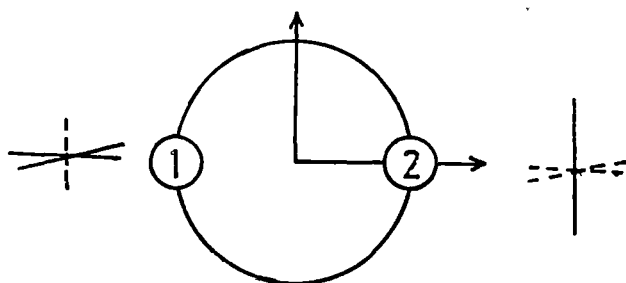
Here the g-values can be related by: $g_{\parallel 2} = 2<g>-g_{\parallel 1}$, $g_{\perp 2} = 2<g>-g_{\perp 1}$, and the least squares fit to the experimental data is shown in figure 8.7b with the three independent fitted parameters being:

$$g_{\parallel 1} = 1.998; \quad g_{\perp 1} = 2.218; \quad E_1 = 0; \quad E_2 = 575 \ cm^{-1}.$$

This centre shows only a small temperature dependence but, again, it is not due to the population of a higher level with an elongated geometry as implied by the S&G model. Rather, the observed temperature dependence will be due to the population of higher vibronic levels within the one well. However, as this well is steep, the electronic properties of these levels will only be slightly different from that of the ground state, making the g-values only slightly temperature dependent.

8.4.2 Motional Averaging of the Orthorhombic Spectrum of Centre (I)

The transition from an orthorhombic to tetragonal g-tensor in Centre (I) is shown in figure 8.3. In the transition region, the orthorhombic spectrum gradually broadens and disappears while the

(8.23)

tetragonal spectrum increases in intensity. This can be easily under-
stood in terms of vibronic relaxation between the two lowest levels.
At low temperatures this rate of relaxation, or exchange, between the
vibronic levels will be slow on the ESR time scale, resulting in the
superposition of the ESR spectrum.from the individual levels. At
higher temperatures this rate increases so that exchange between the
levels is fast on the ESR timescale and an averaged signal is ob-
served.

The implication of the present study is that the g-values at
temperatures lower than 4.2K would be the same as those at 4.2K and
represent the static geometry of the lowest level. This is not
predicted by the simple Boltzmann population of fast exchanging levels
in the Silver and Getz model. Bill (1984, p771) has pointed out the
necessity of measurements at lower temperatures to investigate this,
but the measurements between 4-20K given in figure 8.3a are sufficient
to verify the point.

The orthorhombic to tetragonal coalescence occurs at ~20K and
this can approximately be related to the rate constant for the lowest
levels (Sandstrom 1982):

$$K_{12} = \frac{\pi}{\sqrt{2}} \, \Delta\nu = \nu_o \exp(-\Delta E/kT) \qquad (8.16)$$

where $\Delta\nu$ is the frequency difference between the two exchanging
spectral lines in s^{-1}. Using the above Arrhenius law for the rate
constant, there are a family of curves that satisfy (8.16) at $T=20K$
for different values of ν_o and ΔE. The variation of the g-values with
temperature are shown in figure 8.8b,d for two such rate constants.

However, the observed motional narrowing is difficult to properly
quantify for a number of reasons. Firstly, the orthorhombic →
tetragonal transition temperature seems to be sample dependent to some
extent. Steffen and Reinen (1986) observed weak signals of the
tetragonal spectrum even down to 4.2K, while Watanabe and Abe (1975b)
first observed this spectrum to appear at ~50K. As well as this,
Steffen and Reinen (1986) observed the orthorhombic spectrum to disap-
pear at ~30K, while Watanabe and Abe continued to observe weak signals
up to ~150K.

In both these studies the two types of spectra were observed to
coexist over a temperature range (4-30K and 50-150K respectively)
although only the spectrum of one signal dominated at any particular
temperature. As shown in figures 8.8b,d, the motional narrowing

(8.24)

mechanism does not allow such a coexistence of the two types of spectra. The observed coexistence would imply that the "energy barrier" to the relaxation rate in equation (8.16) is spread over a range of energies, either distributed amoung the centres or within the one centre. The first possibility could be caused by random strain, while the second may be due to the relaxation pathway being a continuum rather than a discrete level. To illustrate that this type of mechanism can account for the observed behaviour, the "activation energy" is spread ± 20 cm^{-1} from the mean values in the plot of figure 8.8b,d, and the results are shown in figure 8.8c,e. The effect of a finite spread in the random strain would actually be more complicated than this as it would cause a spread in the energies and wavefunctions of the vibronic levels as well as the energy of the relaxation pathways.

These complications are ignored, and although it is difficult to be quantitative in the present study, a relaxation rate of the order shown in figures 8.8b-e must be present. Figure 8.8a show the behaviour for very fast relaxation that essentially results in a Boltzmann average over the levels. On the other extreme, no relaxation would result in the g-values of the individual levels appearing as they are thermally populated. The spectrum in figure 8.8b, which has the relaxation rate $K = 1.9 \times 10^{10} exp(-50/kT)$ s^{-1}, roughly gives the correct behaviour. As observed, the orthorhombic g-values move slightly closer together before they coalesce. If the activation energy is much higher, then an unreasonably large spread must be used to explain the observed coexistence of the two types of spectra.

Any attempt to further quantify the relaxation rate in this system would require a careful temperature dependent study of the intensities and halfwidths. However, both of these features may have other contributions, such as spin-lattice relaxation or instrumental factors, to their temperature dependence in addition to just the motional narrowing.

The effect of the slow relaxation at low temperatures is to "delay" the coalescence of the orthorhombic spectrum. This sort of behaviour is usually observed when there are two or more close lying levels which have different magnetic properties, and are separated by a barrier. These conditions are fulfilled in the $Cu(II)/ZnSiF_6.6H_2O$ system, where the tetragonal $\rightarrow$ isotopic transition occurs at ~20K

(8.25)
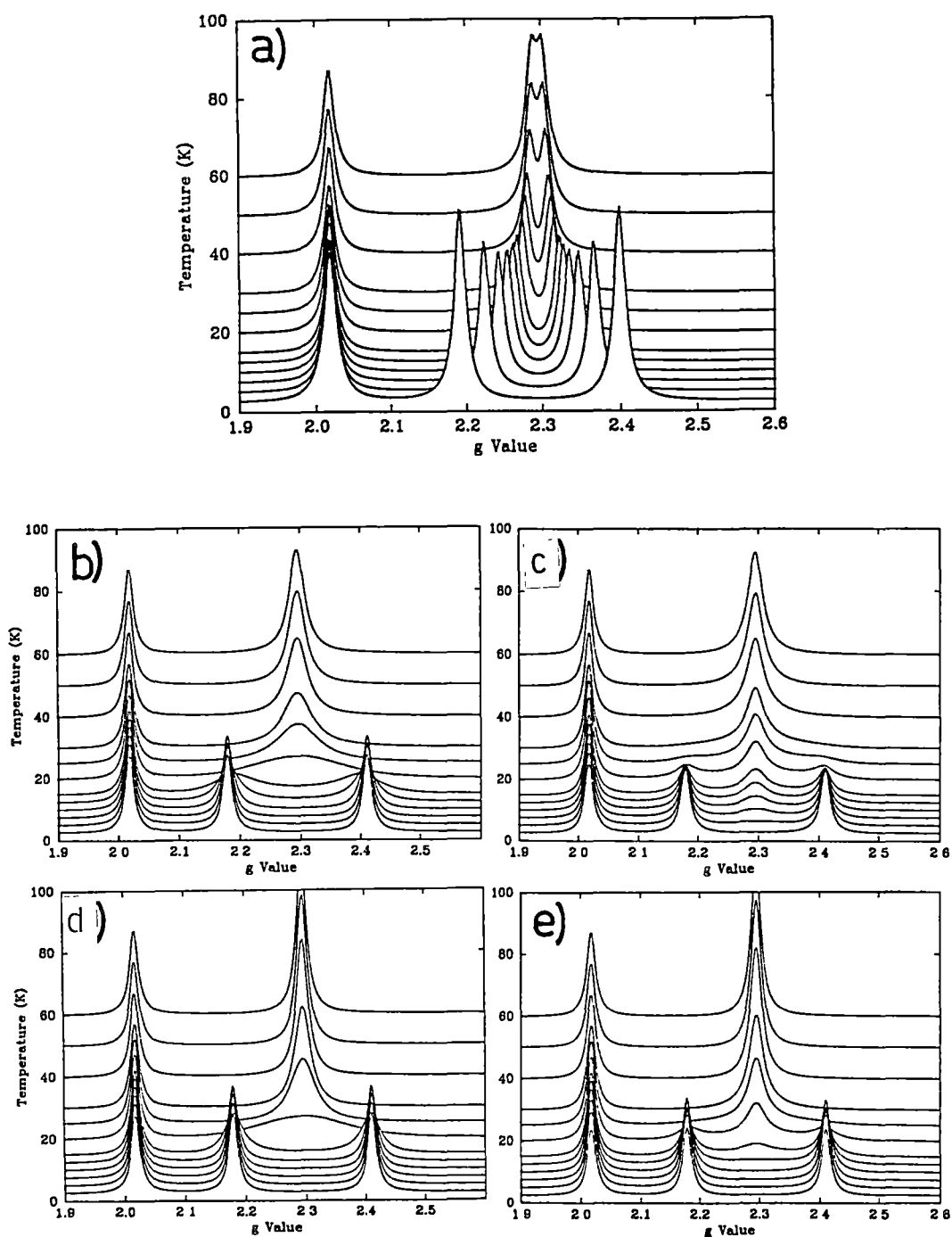
Figure 8.8 Vibronic relaxation in centre (I).

a) $K = 10^{14}s^{-1}$ corresponding to a Boltzmann average of the levels.

b) $K = 1.7 \times 10^{10} \exp(-50/kT)$ s^{-1}

c) As above, except the activation energy is spread 50 ± 20 cm^{-1}.

d) $K = 6.8 \times 10^{11} \exp(-100/kT)$ s^{-1}

e) as above, except the activation energy is spread 100 ± 20 cm^{-1}.

(Dang etal 1974). In the copper doped Tutton salts of the previous chapter, the levels are sufficiently separated so that the relaxation rate is fast at the temperature where the spectrum of individual levels would be expected to be observed. A motionally average ESR spectrum is observed except for the effect on the hyperfine linewidths which are more sensitive to the motional narrowing.

In fitting the experimental g-values of centre (I), a Boltzmann average of the g-values of the individual levels will be used. However, the spectrum will be calculated such that the orthorhombic spectrum observed at 4.2K will be reproduced at zero Kelvin, and the averaged tetragonal spectrum reproduced at ~40K. Although the experimental values in the intermediate temperature region where the orthorhombic → tetragonal transition occurs will not be reproduced, the application a less than infinite relaxation rate (equation 8.16) would correctly give this.

The activation energy of ~50 cm^{-1} is not easily related to the barrier height between the two lowest levels. As discussed in section 5.5, it is usually associated with an excited vibronic level that is to some extent delocalised over both wells, thus providing a relaxation pathway. A very approximate value of ~100 cm^{-1} can be estimated for the barrier height in this study.

8.4.3 The Sorokin and Chirkin Model.

A one dimensional vibronic coupling model was applied to the Cu(II)/NH$_4$Br system by Sorokin and Chirkin (1979). This model ignores anharmonic coupling between different vibrations, and so the two electronic states $^2A_{1g}(z^2)$ and $^2B_{1g}(x^2-y^2)$ are coupled by vibrations of b$_{1g}$ symmetry. For the CuX$_2$Cl$_4^{2-}$ species, there is only one vibration of b$_{1g}$ symmetry and this has the same symmetry coordinates as the orthorhombic component of the e$_g$ vibration of the parent octahedral complex. [Similar arguments hold in the C$_{4v}$ point group of centre (III): the $^2A_1(z^2)$ and $^2B_1(x^2-y^2)$ electronic states are coupled by a single vibration of b$_1$ symmetry.]

This one dimensional pseudo Jahn-Teller model is appealing as it requires only three parameters to be specified and allows their determination uniquely from experiment. Neglecting the kinetic energy operator for the moment, the vibronic equations are:

(8.26)

$$\begin{bmatrix} & |{}^2A_{1g}\!> & |{}^2B_{1g}\!> \\ S + \frac{1}{2} hv \ Q^2 - E & A_1Q \\ A_1Q & -S + \frac{1}{2} hv \ Q^2 - E \end{bmatrix} = 0 \qquad (8.17)$$

The dimensionless coordinate Q and vibrational energy hv refer to the normal mode of b_{1g} symmetry, and the separation of the pseudo degenerate electronic states $|{}^2A_{1g}\!>$ and $|{}^2B_{1g}\!>$, is equal to $2S$.

The lower adiabatic potential surface, found by diagonalising (8.17), is:

$$\varepsilon^- = \frac{1}{2} hv \ Q^2 - [A_1^2Q^2 + S^2]^{1/2} \qquad (8.18)$$

The electronic part of the adiabatic wavefunction that can be associated with this surface is:

$$\psi^- = \sin(\tfrac{z}{2}) \ |A_{1g}\!> + \cos(\tfrac{z}{2}) \ |B_{1g}\!>; \quad z = \tan^{-1}[(A_1Q)/S] \qquad (8.19)$$

The potential surface in (8.18) will have two symmetric minima for $S < A_1^2/hv$. In this case the minima, Q_0; barrier height between the minima ΔB; and the energy separation of the electronic states at the minima, ΔE, are given respectively by:

$$Q_0 = \pm [\ (A_1/hv)^2 - (S/A_1)^2 \ ]^{1/2} \qquad (8.20)$$

$$\Delta B = -|S| + \tfrac{1}{2}hv \ [\ (S/A_1)^2 + (A_1/hv)^2 \ ] \qquad (8.21)$$

$$\Delta E = 2 \ [\ A_1^2Q_0^2 + S^2 \ ]^{1/2} \qquad (8.22)$$

These quantities are shown in figure 8.9a.

When $S > A_1^2/hv$, a single minima at $Q_0 = 0$ results, and the separation of the electronic states is then equal to $2S$. This tetragonal splitting of the electronic states has a different meaning to the tetragonal strain given in section 8.3.3. In that section the tetragonal strain referred to the hypothetical $CuX_2Cl_4^{2-}$ unit <u>before</u> vibronic interactions. Here the quantity $2S$ represents the splitting of the $|A_{1g}\!>$ and $|B_{1g}\!>$ electronic states at the equilibrium tetragonal geometry ($Q_0=0$ in figure 8.9).
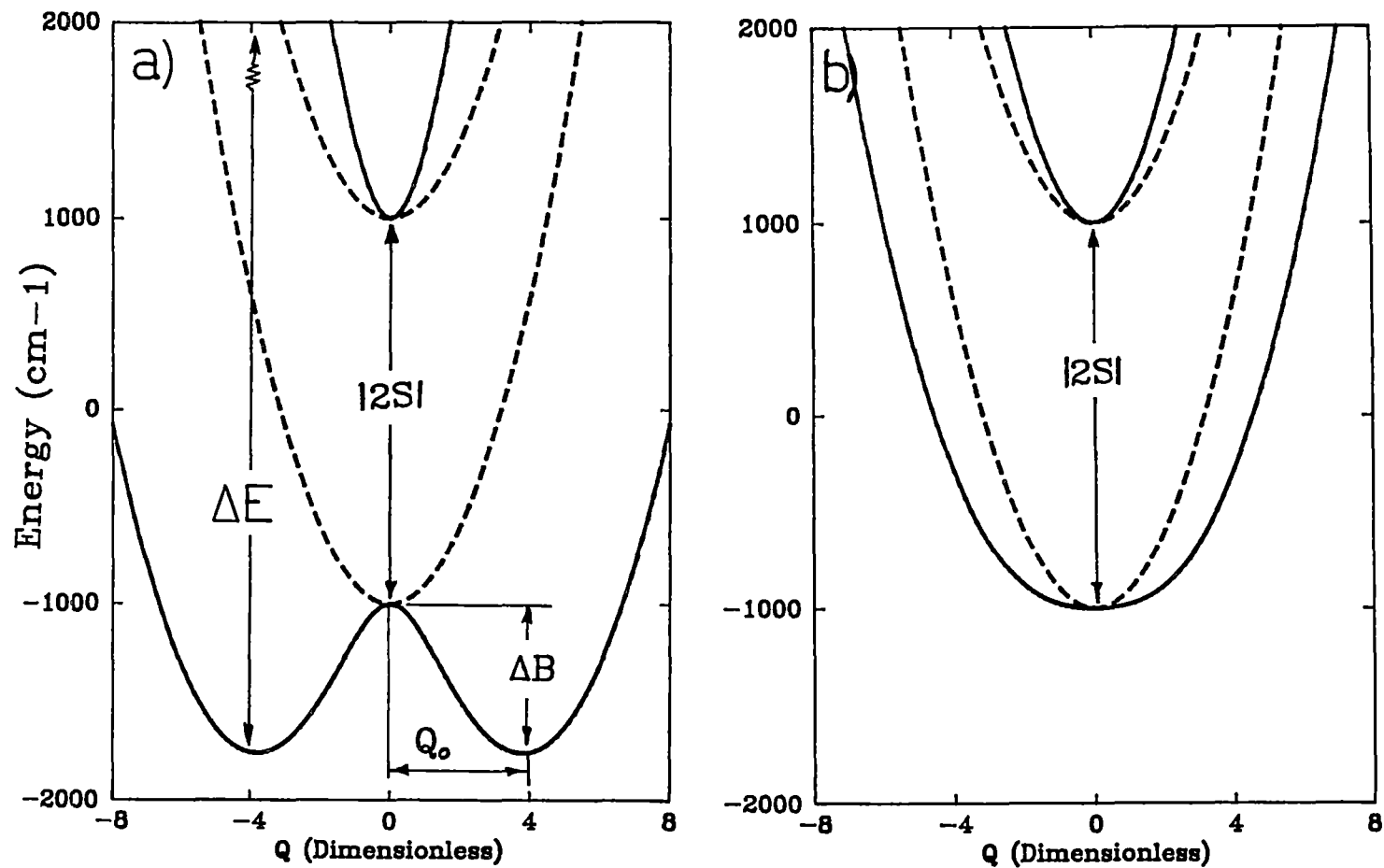
Figure 8.9 Pseudo Jahn-Teller Potentials.

a) Parameters: $h\nu = 200$ cm^{-1}; S = -1000 cm^{-1}; $A_1 = 800$ cm^{-1}.

b) Parameters: $h\nu = 200$ cm^{-1}; S = -1000 cm^{-1}; $A_1 = 400$ cm^{-1}.

The fitting of centre (I) is as follows. The orthorhombic low temperature g-values imply that this centre has a double minima potential where random strain will localise the lowest vibronic wavefunction into one of the wells. The transition to the upper surface, ΔE, can be related to two of the parameters from (8.22):

$$\Delta E = 9,300 \text{cm}^{-1} = 2A_1^2/h\nu \qquad (8.23)$$

The requirement that z ~152° in the wavefunction to fit the low temperature g-values can be used to further relate the three parameters. Using (8.19) and some algebra, one obtains:

$$\sec (z) = A_1^2/(S.h\nu) \qquad (8.24)$$

For the particular values of $h\nu$ and A_1 that satisfy equation (8.23), the parameter S can take only a single value from equation (8.24). This also uniquely defines the barrier height in (8.21). Example results for a range of $h\nu$ are given in table 8.6.

TABLE 8.6   Centre (I) Sorokin and Chirkin Model.

$h\nu/\text{cm}^{-1}$	A_1/cm^{-1}	S/cm^{-1}	$\Delta B/\text{cm}^{-1}$
50	482	−4106	31.9
100	682	"	"
150	835	"	"
200	964	"	"
250	1078	"	"

Although S and ΔB are uniquely defined, many different pairs of $(h\nu, A_1)$ satisfy the experimental data. The frequency, $h\nu$, is not the same as that of the hypothetical complex before vibronic interactions as discussed in section 8.3.2. Rather it is the frequency at the relaxed tetragonal geometry, or that due to the potential along the Q_b coordinate at the minimum of the two dimensional potential in figure 8.6b.

Although this frequency is likely to be lower than the ~200 cm^{-1}

(8.28)

given for the hypothetical vibrational frequency, it would be difficult to quantify. Rather than test pairs of $(h\nu, A_1)$ against the temperature of the g-values, the other centres are first considered.

The application of the Sorokin and Chirkin model to centres (II) and (III) can be made in a manner similar to that used in treating $Cu(II)/K_2ZnF_4$ in chapter 6. Here, the low temperature g-values and their small temperature dependence is due to the dynamic mixture of $d(x^2-y^2)$ into the predominantly $d(z^2)$ ground state in the lowest and higher vibronic levels respectively. By calculating the g-values that would be expected for pure $d(z^2)$ and $d(x^2-y^2)$ electronic states, the fractional electronic mixture of the lowest vibronic level can be obtained. For centre (III), the low temperature g-values imply ~4.5% $d(x^2-y^2)$ in the ground vibronic state.

The value of S is fixed at ~ -4750 cm^{-1} to reproduce the transition to the upper Jahn-Teller surface, and figure 8.10a shows the fraction of $d(x^2-y^2)$ character in the ground vibronic state as a function of A_1 and $h\nu$. As in centre (I), pairs of $(h\nu, A_1)$ give the correct mixture of $d(x^2-y^2)$ character for centre (III). The values of A_1, for each $h\nu$ obtained for centre (I) in table 8.6 are also shown as the large circles. Remarkable agreement is seen for the two centres: for a particular value of $h\nu$, the same value of A_1 is predicted for centres (I) and (III).

The obvious step now would be to try to fit the temperature dependence of the g-values and thereby find a unique pair of $(h\nu, A_1)$ that reproduces all the experimental data. For centre (I), neither the low temperature or temperature dependent g-values are reproduced, even though the potential was chosen, in table 8.6, to give minima that correspond to the correct static mixture of the electronic composition.

This is because the barrier height between the minima is so low that the lowest vibronic wavefunctions are delocalised over both wells even when quite a large linear term is added to the potential to mimic the random strain by making these wells inequivalent. The fact that the vibronic states cannot be localised at the minima means that the low temperature g-values cannot be reproduced. Figure 8.10b shows the barrier height and splitting of the lowest vibronic states as a function of the wavefunction parameter z. To obtain a small splitting at z ~150° implies that the value of $h\nu < 80$ cm^{-1}.
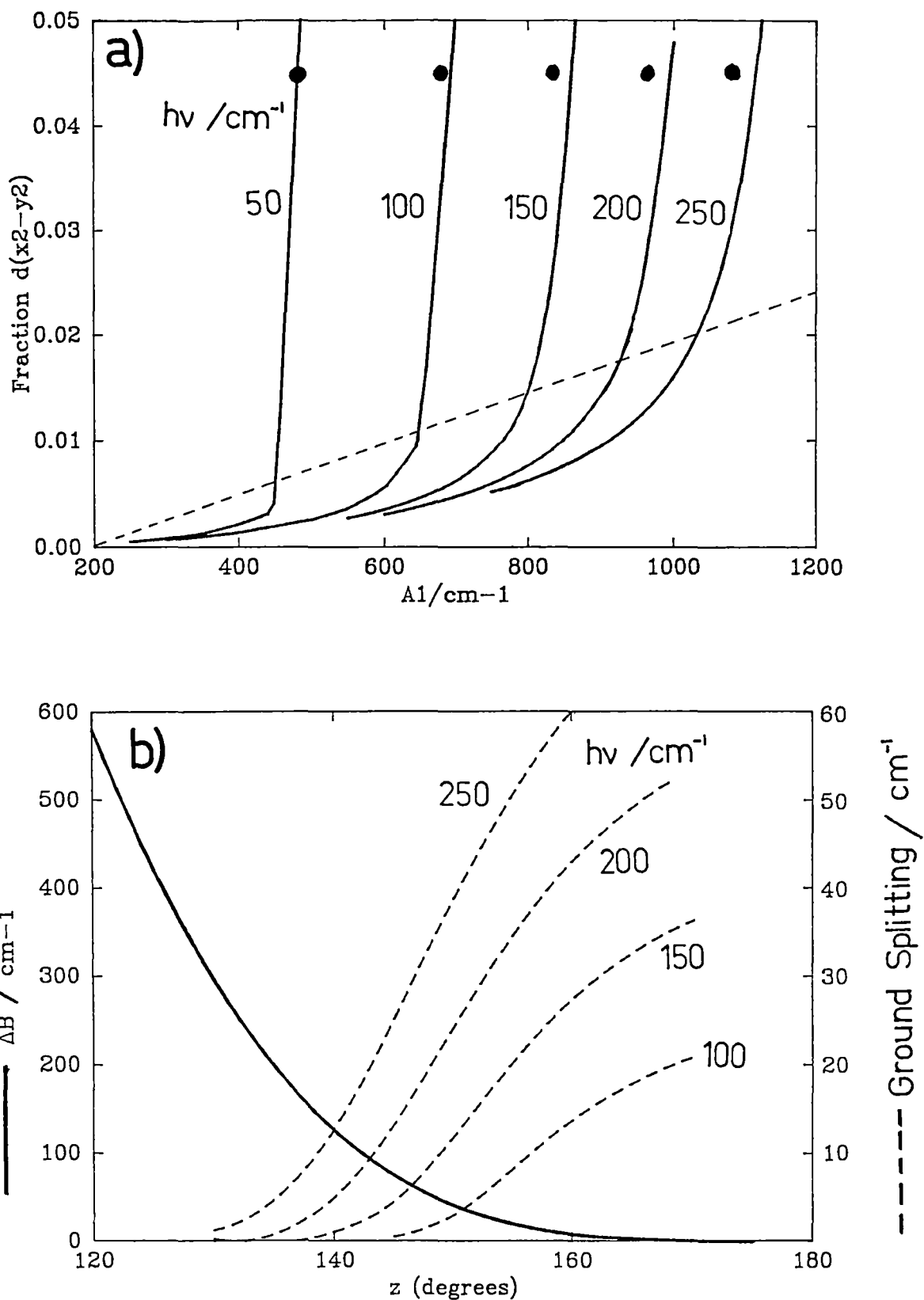
Figure 8.10 **Fraction of d(x^2-y^2) in the Ground Vibronic State.**

a) For different values of hv in centre (III), (S is fixed at 4250 cm^{-1}).

— — — Approximately above this line, the potential becomes a double minima.

● Values of (hv,A_1) pairs that satisfy centre (I).

b) The barrier height and splitting of the lowest levels as a function of z.

The g-values of centre (III) can be fitted using $S = -4750cm^{-1}$ and the appropriate data from figure 8.10a which gives $\%d(x^2-y^2)=4.5$. However, the potentials from which these g-values are calculated are double minima potentials. This form of potential, although giving the correct calculated g-values, would unlikely to occur in practice as the "random strain" would tend to make these wells slightly inequivalent resulting in orthorhombic g-values at low temperature, like those seen in centre (I). The dotted line in figure 8.10a shows the values of the parameters where double minima occur. This implies that to have the correct mixture of $d(x^2-y^2)$ in the ground state, while keeping the potential with a single minimum, hv must be substantially larger than 250 cm^{-1}.

This is the opposite to what would be required to fit centre (I). Both centres could be fitted if an extra parameter controlling the even order anharmonicity around the equilibrium geometry $Q = 0$. To fit the experiment, this "anharmonicity" would be required to soften the potential for centre (I), and stiffen it for centre (III). This then corresponds to making the wells deeper in centre (I), and making them disappear in centre (III).

However, it is not clear what this "anharmonicity" corresponds to physically, nor why it should be so different for the two centres. In the following section the equivalent of this anharmonicity is determined by both the warping and strain terms of the Mexican hat potential surface. The parameters are then related to the physical properties of the centres in a straightforward manner. Since the one dimensional model of Sorokin and Chirkin would require additional parameters it will not be pursued further here.

8.4.4 The Jahn-Teller model.

In this section the cubic E×e Jahn-Teller vibronic Hamiltonian is applied to the three copper(II) centres in NH_4Cl, where the large strain terms are used to differentiate between the different centres. Since a quantitative fit to the experimental data is desired, a systematic approach to obtaining "best fit" parameters is outlined here in detail.

As previously described in chapter 5, the electronic and geometric properties of each vibronic level, obtained from the
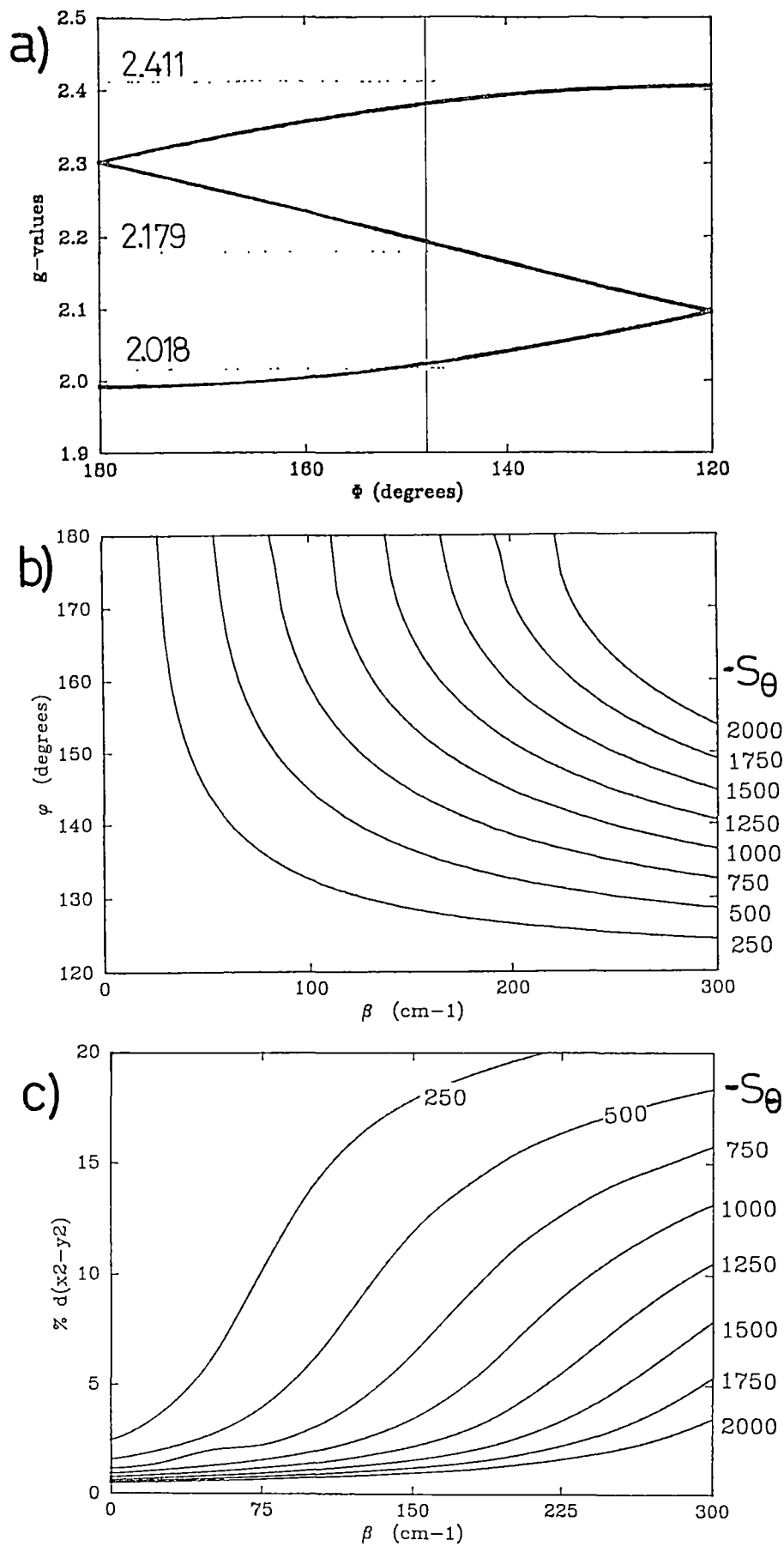
Figure 8.11 Fitting the g-values.

a) The g-values calculated using a static wavefunction in equation (8.2).

b) The position of the orthorhombic minima as a function of β and S_θ.

c) The dynamic mixture of $d(x^2-y^2)$ character in the ground vibronic state due to the zero point motion as function of β and S_θ.

diagonalisation of the vibronic Hamiltonian, is placed in a ligand field matrix. The numerical diagonalisation of these matrices gives the d-orbital mixture caused by spin-orbit coupling, and the application of the Zeeman operator then gives a particular set of g-values for each vibronic level. Covalency is taken into account by the used of orbital reduction parameters and if isotropic values are used, only the electronic properties of the vibronic states are needed. However, it was found that centre (I) requires additional anisotropy and so the expectation values of the geometry of the vibronic levels are also required.

In fitting the g-values, it is convenient to first consider the low temperature g-values as this requires the calculation of only the lowest vibronic level. If many different sets of parameters are found to fit these low temperature values, then the temperature dependence can be used to chose the best set. Similar calculation to those described in chapter 6 show that the $g_\parallel$ values of the tetragonal centres (II) and (III) require the dynamic mixture of ~1.5% and ~4.5% $d(x^2-y^2)$ character in the predominately $d(z^2)$ ground vibronic state from the zero point vibration. A very rough guide to the composition of centre (I) can be obtained from the adiabatic electronic wavefunction given in equation (8.2) at the static geometry around the trough of the Mexican hat potential surface. The calculated g-values as a function of this angle is shown in figure 8.11a. It can be seen that the value of $\phi_o = 152^o$ obtained from the least squares fit in section 8.3.4, does not reproduce the low temperature g-values at all well. Another important aspect of the potential that must be reproduced for centre (I), is a barrier that separates the two lowest vibronic states such that an "inversion splitting" of ~2 cm^{-1} to reproduce the tetragonally averaged spectrum at ~20K. In addition, the barrier height has been very approximately estimated, in section 5.4.2, as ~100 cm^{-1} from the motional averaging of the orthorhombic spectra.

The harmonic vibration of the vibrational basis functions (the hypothetical e_g vibration of the "cubic" $CuX_2Cl_4^{2-}$ species), is taken as $h\nu = 210$ cm^{-1} for all the centres, which is the average of the values obtained from the normal coordinate analysis in section 8.3.2. The linear coupling constant is fixed at $A_1 = 900cm^{-1}$ for all centres, which roughly fits the observed transitions to the upper surface of the Jahn-Teller potential. The warping parameter, β, and the strain

(8.31)
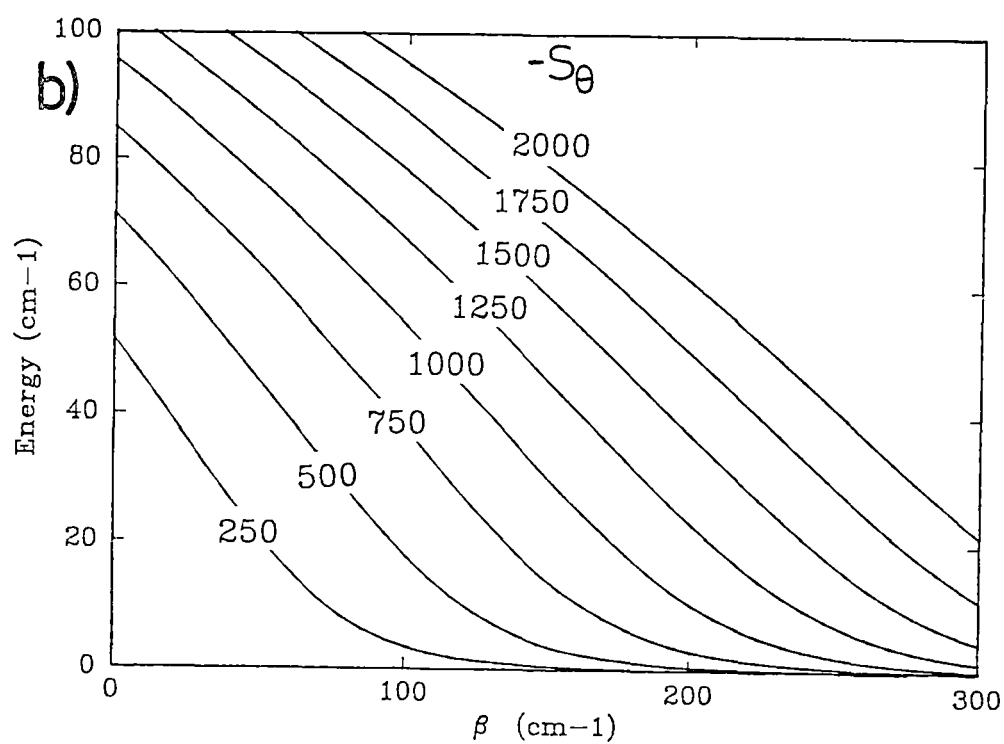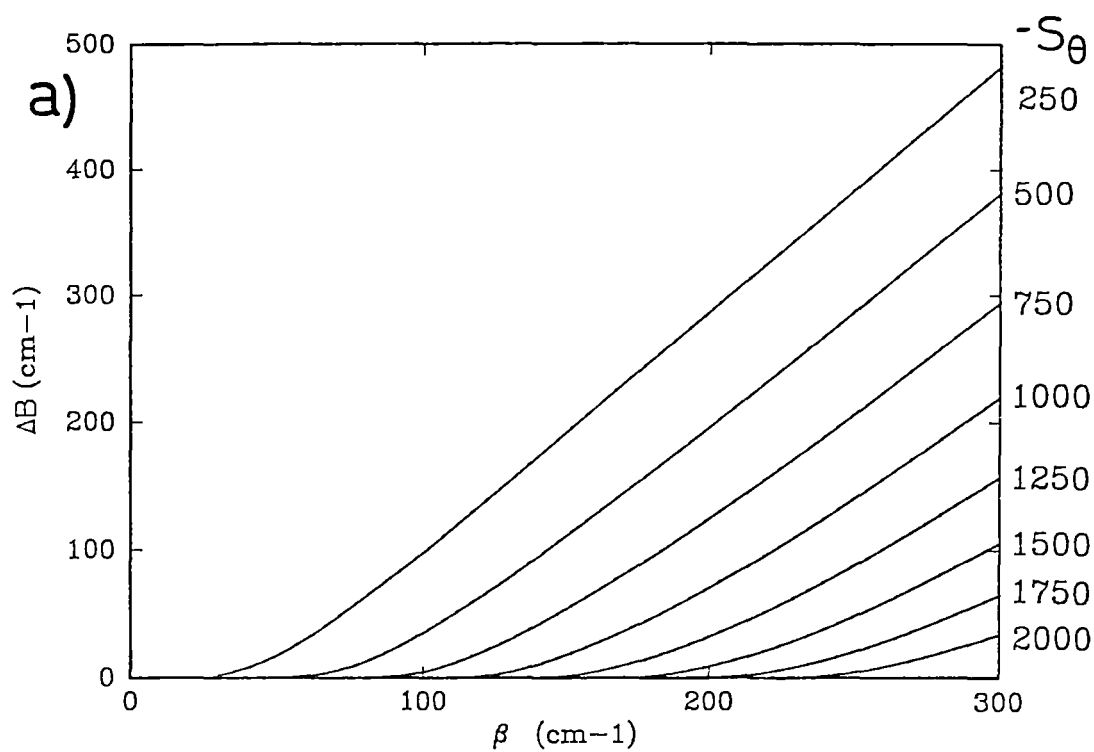
Figure 8.12 a) The barrier height between the orthorhombic minima.
b) The splitting of the two lowest vibronic levels.

terms are allowed to vary. Family of curves are shown in figures 8.11b,c for various values of the tetragonal strain as a function of β. These are plotted against the position of the orthorhombic minima and the % $d(x^2-y^2)$ electronic character in the ground vibronic state respectively. In figure 8.12 similar curves are shown for the barrier height between the minima, ΔB, and the splitting of the two lowest vibronic states.

For a particular value of β, the values of S_θ must be chosen for the centres such that centre (I) has two minima, with a barrier height of ~100 cm^{-1}, and an energy separation of the two lowest levels of ~2 cm^{-1}. The orthorhombic strain that is used to make the wells inequivalent and the localise the wavefunctions in the separate minima, will further slightly split these two levels. For the same value of β, centres (II) and (III) must take values of S_θ such that the potential has a single minima at $\phi=180°$, and have ~1.5% and ~4.5% $d(x^2-y^2)$ electronic character.

Table 8.7 Fitting the Low Temperature Spectra

β/cm^{-1}	A_2/cm^{-1}	$A_1(T)/cm^{-1}$	Tetragonal Strain (S_θ/cm^{-1})		
			(I)	(II)	(III)
100	5.44	-300	-200	-1000	-600
150	8.166	-200	-350	-1500	-875
200	10.88	-160	-600	-1750	-1150

Many sets of values satisfy the above requirements, and several of these are given in table 8.7. As the g-values of centres (II) and (III) have only a small temperature dependence, centre (I) will be initially used to determine the best fit. The calculated and experimental g-values are shown for centre (I) are shown in figure 8.13 for the values given in table 8.7. The anisotropic orbital reduction factors: $k_x=k_y=0.9$, $k_z=0.7$ were required as well as a non-zero linear Jahn-Teller constant for the triplet state, $A_1(T)$. These values are also given in table 8.7 and results in the splitting of the triplet states by $\frac{3}{2}A_1(T)\rho_0$ at an elongated or compressed geometry. The calculated splitting of the triplet state for the values of $A_1(T)$ used are

(8.32)
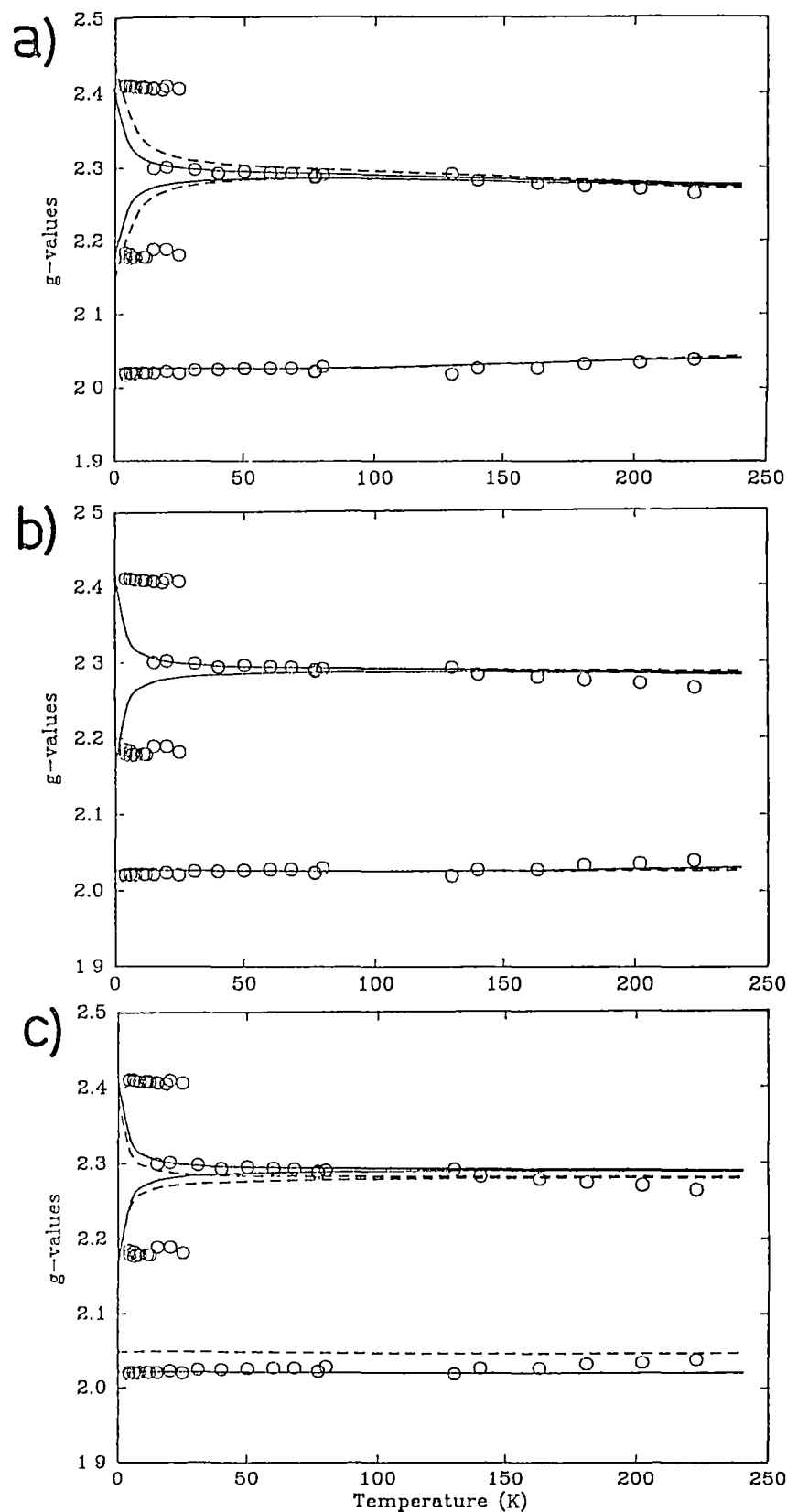
Figure 8.13 Fitting centre (I) using the parameters in table 8.7.

a) $\beta = 100 \text{cm}^{-1}$: ——— $S_\varepsilon = 1.5 \text{cm}^{-1}$; ———— $S_\varepsilon = 3.0 \text{cm}^{-1}$.

b) $\beta = 150 \text{cm}^{-1}$: ——— Basis = 992×992, 35 levels.

——— Basis = 650×650, 20 levels.

—·—·— Basis = 992×992, 35 levels.

c) $\beta = 200 \text{cm}^{-1}$: ——— $k_x = k_y = 0.9$, $k_z = 0.7$, $A_1(T) = -160 \text{cm}^{-1}$.

———— $k_x = k_y = k_z = 0.9$, $A_1(T) = 0$.
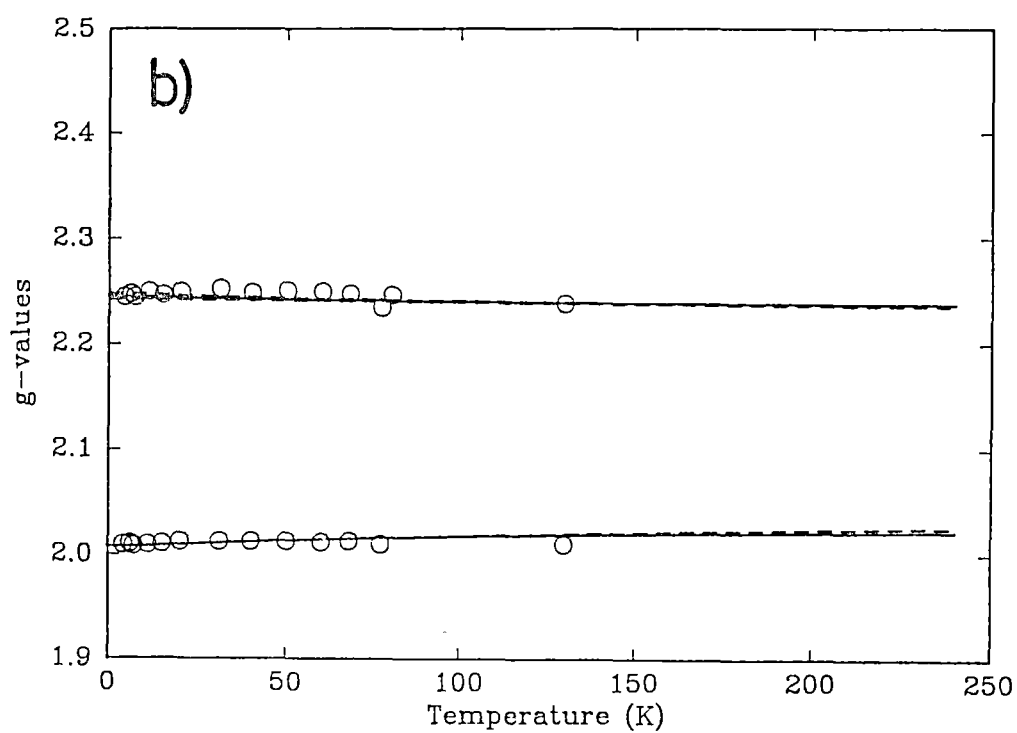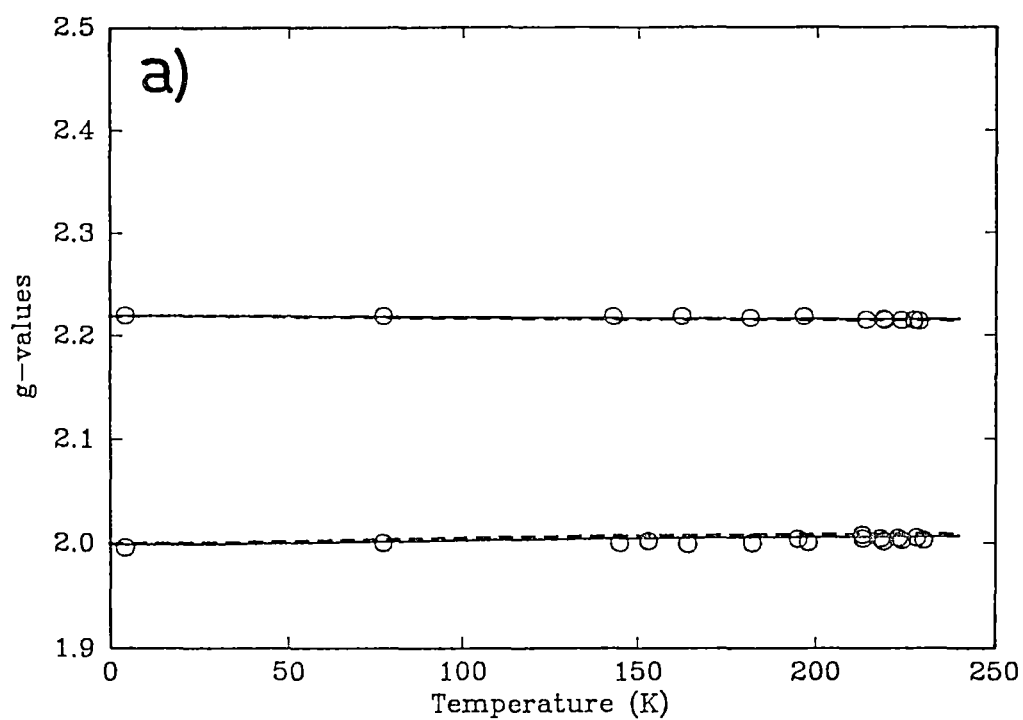
Figure 8.14 Calculated and experimental g-values for:

a) Centre (II): —————— $S_\theta = -1200\ cm^{-1}$, — — — — $S_\theta = -1000\ cm^{-1}$.

b) Centre (III): —————— $S_\varepsilon = 0\ cm^{-1}$, — — — — $S_\varepsilon = 1.5\ cm^{-1}$.

in the range $1,100-2,000 \text{cm}^{-1}$, agreeing well with the experimentally observed value of $1,200 \text{ cm}^{-1}$, since this splitting is at an orthorhombic geometry of the Mexican hat potential, and so is reduced from that expected at a tetragonal geometry. However, it is likely that the introduction of this anisotropy will also contain contributions from the variation of the orbital reduction factors with bondlength.

Additional plots are shown in figure 8.13 to illustrate various aspects of the calculation. The dashed line in figure 8.13a shows the effect of doubling the "random strain". This both causes the tetragonal spectrum to appear at a higher temperature than observed, and the low temperature g-values to be different from what is observed. The former effect is due to additional splitting caused to the lowest vibronic levels, while the latter shows that these wavefunctions are not completely localised within single wells.

Figure 8.13b shows the effect of basis truncation and the error that can be introduced by not including all the populated levels in the Boltzmann sum. The dashed line plot in figure 8.13c shows the effect of using isotropic k values. The most noticeable discrepancy here is that g_x is too low and g_z too high. It is easy to increase g_x by increasing the (negative) $A_1(T)$, but the only way to decrease g_z, without reducing k_z, is to move the position of the minima towards the $\phi=180^\circ$ position, as shown in the static g-values of figure 8.11a. However, it is impossible to do this in the present case, because when the strain is increased, the barrier height between the minima decreases (figure 8.12a) so that the energy splitting of the two lowest states increases (figure 8.12b), and the lowest wavefunctions cannot be localised within the one well. After many trial calculations, it was concluded that centre (I) cannot be fitted with an isotropic k value within the present model.

The temperature dependence of the tetragonal spectrum of centre (I) above ~ 50K is best fitted by the values of $\beta = 100 \text{cm}^{-1}$, $S_\theta = -200 \text{cm}^{-1}$. This can be understood by considering the behaviour of the higher vibronic levels. For large values of the tetragonal strain the potential outside of the double well is steep, whereas for small values it is quite shallow. This means that quite a small value of the tetragonal strain is required to fit this temperature dependence.

If this value of $\beta=100 \text{cm}^{-1}$ is used with the other centres with the strain values given in table 8.7, the g-values shown in figure

(8.33)

8.14 result. Excellent agreement is obtained in both cases, without requiring anisotropic k values. Figure 8.14a shows that centre (II), which has a very small $d(x^2-y^2)$ component, is rather insensitive to the tetragonal strain. Although the potential of centre (III) has a slight double minima (figure 8.12a), the lowest vibronic levels are above the barrier. If the same random strain that was used to fit centre (I) is added to the potential ($S_\varepsilon=1.5cm^{-1}$), then it produces only a very small orthorhombic splitting of $g_\perp$ (figure 8.14b), which would not be detected experimentally. For centre (II), the inclusion of this orthorhombic strain has essentially no effect at all. While these parameters appear capable of fitting the experimental data, the values will only be as meaningful as the model, and they are discussed further in the following section.

8.4.5 The Fitted Parameters.

The parameters arrived at in the previous section are given below:

Table 8.8 The fitted parameters.

$hv = 210$ cm^{-1} $A_1 = 900$ cm^{-1} $A_2 = 5.444$ cm^{-1} ($\beta=100cm^{-1}$)	$S_\theta = -200$ cm^{-1} centre(I) $= -600$ cm^{-1} centre (III) $=-1200$ cm^{-1} centre (II) $S_\varepsilon = 1.5$ cm^{-1}

The lower adiabatic potential surfaces can be found from the vibronic Hamiltonian by diagonalising the potential energy operators, and are shown in figure 8.15. It is interesting to note that the minima in the potentials of centres (I) and (II) correspond to the geometries that are found for $Cu(H_2O)_2Cl_4^{2-}$ and $Cu(NH_3)_2Cl_4^{2-}$ entities in the structures of some pure copper compounds, and this is discussed in the following section. The effectively single minimum in centres (II) and (III) means that the electronic and vibrational parts of the vibronic functions will be very similar to those found for the $Cu(II)/K_2ZnF_4$ system shown in figures 6.6,7.

The basic shape of the potential of centre (I) along the angular coordinate is essentially the same as the one dimensional model of Sorokin and Chirkin. In fact there is a direct mathematical connection
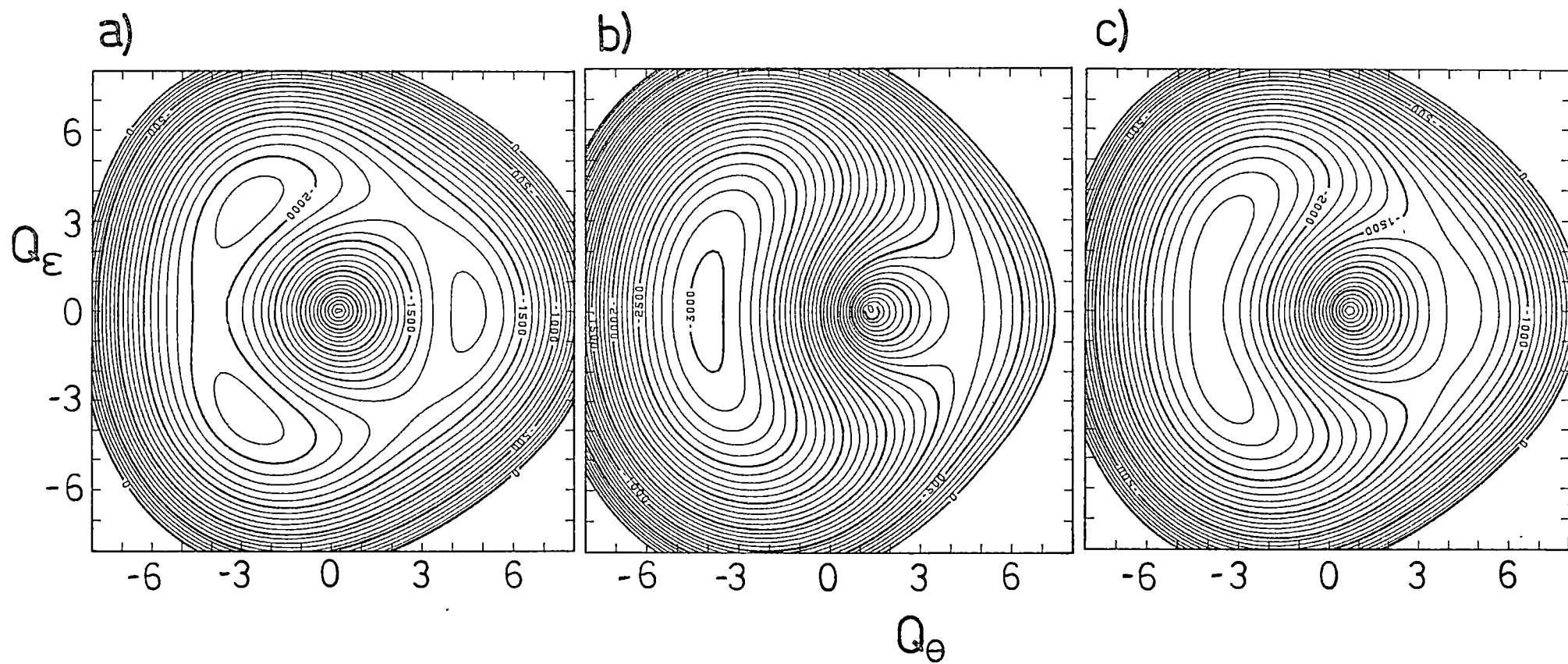
Figure 8.15 The lower adiabatic potential surfaces for the parameters given in table 8.8. a) Centre (I), b) Centre (II), c) Centre (III).

144.6

97.0

74.0

3.0

0.0

Energy
(cm−1)

Q_ϵ

Q_θ

Z

X

Y
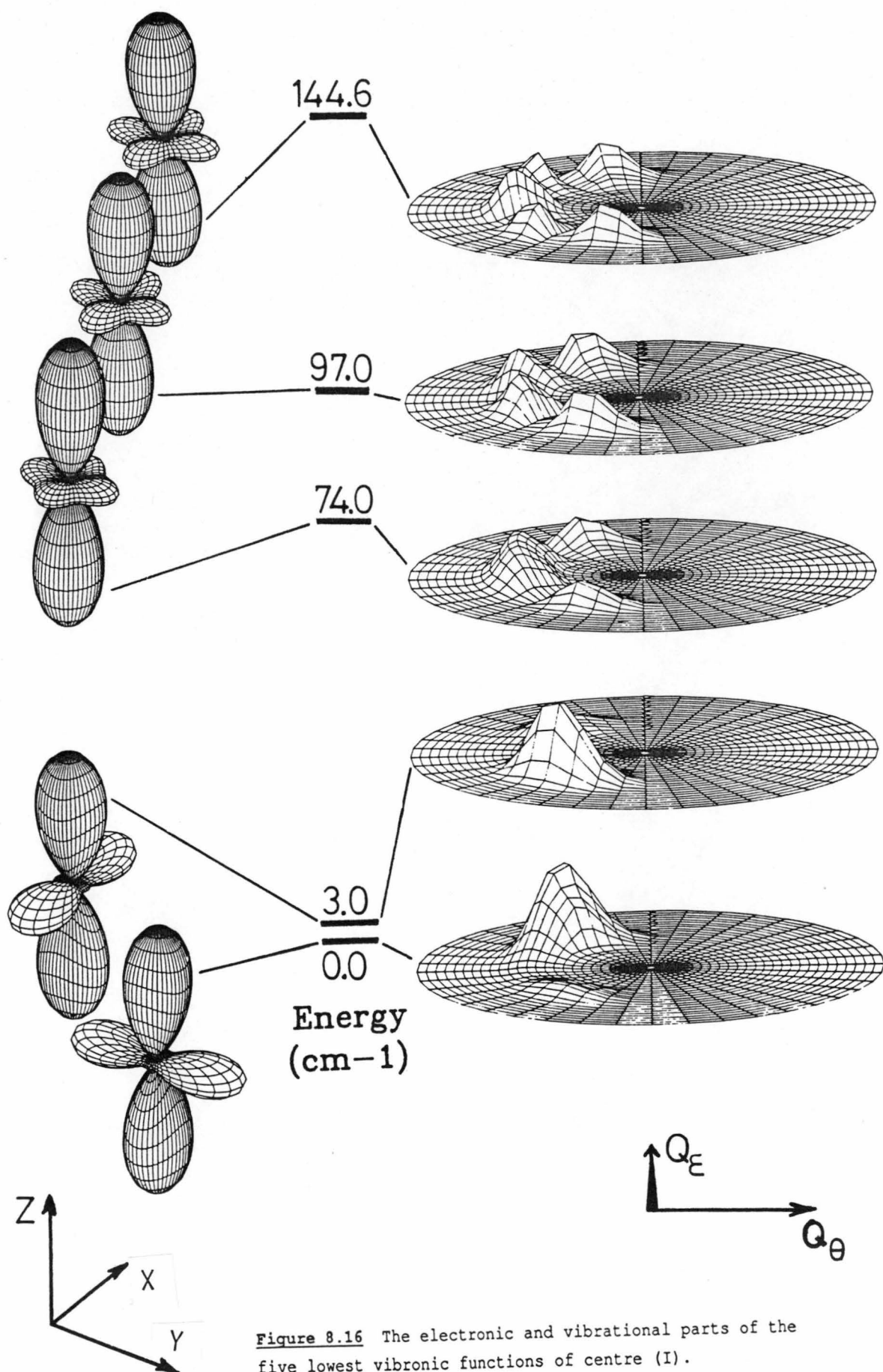
Figure 8.16 The electronic and vibrational parts of the
five lowest vibronic functions of centre (I).

in that, if a change of origin is made to the saddle point between the minima, then part of the second order coupling which causes the double minima in the two dimensional potential becomes a first order coupling constant. While it could be argued group theoretically that the problem should start from this geometry in the first place, the present model provides a rationale as to <u>why the molecule adopts this initial compressed geometry</u>.

The electronic and vibrational parts of the five lowest vibronic wavefunctions are shown in figure 8.16 for centre (I). The g-values are also given for these levels, and can be simply understood from the extension of the d-orbital lobes along the appropriate molecular axes. The two lowest levels are below the barrier height and are localised to a large extent in the separate wells by the random strain $(S_\varepsilon=1.5cm^{-1})$. The lowest wavefunction is localised in the second quadrant $(90^\circ<\phi<180^\circ)$ of the Mexican hat potential, because the orthorhombic strain used to represent the random strain, has been (arbitrarily) chosen to be positive. It is heartening to note that an excited vibronic level at 74 cm^{-1} is completely delocalised over both wells, providing the relaxation pathway between the wells, and the energy of this is close to that predicted $(\sim50cm^{-1})$ by the simulation of the orthorhombic → tetragonal transition region.

However, there are several criticisms that can be made of these results. First, the two lowest levels are not completely localised within their separate wells, but have a small overlap with the other. This is undesirable because a) it would provide a relaxation pathway and an averaged tetragonal spectrum would be expected at all temperatures; and b) the low temperature g-values, if they stay unaveraged, would be dependent on fluctuations of the random strain. This latter point was illustrated in figure 8.12a where a doubling of the random strain caused the low temperature g-values to change.

Since both of the above points conflict with what is observed experimentally, it is almost certain that these wavefunctions are only qualitatively correct. A larger value of β would seem to be required to increase the barrier height between the wells. Connected with this point is the magnitude of the tetragonal strains that have been arrived at. While certainly these appear qualitatively correct, both from the point of view of chemical bonding and their ability to reproduce the ESR data, the value of $S_\theta = -200$ cm^{-1} for centre (I)

(8.35)

seems too low. However, as shown previously, the larger values of S_θ (and correspondingly larger value of β) fails to reproduce the temperature dependence of the higher temperature dependence of the tetragonal g-values of centre (I).

Both the above anomalous points, the magnitude of the S_θ and the barrier height, can be explained by the form of the warping terms. In this formally low symmetry system, the warping terms need not take the cubic form (regardless of whether it caused by anharmonicity or second order electronic coupling). That is, it need not be such that it produces tetragonal minima at $\phi = 0^\circ$, 120° and 240° in the absence of strain. What is needed is a larger barrier height and the minima closer to 180°:
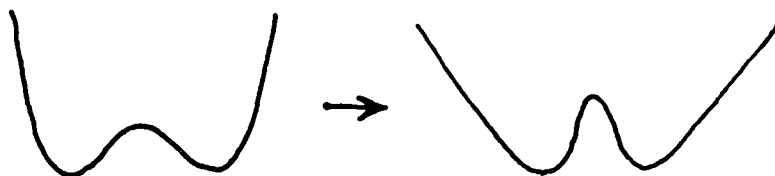
This would then both allow the lowest wavefunctions to be fully localised and the correct temperature dependence of the tetragonal g-values to be calculated with a larger value of the strain. However, it is felt that the basic interpretation of the dynamics of these three centres is correct, and little could be gained by considering the non-cubic forms of the warping terms. The following section considers the effects of using non-cubic forms of the linear coupling and harmonic terms.

It is also noted that there is a level calculated for centre (I) that is 311 cm^{-1} above the ground vibronic state that is localised in the upper well of the potential shown in figure 8.15a. This is similar to the energy of the third level in the Silver and Getz model described in section 8.4.1. The existence of such a level would not be predicted from the one-dimensional pseudo Jahn-Teller model, it makes a small, but significant contribution to the temperature dependence of the g-values.

(8.36)

8.5 DISCUSSION

8.5.1 Comparison of the models.

Although the two dimensional Jahn-Teller model appears to be much more successful in reproducing the observed experimental data than the one dimensional model, the sceptic might say that this is because there are extra parameters in the model that one can vary. However, these parameters are not really free parameters in the sense that it is possible to estimate their magnitudes from the arguments given in section 8.3.

The same cannot be said for the one dimensional Sorokin and Chirkin model, as it is difficult to gain an a priori estimate of the parameters involved. The vibrational frequency in this model would be expected to be reduced from the value of 210 cm^{-1} at the relaxed compressed geometry, as the equatorial bonds involved in the vibration would have lengthen. However, it is difficult estimate how much this reduction would be, although it is unlikely to be as low as ~75 cm^{-1} or greater than 250 cm^{-1}, as suggested from fitting centre (I) and (III) respectively to this model.

The strain parameters of -4,100 and -4750 cm^{-1} for centres (I) and (III) respectively give the difference in the sigma bonding of the axial ligands as $e_\sigma(NH_3)$ - $e_\sigma(H_2O)$ as 325 cm^{-1} which disagrees with the value of 1,000 cm^{-1} obtained from the strain parameters of the Jahn-Teller model. In addition to this, it is difficult to predict the linear coupling constant in the Sorokin and Chirkin model, although the large separation of the electronic states at tetragonal symmetry might suggest that it would be less than what occurs in cubic systems.

The main deficiency suggested for the Jahn-Teller model was that the warping terms were restricted to the cubic form. A non-cubic form of the first order coupling and the harmonic terms might also be expected to have some effect on the potentials. Figure 8.6a shows such a potential which has been constructed from terms estimated from the AOM. However, this potential is of the opposite form that is desired as it will tend to decrease the barrier height in much the same way as the tetragonal strain does.

(8.37)

By keeping the cubic warping term, and varying the harmonic and linear coupling parameters in many trial calculations, no improvement to section 8.4.3 was obtained. It is concluded that the warping is again the most important term in determining the properties of the lowest vibronic levels, and the fact that it is restricted to a high symmetry form is mainly responsible for the difficulty encountered in fitting the experimental data.

8.5.2 Comparison with other $CuX_2Cl_4^{2-}$ entities.

It is instructive to compare the geometry of the doped copper centres predicted from the analysis given here with known structures of pure copper compounds. Table 8.9 shows the bondlengths from published structures of the $Cu(H_2O)_2Cl_4^{2-}$ and $Cu(NH_3)_2Cl_4^{2-}$ units which correspond to centres (I) and (II) respectively for copper doped NH_4Cl. For both types of coordination the structures are very consistent with each other and also with the predictions given by the present study. In particular, orthorhombic bondlengths are found for the centre (I) type compounds with short, medium and long bonds corresponding to pairs of H_2O, Cl and Cl ligands respectively. As suggested by Hagen and Trappeniers (1973), this complex may have an intrinsic tendency to assume this orthorhombic geometry. The present study would imply that the origin of this tendency is vibronic in nature.

This is more convincing in the doped NH_4Cl systems where cooperative effects should be minimal. However, the similar orthorhombic geometry of the pure compounds may suggest a similar vibronic interpretation. That is, the quite drastic difference of the inequivalent Cu-Cl bondlengths is due to the fact that H_2O is a slightly stronger bonding ligand compared to Cl^-, which results in a small tetragonal compression of the warped Mexican hat.

It would be interesting to study the low temperature ESR spectrum of copper doped $CdCl_2.4H_2O$ to see if it also shows orthorhombic g-values. The non-cubic nature of this host (table 8.9) would probably result in the equivalent orthorhombic minima being substantially different in energy so that the orthorhombic to tetragonal motional averaging would be unlikely to occur.

(8.38)

Table 8.9 $CuX_2Cl_4^{2-}$ Structures.

$Cu(H_2O)_2Cl_4^{2-}$ Units:	r_x/pm	r_y/pm	r_z/pm
a) $K_2CuCl_4 \cdot 2H_2O$	228.5(3)	289.5(4)	197.1(6)
b) $CuCl_2 \cdot 2H_2O$	229.0(4)	294.0(6)	195.7(5)
c) $(NH_4)_2CuCl_4 \cdot 2H_2O$	227.1(1)	297.1(1)	195.4(3)
$Cu(NH_3)_2Cl_4^{2-}$ Units:			
d) $(NH_4)_2Cu(NH_3)_2Cl_4$	276(1)	276(1)	196(1)
e) $(NH_4)Cu(NH_3)_2Cl_3$	275.8(1)	275.8(1)	195.0(1)
f) $Cu(NH_3)_2Cl_4$	276(1)	276(1)	195(1)
Others:			
g) $CdCl_2 \cdot 4H_2O$	Cd-Cl = 259.3(7), 258.8(7), 260.6(7), 257.6(7)		
	Cd-OH_2= 235(1), 236(1)		
h) $Cu(NH_3)_4SO_4 \cdot H_2O$	Cu-N = 2.06 (x2), 2.04 (x2)		
	Cu-OH_2= 2.59, 3.37		

a) (Chidambaram 1970) Isolated $Cu(H_2O)_2Cl_4^{2-}$ units.

b) (Engberg 1970) Planar $Cu(H_2O)_2Cl_2$ columns tilted so axial Cl coordination is ~91.2° from $Cu(H_2O)_2Cl_2$ plane.

c) (Bhakay-Tamhane 1980) Isolated $Cu(H_2O)_2Cl_4^{2-}$ units. Basic NH_4Cl structure diluted stoichiometricly by $Cu(H_2O)_2Cl_4^{2-}$. Chains of NH_4^+ along the **c** axis, partial ordering at RT, complete ordering at 115K.

d) (Clayton and Meyers 1976b) Isolated $Cu(NH_3)_2Cl_4$ units. Basic NH_4Cl structure diluted stoichiometricly by $Cu(NH_3)_2Cl_4$.

e) (Clayton and Meyers 1976c) Structure as above.

f) (Hanic and Cakajdova 1958)

g) (Leligny 1979) Chains of $Cd(H_2O)_2Cl_4^{2-}$ each sharing two Cl-Cl edges.

h) (Mazzi 1955) Showing that NH_3 is a stronger ligand than H_2O.

In the centre (II) type structures, all three sets of published bondlengths show a compressed tetragonal geometry in agreement with the ESR data. These three structures are part of a series:

$$NH_4Cl, \quad (NH_4)_2Cu(NH_3)_2Cl_4, \quad (NH_4)Cu(NH_3)_2Cl_3, \quad Cu(NH_3)_2Cl_2,$$

which all have the basic NH_4Cl structure. The Cu(II) ions are randomly distributed over the face centred positions of the unit cell and the two NH_4^+ ions in the axial positions are replaced by two NH_3 ligands (Clayton and Meyers 1976a), exactly as in the doped centres studied here. It is curious that these compounds follow simple stoichiometry rather than a continuous range of mixed crystals that might be expected. Since the above series has the following stoichiometry:

$$NCl.\frac{1}{\infty}Cu, \quad NCl.\frac{1}{4}Cu, \quad NCl.\frac{1}{3}Cu, \quad NCl.\frac{1}{2}Cu,$$

it might be expected that $NCl.\frac{1}{5}$, corresponding to $(NH_4)_3Cu(NH_3)_2Cl_5$, would also form a stable compound.

Although the crystal structure determinations were successful using a model where the Cu atoms (therefore NH_3 molecules) are randomly distributed about the NH_4Cl lattice (Clayton and Meyers 1976a,b,c), there is no reason why this should result in the observed stoichiometric compounds. Presumably, there must be some sort of cooperative effect occurring to explain these intriguing facts, although these effects are assumed to disappear in the present case with the high dilution.

This series of compounds would then be ideal to study such cooperative effects, as the cell constants remain the same for all concentrations of copper, the basic NH_4Cl lattice acting like a "sponge". Any concentration dependence of the ESR spectrum would then be due to cooperative interactions.

Finally, the bondlengths of $Cu(NH_3)_4(H_2O)_2^{2+}$ in $Cu(NH_3)_4SO_4.H_2O$ are given in table 8.9 to illustrate the stronger bonding properties of ammonia over water, in agreement with the sign and magnitude of the strain parameters found in the present study.

(8.39)

8.6 CONCLUSIONS

The temperature dependent ESR spectrum of the different centres of copper doped NH_4Cl over the temperature range 4.2-240K has been rationalised in terms of vibronic interactions. Over this temperature range, it is then the local dynamics of the centres, rather than the influence of the bulk dynamics of the host lattice, that is responsible for the observed properties. The consistency of the present interpretation has allowed the coordination of the previously uncharacterised centre (III) to be postulated.

The system has proved ideal to test the validity of a vibronic approach to low symmetry systems. Although perfect agreement with experiment was not found, and indeed not sought, it appears that the "chemistry" of the system is well understood within the present formalism. It has also been of interest to examine the various approximations inherent in the different levels of interpretations of such an approach. Although the strain terms dominate the potential of the complexes, it was found that the warping terms are again crucial in determining the properties of the lowest vibronic levels. These are difficult to quantify even in the case of cubic systems, and the assumption that these low symmetry systems retain the cubic form of this warping seems to be the major limitation of the present approach.

However, within this limitation, the model was able to describe the different temperature dependent ESR spectra by allowing only the bonding characteristics of the axial ligands to vary between the three centres. The resulting parameters are chemically reasonable and consistent. Moreover, it provides a rationale as to why the radically different geometries of centres (I) and (II), (III) are adopted in identical environments. A comparison with the geometry in the crystal structures of several analogous pure compounds suggests that this type of interpretation could also be applied to pure systems.

There is no group theoretic reason why an isolated molecule in a non-degenerate state should adopt the maximum symmetry of its coordination. If a molecule does not have the maximum symmetry, it is usual to invoke pseudo Jahn-Teller vibronic coupling with a higher excited state to explain the descent in symmetry. It is felt, however, that the present approach offers a better description of what is actually occurring physically.

(8.40)

For centre (I) Sorokin and Chirkin (1979) expressed surprise at finding a pseudo Jahn-Teller effect between states that are separated by ~10,000 cm^{-1} at the tetragonal geometry. In the present interpretation the problem is viewed as a pseudo Jahn-Teller effect between states separated by ~1,000 cm^{-1} at a hypothetical "octahedral" geometry. The fact that $Cu(H_2O)_2Cl_4^{2-}$ complexes seem to adopt an orthorhombic geometry as a rule, is then not because it has a strong tendency to undergo a pseudo Jahn-Teller effect with a state ~10,000 cm^{-1} distant, but rather is a consequence of the axial water ligands being only a marginally stronger ligand than the chloride ions. This then results in a small tetragonal compression which is of the same order as the warping terms in the conventional Mexican hat potential surface, which leads to the orthorhombic geometry.

(8.41)

CHAPTER 9   THE TEMPERATURE DEPENDENCE OF THE ELECTRONIC SPECTRUM
OF SQUARE PLANAR COPPER TETRACHLORIDE

9.1   INTRODUCTION

The temperature dependent vibronically induced electronic spectrum of the square planar $CuCl_4^{2-}$ species has recently been studied by McDonald and Hitchman (1986) in some detail. It was found that the temperature dependence of both the intensities and the shift in the band maxima deviated quite strongly from the behaviour expected from the generally accepted models.

These deviations have previously been observed in Ni^{2+}/ $KMgCl_3$ by Brynstead etal (1966) over the temperature range 80-763K, although no explanation was put forward. The observed deviation in the case of $CuCl_4^{2-}$ is even more dramatic over the limited temperature range 10-300K, and represents an excellent opportunity for investigating the causes of the observed discrepencies.

An investigation of this type is of considerable interest as it is a direct probe of the adiabatic potentials involved. As stressed by Bacci (1984) these potentials, describing metal-nearest neighbour interactions, are important in modulating the active site in metalloproteins and temperature dependent phenomena can be used to investigate their form. The planar $CuCl_4^{2-}$ ion represents an advantageous model compound because of its high symmetry and relatively few normal modes.

9.1.1 Background.

The d-d electronic transitions of centrosymmetric $CuCl_4^{2-}$ are parity forbidden, and the relatively weak intensity observed (McDonald and Hitchman 1986) is due to vibronic coupling. This leads to the transition moment being a function of the nuclear geometry and therefore temperature dependent. The theory of this temperature dependence is discussed in chapter 3. An important result found in appendix 3.A1 was that the temperature dependence of the intensity of a vibronically induced transition will depend only on the ground state potential

surface, and the way the electronic transition moment varies along this surface.

This allows the present study to be conveniently divided into two sections. These are: a) the temperature dependence of the intensity, which depends only on the form of the ground state potential surface and b) the temperature dependence of other spectral phenomena, which depends on the form of both the ground and excited state potential surfaces. In the present model compound there is sufficient experimental data to quantify these ground and excited state properties.

9.1.2 Sources of Experimental Data.

The spectrum of the complex $(meth)_2CuCl_4$ [meth=methadonium] is shown in figures 9.1a,b for light with the electronic vector polarised along the **b** and **c** crystal axes respectively. These directions correspond closely to the z and xy molecular axes indicated in figure 9.A1. All the temperature dependent experimental data used in this chapter was provided by McDonald (1986). Additional spectra of the $(NmpH)_2CuCl_4$ [NmpH=N-methylphenethylammonium] compound were taken at 4.2K by a 3 metre Hilger spectrograph with an immersion liquid helium Dewar.

The most obvious variation of the spectrum with increasing temperature is the increase in the intensity, which is typical of a vibronically induced transition. The source of this intensity is from coupling with higher energy charge transfer states (Desjardins etal 1983). However, it is only the relative intensity that is of interest in the present study. The intermediate states and the source of the vibronic intensity will be briefly considered in appendix 9.A3.

The other temperature dependent features are the shift of the band maxima to lower energies and the increase in the band widths with increasing temperature. Since the overall spectral band shape of the transitions could be well fitted to a Gaussian line shape, the band maxima and band width can be related to the mean energy and variance respectively (see section 3.6). The higher spectral moments (relating to skewness, kurtosis, etc) are small.

Since it would be tedious to analyse the spectra shown in figures 9.1a,b fully, only the highest energy transition $^2B_{1g}(x^2-y^2)$ $\rightarrow$ $^2A_{1g}(z^2)$, will be considered in detail. This transition has been
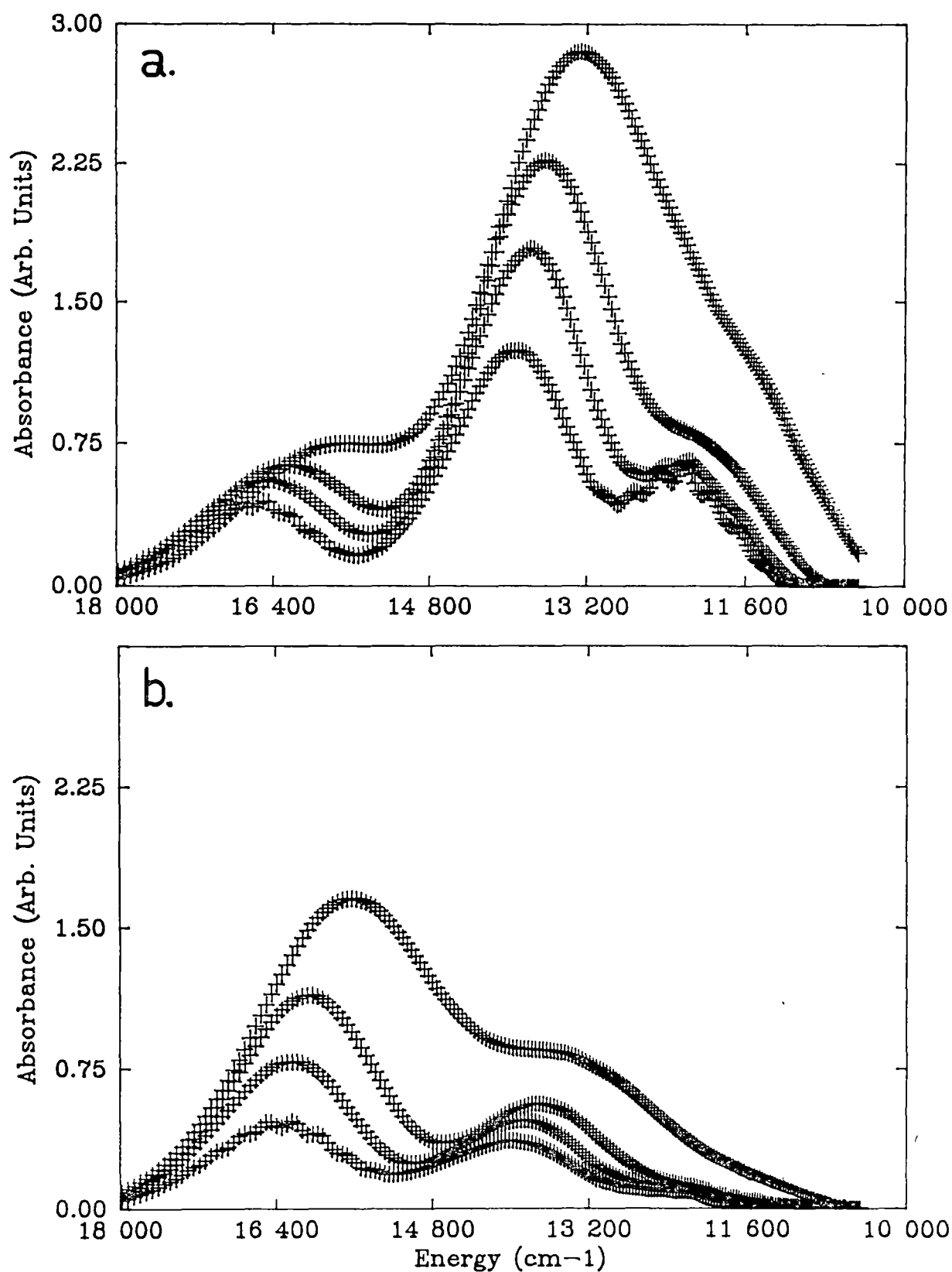
Figure 9.1 The spectrum of (methadonium)$_2$CuCl$_4$ d-d transitions,
The electric vector is polarised a) ||b and b) ||c crystal axes.
The temperatures are 10, 70, 140, 265K for increasing intensity.

chosen because it is the easiest to separate from the other transi-
tions, and also because it lacks complicating features such as
electronic degeneracy or normal modes of more than one symmetry induc-
ing the intensity in each polarisation. In addition it contains the
typical behaviour of all the transitions; that is, in the two
polarisations, a very different behaviour of the intensity, but a
similarly large band shift, was observed as a function of temperature.
The full spectrum is then considered to rationalise the different
trends for the different transitions.

9.2 TEMPERATURE DEPENDENCE OF THE INTENSITIES: A MOMENTS ANALYSIS.

The experimental spectrum of the $^2B_{1g}(x^2-y^2) \rightarrow {}^2A_{1g}(z^2)$ transition is shown in figure 9.2. For this particular transition, modes of only one symmetry are allowed in each polarisation so one dimensional potentials can be used to investigate the deviations from the usual "coth rule" model. There are two schools of thought on the breakdown of the coth rule. Ferguson (1970) has suggested that the inducing mode may be more active in higher vibrational levels than that given by a linear dependence. Englman (1960), and more recently Bacci (1984), have argued that anharmonicity will be important.

Here both schemes are investigated, not because of the importance of explaining the small deviation of the temperature dependence from the harmonic "coth rule", but more because it is necessary to know the relative importance of the two effects when considering the shift in the band maxima.

9.2.1 The Harmonic Approximation.

Vibronic selection rules allow vibrations of only one symmetry to induce intensity in each of the xy and z polarisations. These are the e_u (ν_6, ν_7) and b_{2u} (ν_5) modes respectively that are shown in figure 9.A1. A family of curves can be obtained from different frequencies of these inducing modes by using the "coth rule" of (3.54). Fair agreement with experiment can be obtained when the vibrations take the values $\nu_7 = 165 \text{cm}^{-1}$ and $\nu_5 = 65 \text{cm}^{-1}$, with the stretching vibration of e_u symmetry apparently inactive. The experimental values, and those calculated with the coth rule are the symbols and dashed lines respectively in figure 9.3. It can be seen that the observed intensity rises more quickly than expected from the coth rule at low temperatures, and slower than expected at higher temperatures. The conditions under which the coth rule is derived are now relaxed in an attempt to improve this agreement.

(9.4)
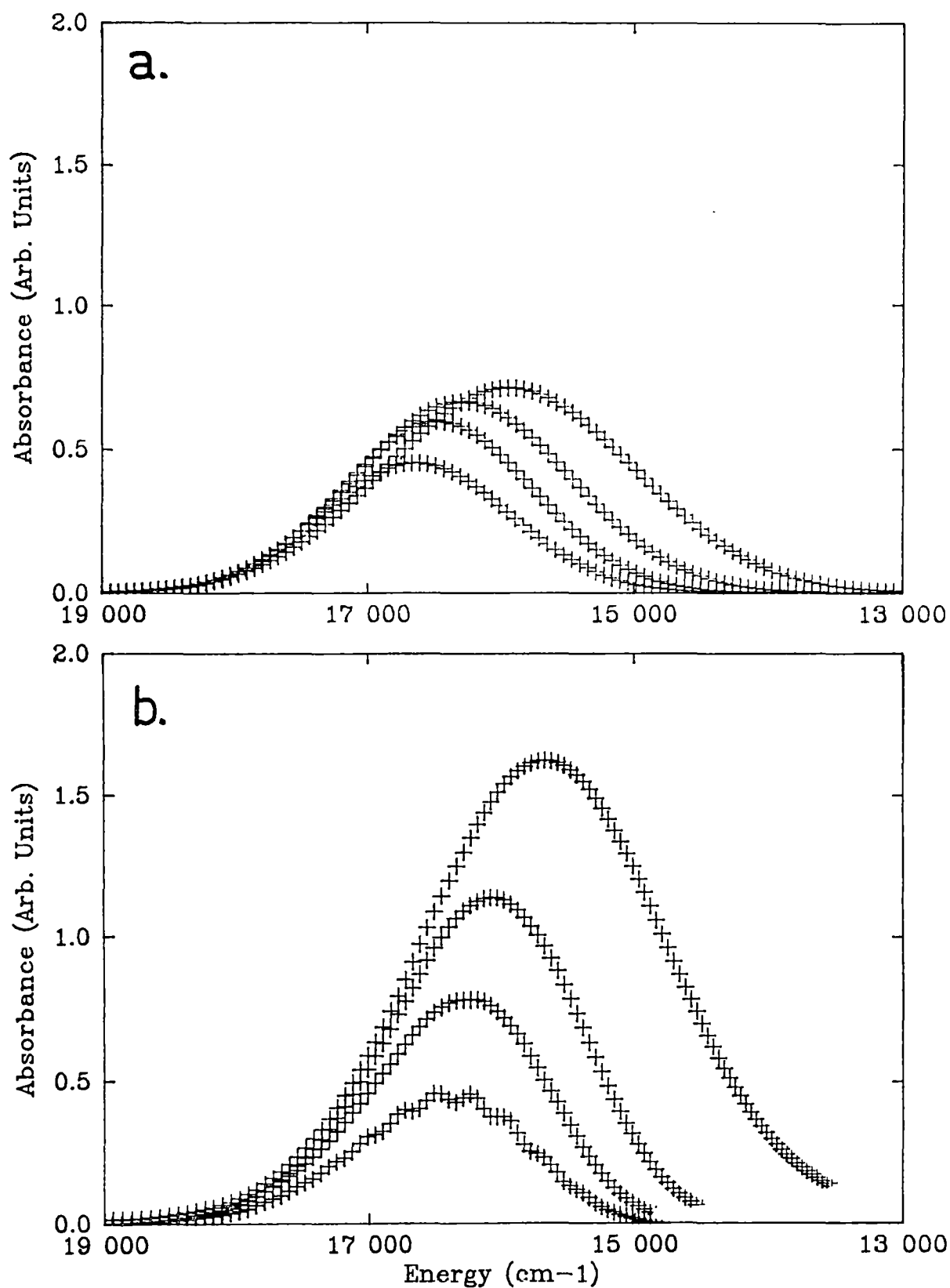
Figure 9.2 The $^2B_{1g}(x^2-y^2) \rightarrow {}^2A_{1g}(z^2)$ transition.

Electric vector polarised a) ||xy and b) ||z molecular axes.

The temperatures are 10, 70, 140, 265K for increasing intensity.
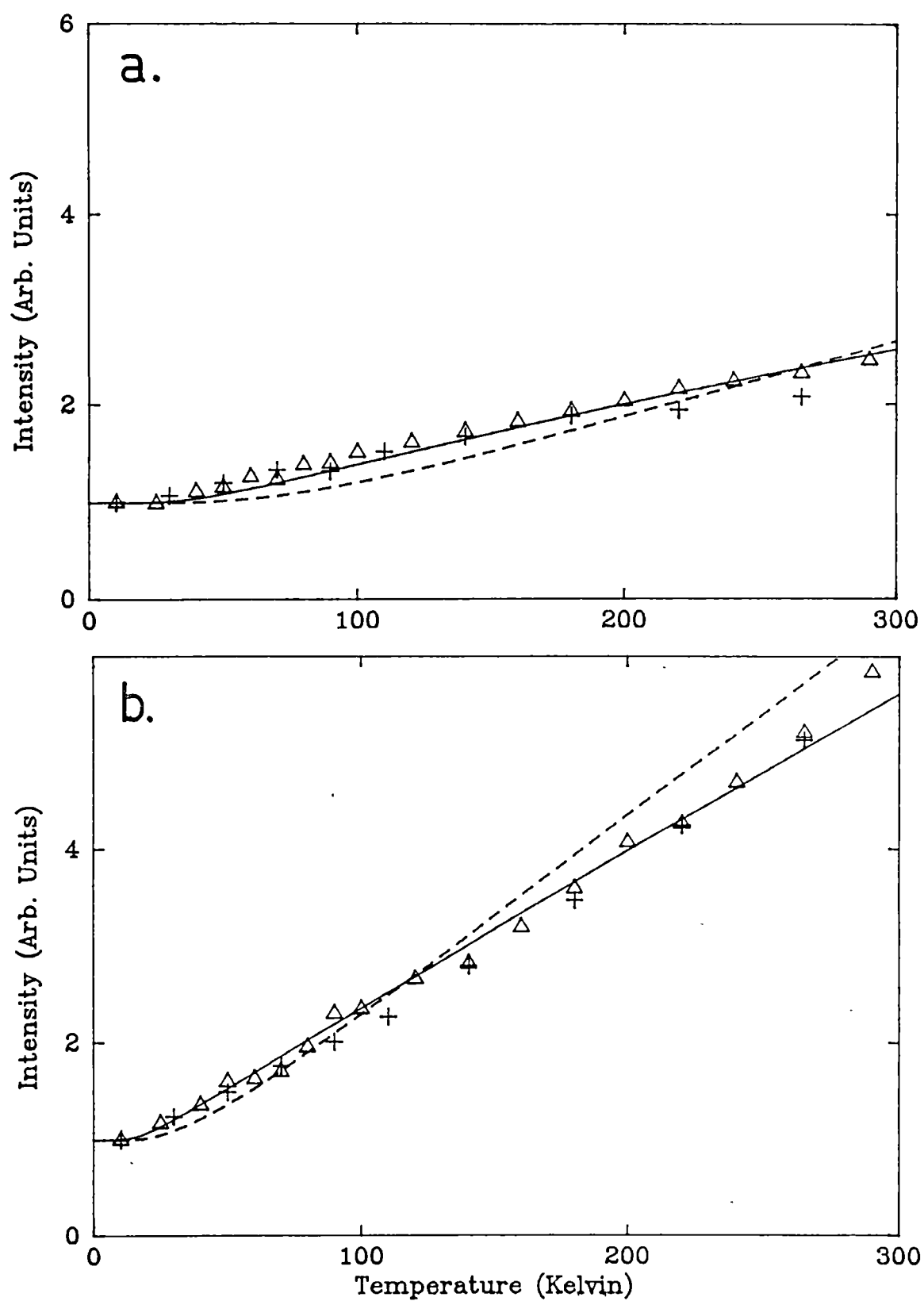
Figure 9.3 The temperature dependence of the intensity.

a) ||xy ---harmonic, hv=165cm^{-1}; —— anharmonic, (equation (9.1)).

b) ||z ---harmonic, hv=65cm^{-1}; —— anharmonic, (equation (9.1)).

9.2.2 The Non-Linear Dependence of the Transition Moment.

If the expansion of the electronic transition moment is taken to second order, the quadratic coth rule of (3.55) is obtained. The application of this formula to the temperature dependence of the intensity is shown in figure 9.4 for the z polarised spectrum. The effect of the additional $\coth^2$ term is to increase the intensity at higher temperatures. Therefore a higher harmonic frequency of $v_5 = 75 \text{cm}^{-1}$ is used, and the I_{01}, I_{02} constants are given the pairs of values 1.0,0.0; 0.95,0.05; 0.90,0.10 to allow the curves to pass on either side of the experimental points. Clearly the wrong sort of behaviour is observed, so that this mechanism cannot account for the intensities in the lower temperature range.

In passing, it is noted that this is exactly the type of deviation from the coth rule that was observed by Brynstead etal (1966), which in turn was the experimental evidence cited by Ferguson (1970) when he suggested this as a possible mechanism. This indeed may be the cause for the deviation from the coth rule in this particular compound [Ni(II)/KMgCl$_3$], although as Brynstead etal (1966) have themselves suggested, this sort of behaviour can also be explained by a quartic anharmonicity. For the present compound however, the above mechanism cannot account for the observed deviations from the coth rule.

9.2.3 Anharmonicity.

The type of anharmonicity likely to account for the deviation from the coth rule in the present case, is one in which the energy separation between the vibrational levels increases for higher levels. This is the same conclusion drawn by Englman (1960), when looking at the temperature dependence of the intensity of $Ni(H_2O)_6^{2+}$. He argued that inter-ligand repulsion would cause the harmonic potential of the bending modes to become steeper at high amplitudes and used a "Poschl-Teller" potential to approximate this effect.

In the present case it is not clear what is causing the anharmonicity, as axial ligands are absent and interligand repulsion should decrease as the angular distortion increases along the out-of-plane b_{2u} coordinate. However, the potentials of the angular vibrations may

(9.5)
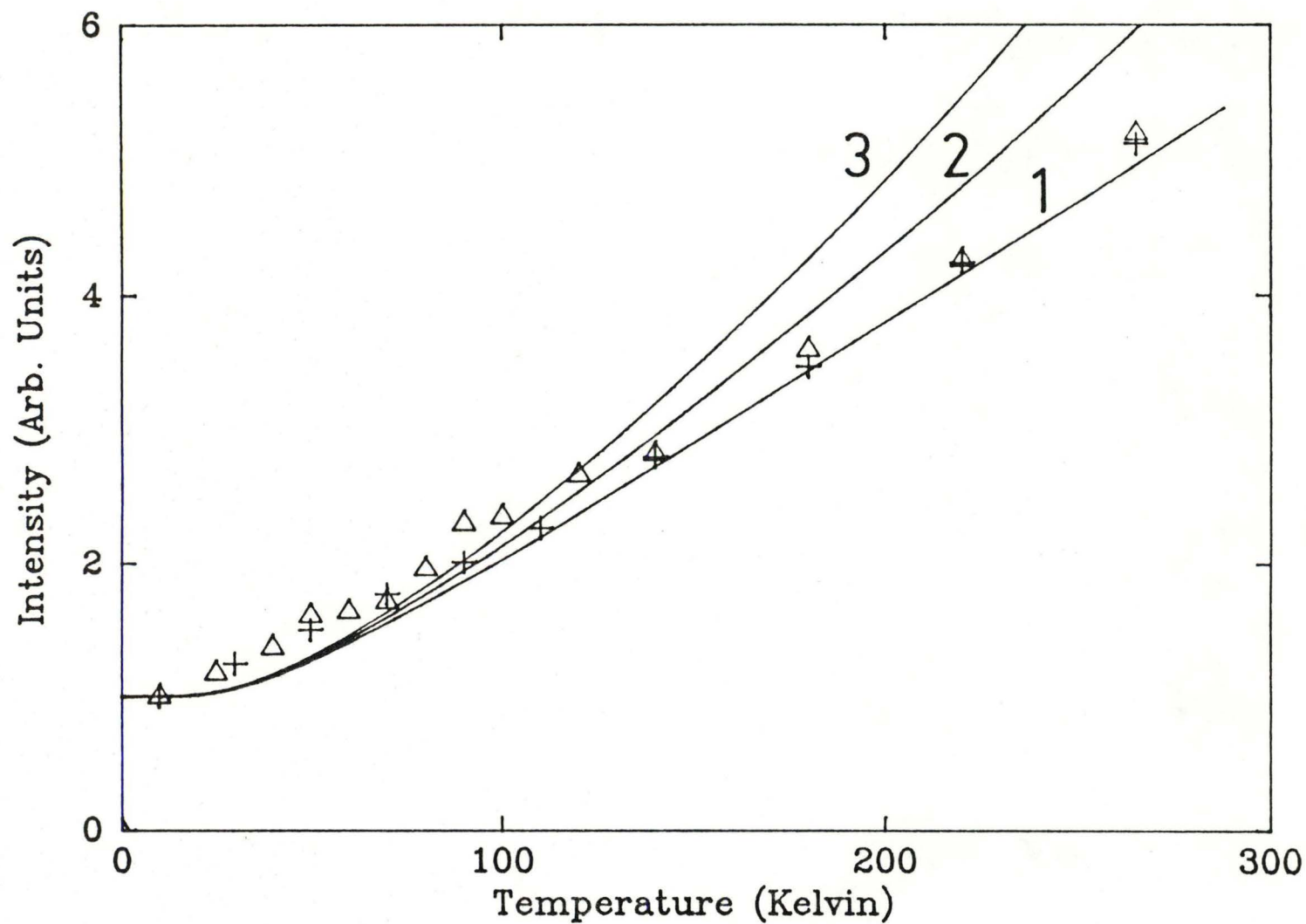
Figure 9.4 The temperature of the intensities with second order dependence of the transition moment on Q. Equation (9.55), $h\nu=75cm^{-1}$, $I_{01}=1.0, 0.95, 0.90$; $I_{02}=0.0, 0.05, 0.10$ for the curves 1,2,3 respectively.

be perturbed by the hydrogen bonding with the methadonium cation which stabilises the planar geometry of these complexes (Harlow etal 1974). Alternatively, such an anharmonicity can be rationalised in terms of vibronic coupling in the ground state potential (see section 9.5). While the actual cause of the anharmonicity cannot be given with certainty, it is clear what form it should take if it is to explain the observed temperature effects.

Calculations of the temperature dependent intensity were done by the variational method for various potentials where the anharmonicity introduced is slight. Again a family of curves were examined, and it became clear that by altering the potential to reproduce the low temperature experimental points, the frequency of the harmonic potential must be lowered to reproduce the higher temperature data. The best fit temperature dependent intensity is shown in figure 9.5 by solid lines. These were obtained with the potentials:

$$V(\xi) = 0.5\xi^2 + 2.0\exp(-0.25\xi^2); \quad h\nu = 165\text{cm}^{-1}, \qquad (9.1)$$
$$V(\xi) = 0.5\xi^2 + \exp(-0.5\xi^2); \qquad h\nu = 60\text{cm}^{-1}$$

for xy and z polarisations respectively. These potentials are shown in figure 9.5 along with the best fit harmonic potentials for comparison.

It can be seen that the curves are an improvement on the "coth rule" and certainly account for the deviation better than the non-linear dependence of the transition moment. For this reason the latter mechanism will not be considered when analysing the larger deviation from expected behaviour of the shift of band maxima with temperature.

9.2.4 Are the Ground States Unique?

It is not clear that the potentials that result in fitting the experimental data in figure 9.3 are unique. Although these potentials represent a small deviation from the best fit harmonic potential of the "coth plots", a far from harmonic potential might also fit the experimental data. The cause of this uncertainty arises because the absolute intensities are not being calculated, but rather the intensities relative to the intensity at absolute zero. This means that different potentials could give the same relative change in the RMS value of the inducing coordinate, which would then give the same
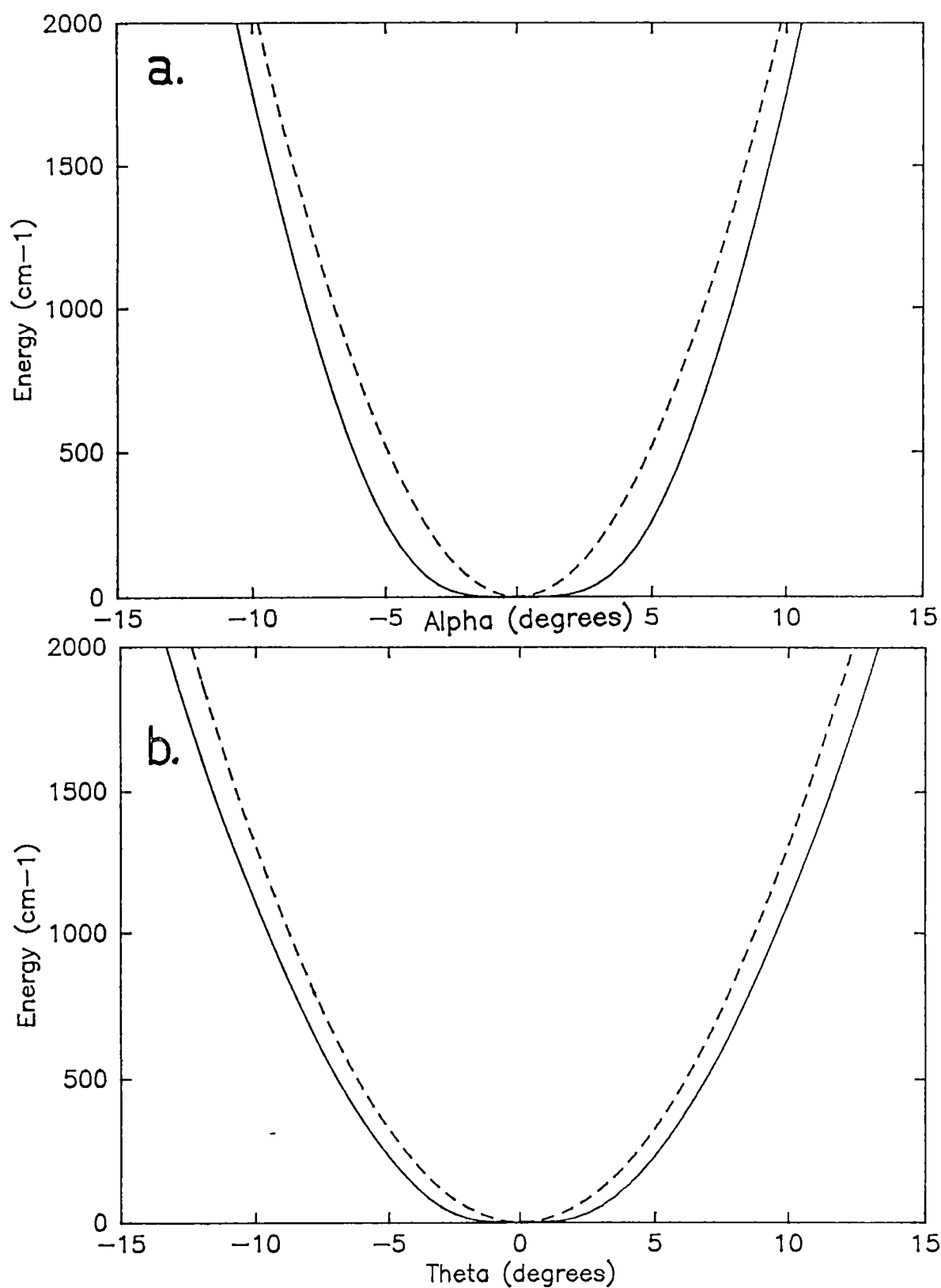
Figure 9.5 Ground state potentials corresponding to the temperature dependence shown in figure 9.3.for a) the e_u(b) and b) the b_{2u} normal coordinates. – – – – Harmonic ———— Anharmonic (equation (9.1)).

relative change in the intensity. Several alternate potentials are therefore investigated at this point. Here, only the potential of the b_{2u} mode, or z polarised data of figure 9.3 is considered for illustration. Potentials given below have been chosen to have a large root-mean-squared amplitude in the lowest vibrational level and are shown in figure 9.6a.

$$
\begin{align}
V_1(\xi) &= 0.5\xi^2 & , \ h\nu &= 70 \ cm^{-1} & (9.2)\\
V_2(\xi) &= 0.2\xi^2 + \exp(-0.4\xi^2) & , \ h\nu &= 65 \ cm^{-1}\\
V_3(\xi) &= 0.5\xi^2 + 5.0 \ \exp(-0.1\xi^2) & , \ h\nu &= 49 \ cm^{-1}\\
V_4(\xi) &= -0.5\xi^2 + 0.00625\xi^4 & , \ h\nu &= 20 \ cm^{-1}
\end{align}
$$

These potentials have been chosen to give the same relative intensity of 6.0 at a temperature of 300K reflecting the experimentally observed values for the z polarisation (see figure 9.3b). The temperature dependence calculated for these potentials is shown in figure 9.6b and it can be seen that while it agrees with experimental data at low and high temperatures, the deviation at intermediate temperatures is much larger than experimentally observed. The potential that comes closest to reproducing the observed behavior is potential number two which is very similar to the potential already arrived at in the previous section.

The reasons why the other potentials fail to give the correct behaviour can be illustrated classically. Table 9.1 gives the square root of the Boltzmann averaged mean-square value of the angle theta (see figure 9.A1 for the definition of θ) at various temperatures for the different potentials. Since the vibronic mixing is assumed to depend linearly on θ, a molecule at a particular temperature can be thought of as being "statically" at the RMS geometry. This will give a "static" mixture of allowed character into the wavefunctions and a static contribution to the intensity.

Notice that the ratio of the RMS value at 300K to that at 0K is the same for all potentials as they have been chosen to reproduce experiment at low and high temperatures. At intermediate temperatures the relative RMS values deviate from the harmonic values in much the same way as the intensity deviates in figure 9.6b. In fact the connection is stronger; the square of these relative RMS values is <u>exactly equal</u> to the relative intensities if the electronic transition moment

(9.7)
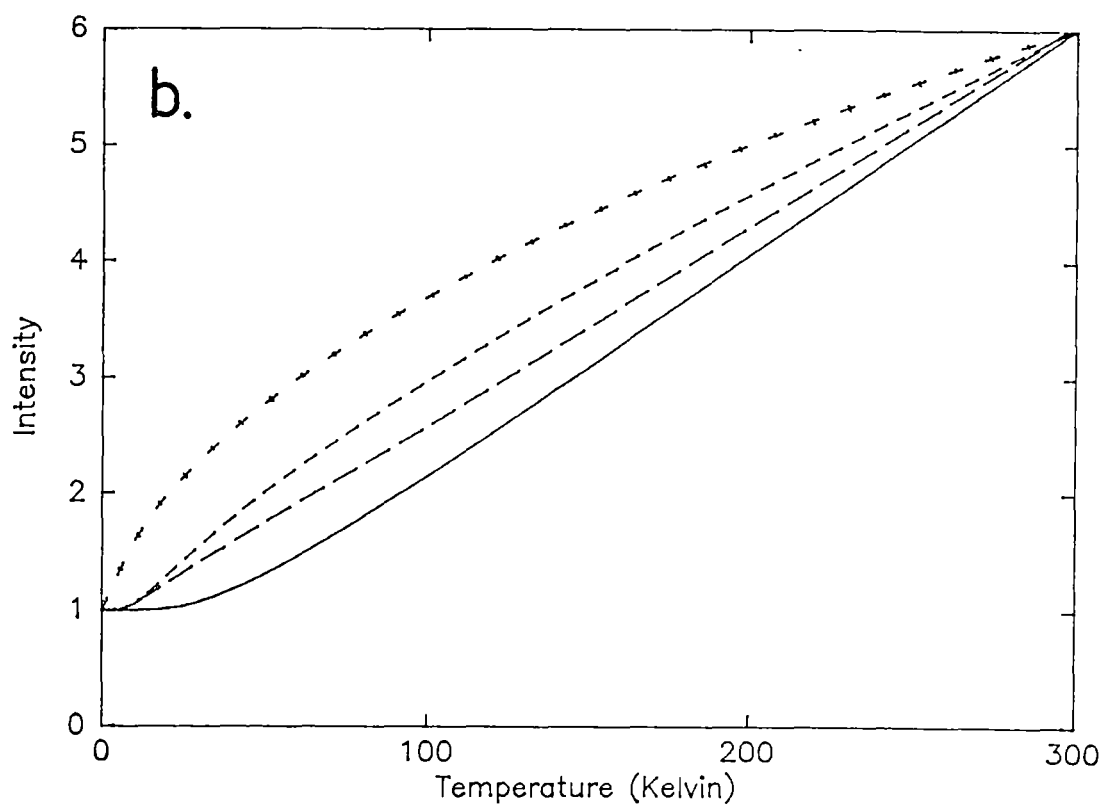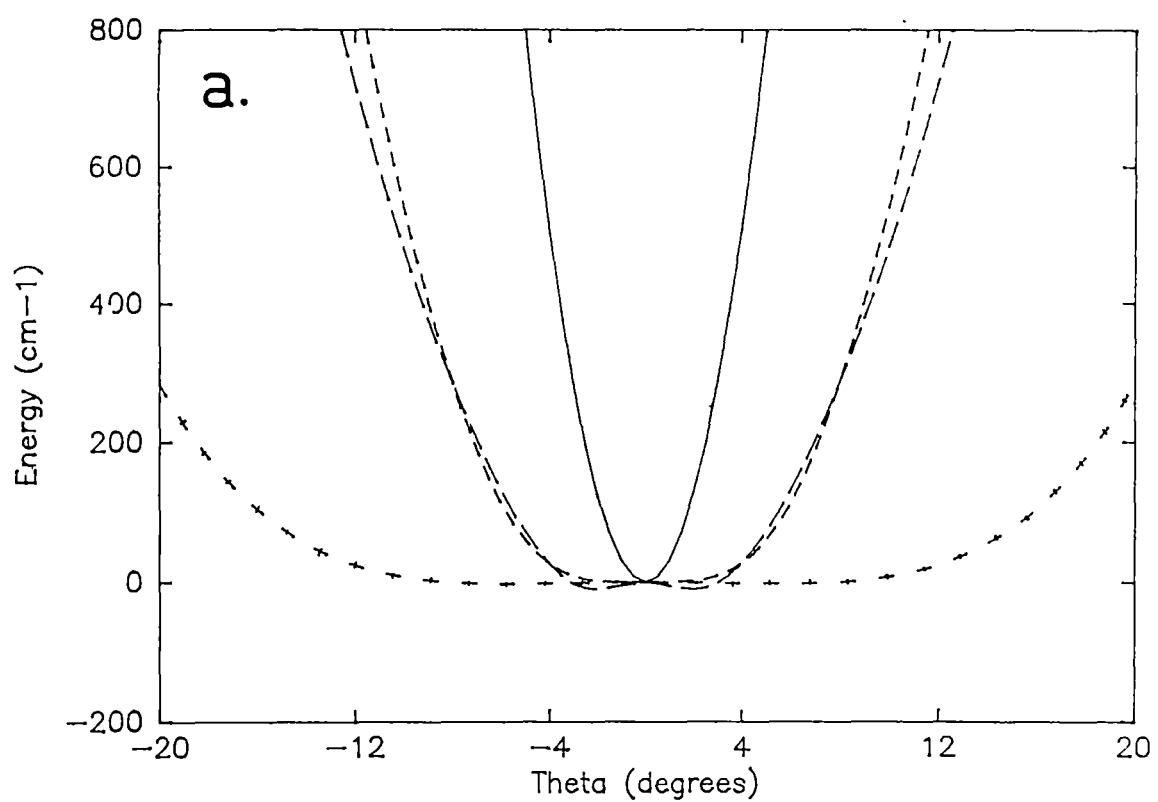
Figure 9.6 a) Trial potentials: 1———,2 —— ,3 ---- ,4 ++++.
b) Temperature dependence of the intensities for the above potentials.

depends linearly on the coordinate. This can easily be proved by using the closure relationship or "sum rule" as shown by Albrecht (1960). Said again: The relative mean-square value of θ is exactly equal to the relative intensity, no matter what form the ground and excited state potentials take. Therefore although a "static" picture of the intensity mechanism is helpful conceptionally, it gives no computational advantage, as the calculation is essentially the same.

Table 9.1   RMS values $<\theta^2>^{1/2}$ (degrees)

	Absolute				Relative			
Temp/K:	0	100	200	300	0	100	200	300
1	1.05	1.54	2.11	2.57	1.0	1.47	2.01	2.45
2	1.86	2.99	3.86	4.58	1.00	1.61	2.07	2.46
3	1.81	3.13	3.88	4.45	1.00	1.72	2.14	2.45
4	4.37	8.41	9.79	10.73	1.00	1.92	2.24	2.45

The reason why the above potentials cannot be made to fit the experimental data is because a potential that is flattened to give a large RMS geometry in the lowest level also gives levels that are very close to the ground vibrational level. Population of these low lying levels occurs at quite low temperatures and gives a larger increase in intensity than observed experimentally in figure 9.6. This conclusion is in agreement with a study of the anisotropic temperature factors from the crystal structures of planar $CuCl_4^{2-}$ (see appendix 9.A1), which gives a RMS value for theta of $\sim 3^{\circ}$ at 300K, compared to the $\sim 11^{\circ}$ predicted by potential 4 in table 9.1 above.

From the above arguments it is felt that reasonably accurate ground state potentials have been found. This is not to say that an exact potential has been obtained, the flatten potentials of figure 9.4 may be double well potentials with a small barrier separating the minima. If this is the case, a temperature dependent study of the crystal structure of square planar $CuCl_4^{2-}$ would be of interest as such a double minima ground state may cause a phase transition to occur at low temperatures if the $CuCl_4^{2-}$ ion were frozen into one well and thereby losing it's inversion symmetry.

9.3 THE TEMPERATURE DEPENDENCE OF THE BAND MAXIMA: A MOMENTS ANALYSIS

9.3.1 The Harmonic Approximation.

In calculating details of the spectrum other than just the integrated intensity, the excited state potentials must also be considered. The a_{1g} potential is known to be displaced and slightly reduced in frequency compared to the ground state from a Franck-Condon analysis of the spectrum at low temperature (McDonald and Hitchman 1986). The potential appropriate to this mode in dimensionless units is given in table 9.2. This corresponds to the frequencies $275cm^{-1}$ and $265cm^{-1}$ for the ground and excited states respectively, and a displacement of $\Delta S(a_{1g}) = 21.4pm$. The potentials of all the other modes are required to be undisplaced by group theory (see section 3.2) and initially these potentials are considered to be harmonic and of the same frequency as the ground state.

In this approximation, the equations (3.56) and (3.57) can be used to calculate the contribution from each normal mode to the bandshift and halfwidth respectively. These calculations are shown in table 9.2 for both the z and xy polarised spectrum at low (T=0K) and room (T=300K) temperatures. As discussed in section 3.6, contributions to the shift in the band maxima occur only from the inducing modes or modes of different frequencies in the ground and excited states. These are the b_{2u} and a_{1g} modes in the z polarisation and the e_u(b) and a_{1g} modes in the xy polarisation. Similarly, the halfwidth is determined from these same modes; the largest contribution coming from the a_{1g} mode, which is displaced with respect to the ground state.

The results that are calculated using this harmonic approximation are shown as solid lines in figures 9.7 and 9.8, along with the experimental data. A constant energy term has been added to these results representing the vertical electronic transition so that the low temperature band maximum in z polarisation agrees with experiment. Clearly the experimental results cannot be explained in this approximation. Consider the band maxima in figure 9.7: the low temperature band maximum in z polarisation fits the experimental value only because the vertical transition energy difference was chosen to do so. In xy polarisation the band maximum at low temperature is

(9.9)

correctly calculated as higher in energy than in z polarisation, but is not as high as is observed experimentally. The overall temperature dependence in both polarisations shows only a fraction of the decrease in the energy of the band maxima that is experimentally observed.

TABLE 9.2: Temperature dependence of band maximum and halfwidth.
Harmonic gound and excited state potentials with equal frequencies.

	v_1 a_{1g}	v_2 b_{1g}	v_3 a_{2u}	v_4 b_{2g}	v_5 b_{2u}	v_6 $e_u(s)$	v_7 $e_u(b)$
hv	275	195	159	181	65	290	165
a_1'	-3.6385	0.0	0.0	0.0	0.0	0.0	0.0
a_2'	0.4643	0.5	0.5	0.5	0.5	0.5	0.5

z polarisation

$E(0)$	-4.9	0.0	0.0	0.0	65.0	0.0	0.0
$E(300)$	-8.5	0.0	0.0	0.0	10.1	0.0	0.0
$H(0)$	833.1	0.0	0.0	0.0	0.0	0.0	0.0
$H(300)$	1095.8	0.0	0.0	0.0	75.6	0.0	0.0

$E_{tot}(0) = 60.1$, $E_{tot}(300) = 1.6$, $\Delta E_{tot} = -58.5$

$H_{tot}(0) = 833.1$, $H_{tot}(300) = 1171.4$, $\Delta H_{tot} = 338.3$

xy polarisation

$E(0)$	-4.9	0.0	0.0	0.0	0.0	0.0	165.0
$E(300)$	-8.5	0.0	0.0	0.0	0.0	0.0	62.1
$H(0)$	833.1	0.0	0.0	0.0	0.0	0.0	0.0
$H(300)$	1095.8	0.0	0.0	0.0	0.0	0.0	180.0

$E_{tot}(0) = 160.1$, $E_{tot}(300) = 53.6$, $\Delta E_{tot} = -106.5$

$H_{tot}(0) = 833.1$, $E_{tot}(300) = 1275.8$, $\Delta H_{tot} = 442.7$

All units are in cm^{-1} except for a_1', a_2' which are dimensionless.

The calculated halfwidth at low temperature in xy polarisation (figure 9.8) agrees very well with experiment. However, the experimental observation that the halfwidth in z polarisation is ~100cm^{-1} greater than in xy polarisation is not reproduced. It should be noted however, that the contribution from these inducing modes can only be considered to be qualitative since the spectra due to these

(9.10)
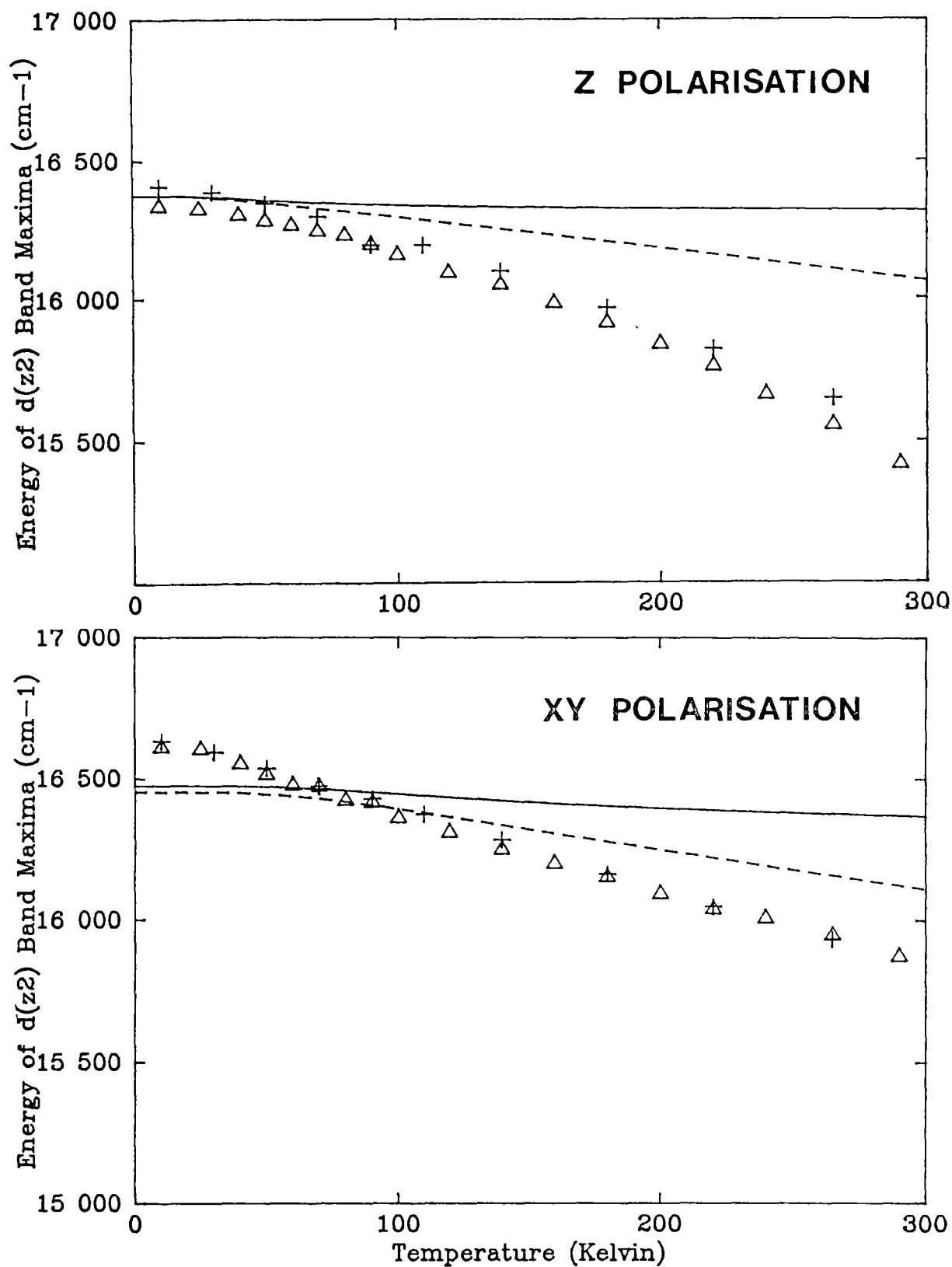
Figure 9.7 The temperature dependence of the band maxima.
Harmonic potentials with ———— hv′=hv; and — — — — hv′=0.75hv.

modes is far from Gaussian, and this is a condition under which the harmonic formulae were derived (section 3.6).

Still within the harmonic approximation, the same calculations were carried out except that the frequencies in the excited states were set to 75% of their ground state values (except the a_{1g} mode, where the known excited state potential was used as before). Even though this is probably an unrealistically large reduction, it will be shown that even this cannot account for the observed behaviour.

TABLE 9.3: Temperature dependence of band maximum and halfwidth.
Harmonic excited state potentials with frequency reduced by 0.75.

	v_1 a_{1g} 275	v_2 b_{1g} 195	v_3 a_{2u} 159	v_4 b_{2g} 181	v_5 b_{2u} 65	v_6 $e_u(s)$ 290	v_7 $e_u(b)$ 165
hv							
a_1'	-3.6385	0.0	0.0	0.0	0.0	0.0	0.0
a_2'	0.4643	0.2813	0.2813	0.2813	0.2813	0.2813	0.2813
z polarisation							
E(0)	-4.9	-21.3	-17.4	-19.8	43.7*	-31.7	-18.1
E(300)	-8.5	-48.9	-47.8	-48.4	-127.9*	-52.7	-48.0
H(0)	833.1	35.5	29.0	33.0	20.5*	52.8	30.1
H(300)	1095.8	81.4	79.6	80.7	152.6*	87.8	79.9
$E_{tot}(0)$ =-69.5,		$E_{tot}(300)$ =-382.2,		ΔE_{tot}= -312.7			
$H_{tot}(0)$ =1033.9,		$H_{tot}(300)$ =1657.8,		ΔH_{tot}= 623.9			
xy polarisation							
E(0)	-4.9	-21.3	-17.4	-19.8	-7.1	-31.7	110.9*
E(300)	-8.5	-48.9	-47.8	-48.4	-46.0	-52.7	-81.8*
H(0)	833.1	35.5	29.0	33.0	11.8	52.8	52.1*
H(300)	1095.8	81.4	79.6	80.7	76.6	87.8	227.0*
$E_{tot}(0)$ = 8.6,		$E_{tot}(300)$ =-334.2,		ΔE_{tot}=-342.8			
$H_{tot}(0)$ = 1047.2,		$E_{tot}(300)$ = 1728.9,		ΔH_{tot}= 681.6			

All units are cm^{-1} except a_1', a_2' which are dimensionless.
* These results are from a variational calculation.

(9.11)
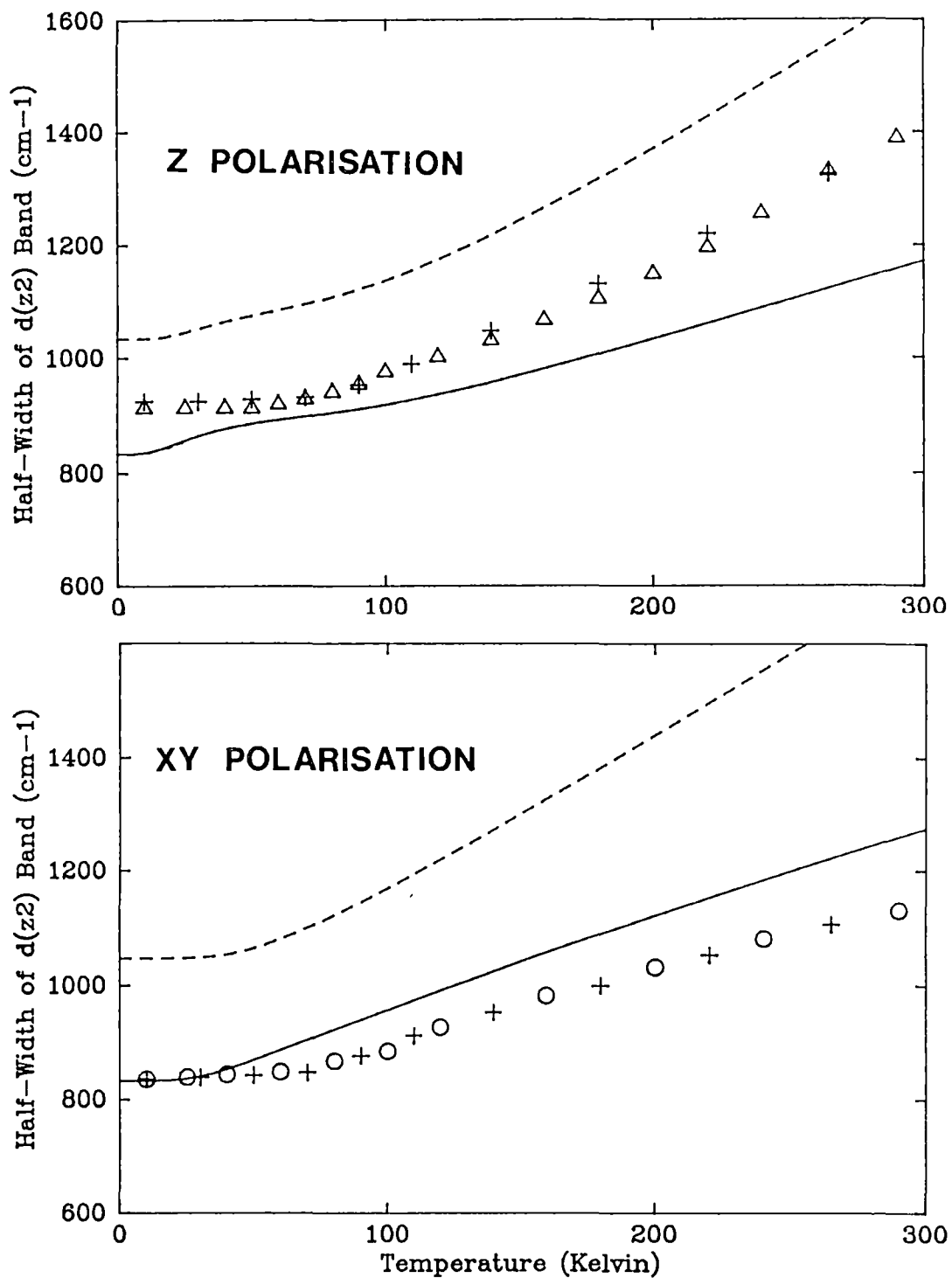
Figure 9.8 The temperature dependence of the halfwidth.
Harmonic potentials with ———— hν′=hν; and ———— hν′=0.75hν.

Equations (3.56) and (3.57) are again used for the non-inducing modes. The contribution from the inducing modes must now be calculated from the variational method, as the above equations assume harmonic potentials of equal frequency in the ground and excited states for these modes. The individual contributions are shown in table 9.3 and as dashed lines in figures 9.7 and 9.8.

The calculated shift in the band maxima is now closer to that observed experimentally. For instance, in z polarisation an overall shift of $\sim 300 \text{cm}^{-1}$ was calculated (cf. $\sim 60 \text{cm}^{-1}$ shift calculated for harmonic potentials of the same frequency) while a shift of $\sim 900 \text{cm}^{-1}$ is observed experimentally between 10-300K. However, the position of the band maximum in xy polarisation is again predicted at too low an energy.

From the above calculations, it is shown that the experimental temperature dependence of the band maxima of planar $CuCl_4^{2-}$ cannot be reconciled with harmonic excited state potentials. There is little difference in the results if the anharmonic ground state potentials given by (9.1) are used in the above calculations. Anharmonicity (in the conventional sense) in the excited state potentials will also make little difference. No anharmonicity was experimentally observed in the a_{1g} progression, and can only enter as even order terms in the normal coordinates of all other modes.

9.3.2 The Angular Overlap Potentials.

The bandshift and halfwidth of the $^2B_{1g}(x^2-y^2) \to {}^2A_{1g}(z^2)$ transition are now calculated using excited state potentials that have been derived using the angular overlap model. The ground state potentials are those found to reproduce the temperature dependence of the intensity in section 9.2. To these potentials are added the variation of the energy of the d-orbitals change relative to the ground state as a function of the appropriate symmetry coordinate. The way these potentials have been obtained is outlined in appendix 9.A2.

It should be noted that the stretching vibrations have not been considered. This is because they are of higher energy and therefore of less importance than the bending vibrations in the temperature range under consideration. Also, the excited state potentials are unlikely

to be very different to those of the ground state along these coordinates. [See appendix 9.A2 for a justification of this latter point.] The $\nu_1(a_{1g})$ potential is used as before.

TABLE 9.4: Temperature dependence of band maximum and halfwidth.
Excited state potentials from the angular overlap model.

	ν_1 a_{1g}	ν_3 a_{2u}	ν_4 b_{2g}	ν_5 b_{2u}	ν_5^* b_{2u}	ν_7 $e_u(b)$	ν_7^* $e_u(b)$
$h\nu$	275	159	181	65	65	165	165
a_1'	-3.6385	0.0	0.0	0.0	0.0	0.0	0.0
a_2'	0.4643	0.2408	0.5380	-0.0632	-0.0632	0.3224	0.3224
a_4'	0.0	0.00024	0.0012	0.00043	0.00043	-0.0005	-0.0005
E(0)	-4.9	-20.6	3.6	-23.2	-21.3	-23.8	35.9
E(100)	-5.1	-21.0	4.2	-54.7	-123.0	-33.0	-11.5
E(200)	-6.5	-39.8	6.5	-92.2	-237.0	-47.7	-67.0
E(300)	-8.5	-56.4	9.4	-129.6	-350.4	-61.2	-111.8
H(0)	833.1	34.2	6.3	36.6	53.6	37.2	44.6
H(100)	849.2	41.9	7.4	81.0	132.5	48.7	109.7
H(200)	957.5	66.0	11.7	140.7	233.6	68.1	152.9
H(300)	1095.8	93.6	17.4	201.8	337.8	87.3	184.7

TOTAL BAND-SHIFT:

Temperature	Z	XY
0	-67.0	-9.2
100	-182.0	-92.3
200	-324.5	-199.0
300	-467.1	-296.9

TOTAL HALFWIDTH:

0	964.4	954.8
100	1079.7	1089.2
200	1336.9	1328.8
300	1631.9	1593.3

* Indicates that this mode is inducing.
This will be ν_5 in z, and ν_7 in xy polarisations.

(9.13)

The excited state potentials used in this calculation are given in table 9.4. The ground state potentials are all assumed harmonic except for the v_5 and v_7 modes which are given by equation (9.1) from temperature dependence of the intensities. Also shown in table 9.4 are the individual contributions from these modes as well as the total band-shift and halfwidth for several temperatures. The total band-shift and halfwidth are compared with experimental values in figure 9.9. Again, agreement with experiment is not particularly good, though it is much better than that obtained with the harmonic potentials of the previous section. However, there are four main features in the figures 9.9a,b that qualitatively reproduce the experimental behaviour quite well. These features are:

i)   At low temperature the band maximum is at a lower energy in z polarisation than in xy polarisation.

ii) With increasing temperature the band maximum decreases in energy to a slightly greater extent in z polarisation than in xy polarisation.

iii) At low temperature the halfwidth is greater in z polarisation than in xy polarisation.

iv) With increasing temperature, the halfwidth increases to a slightly greater extent in z polarisation than in xy polarisation.

From table 9.4 it is seen that the greatest contribution to the shifts in the band maxima is made by the $v_5(b_{2u})$ vibrational mode. This is for two reasons: first this mode is of low energy and will be populated to a greater extent at a particular temperature; and second, the excited state potential derived from AOM considerations has a double minimum.

This potential has its two equivalent minima at a D_{2d} geometry along the b_{2u} symmetry coordinate (see figure 9.13). This coordinate is the one that takes the square planar configuration towards a tetrahedral geometry. A D_{2d} geometry is the one commonly adopted by the $CuCl_4^{2-}$ ion, the square planar compounds studied here being exceptions. It is therefore not surprising that in the excited states where an electron is promoted to the $d(x^2-y^2)$ anti-bonding orbital, the molecule adopts the preferred D_{2d} geometry. It should be noted that the excited state potential is not <u>displaced</u> along the b_{2u} symmetry coordinate. This would require linear term in the potential, and such

(9.14)
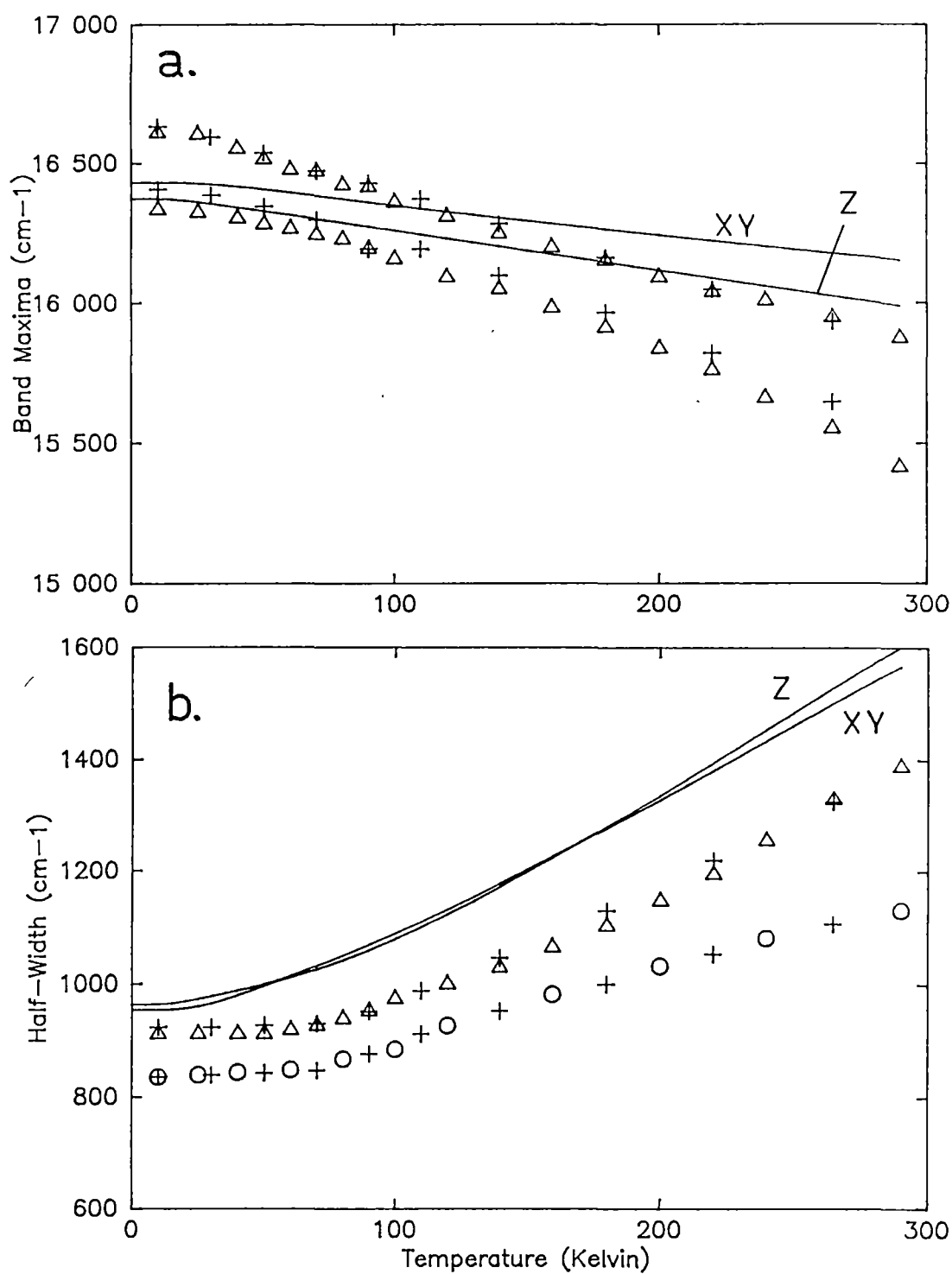
Figure 9.9 The temperature dependence of the spectrum using angular overlap potentials. a) Band Maxima. b) Halfwidths.

a term must be zero by group theory. A double minima potential however is allowed by group theory because it is made of even order terms (see section 3.2).

To improve the agreement to the experimental data, all seven potentials of the normal modes could be varied to "fit" the data, but the problem would be impossibly underdetermined. From the above calculations it can be seen that it is the low frequency b_{2u} mode that is by far the most important in determining the temperature dependent phenomena, and in the following section this potential will be allowed to vary. A discussion of why the AOM potentials are apparently inadequate in reproducing the exact behaviour that is observed will be given in section 9.5.

9.3.3 Improving the fit.

In this section the basic double well excited state potential of the b_{2u} mode is retained, and the effects of varying the position and depth of the two wells are examined. All other potentials are kept the same as in table 9.4. Figure 9.10a shows the red shift of the band maxima between low (T=0K) and room (T=300K) temperatures for several different potentials. Here E_{min} represents the well depth and three sets of curves where E_{min}= -500,-1000,-1500 cm^{-1} are shown for both xy and z polarisations. The abscissa in figure 9.10, θ_{min}, is the position of these minima along the b_{2u} coordinate. These two quantities are simply related to the dimensioned coefficients that make the double minima potential (the relationship between the dimensioned (c_2, c_4) and dimensionless (a_2, a_4) are given in appendix 9.A2):

$$\theta_{min} = \left(\frac{c_2}{2c_4}\right)^{1/2}, \quad E_{min} = -\frac{c_2^2}{4c_4} \quad (9.3)$$

As might be expected, the red shift is greater in z polarisation, where the double well is an inducing mode, than in xy polarisation where it is not. This is because in the former case the overlaps are dependent on the coordinate and are calculated greater for the higher ground state vibrational levels, while in the later case the overlaps are the normal Franck-Condon factors. This shift in the curves of figure 9:10a are seen to increase as the minima become closer.

(9.15)
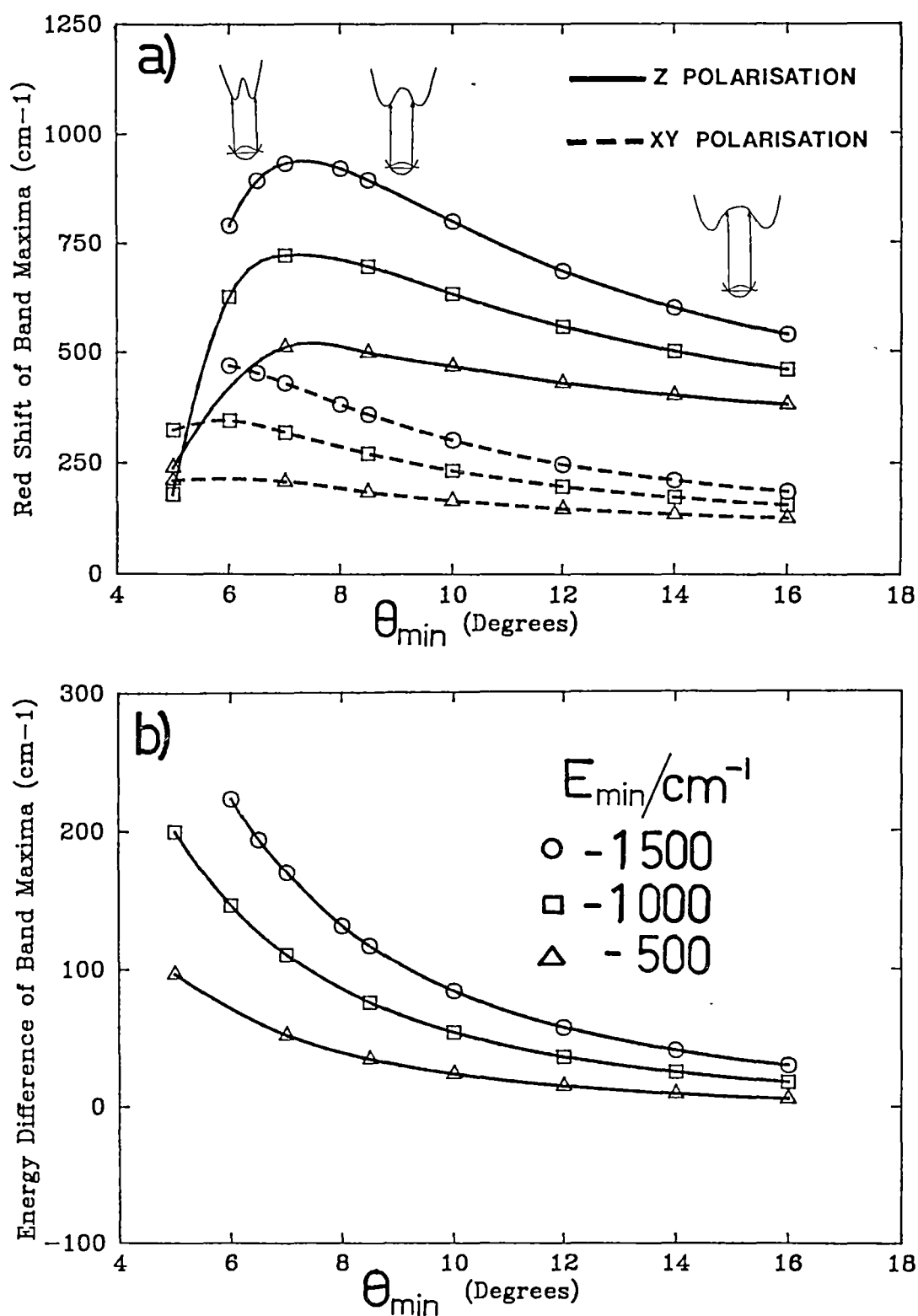
Figure 9.10 The spectrum obtained from various b_{2u} potentials.
a) Shift of band maxima in xy and z polarisations.
b) Difference of band maximum in xy and z polarisations

Classically this can be visualised as due to the "time averaged" or root-mean-square geometry at higher temperatures cutting the excited state potential at a lower energy as the minima move closer together. That is, the slope of the excited state potential becomes steeper in the region of the coordinate that is populated in the ground state. There reaches a point, however, where this trend reverses as overlaps on the outside of the wells become important. This is indicated schematically in figure 9.10a. Note that this occurs sooner in z polarisation because, again, the "outside" overlaps (ie those from higher ground state vibrational levels) are weighted more.

If this is carried to an extreme, by moving the minima close together, the transition will shift to <u>higher</u> energies (ie blue shift) between 0 and 300K. Calculation of the intermediate temperature dependence reveals that the spectrum will first shift to lower energies and then reverse to higher energies. This type of behaviour also occurs for a harmonic inducing mode that is of higher frequency in the excited state (Lohr 1970). This illustrates that the shape of the curve representing the temperature dependence of the band-shift can be controlled to some extent by varying θ_{min}.

Figure 9.10b shows the difference of the mean energy in xy and z polarisations at low temperatures (0K). For all values of θ_{min} the band maximum is seen to be of higher energy in the xy than the z polarisation. This is again a consequence of the fact that the overlaps of the higher ground state levels are weighted more when the potential is inducing. This agrees with what is observed experimentally, and the calculation of this splitting can again be controlled by varying θ_{min}.

The approach to finding the appropriate potential was as follows: Three main experimental observables must be fulfilled: a red shift of ~920cm^{-1} in z polarisation, and ~800cm^{-1} in xy polarisation between 10 and 290K, and the xy polarised band maximum ~200cm^{-1} higher in energy than that in z. From table 9.4 it can be found that, not counting the a_{1g} and b_{2u} modes, the potentials of all the remaining modes contribute 71cm^{-1}, 181cm^{-1} and 60cm^{-1} respectively to the above three quantities. Therefore, to fit experiment, the differences must be made up by the contribution of the b_{2u} mode.

The required ~850cm^{-1} for the band-shift in z polarisation, must come from the E_{min}=-1500cm^{-1} curve as neither of the other two curves

(9.16)
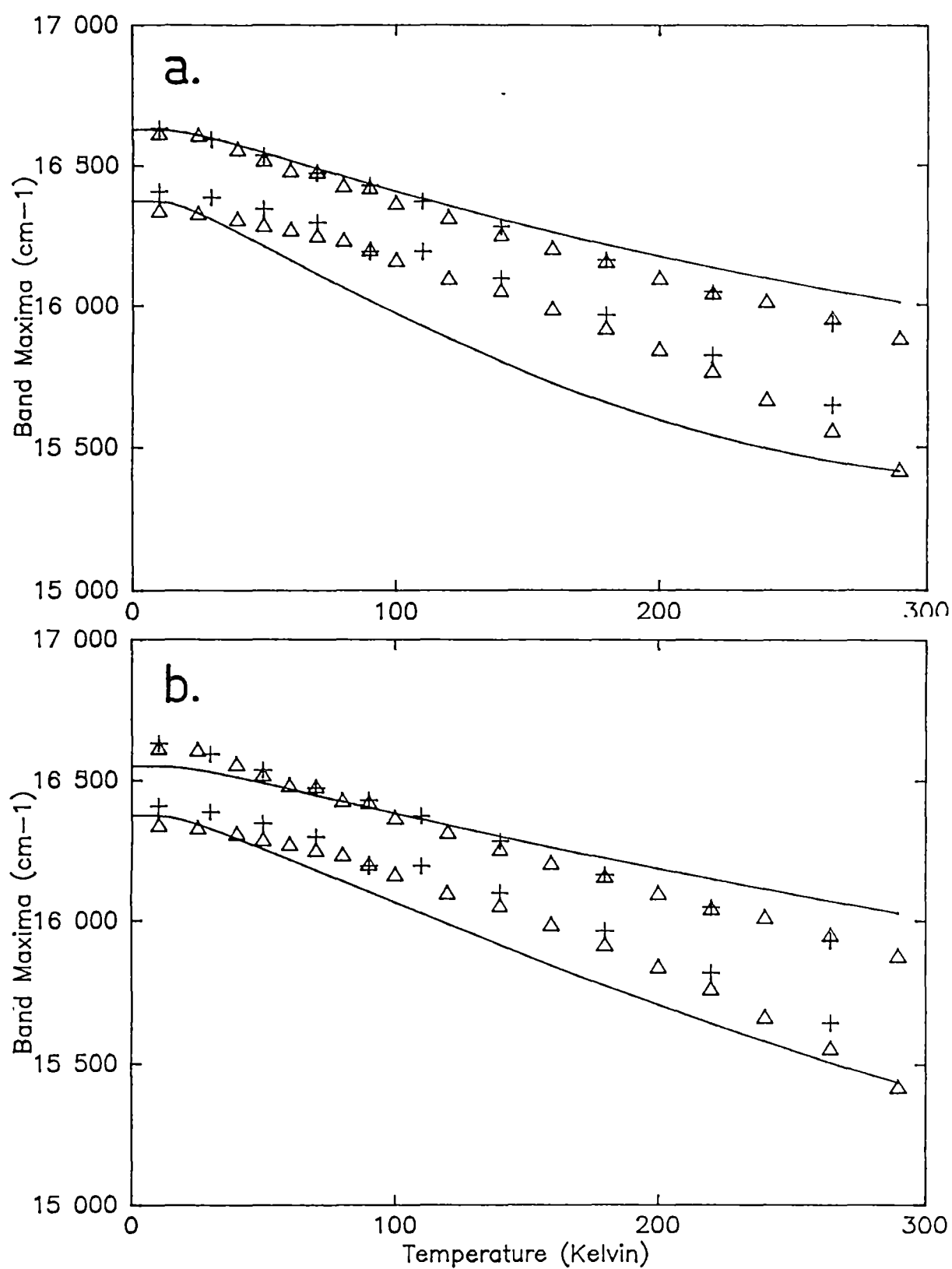
Figure 9.11 The temperature dependence of the band maxima using $E_{min} = -1500 \ cm^{-1}$ and a) $\Theta_{min} = 6.5^{\circ}$ or b) $\Theta_{min} = 8.5^{\circ}$.

approach this value. Values of θ_{min}= 6.5, 8.5 degrees (marked by arrows in figure 9.10) roughly fit the desired quantities, and the temperature dependence of the band-shift using these two potentials are shown in figure 9.11. All three of the above experimental observables are well accounted for, but the potential with θ_{min}= 8.5° appears to better reproduce the shape of the curves at intermediate temperatures. The ground and excited state b_{2u} potentials used in this calculation are shown in figure 9.13 along with the angular overlap potential of the previous section for comparison.

It is not really possible to improve this fit by further adjusting the excited state potential of just the b_{2u} coordinate. The correct downward curvature observed experimentally in figures 9.11 can only be reproduced with a potential with a larger θ_{min}. As can be seen from figure 9.10, this will increase the disagreement with the band-shift in xy polarisation and also the energy difference of the band maxima at low temperature. This can be rectified by varying the e_u(b) potential so that it contributes more to the band shifts (but this time to a greater extent in xy than in z polarisation).

This has not been done because an exact fitting of the calculated and experimental spectrum is not desired, but rather a model that can explain these unusual features. It is felt that the less free parameters used, the more meaningful (and believeable) the model becomes. In the present case the gross features of the temperature dependence of the spectrum can be reproduced by allowing only the two parameters, E_{min}, θ_{min} to vary; all other potentials being determined by the angular overlap model. [The small anharmonicity introduced to explain the deviation of the coth rule in section 9.2 has little effect on the above calculations. It is therefore essentially an independent problem.]

Turning finally to the variation of the halfwidth with temperature, it can be seen in figure 9.12 that the halfwidth for both potentials with θ_{min}= 6.5°, 8.5° grossly overestimate the observed values. As discussed in section 3.6.1, this is because the non-totally symmetric modes contribute a non-Gaussian spectrum and so the halfwidth is not simply related to the second spectral moment. This can be seen in figure 9.12 where, contrary to experiment, an early increase in the halfwidth between 0-100K is due to the calculated contribution from a low frequency mode. In the present study a moments

(9.17)
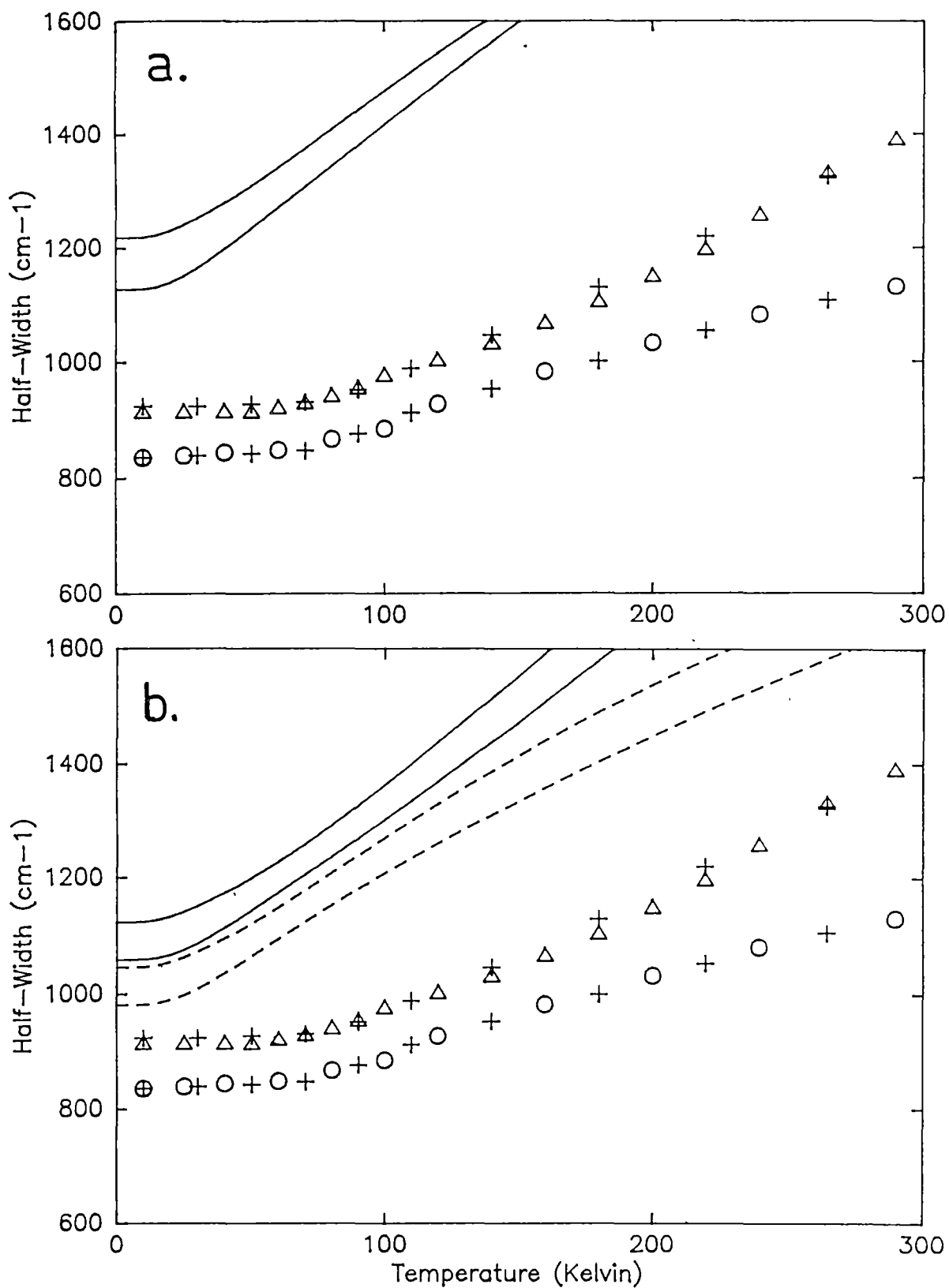
Figure 9.12 The temperature dependence of the halfwidths for potentials as in figure 9.11. ———$\Delta S(a_{1g})=21.4$pm, — — —$\Delta S(a_{1g})=19.4$pm.
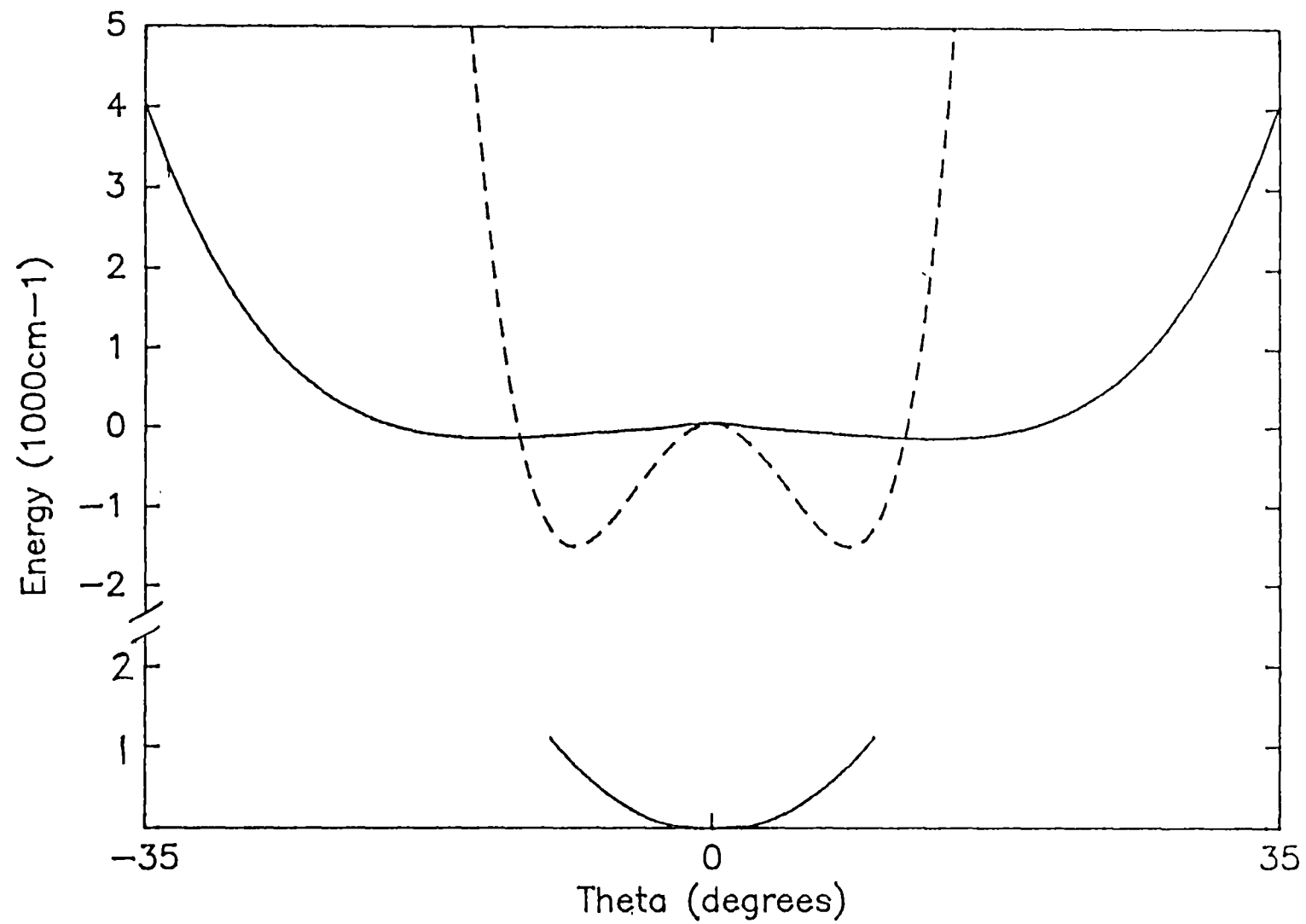
Figure 9.13 The b_{2u} excited state potentials.
——— AOM derived. — — — Experimentally derived.

analysis is inappropriate to the calculation of the halfwidth. Simulating the spectra, which involves plotting the energy and intensity of each vibronic transition, provides a clearer picture of what is occurring.

The non-totally symmetric vibrations will have some contribution to the halfwidth, and this then means that one must be careful when a Franck-Condon analysis is performed on a structureless band using the halfwidth of the spectrum. The true displacement may then be overestimated. The dotted curves in figure 9.12b show the same calculation for $\Delta S(a_{1g}) = 19.4pm$ instead of $\Delta S(a_{1g}) = 21.4pm$.

9.4 SPECTRAL SIMULATION

9.4.1 The Low Temperature Spectrum.

In this section the low temperature spectrum shown in figure 9.2 is reproduced by considering only the spectrum due to the displacement of the potential surface of the a_{1g} mode built on a single vibronic origin. This procedure is known as Franck-Condon analysis and provides information about the geometry change in the excited state.

From vibrational studies and the spacing of the progression in the low temperature vibronic spectra, the ground and excited state frequencies are found to be $v_1(a_{1g}) = 275cm^{-1}$ and $v_1'(a_{1g}) = 265cm^{-1}$ respectively. The spectra calculated with various values for the displacement of the a_{1g} symmetry coordinate are shown in figure 9.14. Optimum agreement was found with $\Delta S(a_{1g}) = 20.8pm$ (figure 8.14b), which is close to the value reported in the literature ($\Delta S(a_{1g}) = 21.2pm$, McDonald and Hitchman 1986). The experimental vibrational frequencies and a displacement of 20.8pm correspond to the following potentials:

$$V_g(S) = 3.975\ S^2 \qquad S \equiv S(a_{1g}) \qquad (9.4)$$
$$V_e(S) = 3.690\ S^2 - 153.541\ S$$

These potentials can be reexpressed in terms of the dimensionless coordinates that are appropriate to a variational calculation:

$$V_g(\xi) = 0.5\ \xi^2 \qquad (9.5)$$
$$V_e(\xi) = 0.4643\ \xi^2 - 3.284\ \xi$$

The energy units are $hv = 275cm^{-1}$, and the interconversion of these "force constants" are given by equation (9.A7) in appendix 9.A2. The appropriate mass M to use in this equation is that of one chloride ligand. A displacement of $\Delta S(a_{1g}) = 20.8pm$ implies that the individual Cu-Cl bondlengths change by $\Delta r = 10.4pm$ in this excited state. The actual Franck-Condon overlaps that were calculated in this case (figure 9.14b) are given in table 9.5 below for reference.

(9.19)
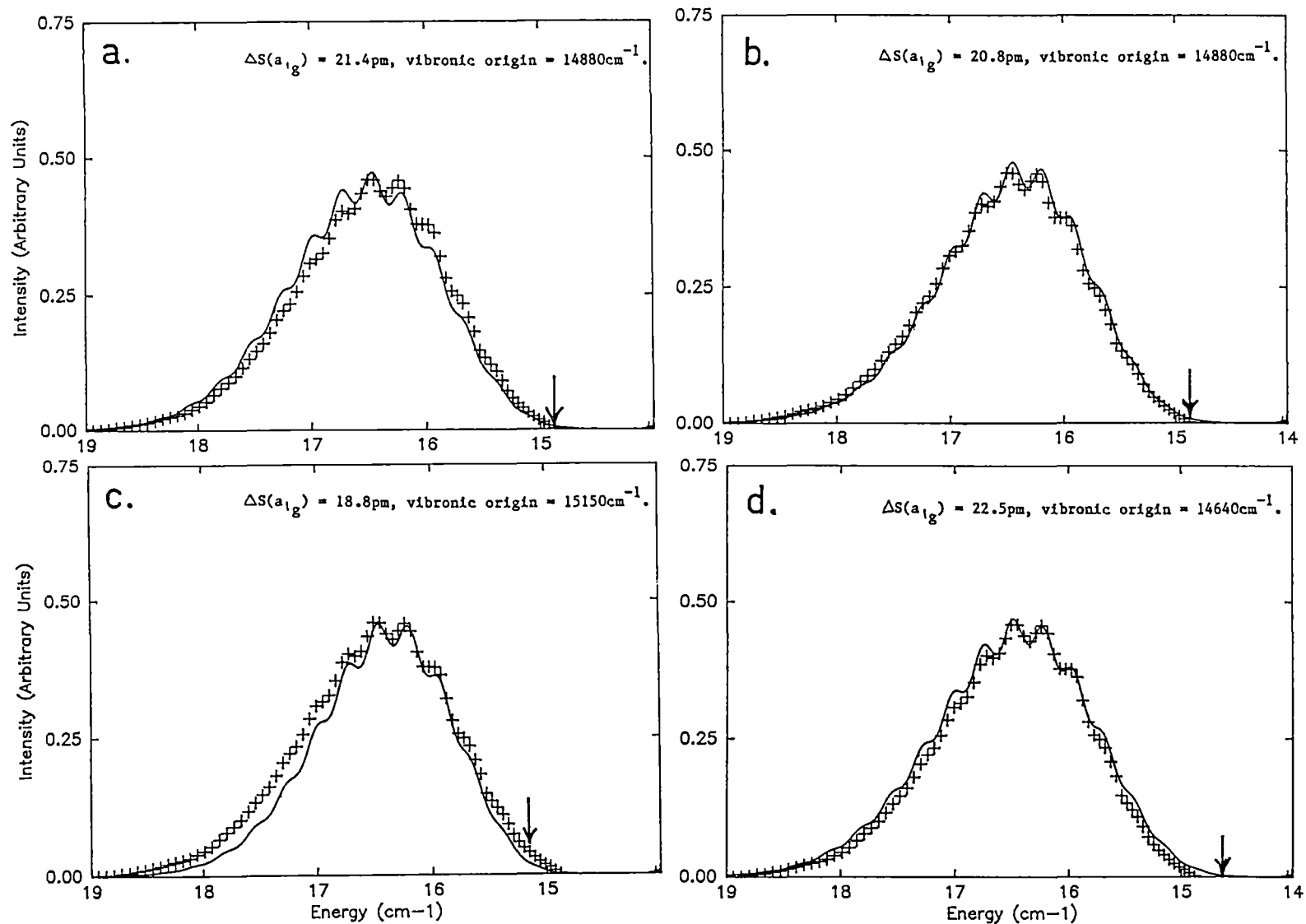
Figure 9.14 Franck-Condon analysis of the low temperature spectrum.
$h\nu_g = 275\text{cm}^{-1}$, $h\nu_e = 265\text{cm}^{-1}$, halfwidth (HWHH) = 135cm^{-1}.

Table 9.5

Franck-Condon overlaps for $h\nu=275cm^{-1}$, $h\nu'=265cm^{-1}$, $\Delta S(a_{1g})=20.8pm$

n	0	1	2	3	4
$\langle 0\|n\rangle$	0.04648	-0.11621	0.20483	-0.29392	0.36414
n	5	6	7	8	9
$\langle 0\|n\rangle$	-0.40229	0.40446	-0.37531	0.32475	-0.26410

These overlaps can either be calculated from the recursion relationship in equation (3.17), the formula in equation (3.18), or from variational methods. It must be remembered that the absorption and emission of radiation are frequency dependent, and a frequency factor must be included in the expression for the intensity when the spectrum is simulated.

As a note of warning figures 9.14c,d also show quite a good fit to the experimental spectra using $\Delta S(a_{1g}) = 18.8pm$ and $\Delta S(a_{1g}) = 22.5pm$. This is achieved with a shift in the electronic origin as indicated by the arrows. Therefore, if the vibronic origin of the progression is not definitely known, as in the present case due to the overlapping bands, then there is some ambiguity as to the magnitude of the displacement. It can be seen that the shape of the spectrum does not change much when the displacement takes the values 18.8pm, 20.8pm, 22.5pm (intermediate values will give the wrong relative intensities of the peaks), the bandwidth becoming slightly greater with increasing displacement. Classically this can be rationalised by noting that for an excited state parabola that has a large displacement (as in the present case) further displacements do not greatly change the slope of the excited state parabola that lies vertically above the minima of the ground state.

The Franck-Condon analysis of a low temperature spectrum is reasonably straightforward and is commonly used to extract information about the excited state geometry along totally-symmetric coordinates. It is less common to find information about the excited state geometry along non-totally symmetric coordinates, as in the present case from an analysis of the temperature dependence of a spectrum.

(9.20)

9.4.2 The Temperature Dependent Spectrum.

In simulating the temperature dependent spectrum, the potential surfaces of only two of the normal modes are considered. These are the potentials of the totally symmetric mode $v_1(a_{1g})$ and the inducing mode, $v_5(b_{2u})$ and $v_7(e_u(b))$ in the z and xy polarisations respectively. The first provides the low temperature envelope of the displaced a_{1g} surface, and the later provides the intensity and vibronic origins that the former are built on. Both will be temperature dependent, the later being more so. The effect of the other normal modes cannot be ignored (especially the b_{2u} mode in xy polarisation, see table 9.4), so energy shifts due to these modes are included. Note that these "other" modes are all "non-inducing" and contribute nothing to the intensity.

The calculated line spectrum is then given a finite halfwidth to compare with the experimental spectrum. A halfwidth is chosen to fit the low temperature spectrum (ie see previous section) and this is then kept constant for simulating the spectra at all other temperatures. As before the electronic origin is chosen to reproduce the low temperature spectrum in z polarisation.

The spectrum calculated from the AOM potentials (table 9.4) is compared to experiment in figure 9.15. The intensity variation with temperature is well reproduced because the ground state has been chosen in section 9.2 to do this. The failing of these potentials is the same as found in the moments analysis, but here it is particularly easy to see that:

    i)   The band shift is far too small in both polarisations.

    ii)   The low temperature spectrum in xy polarisation is too low in energy.

    iii) The vibrational fine structure does not disappear as fast as is observed experimentally.

The simulated spectra using the potential obtained in section 9.3 for the b_{2u} mode are shown in figure 9.16, where all that is changed in the various curves is the temperature. In z polarisation the intensity, bandshift and disappearance of the vibrational structure are all well reproduced. The agreement is also good in the xy polarisation in
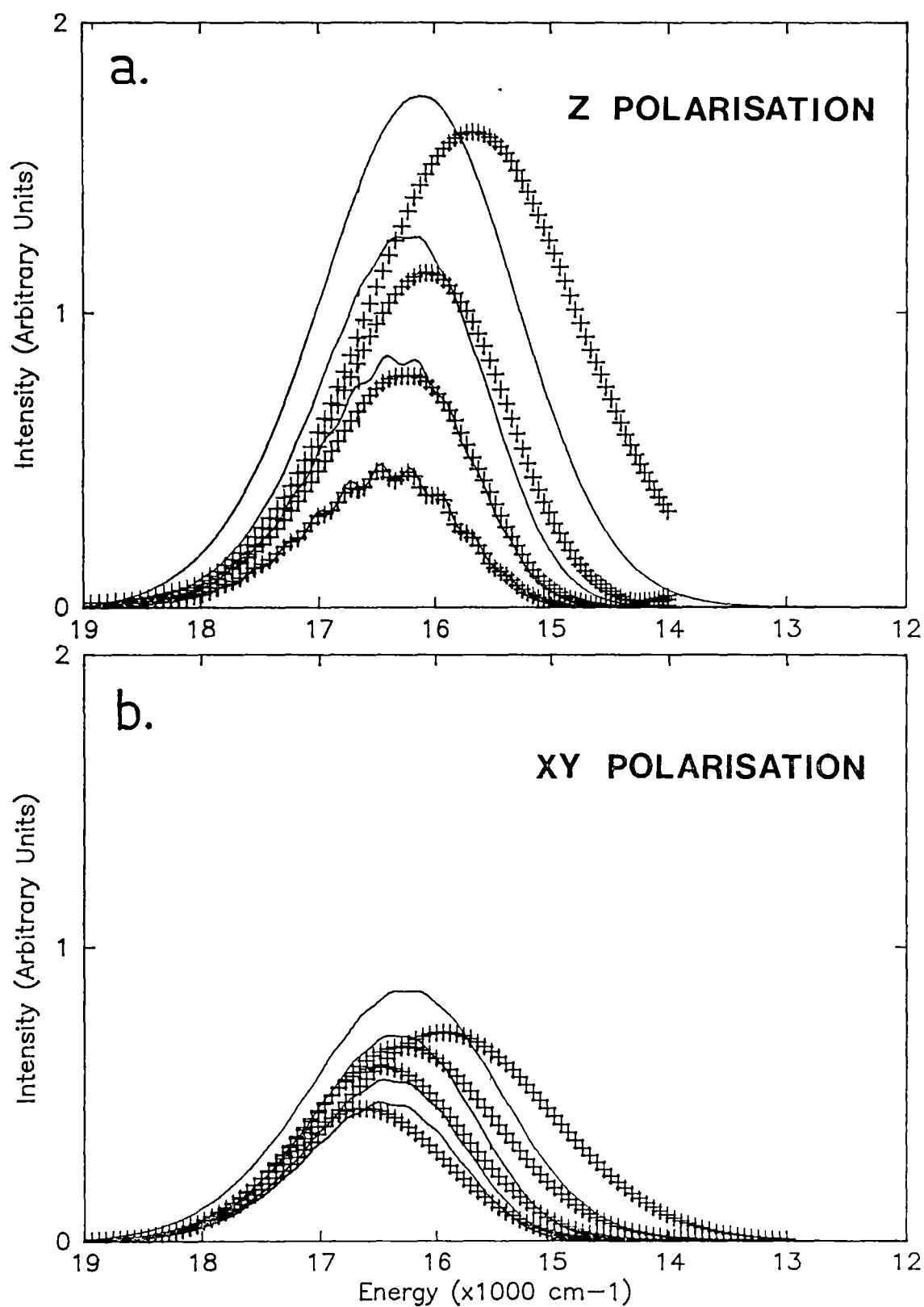
Figure 9.15 Experimental spectra of the $^2B_{1g}(x^2-y^2) \to {}^2A_{1g}(z^2)$ transition and the spectrum calculated from the AOM potentials. a) z polarisation, b) xy polarisation.
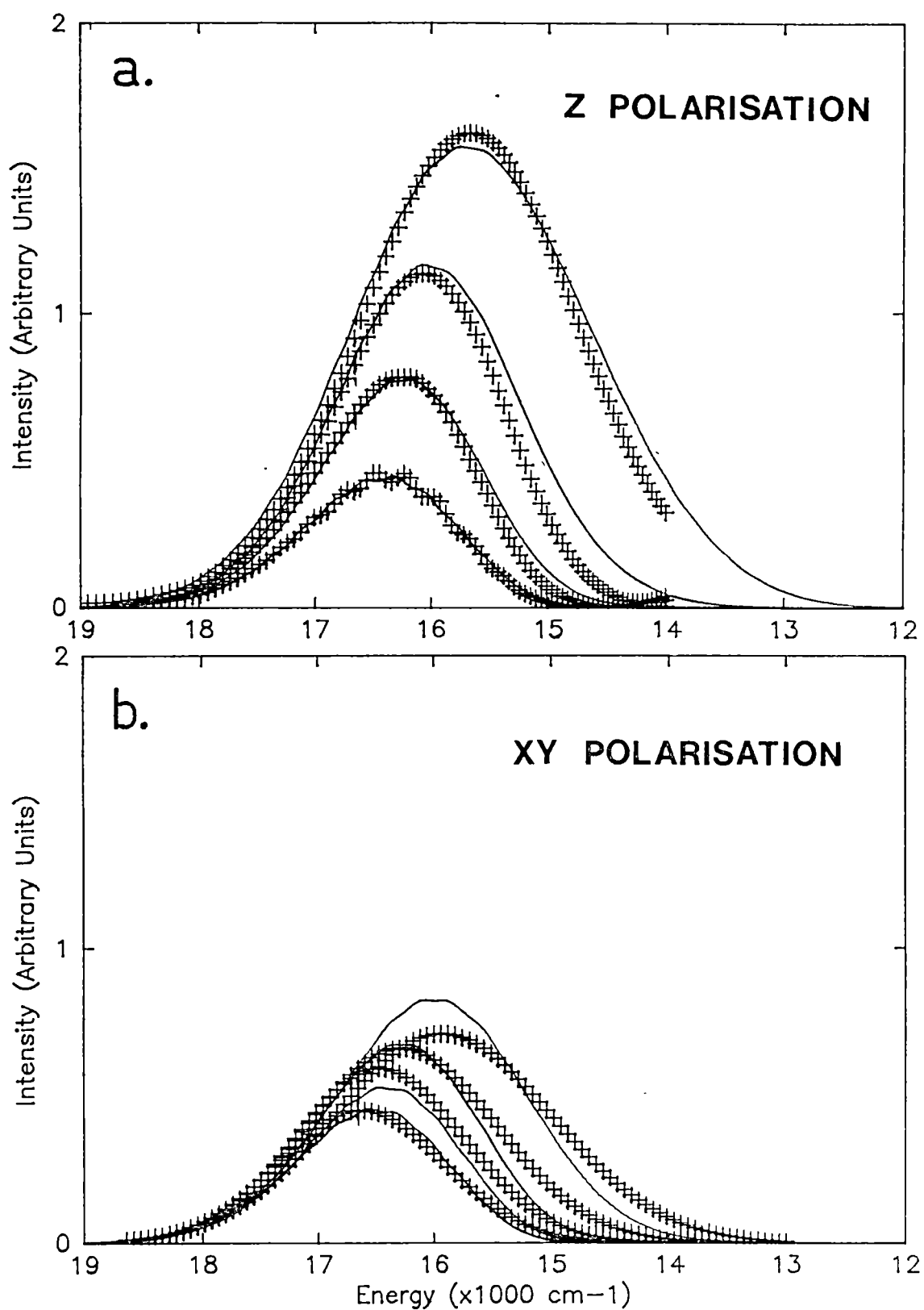
Figure 9.16 Experimental spectrum of the $^2B_{1g}(x^2-y^2) \rightarrow {}^2A_{1g}(z^2)$ transition and the spectrum calculated from the AOM potentials and a b_{2u} potential as in figure 9.11b.

a) z polarisation, b) xy polarisation.

terms of the position of the low temperature spectrum, and the variation of the intensities and bandshift with temperature. However, at higher temperatures, the experimental spectrum is much broader than the calculated one. This is as one would expect because in this polarisation, the b_{2u} mode is non-inducing and only the contribution to the band shift has been included from it. A substantial contribution to the increase in the halfwidth with temperature would be expected from this mode.

In principle the effect of all modes should be considered in both polarisations, as they will contribute to both the shift in the band maximum and the increase in halfwidth (but not to the intensity). However, this becomes a huge calculation as each vibronic transition within one mode acts as a vibronic origin for the "progression" in all other modes. However the two mode model use here to calculate figures 9.15-16 seem to work quite adequately as long as its limitations are realised.

9.4.3 Implications for the Vibrational Fine Structure.

In the previous section it was shown that the structure due to the low temperature a_{1g} progression was correctly calculated to broaden with increasing temperature. To illustrate how this occurs figure 9.17a shows the calculated temperature dependence of the spectrum due only to transitions between the b_{2u} vibrational levels in z polarisation. Here the "vibronic origin" is seen to both increase in intensity and halfwidth as well as shifting to the red. [The unusual bump seen in the highest temperature spectrum in figure 9.17a is superfluous and provides a good example of the effects of truncation error. The basis size (60×60 in this case) in the variational calculation was insufficient to converge all the eigenvectors in the overlaps between the populated levels at this temperature.] If the halfwidth of the vibronic lines that make up the band in figure 9.17a is made very small, the rich underlying structure of 9.17b is revealed. The "vibronic origin" in figure 9.17a is actually composed of thousands of vibronic lines, each which can serve as an origin for the a_{1g} progression.

What is of interest in this section is whether any effects due to underlying structure of the sort shown in figure 9.17b can be detected

(9.22)
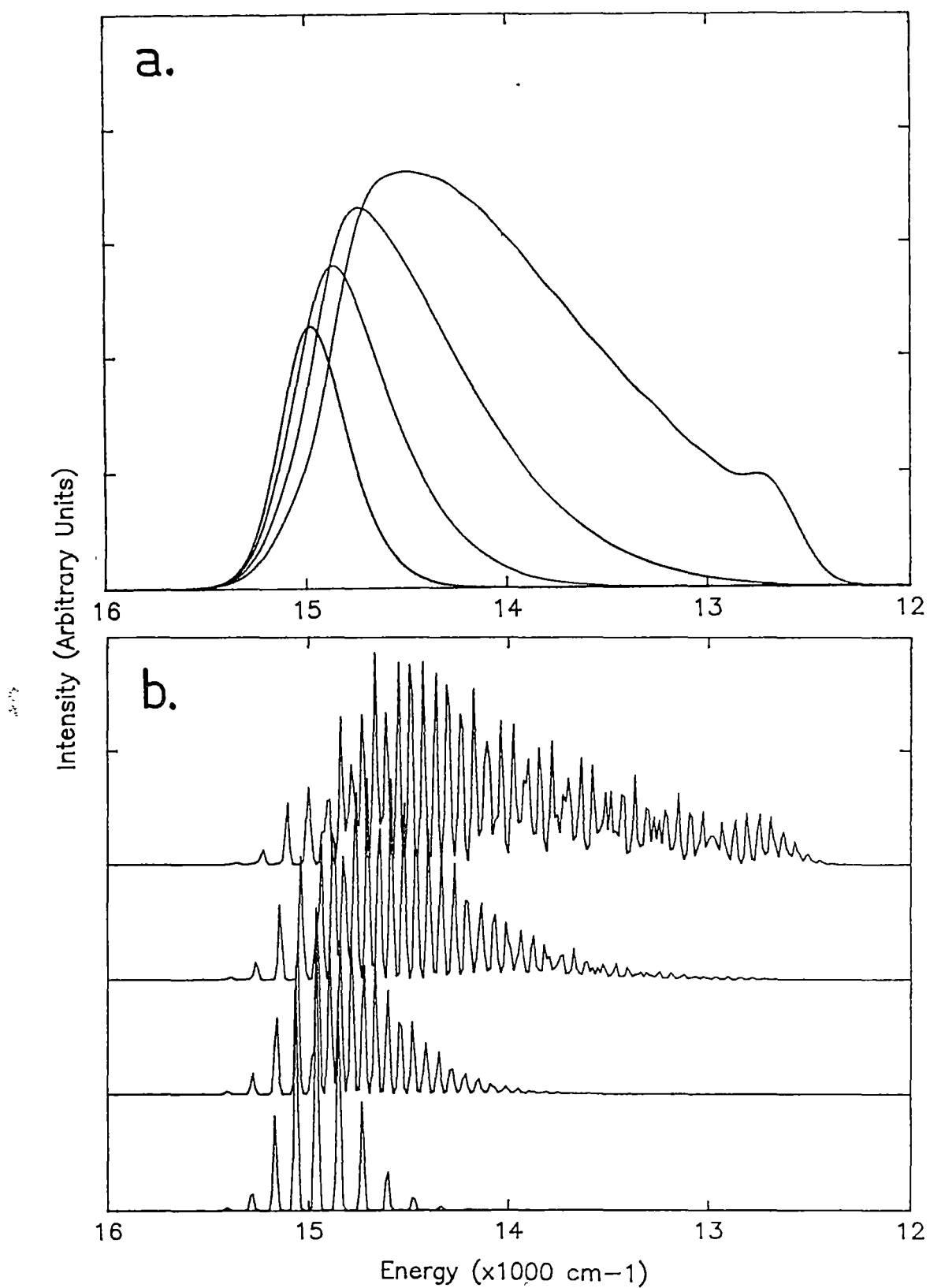
Figure 9.17 The spectrum due to the b_{2u} mode only.
a) Low resolution (HWHH=135cm^{-1}), b)High resolution (HWHH=12cm^{-1}).

in the vibrational fine structure of the spectrum. In particular, it is of interest to investigate what sort of deviations could be expected from the usual model where equal harmonic frequencies are assumed for both the ground and excited states of the non-totally symmetric modes.

To show that such a "high resolution" study may be feasible, figure 9.18 shows the spectrum of this same $^2B_{1g}(x^2-y^2) \rightarrow\ ^2A_{1g}(z^2)$ transition in the complex $(NmpH)_2CuCl_4$ which also contains planar $CuCl_4^{2-}$ species. This spectrum was taken at 4.2K and is considerable more resolved than those shown in the previous figures. This structure may sharpen even more at lower temperatures.

Some effects from different potentials are investigated where a small halfwidth is used to make these changes more obvious, and the electronic origin is held fixed at 15,000cm^{-1}. The a_{1g} potential corresponding to hv=275cm^{-1}, hv'=265cm^{-1} and $\Delta S(a_{1g})$=20.8pm (equation (9.5)) is used throughout.

Figure (9.19a) shows the behaviour when the inducing mode has equal frequencies, hv=60cm^{-1}, in both the ground and excited states. The inset shows the spectrum due to this mode alone. Here the intensity of the n $\rightarrow$ n+1 and the lower energy n $\rightarrow$ n-1 transitions both increase with temperature, and in the limiting case at high temperature these two vibronic peaks approach equal intensity. In the complete spectrum, if the components of the a_{1g} envelope were sharp "lines", then a new a_{1g} envelope shifted 2hv=120cm^{-1} to lower energies would be expected to grow with temperature. However, as these components have a finite halfwidth, when the two envelopes are added then the effect of the n $\rightarrow$ n-1 transitions is to make these components appear to gradually shift to the red and increase in halfwidth.

If the same calculation is performed with a much reduced excited state frequency (hv=60cm^{-1}, hv'=30cm^{-1}) for the inducing mode, then spectrum shown in figure 9.19b is obtained. The spectrum due to the inducing mode shown in the inset. This spectrum shows different behaviour than the previous case, as the n $\rightarrow$ n±1 selection rule breaks down and are replaced by a n $\rightarrow$ n±1,±3,±5,.. type selection rule, as discussed in section 3.4. The overall effect when the many transitions are given halfwidths and summed is, in the terminology of the previous spectrum, that the n $\rightarrow$ n+1 type peak <u>decreases</u> while the n $\rightarrow$ n-1 type peak increases with temperature. The total spectrum appears similar to
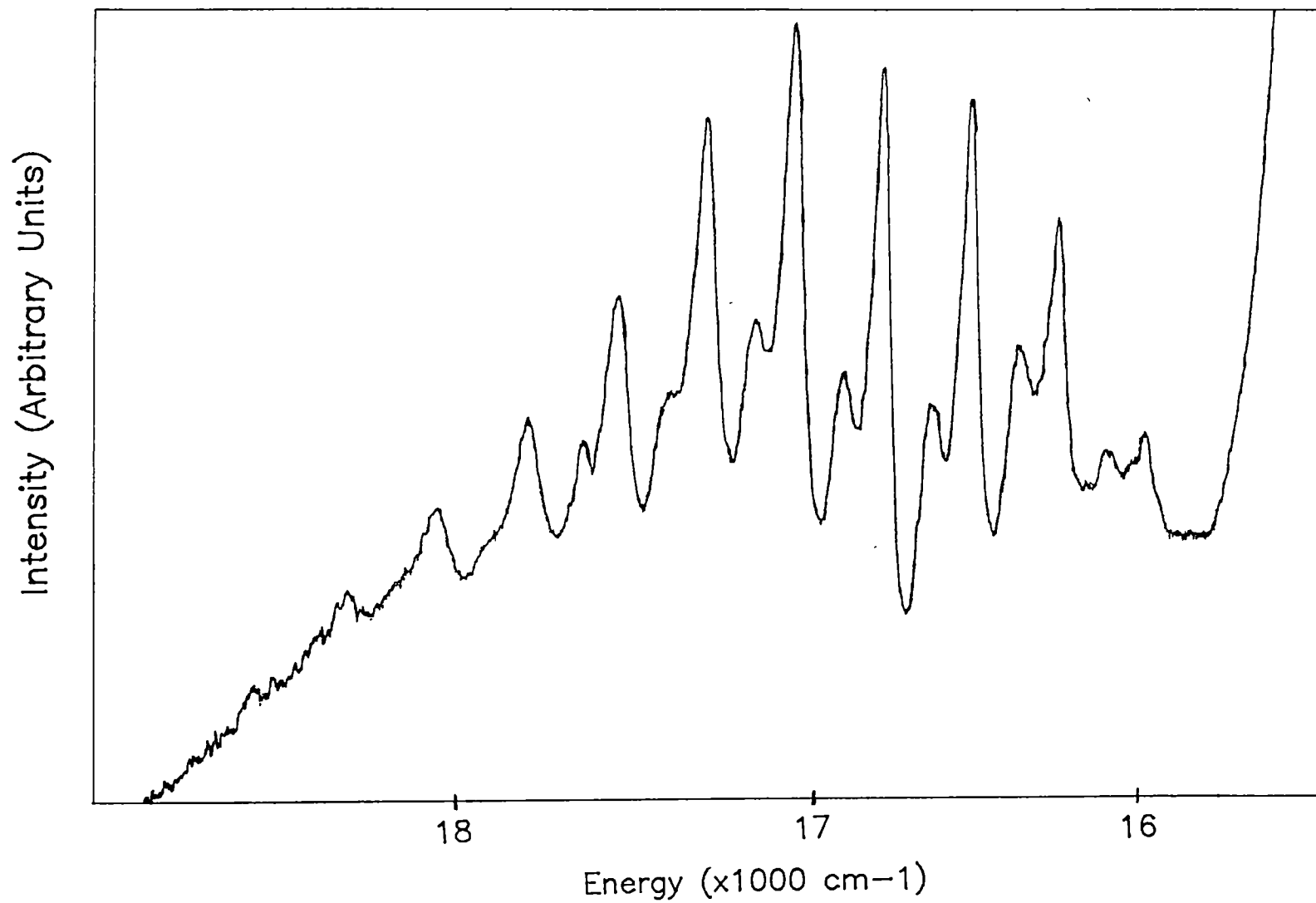
Figure 9.18 Experimental spectrum of (NmpH)$_2$CuCl$_4$ at 4.2K.
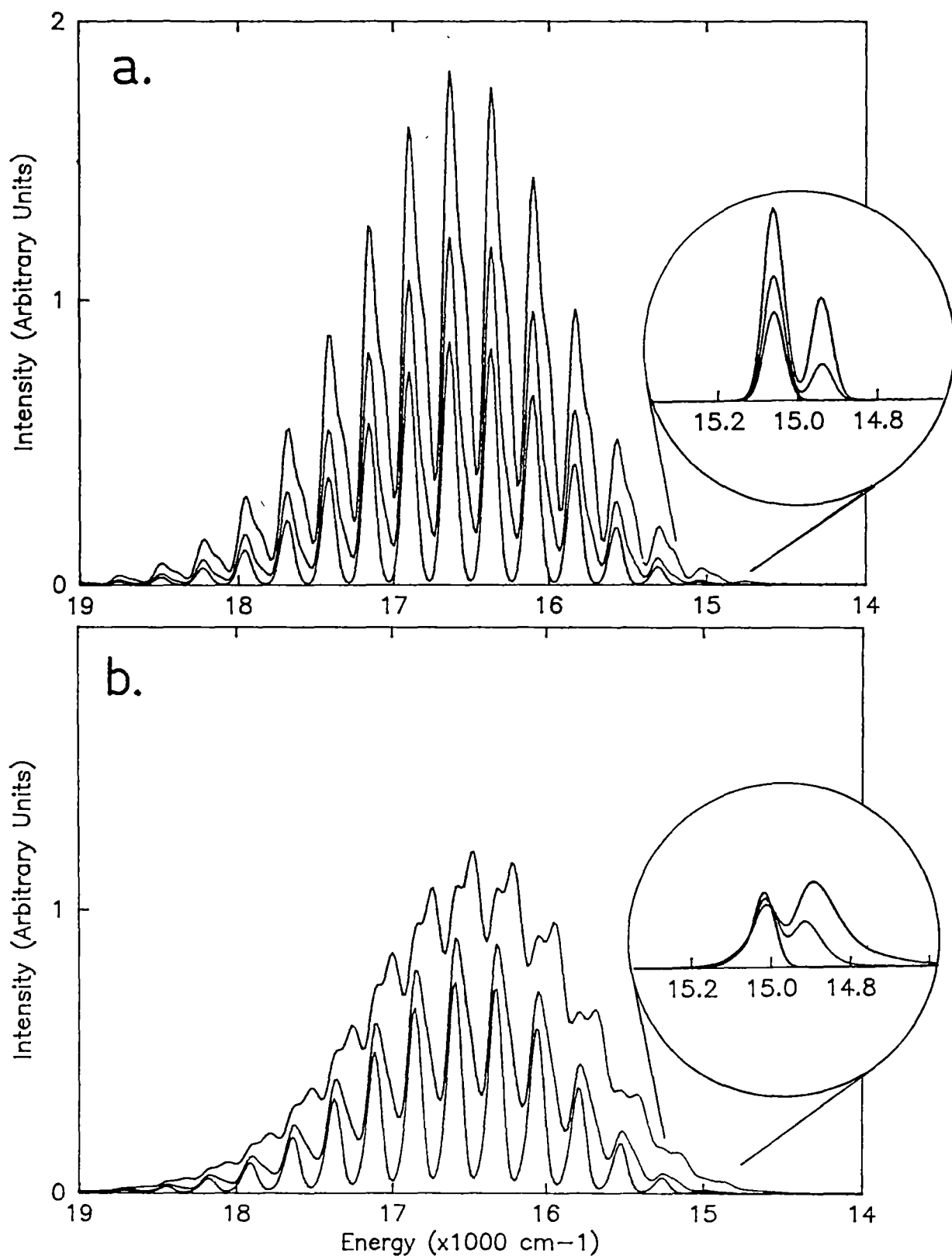
Figure 9.19 Temperature dependence of the structure of the spectrum with a harmonic inducing mode. The insets show the specta due to the inducing mode only. The a_{1g} potential as for figure 9.14b except halfwidth = $60cm^{-1}$. a) $hv'=hv=60cm^{-1}$, b) $hv=60cm-1$, $hv'=30cm^{-1}$. Temperatures = 0, 75, 150K with increasing intensity.

the previous example where the components of the a_{1g} progression appear to broaden and shift to lower energies. However, there are subtle differences. In the previous example, the spectrum at the energies where the maxima of the components were located at low temperature increased substantially in intensity with temperature. In the second example, however, the positions in the spectrum that were the low temperature peaks do not change very much and can actually <u>decrease</u> in intensity with increasing temperature. This behaviour can be understood simply by looking at the spectrum of the vibronic origins of the inducing modes alone in the insets of figure 9.19, and observing their intensity variation with temperature. Behaviour of this second type has been observed (Hitchman 1986).

The spectrum calculated with the double well potential of the b_{2u} mode that was found to reproduce the experimental data in section 9.3, is given in figure 9.16. If this calculation is repeated using a smaller halfwidth, then the hypothetical spectrum of planar $CuCl_4^{2-}$ at high resolution is obtained in figure 9.20. This spectrum shows some similarities to the experimental spectrum at 4.2K shown in figure 9.18, both in that the a_{1g} progression appears to be based on two origins, and that the intensity distribution in these two progressions are different. The intensity distribution is expected to be the same for both origins as there is only one a_{1g} potential surface. Examining the spectrum due to the b_{2u} mode alone in the inset of figure 9.20, it is not obvious why two "origins" appear in the convoluted spectrum, but appears to be the result of an interference pattern. Such vibronic structure is similar to the that seen in the MIME effect that was discussed in section 3.7. Such an interference pattern would be sensitive small changes in the potentials, and therefore might be expected to differ for different planar $CuCl_4^{2-}$ complexes. However, the same is true for lattice vibrations and the spectrum shown in figure 9.18 has previously been interpreted in terms of the participation of three lattice vibrations of b_{2u} symmetry (Hitchman and Cassidy 1979).

The above three examples show only some of the effects that are possible in the vibrational fine structure which deviate from a simple Frank-Condon envelope typical of a diatomic molecule. The ability to simulate a spectrum that appears to be based on the vibronic origins of two inducing modes with just a single inducing mode is quite unexpected, and in a sense unwanted. It is a sad fact that while all the

(9.24)
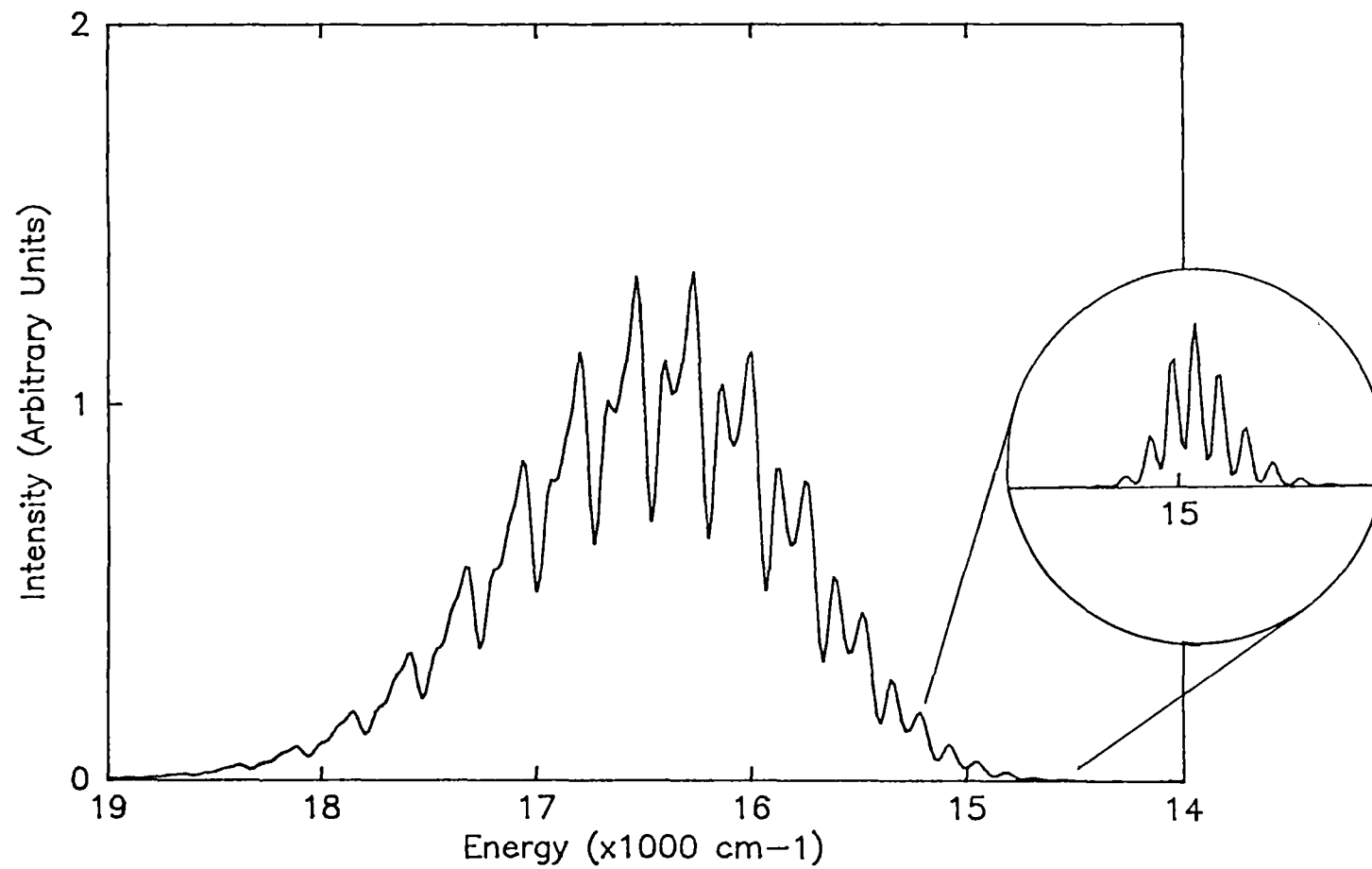
Figure 9.20   The "best fit" calculated spectrum of figure 9.16
at high resolution, halfwidth = 60cm^{-1}.

features of vibrational fine structure can be interpreted in terms of transitions between potential surfaces, often these surfaces will give more questions than answers. Ideally, with an infinitely resolved spectrum, every potential surface of a molecule could be derived to the accuracy of fitting every spectral line. This situation is sometimes approached in the gas phase spectra of small molecules but experimental spectra in the solid state are never resolved as one would wish. It is therefore only the trends due to the different types of potentials that can be talked about with any degree of confidence.

While the potentials (other than the a_{1g} potential) cannot be chacterised by direct observation of fine structure, the previously derived potentials from the "bulk" spectral features (intensity, energy, halfwidth ...) are fully consistent with the expected behaviour of the vibrational fine structure.

9.5 SUMMARY

9.5.1 Discussion.

The general trends in the $^2B_{1g}(x^2-y^2) \rightarrow {}^2A_{1g}(z^2)$ transition studied here are found in the other d-d transitions of square planar $CuCl_4^{2-}$. Although large red-shifts of the band maxima with temperature were also found, they are in all cases less than that observed for the $^2B_{1g} \rightarrow {}^2A_{1g}$ transition in z polarisation. This is consistent with the importance of the b_{2u} potential that is implied in this study, as this is the only vibronically active mode for this transition in this polarisation. It should be noted that the proposed double minima potential surface for the b_{2u} potential will cause a red-shift even when it is not active.

The general trend of the bandshifts in the three transitions is in the same order as their transition energies, the largest bandshift being seen for the $^2B_{1g}(x^2-y^2) \rightarrow {}^2A_{1g}(z^2)$ transition. There are two ways of rationalising this observation. First, simply from the way the d-orbital energies change relative to the ground state as a function of the b_{2u} coordinate (figure 2.A2), this trend would be expected. However, since the AOM was not found to give a realistic potential, this argument cannot really be used with confidence.

Similar arguments about the effects of promoting an electron to an anti-bonding orbital have been put forward to explain a double minima excited state in SO_2, however it has recently been shown (Innes 1986) that vibronic (pseudo Jahn-Teller) coupling provides a better explanation. Strong vibronic coupling would also give a convincing explanation in the present case as simple bonding arguments from the AOM have not found to be adequate. This would also explain why the bandshifts are in the observed order, as higher energy states would be expected to be involved in stronger vibronic coupling. Weak coupling with the ground state would also explain the form of the "anharmonicity" that was required to reproduce the experimental temperature dependent intensity.

It might be argued that the above explanation cannot be true since the b_{2u} mode is not vibronically active in all transitions. However, all the excited d-d electronic states can be coupled to the

higher energy charge transfer states by the b_{2u} mode. The vibronic selection rules merely mean that it is just the $^2A_{1g}(z^2)$ and the $^2E_g(xz,yz)$ states that are coupled to charge transfer states that are allowed (in z and xy polarisations respectively). Appendix 9.A3 discusses this in more detail along with the source of the vibronic intensity.

The $^2B_{1g}(x^2-y^2) \rightarrow ^2E_g(xz,yz)$ transition has been observed to be split in the $(NmpH)_2CuCl_4$ complex (Hitchman and Cassidy 1979). It has been suggested that the degeneracy will be removed by either the slight inequivalence of the bondlengths, spin-orbit coupling, or the Jahn-Teller effect (McDonald and Hitchman 1986). However, the latter mechanism is likely to be small as a splitting of only $82cm^{-1}$ is predicted at the RMS geometry of the Jahn-Teller active b_{2g} mode using the coupling constants given by the AOM in appendix 9.A2.

It is interesting to note that the congestion which gradually reduces the structure that is present at low temperatures in the present study may explain the fact that the d-d spectra of $CuCl_4^{2-}$ complexes of D_{2d} symmetry, such as Cs_2CuCl_4, are featureless. In this point group there are two vibrational modes of a_{1g} symmetry (they correlate to the a_{1g} and b_{2u} modes of the D_{4h} $CuCl_4^{2-}$). Displacement along both of these coordinates would result in two Franck-Condon envelopes, and the convolution of these would give rise to the featureless bands that are observed at low temperatures. It is interesting to speculate whether the excited state potentials of D_{2d} $CuCl_4^{2-}$ might be similar to the potentials of planar $CuCl_4^{2-}$. The excited state of the D_{2d} $CuCl_4^{2-}$ would then be distorted towards a planar geometry, compared to the $\theta_{min} \sim 28^{\circ}$ in the ground state (McGinnety 1972). The difference in the two complexes would then be as follows: in the planar complex the excited state along the b_{2u} coordinate would have zero slope above the ground state, while in the distorted tetrahedral complex there would be a very steep slope along this coordinate above the ground state. In agreement with group theory, this corresponds to the absence and presence, respectively, of a linear term in the potential. This would then account for the structured low temperature spectrum of the former complex and the lack of it in the latter.

9.5.2 Conclusions.

The temperature dependence of the electronic spectrum of square planar $CuCl_4^{2-}$ has been analysed in terms of various non-harmonic ground and excited state potential surfaces. It was found that only a relatively small perturbation to the harmonic ground state was necessary to account for the experimentally observed temperature variation of the intensity. This conclusion is independently supported by an analysis of the anisotropic temperature factors from published crystal structures in appendix 9.A1.

By constraining the ground state potentials in this manner, it was then possible to consider various possible excited state potentials to explain the unusually large shift in the band maxima with temperature. It was concluded that the form of the excited state potentials that was consistent with experiment are ones in which there is a double minima along the b_{2u} coordinate. Although qualitatively supporting this conclusion, the AOM failed to give excited state potentials which reproduce the experimental data. This may be a general failing of ligand field theory where coupling occurs to states outside of the d-orbital basis.

A distorted tetrahedral geometry in the $^1B_{2g}$ excited state of $Ni(CN)_4^{2-}$ has also been suggested by Ballhausen etal (1965) to explain the anomalous polarisation properties in the electronic spectrum of this complex. It is noted here that such a distortion must, by group theory, result from a double minima rather than from a displaced potential surface.

It was then shown that such a double minimum potential surface will have implications for the vibrational fine structure, and may possibly provide an explanation for the variety of fine structure that is observed in different planar $CuCl_4^{2-}$ complexes. Finally the source of the vibronic intensity, although not directly related to the central concerns of this chapter, has been considered in appendix 9.A3.

APPENDIX 9.A1   THE ANISOTROPIC TEMPERATURE FACTORS

An alternative explanation for the temperature dependence of the intensity and band shift was investigated in section 9.2. This alternative model was essentially that the ground state b_{2u} potential was very anharmonic so the bandshift could be rationalised in terms of the energy differences of the d-orbitals predicted by the AOM for distortions along this coordinate. However, it was shown in section 9.2 that while such a potential could also be capable of reproducing the experimental intensities at 0 and 300K, it was impossible to reproduce the experimental intensities at intermediate temperatures.

This appendix will provide additional support for rejecting this alternative model from an analysis of the anisotropic thermal parameters of the $CuCl_4^{2-}$ ion in published crystal structures. The anharmonic model would predict a RMS angular distortion of the Cl^- ions out of the $CuCl_4^{2-}$ plane of ~10° at 300K, whereas a value of ~3° is obtained from the analysis below.

The anisotropic temperature factors for $(creat)_2CuCl_4$ [creat = creatinium] and $(NmpH)_2CuCl_4$ have been reported by Udupa and Krebs (1979) and Harlow etal (1974) respectively. These quantities are listed in table 9.A1 in terms of the dimensionless β matrix (Willis and Pryor 1975; pg 99) for an anisotropic temperature factor of the form:

$$exp-(\beta_{11}h^2 + \beta_{22}k^2 + \beta_{33}l^2 + 2\beta_{12}hk + 2\beta_{13}hl + 2\beta_{23}kl) \qquad (9.A1)$$

In both structures the Cu atom occupies a centrosymmetric site and there are two independent Cl atoms. Following the procedure outlined by Willis and Pryor (1975, section 4.4), the β matrices can be converted into the mean square displacement matrices, B, which are also given in table 9.A1. These B matrices represent ellipsoids where there is 50% probability of finding the atoms within. The square root of the principal values of these ellipsoids correspond to the root mean-square displacement of the atoms along the principal axes (Willis and Pryor 1975, pp 97-8). Diagonalisation of the B matrices gives eigenvectors which show that the major principal axis is approximately along the z molecular axis. The RMS displacements of the atoms along these axes are given in table 9.A2.

TABLE 9.A1 The anisotropic temperature factors

	β_{11} [a)	β_{22}	β_{33}	β_{12}	β_{13}	β_{23}
(creat)$_2$CuCl$_4$						
Cu	96.9	73.8	61.9	-9.9	21.0	-1.5
Cl1	119.8	80.3	143.7	-13.0	27.1	9.5
Cl2	114.3	106.0	115.2	-3.9	-7.2	6.3
(NmpH)$_2$CuCl$_4$						
Cu	206	17.9	143	1	69	-2
Cl1	335	31.7	235	-41	173	-41
Cl2	336	19.2	179	-12	138	-5
	B_{11} [b)	B_{22}	B_{33}	B_{12}	B_{13}	B_{23}
(creat)$_2$CuCl$_4$						
Cu	268	229	563	-29	-8.6	4.5
Cl1	331	249	1351	-38	-4.8	69
Cl2	316	329	1226	-11	-177	40
(NmpH)$_2$CuCl$_4$						
Cu	355	466	448	6.7	1.2	-23
Cl1	578	826	586	-275	156	-270
Cl2	579	500	464	-80	67	-9.9

a) (x 10^{-4}); b) (x 10^{-4} pm^2)

TABLE 9.A2 RMS Displacements along the Principal Axes

	X/pm	Y/pm	Z/pm	$<\theta>^{1/2}$/deg.
(creat)$_2$CuCl$_4$				
Cu	16.8	14.6	23.7	
Cl1	18.6	15.2	36.8	3.34
Cl2	16.8	18.1	35.5	3.00
(NmpH)$_2$CuCl$_4$				
Cu	18.8	20.8	22.0	
Cl1	19.8	20.6	34.1	3.08
Cl2	21.7	20.5	25.5	0.89

The RMS displacements will be due to both internal and external motions of the $CuCl_4^{2-}$ unit, where the external translational and librational motions of the $CuCl_4^{2-}$ unit as a whole makes the greatest contribution at room temperature (Willis and Pryor 1975; pp191-3). The approximation is now made that these external motions can be removed from the problem by subtracting the principal values of the Cu atom from those of the Cl atoms. This results in the largest remaining motion of the Cl relative to the Cu atoms being in the molecule z direction, or out of the $CuCl_4^{2-}$ plane. The RMS angular displacements can be found using a Cu-Cl bondlength of 225pm and are also given in table 9.A2.

Consistent values of ~3° where obtained except for the Cl2 atom in the $(NmpH)_2CuCl_4$ complex, which is far too low. No explanation can be given for this discrepancy, although it was noted that in this complex, the principal axes of the thermal ellipsoids are only roughly parallel with each other when compared to the $(creat)_2CuCl_4$ complex. If out-of-plane motion is assumed to be only caused by the vibration of b_{2u} symmetry, then this corresponds to a harmonic frequency of ~60 cm^{-1}, which is pleasingly close to that obtained from the analysis of the temperature dependent intensity in section 9.2.

However, it should be stressed that the above procedure has many drastic approximations, some of which are outlined below:

a) The subtraction of the translational motion of the $CuCl_4^{2-}$ unit assumes a parallel correlated motion of the Cu and Cl atoms (Willis and Pryor 1975; pg 116). This assumption will tend to underestimate the true RMS geometry.

b) The neglect of the librational motions about axes lying in the $CuCl_4^{2-}$ plane will tend to overestimate the true RMS value.

c) The RMS angular displacement of the Cl atoms by internal vibrations will also receive contributions from the out-of-plane a_{2u} bending vibration. Using the relationships given by Cyvin (1968; pg 76), and the harmonic frequencies 60 and 160 cm^{-1} for the b_{2u} and the a_{2u} modes respectively; the RMS angular displacement at 300K is calculated to be 3.0° and 3.65° when taking into account just the b_{2u} mode and both modes respectively.

With the above approximations it is somewhat surprising that such a good value of $<\theta>^{1/2}$ ~ 3° was found. However, the neglect of the antiparallel correlated motion of the Cu and Cl atoms in approximation

a) above will be approximately cancelled by the neglect of the a_{2u} contribution in approximation b), since this vibration represents a pure antiparallel correlation of the Cu and Cl atoms. The present study seems to be particularly favourable case for determining the energy of an internal vibration from RMS values of a crystal structure. A low temperature study of the temperature factors of these complexes would be interesting as the contribution from the external motions would be greatly reduced.

In the present context, a RMS value of ~3° for the out-of-plane motion of the Cl atoms in $CuCl_4^{2-}$ means that the anharmonic model considered in section 9.2 is incapable of providing an explanation for both the temperature dependence of the intensity and bandshift while remaining consistent with the anisotropic temperature factors of their crystal structures.

APPENDIX 9.A2   ELECTRONIC POTENTIALS FROM THE ANGULAR OVERLAP MODEL.

In this appendix ligand field theory, in the form of the angular overlap model (AOM), is used to gain a qualitative understanding of the form of the excited state potentials. This is done by assuming a particular ground state potential to which is added the energy difference between electronic states along the particular symmetry coordinate to determine the excited state potentials. That is, the energy differences in the ligand field electronic states are allowed to determine the differences in the excited state potentials to the ground state potentials. This is clearly a big approximation because the vibrational force constants depend on the electronic distribution of the molecule; and secondly, the normal coordinates of the molecule are not exactly the same as the symmetry coordinates given in figure 9.A1. This second point will mean that the bending modes will not be independent of the stretching modes, and a "non-rigid inverter" model should strictly be used for the low frequency bending modes (see Papousek 1983).

However, setting aside these objections, the above simple approach has been found to give very good agreement with experiment for calculating both the displacement of the excited state along a_{1g} modes (Hitchman 1982), and Jahn-Teller coupling constants (Deeth and Hitchman 1986). It is therefore hoped that this same approach will at least provide some insight into the present problem.

The Vibrations.

The choice of molecular axes and symmetry coordinates for the $CuCl_4^{2-}$ species are shown in figure 9.A1. It is important to note the conventions adopted. This figure also defines the phase of the vibrations and the relationships between the internal coordinates (r,θ,α) and the symmetry coordinates S. Following the recommendations of Cyvin (1968, pg101), all symmetry coordinates involving angular displacement are multiplied by the equilibrium bondlength R. This will mean that all the symmetry coordinates are in units of length (pm) and the quadratic force constants will have the units $cm^{-1}pm^{-2}$. The internal coordinates can be expressed in terms of the symmetry coordinates by

$\nu_1 : a_{1g}$

$S_{a_{1g}} = \frac{1}{2}\left(r_1 + r_2 + r_3 + r_4\right)$

$\nu_2 : b_{1g}$

$S_{b_{1g}} = \frac{1}{2}\left(r_1 - r_2 + r_3 - r_4\right)$

$\nu_3 : a_{2u}$

$S_{a_{2u}} = \frac{R}{2}\left(\theta_1 + \theta_2 + \theta_3 + \theta_4\right)$

$\nu_4 : b_{2g}$

$S_{b_{2g}} = \frac{R}{2}\left(\alpha_{12} - \alpha_{23} + \alpha_{34} - \alpha_{41}\right)$

$\nu_5 : b_{2u}$

$S_{b_{2u}} = \frac{R}{2}\left(\theta_1 - \theta_2 + \theta_3 - \theta_4\right)$

$\nu_6 : e_u(s)$

$S^1_{e_u(s)} = \sqrt{\frac{1}{2}}\left(r_1 - r_3\right)$

$S^2_{e_u(s)} = \sqrt{\frac{1}{2}}\left(r_2 - r_4\right)$

$\nu_7 : e_u(b)$

$S^1_{e_u(b)} = \frac{R}{2}\left(\alpha_{12} - \alpha_{23} - \alpha_{34} + \alpha_{41}\right)$

$S^2_{e_u(b)} = \frac{R}{2}\left(\alpha_{12} + \alpha_{23} - \alpha_{34} - \alpha_{41}\right)$
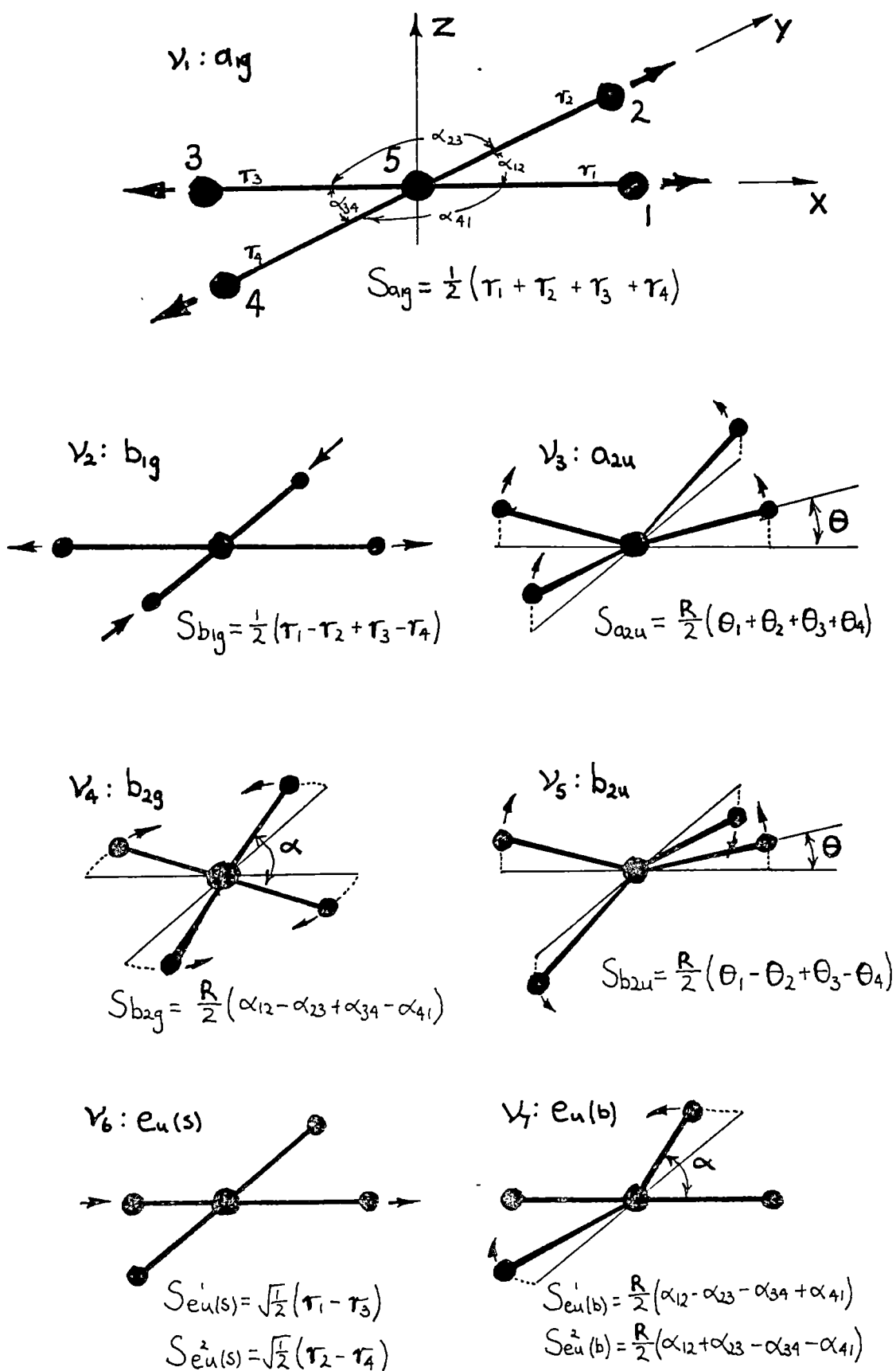
Figure 9.A1 Molecular Axes and Symmetry Coordinates for $CuCl_4^{2-}$. R is the equilibrium Cu-Cl bond length.

inverting the U matrix (see Cyvin 1968; pp64-67) and, for example, one can find:

$$r_1 = \frac{1}{2} S(a_{1g}) + \frac{1}{2} S(b_{1g}) + \frac{1}{2} S(e_u^1(s))$$

$$\alpha_{12} = -\frac{1}{2R} S(b_{2g}) - \frac{1}{2R} S(e_u^1(b)) + \frac{1}{2R} S(e_u^2(b))$$

$$\theta_1 = \frac{1}{2R} S(a_{2u}) + \frac{1}{2R} S(b_{2u}) \qquad\qquad (9.A2)$$

In the present study only bending vibrations are investigated. This is because of the stretching vibrations, the displacement and excited state force constant of the a_{1g} mode is determined by the experimental spectra. The b_{1g} and e_u stretch modes are "even" vibrations where positive and negative displacements along their coordinates are equivalent. The overall effect of adding a potential where a bond compression raises the energy higher than an extension (ie an inverse power or overlap calculated potential) would be to increase the frequency in the excited state. Since this cannot be an explanation for the present problem, only the bending modes are considered.

The Potentials.

The instantaneous point groups of the vibrations are shown in table 9.A3 along with the irreducible representations of the real d-orbitals basis functions. [Note: For distortions along the b_{2u} and b_{1g} coordinates, the instantaneous point groups differ from the standard ones normally used due to the non-conventional orientation of the molecular axes.]

Because each d-orbital belongs to a different irreducible representation for distortions along the a_{2u} or b_{2u} symmetry coordinates, the ligand field will not mix them and analytic formula can be given for the energies of the electronic states in terms of pure d-orbitals. These two distortions are equivalent in terms of the AOM model and the energies of the electronic states as a function of θ have been derived by Smith (1977) and are given in table 9.A4. For the b_{2g} and $e_u(b)$ instantaneous point groups, however, repeated representations occur and the $d(z^2),d(xy)$ and $d(z^2),d(x^2-y^2)$ pairs respectively will be

mixed by the ligand field. The non zero matrix elements are given in table 9.A4 and diagonalisation of the ligand field matrix must now be done to obtain the energy of the electronic states (which now will not all be pure d-orbitals). In addition, the d-orbitals that transform as totally symmetric have been shown to be depressed by configuration interaction with the metal 4s orbital (Smith 1977). The perturbative approach by Smith (1977) along with group overlap integrals (Kettle 1965) has been used to include this effect and the results are included in table 9.A4 where necessary.

<center>**TABLE 9.A3**</center>

Vibration	Instantaneous Point groups	Irreducible Representations $d(z^2)$ $\quad$ $d(x^2-y^2)$ $\quad$ $d(xy)$ $\quad$ $d(xz)$ $\quad$ $d(yz)$				
v_1 (a_{1g})	D_{4h}	A_{1g}	B_{1g}	B_{2g}	E_g	
v_2 (b_{1g})	D_{2h}	A_g	A_g	B_{1g}	B_{2g}	B_{3g}
v_3 (a_{2u})	C_{4v}	A_1	B_1	B_2	E	
v_4 (b_{2g})	D_{2h}^*	A_g	B_{1g}	A_g	B_{2g}, B_{3g}	
v_5 (b_{2u})	D_{2d}	A_1	B_2	B_1	E	
v_6 $(e_u(b))$	C_{2v}	A_1	A_1	B_1	B_2	A_2
v_7 $(e_u(s))$	C_{2v}	A_1	A_1	B_1	B_2	A_2

*Denotes a "non-standard" point group, the molecular axes are as defined in figure 9.A1.

The three AOM parameters e_σ, e_π and e_{ds} take the values 5250, 900 and 1500 cm^{-1} respectively from the observed electronic transitions of the planar complex. The transitions of $CuCl_4^{2-}$ in the more commonly observed D_{2d} geometry have been found to lie along the calculated curves of the b_{2u} coordinate (McDonald and Hitchman 1986). The energy differences of these electronic states, calculated from the matrix elements given in table 9.A4, are shown in figure 9.A2. The appropriately dimensioned harmonic ground state potential is also included for comparison. These curves are now fitted to a fourth order polynomial by the least squares method and the results are presented in table 9.A5.

<center>(9.34)</center>

TABLE 9.A4 AOM matrix elements for angular distortions.

a_{2u} and b_{2u} type distortions.

$$\langle z^2|V|z^2\rangle = \tfrac{1}{4}(1 - 3\cos 2\theta)^2 e_\sigma + 3\sin^2 2\theta\, e_\pi - 16(\sin^2\theta - \tfrac{1}{2}\cos^2\theta)^2 e_{ds}$$

$$\langle x^2-y^2|V|x^2-y^2\rangle = \tfrac{3}{4}(1 + \cos 2\theta)^2\, e_\sigma + \sin^2 2\theta\, e_\pi$$

$$\langle xy|V|xy\rangle = 4\cos^2\theta\, e_\pi$$

$$\langle xz|V|xz\rangle = \tfrac{3}{2}\sin^2 2\theta\, e_\sigma + 2(\sin^2\theta + \cos^2 2\theta)\, e_\pi$$

$$\langle yz|V|yz\rangle = \tfrac{3}{2}\sin^2 2\theta\, e_\sigma + 2(\sin^2\theta + \cos^2 2\theta)\, e_\pi$$

---

b_{2g} type distortion

$$\langle z^2|V|z^2\rangle = e_\sigma - 4e_{ds}$$

$$\langle x^2-y^2|V|x^2-y^2\rangle = 3\sin^2\alpha\, e_\sigma + 4\cos^2\alpha\, e_\pi$$

$$\langle xy|V|xy\rangle = 3\cos^2\alpha\, e_\sigma + 4\sin^2\alpha\, e_\pi - 48\cos^2\alpha\, e_{ds}$$

$$\langle xz|V|xz\rangle = 2\, e_\pi$$

$$\langle yz|V|yz\rangle = 2\, e_\pi$$

$$\langle xz|V|yz\rangle = \langle yz|V|xz\rangle = 2\cos\alpha\, e_\pi$$

$$\langle z^2|V|xy\rangle = \langle xy|V|z^2\rangle = -\sqrt{3}\cos\alpha\, e_\pi$$

$e_u(b)$ type distortion

$$\langle z^2|V|z^2\rangle = e_\sigma - 4\, e_{ds}$$

$$\langle x^2-y^2|V|x^2-y^2\rangle = \tfrac{3}{2}(1 + \cos^2 2\alpha)\, e_\sigma + 2\sin^2 2\alpha\, e_\pi - 48\cos^4\alpha\, e_{ds}$$

$$\langle xy|V|xy\rangle = \tfrac{3}{2}\sin^2 2\alpha\, e_\sigma + 2(1 + \cos^2 2\alpha)\, e_\pi$$

$$\langle xz|V|xz\rangle = 2(1 + \cos^2\alpha)\, e_\pi$$

$$\langle yz|V|yz\rangle = 2\sin^2\alpha\, e_\pi$$

$$\langle z^2|V|x^2-y^2\rangle = \langle x^2-y^2|V|z^2\rangle = -\tfrac{\sqrt{3}}{2}(1 + \cos 2\alpha)\, e_\sigma$$

Note: The internal coordinates Θ, α are defined in figure 9.A1.
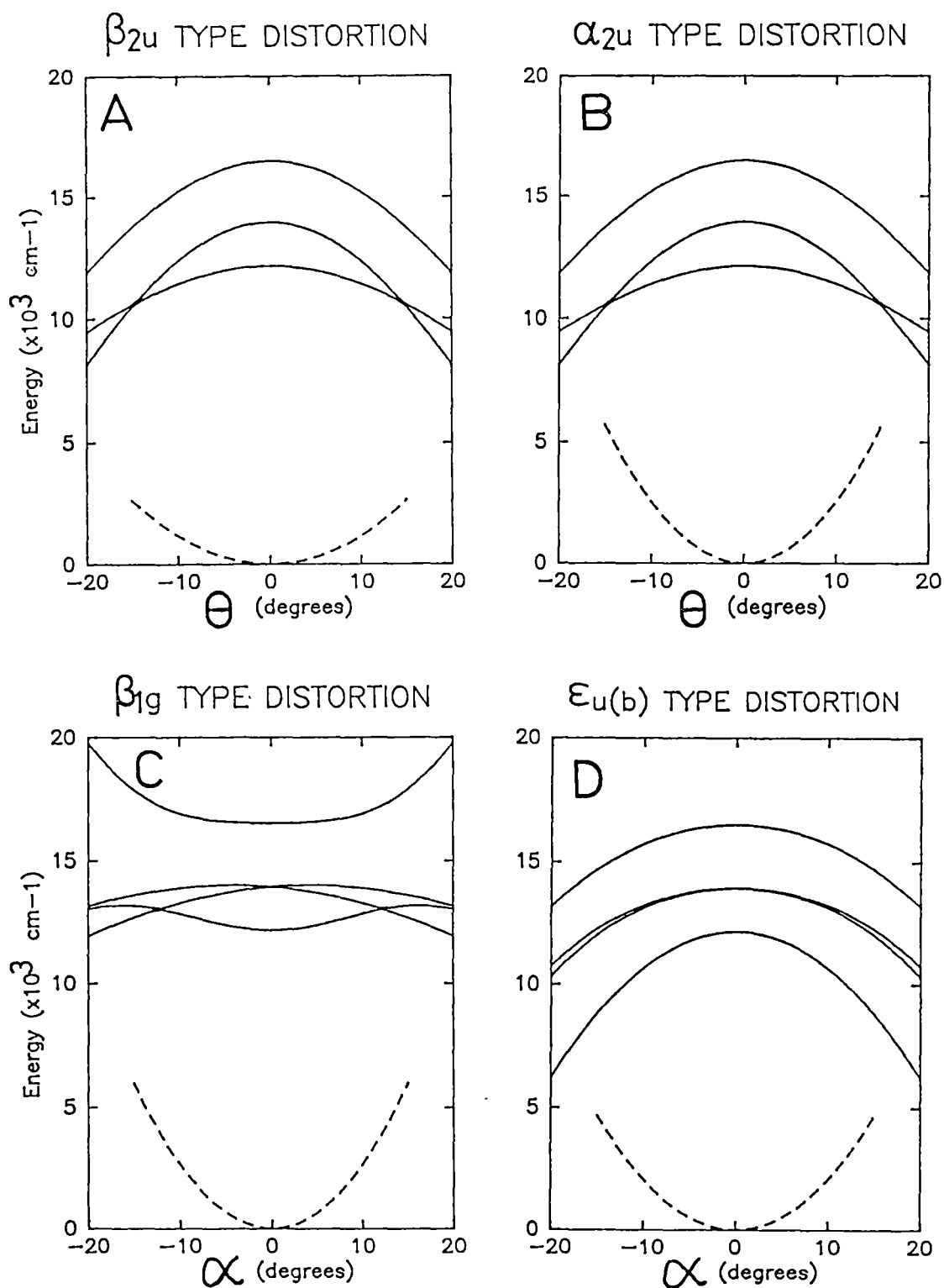
Figure 9.A2 The d-orbital energies relative to the ground state as a function of: a) b_{2u}, b) a_{2u}, c) b_{1g} and d) $e_u(b)$ symmetry coordinates. The ground state vibrational potentials are also shown for comparison.

Care must be taken both when converting from internal coordinates (θ, α), symmetry coordinates, and dimensionless coordinates (ξ); and also when converting their coefficients. To avoid confusion these conversions are outlined in detail. For the b_{2u} mode the potentials can be defined as:

$$V(\theta) \quad = c_0 + c_1\theta + c_2\theta^2 + \ldots \qquad (9.A3)$$

$$V(S_{b2u}) = b_0 + b_1 S_{b2u} + b_2 S_{b2u}^2 + \ldots \qquad (9.A4)$$

$$V(\xi) \quad = a_0 + a_1\xi + a_2\xi^2 + \ldots \qquad (9.A5)$$

The coefficients have the dimensions: c_i ($cm^{-1}deg^{-i}$), b_i ($cm^{-1}pm^{-i}$) , a_i (dimensionless), and are related by the following expressions:

$$a_i = (\tfrac{1}{x})^i \tfrac{1}{h\nu} b_i = (\tfrac{180}{2\pi R x})^i \tfrac{1}{h\nu} c_i \qquad (9.A6)$$

and the coordinates by: $\theta = (\tfrac{180}{2\pi R}) S_{b2u} = (\tfrac{180}{2\pi R}) \tfrac{1}{x} \xi \qquad (9.A7)$

Here R is the equilibrium bondlength and x is given by (Cyvin 1968):
$x = 1.722 \times 10^{-3} (Mh\nu)^{1/2}$ pm^{-1} where M is the mass of the chloride ion in amu and $h\nu$ is the frequency of the vibration in cm^{-1}.

For the other bending modes the above equations are identical, making the appropriate substitutions ($\theta \rightarrow \alpha$, $S(b_{2u}) \rightarrow S(b_{2g})$ for example), except for the mass used M. This is actually the inverse of the appropriate element of the G matrix (see Cyvin 1968) and will differ for each mode[*]:

$$b_{2u}: \quad M = m(Cl) \qquad a_{2u}: \quad M = \frac{m(Cl)m(Cu)}{[4m(Cl)+m(Cu)]} \qquad (9.A8)$$

$$b_{2g}: \quad M = \frac{m(Cl)}{4} \qquad e_u(b): \quad M = \frac{m(Cl)m(Cu)}{[4m(Cl)+2m(Cu)]}$$

[* The e_u(b) mode is actually more complicated as the G matrix couples the e_u bending and the e_u stretching vibrations. Here it is assumed that such coupling is small enough to be ignored.]

TABLE 9.A5 * Least squares fit to the AOM potentials.

Vibration Symmetry Frequency (cm^{-1})	ν_3 a_{2u} 159	ν_4 b_{2g} 181	ν_5 b_{2u} 60	ν_7 e_u(b) 165
a_2	0.5	0.5	0.5	0.5
b_2 (cm^{-1} pm^{-2}) **	0.4112	0.4305	0.1892	0.3382
c_2 (cm^{-1} deg^{-2})	25.37	26.55	11.67	20.86
→ d(z^2) transition				
c_2 (cm^{-1} deg^{-2})	-13.148	2.020	-13.148	-7.408
c_4 (cm^{-1} deg^{-4})	0.00392	0.01864	0.00392	-0.00258
a_2	-0.2592	0.0380	-0.5632	-0.1776
a_4	0.00024	0.00120	0.00043	-0.00055
→ d(xz) transition***				
c_1 (cm^{-1} deg^{-1})	0.0	31.416	0.0	0.0
c_2 (cm^{-1} deg^{-2})	-16.435	-3.701	-16.435	-6.859 (-7.956)
c_3 (cm^{-1} deg^{-3})	0.0	-0.00159	0.0	
c_4 (cm^{-1} deg^{-4})	0.00484	0.00037	0.00484	-0.00312 (-0.003)
a_1	0.0	0.3204	0.0	
a_2	-0.324	-0.069	-0.704	-0.164 (-0.191)
a_3	0.0	-0.00006	0.0	
a_4	0.00030	0.00002	0.0053	-0.00030 (-0.00029)
→ d(xy) transition				
c_2 (cm^{-1} deg^{-2})	-7.397	8.809	-7.397	-14.807
c_4 (cm^{-1} deg^{-4})	0.00181	-0.0197	0.00181	-0.00013
a_2	-0.1458	0.1659	-0.3169	-0.3549
a_4	0.00011	-0.00127	0.00020	-0.00001

* Only non-zero coefficients are given. A least squares polynomial of degree 4 is fitted to 31 points in the range $\pm15°$.

** 1.0 mdyneÅ^{-1} = 5.035 cm^{-1} pm^{-2}

*** For the → d(yz) transition change the sign of c_1, c_3 and use the bracketed quantities for c_2, c_4.

Discussion.

The dimensionless coefficients, a_i, given in table 9.A5 are those required for use in section 9.3.2. Several comments can be made at this stage however. The pair of d-orbitals d(xz), d(yz) that are degenerate in D_{4h} symmetry are split along the b_{2g} and $e_u(b)$ symmetry coordinates. This is exactly as given by group theory in terms of the instantaneous point groups given in table 9.A1.

The antisymmetric direct product $\{E_g \underline{x} E_g\} = b_{1g} \underline{+} b_{2g}$ gives b_{1g}, b_{2g} as Jahn-Teller active coordinates (Ballhausen 1965), and from table 9.A5 a linear Jahn-Teller coupling constant of $A_1 = 4.00$ cm^{-1}pm^{-1} for the b_{2g} mode is calculated. This of course could be immediately calculated from the matrix element in a manner similar to that outlined by Bacci (1979), which gives $A_1 = {}^e\pi/R$. It is interesting to note that along the b_{1g} coordinate the d_{xz}, d_{yz} orbitals are not mixed, whereas they are mixed along the b_{2g} coordinate, analogous to the behaviour of the Q_θ and Q_ε components, respectively, of the e_g vibration in an octahedral E_g state.

The only active Renner-Teller vibrations will be those whose direct product with itself contains either of the b_{1g}, b_{2g} representations. This will only occur for the e_u vibrations. From table 9.A5 the second-order Jahn-Teller (or Renner-Teller) coupling constant for the $e_u(b)$ mode is calculated as $A_2 = 0.0178$ cm^{-1}pm^{-2}. Again this could have been calculated directly from the matrix element $A_2 = {}^e\pi/R^2$. Herzberg (1966, pp42-5) has discussed the Renner-Teller effect in non-linear molecules.

It is heartening that the qualitative behaviour of matrix elements <u>required</u> to be non-zero by group theory is correctly reproduced within a ligand field model. Returning now to the immediate problem, the electronic "difference" potentials are added on to the ground state vibrational potentials in table 9.A5 to form the excited state vibrational potentials. In $d(x^2-y^2) \rightarrow d(z^2)$ transition, the b_{2u} excited state vibrational potential dramatically deviates from a harmonic parabola. Indeed, it forms a "double well" potential where the minima are at $\pm 14°$ and are depressed by 140 cm^{-1} from the minima of a harmonic potential. The b_{2u} mode is the only one that displays a potential of this form. This is due partly to the steepness that the

electronic "difference" energies fall along this coordinate, and to the low frequency (or large amplitude) of this vibration.

The fourth order term for distortions along the e_u(b) coordinate is negative, which will eventually cause the potential to turn negative and become unrealistic. This will occur at quite large distortions and will not have any effect on the present problem at the temperatures to be studied. However, in practise this term is set to zero in the numerical calculations because the diagonalisation routines will attempt to calculate "unbound states" outside of the potential for large basis sizes.

(9.37)

9.A3   THE SOURCE OF THE VIBRONIC INTENSITY

The intensity of the forbidden d-d transitions in this centrosymmetric complex is vibronic in nature, although this chapter has not been concerned with the source of this intensity. When the intermediate "lending" states are not of interest, then the usual vibronic selection rules in equation (3.27) can be applied to D_{4h} $CuCl_4^{2-}$ and the results given in table 9.6 are obtained.

The electronic selection rules of the complex with a static distortion along each of these inducing modes gives exactly the same results as the vibronic selection rules of table 9.6. This can easily be shown to be true for molecules of any point group. Distortions along a particular symmetry coordinate Q, causes this coordinate to transform as totally symmetric in the new point group. Substitution of $\Gamma_Q = A_{1g}$ into the vibronic selection rule of equation (3.27) results in the electronic selection rule, so that transitions that are vibronically allowed become electronically allowed with a static distortion along their inducing coordinates.

The static selection rules can be found by noting how the d-orbitals and the electric dipole vector transform in the "instantaneous" point groups (subgroups of the parent D_{4h} group) resulting from distortions along the normal modes. [These are given in table 9.A3 of appendix 9.A2.] Although these above two approaches give identical selection rules, it will be shown in the following sections that they give very different interpretations as to the source of the vibronic intensity.

Vibronic Approach.

If the nature of the intermediate charge transfer states are of interest, then the separate selection rules in equations (3.25) and (3.26) for the relevant pair of integrals in the transition moment of (3.24) are considered. The first integral gives the possible mixtures of the charge transfer states into the "d-orbital" states, while the second integral determines whether the charge transfer states that are mixed into the wavefunctions are themselves allowed.

(9.38)

TABLE 9.A6: Vibronic Selection Rules for $CuCl_4^{2-}$.

Inducing Mode	Vibronically Allowed Transition	Polarisation	"Lending" CT Transition
a_{2u}	$^2B_{1g}(x^2-y^2) \to {}^2E_g(xz,yz)$	xy	$^2B_{1g}(x^2-y^2) \to {}^2E_u$
b_{2u}	$\to {}^2E_g(xz,yz)$	xy	$\to {}^2E_u$
	$\to {}^2A_{1g}(z^2)$	z	$\to {}^2B_{2u}$
e_u	$\to {}^2B_{2g}(xy)$	xy	$\to {}^2E_u$
	$\to {}^2A_{1g}(z^2)$	xy	$\to {}^2E_u$
	$\to {}^2E_g(xz,yz)$	z	$\to {}^2B_{2u}$

Table 9.A7: The Vibronic Selection Rules

at Various Levels of Approximation.

Transition	Inducing Vibrations					
	I		II		III	
	xy	z	xy	z	xy	z
$B_{1g} \to B_{2g}$ $[x^2-y^2 \to xy]$	$e_u(E_u)$	–	–	$b_{2u}(A_{1u})$	$e_u(E_u)$	–
$B_{1g} \to E_g$ $[x^2-y^2 \to xz$ $\to yz]$	$a_{2u}(E_u)$ $b_{2u}(E_u)$	$e_u(B_{2u})$ –	– –	$e_u(A_{1u})$ $e_u(A_{2u})$	$a_{2u}(B_{2u})$ $b_{2u}(A_{2u})$	$e_u(E_u)$ –
$B_{1g} \to A_{1g}$ $[x^2-y^2 \to z^2]$	$e_u(E_u)$	$b_{2u}(B_{2u})$	–	$a_{2u}(A_{2u})$	$e_u(E_u)$	$b_{2u}(A_{2u})$

Note: All the electronic states above are doublets. ie $B_{1g} \equiv {}^2B_{1g}$

The "d-orbital" states are:

$$\Psi_g(B_{1g}) = B_{1g}(x^2-y^2) + c(a_{2u})B_{2u} + c(b_{2u})A_{2u} + c(e_u)E_u \qquad (9.A9)$$

$$\psi(B_{2g}) = B_{2g}(xy) \quad + c(a_{2u})B_{1u} + c(b_{2u})A_{1u} + c(e_u)E_u$$

$$\psi(E_g) = E_g(xz,yz) + c(a_{2u})E_u \quad + c(b_{2u})E_u$$

$$+ c(e_u)(A_{1u} + A_{2u} + B_{1u} + B_{2u})$$

$$\psi(A_{1g}) = A_{1g}(z^2) \quad + c(a_{2u})A_{2u} + c(b_{2u})B_{2u} + c(e_u)E_u$$

Here, the lower case letters refer to vibrations and the upper case letters to states, so for example, $c(a_{2u})$ represents a mixing coefficient dependent on the a_{2u} symmetry coordinate. From the above mixture of the ground state wavefunction, the following allowed transitions are possible:

xy	**z**	
$B_{1g} \rightarrow E_u$	$B_{1g} \rightarrow B_{2u}$	(9.A10)
$B_{2u} \rightarrow E_g$	$B_{2u} \rightarrow B_{1g}$	
$A_{2u} \rightarrow E_g$	$A_{2u} \rightarrow A_{1g}$	
$E_u \rightarrow A_{1g}$	$E_u \rightarrow E_g$	
$\rightarrow A_{2g}$		
$\rightarrow B_{1g}$		
$\rightarrow B_{2g}$		

Note that the transitions all involve a change in parity, both transitions from charge transfer to charge transfer states and d-d transitions are forbidden by symmetry. The vibronic selection rules are now derived in three different cases:

I. In the first case the ground state is considered to be a pure $d(x^2-y^2)$ orbital, and only the excited states are allowed to mix with charge transfer states. Further, only electronically allowed charge transfer transitions are assumed to contribute intensity. Using equations (9.A9) and (9.A10), the selection rules given in column I of table 9.A7 are derived. Here, for each polarisation, the symmetry of the inducing mode is given, as well as that of the charge transfer states (in brackets) from which the intensity is "borrowed". These are

(9.39)

the same selection rules as given in table 9.A6, however, now the intermediate states are identified.

The charge transfer spectrum of planar $CuCl_4^{2-}$ has been studied by Desjardins etal (1983). The following three transitions were assigned: $^2B_{1g} \rightarrow {}^2A_{2g}$ (23,700cm^{-1}), $^2B_{1g} \rightarrow {}^2E_u$ (26,400cm^{-1}), $^2B_{1g} \rightarrow {}^2E_u$ (35,900cm^{-1}), all of which were observed to be almost totally xy polarised. In particular, the $^2B_{1g} \rightarrow {}^2B_{2u}$ transition that is formally allowed in z polarisation, was calculated to have zero intensity and was not observed. This creates a problem, as although the d-d spectrum is more intense in xy than z polarisation (see figure 9.1), the difference is nowhere near as great as that observed in the charge transfer spectrum. A question one might ask is then: where does this z polarised intensity come from?

II. In the second case to be considered, the ground state is again assumed to be a pure $d(x^2-y^2)$ orbital but the mixing with charge transfer states that are electronically forbidden in (9.A9) are allowed to provide some intensity. This is justified by the fact that the forbidden $^2B_{1g} \rightarrow {}^2A_{2g}$ charge transfer transition is observed to be much more intense than the d-d transitions although it is allowed only through vibronic coupling with the ^2E_u states (Desjardins etal 1983). This mechanism can then be described as "vibronic coupling with vibronically allowed charge transfer states". The transitions to these states are only electric dipole forbidden, not parity forbidden as are the d-d transitions. The following transitions of (9.A9) that have not yet been considered become vibronically allowed by b_{2g}, b_{1g} vibrations:

Charge Transfer Transition	Inducing vibration	
	xy	z
$B_{1g}(x^2-y^2) \rightarrow B_{1u}$	–	–
$\rightarrow A_{1u}$	–	$b_{2g}(B_{2u})$
$\rightarrow A_{2u}$	–	$b_{1g}(B_{2u})$

Again by using (9.A9) the additional selection rules that result from coupling to these states are found and are given in column II of table 9.A7. The total selection rules in this approximation are given

(9.40)

by both columns I and II. It should be noted that the charge transfer transitions under consideration here gain their intensity via vibronic coupling to the allowed $^2B_{2u}$ states, and these states were not observed experimentally. Therefore this mechanism does not provide an explanation for the anomalous z polarised intensity discussed previously.

III. In the final case considered, the ground state is allowed to be vibronically coupled to the ungerade charge transfer states in (9.A9). The additional selection rules, which involve transitions between the ligand character in the ground state and the d-orbital part of the excited d states in (9.A9), are given in column III of table 9.A7. The total selection rules in this approximation are then given by both columns I and III. Note that the selection rules for the inducing vibrations are exactly the same as in column I, the only difference being in the intermediate "lending" states. This third mechanism does provide an explanation for the intensity observed in the z polarisation of the d-d spectra.

Where is the intensity being "stolen" from? From the $^2B_{2u} \rightarrow {}^2E_g$ type transitions in (9.A10), ie the integrals involving the <u>excited</u> d orbitals and the charge transfer states. Therefore, even though an intense z polarised charge transfer spectrum is not seen, there is still vibronic coupling with the z polarised "virtual" excited state charge transfer spectrum. This is a perfectly logical conclusion but not one that is usually considered. This is because popular vibronic coupling interpretations talk in terms of "borrowing" from intense transitions, when it is of course the coupling of the states that is important. The idea of "borrowing" intensity can be a misleading conceptional idea when, as in the present case, the vibronic coupling is such that the intensity is being "borrowed" from an excited state transition that is not observed in a normal electronic spectrum.

The excited state absorption spectra would provide useful data on the intensities of these "virtual" transitions and the importance of this mechanism. The excited state absorption spectrum of K_2PtCl_4 in a triplet state has been studied (Viaene etal 1985); however short lifetimes in the present case would make such a study difficult.

A Static Approach.

In square planar $CuCl_4^{2-}$, the most intense d-d transition in z polarisation at all temperatures is the $d(x^2-y^2) \to d(z^2)$ transition which is vibronically allowed only by modes of b_{2u} symmetry. Instead of asking where the z polarised vibronic intensity is coming from, it is instructive to consider where the intensity is coming from for a small distortion away from D_{4h} symmetry along the b_{2u} coordinate. To do this, a semi-empirical approach using the σ and π bonding properties of the p orbitals of the chlorine ligands was used (unpublished results). In agreement with others (Van der Avoird and Ros 1963, Fenske and Sweeney 1964) it was found that the intensity is mainly derived from the single ligand(σ) $\to$ ligand(σ) type transition, $^2B_2 \to \,^2A_1$ in the D_{2d} point group, from the ligand component of the molecular orbitals. However, it was somewhat surprising to find that this is also the case at quite small departures from D_{4h} symmetry in the region where Herzberg-Teller theory assumes that the dominant intensity contribution comes from the metal $\to$ ligand type transitions.

Extrapolating back to D_{4h} symmetry, this intensity contribution corresponds to the ligand-ligand transition $^2A_{2u} \to \,^2B_{2u}$. However, this transition is electric dipole forbidden at D_{4h} symmetry, and so strictly cannot provide any intensity at the square planar geometry. The four possible contributions to the $d(x^2-y^2) \to d(z^2)$ transition due to mixing from the b_{2u} coordinate are:

$$
\begin{array}{llll}
1) & ^2B_{1g} \to \,^2A_{1g} & (M\text{-}M) & \text{forbidden} \\
2) & ^2B_{1g} \to \,^2B_{2u} & (M\text{-}L) & \text{allowed} \\
3) & ^2A_{2u} \to \,^2A_{1g} & (L\text{-}M) & \text{allowed} \\
4) & ^2A_{2u} \to \,^2B_{2u} & (L\text{-}L) & \text{forbidden}
\end{array}
\qquad (9.\text{A}11)
$$

The first and fourth contributions are forbidden by symmetry, and the second is vanishingly small, as observed by the absence of the $^2B_{1g} \to \,^2B_{2u}$ transition in the charge transfer spectrum (Desjardins et al 1983). As argued in the vibronic approach above, the third mechanism does provide a plausible explanation for the source of the z polarised intensity. The intensity that is being "stolen" cannot be

directly observed as in corresponds to the $^2A_{2u} \rightarrow \, ^2A_{1g}$ ligand to metal charge transfer transition.

However, even though the fourth $^2A_{2u} \rightarrow \, ^2B_{2u}$ (L-L) contribution is symmetry forbidden at a D_{4h} geometry, the semi-empirical calculations show that for a small static distortion along the b_{2u} coordinate, this mechanism makes the greatest contribution to the intensity. Therefore, as far as the source of the z polarised intensity is concerned, it may be more profitable to view the square planar $CuCl_4^{2-}$ ion at the static RMS geometry along the b_{2u} coordinate. This is then an example of "dynamical symmetry breaking" which has recently been of interest in the literature (Kellman 1983, Levine 1985). It does not represent a breakdown of the Born-Oppenheimer approximation, but rather is due to the fact that this approximation is obeyed. The electronic transition, which takes place on a much faster timescale than the vibrational motions of the molecule, will occur at the D_{2d} geometry that the molecule will have (considering just this one coordinate) at any instant of time.

This approach has many similarities to the work of Kellman (1983), where the overtone spectrum of the C-H stretch vibrations in benzene are interpreted in terms of the C_{2v} point group of the local modes rather than the full D_{6h} point group of the molecule. As Kellman notes, the D_{6h} geometry can be viewed as permutation-inversion group of which C_{2v} is a subgroup. "Dynamical tunnelling" will occur to restore the D_{6h} point group, although there is no "barrier" between the six equivalent C_{2v} geometries. The point group that is the best to view the molecule is then dependent on the timescale of the experiment.

If this mechanism for the z polarised intensity in $CuCl_4^{2-}$ is correct, then it is pertinent to ask why it is necessary in this case when molecular point groups generally work so well in spectroscopy. The reason may be two fold. First, the frequency of this out-of-plane b_{2u} vibration is low and so the RMS angular distortions are quite large; and secondly, the normal Herzberg-Teller intensity source (ie: the $^2B_{1g} \rightarrow \, ^2B_{2u}$ contribution) is very weak.

CHAPTER 10: GENERAL CONCLUSIONS

In the experimental systems considered in this thesis, vibronic coupling was found to be essential in the interpretation of their spectroscopic properties. This has led to the re-interpretation of many previous studies and stresses the importance of including vibronic interactions in the study of transition metal spectroscopy.

It was found that the temperature dependent g-values of six coordinate copper(II) complexes could be successfully explained using a Jahn-Teller Hamiltonian appropriate to a cubic system with strain terms describing the departure from high symmetry. These strain terms result, to a large extent, in the quenching of the dynamic nature of the vibronic wavefunctions that occur in cubic systems. However, the formalism developed here gives a convenient method of calculating the electronic and geometric properties of the vibronic energy levels in low symmetry complexes. The parameters used in the model can be re-lated to the bonding properties of the ligands in a consistent manner.

The d-d electronic spectrum of square planar $CuCl_4^{2-}$ was also successfully interpreted in terms of vibronic interactions, both as a source of intensity and as the cause of unusual temperature effects. A double minima excited state potential was found to be necessary to explain the shift in the band maxima that was experimentally observed.

Although only a small number of experimental systems have been considered here, it is clear from their spectral properties, that vibronic interactions in general can be crucial in determining the electronic and geometric properties of transition metal complexes.

Finally, as much of chemistry finds justification in biological applications, it is noted that there has recently been much interest in the temperature dependent spectroscopy of proteins with transition metal centres. It has been thought (Bacci and Cannistraro 1987) that vibronic coupling could play an important role in the active site dynamics of such biomolecules.

CHAPTER 11   REFERENCES:

Abragam A. and Bleaney B., "Electron Paramagnetic Resonance of Transition
          Metal Ions", Claredon Press, Oxford, (1970).

Abramowitz M. and Stegun I.A., "Handbook of Mathematical Functions",
          Dover, New York, (1972).

Adams D.M. and Trumble W.R. Inorg.Chim.Acta, $\underline{10}$, 235, (1974).

Albrecht A.C., J.Chem.Phys., $\underline{33}$, 156, (1960).

Alcock N.W., Duggan M., Murray A., Tyagi S., Hathaway B.J. and Hewat A.,
          J.Chem.Soc. Dalton Trans., 7, (1984).

Alder-Golden S.M., J.Chem.Phys., $\underline{89}$, 964, (1985).

Almgren F.J. and Taylor J.E., Sci.Am., July, 82, (1976).

Ammeter J.H., Burgi H.B., Gamp E., Meyer-Sandrin V. and Jensen W.P.,
          Inorg.Chem., $\underline{18}$, 733, (1979).

Ansbacher F., Z.Naturforsch., $\underline{14A}$, 889, (1959).

Atkins P.W., "Physical Chemistry", 2nd Ed, Ox.Uni.Press, Oxford, (1982).

Bacci M., Chem.Phys.Lett., $\underline{58}$, 537, (1978).

_____, Chem.Phys., $\underline{40}$, 237, (1979).

_____, Chem.Phys., $\underline{88}$, 39, (1984).

_____ and Cannistraro S., Chem.Phys.Lett., $\underline{133}$, 109, (1987).

Bagguley D.S. and Griffiths J.H.E., Proc.Roy.Soc.(Lond), $\underline{65A}$, 594,(1952).

Ballhausen C.J., "Introduction to Ligand Field Theory", McGraw-Hill,
          New York, (1962).

_____, Theoret.Chim.Acta., $\underline{3}$, 368, (1965).

_____, in: "Semi-Emperical Methods of Electronic Structure
          Calculation, Part B: Applications", G.A. Segal (Ed.),
          Plenum Press, New York, (1977); pg 159.

_____ and Hansen A.E., Ann.Rev.Phys.Chem., $\underline{23}$, 15, (1972).

_____, Bjerrum N., Dingle R., Eriks K. and Hare C.R.,
          Inorg.Chem., $\underline{4}$, 514, (1965).

Balsa R., Plo M., Esteve J.G. and Pacheco A.F.,Phys.Rev.D,$\underline{28}$,1945,(1983).

Barentzen H., Olbich G. and O'Brien M.C.M., J.Phys.A, $\underline{14}$, 111, (1981).

Bates C.A., Phys.Reports, $\underline{35}$, 188, (1978).

Bechtle B., Boettcher F. and Spaeth J.M., phys.stat.solidi(b), $\underline{43}$,
          K169, (1971).

Bersuker I.B., Coord.Chem.Rev., $\underline{14}$, 357, (1975).

_____, "The Jahn-Teller Effect and Vibronic Interactions in
    Modern Chemistry", Plenum, New York, (1984a).

_____, "The Jahn-Teller Effect: A Bibliographic Review",
    Plenum, New York, (1984b).

_____ and Polinger V.Z., Adv.Quant.Chem., $\underline{15}$, 85, (1982).

_____, pg 21 in: Perlin and Wagner (1984).

Bertini I., Gatteschi D. and Scozzafava A., Coord.Chem.Rev.,$\underline{29}$,67,(1979).

Bethe H.A., Ann.Physik, $\underline{3}$, 133, (1929).

Bhakay-Tamhane S.N., Sequeira A. and Chidambaram R., Acta Cryst.,$\underline{B36}$,2925,(1980).

Bill H., pg 709 in: Perlin and Wagner (1984).

Billing D.E., Hathaway B.J. and Tomlinson A.G., J.Chem.Soc.A,2839,(1971).

Binsch G., Mol.Phys., $\underline{15}$, 469, (1968).

_____, in: "Dynamic Nuclear Magnetic Resonance Spectroscopy",
    Academic Press, New York, (1975).

Bjorck A., Plemmons R.J. and Schneider H. (Eds.), "Large Scale Matrix
    Problems", North Holland, New York, (1981).

Bleaney B., Bowers K.D. and Ingram D.J.E.,Proc.Roy.Soc.,$\underline{A228}$,147,(1955a).

_____ and Trenam R.S., Proc.Roy.Soc., $\underline{A228}$,157,(1955b).

_____ and Pryce M.H.L., Proc.Roy.Soc.,$\underline{A228}$,166,(1955c).

_____ and Ingram D.J.E., Proc.Phys.Soc., $\underline{A63}$, 408, (1950).

Boatner L.A., Reynolds R.W., Chen Y. and Abraham M.M., Phys.Rev.,
    $\underline{B16}$, 86, (1977).

Boettcher F. and Spaeth J.M., phys.stat.solidi(b), $\underline{61}$, 465, (1974a).

_____, phys.stat.solidi(b), $\underline{62}$, 65, (1974b).

Born M. and Oppenheimer J.R., Ann.Phys., $\underline{84}$, 457, (1927).

Brown G.M. and Chidambaram R., Acta Cryst., $\underline{B25}$, 676, (1969).

Brynstead J., Yakel H.L. and Smith G.P., J.Chem.Phys., $\underline{45}$, 4652, (1966).

Carnahan B., Luther H.A. and Wilkes J.O., "Applied Numerical Methods",
    Wiley, New York, (1966).

Carrington A. and McLachlan A.D., "Introduction to Magnetic Resonance",
    Harper and Row, New York, (1967).

Ceulemans A., Beyens D. and Vanquickenborne L.G., JACS, $\underline{106}$, 5824,(1984).

Chan S.I. and Stelman D., J.Chem.Phys., $\underline{39}$, 545, (1963b).

_____, J.Mol.Spect., $\underline{10}$, 278, (1963a).

Chidambaram R., Navarro Q.O., Garcia A., Linggoatmodjo K., Shi-Chien L., Suh I., Sequeira A. and Srikanta S., Acta Cryst., <u>B26</u>, 827, (1970).

Choudhury P., Gnosh B., Patel M.B. and Bist H.D., J.Raman Spect., <u>16</u>, 149, (1985).

Clayton W.R. and Meyers E.A., Cryst.Struct.Comm., <u>5</u>, 57, (1976a).

_____, Cryst.Struct.Comm., <u>5</u>, 61, (1976b).

_____, Cryst.Struct.Comm., <u>5</u>, 63, (1976c).

Coffman R.E., J.Chem.Phys., <u>48</u>, 609, (1968).

_____, Lyle D.L. and Mattison D.R., J.Phys.Chem., <u>72</u>, 1392,(1968).

Cohen-Tannoudji C., Dui B. and Lahoe F., "Quantum Mechanics", (Two volumes), Wiley, New York, (1977).

Condon E.U. and Shortley G.H., "The Theory of Atomic Spectra", Cambridge University Press, (1935).

Cotton F.A., "Chemical Applications of Group Theory", Interscience, New York, (1963).

Craig D.P., J.Chem.Soc., 2146, (1950).

_____ and Small G.J., J.Chem.Phys., <u>50</u>, 3827, (1969).

Cullen D.L. and Lingafelter E.C., Inorg.Chem., <u>10</u>, 1264, (1971).

Cullum J. and Willoughby R.A., J.Comp.Phys., <u>44</u>, 359, (1981).

Cyvin S.J., "Molecular Vibrations and Mean Square Amplitudes", Elsevier, Amsterdam, (1968).

Dang L.S., Buisson R. and Williams F.I.B., J.Phys.(Paris), <u>35</u>, 49,(1974).

Davis M.J. and Heller E.J., J.Chem.Phys., <u>75</u>, 3922, (1981).

De D.K., Rubins R.S. and Black T.D., Phys.Rev., <u>B29</u>, 71, (1984).

Deeth R.J. and Hitchman M.A., Inorg.Chem., <u>25</u>, 1225, (1986).

Desjardins S.R., Penfield K.W., Cohen S.L., Musselman R.L. and Solomon E.I., JACS, <u>105</u>, 4590, (1983).

Dirac P.A.M., "The Principles of Quantum Mechanics", 4th Ed., Oxford University Press, New York, (1958).

Distler T. and Vaughan P.A., Inorg.Chem., <u>6</u>, 126, (1967).

Doktorov E.V., Malkin I.A. and Man'ko V.I., J.Mol.Spect., <u>77</u>, 178,(1979).

Dongarra J.J., Moler C.B., Bunch J.R. and Stewart G.W., LINPACK User's Guide, SIAM, Philadelphia, (1979).

Dreybrodt W. and Fussgaenger K., phys.stat.sol.(b), <u>18</u>, 133, (1966).

Duggan M., Murphy A. and Hathaway B.J., Inorg.Nucl.Chem.Lett., <u>15</u>, 103, (1979).

Dushinsky F., Acta Phys.Chim.URSS, 7, 551, (1937).

Engberg A., Acta Cryst.Scand., 24, 3510, (1970).
Englman R., Mol.Phys., 3, 23, (1960).
_____, "The Jahn-Teller Effect in Molecules and Crystals",
        Wiley-Interscience, London, (1972).
_____ and Halperin B., Phys.Rev.B, 2, 75, (1970).

Feiner L.F., J.Phys.C, 14, 1955, (1981).
Fender B.E.F., Figgis B.N. and Forsyth J.B., Aust.J.Chem.,39,1023,(1986).
Fenske R.F. and Sweeney C.C., Inorg.Chem., 3, 1105, (1964).
Ferguson J., Prog.Inorg.Chem., 12, 159, (1970).
Ferre J., Regis M., Farge Y. and Kleemann W., J.Phys.C, 12, 2671, (1979).
Fischer G., "Vibronic Coupling", Academic Press, London, (1984).
Figgis B.N., "Introduction to Ligand Fields", Interscience,
            New York, (1966).
Flügge S., "Practical Quantum Mechanics",Springer-Verlag,New York,(1974).
Flurry Jr, R.L., in: Maruani and Serre (1983), pp113-132, (1983).
Fredericks G.E., Phys.Rev.B, 4, 911, (1971).
Freeman T.E. and Pilbrow J.R., J.Phys.C, 7, 2365, (1974).
Friebel C., Propach V. and Reinen D., Z.Naturforsch, 31B, 1574, (1976).
Fuhrer H., Kartha V.B., Kidd K.G., Krueger P.J. and Mantsch H.H.,
        "Normal Coordinate Analysis", NRCC Bulletin, 15, (1976).
Fussgaenger K., Martienssen W. and Bilz H., phys.stat.solidi(b), 12,
            383, (1965).

Gans P., Advances in IR and Raman Spectroscopy, 3, 87, (1977).
Gauthier N. and Walker M.B., J.Can.Phys., 54, 9, (1976).
Gerloch M., "Magnetism and Ligand Field Analysis",
        Cambridge Uni.Press, Cambridge, (1983).
_____ and McMeeking R.F., J.Chem.Soc.Dalton, 2443, (1975).
_____ and Slade R.C., "Ligand Field Parameters",
        Cambridge Uni. Press, Cambridge, (1973).
Getz D. and Silver B.L., J.Chem.Phys., 61, 630, (1974).
Golding R.M., "Applied Wave Mechanics", Van Nostrond, London, (1969).
Goldstein H., "Classical Mechanics", Addison-Wesley, Reading, (1980).
Griffith J.S., "The Theory of Transition Metal Ions",
            Cambridge Uni. Press, Cambridge, (1961).

Griller D. and Preston K.F., JACS, <u>101</u>, 1975, (1976).

Grimes N.W., Kay H.F. and Webb M.W., Acta Cryst., <u>16</u>, 823, (1963).

Hagen S.H. and Trappeniers N.J., Physica, <u>47</u>, 165, (1970).

                , Physica, <u>66</u>, 166, (1973).

Ham F.S., Phys.Rev., <u>138</u>, A1727, (1965).

       , Phys.Rev., <u>166</u>, 307, (1968).

       , in: "Electron Paramagnetic Resonance",
S.Geschwind (Ed.), Plenum, New York, (1972).

Hanic V.F. and Cakajdova I.I.A., Acta Cryst., <u>11</u>, 610, (1958).

Harlow R.L., Wells W.J., Watt G.W., and Simonsen S.H., Inorg.Chem.,
<u>13</u>, 2106, (1974).

Harriman J.E., "Theoretical Foundations of Electron Spin Resonance",
Academic Press, New York, (1978).

Harris D.C. and Bertolucci M.D., "Symmetry and Spectroscopy",
Oxford University Press, New York, (1978).

Hathaway B.J., Duggan M., Murphy A., Mullane J., Power C., Walsh A. and
Walsh B., Coord.Chem.Rev., <u>36</u>, 267, (1981).

            and Hewat A.W., J.Sol.State Chem., <u>51</u>, 364, (1984).

Hayes W. and Wilkins J., Proc.Roy.Soc., <u>281A</u>, 340, (1964).

Heinzer J., Mol.Phys., <u>22</u>, 167, (1971).

Heilbronner E., Gunthard H.H. and Gerdil R., Helv.Chim.Acta, <u>39</u>,
1171, (1956).

Heller E.J., Acc.Chem.Res., <u>14</u>, 368, (1981).

Henderson J.R., Muramoto M. and Willett R.A.,J.Chem.Phys.,<u>41</u>,580,(1964a).

           , Willett R.A., Muramoto M. and Richardson D.R., "A Table
of Franck-Condon Overlap Integrals Including Displacement
of the Normal Coordinates", Douglas Report, SM-45807,
Jan.,(1964b).

Henneker W.H., Pawlikowski M., Siebrand W. and Zgierski M.Z.,
J.Chem.Phys., <u>87</u>, 4805, (1983).

           , Siebrand W. and Zgierski M.Z.,Chem.Phys.Lett.,<u>68</u>,5,(1979).

Herdtweck E. and Babel D., Z.Krist., <u>153</u>, 189, (1980).

Herzberg G., "Spectra of Diatomic Molecules", Van Nostrand, N.Y., (1950).

           , "Electronic Spectra and Electronic Structure of Polyatomic
Moleclues", Van Nostrand, New York, (1966).

Hitchman M.A., J.Chem.Soc.(A), 4, (1970).

_____, Inorg.Chem., 21, 821, (1982).

_____, Trans.Metal Chem., 9, 1, (1985a).

_____, Inorg.Chem., 24, 4762, (1985b).

_____, personal communication, (1986).

_____ and Cassidy P.J., Inorg.Chem., 18, 1745, (1979).

_____ and Waite T.D., Inorg.Chem., 15, 2150, (1976).

_____, McDonald R.G. and Reinen D., Inorg.Chem., 25, 519, (1986).

Hodgeson P.G., Whitnall J., Kennard C.H.L. and Moore F.H.,
        Cryst.Struct.Comm., 4, 713, (1975).

Hutchisson E., Phys.Rev., 36, 410, (1930).

Innes K.K., J.Mol.Spect., 120, 1, (1986).

Isaacs N.W. and Kennard C.H.L., J.Chem.Soc A, 386, (1969).

Jahn H.A., Proc.Roy.Soc.(London), A164, 117, (1938).

_____ and Teller E., Proc.Roy.Soc.(London), A161, 220, (1937).

Jenkins T.E. and Lewis J., Spect.Acta, 37A, 47, (1981).

Judd B.R., Can.J.Phys., 52, 999, (1974).

_____, J.Chem.Phys., 67, 1174, (1977).

_____, J.Phys.C, 12, 1685, (1979).

Kannon K.K. and Viswamitra M.A., Z.Kristallogr., 122, 161, (1965).

Kaplan J.I. and Fraenkel G., "NMR of Chemically Exchanging Systems",
        Academic Press, New York, (1980).

Kellman M.E., J.Phys.Chem., 87, 2161, (1983).

Kettle S.F.A., Inorg.Chem., 4, 1821, (1965).
        Note: There is a misprint in Table I; $\cos\theta_n$ in the
        expression for $G(d_{yz})$ should read $\sin\theta_n$.

Kleemann W. and Farge Y., J.Physique, 36, 1293, (1975).

Kojima K. and Matsuda J., Bull.Chem.Soc.Japan, 59, 859, (1986).

Koningstein J.A., Vib.Spectra and Struct., 9, 115, (1980).

Köning E. and Kremer S., "Ligand Field Energy Diagrams",
        Plenum Press, New York, (1977).

Koster G.F., Dimmock J.O., Wheeler R.G. and Statz H., "Properties of the
        Thirty-Two Point Groups", MIT Press, Cambridge Mass.,(1963).

Kubo R. and Toyozawa Y., Prog.Theor.Phys., 13, 160, (1955).

Kupka H. and Cribb P.H., J.Chem.Phys., <u>85</u>, 1303, (1986).

Kuroda N. and Kawamori A., J.Phys.Chem.Solids, <u>32</u>, 1233, (1971).

Kurzynski M., J.Phys.C, <u>8</u>, 2749, (1975).

_____, Acta.Phys.Polonica, <u>A52</u>, 647, (1977).

Laiho R., phys.stat.solidi(b), <u>69</u>, 579, (1975).

_____ and Treshchalov A., Chem.Phys.Lett., <u>80</u>, 576, (1981).

Landau L.D. and Lifshitz E.M., "Quantum Mechanics", 3rd Ed.,
        Pergamon Press, Oxford, (1977).

Larsen E. and La Mar G.N., J.Chem.Ed., <u>51</u>, 633, (1974).
        Note: There are misprints in table 1 of this reference.
        See Schaffer (1968) table 2b for the correct expressions.

Lee S.Y., J.Chem.Ed., <u>62</u>, 561, (1985).

Leligny P.H. and Monier J.C., Acta Cryst., <u>B35</u>, 569, (1979).

Lever A.B.P., "Inorganic Spectroscopy", 2nd Ed.,
        Elsevier, Amsterdam, (1984).

Levine R.D., J.Phys.Chem., <u>89</u>, 2122, (1985).

Liehr A.D., J.Phys.Chem., <u>67</u>, 389, (1963).

_____ and Ballhausen C.J., Ann.Phys., <u>3</u>, 304, (1958).

Longuet-Higgins H.C., Advanc.Spectros., <u>2</u>, 429, (1961).

_____, Mol.Phys., <u>6</u>, 445, (1963).

_____, Öpik U., Pryce M.H.L. and Sack R.A., Proc.Roy.Soc.,
        <u>A244</u>, 1, (1958).

Lohr L.L., J.Chem.Phys., <u>50</u>, 4596, (1969).

_____, JACS, <u>92</u>, 2210, (1970).

Mabbs F.E. and Machin D.J., "Magnetism and Transition Metal Complexes",
        Chapman and Hall, London, (1973).

Marechal Y., J.Chem.Phys., <u>83</u>, 247, (1985).

Margulis T.N. and Templeton D.H., Z.Kristallogr., <u>117</u>, 344, (1962).

Markham J.J., Rev.Mod.Phys., <u>31</u>, 956, (1959).

Martin Jr. D.S., Tucker M.A. and Kassman A.J., Inorg.Chem.,<u>4</u>,1682,(1965).

Maruani J. and Serre J., "Symmetries and Properties of Non-Rigid
        Molecules", Elsevier, Amsterdam, (1983).

Mazzi F., Acta Cryst., <u>8</u>, 137, (1955).

McDonald R.G., personal communication, (1986).

_____ and Hitchman M.A., Inorg.Chem., <u>25</u>, 3273, (1986).

McGarvey B.R., Trans.Metal Chem., <u>3</u>, 89, (1966).

McGinnety J.A., JACS, 94, 8406, (1972).

McIntosh H.V. and Beebe N.H.F., "<PLOT79>: A Graphics Software Package", University of Utah, Salt Lake City, (1979).

McLachlan A.D., Mol.Phys., 5, 417, (1961).

Mills I.M., J.Phys.Chem., 88, 532, (1984).

Monge A. and Gutierrez-Puebla E., Acta Cryst., B37, 427, (1981).

Montgomery H., Chastain R.V. and Lingafelter E.C., Acta Cryst., 20, 731, (1966).

_____, Natt J.J., Witkowska A.M. and Lingafelter E.C., Acta Cryst., 22, 775, (1967).

_____ and Lingafelter E.C., Acta Cryst., 17, 1295, (1964a).

_____, Acta Cryst., 17, 1478, (1964b).

_____, Acta Cryst., 20, 659, (1966a).

_____, Acta Cryst., 20, 728, (1966b).

Morales J., Palma A. and Berrondo M., Int.J.Quat.Sym., 18, 57, (1984).

Moule D.C., Vib.Spectra and Struct., 6, 227, (1977).

Mulliken R.S., J.Chem.Phys., 55, 309, (1971).

Nakagawa I. and Shimanouchi T., Spect.Acta, 20, 429, (1964).

Nelson H.C., Simonsen S.H. and Watt G.W., J.Chem.Soc.Comm., 632, (1979).

Noda C. and Zare R.N., J.Mol.Spect., 95, 254, (1982).

O'Brien M.C.M., Proc.Roy.Soc.(London), A281, 323, (1964).

_____, J.Phys.C, 5, 2045, (1972).

_____, Vib.Spectra and Struct., 10, 321, (1981).

_____, J.Phys.C, 16, 85, (1983).

_____, J.Phys.C, 17, 3449, (1984).

_____ and Evangelou S.N., J.Phys.C, 13, 611, (1980).

Öpik U. and Pryce M.H.L., Proc.Roy.Soc., A238, 425, (1957).

Orlandi G., Chem.Phys.Lett., 19, 459, (1973).

_____ and Siebrand W., Chem.Phys.Lett., 15, 465, (1972).

_____, J.Chem.Phys., 58, 4513, (1973).

Papousek D. and Aliev M.R., "Molecular Vibrational-Rotational Spectra", Elsevier, Amsterdam, (1983).

Parlett B.N., "The Symmetric Eigenvalue Problem", Prentice-Hall, Englewood Cliffs, (1980).

_____ and Reid J.K., AERE Report CSS 83, Harwell, (1980).

Pease M.C., "Methods of Matrix Algebra", Academic Press, New York,(1965).

Pelikan P., Breza M. and Boca R., Polyhedra, 4, 1543, (1985).

Perlin Yu.E. and Wagner M. (Eds.), "The Dynamical Jahn-Teller Effect in
            Localised Systems", North Holland, Amsterdam, (1984).

Perry C.H. and Lowndes R.P., J.Chem.Phys., 51, 3648, (1969).

Petrashen V.E., Yablakov Yu.V. and Davidovitch R.L., phys.stat.solidi(b),
            101, 117, (1980).

Piepho S.B. and Schatz P.N., "Group Theory in Spectroscopy with
            Applications to MCD", Wiley, New York, (1983).

Pilbrow J.R. and Spaeth J.M., phys.stat.solidi(b), 20, 225, (1967a).

_____, phys.stat.solidi(b), 20, 237, (1967b).

Pissanetsky S., "Sparse Matrix Technology", Academic Press,London,(1984).

Poole C.P. and Farach H.A., "The Theory of Magnetic Resonance",
            Wiley, New York, (1972).

Poupko R. and Luz Z., J.Chem.Phys., 57, 3311, (1972).

Prassides K. and Day P., J.Chem.Soc.Farad.Trans.2, 80, 85, (1984).
            Note: There is a misprint in equation 3 of this paper.
            See equation (3.57) for the correct expression.

Reddy T.R. and Srinivasan R., Phys.Lett., 22, 143, (1966).

Reik H.G., in: Perlin and Wagner (1984), pp117-153, (1984).

_____ and Doucha M., Chem.Phys.Lett., 127, 413, (1986).

Reinen D. and Friebel C., Struct.Bond., 37, 1, (1979).

_____ and Krause S., Inorg.Chem., 20, 2750, (1981).

Reynolds R.W. and Boatner L.A., Phys.Rev.B, 12, 4735, (1975).

_____, Boatner L.A., Abraham M.M. and Chen Y., Phys.Rev.B, 10,
            3802, (1974).

Riley M.J., Hitchman M.A. and Reinen D., Chem.Phys., 102, 11, (1986).

Robinson D.J. and Kennard C.H.L., Cryst.Struct.Comm., 1, 185, (1972).

Roche M. and Jaffe H.H., Chem.Soc.Rev., 5, 165, (1976).

Rorison J. and O'Brien M.C.M., J.Phys.C, 17, 3449, (1984).

Rubins R.S., Tello L.N., De D.K. and Black T.D. J.Chem.Phys., 81,
            4230, (1984).

Sakamoto N., J.Phys.C, 15, 6379, (1982).

Sandström J., "Dynamic NMR Spectroscopy", Acad.Press, London, (1982).

Schäffer C.E., Struct.and Bond., 5, 68, (1968).

_____, Pure and App.Chem., 24, 361, (1970).

Schiff L.I., "Quantum Mechanics", McGraw-Hill, New York, (1968).

Schmidt K.H. and Muller A., Coord.Chem.Rev., $\underline{19}$, 41, (1976).

_____, Inorg.Chem., $\underline{14}$, 2183, (1975).

Setser G.G., Barksdale A.O. and Estle T.L., Phys.Rev.B, $\underline{12}$, 4720, (1975).

_____ and Estle T.L., Phys.Rev.B, $\underline{17}$, 999, (1978).

Shaffer W.H. and Krohn B.J., J.Mol.Spect., $\underline{63}$, 323, (1976).

Shashkin S.Yu. and Goddard III W.A., Phys.Rev., $\underline{33}$, 1353, (1986).

Shields K.G. and Kennard C.H.L., Cryst.Struct.Comm., $\underline{1}$, 189, (1972).

_____, Van der Zee J.J. and Kennard C.H.L., Cryst.Struct.Comm.,
       $\underline{1}$, 371, (1972a).

_____, Kennard C.H.L. and Moore F.H.,
       personal communication, (1972b).

Silver B.L. and Getz D., J.Chem.Phys., $\underline{61}$, 638, (1974).

Slichter C.P., Seidel H., Schwartz P. and Fredericks G., Phys.Rev.B,
       $\underline{4}$, 907, (1971).

Sloane C.S. and Silbey R., J.Chem.Phys., $\underline{56}$, 6031, (1972).

Slonczewski J.C., Phys.Rev., $\underline{131}$, 1596, (1963).

Small G.J., J.Chem.Phys., $\underline{54}$, 3300, (1971).

Smith B.T., Boyle J.M., Garbow B.S., Ikebe Y., Klema V.C. and Moler C.B.,
       "EISPACK guide",in: Lecture Notes in Computer Science, Vol.6,
       2nd.Ed., Springer-Velag, Berlin, (1976).

Smith D.W., Inorg.Chem.Acta, $\underline{22}$, 107, (1977).
       Note: There is a misprint on page 108 in the expression for
       $E(^2B_2 \rightarrow ^2E)$. The last term $\cos^2\theta$ should read $2\cos^2\theta$.

Smith G., Moore F.H. and Kennard C.H.L., Cryst.Struct.Comm., $\underline{4}$,
       407, (1975).

Somorjai R.L. and Hornig D.F., J.Chem.Phys., $\underline{36}$, 1980, (1962).

Sorokin M.V. and Chirkin G.K., Sov.Phys.Sol.State, $\underline{21}$, 1720, (1979).

Spiegel M.R., "Advanced Mathematics for Engineers and Scientists",
       McGraw-Hill, New York, (1971).

Spirko V., Civis S., Ebert M. and Danielis V., J.Mol.Spect., $\underline{119}$,
       426, (1986).

Steffen G. and Reinen D., personal communication, (1986).

Strickler S.J., J.Phys.Chem., $\underline{80}$, 2149, (1976).

Stround A. and Secrest D., "Gaussian Quadrature Formulas",
       Prentice-Hall, Englewood Cliffs, New Jersey, (1966).

Struck C.W. and Herzfeld F., J.Chem.Phys., $\underline{44}$, 464, (1966).

Sturge M.D., Solid State Phys., $\underline{20}$, 91, (1967).

Syoyama S. and Osaki K., Acta Cryst., B28, 2626, (1972).

Thompson T.C., Truhlar D.G. and Mead C.A., J.Chem.Phys., 82, 2408,(1985).

Thorson W. and Moffitt W., Phys.Rev., 168, 362, (1968).

Trappeniers N.J. and Hagen S.H., Physica, 31, 122, (1965).

_____, Stibbe F.S. and Rao J.L., Chem.Phys.Lett.,56,10,(1978).

Tutt L., Tannor D., Heller E.J. and Zink J.I., Inorg.Chem.,
        21, 3859, (1982).

_____, Schindler J., Heller E.J. and Zink J.I.,
        J.Phys.Chem., 87, 3017, (1983).

_____, Zink J.I. and Heller E.J., Inorg.Chem., (in press), (1987).

Udupa M.R. and Krebs B., Inorg.Chim.Acta, 33, 241, (1979).

Van der Avoird A. and Ros., Theor.Chim.Acta, 4, 13, (1963).

Van der Valk P.J. and Trappeniers N.J., Chem.Phys.Lett., 52, 255, (1977).

Van der Zee J.J., Shields K.G., Graham A.J. and Kennard C.H.L., Cryst.
        Struct.Comm., 1, 367, (1972).

Viaene L., Ceulemans A., and Vanquickenborne L.G., Inorg.Chem., 24,
        1713, (1985).

Vincent A., "Molecular Symmetry and Group Theory", Wiley, London, (1977).

Waite T.D. and Hitchman M.A., Inorg.Chem., 15, 2150, (1976).

Waldenstrom S. and Naqvi K.R., Chem.Phys.Lett., 85, 581, (1982).

Wan Mohamed W.A., Honours Thesis, University of Tasmania, (1985).

Watanabe K. and Abe H., phys.stat.solidi(b), 72, 275, (1975a).

_____, J.Phys.Soc.Japan, 38, 755, (1975b).

Webb M.W., Kay H.F., and Grimes N.W., Acta Cryst., 18, 740, (1965).

Weissbluth M., "Atoms and Molecules", Academic Press, New York, (1978).

Wells A.F., Acta Cryst., 2, 175, (1949).

Wertz J.E. and Bolton J.R., "Electron Spin Resonance: Elementary Theory
        and Applications", McGraw-Hill, New York, (1972).

Whitnall J., Kennard C.H.L., Nimmo J. and Moore F.H., Cryst.Struct.
        Comm., 4, 709, (1975a).

_____, Cryst.Struct.
        Comm., 4, 717, (1975b).

Williams F.I.B., Krupka D.C. and Breen D.P., Phys.Rev., 179, 225, (1969).

Willis B.T.M. and Pryor A.W., "Thermal Vibrations in Crystallography", Cambridge University Press, (1975).

Wilson E.B., Decius J.C. and Cross P.C., "Molecular Vibrations", Dover, New York, (1955).

Woolley R.G., Chem.Phys.Lett., 79, 395, (1981).

Yamatera H., Acta Chem.Scand.A, 33, 107, (1979).

Yersin H., Otto H., Zink J.I. and Gliemann G., JACS, 102, 951, (1980).
    Note: There are misprints in equations 2b,3b,4a,4b and in the expressions for the constants C and D in this paper. The correct expressions are given by equation (3.17).

Zaitdinov A.M., Davidovitch R.L., Shevchenko V.Ya. and Yablokov Yu.V., Koord.Khim., 9, 1644, (1983).

_____, Zaripov M.M., Yablokov Yu.V. and Davidovitch R.L., phys.stat.solidi (b), 78, K69, (1976).

Zaripov M.M. and Chirkin G.K., Sov.Phys.Sol.State, 6, 1290, (1964).

Ziegler L. and Albrecht A.C., J.Chem.Phys., 60, 3558, (1974).

Zwanziger J.W., Grant E.R. and Erza G.S., J.Chem.Phys., 85, 2089, (1986).